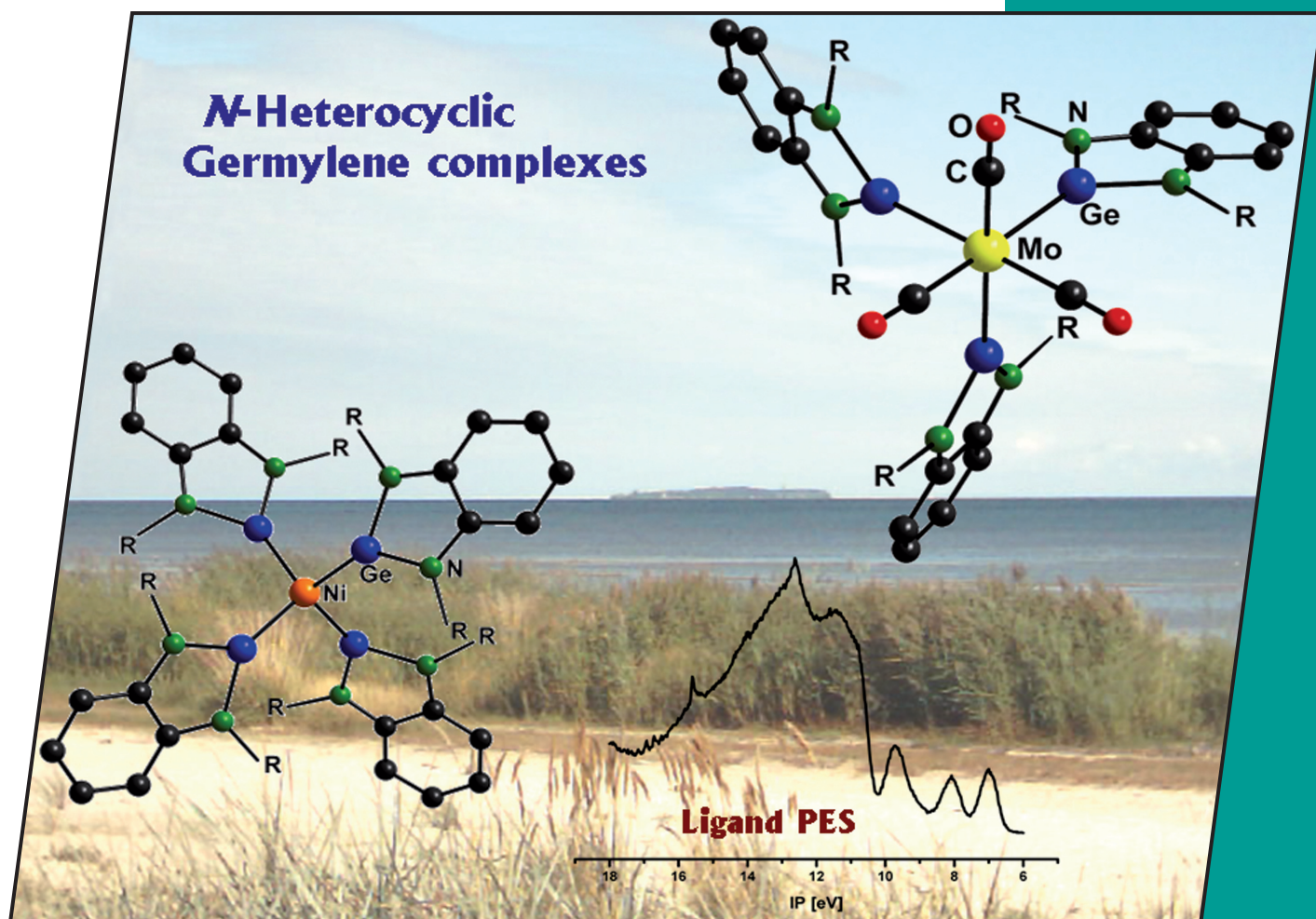


2/2009
2nd January Issue

EurJIC
European Journal of
Inorganic Chemistry

**N-Heterocyclic
Germylene complexes**



Cover Picture

Tamas Veszprémi, Joachim Heinicke et al.
Transition Metal Complexes of N-Heterocyclic Germylenes

Microreview

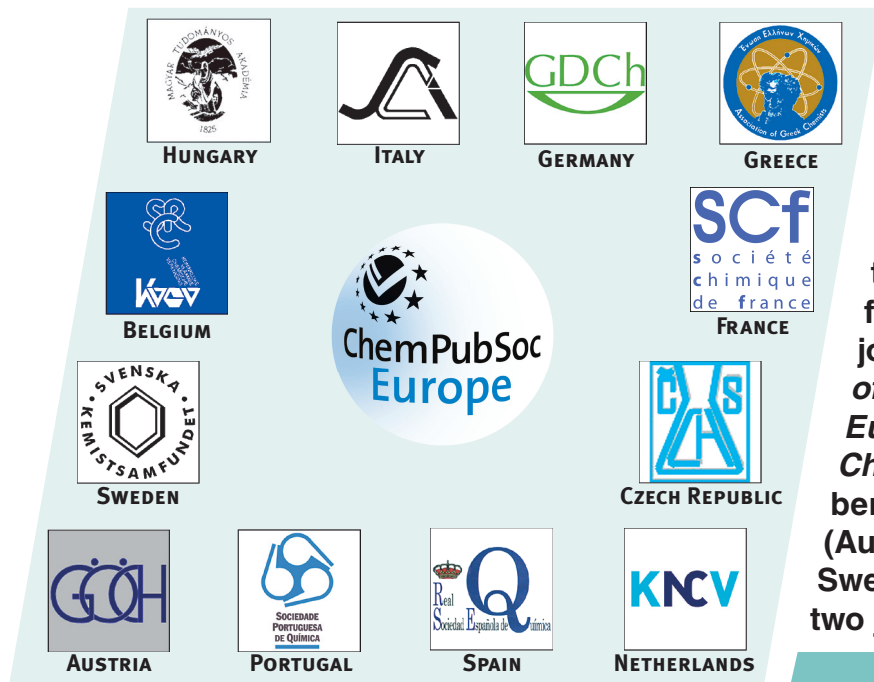
Arjan W. Kleij
Nonsymmetrical Salen Ligands and Their Complexes

WILEY-VCH

www.eurjic.org

A Journal of

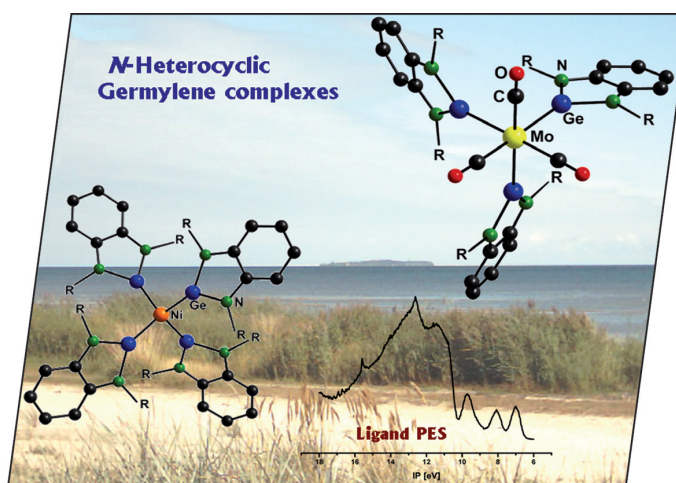


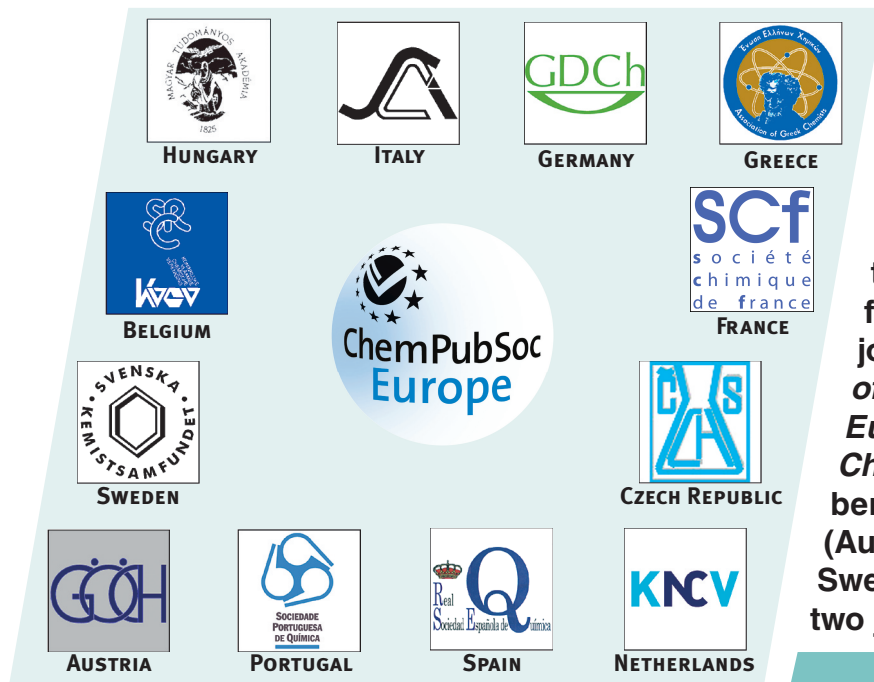


A union formed by chemical societies in Europe (ChemPubSoc Europe) has taken the significant step into the future by merging their traditional journals, to form two leading chemistry journals, the *European Journal of Inorganic Chemistry* and the *European Journal of Organic Chemistry*. Three further members of ChemPubSoc Europe (Austria, Czech Republic and Sweden) are Associates of the two journals.

COVER PICTURE

The cover picture shows the X-ray crystal structures of new benzo-anellated N-heterocyclic germylene complexes with nickel(0) and molybdenum(0). The low bathochromic shift of the valence vibration of CO in the *trans* position of the germylene ligands of *fac*-(bnNHGe)₃Mo(CO)₃ indicates weak donor properties, the relatively short Mo–Ge^{II} bonds indicate stabilization by back-bonding. The ligand properties contrast strongly with those of the homologous N-heterocyclic carbene ligand (bnNHC) because of the different electronic structures, which can also be recognised from the photoelectron spectrum of the germylene ligand. The Ge^{II} electron lone pair is bound firmly, and according to quantum chemical calculations represents only the third band, whereas in bnNHC the lone electron pair is the HOMO. The extreme air and moisture sensitivity of the NHGe complexes is in sharp contrast with the background, depicting the Baltic Sea with the small island Greifswalder Oie at the seaside entrance to the site of one of the oldest universities in northern Europe. Details are discussed in the article by T. Veszprémi, J. Heinicke et al. on p. 221ff. We thank Prof. Dr. Martin Köckerling (Rostock) and Dr. Lutz Wolf (Kahla) for support in designing this picture.

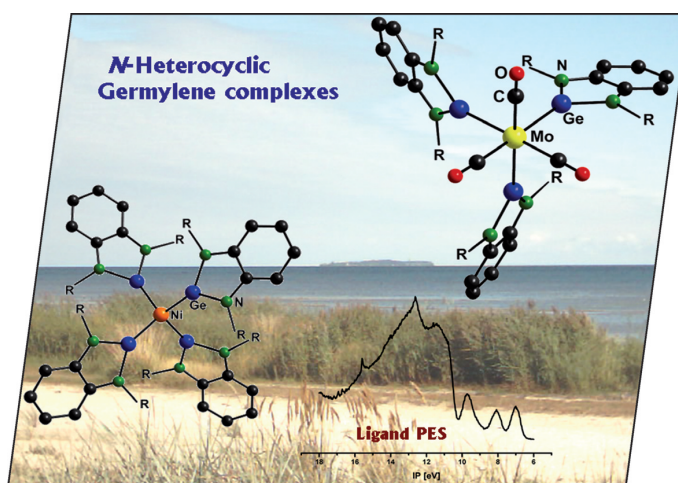




A union formed by chemical societies in Europe (ChemPubSoc Europe) has taken the significant step into the future by merging their traditional journals, to form two leading chemistry journals, the *European Journal of Inorganic Chemistry* and the *European Journal of Organic Chemistry*. Three further members of ChemPubSoc Europe (Austria, Czech Republic and Sweden) are Associates of the two journals.

COVER PICTURE

The cover picture shows the X-ray crystal structures of new benzo-anellated N-heterocyclic germylene complexes with nickel(0) and molybdenum(0). The low bathochromic shift of the valence vibration of CO in the *trans* position of the germylene ligands of *fac*-(bnNHGe)₃Mo(CO)₃ indicates weak donor properties, the relatively short Mo–Ge^{II} bonds indicate stabilization by back-bonding. The ligand properties contrast strongly with those of the homologous N-heterocyclic carbene ligand (bnNHC) because of the different electronic structures, which can also be recognised from the photoelectron spectrum of the germylene ligand. The Ge^{II} electron lone pair is bound firmly, and according to quantum chemical calculations represents only the third band, whereas in bnNHC the lone electron pair is the HOMO. The extreme air and moisture sensitivity of the NHGe complexes is in sharp contrast with the background, depicting the Baltic Sea with the small island Greifswalder Oie at the seaside entrance to the site of one of the oldest universities in northern Europe. Details are discussed in the article by T. Veszprémi, J. Heinicke et al. on p. 221ff. We thank Prof. Dr. Martin Köckerling (Rostock) and Dr. Lutz Wolf (Kahla) for support in designing this picture.



CONTENTS

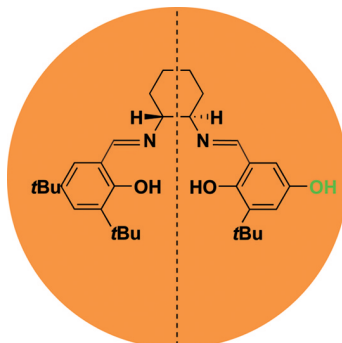
MICROREVIEW

Unsymmetrical Salen Derivatives

A. W. Kleij* 193–205

Nonsymmetrical Salen Ligands and Their Complexes: Synthesis and Applications

Keywords: Asymmetric catalysis / Ligand design / N,O ligands / Nonsymmetrical ligands



How to break symmetry ...

Nonsymmetrical (metallo)salen compounds are highly useful synthons for innovative homogeneous catalysis and the construction of macromolecular/supramolecular structures. This review focuses on the recent advances in synthetic salen chemistry devoted to unsymmetrical derivatives, and fascinating examples of their application potential are presented.

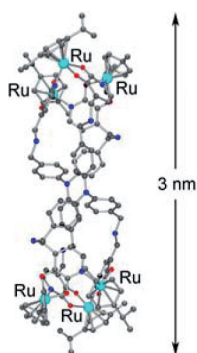
SHORT COMMUNICATIONS

Cylindrical Nanostructures

C. Olivier, R. Scopelliti,
K. Severin* 207–210

Expanding the Size of Organometallic Nanostructures: A Hexanuclear (Cymene)Ru Cylinder with a Length of More Than 3 nm

Keywords: Macrocycles / Nanostructures / Organometallic complexes / Ruthenium / Self-assembly



A cylindrical nanostructure containing six (*p*-cymene)Ru fragments and two bridging ligands was obtained by base-assisted reaction of a tris(dihydroxypyridine) ligand with [(*p*-cymene)RuCl₂]₂.

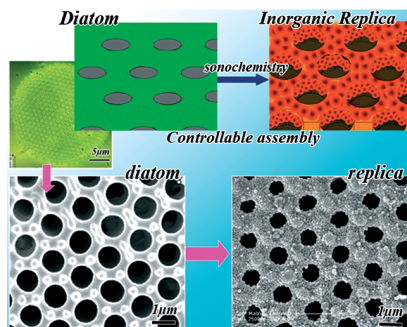
Photonic Nanostructures

H. Zhou, T. Fan,* X. Li, J. Ding,
D. Zhang,* X. Li, Y. Gao 211–215



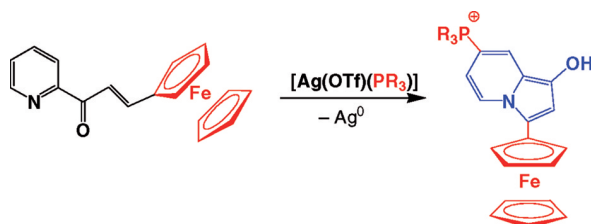
Bio-Inspired Bottom-Up Assembly of Diatom-Templated Ordered Porous Metal Chalcogenide Meso/Nanostructures

Keywords: Chalcogens / Sonochemistry / Mesoporous materials / Nanostructures



A controllable assembly of metal chalcogenide nanoparticles onto ordered porous diatom meso/nanostructures by a sonochemical method has been developed. The inorganic replicas copy the morphology of the ordered porous structure and inherit its optical property. Photonic properties in the replicas can be tuned by assembly of various metal chalcogenide semiconductors of different refractive indexes.

Ferrocene-Containing Indolizines



Silver salts are used as promoters for the cyclization to novel ferrocene-containing indolizine systems in only one step and

with the simultaneous activation of the 7-position of the heterocyclic ring.

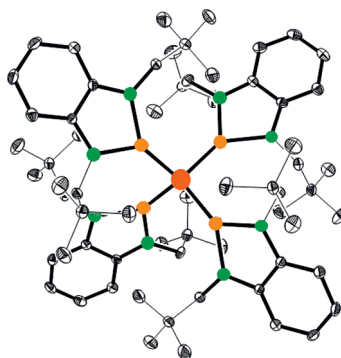
J. E. Aguado, C. Cativiela,
M. C. Gimeno,* P. G. Jones, A. Laguna,
C. Sarroca 216–219

Unexpected Formation of Ferrocene-Containing Indolizines by Tandem Cyclization–Activation Reactions Induced by Silver Salts

Keywords: Heterocycles / Cyclization / Silver / Phosphonium salts / Ferrocene derivatives

FULL PAPERS

The CO valence vibrations and short Ge^{II}–Mo bonds in *fac*–[(NHGe)₃Mo(CO)₃] and [Ni(NHGe)₄], both of which contain N-heterocyclic germylene ligands, indicate the weak donor and good π -acceptor properties of these ligands, in line with quantum chemical studies and their PES orbital ionization potentials. The ligand bending in the complexes may be due to packing effects.



Germylene Complexes

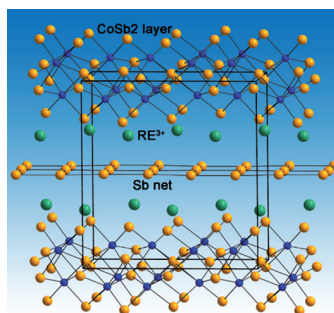
F. Ullah, O. Köhl, G. Bajor, T. Veszprémi,*
P. G. Jones, J. Heinicke* 221–229

Transition Metal Complexes of N-Heterocyclic Germylenes

Keywords: Germanium / Molybdenum / Nickel / Carbenoids / Quantum chemical calculations

Rare-Earth Cobalt Antimonides

Five new ternary cobalt antimonides β -RECoSb₃ (RE = La–Nd, Sm) have been synthesized and characterized. The structural relationship among parent, α - and β -type of RE₂Sb₃ has been elucidated. The TB-LMTO calculations revealed that LaCoSb₃ is an anisotropic metal and no spin-polarization occurred around the Fermi level.



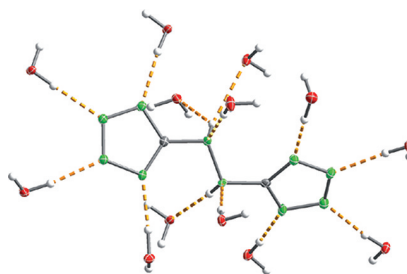
W.-Z. Cai, L.-M. Wu, L.-H. Li,
L. Chen* 230–237

Syntheses, Structures, and Theoretical Studies of New Ternary Antimonides β -RECoSb₃ (RE = La–Nd, Sm)

Keywords: Transition metals / Rare earth metal compounds / Cobalt / Antimony / Electronic structure / Calculations / Tight-binding linear muffin-tin orbital method

Pyrotechnics

Salts with the nitrogen-rich 5,5'-hydrazine-1,2-diylbis(tetrazolate) anion and alkaline earth metals were synthesized and fully characterized. The great thermal stability in combination with a high nitrogen content make the compounds interesting as ingredients for environmentally friendly pyrotechnic compositions.



K. Karaghiosoff, T. M. Klapötke,*
C. M. Sabaté 238–250

Nitrogen-Rich Compounds in Pyrotechnics: Alkaline Earth Metal Salts of 5,5'-Hydrazine-1,2-diylbis(1H-tetrazole)

Keywords: Nitrogen heterocycles / Nitrogen-rich compounds / Alkaline earth metals / Pyrotechnics

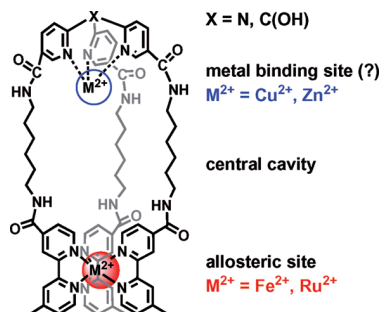
CONTENTS

Supramolecular Cages

H. Szelke, H. Wadepohl, M. Abu-Youssef,
R. Krämer* 251–260

Toward an Allosteric Metallated Container

Keywords: Allosterism / Supramolecular chemistry / Cage compounds / Iron / Ruthenium



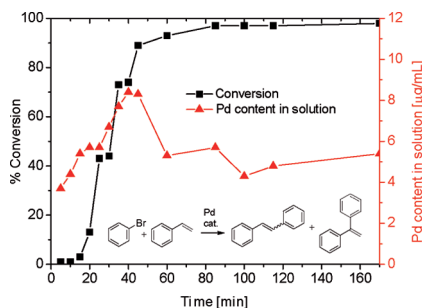
To mimic effective shielding of reactive metal sites in metalloproteins, new polytopic ligands were prepared, and they form a cage-like structure upon coordination of Fe^{2+} and Ru^{2+} . However, binding of Zn^{2+} and Cu^{2+} biometals to a vacant tris(pyrid-2-yl) site in the interior of the container appears to be disfavoured, indicating a negative allosteric effect.

Supported Palladium Catalysts

W. Kleist, J.-K. Lee,
K. Köhler* 261–266

Pd/MO_x Materials Synthesized by Sol-Gel Coprecipitation as Catalysts for Carbon–Carbon Coupling Reactions of Aryl Bromides and Chlorides

Keywords: C–C Coupling / Heck reaction / Palladium / Sol-gel processes / Supported catalysts



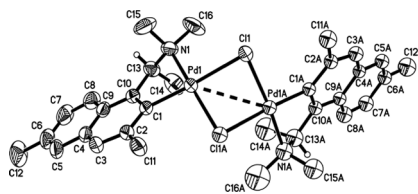
Coprecipitation of Pd/MO_x via sol-gel routes leads to a strong Pd-support interaction. These catalysts are efficient in Heck reactions where the catalytically active species is generated by dissolution of Pd from the support. In consequence of the strong Pd-support interaction, this occurs only at high temperatures ($\geq 160^\circ\text{C}$) which are necessary for the activation of aryl bromides and chlorides.

Chiral Palladacycles

Y. Ding, Y. Li, S. A. Pullarkat,
S. L. Yap, P.-H. Leung* 267–276

Rational Design of a Novel Chiral Palladacycle: Synthesis, Optical Resolution, and Stereochemical Evaluation

Keywords: Asymmetric synthesis / Palladium / Chiral resolution / Cycloaddition



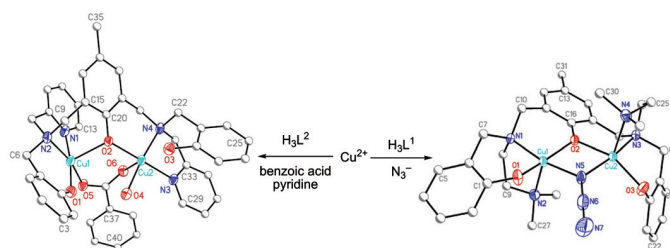
A racemic cyclopalladated complex was efficiently resolved through the formation of its (*S*)-prolinato derivatives. The new chiral palladacycle showed high stereoselectivity in the chiral template-promoted asymmetric Diels–Alder reaction of coordinated 3,4-dimethyl-1-phenylphosphole and *N,N*-dimethylacrylamide.

Binucleating Ligands

A. Banerjee, R. Singh, E. Colacio,
K. K. Rajak* 277–284

Binuclear Copper(II) Chelates with Heptadentate Ligands: Synthesis, Structure, Magnetic Properties, DFT Studies, and Catecholase and Hydrolytic DNA Cleavage Activity

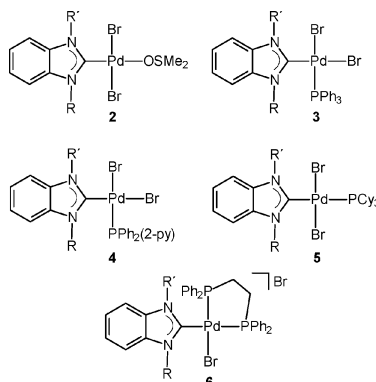
Keywords: Copper / Magnetic properties / Density functional calculations / DNA cleavage



Heterobridged μ -phenoxido, $\mu_{1,1}$ azido, and μ -phenoxido $\mu_{sym-sym}$ -benzoato-bridged binuclear copper(II) complexes with N_4O_3 coordinating heptadentate ligands were synthesized and characterized. The variable-temperature magnetic moments of the

complexes were confirmed by using BS-DFT calculations. The benzoato-bridged Cu^{II} complex exhibits both catecholase and hydrolytic DNA cleavage activity.

Palladium(II) complexes with phosphane and symmetrically and unsymmetrically substituted benzimidazolin-2-ylidene ligands of types **2–6** were prepared and selected derivatives were characterized by X-ray diffraction. The NHC–phosphane complexes with unsymmetrically substituted NHC ligands of type **6** exhibit good catalytic activity in Mizoroki–Heck C–C coupling reactions.



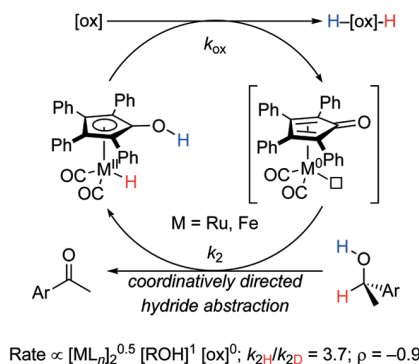
H. Türkmen,* T. Pape, F. E. Hahn,*
B. Çetinkaya 285–294

Palladium(II) Complexes with Benzimidazolin-2-ylidene and Phosphane Ligands and their Catalytic Activity in Mizoroki–Heck Coupling Reactions

Keywords: N ligands / Phosphanes / Palladium / Carbene ligands / Cross-coupling

Hydride Abstraction

Hydride is abstracted from alcoholic C–H groups by cyclopentadienone-ligated ruthenium(0) and iron(0) complexes. The reactions take place under mild conditions – even with an oxidant as weak as acetone – and show no kinetic order in re-oxidation of the metal hydride mediator. These mechanistic findings pave the way for more general and environmentally more benign C–H activation methods.



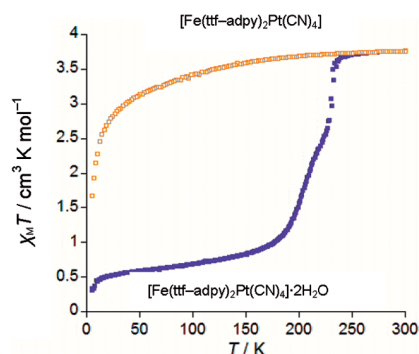
M. K. Thorson, K. L. Klinkel, J. Wang,
T. J. Williams* 295–302

Mechanism of Hydride Abstraction by Cyclopentadienone-Ligated Carbonylmetal Complexes (M = Ru, Fe)

Keywords: Cyclopentadienone ligands / C–H bond activation / Oxidation / Hydrides / Reaction mechanisms

Spin-Crossover MOFs

A tetrathiofulvalene ligand containing an amidopyridine moiety was prepared and its reaction with $\text{Fe}(\text{BF}_4)_2 \cdot 6\text{H}_2\text{O}$ and $[\text{M}(\text{CN})_4]^{2-}$ counterions led to the 2D polymers $\{\text{Fe}(\text{tff-adpy})_2[\text{M}(\text{CN})_4]\} \cdot n\text{H}_2\text{O}$ ($\text{M}^{\text{II}} = \text{Ni}, \text{Pd}$ and Pt). The hydrated compounds present a complete thermally induced two-step spin transition, whereas the nonhydrated materials are paramagnetic in the studied temperature range.

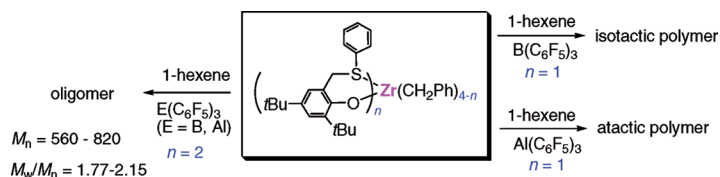


V. Martínez, A. B. Gaspar,* M. C. Muñoz,
R. Ballesteros, N. Ortega-Villar,
V. M. Ugalde-Saldivar, R. Moreno-Esparza,
J. A. Real* 303–310

Spin-Crossover 2D Metal–Organic Frameworks with a Redox-Active Ligand: $[\text{Fe}(\text{tff-adpy})_2\text{M}(\text{CN})_4] \cdot n\text{H}_2\text{O}$ (tff-adpy = 4-Tetrathiafulvalenylcarboxamidopyridine; $\text{M}^{\text{II}} = \text{Ni}, \text{Pd}, \text{Pt}$)

Keywords: Metal–organic frameworks / Polymers / Spin crossover / Cooperative effects / Conducting materials

Group 4 Polymerization Catalysts



Group 4 metal catalysts containing a [OS]-type bidentate phenolate ligand were synthesized. On benzyl abstraction, the di-benzyl zirconium catalyst gives oligo(1-

hexene) with a 2,1 regioselectivity. The tri-benzyl zirconium catalyst produces isotactic poly(1-hexene) with high molecular weight.

B. Lian, K. Beckerle, T. P. Spaniol,
J. Okuda* 311–316

Group 4 Metal Complexes That Contain a Thioether-Functionalized Phenolate Ligand: Synthesis, Structure, and 1-Hexene Polymerization

Keywords: Hafnium / Zirconium / Titanium / Oligomerization / Polymerization / Regioselectivity

* Author to whom correspondence should be addressed.

Supporting information on the WWW (see article for access details).

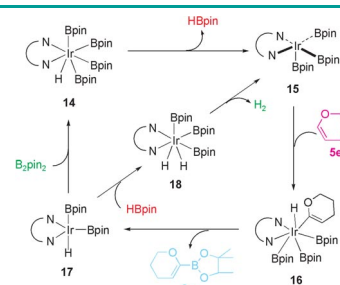


Cross-Coupling

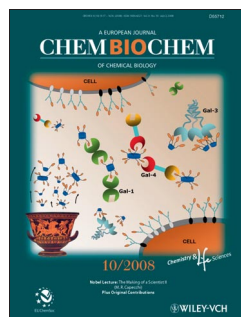
T. Kikuchi, J. Takagi, H. Isou, T. Ishiyama,* N. Miyaura*

Vinyl C–H Borylation of Cyclic Vinyl Ethers with Bis(pinacolato)diboron Catalyzed by an Iridium(I)-dtbpy Complex

A simple cycle: Vinyl C–H borylation of cyclic vinyl ethers by bis(pinacolato)diboron or pinacolborane was effectively catalyzed by iridium complexes comprised of $1/2[\text{Ir}(\text{OMe})(\text{cod})]_2$ and 4,4'-di-*tert*-butyl-2,2'-bipyridine in hexane or octane to give the corresponding vinylboron compounds in good yields.



Chem. Asian J.
DOI: 10.1002/asia.200800157

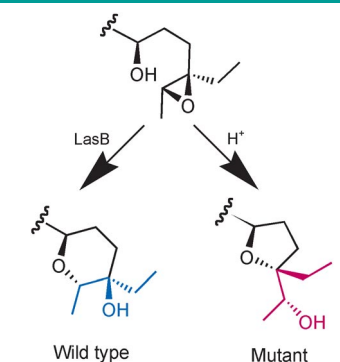


Biosynthesis

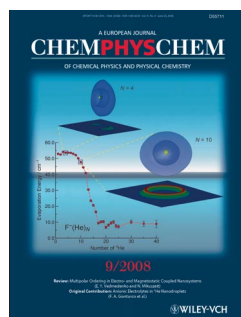
L. Smith, H. Hong, J. B. Spencer, P. F. Leadlay*

Analysis of Specific Mutants in the Lasalocid Gene Cluster: Evidence for Enzymatic Catalysis of a Disfavoured Polyether Ring Closure

Baldwin's rules bent: The biosynthesis of the polyether ionophore lasalocid in *Streptomyces lasaliensis* involves a kinetically disfavoured ring closure to form a six-membered tetrahydropyran. In a mutant lacking the novel epoxide hydrolase LasB, the intermediate instead forms the five-membered ring product predicted by Baldwin's rules; this shows the key role of LasB in stereocontrol.



ChemBioChem
DOI: 10.1002/cbic.200800585

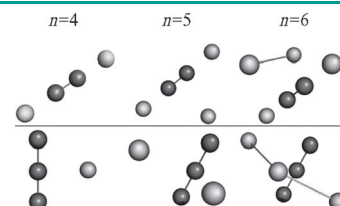


Helium Clusters

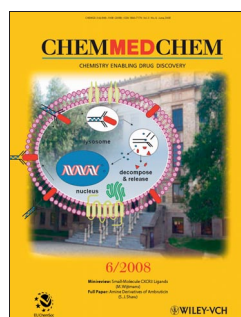
F. Marinetti, E. Bodo, F. A. Gianturco,* E. Yurtserver

Energetics and Structures of Charged Helium Clusters: Comparing Stabilities of Dimer and Trimer Cationic Cores

Three in a row: The ionization of small cationic helium clusters is analyzed by investigating the equilibrated cluster structural energy obtained after their optimization in the presence of two competing cores (see picture). The results show that upon equilibration of the ionized clusters, the trimeric ionic core should be the more abundant residual species.



ChemPhysChem
DOI: 10.1002/cphc.200800457

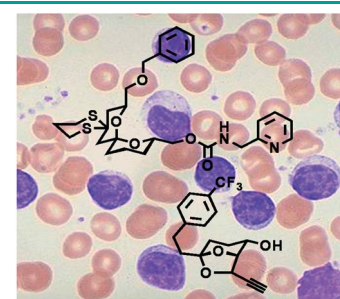


Drug Design

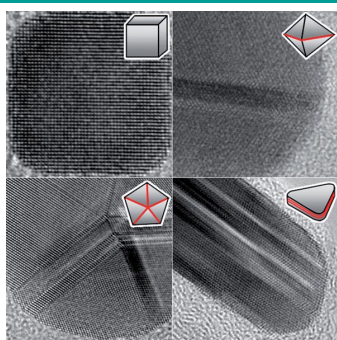
L.-G. Milroy, G. Zinzalla, F. Loiseau, Z. Qian, G. Prencipe, C. Pepper, C. Fegan, S. V. Ley*

Natural-Product-Like Spiroketal and Fused Bicyclic Acetals as Potential Therapeutic Agents for B-Cell Chronic Lymphocytic Leukaemia

The guiding principle of natural products is applied with success to the rapid identification of a new series of small molecules with activity against chronic lymphocytic leukaemia. These compounds are shown to induce apoptosis via a classical intrinsic drug-induced pathway with superior activity to market leader chemotherapeutics in similar screens.



ChemMedChem
DOI: 10.1002/cmdc.200800265



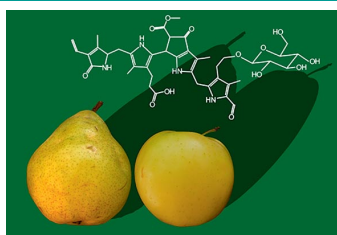
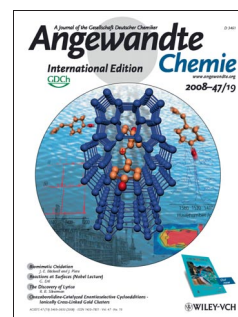
Angew. Chem. Int. Ed.
DOI: 10.1002/anie.200802248

Nanostructures

Y. Xia,* Y. Xiong, B. Lim, S. E. Skrabalak

Shape-Controlled Synthesis of Metal Nanocrystals: Simple Chemistry Meets Complex Physics?

Function follows form: Controlling the shape of nanocrystals may initially seem like a scientific curiosity, but its goal goes far beyond aesthetic appeal. For metal nanocrystals, shape not only determines their intrinsic physical and chemical properties but also their relevance for electronic, magnetic, optical, catalytic, and sensing applications.



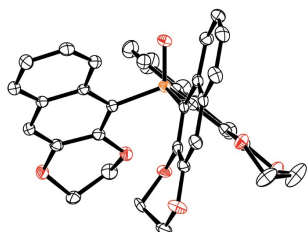
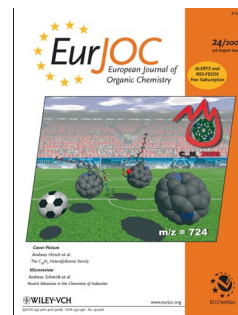
Eur. J. Org. Chem.
DOI: 10.1002/ejoc.200800804

Chlorophyll Catabolites

S. Moser, T. Müller, M. Oberhuber, B. Kräutler*

Chlorophyll Catabolites – Chemical and Structural Footprints of a Fascinating Biological Phenomenon

The elucidation of the chemical nature of chlorophyll catabolites has allowed the first structural insights into chlorophyll breakdown, assisting in developing understanding of the molecular basis and possible roles of this biological phenomenon. Current knowledge on chlorophyll catabolites in higher plants is outlined, as are their properties. Their antioxidant activity may give added value to fresh fruit.



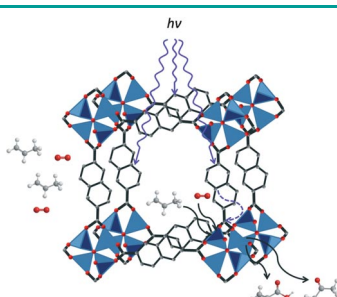
Chem. Eur. J.
DOI: 10.1002/chem.200801489

Chirality

T. Benincori, A. Marchesi, P. R. Mussini, T. Pilati, A. Ponti, S. Rizzo, F. Sannicolò*

Chirality in the Absence of Rigid Stereogenic Elements: The Absolute Configuration of Residual Enantiomers of C₃-Symmetric Propellers

Which enantiomer? The enantiopure residual antipodes of phosphane oxide shown here were obtained by quartz-induced crystallisation of the racemate and their absolute configuration was determined by anomalous X-ray diffraction scattering measurements. Configurational descriptors are suggested for propeller-shaped residual enantiomers.



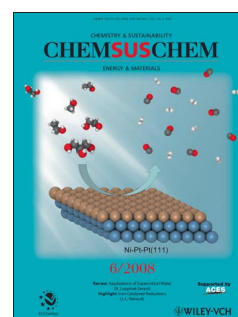
ChemSusChem
DOI: 10.1002/cssc.200800203

Metal-Organic Frameworks

J. Gascon,* M. D. Hernández-Alonso, A. R. Almeida, G. P. M. van Klink, F. Kapteijn, G. Mul

Isorecticular MOFs as Efficient Photocatalysts with Tunable Band Gap: An Operando FTIR Study of the Photoinduced Oxidation of Propylene

Photo frame(work): The first spectroscopic evidence of metal-organic frameworks (MOFs) acting as photocatalysts has been obtained. Isorecticular MOFs act as efficient photocatalysts in the photooxidation of propylene. The band gap energy can be tuned by changing the organic linker. Among the MOFs tested, the 2,6-naphthalenedicarboxylic acid based IRMOF was the most active, showing a higher activity than ZnO.



Nonsymmetrical Salen Ligands and Their Complexes: Synthesis and Applications

Arjan W. Kleij^{*[a,b]}

Keywords: Asymmetric catalysis / Ligand design / N,O ligands / Nonsymmetrical ligands

The importance of salen ligands in homogeneous catalysis and material chemistry has unambiguously been demonstrated over the last two decades. In the majority of the existing studies, C_2 -symmetrical salen complexes have been used as catalysts for many organic conversions; however, the amount of structures that can become available for catalyst fine-tuning by changing the peripheral groups on the bridging unit and the aryl side groups is limited. In order to widen their scope in catalytic procedures new designs of salen structures have been probed, and above all unsymmetrical versions. In this respect, it has become increasingly important to develop reliable and efficient preparative methods for these nonsymmetrical salen compounds, and more particu-

larly ligands with two differently substituted salicylideneimine groups. The presence of a single functional group suitable for connection to various supports has great advantages, since full access of the catalytic sites in the supported structure may be preserved and new and/or improved catalytic properties can be tailored. On the other hand, different functions on both sides of the central N_2O_2 unit can be used to force the formation of specific (supramolecular) architectures. This review discloses the general methods available for the preparation of unsymmetrical salen ligands/complexes and the most important fields of their application.
(© Wiley-VCH Verlag GmbH & Co. KGaA, 69451 Weinheim, Germany, 2009)

1. Introduction

Salen ligands^[1] are comprised of a potentially tetradentate N_2O_2 donor set usually obtained through a double condensation reaction between a diamine and two equivalents of a salicylaldehyde. The early work of Jacobsen and Katsumi^[2] has led to the discovery of powerful oxidation catalysts based on Mn^{III} -centered salen compounds, of which the properties are easily altered by structural changes in the diamine and/or salicylaldehyde components.^[3] This offers great diversity in the salen ligands that may be obtained and offers a valuable toolkit for the fine-tuning of the steric and electronic properties. Also, appropriate selection of chiral modules provides the opportunity to vary the non-sym-

metrical environment of the metal centre. Typical and general advantages related to the application of metallosalen systems in homogeneous catalysis are the easy access to various structures, their cost-effective synthesis and the amount of materials that can be produced as opposed to other comparable planar ligand structures such as porphyrins. These properties make the salen system highly competitive for application in homogeneous catalysis. The first generation of salen ligands with C_2 symmetry were constructed with the two salicylidene fragments having the same substitution pattern on the aromatic side rings. Although the use of various salicylaldehydes can create a way to vary the ligand properties to some extent, the diversity of structures that can be accessed in this way is limited. The presence of two distinct salicylideneimine groups could be beneficial for different reasons. First of all, immobilization of salen ligands onto heterogeneous and homogeneous supports allows recovery of the catalyst systems and thus a potential reuse in subsequent catalytic campaigns.^[4] Unsymmetrical

[a] Institute of Chemical Research of Catalonia (ICIQ),
Av. Països Catalans 16, 43007 Tarragona, Spain
Fax: +34-977-920-224
E-mail: akleij@iciq.es

[b] Institució Catalana de Recerca i Estudis Avançats (ICREA),
Pg. Lluís Companys 23, 08010 Barcelona, Spain



Arjan W. Kleij (1971) received his MSc and PhD from the University of Utrecht, The Netherlands, under the supervision of Prof. Gerard van Koten working on dendrimer-supported homogeneous catalysis. Afterwards he was a NWO Talent postdoctoral fellow in the group of Prof. Javier de Mendoza (Madrid, Spain) and a postdoctoral associate with Prof. Joost Reek and Prof. Piet van Leeuwen (University of Amsterdam, The Netherlands) focusing on supramolecular chemistry and catalysis. He also spent three years in industry working in various principal research scientist positions at Avantium Technologies (Pharma division) and Hexion Specialty Chemicals (Epoxy Resins & Coatings Division). Since 2006, he is a Group Leader and ICREA fellow in the Institute of Chemical Research of Catalonia (ICIQ, Tarragona, Spain). His current research interests encompass the use of salen complexes in homogeneous cooperative catalysis, utilization of new reactivity behaviour of metallosalen complexes and (supramolecular) materials based on multimetallic and macrocyclic salen structures.

salen ligands equipped with a single functional group useful for such immobilization procedures would thus be required. The presence of a single connection to polymer,^[5] dendritic^[6] and other supports^[7] permits the substrates to freely access the catalytic sites which may be difficult in doubly immobilized, symmetrical salen derivatives eventually leading to lower reaction rates and selectivities.

Another advantage of nonsymmetry within the salen scaffold is the possibility of further fine-tuning its structure by introducing different electron-withdrawing and/or donating groups on the periphery of both salicylideneimine units. In the latter situation, a faster optimization of the structure–reactivity relationship in homogeneous catalysis may be foreseen. Lastly, the desymmetrization of the salen ligand has been reported to give, at least in some cases, improved enantioselective behaviour in various organic transformations as compared to their symmetrical derivatives.^[8] In the last decade, numerous groups have devoted part of their research programs to the preparation and application of nonsymmetrical salen ligands and complexes. This review intends to give a concise overview of the latest developments in the field of synthetic salen chemistry with a particular focus on the various methods that have proven to be successful for the isolation of these structures, the complications and challenges met in the synthetic procedures and the most important fields of application of these unsymmetrical systems. Although this review is intended to give a broad overview, salen systems that have a nonsymmetrical bridging unit between the two salicylideneimine groups, and those systems that resemble salen ligands will not be discussed here in detail.

2. Direct Preparation of Non-Symmetrical Salen Derivatives

“Direct” preparation is here defined as the reaction between the double Schiff base precursors without the use of templating metal ions or any other (in)organic reagent or protection/deprotection sequences in the condensation stage(s). This part will focus on particular and illustrative examples of successful approaches toward nonsymmetrical (metal) salen compounds rather than to treat each individual report separately.

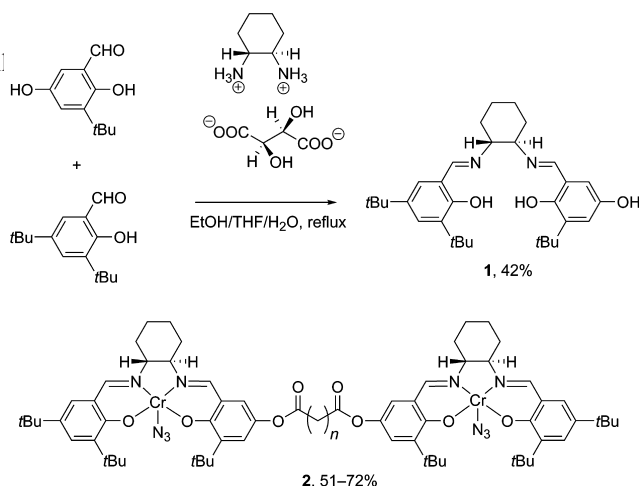
Direct synthesis is probably the easiest way to target nonsymmetrical salen structures and is generally carried out using a double stage Schiff base formation between a diamine precursor and two distinct salicylaldehydes in a stoichiometric one-pot approach. The main problem encountered in the unassisted, step-wise condensation approach is the labile nature of the imine bond towards hydrolysis. In most cases this leads to undesired formation of a (statistical) mixture of the unsymmetrical and C_2 -symmetrical derivatives, which need to be separated prior to their use in further synthesis. Nonsymmetrical salen compounds may also be accessed using an adapted method that is based on the isolation of a mono-imine intermediate (see for successful examples section 4) and the reaction stoichiometry here

plays a crucial role. The principal issue in the latter approach is the nature of the equilibrium between all species which needs to be controlled effectively; otherwise mixtures of diamine and mono/diimines are obtained which are inadequate for the metal insertion stage.

One of the first successful syntheses of a nonsymmetrical (metallo)salen was provided by Atkins et al.^[9] They used a stepwise condensation approach, starting with the reaction between 5-chloro-2-hydroxybenzophenone and 1,2-diaminobenzene to afford the mono-ketimine product.^[10] Hereafter, addition of salicylaldehyde furnished the salen ligand in high yield (80–90%), and metal ions (Cu, Ni) could be conveniently introduced.

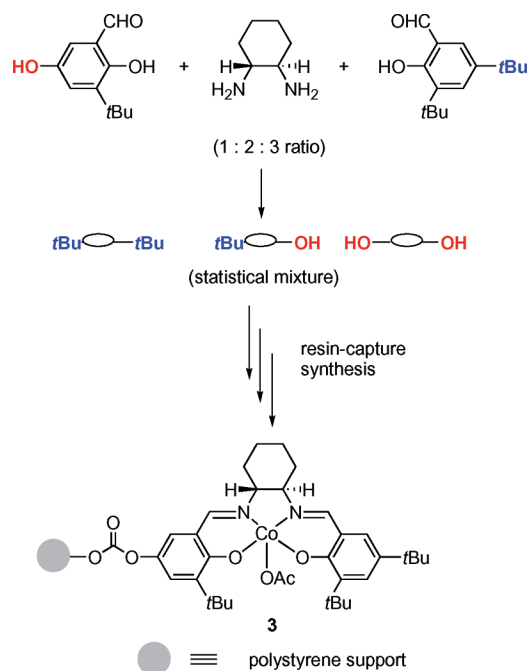
Kol and co-workers reported the synthesis of a hybrid salan/salen (i.e., salalen) ligands prepared in moderate yields (36–53%) in a two-step sequence.^[11] They utilized a mono-*N*-substituted diamine, of which the primary amine group was treated with a salicylaldehyde to form the “half-salen” part. Then, the (unreacted) secondary amine group of the “half-salen” was treated with formaldehyde and a substituted phenol in a Mannich condensation step to complete the “half-salan” unit.

Another account on the direct preparation of nonsymmetrical salen derivatives was presented by the group of Jacobsen.^[12a] The preparation of the dissymmetric salen ligand **1** was reported with two distinct salicylideneimine groups, of which one encompasses an additional phenol group that was subsequently used for the preparation of tethered bimetallic complexes **2** (Scheme 1)^[12] that differ in the length of the linking unit. These bimetallic bis- Cr^{III} derivatives find useful application in the field of (cooperative) homogeneous catalysis. The statistical mixture of salen ligands (both homo-combinations as well as the hetero-combination) was separated using column chromatography. Although the reported yield of **1** was only moderate (42%), it already showed the high potential of nonsymmetrical ligands for the preparation of multimetallic salen catalysts using difunctional linkers.



Scheme 1. Synthesis and application of a nonsymmetrical salen ligand for the construction of bimetallic catalysts.

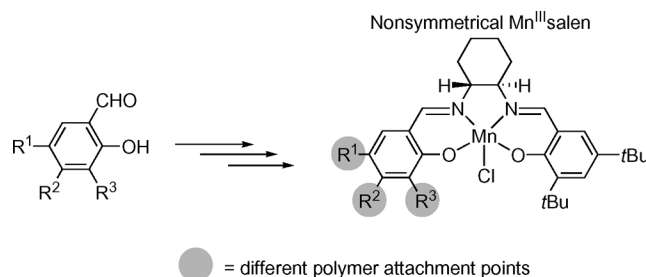
In another contribution^[13a] this concept was extended to polymer- and silica-supported chiral catalysts based on Co(salen) complexes. Polystyrene-bound Co^{III}-salen derivatives of type **3** (see Scheme 2) were obtained after a resin-capturing approach. Since the bis-*t*Bu version of the salen ligand will not react with the resin precursor this allows (upon choosing the appropriate stoichiometry) an effective capturing of the OH-functionalized ligands.^[14] The non-bound ligands are then simply removed through subsequent washing stages. Although the direct attachment of the mono-OH salen derivative onto polystyrene beads^[13] was also accomplished, chromatographic purification was additionally needed for this particular ligand prior to immobilization. Nonetheless, both approaches afforded catalytic systems with comparable reaction rates and enantioselectivities in the hydrolytic kinetic resolution (HKR) of terminal epoxides such as epichlorohydrin, and the catalyst could be at least recycled 5 times without observable loss of activity and/or enantioselectivity.



Scheme 2. Polystyrene-supported chiral Co(salen) catalysts derived from nonsymmetrical ligand **1**.

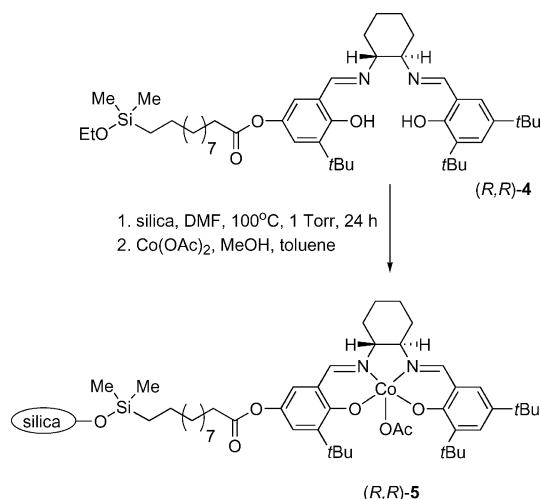
A similar strategy was employed by Sherrington and co-workers^[15a] who used a series of polymer supported^[15] analogues of Jacobsen's catalyst (Scheme 3) with the aim to design a catalyst that would retain the original features of the unsupported system. The polymer resin catalysts based on Mn^{III}-salen complexes were prepared using a direct approach starting with immobilized salicylaldehyde precursors. The salen structure was subsequently completed by the stepwise introduction of the chiral diamine and a second salicylaldehyde reagent. In the last step the Mn^{III}-centred catalyst was obtained using standard reaction conditions. The polymeric catalysts were tested in the asymmetric epoxidation of 1-phenylcyclohex-1-ene and results were evaluated against a commercial sample of Jacobsen's catalyst.

The best result was obtained with a heavily cross-linked macroporous resin modified with Mn^{III}-salen units having a low Mn-loading amounting to 0.08 mmol/g, and showing an enantioselectivity of more than 90%.



Scheme 3. Polymer resins modified with Jacobsen's catalyst for enantioselective epoxidation reactions.

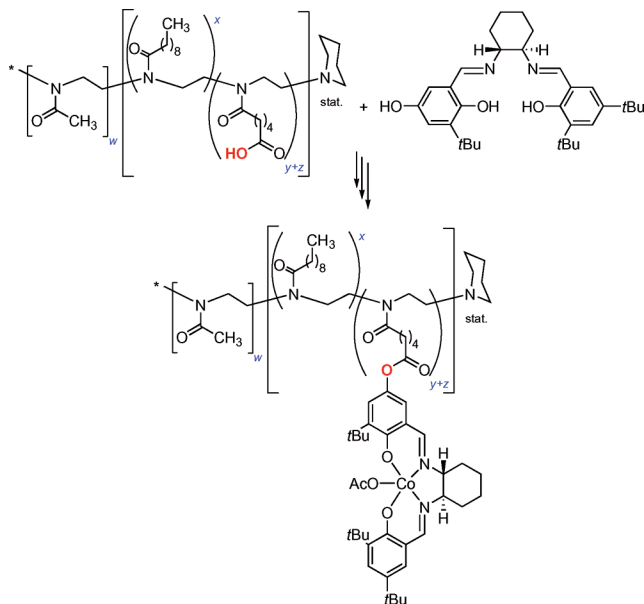
Silica-immobilized Co^{III}-salen complexes were prepared via a tethering strategy using modified salen precursor **4** (Scheme 4).^[13a] The silyl ether **4** was attached to the silica support using previously reported conditions and then converted into its Co^{III}-salen complex **5**. The supported catalyst was tested in the HKR of styrene oxide and provided an efficient and highly enantioselective catalytic process. More importantly, this silica-bound Co^{III}-salen complex was also probed for its efficacy to act as a HKR catalyst in a continuous flow system, and the results nicely demonstrated the successfulness of this approach with respect to catalyst recycling and separation from the product stream in a continuous mode.



Scheme 4. Immobilization of a nonsymmetrical Co^{III}-salen complex onto a silica support using a tethering strategy.

Self-assembled nanoreactors composed of amphiphilic block copolymers functionalized with pendant Co^{III}-salen units covalently attached to the hydrophobic part were reported by the group of Weberskirch (Scheme 5).^[16] The principal idea was to create, through micellar aggregation, a nanoenvironment in which a high local concentration of

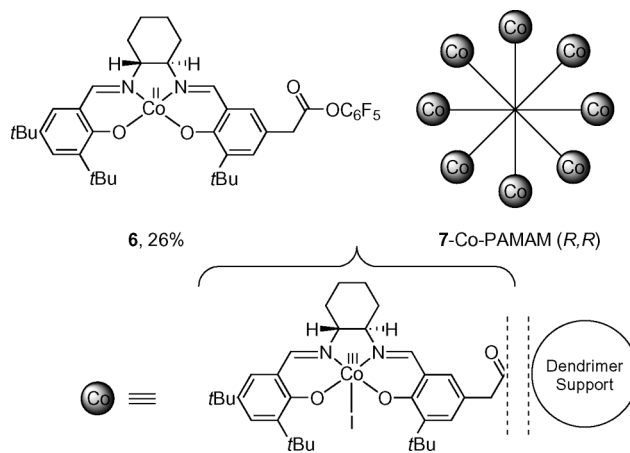
the catalytic Co^{III} -salen complex inside the hydrophobic core would be present while the hydrophilic outer shell would ensure water-solubility. The salen moiety was attached to the block copolymer using a hydroxy-function-alized precursor which was subsequently metalated. The resultant micellar, nanocatalyst was used in the HKR of various racemic aromatic terminal epoxides in water. This catalysts species could be recycled at least four times without any loss of enantioselectivity.



Scheme 5. A block copolymer-supported Co^{III} -salen catalyst that is able to self-assemble into a nanoscale micellar aggregate.

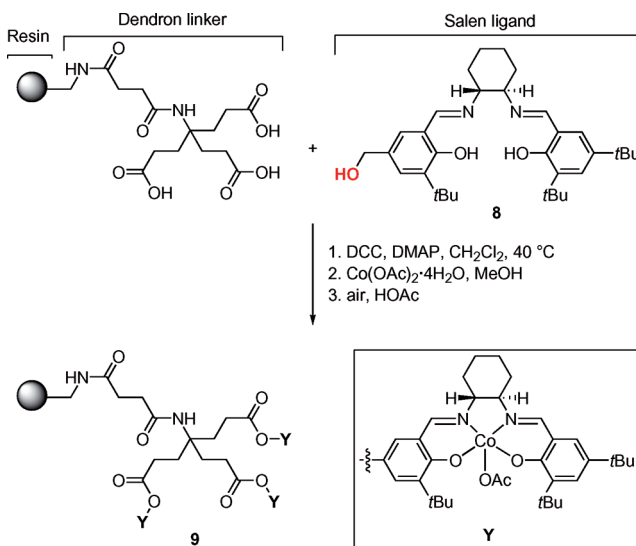
Well-defined dendrimers may give advantageous properties to the Co^{III} -salen system upon immobilization since the regularly branched dendrimer structure allows precise control over the amount and location of the catalytic units. Jacobsen et al. prepared the pentafluorophenyl ester **6** (Scheme 6) that was attached via peptide coupling procedures to different generations of commercially available PAMAM (PAMAM = polyamidoamine) dendrimers.^[6a] The Co^{II} complex **6** was prepared in six steps (26% overall yield) and oxidized with molecular I_2 to yield the catalytically active Co^{III} dendrimer **7-Co-PAMAM-(R,R)**. The catalytic results showed a positive influence on the reaction, i.e. a higher overall reaction rate was noted for the dendrimeric catalysts. This effect was ascribed to a higher effective molarity of the Co^{III} -salen units and the second-order kinetic dependence of the HKR reaction.

A highly active, dendronized $\text{Co}(\text{salen})$ catalyst for the HKR of terminal epoxides was reported by Weck et al. (Scheme 7).^[17] Their catalyst system consists of three components, viz. a polystyrene resin,^[18] a dendron-based linking unit and the Co^{III} -salen complex. The commercially available, selected aminotriester dendron allowed introduction of three distinct catalytic sites via covalent attachment, and forcing these sites in close proximity along the dendron's periphery. This close proximity highly favours cooperativity between the Co^{III} centres and thus an excellent



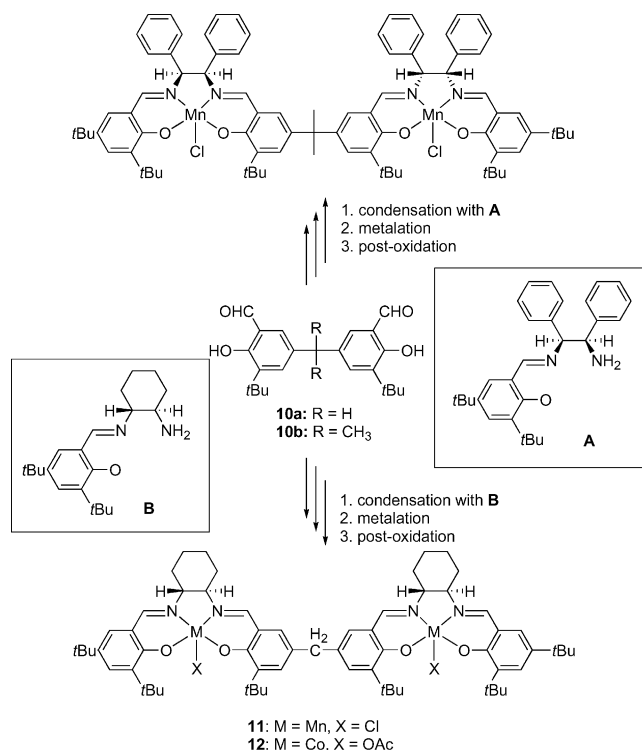
Scheme 6. Attachment of the nonsymmetrical Co^{II} -salen complex **6** to a PAMAM dendrimer and schematic drawing of its post-oxidized Co^{III} iodide complex **7-Co-PAMAM (R,R)**.

catalytic performance. The authors furthermore demonstrated that these catalytic systems, as a result of their immobilization, are easily filtered from the product solution and recycled without loss of activity and enantioselectivity. The nonsymmetrical salen ligand was attached to the resin via precursor **8**^[19] and then metalated and oxidized to **9**. The synthetic outline is presented in Scheme 7.



Scheme 7. A dendronized, resin-supported Co^{III} -salen complex.

The group of Kureshy has reported several examples of binuclear complexes that comprise nonsymmetrical salen ligands (Scheme 8).^[20] The general strategy employs the condensation of bis-salicylaldehyde precursors **10** and a monoimine intermediates **A** and **B** to give homochiral, dimetallic bis-salen complexes that are useful as recyclable catalysts for enantioselective epoxidation ($\text{M} = \text{Mn}$, e.g. **11**) and HKR of racemic epoxides ($\text{M} = \text{Co}$, e.g. **12**).



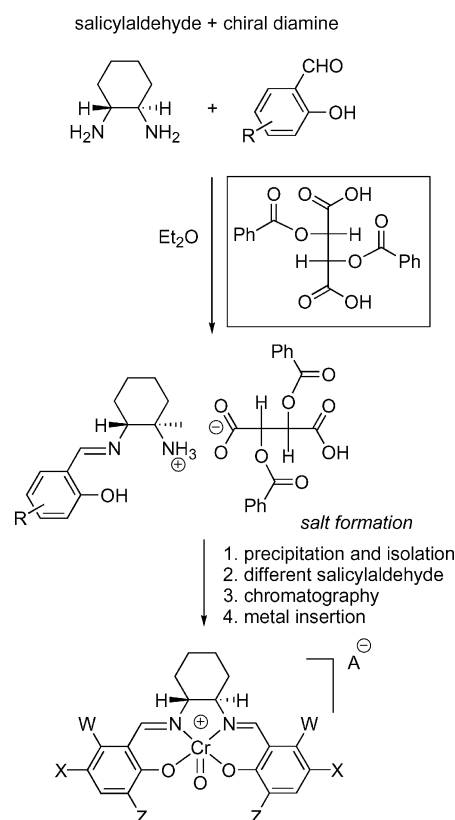
Scheme 8. Synthesis of binuclear homochiral metallosalen complexes via step-wise condensation.

3. Synthesis of Nonsymmetrical Salen Compounds Using a Protecting Group Approach

The preparation of nonsymmetrical salen derivatives via a protecting group approach is classified as the selective protection of one of the two secondary amine groups in the diamine reagent. The protected reagent is then subjected to a step-wise condensation with distinct salicylaldehydes to give the nonsymmetrical salen ligands; the second Schiff base function is introduced after (in situ) deprotection of the protected amine group. Currently, many different protected reagents based on (chiral) diamines have been reported and this section intends to provide the most illustrative examples reported together with their application potential.

So far, most described protected diamine reagents are chiral and are based on the 1,2-cyclohexane backbone. One of the earliest studies devoted to the use of protected mono-imine intermediates in the synthesis of nonsymmetrical chiral salen structures was carried out by the group of Gilheany.^[21] The formation of bis-imine ligands from aldehyde and diamine reagents is under thermodynamic control: when a 1:1 mixture of salicylaldehyde and diamine in ethanol are mixed often a mixture of products is obtained comprising small amounts of the mono-imine derivative, as well as the bis-imine product and starting diamine precursor. However, in some cases the selective formation of mono-imines is favoured, in particular in reactions that involve salicylaldehydes substituted with electron-withdrawing groups.

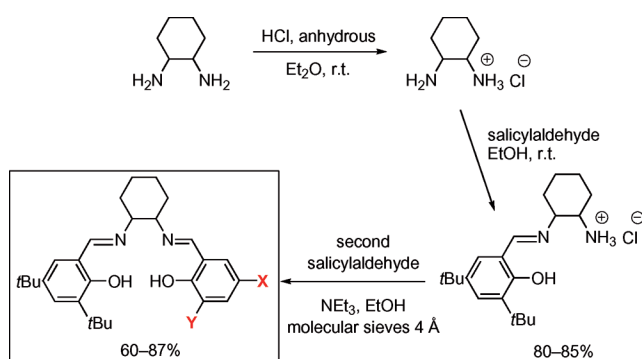
Trapping the mono-imine intermediate with a reagent that would react with the remaining amine groups should allow for an easy separation of the mono-imine from the bis-imine product, isolation and further reaction with a different salicylaldehyde to give access to unsymmetrical salen compounds. Gilheany and co-workers found that (+)-*O,O'*-dibenzoyltartaric acid was quite effective to isolate the mono-imine derivative in this way since it is insoluble in ether and can be collected by filtration. In subsequent syntheses, due to equilibration of the unsymmetrical salen, chromatography was still needed to isolate the pure, nonsymmetrical ligands (Scheme 9) which was achieved in very low yields.^[22] These ligands were used to produce their Cr^{III} complexes, that were applied as stoichiometric reagents in the enantioselective epoxidation of *E*- β -methylstyrene.



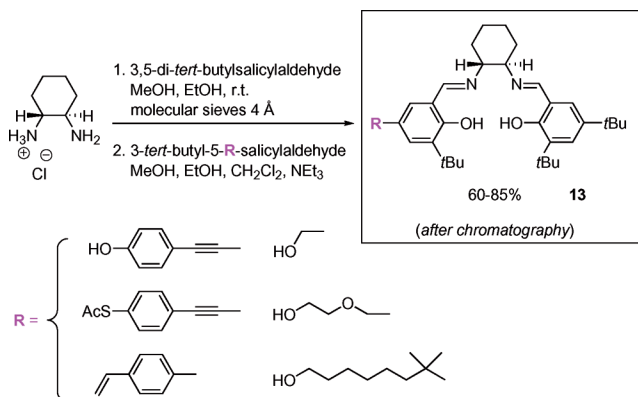
Scheme 9. Nonsymmetrical salen ligands using (+)-*O,O'*-dibenzoyltartaric acid as a trapping agent.

In another contribution, Nguyen reported on a general and high-yielding synthesis of nonsymmetrical salen derivatives using a mono-ammonium salt derived from diamines and anhydrous hydrochloric acid.^[23] The ammonium salts are rather insoluble in ether and can be isolated and treated with one equivalent of salicylaldehyde to yield mono-imine reagents in high yield. The mono-imino ammonium salt can in turn be added to a second salicylaldehyde in the presence of triethylamine to produce the desired unsymmetrical salen ligands in high isolated yields (Scheme 10). The major advantage of this procedure is that large-scale syntheses may

be carried out without the need for tedious chromatographic and/or crystallization procedures. This procedure was eventually further improved and the scope broadened by Weck et al. (Scheme 11).^[19]



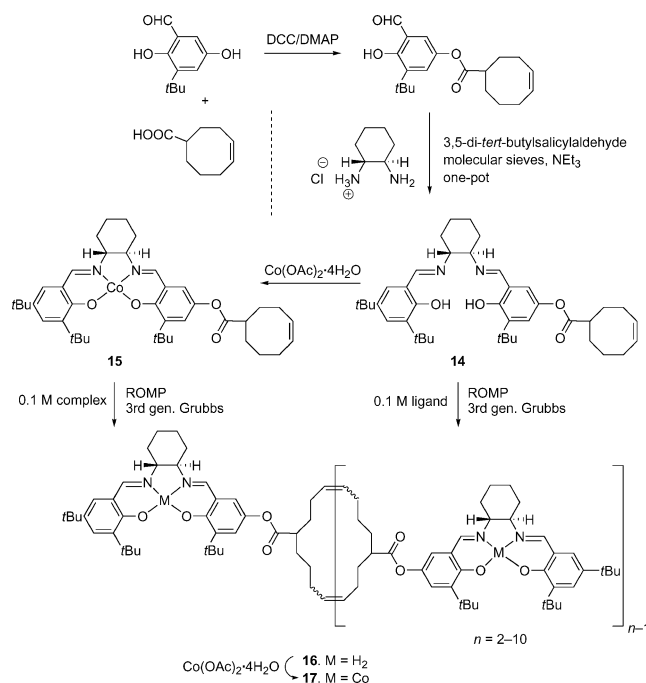
Scheme 10. Synthesis of nonsymmetrical salen derivatives via a mono-imine ammonium salt.



Scheme 11. Weck's one-pot procedure for unsymmetrical salen compounds.

This one-pot procedure towards enantiopure nonsymmetrical salen systems proved to be widely applicable as demonstrated by the Weck group. Their major focus within this field is the use of this synthetic methodology for polymer-supported catalysis. An interesting ring-expanding olefin metathesis of mono-(cyclooct-4-ene-1-yl)-functionalized salen ligand **14** or Co^{II} complex **15**^[24] at typically low monomer concentrations with third generation Grubbs' catalyst^[25] furnished unsymmetrical macrocyclic oligomers **16** and **17**, respectively, in virtually quantitative yields (Scheme 12). These results show that this approach is highly versatile since post-metalation of the macrocyclic oligosalen ligand with different metal reagents can give access to various supported catalyst systems. The macrocyclic Co^{II}-salen complexes were oxidized aerobically under acidic conditions, and the resultant Co^{III} derivatives **17** applied as HKR catalysts for various racemic terminal epoxides using very low catalyst loadings. An important feature brought about by the architecture of the macrocyclic systems is that the catalytic sites are highly accessible, and a high local concentration of the Co^{III} centres provokes bimetallic cooperative

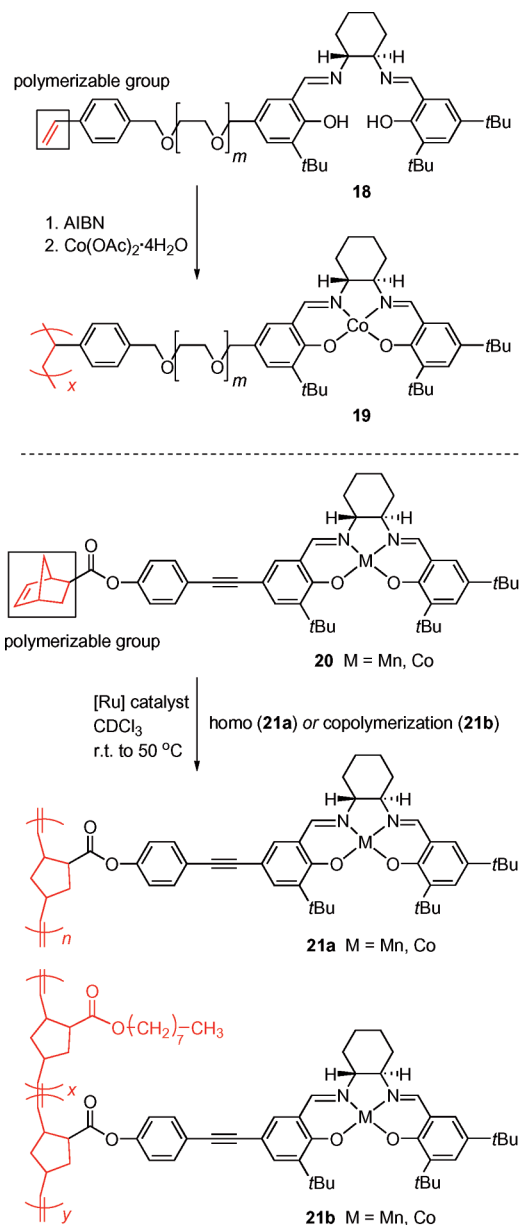
interactions. As compared to polymeric analogues, the macrocyclic catalyst systems **17** proved to be superior in terms of reaction rate.



Scheme 12. Ring-expanding olefin metathesis of nonsymmetrical salen compounds to afford macrocyclic oligomeric Co-salen catalysts for HKR of epoxides.

The same authors have used similar principles for the fabrication of various other polymer supported unsymmetrical metallosalen complexes: in each case the followed strategy makes use of a one-pot synthesis of an unsymmetrical salen compound (cf., Scheme 10 and Scheme 11) that is functionalized with a suitable monomer group that upon appropriate conditions can be polymerized (Scheme 13). Thus, AIBN free radical polymerization of **18**^[26,27] affords the oligosalen compounds, and metalation with [Co^{II}(OAc)₂·4H₂O] provides then the polystyrene-supported Co^{II} complexes **19**. Alternatively, norbornene-functionalized unsymmetrical metallosalen derivatives^[28] are also easily polymerized. Using the latter procedure, chemically inert C–C linkages were used as to minimize catalyst degradation in the case of Mn species. Variations of the catalyst density is readily achieved by either homo- or copolymerization of the metallosalen monomer **20** by ROMP yielding metallosalen polymers **21**.

Highly active, recyclable poly(norbornene)-supported Al^{III}-salen catalysts for the enantioselective 1,4-conjugate addition of cyanide to α,β -unsaturated imides^[29] were also developed by Weck.^[30] Unsupported Al^{III}-salen catalysts usually require catalyst loadings between 10–15 mol-%, while their polymeric catalyst proved to be more active at lower Al^{III}-loading (5 mol-%). Again, the assumption that a non-random distribution of catalytic sites in the polymeric catalyst would favour a bimetallic cooperative pathway was fully supported by the catalysis results.



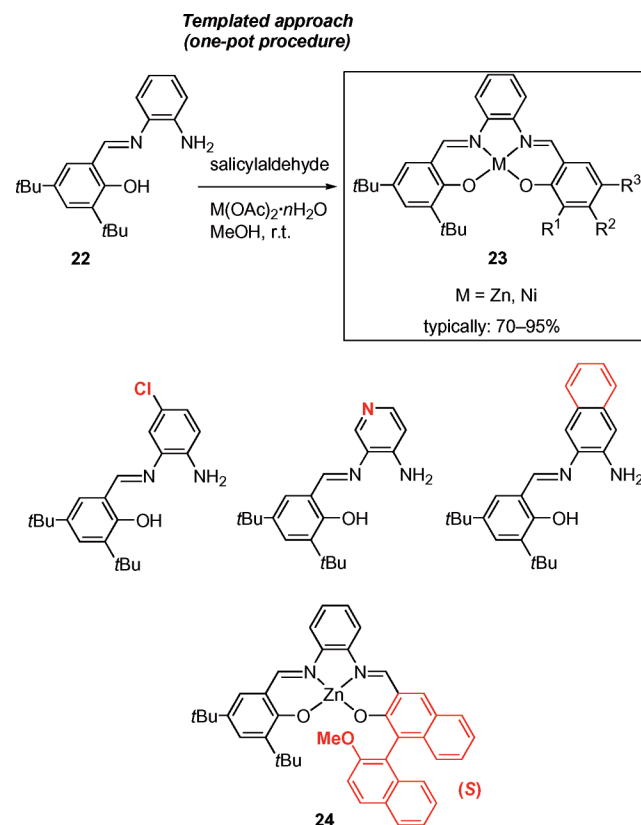
Scheme 13. Polymerization of monomer-functionalized unsymmetrical salen compounds: access to polymer-supported catalyst systems.

4. Nonsymmetrical Salen Derivatives via Monoimine Precursors

Nonsymmetrical salen structures can also be prepared by the use of pre-isolated mono-imine precursors. In order to arrive at nonsymmetrical salen compounds, the equilibrium between mono- and diimine species, and the diamine upon dissolution in subsequent stages needs to be controlled. One way to control the equilibrium during the second condensation step is to make use of templation, and in this section typical examples are discussed where metal ions are primarily applied as templating agents.

The group of Atwood reported the high-yield preparation of an interesting mono-imine, “half-salen” synthon constructed from *ortho*-phenylenediamine and 3,5-di-*tert*-

butylsalicylaldehyde (Scheme 14, **22**).^[31] The mono-imine was used by the authors as a potentially tridentate ligand for Al^{III} and Ga^{III} ions.

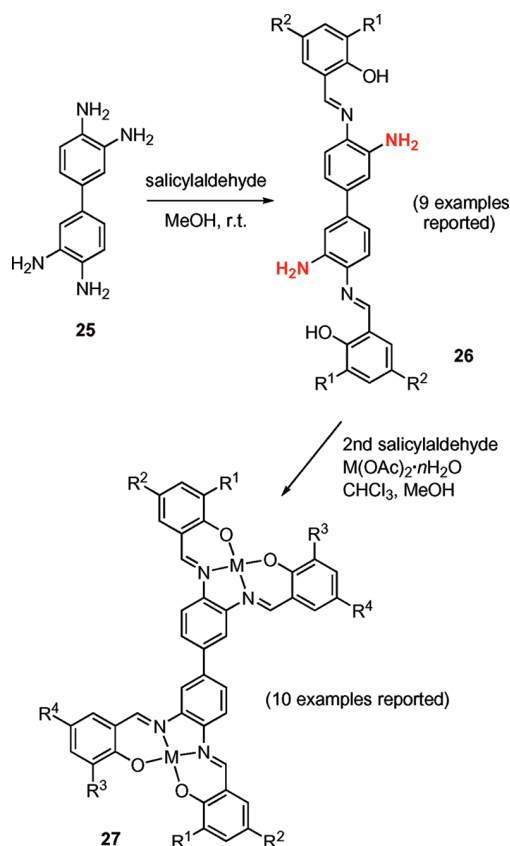


Scheme 14. Synthesis of nonsymmetrical salen derivatives via a metal templated approach.

Kleij et al. have used this mono-imine synthon to prepare, in a one-pot procedure, nonsymmetrical salphen [salphen = *N,N'*-1,2-phenylene-bis(salicylideneimine)] complexes using a templating approach with metal ions (Scheme 14).^[32] The procedure proved to be useful for both systems having the asymmetry within the bridging unit (including salpyr compounds)^[33] as well as for nonsymmetrical salen derivatives with two distinct phenyl side groups (Scheme 14). In general, the mono-imine reactant **22** is treated with a mixture of another salicylaldehyde and a metal salt to afford exclusively the nonsymmetrical salen complexes **23** (Scheme 14) in high isolated yield. Depending on the conditions (cf. solvent) used, isolation may be performed by one simple filtration step to directly furnish the pure compounds. This template approach has also proven to be practical when using other mono-imine precursors, and even allowed the isolation of a unique chiral Zn^{II}-(salphen) complex **24** with the chiral unit being present in the aromatic side chain.

Further extension of this methodology has led to the preparation of nonsymmetrical, bis-metallosalphen building blocks (Scheme 15).^[34] In order to introduce a non-symmetry within each salen unit, bis-imine reagents **26** were prepared based on the 3,3'-diaminobenzidine backbone (**25**). Hereafter, the bis-imine compounds were subjected to

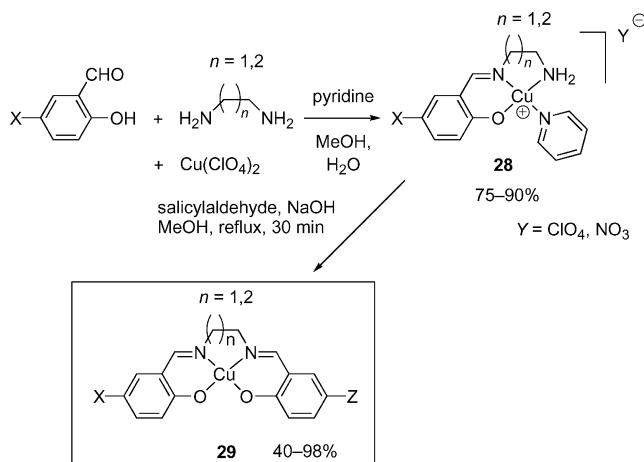
one-pot condensation-metalation procedure to afford non-symmetrical bimetallic synthons **27** potentially useful as supramolecular building blocks.^[35–38] Since both the structure of the diimine species, the second aldehyde reagent and the metal ion may be varied with ease, a versatile modular approach has become available for this category of building block.



Scheme 15. Nonsymmetrical bimetallic salen complexes (within the salen unit) derived from 3,3'-diaminobenzidine.

Other authors have also used metal templation to construct unsymmetrical salen compounds. For instance, Rigamonti et al. communicated the preparation of Cu^{II} complexes of salen analogues with two distinct phenyl side groups.^[39] These salen complexes have a so called push-pull charge asymmetry, and the substitution has a particular effect on the Cu-phenolato coordination bond. The complexes were studied as to gather information about the modulation of electronic asymmetry and nonlinear optical properties of these systems. The synthetic route toward these Cu^{II} -centred salen species is outlined in Scheme 16. The templated synthesis starts off with the selective isolation of the monocondensated “half-unit” Schiff base **28**^[40] by reaction of a 1:1:1 stoichiometry of salicylaldehyde, a diamine and copper perchlorate or nitrate in the presence of pyridine. This reaction could also be regarded as a one-pot, multi-component (MCR) reaction. The mononuclear Cu^{II} intermediates **28** can be conveniently converted into the

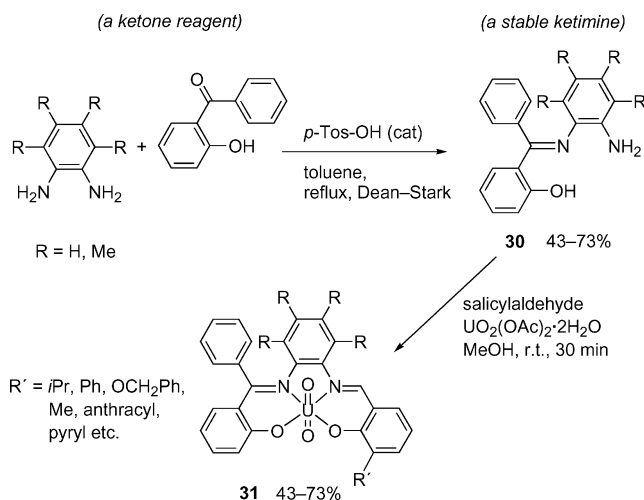
Cu^{II} -salen species **29** in high isolated yield upon treatment with a second salicylaldehyde in the presence of aqueous NaOH.



Scheme 16. Push-pull Cu^{II} -salen systems obtained via templated synthesis.

A similar intermediate^[41] like Cu^{II} complex **28** (Scheme 16) was used by Tao et al. to yield an unsymmetrical Cu^{II} -salen with a pendant carboxylic acid group.^[42] The presence of the $-\text{COOH}$ fragment was utilized for the preparation of heterotrinnuclear complexes and their magnetic properties were evaluated.

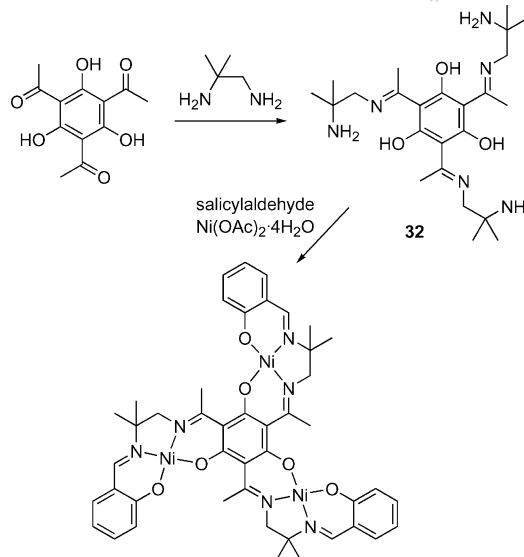
(Un)symmetrical uranyl-salphen complexes have been reported by Mandolini and co-workers.^[43–48] These uranyl-salphen derivatives are excellent candidates for molecular receptors^[43–46] and homogeneous catalysts.^[47–48] These authors employed two major strategies for the preparation of the unsymmetrical versions (for some examples see Scheme 17) of these $\text{UO}_2(\text{salen})$ complexes, though generally both may be considered metal-mediated procedures.



Scheme 17. Preparation of nonsymmetrical $\text{UO}_2(\text{salen})$ derivatives. Only a selection of the synthesized structure is shown here.

Combination of two distinct salicylaldehydes with 1,2-diaminobenzene and $\text{UO}_2(\text{OAc})_2 \cdot 2\text{H}_2\text{O}$ affords a statistical mixture^[13a] of uranyl-salen complexes which require separation by column chromatography: consequently only low yields are obtained for the targeted compounds. Alternatively, and perhaps more attractive from a time-management and purification point of view, step-wise condensation using metal templation in the second condensation stage gives smooth access to various substituted nonsymmetrical $\text{UO}_2(\text{salen})$ compounds (Scheme 17).^[43]

Lastly, it has been reported by Ambroziak and Szypa^[49] that unsymmetrical salen structures may be easily obtained by a step-wise condensation method using in the first stage 2-hydroxynaphthaldehyde. In this case, the pure mono-imine reagent needed for the second condensation stage involving various salicylaldehydes was isolated in high yield (92%). This exemplifies that subtle changes in the structure of the desired mono-imine provides a tool to stir the mono- vs. dimine equilibrium in favour of the former.



Scheme 18. A tri-metallosalen complex obtained via a selective step-wise synthesis.

5. Miscellaneous Systems

In the preceding sections the synthetic methods for nonsymmetrical (metallo)salen complexes have been discussed. In this section, some attention is given to the application of these synthons in other fields than already discussed, and on specially selected examples of systems of which the origin of asymmetry is induced by an external module/structure.

The group of Glaser constructed a tri-salen ligand^[50] by making use of the difference in reactivity of both amine groups within a mono-*N*-substituted diamine reagent.^[11] The sterically more hindered amine group does not react with ketones thus giving rise to the selective formation of the tri-imine/tri-amine intermediate **32** (Scheme 18), which can then be used to complete the three metallosalen moieties by treatment with a salicylaldehyde and a subsequent post-metallation step. Such multimetallics may find use in the design of magnetically interesting molecules and other types of materials based on salen scaffolds.^[1e,51]

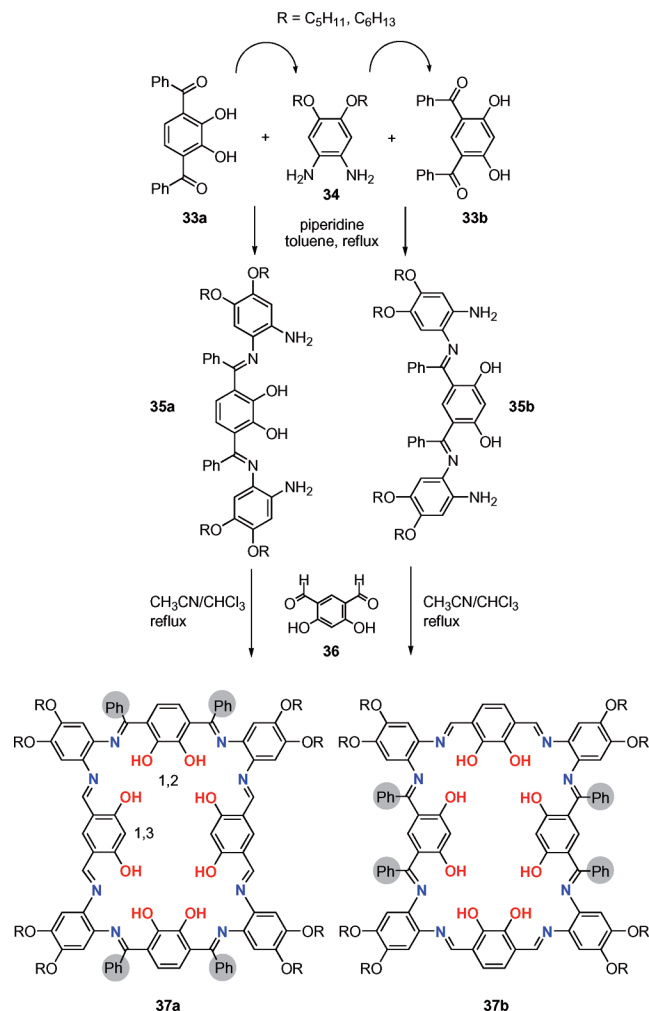
Schiff base macrocycles^[52] are usually multimetallic in nature and can display interesting (supramolecular) properties.^[53] Nonsymmetrical versions of (macrocyclic) multimetallic salen derivatives, however, have rarely been reported. Interesting macrocyclic salen isomers which comprise four separate unsymmetrical salphen coordination pockets for metal ions were reported by MacLachlan et al. (Scheme 19).^[54] They elegantly used the fact that diphenyl ketone structures only react once with diamines unless harsh reaction conditions are applied.^[9] Thus, reaction of the diketone **33a** with *ortho*-phenylenediamine **34** affords diketimine precursors **35a**, and subsequent treatment with dialdehyde **36** the macrocyclic tetrasalphen derivative **37a** is obtained. Likewise, using diketone **33b** and following a similar strategy the isomeric macrocycle **37b** was constructed. Each salen unit in both macrocycles **37** incorporates one ald-

imine and one ketimine, and the difference between the two macrocycles **37a** and **37b** is the relative position of the phenol OH groups (1,2 vs. 1,3; see Scheme 19).

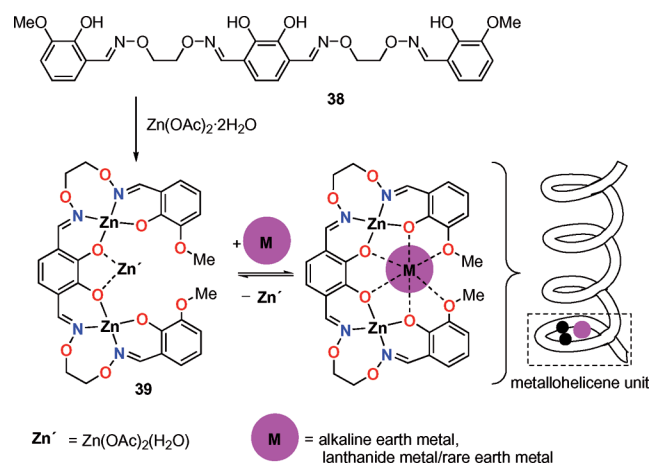
Nabeshima and co-workers designed a helical metall-ohost based on oxime-derived (unsymmetrical) salen compounds.^[55] The strategy is based on the use of oxime precursor **38** which after treatment with $\text{Zn}^{\text{II}}(\text{OAc})_2$ results in formation of homotrimeric **39** with a C-shaped O_6 cavity. This cavity proved to be useful for binding of various rare earth and alkaline earth metal ions after exchange of the central Zn^{2+} ion in **39** upon which the consequential helical shape of the hetero-trinuclear complex can be fine-tuned. For small guest metal cations, a tighter helix is formed, while for the larger cations a loose helix prevails. The authors have suggested application potential in fields such as selective ion recognition, new magnetic materials and catalysis.

So far, nonsymmetrical salen systems have been discussed with the asymmetry arising from the presence of two different salicylideneimine groups. A number of groups have recently designed functional metallosalen complexes in which the asymmetry originates from either the bridging unit or another component (Scheme 20). The first example is a bifunctional catalyst system that constitutes the merge between both a Lewis acid [Co^{II} center] as well as a Lewis base site (tertiary amine group from quinine).^[56]

Covalent attachment of the quinine unit to the Co^{II} -salen framework using an ester linkage onto the bridging ethylenediamine group was accomplished through Boc-protected (\pm)-2,3-diaminopropionic acid (Scheme 21). This gave a 1:1 diastereomeric mixture of ester **40** in high yield (87%). The Boc groups were then removed by TFA, followed by a double condensation with a salicylaldehyde to yield the unsymmetrical salen ligand (92%). A series of metal complexes were prepared to screen for bifunctional catalytic activity in the Wynberg reaction of 2-benzyloxyacetaldehyde

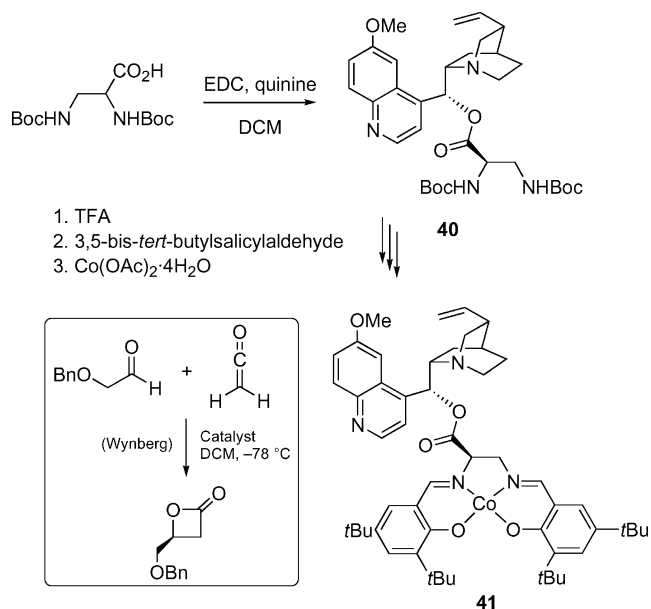


Scheme 19. Macrocyclic Schiff bases with four unsymmetrical salen pockets.



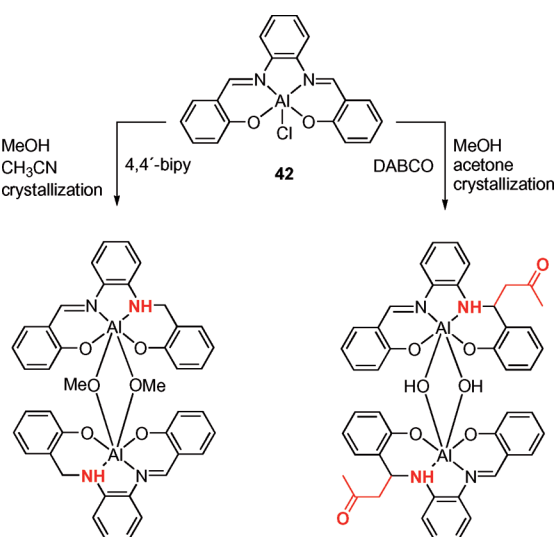
Scheme 20. Metallohelix structures build from an oxime-based, nonsymmetrical salen derivative.

with an in situ generated ketene giving a chiral β -lactone product (Scheme 21). Among these metallosalen derivatives, the Co^{II} complex **41** proved to be superior in terms of reaction rate and enantioselectivity.



Scheme 21. A bifunctional nonsymmetrical Co^{II}-salen catalyst based on a Lewis acid and Lewis base site.

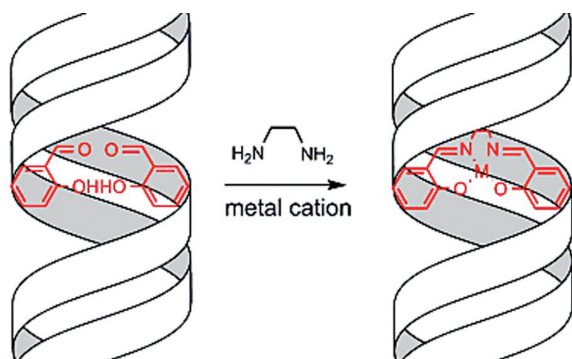
Dalla Cort found that Al^{III}-salphen complex **42** (Scheme 22) can undergo facile hydride and enolate addition to the imine bond under mild conditions.^[57a] The Al^{III} complex **42** was subjected to crystallization from a 2:1 mixture of MeOH/CH₃CN in the presence of 4,4'-bipyridine in order to investigate the formation of sandwich type, supramolecular coordination complexes. Alternatively, formation of 2:1 assemblies was also attempted using DABCO (1,4-diazabicyclo[2.2.2]octane) in CH₃OH/acetone (2:1). In both situations, crystals were obtained and X-ray molecular structures determined. Surprisingly, when using the former crystallization conditions, a dimeric complex was obtained which has in each salphen unit one of the CH=N imine bonds reduced to a single bond. This was explained by a



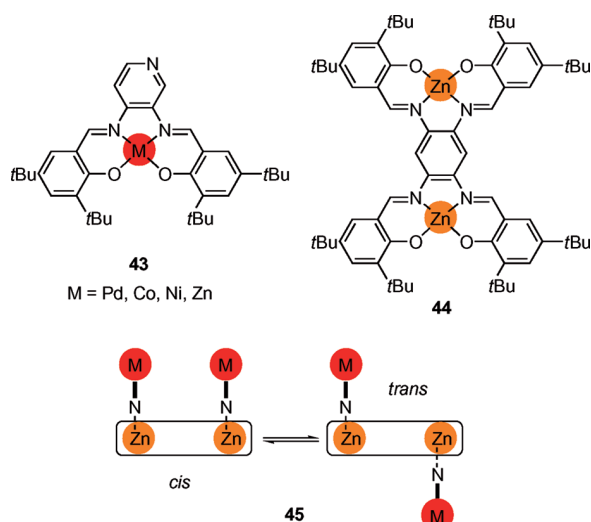
Scheme 22. Desymmetrization of Al^{III}-salphen complexes via hydride/enolate addition to one of the imine bonds.

proposed Meerwein–Ponndorf–Verley reduction. In the second case, acetone (one of the crystallization solvents) is added to the imine bond. The key factor that determines the outcome of the crystallization process is the coordination and subsequent activation (base-assisted deprotonation) of MeOH and acetone, respectively, by the Lewis acidic Al^{III} centre.

Axial ligand binding has been employed by Nguyen and co-workers for the induction of asymmetry in the Ru^{II} -salen catalyzed olefin cyclopropanation.^[58] Achiral Ru^{II} -salen complexes were axially decorated with chiral sulfoxide ligands and thus provided a nonsymmetrical environment for the salen system. An even more elegant way to afford such a nonsymmetry around a symmetrical salen framework was reported by Carell and others.^[59–61] For instance, Carell^[59] reported the synthesis of a salen-based metal-base pair inside a DNA duplex (Scheme 23), with the metal inbedded in the duplex structure. Assembly of the salen-oligonucleotide hybrid resulted in the tremendous stabilization of the duplex structure. The incorporation of multiple cations inside the DNA duplex^[61] is currently also a topic that attracts huge interest in the field of bio-inspired nanotechnology.



Scheme 23. Schematic duplex formation by assembly of two salicylaldehyde-derived oligonucleotides.



Scheme 24. Supramolecular hetero-tetrametallic salen structures potentially useful for cooperative catalysis.

Salen derivatives equipped with one or more pyridine groups are well-suited for supramolecular assembly formation.^[33,62] Kleij and co-workers have shown that immobilization of metallosalen complexes can, in contrast to covalent attachment (see sections 2 and 3), also be accomplished via supramolecular coordination motifs.^[63] For instance, metallo-salpyr complexes of type **43** were simply mixed with bis- Zn^{II} (salphen) complex **44** to cleanly give the supramolecular system **45** in quantitative yield (Scheme 24). The relative position of both salpyr complexes may be *cis* or *trans* due to the dynamic nature of the $\text{Zn}-\text{N}_{\text{pyr}}$ bond, but nonetheless it offers new opportunities to design and develop new systems for cooperative catalysis.^[14]

6. Conclusion

This review has shown that the field of nonsymmetrical salen compounds has matured significantly during the last decade. Principal problems in the construction of unsymmetrical versions of (metallo)salen derivatives with two different salicylideneimine groups have been addressed using either step-wise condensation approaches, partial protection of diamine intermediates or metal templation. Other useful routes start off with the use of a mono-*N*-substituted diamine precursor, thereby exploiting the difference in reactivity of secondary and primary amine functions. Also, several research groups have utilized ketones as key reagents to make “half-salen” (i.e., ketimine) derivatives which are then conveniently converted into salen derivatives by treatment with a salicylaldehyde in a second condensation stage (i.e., formation of the aldimine part). These unsymmetrical salen ligands and their complexes have found widespread application in the field of catalysis, where improved selectivities have frequently been encountered as opposed to their symmetrical counterparts. The nonsymmetrical salen derivatives have demonstrated to be vital for the preparation of various polymer-supported catalysts that show improved properties (catalyst recycling, higher activities) as compared with parent mono-nuclear complexes. A more recent tendency focuses on the use of unsymmetrical salen compounds as building blocks of (bio-inspired) macromolecular and/or supramolecular structures,^[1c,1g] a development that will arouse renewed and amplified interest for these intriguing molecules.

Acknowledgments

I am grateful to the Institució Catalana de Recerca i Estudis Avançats (ICREA), the Institute of Chemical Research of Catalonia (ICIQ) and the Ministerio de Educación y Ciencia (MEC) (project CTQ2008-02050/BQU) for their financial support to this work.

[1] The term “salen” here will be used throughout this review as a general name for this kind of ligand. Where needed, the exact nature of the ligand will be structurally detailed. For selected reviews on this subject see: a) L. Canali, D. C. Sherrington, *Chem. Soc. Rev.* **1999**, 28, 85–93; b) J. F. Larrow, E. N. Ja-

- cobson, *Top. Organomet. Chem.* **2004**, *6*, 123–152; c) T. Katsuki, *Adv. Synth. Catal.* **2002**, *344*, 131–147; d) P. G. Cozzi, *Chem. Soc. Rev.* **2004**, *33*, 410–421; e) S. J. Wezenberg, A. W. Kleij, *Angew. Chem. Int. Ed.* **2008**, *47*, 2354–2364; f) E. M. McGarrigle, D. G. Gilheany, *Chem. Rev.* **2005**, *105*, 1563–1602; g) A. W. Kleij, *Chem. Eur. J.* **2008**, early view (DOI: 10.1002/chem.200801149); h) D. A. Atwood, M. J. Harvey, *Chem. Rev.* **2001**, *101*, 37–52; i) D. J. Darensbourg, *Chem. Rev.* **2007**, *107*, 2388–2410; j) T. Katsuki, *Coord. Chem. Rev.* **1995**, *140*, 189–214; k) E. N. Jacobsen, *Acc. Chem. Res.* **2000**, *33*, 421–431; l) A. Dalla Cort, C. Pasquini, L. Schiaffino, *Supramol. Chem.* **2007**, *19*, 79–87; m) T. Katsuki, *Chem. Soc. Rev.* **2004**, *33*, 437–444; n) N. Madhavan, C. W. Jones, M. Weck, *Acc. Chem. Res.* **2008**, *41*, 1153–1165.
- [2] a) W. Zhang, J. L. Loebach, S. R. Wilson, E. N. Jacobsen, *J. Am. Chem. Soc.* **1990**, *112*, 2801–2803; b) R. Irie, K. Noda, Y. Ito, N. Matsumoto, T. Katsuki, *Tetrahedron Lett.* **1990**, *31*, 7345–7348.
- [3] See for instance: a) J. F. Larrow, E. N. Jacobsen, Y. Gao, Y. Hong, X. Nie, C. M. Zepp, *J. Org. Chem.* **1994**, *59*, 1939–1942; b) M. Palucki, N. S. Binney, P. J. Pospisil, M. L. Güler, T. Ishida, E. N. Jacobsen, *J. Am. Chem. Soc.* **1998**, *120*, 948–954; For recent theoretical studies devoted to electronic effects in these systems: c) L. Cavallo, H. Jacobsen, *J. Org. Chem.* **2003**, *68*, 6202–6207.
- [4] For a few examples of polymer-supported (symmetrical) metallosalen catalyst see: a) F. Minutolo, D. Pini, P. Salvadori, *Tetrahedron: Asymmetry* **1996**, *7*, 2293–2302; b) F. Minutolo, D. Pini, P. Salvadori, *Tetrahedron Lett.* **1996**, *37*, 3375–3378.
- [5] Please refer to section 2.
- [6] For examples of dendritic catalysts with metallosalen fragments: a) R. Breinbauer, E. N. Jacobsen, *Angew. Chem. Int. Ed.* **2000**, *39*, 3604–3607; b) H. Sellner, J. K. Karjalainen, D. Seebach, *Chem. Eur. J.* **2001**, *7*, 2873–2887.
- [7] Please refer to section 2.
- [8] a) G.-J. Kim, J.-H. Shin, *Catal. Lett.* **1999**, *63*, 83–90; b) M. F. Renehan, H.-J. Schanz, E. M. McGarrigle, C. T. Dalton, A. M. Daly, D. G. Gilheany, *J. Mol. Catal. A* **2005**, *231*, 205–220.
- [9] R. Atkins, G. Brewer, E. Kokot, G. M. Mockler, E. Sinn, *Inorg. Chem.* **1985**, *24*, 127–134.
- [10] For similar approaches through mono- and/or diketimine intermediates see: a) X.-D. Du, X.-D. Yu, *J. Mol. Catal. A* **1997**, *126*, 109–133; b) D. M. Boghaei, S. Mohebi, *Tetrahedron* **2002**, *58*, 5357–5366; c) A. Böttcher, H. Elias, B. Eisenmann, E. Hilms, A. Huber, R. Kniep, C. Röhr, M. Zehnder, M. Neuburger, J. Springborg, *Z. Naturforsch., Teil B* **1994**, *49*, 1089–1100; d) A. Huber, L. Müller, H. Elias, R. Klement, M. Valko, *Eur. J. Inorg. Chem.* **2005**, 1459–1467; e) R. I. Kureshy, N. H. Khan, S. H. R. Abdi, A. K. Bhatt, *J. Mol. Catal. A* **1996**, *110*, 33–40; f) R. I. Kureshy, N. H. Khan, S. H. R. Abdi, P. Iyer, A. K. Bhatt, *J. Mol. Catal. A* **1997**, *120*, 101–108; g) R. I. Kureshy, N. H. Khan, S. H. R. Abdi, P. Iyer, S. T. Patel, *Polyhedron* **1996**, *110*, 33–40.
- [11] A. Yeori, S. Gendler, S. Groysman, I. Goldberg, M. Kol, *Inorg. Chem. Commun.* **2004**, *7*, 280–282.
- [12] a) R. G. Konsler, J. Karl, E. N. Jacobsen, *J. Am. Chem. Soc.* **1998**, *120*, 10780–10781. For a recent contribution describing a similar approach with dinuclear Al^{III}salen complexes useful in cooperative catalysis see: b) C. Mazet, E. N. Jacobsen, *Angew. Chem. Int. Ed.* **2008**, *47*, 1762–1765.
- [13] a) D. Allen Annis, E. N. Jacobsen, *J. Am. Chem. Soc.* **1999**, *121*, 4147–4154. For another interesting example see: b) U. K. Anyanwu, D. Venkataraman, *Tetrahedron Lett.* **2003**, *44*, 6445–6448.
- [14] Co^{III}-salen complexes with two pending hydroxy groups in the 5 and 5' position of the phenyl side groups have been used to construct symmetrical, cyclic oligosalen catalysts useful in cooperative campaigns. See: a) J. M. Ready, E. N. Jacobsen, *J. Am. Chem. Soc.* **2001**, *123*, 2687–2688; b) J. M. Ready, E. N. Jacobsen, *Angew. Chem. Int. Ed.* **2002**, *41*, 1374–1377; c) D. E. White, E. N. Jacobsen, *Tetrahedron: Asymmetry* **2003**, *14*, 3633–3638.
- [15] a) L. Canali, E. Cowan, H. Deleuze, C. L. Gibson, D. C. Sherrington, *Chem. Commun.* **1998**, 2561–2562. For other examples using a direct approach for nonsymmetrical salen derivatives attached to polymeric and other supports see: b) C. Baleizão, H. García, *Chem. Rev.* **2006**, *106*, 3987–4043 and references cited therein; c) A. Corma, H. García, *Adv. Synth. Catal.* **2006**, *348*, 1391–1412; d) M. Alvaro, C. Baleizão, E. Carbonell, M. El Ghoul, H. García, B. Gigante, *Tetrahedron* **2005**, *61*, 12131–12139; e) M. D. Angelino, P. E. Laibinis, *Macromolecules* **1998**, *31*, 7581–7587; f) D. C. Sherrington, *Catal. Today* **2000**, *57*, 87–104 and references cited therein; g) M. Nielsen, K. V. Gothelf, *J. Chem. Soc. Perkin Trans. 1* **2004**, 2440–2444.
- [16] B. M. Rossbach, K. Leopold, R. Weberskirch, *Angew. Chem. Int. Ed.* **2006**, *45*, 1309–1312.
- [17] P. Goyal, X. Zheng, M. Weck, *Adv. Synth. Catal.* **2008**, *350*, 1816–1822.
- [18] For similar, but less active resin-supported Co^{III}-salen systems, see: a) ref.^[10a]; b) W. Solodenko, G. Jas, U. Kunz, A. Kirschning, *Synthesis* **2007**, 583–589.
- [19] M. Holbach, X. Zheng, C. Burd, C. W. Jones, M. Weck, *J. Org. Chem.* **2006**, *71*, 2903–2906.
- [20] a) R. I. Kureshy, N. H. Khan, S. H. R. Abdi, S. Singh, I. Ahmad, R. V. Jasra, A. P. Vyas, *J. Catal.* **2004**, *224*, 229–235; b) R. I. Kureshy, N. H. Khan, S. H. R. Abdi, S. T. Patel, R. V. Jasra, *J. Mol. Catal. A* **2002**, *179*, 73–77; c) R. I. Kureshy, N. H. Khan, S. H. R. Abdi, S. T. Patel, R. V. Jasra, *Tetrahedron: Asymmetry* **2001**, *12*, 433–437.
- [21] a) A. M. Daly, C. T. Dalton, M. F. Renehan, D. G. Gilheany, *Tetrahedron Lett.* **1999**, *40*, 3617–3620; b) see also ref.^[8b] for a full account.
- [22] Although an earlier report exists on the high yield synthesis of nonsymmetrical salen derivatives, several groups have reported problems with the reproducibility of these results: J. Lopez, S. Liang, X. R. Bu, *Tetrahedron Lett.* **1998**, *39*, 4199–4202.
- [23] E. J. Campbell, S. T. Nguyen, *Tetrahedron Lett.* **2001**, *42*, 1221–1224.
- [24] X. Zheng, C. W. Jones, M. Weck, *J. Am. Chem. Soc.* **2007**, *129*, 1105–1112.
- [25] J. A. Love, J. P. Morgan, T. M. Trnka, R. H. Grubbs, *Angew. Chem. Int. Ed.* **2002**, *41*, 4035–4037.
- [26] X. Zheng, C. W. Jones, M. Weck, *Adv. Synth. Catal.* **2008**, *350*, 255–261. For symmetrical metallosalen complexes equipped with styrene functions that can be polymerized see ref.^[6b]
- [27] X. Zheng, C. W. Jones, M. Weck, *Chem. Eur. J.* **2006**, *12*, 576–583.
- [28] M. Holbach, M. Weck, *J. Org. Chem.* **2006**, *71*, 1825–1836.
- [29] For some representative examples of 1,4-conjugate additions see: a) M. S. Sigman, E. N. Jacobsen, *J. Am. Chem. Soc.* **1998**, *120*, 5315–5316; b) M. S. Taylor, E. N. Jacobsen, *J. Am. Chem. Soc.* **2003**, *125*, 11204–11205; c) M. Gandelman, E. N. Jacobsen, *Angew. Chem. Int. Ed.* **2005**, *44*, 2393–2397; d) M. Bandini, M. Fagioli, M. Garavelli, A. Melloni, V. Trigari, A. Umani-Ronchi, *J. Org. Chem.* **2004**, *69*, 7511–7518.
- [30] N. Madhavan, M. Weck, *Adv. Synth. Catal.* **2008**, *350*, 419–425.
- [31] M.-A. Muñoz-Hernández, T. S. Keizer, S. Parkin, B. Patrick, D. A. Atwood, *Organometallics* **2000**, *19*, 4416–4421.
- [32] A. W. Kleij, D. M. Tooke, A. L. Spek, J. N. H. Reek, *Eur. J. Inorg. Chem.* **2005**, 4626–4634.
- [33] Salpyr compounds are defined as salen derivatives with a pyridine bridging group. See for the use of Zn^{II}-salpyr compounds: a) A. W. Kleij, M. Kuil, D. M. Tooke, A. L. Spek, J. N. H. Reek, *Inorg. Chem.* **2007**, *46*, 5829–5831; b) G. Li, W. Yu, J. Ni, T. Liu, Y. Liu, E. Sheng, Y. Cui, *Angew. Chem. Int. Ed.* **2008**, *47*, 1245–1249; c) K.-H. Chang, C.-C. Huang, Y.-H. Liu, Y.-H. Hu, P.-T. Chou, Y.-C. Lin, *Dalton Trans.* **2007**, 1731–1738; d) K.-L. Kuo, C.-C. Huang, Y.-C. Lin, *Dalton Trans.* **2008**, 3889–3898.

- [34] a) S. Curreli, E. C. Escudero-Adán, J. Benet-Buchholz, A. W. Kleij, *J. Org. Chem.* **2007**, 72, 7018–7021; b) S. Curreli, E. C. Escudero-Adán, J. Benet-Buchholz, A. W. Kleij, *Eur. J. Inorg. Chem.* **2008**, 2863–2873.
- [35] A. W. Kleij, D. M. Tooke, M. Kuil, M. Lutz, A. L. Spek, J. N. H. Reek, *Chem. Eur. J.* **2005**, 11, 4743–4750.
- [36] A. W. Kleij, M. Lutz, A. L. Spek, P. W. N. M. van Leeuwen, J. N. H. Reek, *Chem. Commun.* **2005**, 3661–3663.
- [37] A. W. Kleij, M. Kuil, M. Lutz, D. M. Tooke, A. L. Spek, P. C. J. Kamer, P. W. N. M. van Leeuwen, J. N. H. Reek, *Inorg. Chim. Acta* **2005**, 359, 1807–1814.
- [38] M. Kuil, P. E. Goudriaan, A. W. Kleij, D. M. Tooke, A. L. Spek, P. W. N. M. van Leeuwen, J. N. H. Reek, *Dalton Trans.* **2007**, 2311–2320.
- [39] L. Rigamonti, F. Demartin, A. Forni, S. Righetto, A. Pasini, *Inorg. Chem.* **2006**, 45, 10976–10989.
- [40] For further experimental details see also: J.-P. Costes, F. Dahan, M. B. Fernandez Fernandez, M. I. Fernandez Garcia, A. M. Garcia Deibe, J. Sanmartin, *Inorg. Chim. Acta* **1998**, 274, 73–81.
- [41] C. Benelli, A. Caneschi, D. Gatteschi, O. Guillou, L. Pardi, *Inorg. Chem.* **1990**, 29, 1750–1755.
- [42] R.-J. Tao, C.-Z. Mei, S.-Q. Zang, Q.-L. Wang, J.-Y. Niu, D.-Z. Liao, *Inorg. Chim. Acta* **2004**, 357, 1985–1990.
- [43] A. Dalla Cort, L. Mandolini, G. Palmieri, C. Pasquini, L. Schiaffino, *Chem. Commun.* **2003**, 2178–2179. See also ref.^[11] for a review on uranyl-salen chemistry.
- [44] M. Cametti, M. Nissinen, A. Dalla Cort, L. Mandolini, K. Rissanen, *J. Am. Chem. Soc.* **2005**, 127, 3831–3837.
- [45] V. van Axel Castelli, A. Dalla Cort, L. Mandolini, V. Pinto, D. N. Reinhoudt, F. Ribaudou, C. Sanna, L. Schiaffino, B. H. M. Snellink-Ruël, *Supramol. Chem.* **2002**, 14, 211–219.
- [46] A. Dalla Cort, J. I. Miranda Murua, C. Pasquini, M. Pons, L. Schiaffino, *Chem. Eur. J.* **2004**, 10, 3301–3307.
- [47] A. Dalla Cort, L. Mandolini, L. Schiaffino, *Chem. Commun.* **2005**, 3867–3869.
- [48] V. van Axel Castelli, A. Dalla Cort, L. Mandolini, V. Pinto, L. Schiaffino, *J. Org. Chem.* **2007**, 72, 5383–5386.
- [49] K. Ambroziak, M. Szypa, *Tetrahedron Lett.* **2007**, 48, 3331–3335.
- [50] T. Glaser, M. Heidemeier, T. Lügger, *Dalton Trans.* **2003**, 2381–2383.
- [51] See for the use of (multimetallic)salen complexes as adsorption materials and sensors: a) E. C. Escudero-Adán, J. Benet-Buchholz, A. W. Kleij, *Inorg. Chem.* **2008**, 47, 4256–4263; b) S. J. Wezenberg, E. C. Escudero-Adán, J. Benet-Buchholz, A. W. Kleij, *Org. Lett.* **2008**, 10, 3311–3314; c) A. Dalla-Cort, L. Mandolini, C. Pasquini, K. Rissanen, L. Russo, L. Schiaffino, *New J. Chem.* **2007**, 31, 1633–1638; d) M. E. Germain, T. R. Vargo, P. G. Khalifah, M. J. Knapp, *Inorg. Chem.* **2007**, 46, 4422–4429; e) M. E. Germain, M. J. Knapp, *J. Am. Chem. Soc.* **2008**, 130, 5422–5423.
- [52] a) N. E. Borisova, M. D. Reshetova, Y. A. Ustynyuk, *Chem. Rev.* **2007**, 107, 46–79; b) P. A. Vigato, S. Tamburini, L. Bertolo, *Chem. Rev.* **2007**, 107, 1311–1492.
- [53] For a recent example: P. D. Frischmann, A. J. Gallant, J. H. Chong, M. MacLachlan, *Inorg. Chem.* **2008**, 47, 101–112.
- [54] P. D. Frischmann, J. Jiang, J. K.-H. Hui, J. J. Grzybowski, M. J. MacLachlan, *Org. Lett.* **2008**, 10, 1255–1258.
- [55] S. Akine, T. Taniguchi, T. Nabeshima, *J. Am. Chem. Soc.* **2006**, 128, 15765–15774.
- [56] Y.-M. Lin, J. Boucau, Z. Li, V. Casarotto, J. Lin, A. N. Nguyen, J. Ehrmantraut, *Org. Lett.* **2007**, 9, 567–570.
- [57] a) M. Cametti, A. Dalla Cort, M. Colapietro, G. Portalone, L. Russo, K. Rissanen, *Inorg. Chem.* **2007**, 46, 9057–9059; b) For another similar example: Y. Wang, S. Parkin, D. A. Atwood, *Inorg. Chem.* **2002**, 41, 558–565.
- [58] J. A. Miller, B. A. Gross, M. A. Zhuravel, W. Jin, S. T. Nguyen, *Angew. Chem. Int. Ed.* **2005**, 44, 3885–3889.
- [59] a) G. H. Clever, K. Polborn, T. Carell, *Angew. Chem. Int. Ed.* **2005**, 44, 7204–7208; b) G. H. Clever, Y. Sörtl, H. Burks, W. Spahl, T. Carell, *Chem. Eur. J.* **2006**, 12, 8708–8718.
- [60] For some other salen-based DNA templated systems see: a) J. L. Czapinski, T. L. Sheppard, *J. Am. Chem. Soc.* **2001**, 123, 8618–8619; b) J. L. Czapinski, T. L. Sheppard, *ChemBioChem* **2004**, 5, 127–129.
- [61] K. Tanaka, G. H. Clever, Y. Takezawa, Y. Yamada, C. Kaul, M. Shionoya, T. Carell, *Nat. Nanotechnol.* **2006**, 1, 190–194.
- [62] For an example see: S.-S. Sun, C. L. Stern, S. T. Nguyen, J. T. Hupp, *J. Am. Chem. Soc.* **2004**, 126, 6314–6326.
- [63] S. J. Wezenberg, E. Escudero-Adán, J. Benet-Buchholz, A. W. Kleij, *Inorg. Chem.* **2008**, 47, 2925–2927.

Received: September 19, 2008

Published Online: November 28, 2008

Expanding the Size of Organometallic Nanostructures: A Hexanuclear (Cymene)Ru Cylinder with a Length of More Than 3 nm

Céline Olivier,^[a] Rosario Scopelliti,^[a] and Kay Severin*^[a]

Keywords: Macrocycles / Nanostructures / Organometallic complexes / Ruthenium / Self-assembly

Coordination cages based on organometallic half-sandwich complexes are of interest, because they can display unique structures and host properties. This communication describes the synthesis and structure of a cylindrical nanostructure containing six (*p*-cymene)Ru^{II} fragments. The complex was

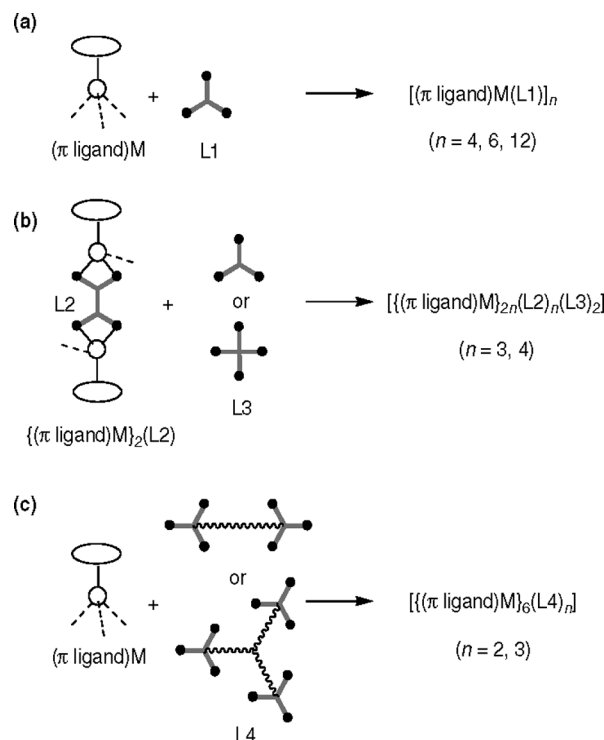
obtained by reaction of [(*p*-cymene)RuCl₂]₂ with a novel C₃-symmetrical ligand containing a triarylamine core and three dihydroxypyridine groups in its periphery.

(© Wiley-VCH Verlag GmbH & Co. KGaA, 69451 Weinheim, Germany, 2009)

Introduction

(Arene)Ru^{II} and (cyclopentadienyl)M (M = Ru^{II}, Rh^{III}, Ir^{III}) complexes are versatile building blocks in supramolecular coordination chemistry.^[1] The π ligands in these complexes are relatively inert and can be used to modulate the stability, solubility, and redox potential of the resulting assemblies. Opposite the π ligands are three available coordination sites. Reactions with polyfunctional ligands allow macrocycles and cages to be built.

For the construction of coordination cages based on (arene)Ru^{II} and (cyclopentadienyl)M (M = Ru^{II}, Rh^{III}, Ir^{III}) complexes, three main strategies have been employed. Tetra-,^[1c,2] hexa-,^[3,4] and dodecanuclear^[3b] cages were obtained by combining half-sandwich complexes with trifunctional ligands (Scheme 1a). The ligands themselves can be metal complexes, as in the case of molecular cubes that were formed by reactions of half-sandwich complexes with cyanometallates (e.g. [CpCo(CN)₃]).^[1c] The groups of Jin and Therrien have utilized dinuclear half-sandwich complexes as building blocks for the construction of cages (Scheme 1b).^[5,6] First, two (π ligand)M fragments were linked by oxalato or dihydroxybenzoquinonato ligands. In a second step, these molecular clips were treated with tri- or tetrafunctional ligands to afford prismatic boxes containing six or eight (π ligand)M units.^[7] Our group has recently started to explore a third approach. Trifunctional ligands, which are known to form stable macrocyclic complexes with (π ligand)M fragments, were linked by linear or branched spacers. This strategy has allowed us to prepare hexanuclear complexes (Scheme 1c).^[8]



Scheme 1. Three main routes for the construction of coordination cages based on (arene)Ru^{II} or (cyclopentadienyl)M (M = Ru^{II}, Rh^{III}, Ir^{III}) complexes. The number of donor atoms of the ligands L1–L4 is indicated by black dots. Charges are not shown for clarity.

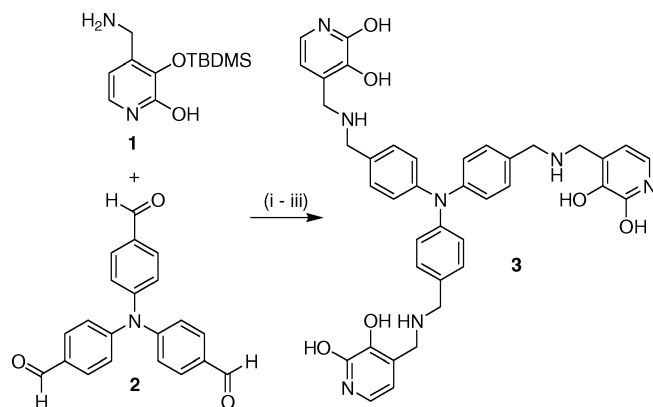
The coordination cages described above are not only appealing from a structural point of view, but they can also display interesting host–guest chemistry. This includes the selective complexation of alkali metal ions in the interior^[1c,2] or on the surface^[3] of cages, the binding of phosphate and acetate ions in aqueous solution,^[8b] and the encapsulation and solubilization of antitumor drugs.^[6b]

[a] Institut des Sciences et Ingénierie Chimiques, École Polytechnique Fédérale de Lausanne (EPFL), Lausanne, Switzerland
Fax: +41-21-6939305
E-mail: kay.severin@epfl.ch

Below we describe the synthesis and structure of a cylindrical nanostructure containing six (*p*-cymene)Ru^{II} fragments. The complex was obtained by route c (Scheme 1) with a novel C₃-symmetrical ligand containing a triarylamine core and three dihydroxypyridine groups in its periphery.

Results and Discussion

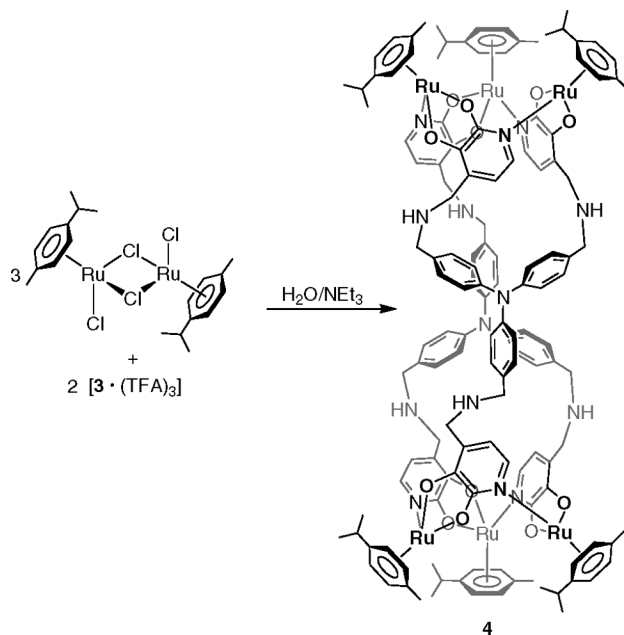
For the construction of an organometallic nanocylinder, we have first synthesized the novel ligand **3**. This was accomplished by reductive amination of 4,4',4''-triformyltriphenylamine with amine **1**, followed by deprotection of the *tert*-butyldimethylsilyl (TBDMS) protecting groups (Scheme 2). The C₃-symmetrical ligand **3** has three 1,2-dihydroxypyridine groups in its periphery. These groups are known to form very stable trinuclear metallamacrocycles with (π ligand)M complexes.^[9] The overall design of ligand **3** is related to that of a previously described ligand, which was obtained by reductive condensation of amine **1** with 1,3,5-triformylbenzene.^[8a] However, the utilization of 4,4',4''-triformyltriphenylamine instead of 1,3,5-triformylbenzene was expected to result in significantly larger structures.



Scheme 2. Synthesis of ligand **3**. Conditions: (i) MeOH/CHCl₃; (ii) NaBH₄; (iii) BF₃·Et₂O, CHCl₃.

For the reaction of ligand **3** with complex [(*p*-cymene)-RuCl₂]₂, we employed a crystallization protocol, which was previously used with success for the synthesis of organometallic nanostructures.^[8] The trifluoroacetic acid (TFA) adduct of ligand **3** was treated with [(*p*-cymene)RuCl₂]₂ in aqueous solution. The pH of the solution was then slowly raised by vapor diffusion of NEt₃. This resulted in the formation of red crystals of compound **4** in 15% yield (Scheme 3). A fluffy, noncrystalline precipitate was formed along with the crystals, which was separated from the crystals by suspension in the solvent and decantation.

The crystals of **4** were soluble in methanol and chloroform. The ¹H NMR spectrum in CDCl₃ was very complex, which indicated the formation of a structure of low symmetry. By integration of selected signals, it could be deduced that complex **4** contains (*p*-cymene)Ru fragments and



Scheme 3. Synthesis of complex **4**.

ligand **3** in a ratio 3:1. These results are in line with what was observed for (arene)Ru complexes with the 1,3,5-triformylbenzene-based ligand described above. In this case, hexanuclear structures with two deprotonated, bridging ligands were obtained.^[8a] A related structure of formula [(*p*-cymene)Ru]₆(**3**-6H⁺)₂ was therefore anticipated for complex **4**. This was substantiated by the high-resolution ESI-MS spectrum, which showed isotope-resolved M²⁺, M³⁺, and M⁴⁺ peaks for a hexanuclear complex (Figure 1).

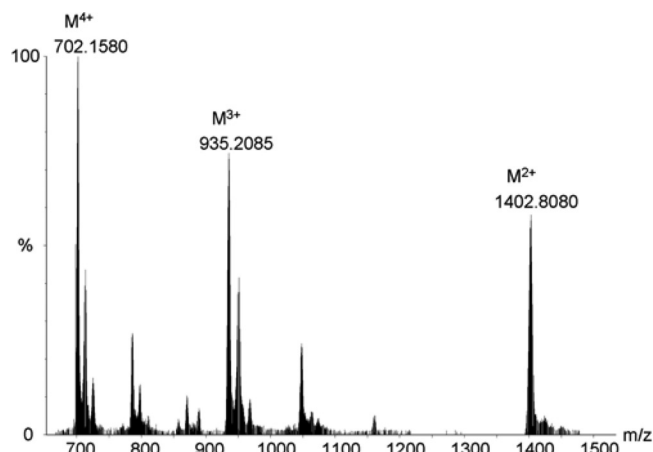


Figure 1. Part of the high-resolution ESI-MS spectrum of complex **4**.

Final confirmation came from a single-crystal X-ray diffraction analysis. Complex **4** can be described as a long cylinder with two (*p*-cymene)Ru trimers at the ends (Figure 2). The concave geometry of these trimers is similar to what has been observed for other 2,3-dihydroxypyridine-based complexes:^[9] the metal centers are bridged by the nitrogen atoms of the pyridine groups and by the two adjacent oxygen atoms, which results in a 12-membered macro-

cycle. The length of the cylinder (maximum C–C distance) is 30.9 Å, making complex **4** one of the longest (arene)Ru-based nanostructures described so far.^[1]

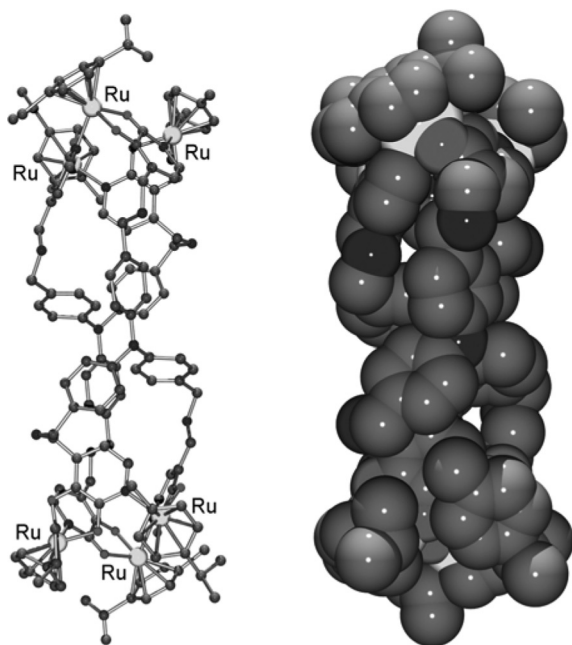


Figure 2. Molecular structure of complex **4** in the crystal. Left: ball-and-stick representation; right: space-filling representation. The hydrogen atoms and the cocrystallized water molecules are not shown for clarity.

The two bridging ligands are no longer C_3 -symmetric: two of the three arms are directed towards one end and the remaining arm towards the other end. The two central triarylamine fragments are packed closely against each other to yield a very compact structure (Figure 2, right side). One should note, however, that the two (*p*-cymene)-Ru trimers are connected by 46-membered macrocycles containing eight methylene and four secondary amine groups. This suggests that the structure displays significant flexibility in solution. Per complex, 22 molecules of cocrystallized water were localized in the crystal. None of the water molecules reside in the interior of the cylinder, but several hydrogen-bonding interactions with the N and O atoms of the ligands were observed.

Complex **4** has a crystallographic inversion center. Consequently, the three stereogenic Ru centers at one end of the cylinder have the opposite relative configuration to that of the three Ru centers at the other end of the cylinder. The ^1H NMR spectrum of **4** in solution is in agreement with the solid-state structure, indicating that crystalline **4** is a single diastereoisomer. Since the crystalline material was obtained in low yield, we are not able to tell whether the formation of **4** is diastereospecific. The ^1H NMR spectrum of the noncrystalline precipitate showed the presence of additional amounts of complex **4** along with numerous peaks of unidentified complexes.

Conclusions

The base-assisted reaction of $[(p\text{-cymene})\text{RuCl}_2]_2$ with the tris(dihydropyridine) ligand **3** resulted in the formation of the cylindrical nanostructure **4** containing six (*p*-cymene)Ru fragments and two bridging ligands. The structure is of interest because of its unusual length of more than 3 nm. So far, cylindrical metal complexes of this length have mainly been observed for helicates.^[10] In addition, complex **4** is further evidence that cylindrical complexes can be obtained from C_3 -symmetrical ligands.^[8a]

Experimental Section

General: Commercial reagents were purchased from Acros, Fluka, or Sigma–Aldrich and were used as received. The half-sandwich complex $[(p\text{-cymene})\text{RuCl}_2]_2$ ^[11] and 4,4',4''-triformyltriphenylamine (**2**)^[12] were synthesized according to literature procedures. The primary amine **1** was synthesized as previously reported.^[8a] The synthesis of complex **4** was carried out under an atmosphere of dry dinitrogen by using standard Schlenk techniques. The ^1H NMR spectra were recorded with a Bruker 400 MHz spectrometer. Chemical shifts (δ) are quoted in parts per million (ppm) and are calibrated relative to residual solvent peaks. High-resolution mass spectra (HRMS) were recorded with a Waters CapLC-coupled Micromass Q-ToF Ultima ESI-instrument.

TBDMS-protected Ligand 3: 4,4',4''-Triformyltriphenylamine (**2**) (0.25 g, 0.76 mmol) and amine **1** (0.58 g, 2.27 mmol; 3 equiv.) were dissolved in MeOH (100 mL) and CH_3Cl (10 mL), and the mixture was stirred overnight at room temperature. NaBH_4 (0.11 g, 2.8 mmol) was then added to the resulting yellow solution of the tris(imine) intermediate. After 2 h of stirring at room temperature, the solvents were removed, and the crude material was washed with Et_2O (50 mL), then dissolved in EtOH (100 mL), and the organic solution was filtered. Evaporation of the solvent afforded a yellow solid that was used without further purification. The TBDMS-protected ligand was obtained in 63% yield (0.50 g, 0.48 mmol). ^1H NMR (400 MHz, $[\text{D}_6]\text{DMSO}$): δ = 11.45 (s, 3 H, NH_{pyr}), 7.18 (d, 3J = 8.0 Hz, 6 H, CH_{Ar}), 7.04 (d, 3J = 5.5 Hz, 3 H, pyr), 6.88 (d, 3J = 8.0 Hz, 6 H, CH_{Ar}), 6.02 (d, 3J = 5.5 Hz, 3 H, pyr), 3.60 (s, 6 H, CH_2N), 3.53 (s, 6 H, NCH_2), 0.90 [s, 27 H, $[(\text{CH}_3)_3\text{C}]\text{Si}$], 0.21 [s, 18 H, $(\text{CH}_3)_2\text{Si}$] ppm. ^{13}C NMR (101 MHz, $[\text{D}_6]\text{DMSO}$): δ = 158.6, 146.0, 142.0 (pyr), 135.3, 134.8, 129.1, 123.2 (Ar), 125.6, 105.4 (pyr), 56.0, 52.0 (CH_2), 26.0 [$\text{SiC}(\text{CH}_3)_3$], 18.6 [$\text{SiC}(\text{CH}_3)_3$], –3.2 [$\text{Si}(\text{CH}_3)_2$] ppm. HRMS ESI: calcd. for $[\text{C}_{57}\text{H}_{82}\text{N}_7\text{O}_6\text{Si}_3]^+$ 1044.5634; found 1044.5865 $[\text{M} + \text{H}]^+$.

Ligand 3 (TFA salt): The TBDMS-protected ligand (0.50 g, 0.48 mmol) was dissolved in dry CHCl_3 (200 mL). $\text{BF}_3 \cdot \text{Et}_2\text{O}$ (0.28 mL, 2.16 mmol) was added dropwise to this solution, and the reaction mixture was stirred and heated to 50 °C for 4 h. Evaporation of the solvent afforded a yellow solid, which was purified by reversed phase HPLC ($\text{H}_2\text{O}/\text{CH}_3\text{CN} + 0.1\%$ TFA). The TFA salt of **3** was obtained as a slightly yellow solid in 50% yield. ^1H NMR (400 MHz, $[\text{D}_6]\text{DMSO}$): δ = 11.85 (s, 3 H, NH_{pyr}), 9.82 (s, 3 H, OH_{pyr}), 9.18 (s, 6 H, H_2N^+), 7.44 (d, 3J = 8.6 Hz, 6 H, CH_{Ar}), 7.02 (d, 3J = 8.6 Hz, 6 H, CH_{Ar}), 6.94 (d, 3J = 6.8 Hz, 3 H, pyr), 6.20 (d, 3J = 6.8 Hz, 3 H, pyr), 4.13 (s, 6 H, CH_2N), 4.00 (s, 6 H, NCH_2) ppm. ^{13}C NMR (101 MHz, $[\text{D}_6]\text{DMSO}$): δ = 157.8, 147.2, 146.0, 131.7, 126.5, 123.7, 123.6, 119.2, 106.2, 49.7, 43.4 ppm. HRMS ESI: calcd. for $[\text{C}_{39}\text{H}_{40}\text{N}_7\text{O}_6]^+$ 702.3040; found 702.1003 $[\text{M} + \text{H}]^+$.

Complex $[(p\text{-cymene})\text{Ru}]_6(\text{C}_{40}\text{H}_{36}\text{N}_7\text{O}_6)_2$ (**4**): A mixture of the half-sandwich complex $[(p\text{-cymene})\text{RuCl}_2]_2$ (13.8 mg, 22.5 μmol) and **3**·(TFA)₃ (15.6 mg, 15 μmol) was stirred in a mixture of degassed water (7 mL) and degassed methanol (7 mL) until a clear solution was obtained. Vapor diffusion of NEt_3 led to the formation of complex **4** in the form of red crystals in 15% yield (3.2 mg, 1.12 μmol). ^1H NMR (400 MHz, CDCl_3): δ = 6.92–6.95 (m, 4 H, CH_{Ar}), 6.60–6.72 (m, 18 H, CH_{Ar}), 5.94 (d, 3J = 6.3 Hz, 2 H, CH_{Ar}), 5.76–5.85 (m, 12 H, CH_{Ar}), 5.62 (d, 3J = 6.3 Hz, 2 H, CH_{Ar}), 5.58 (d, 3J = 5.6 Hz, 2 H, CH_{Ar}), 5.50 (d, 3J = 5.4 Hz, 2 H, CH_{Ar}), 5.40 (d, 3J = 5.6 Hz, 2 H, CH_{Ar}), 5.25–5.33 (m, 8 H, CH_{Ar}), 5.02–5.06 (m, 6 H, CH_{Ar}), 4.16 (d, 3J = 6.3 Hz, 2 H, CH_{Ar}), 3.72–3.91 (m, 12 H, NCH_2), 3.60 (d, 2J = 13.9 Hz, 2 H, NCH_2), 3.58 (d, 2J = 11.2 Hz, 2 H, NCH_2), 3.29–3.36 (m, 6 H, NCH_2), 3.15 (d, 2J = 14.6 Hz, 2 H, NCH_2), 2.68–2.88 (m, 6 H, CH), 2.62 (d, 2J = 11.2 Hz, 2 H, NCH_2), 2.37 (d, 2J = 12.7 Hz, 2 H, NCH_2), 1.86–1.90 (m, 18 H, CH_3), 1.21–1.36 (m, 36 H, CH_3) ppm. HRMS ESI: calcd. for $[\text{C}_{138}\text{H}_{150}\text{Ru}_6\text{N}_{14}\text{O}_{12}]^{2+}$ 1402.8029; found 1402.8080 $[\text{M}]^{2+}$.

Crystallographic Analysis: Diffraction data were collected by using Mo-K_α radiation and a Bruker APEX II CCD up to 22° (θ), because of the extreme weakness of the sample. Data were reduced by EVAL CCD.^[13] The structure was refined by using full-matrix least-squares on F^2 and anisotropically defining all non-hydrogen atoms. The hydrogen atoms were placed in calculated positions by using the “riding model” with $U_{\text{iso}} = a U_{\text{eq}}$ (where a is 1.5 for methyl hydrogen atoms and 1.2 for others). Structure refinement and geometrical calculations were carried out with SHELXTL.^[14] Per complex, 22 water molecules were observed, but the actual number is likely to be higher. The SQUEEZE^[15] algorithm has been used to take into account the electron density due to the diffused and unresolved solvent, whereas the 11 water molecules of the asymmetric unit have been located by the difference map.

Crystal Data for Complex 4·22H₂O: $\text{C}_{138}\text{H}_{194}\text{N}_{14}\text{O}_{34}\text{Ru}_6$, M = 3199.49, monoclinic, a = 12.496(3) Å, b = 28.565(6) Å, c = 20.908(4) Å, β = 100.08(3)°, V = 7348(3) Å³, T = 100(2) K, space group $P2_1/n$, Z = 2, $\mu(\text{Mo-K}_\alpha)$ = 0.71073 Å, 8900 independent reflections, R_1 [$I > 2\sigma(I)$] = 0.1513, wR_2 (all data) = 0.4067. CCDC-705475 contains the supplementary crystallographic data for this paper. These data can be obtained free of charge from The Cambridge Crystallographic Data Centre via www.ccdc.ac.uk/data_request/cif.

Acknowledgments

The work was supported by the Swiss National Science Foundation, by the Claude & Giuliana Foundation, and by the École Polytechnique Fédérale de Lausanne (EPFL).

- [1] For reviews see: a) T. B. Rauchfuss, K. Severin in *Organic Nanostructures*, (Eds.: J. W. Atwood, J. W. Steed), Wiley-VCH, Weinheim, **2008**, pp. 179–203; b) S. Liu, G.-L. Wang, G.-X. Jin, *Dalton Trans.* **2008**, 425–432; c) J. L. Boyer, M. L. Kuhlman, T. B. Rauchfuss, *Acc. Chem. Res.* **2007**, *40*, 233–242; d) K. Severin, *Chem. Commun.* **2006**, 3859–3867; e) R. H. Fish, G. Jaouen, *Organometallics* **2003**, *22*, 2166–2177; f) K. Severin, *Coord. Chem. Rev.* **2003**, *245*, 3–10; g) R. H. Fish, *Coord. Chem. Rev.* **1999**, *185–186*, 569–584.
- [2] a) M. Ramesh, T. B. Rauchfuss, *J. Organomet. Chem.* **2004**, *689*, 1425–1430; b) S. C. N. Hsu, M. Ramesh, J. H. Espenson, T. B. Rauchfuss, *Angew. Chem. Int. Ed.* **2003**, *42*, 2663–2666; c) K. K. Klausmeyer, S. R. Wilson, T. B. Rauchfuss, *J. Am.*

- Chem. Soc.* **1999**, *121*, 2705–2711; d) K. K. Klausmeyer, T. B. Rauchfuss, S. R. Wilson, *Angew. Chem. Int. Ed.* **1998**, *37*, 1694–1696.
- [3] a) S. Mirtschin, E. Krasniqi, R. Scopelliti, K. Severin, *Inorg. Chem.* **2008**, *47*, 6375–6381; b) T. Brasey, R. Scopelliti, K. Severin, *Chem. Commun.* **2006**, 3308–3310.
- [4] M. L. Kuhlman, H. Yao, T. B. Rauchfuss, *Chem. Commun.* **2004**, 1370–1371.
- [5] a) Y.-F. Han, Y.-J. Lin, L.-H. Weng, H. Berke, G.-X. Jin, *Chem. Commun.* **2008**, 350–352; b) Y.-F. Han, Y.-J. Lin, W.-G. Jia, L.-H. Weng, G.-X. Jin, *Organometallics* **2007**, *26*, 5848–5853.
- [6] a) J. Mattson, P. Govindaswamy, J. Furrer, Y. Sei, K. Yamaguchi, G. Süss-Fink, B. Therrien, *Organometallics* **2008**, *27*, 4346–4356; b) B. Therrien, G. Süss-Fink, P. Govindaswamy, A. K. Renfrew, P. J. Dyson, *Angew. Chem. Int. Ed.* **2008**, *47*, 3773–3776; c) P. Govindaswamy, J. Furrer, G. Süss-Fink, B. Therrien, *Z. Anorg. Allg. Chem.* **2008**, *634*, 1349–1352; d) P. Govindaswamy, D. Linder, J. Lacour, G. Süss-Fink, B. Therrien, *Dalton Trans.* **2007**, 4457–4463; e) P. Govindaswamy, D. Linder, J. Lacour, G. Süss-Fink, B. Therrien, *Chem. Commun.* **2006**, 4691–4693.
- [7] Structurally related complexes with (π ligand) $\text{M}(\mu\text{-Cl})_2\text{M}(\pi$ ligand) fragments have been described: a) Y.-F. Han, W.-G. Jia, Y.-J. Lin, G.-X. Jin, *J. Organomet. Chem.* **2008**, *693*, 546–550; b) P. Govindaswamy, G. Süss-Fink, B. Therrien, *Organometallics* **2007**, *26*, 915–924; c) P. Govindaswamy, G. Süss-Fink, B. Therrien, *Inorg. Chem. Commun.* **2007**, *10*, 1489–1492.
- [8] a) C. Olivier, R. Scopelliti, K. Severin, *Inorg. Chem.* **2008**, *47*, 4454–4456; b) C. Olivier, Z. Grote, E. Solari, R. Scopelliti, K. Severin, *Chem. Commun.* **2007**, 4000–4002; c) Z. Grote, S. Bonazzi, R. Scopelliti, K. Severin, *J. Am. Chem. Soc.* **2006**, *128*, 10382–10383.
- [9] a) L. Mimassi, C. Cordier, C. Guyard-Duhayon, B. E. Mann, H. Amouri, *Organometallics* **2007**, *26*, 860–864; b) Z. Grote, H.-D. Witzemann, R. Scopelliti, K. Severin, *Z. Anorg. Allg. Chem.* **2007**, *633*, 858–864; c) Z. Grote, R. Scopelliti, K. Severin, *Eur. J. Inorg. Chem.* **2007**, 694–700; d) Z. Grote, R. Scopelliti, K. Severin, *J. Am. Chem. Soc.* **2004**, *126*, 16959–16972; e) L. Mimassi, C. Guyard-Duhayon, M. N. Rager, H. Amouri, *Inorg. Chem.* **2004**, *43*, 6644–6649; f) Z. Grote, M.-L. Lehaire, R. Scopelliti, K. Severin, *J. Am. Chem. Soc.* **2003**, *125*, 13638–13639; g) M.-L. Lehaire, A. Schulz, R. Scopelliti, K. Severin, *Inorg. Chem.* **2003**, *42*, 3576–3581; h) M.-L. Lehaire, R. Scopelliti, K. Severin, *Angew. Chem. Int. Ed.* **2002**, *41*, 1419–1421; i) M.-L. Lehaire, R. Scopelliti, K. Severin, *Chem. Commun.* **2002**, 2766–2767; j) M.-L. Lehaire, R. Scopelliti, K. Severin, *Inorg. Chem.* **2002**, *41*, 5466–5474; k) H. Piotrowski, K. Severin, *Proc. Natl. Acad. Sci. USA* **2002**, *99*, 4997–5000; l) H. Piotrowski, G. Hilt, A. Schulz, P. Mayer, K. Polborn, K. Severin, *Chem. Eur. J.* **2001**, *7*, 3196–3208; m) H. Piotrowski, K. Polborn, G. Hilt, K. Severin, *J. Am. Chem. Soc.* **2001**, *123*, 2699–2700.
- [10] a) M. Albrecht, I. Janser, R. Fröhlich, *Chem. Commun.* **2005**, 157–165; b) M. Albrecht, *Chem. Rev.* **2001**, *101*, 3457–3497; c) C. Piguet, G. Bernardinelli, G. Hopfgartner, *Chem. Rev.* **1997**, *97*, 2005–2062.
- [11] M. A. Bennett, T.-N. Huang, T. W. Matheson, A. K. Smith, *Inorg. Synth.* **1982**, *21*, 74–78.
- [12] P. Taranekar, Q. Qiao, H. Jiang, I. Ghiviriga, K. S. Schanze, J. R. Reynolds, *J. Am. Chem. Soc.* **2007**, *129*, 8958–8959.
- [13] A. J. M. Duisenberg, L. M. J. Kroon-Batenburg, A. M. M. Schreurs, *J. Appl. Crystallogr.* **2003**, *36*, 220–229.
- [14] G. M. Sheldrick, *SHELXTL*; University of Göttingen, Göttingen, Germany, **1997**; Bruker AXS, Inc., Madison, WI, **1997**.
- [15] SQUEEZE, P. van der Sluis, A. L. Spek, *Acta Crystallogr. Sect. A* **1990**, *46*, 194–201.

Received: October 16, 2008

Published Online: December 5, 2008

Bio-Inspired Bottom-Up Assembly of Diatom-Templated Ordered Porous Metal Chalcogenide Meso/Nanostructures

Han Zhou,^[a] Tongxiang Fan,^{*[a]} Xufan Li,^[a] Jian Ding,^[a] Di Zhang,^{*[a]} Xuesong Li,^[b] and Yahui Gao^[b]

Keywords: Chalcogens / Sonochemistry / Mesoporous materials / Nanostructures

We put forward a novel and straightforward sonochemical process as a generic bottom-up assembly route to produce ordered porous metal chalcogenide meso/nanostructures by templating of diatom frustules. We work with one of the most beautiful species of diatoms, *Coscinodiscus lineatus*, as a representative of diatoms with central symmetry, and with ZnS as the prototype, as it is a high refractive index material and is a typical material widely used in optics and photonics. ZnS replicas have been successfully synthesized from the interaction between the reactive surfaces of the frustules and the precursors under ultrasound. The inorganic replicas copy the

morphology of the ordered porous structure and inherit its optical property, such as the existence of the photonic bandgap of the diatom frustules. It is possible to achieve tunable photonic properties in the replicas by assembly of various metal chalcogenide semiconductors of different refractive indexes. This bio-inspired discovery provides insight into the facile synthesis of elaborate meso/nanostructures from these marine microbes.

(© Wiley-VCH Verlag GmbH & Co. KGaA, 69451 Weinheim, Germany, 2009)

Introduction

We marvel at nature's ability to drive the self-assembly of incredibly complicated structures, and we are even more fascinated by their evolved functions of intelligence, response, and adaptability in optics, electronics, magnetism among others. It is well known that some biological organisms can exhibit sophisticated optical systems, including one-dimensional multilayer reflectors,^[1] two-dimensional diffraction gratings,^[2] and three-dimensional liquid crystals.^[3] These natural optical systems can compete against or even outperform the top-technology products available. Thus, it has become increasingly important to further explore novel photonic nanostructures in nature, to replicate such nanomachineries and the photonic performance, and/or to biomimic these sophisticated nanostructures to construct analogues.

Diatoms are single-celled photosynthetic microorganisms which can make the most effective use of solar energy, converting it into energy-rich compounds.^[4] The reason that diatoms are so efficient in photosynthesis can be attributed to the intricate geometries and spectacular patterns of their

silica-based cell walls. As a typical example, the species *Coscinodiscus granii* have frustules (the cell wall of a diatomic silicate cell) with a diameter of about 150 μm and a thickness of 700 nm. The frustules exhibit hexagonal patterns of holes with a lattice constant of ca. 1 μm . Such systems are commonly denoted as photonic-crystal slabs, which are capable of confining photons coupled into the slab,^[5] thus serving as a convincing explanation for their high efficiency in photosynthesis. A similar assumption could also be extended to other diatom species. As a result, diatom cells are believed to act as natural mini-photonic devices, which can collect and control light intelligently.^[6] However, the biosilica inherent to diatoms does not provide the optimum chemistry/refractive index (of about 1.43) for many applications. The possibility to use and to tailor biological silica for optical devices could offer several advantages over current technologies. Several approaches for altering the chemistry of diatom frustules, while preserving the 3D frustule shape, have been reported. Gas/solid displacement reactions^[7] have generated 3D frustule replicas of non-silica-based oxides (e.g. MgO, TiO₂, and ZrO₂). Hydrothermal reactions^[8] have been used to convert frustules into silicates and non-silicates (e.g. BaTiO₃). Wet chemical coating or impregnation methods, with or without dissolution of the underlying silica frustules, have yielded replicas comprised fully or partially of silicates (e.g. Zn₂SiO₄), other oxides (e.g. ZrO₂, BaTiO₃), polymers, carbon, or metals.^[9] Other methods such as sol-gel synthesis^[10] and the thermal evaporation of metals (e.g. Au, Ag)^[11] have also been applied. To date, there is still no general method to produce 3D frustule replicas of

[a] State Key Lab of Metal Matrix Composites, Shanghai Jiaotong University, Shanghai 200240, P. R. China
Fax: +86-21-34202749
E-mail: txfan@sjtu.edu.cn
zhangdi@sjtu.edu.cn

[b] School of Life Sciences, Xiamen University, Fujian 361005, P. R. China

Supporting information for this article is available on the WWW under <http://www.eurjic.org> or from the author.

metal chalcogenides that commonly possess high refractive indices for wide applications, especially in optics and photonics.^[12] Furthermore, the inherited photonic performance has seldom been discussed, which may have a profound significance both in theory and in applications.

Here, we demonstrate a novel sonochemical process as a general bottom-up assembly technique to synthesize ordered porous metal chalcogenide meso/nanostructures with a 3D scaffold of diatom frustules as templates. We decided to work with one of the most beautiful species of diatoms, *Coscinodiscus lineatus*, as a representative of diatoms with central symmetry, and with ZnS as the prototype, as it is a high refractive index material (about 2.35) and is a typical material widely used in optics and photonics. The as-obtained diatom-templated ZnS replicas have replicated the ordered porous meso/nanostructures of the original diatom frustules well. The possible formation mechanisms based on the interaction between the reactive surfaces of the frustules and the precursors under ultrasound have been proposed. The reflectance spectra measurement demonstrates that the replicas inherit the photonic property of the original diatom frustules. A similar method could also be extended to a large variety of metal chalcogenides replicas, which could probably exhibit tunable photonic properties. This bio-inspired discovery provides insight into the biomimetic synthesis of elaborate meso/nanostructures from these marine microbes and their potential applications in optics and photonics.

Results and Discussion

The geometrical parameters have been obtained by FESEM (field emission scanning electron microscope) and TEM (transmission electron microscope). Figure 1a shows the FESEM image of valve view of a cleaned diatom frustule *C. lineatus*, the total diameter of which is about 40 μm . In the digital microscope image of the diatom frustule (Figure 1b), the frustule appears green because it has several hundred chloroplasts, which are located close to the cell walls, thus allowing them to make full use of the confined light. The girdle view of *C. lineatus* in Figure 1c shows that the diatom has a thickness of about 10 μm . The valves display regularly ordered and circular pores with diameters of about 1000 nm (Figure 1d, e). The size of the holes is nearly constant. The pores of the valves are in a regular repeating hexagonal lattice. Besides, there are smaller pores with sizes of 100 nm to 500 nm, which are also highly symmetrical on the edge of the valve (Figure S1). From the periodic pattern of holes in a slab, the valve band can be regarded as a slab waveguide photonic crystal with distinct symmetries and spectral ranges.

Such a delicate structure given by nature probably contains PBG (photonic bandgap) structures. However, the bi-silica inherent to diatoms does not provide the optimum chemistry/refractive index for many applications. By utilizing such a structure as a template and coating it uniformly with an inorganic dielectric material, it may be possible to

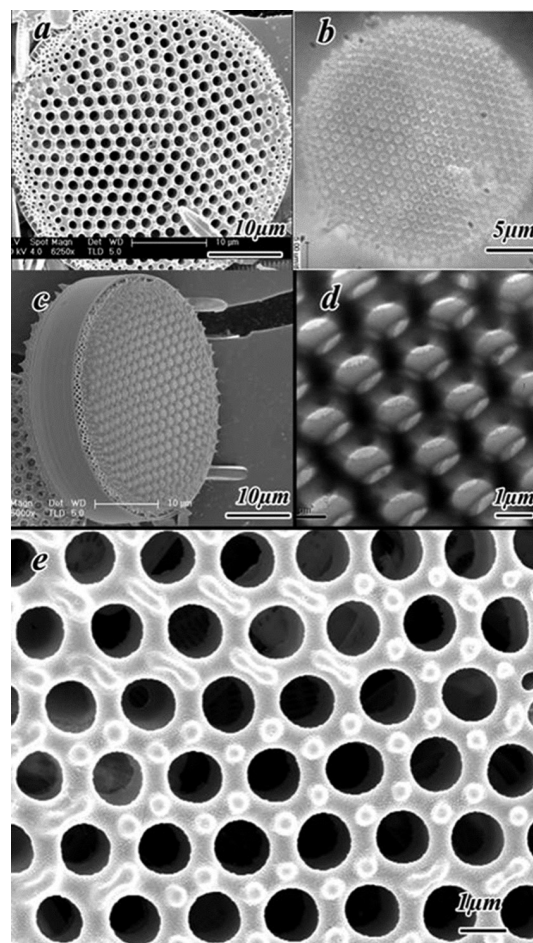


Figure 1. A series of images of the original diatom frustule *Coscinodiscus lineatus*. FESEM images of (a) valve view of a cleaned diatom frustule of *C. lineatus*; (b) valve view of a diatom frustule obtained by a digital light microscope; (c) girdle view of *C. lineatus*. (d) TEM image of the original diatom frustules *C. lineatus*. (e) High resolution FESEM image of *C. lineatus*.

fabricate PBG structures with high reproducibility and low cost. Here, we used a novel sonochemical technique to replicate the delicate structure. After 3 h of sonication, ZnS nanoparticles controllably assemble onto the diatom frustules. Figure 2 shows some typical examples of diatom-templated ZnS replicas. The inorganic replicas replicate the ordered porous structures of the diatom frustules well (Figure 2a). As shown in Figure 2b, the valves display regularly ordered, circular pores with a diameter of about 1000 nm. The pores of the valves are in a regular repeating hexagonal lattice as indicated by the dashed line. A magnified image (Figure 2c) shows the surface clearly, ZnS nanoparticles aggregate into nanoclusters and assemble onto the surfaces of the frustules to form ordered porous meso/nanostructures. The inset shows the corresponding TEM image of the replica. FESEM images of the products from other angles are presented in Figure S2, which indicates that ZnS films deposit not only on the external side of the frustule but also on the internal side. Figure 3 schematically illustrates the formation process of diatom-templated ordered porous ZnS meso/nanostructures assembled from ZnS nanoparticles.

The HRTEM image in Figure 2d shows that the average size of these nanoparticles is estimated to be only 3–5 nm as a result of the sonochemical process at near room temperature. The electron diffraction pattern shows diffuse rings, which indicates that the ZnS nanostructures are polycrystalline, and this result coincides with that from the XRD study (Figure S3).

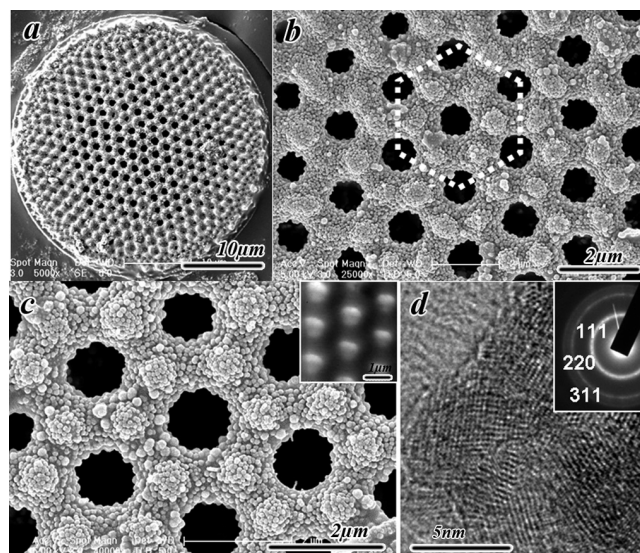


Figure 2. A series of images of the synthesized silica-based ZnS replicas. FESEM images of (a) top view of a whole silica-based ZnS replica; (b) low and (c) high resolution images of the silica-based ZnS replica, the inset of (c) is the corresponding TEM image. (d) HRTEM image of ZnS nanoparticles, the inset shows the SAED pattern.

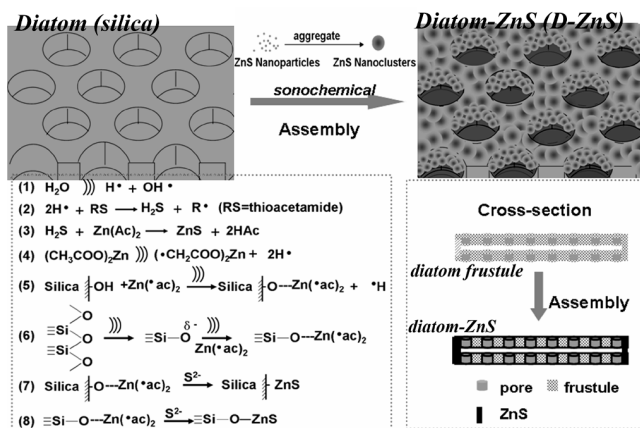


Figure 3. Schematic illustration of the synthesis of diatom-templated ordered porous ZnS meso/nanostructures assembled from ZnS nanoparticles.

A simplified reaction mechanism of the formation of ZnS under sonication is illustrated in Equation (1)–Equation (4). Equation (1) represents the formation of primary radicals from the ultrasound-initiated dissociation of water. Equation (2) and Equation (3) represent the main reactions leading to the formation of the ZnS nanoclusters. The freshly generated ZnS nanoclusters interact with the diatom frustules and form a ZnS-capped diatom composite. We be-

lieve that the acetate ligand plays an important role in the grafting of zinc onto the cell surfaces. The formation of $\cdot\text{CH}_2\text{COO}$ radicals ($\cdot\text{AC}$) for various transition metal acetates, in an appropriate liquid medium, has been known in the literature.^[13] Equation (4) represents the formation of solute radicals under sonochemical conditions, which has already been well established.^[13] The solute radicals formed under the sonochemical conditions can easily react with the reactive surfaces of frustules, thereby yielding metal-implanted cells.

The surfaces of the frustules comprise abundant Si–OH and Si–O–Si bonds, which attribute to the capture of metal ions (Figure S4). The sonochemical implantation of Zn^{2+} into the diatom frustule can probably be visualized in two ways: (i) the reactivity of surface silanol groups (–OH) and solute radicals (this is a consequence of the acidic nature of the silica, the negative polarity of the Si–O bonds, and the reactivity of its hydroxy groups, which allows for an effective interaction with sonochemically formed $\text{Zn}(\text{Ac})_2$), and (ii) the chemical reactivity of Si–O nucleation sites formed by the ultrasonic breakage of the strained siloxane link toward the solute radicals, as illustrated in Equation (5) and Equation (6), respectively. The breakage of the strained siloxane link by ultrasonic cavitation seems to be energetically preferable because it allows the reduction of the structural tension in this fragment (Si–O–Si) owing to the greater length and lower rigidity of the free Si–O bond.^[14] The metal acetate implanted into the cell surface then undergoes ligand exchange, with the generation of sulfide ions according to Equation (7) and Equation (8) to yield ZnS coated on the cells. Once the surface ZnS is formed, this can act as a nucleating site for the further adhesion of the ZnS formed in the bulk solution.

Although the current work is focused on ZnS, we believe that a similar approach is applicable to other metal chalcogenide materials such as ZnSe,^[15] PbS,^[16] PbSe,^[17] PbTe,^[18] CdS,^[19] CdSe,^[20] CuS,^[21] NiS,^[21] MoS,^[22] Ag₂S,^[23] among others, since such materials can also be prepared by the sonochemical method, whereas the precursors probably have a strong interaction with the cell surfaces under ultrasound. As a result, it is probably a general and straightforward route to synthesize various metal chalcogenide semiconductors of ordered porous meso/nanostructures based on diatom frustules.

The reflectance spectra demonstrate that the replica preserves not only the morphological structures but also the photonic property of the original diatom. The reflectance was measured on the diatom frustules and ZnS replicas of the well-ordered region. The scales were manipulated by a microprobe to a side-by-side arrangement and covered an area of $10 \times 10 \mu\text{m}$. The corresponding spectra are summarized in Figure 4. Diatom cell walls probably act as photonic-crystal slabs. Photonic crystals are regular structured materials that possess photonic bandgaps, i.e. frequency ranges in which light propagation does not occur through the material. Obviously, diatom cell walls are regular structured materials of limited thickness. The original diatom frustule exhibits reflection peak of about 990 nm. The well-

ordered region of the ZnS replica shows a reflection peak that is close in value to that of the diatom frustule. However, there is no reflection peak detected for the corresponding poorly ordered region. The appearance of this peak reveals the existence of a PBG in the replicated structure in the well-ordered region, so the replicas inherit the photonic performance of the original diatom frustule successfully. Meanwhile, the bandgap reflectivity is enhanced in the replicas relative to that of the diatom frustules, because of the higher dielectric contrast between the phases.^[24] Theoretical analysis of the reflectance calculations is currently underway. Since our sonochemical process is probably a general and versatile route to produce various metal chalcogenide replicas, so it is possible to achieve tunable photonic properties in the replicas by changing the refractive index and the periodicity constant. The products may have potential applications as photonic devices.

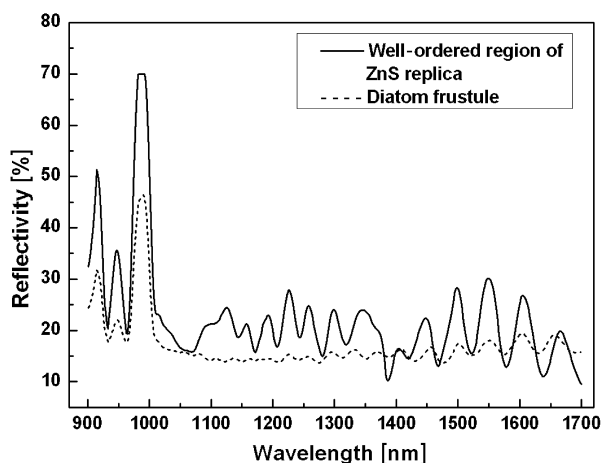


Figure 4. NIR reflectance spectra of the original diatom frustules and of the well-ordered region of silica-based ZnS replica.

Conclusions

In summary, a novel and straightforward sonochemical process has been demonstrated as a generic bottom-up assembly route to produce ordered porous metal chalcogenide replicas by templating diatom frustule meso/nanostructures, which has been inspired by their intricate structures and advanced optical functions. ZnS replicas have been successfully synthesized by the assembly of nanoparticles by the interaction between the reactive surfaces of the frustules and the precursors under ultrasound. Other than a copy of the morphology of the fine meso/nanostructure, optical properties, such as the existence of PBG, was also inherited by the ZnS replicas. It is possible to achieve tunable photonic properties in the replicas by assembly of various metal chalcogenide semiconductors of different refractive indexes. Similar strategies will be adopted for other diatom species with intricate and unique morphologies that are not accessible by conventional fabrication techniques. Thus, this general approach will pave a new pathway for the further extensive study of the specific relationship between the sophisti-

cated meso/nanostructures and their particular photonic properties as well as extend their application potentials in nanophotonic devices. Furthermore, this bio-inspired method will lead to the innovative design and generation of new nanomaterials or nanodevices with elaborate structures and unique properties.

Experimental Section

Materials: The diatom species, *Coscinodiscus lineatus* (*C. lineatus*) was provided by Xiamen University. The cultures were maintained at 25 °C by using a 12 h light/12 h dark cycle whilst stirring. Guillard's medium (*f/2*) was used as a culture. The live diatoms were harvested after 1–2 months of culturing and mixed with concentrated sulfuric acid for 20 min at 60 °C. The mixture was centrifuged and washed with distilled water and ethanol several times to remove the acid. Cleaned frustule valves were stored in 100% ethanol. Zinc acetate [Zn(ac)₂], thioacetamide (TA), and ethanol were provided by Shanghai Chemical Company and were used as received without further purification. Ultrasonic irradiation was performed with an ultrasonic cleaner (with maximum acoustic power of 360 W, frequency of 59 KHz).

Preparation: In a typical procedure, three drops of the cleaned frustule suspension (the concentration of the suspension was about 10³ individuals/drop observed by optical microscopy) was diluted in 50 mL distilled water, and Zn(ac)₂ (55 mg) and TA (18.75 mg) were dispersed into the suspension. The solution was then sonicated with an ultrasonic cleaner at room temperature for 3 h in ambient air. The formation of the ZnS nanoparticles was controlled by the concentrations of the precursors and sonication conditions (time, temperature, power, and frequency). These parameters control the thickness of the ZnS films and the size of ZnS nanoparticles. The resulting white powder was recovered by centrifugation, washed repeatedly with distilled water and ethanol, and then dispersed in ethanol for characterization.

Characterization: The samples were examined by X-ray diffraction (XRD) with a Bruker-AXS D8 Advance instrument operating at a voltage of 40 kV and a current of 40 mA with Cu-K_α radiation ($\lambda = 1.5406 \text{ \AA}$). The investigation of the morphologies and microstructures was carried out by using FESEM (Sirion 200) operated under 5.0 Kv (SE 3.0; WD 5 mm). Transmission electron microscopy (TEM) and high-resolution transmission electron microscopy (HRTEM) images were obtained as a bright-field image and examined by selected area electron diffraction (SAED), conducted on a JEOL JEM-2010 instrument operated at an accelerating voltage of 200 kV and a JEOL JEM-2100F instrument working at an accelerating voltage of 200 kV, respectively. The digital images of the original diatom frustules were obtained from a digital microscope (VHX-100, KEYENCE). Fourier-transform infrared (FTIR) spectroscopy measurements were recorded with a Nicolet NEXUS-670 instrument. The reflectance spectra of the nanostructures were obtained by using a UV/Vis/NIR spectrometer (CRAIC, QDI2010, USA) coupled through optical fibers to an optical microscope (100 \times objective corresponding to an illuminated area of 10 $\mu\text{m} \times 10 \mu\text{m}$).

Supporting Information (see also the footnote on the first page of this article): Additional FESEM and TEM images of pores on the edge of the valve, FESEM images of replicas from various angles, XRD patterns, and FTIR spectra.

Acknowledgments

This work is supported by the National Natural Science Foundation of China (No.50401005 and No.50671065), the Program for New Century Excellent Talents in university (NCET-04-0387), the Major Fundamental Research Project of Shanghai Science and Technology Committee (No. 07DJ14001) and the National Basic Research Program of China (No.2006CB601200). The authors wish to express their thanks to the Instrumental Analysis Center of Shanghai Jiaotong University for XRD, FESEM, TEM and FTIR measurements.

- [1] P. Vukusic, J. R. Sambles, *Nature* **2003**, *424*, 852–855.
- [2] a) D. J. Webb, N. Suginoara, *Nature* **2001**, *409*, 36–37; b) S. Kinashita, S. Yoshioka, *ChemPhysChem* **2005**, *6*, 1442–1459; c) V. C. Sundar, A. D. Yablon, J. L. Grazul, M. Ilan, J. Aizenberg, *Nature* **2003**, *424*, 899–900.
- [3] a) G. Tayeb, B. Gralak, S. Enoch, *Optics Photonics News* **2003**, *40*; b) M. Srinivasarao, *Chem. Rev.* **1999**, *99*, 1935–1961.
- [4] E. G. Vrieling, T. P. M. Beelen, R. A. Van Santen, W. W. C. Gieskes, *J. Biotechnol.* **1999**, *70*, 39–51.
- [5] T. Fuhrmann, S. Landwehr, M. El Rharbi-Kucki, M. Sumper, *Appl. Phys. B* **2004**, *78*, 257–260.
- [6] A. R. Parker, H. E. Townley, *Nature Nanotechnology* **2007**, *2*, 347–353.
- [7] a) K. H. Sandhage, US Pat., No 7067104, June, 27, **2006**; b) S. Shian, Y. Cai, M. R. Weatherspoon, S. M. Allan, K. H. Sandhage, *J. Am. Ceram. Soc.* **2006**, *89*, 694–698; c) Y. Cai, S. M. Allan, K. H. Sandhage, F. M. Zalar, *J. Am. Ceram. Soc.* **2005**, *88*, 2005–2010; d) R. R. Unocic, F. M. Zalar, P. M. Sarosi, Y. Cai, K. H. Sandhage, *Chem. Commun.* **2004**, 796–797; e) K. H. Sandhage, M. B. Dickerson, P. M. Huseman, M. A. Caranna, J. D. Clifton, T. A. Bull, T. J. Heibel, W. R. Overton, M. A. Schoenwaelder, *Adv. Mater.* **2002**, *14*, 429–433.
- [8] a) M. W. Anderson, S. M. Holmes, N. Hanif, C. S. Cundy, *Angew. Chem. Int. Ed.* **2000**, *39*, 2707–2710; b) Y. Cai, M. R. Weatherspoon, E. Ernst, M. S. Haluska, R. L. Snyder, K. H. Sandhage, *Ceram. Eng. Sci. Proc.* **2006**, *27*, 49–55; c) W. Shan, Y. Zhang, Y. Wang, J. Xia, Y. Tang, *Chem. Lett.* **2004**, *33*, 270–273.
- [9] a) J. Zhao, C. S. Gaddis, Y. Cai, K. H. Sandhage, *J. Mater. Res.* **2005**, *20*, 282–287; b) C. S. Gaddis, K. H. Sandhage, *J. Mater. Res.* **2004**, *19*, 2541–2545; c) M. R. Weatherspoon, M. S. Haluska, Y. Cai, J. S. King, C. J. Summers, R. L. Snyder, K. H. Sandhage, *J. Electrochem. Soc.* **2006**, *153*, H34–H37; d) Y. Cai, K. H. Sandhage, *Phys. Status Solidi A* **2005**, *202*, R105–R107; e) N. L. Rosi, C. S. Thaxton, C. A. Mirkin, *Angew. Chem. Int. Ed.* **2004**, *43*, 5500–5503; f) X. Cai, G. Zhu, W. Zhang, H. Zhao, C. Wang, S. Qiu, Y. Wei, *Eur. J. Inorg. Chem.* **2006**, *18*, 3641–3645; g) S. M. Holmes, B. E. Graniel-Garcia, P. Foran, P. Hill, E. P. L. Roberts, B. H. Sakakini, J. M. Newton, *Chem. Commun.* **2006**, 2662–2663.
- [10] M. R. Weatherspoon, S. M. Allan, E. Hunt, Y. Cai, K. H. Sandhage, *Chem. Commun.* **2005**, 651–653.
- [11] a) D. Losic, J. G. Mitchell, N. H. Voelcker, *New J. Chem.* **2006**, *30*, 908–914; b) E. K. Payne, N. L. Rosi, C. Xue, C. A. Mirkin, *Angew. Chem. Int. Ed.* **2005**, *44*, 5064–5067.
- [12] a) S. Wong, M. Deubel, F. P. Willard, S. John, G. A. Ozin, M. Wegener, G. V. Freymann, *Adv. Mater.* **2006**, *18*, 265–269; b) R. J. Ellingson, M. C. Beard, J. C. Johnson, P. Yu, O. I. Micic, A. J. Nozik, A. Shabaev, A. L. Efros, *Nano Lett.* **2005**, *5*, 865–871; c) S. A. McDonald, G. Konstantatos, S. G. Zhang, P. W. Cyr, E. J. D. Klem, L. Levina, E. H. Sargent, *Nat. Mater.* **2005**, *4*, 138–142.
- [13] a) N. Arul Dhas, A. Zaban, A. Gedanken, *Chem. Mater.* **1999**, *11*, 806–813; b) J. A. Norman, C. B. Thomas, M. J. Burrow, *J. Chem. Soc. Perkin Trans. 1* **1995**, 1087.
- [14] A. G. Pelmenchikov, G. Morosi, A. Gamba, *J. Phys. Chem.* **1991**, *95*, 10037–10041.
- [15] J. Zhu, Y. Koltypin, A. Gedanken, *Chem. Mater.* **2000**, *12*, 73–78.
- [16] a) S. F. Wang, F. Gu, M. K. Lu, *Langmuir* **2006**, *22*, 398–401; b) R. Xie, D. Li, D. Yang, M. Jiang, *J. Mater. Sci.* **2007**, *42*, 1376–1380.
- [17] R. Kerner, O. Palchik, A. Gedanken, *Chem. Mater.* **2001**, *13*, 1413–1419.
- [18] Q. Li, Y. Ding, M. Shao, J. Wu, G. Yu, Y. Qian, *Mater. Res. Bull.* **2003**, *38*, 539–543.
- [19] Y. Ma, L. Qi, J. Ma, H. Cheng, W. Shen, *Langmuir* **2003**, *19*, 9079–9085.
- [20] M. J. Murcia, D. L. Shaw, H. Woodruff, C. A. Naumann, B. A. Young, E. C. Long, *Chem. Mater.* **2006**, *18*, 2219–2225.
- [21] H. Wang, J. Zhang, X. Zhao, S. Xu, J. Zhu, *Mater. Lett.* **2002**, *55*, 253–258.
- [22] M. M. Mdleleni, T. Hyeon, K. S. Suslick, *J. Am. Chem. Soc.* **1998**, *120*, 6189–6190.
- [23] N. Du, H. Zhang, H. Sun, D. Yang, *Mater. Lett.* **2007**, *61*, 235–238.
- [24] a) Y. H. Ha, R. A. Vaia, W. F. Lynn, J. P. Costantino, J. Shin, A. B. Smith, P. T. Matsudaira, E. L. Thomas, *Adv. Mater.* **2004**, *16*, 1091–1094; b) C. Lopez, *Adv. Mater.* **2003**, *15*, 1679–1704.

Received: July 31, 2008

Published Online: December 2, 2008

Unexpected Formation of Ferrocene-Containing Indolizines by Tandem Cyclization–Activation Reactions Induced by Silver Salts

Javier E. Aguado,^[a] Carlos Cativiela,^[b] M. Concepción Gimeno,^{*[a]} Peter G. Jones,^[c] Antonio Laguna,^[a] and Cristina Sarroca^[a]

Keywords: Heterocycles / Cyclization / Silver / Phosphonium salts / Ferrocene derivatives

Silver salts are used as promoters for the cyclization to novel ferrocene-containing indolizine systems in only one step and with the simultaneous activation of the 7-position of the heterocyclic ring. The reaction of 2-[3-(ferrocenyl)-1-oxo-prop-2-enyl]pyridine with [Ag(OTf)(PR₃)] (OTf = trifluoro-

methylsulfonate; PR₃ = PPh₃, PPh₂Me) occurs with the precipitation of metallic silver and formation of the indolizine system.

(© Wiley-VCH Verlag GmbH & Co. KGaA, 69451 Weinheim, Germany, 2009)

Introduction

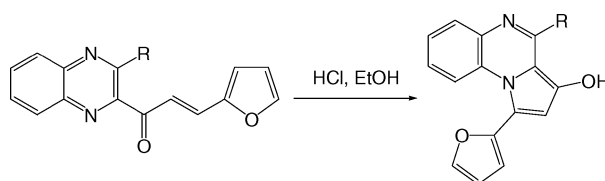
Ferrocene is a very versatile molecule with important properties such as high electron density, aromaticity and redox reversibility. These characteristics, together with the ease of preparation of mono- and 1,1'-disubstituted ferrocene derivatives with a great variety of organic fragments that may contain O, N, S, P, etc. as donor atoms, make ferrocene a suitable building block in many fields of research.^[1–4] These functionalized ferrocene derivatives and the study of their coordination to metal centres is an important topic of research in many areas that seek special properties of such species, e.g. materials with nonlinear optical properties, charge transport, liquid crystals, electrochemical recognition, catalysis, nanoparticles, immunoassay reagents or biological applications.^[1–4]

In the course of our research program, we have focused on the synthesis and studies of ferrocenes functionalized with various heterocyclic moieties, with the intention of using these products as ligands in organometallic chemistry, and we observed the formation of novel indolizine derivatives.

Functionalized pyrrolo[1,2-a]pyridines (indolizines) are common substructures found in biologically important natural products, and they are frequently used as a key scaffold in the pharmaceutical industry, because of the broad spectrum of associated biological activities.

Although a number of methods are available for the synthesis of indolizines,^[5] the development of efficient syntheses for these functionalized heterocyclic compounds is still highly attractive. Of all reported procedures, cyclization reactions starting from pyridine derivatives are probably the most used and, in particular, those that involve the attack of the nitrogen atom at an activated electrophilic carbon. In this context, cyclization reactions of propargylic pyridines have recently attracted considerable attention, particularly in those cases in which the reaction is mediated by metals^[6] (metal-catalyzed cycloisomerizations) or by iodine.^[7]

In principle, a Michael-type cyclization involving the conjugate addition of the pyridine nitrogen to an α,β -unsaturated moiety could also be an interesting alternative. Nevertheless, this system has, to the best of our knowledge, been scarcely used. An acid-catalyzed cyclization of chalcones derived from various nitrogen-containing heteroaromatic compounds was reported several years ago^[8] (Scheme 1), and more recently a thermal cyclization of some 2-pyridyl derivatives (Scheme 2) has been carried out.^[9]



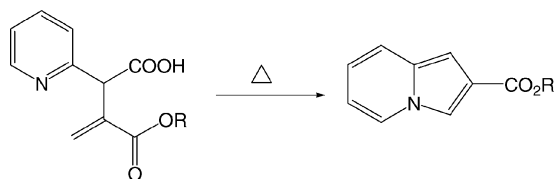
Scheme 1.

Here we describe the use of silver salts in the form of [Ag(OTf)(PR₃)] as promoters for the cyclization to novel ferrocene-containing indolizine systems in only one step and with the simultaneous activation of the 7-position of the heterocyclic ring.

[a] Departamento de Química Inorgánica, Instituto de Ciencia de Materiales de Aragón, Universidad de Zaragoza-CSIC, 50009 Zaragoza, Spain

[b] Departamento de Química Orgánica, Instituto de Ciencia de Materiales de Aragón, Universidad de Zaragoza-CSIC, 50009 Zaragoza, Spain

[c] Institut für Anorganische und Analytische Chemie der Technischen Universität, Postfach 3329, 38023 Braunschweig, Germany

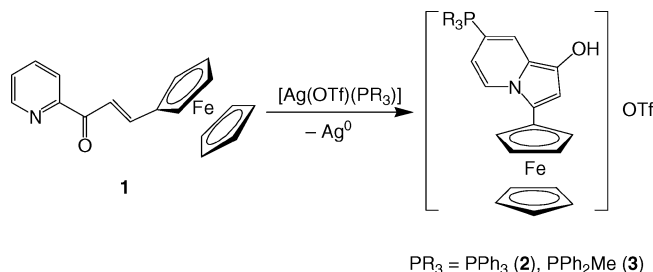


Scheme 2.

Results and Discussion

We have studied the behaviour of 2-[3-(ferrocenyl)-1-oxoprop-2-enyl]pyridine (**1**) with various complexes from the point of view of competitive coordination with different metal centres. This compound can be easily prepared from ferrocenecarbaldehyde and 2-acetylpyridine in ethanol as previously reported.^[10]

Compound **1** can coordinate to metal centres through the nitrogen or oxygen atoms, and silver can act as a metal centre. However, the reaction of **1** with [Ag(OTf)(PR₃)] (PR₃ = PPh₃, PPh₂Me) involved reduction to metallic silver. After the corresponding workup, yellow solids were obtained, which, after purification, were identified as the new compounds **2** or **3** (see Scheme 3) with an unexpected structure that was confirmed by spectroscopic data and X-ray diffraction analysis of crystals, easily obtained from a solution of compound **2** in dichloromethane/hexane. Compounds **2** or **3** were obtained in moderate yield (ca. 40%) after column chromatography along with the starting material (ca. 30%) and some unidentified compounds that were obtained in very low yield (<5%). Longer reaction times did not improve the reaction yield significantly.

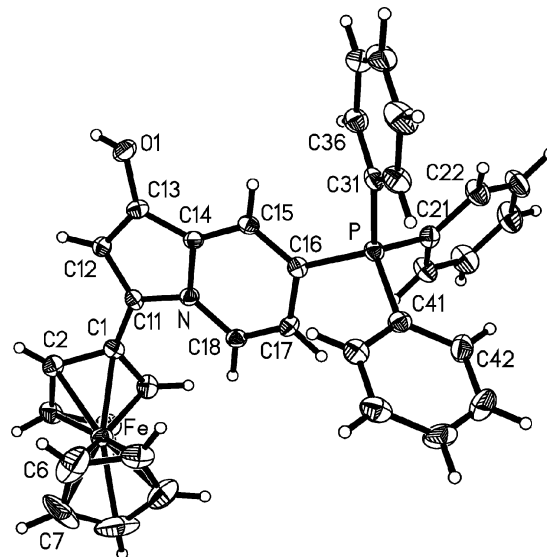


Scheme 3.

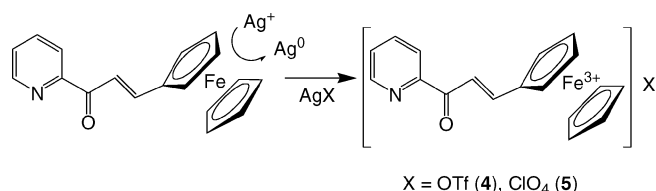
The ¹H NMR spectra of **2** and **3** show a singlet for the unsubstituted cyclopentadienyl ring and two multiplets for the α and β protons of the substituted cyclopentadienyl unit. The four protons assigned to the planar rings of the indolizine moiety and the phenyl protons appear as multiplets between 6.0 and 8.5 ppm. The hydroxy proton appears at about 10.5 ppm. The ³¹P{¹H} NMR spectrum presents a single resonance at 22.0 (**2**) or 19.2 (**3**) ppm, characteristic of phosphonium salts. The liquid secondary-ion mass spectra (LSIMS+) present the cation molecular peaks at *m/z* = 578 (**2**) or 516 (**3**).

The structure of **2** has been established by an X-ray diffraction study; the molecule is shown in Figure 1. A selection of bond lengths and angles are collected in Table 1. The two rings of the indolizine system are planar with mean

deviations from the best plane of 0.001 (five-membered ring) and 0.012 Å (six-membered ring). The C–C bond lengths correspond to a delocalized system, whereas the N–C distances are dissimilar: N–C11 1.367(3), N–C18 1.378(3) and N–C14 1.425(3) Å. The OH group forms hydrogen bonds to a triflate oxygen, with O...O 2.696 Å, H...O 1.86 Å and O–H...O 173°.

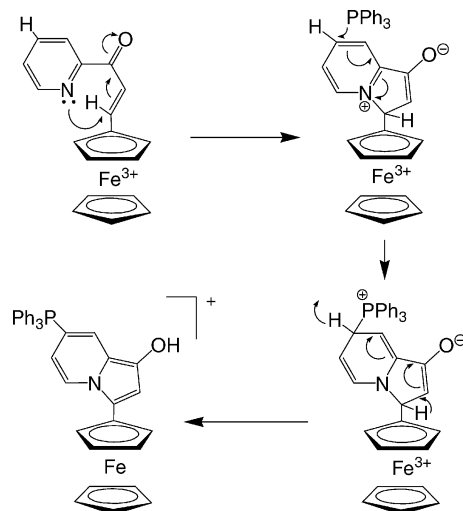


pounds prompted us to consider a plausible mechanism. We believe that the first step is the oxidation of the ferrocene derivative to ferrocenium and the reduction of Ag^{I} to metallic silver (see Scheme 4). Indeed, in a separate experiment we carried out the reaction of **1** with $\text{Ag}(\text{OTf})$ or $\text{Ag}(\text{ClO}_4)$ and obtained the ferrocenium derivative **4** or **5**. These compounds do not react further by themselves to form the indolizine species even under reflux; thus the presence of a nucleophile seems essential. Compounds **4** and **5** are the oxidized form of the ligand **1** and are paramagnetic, consequently they show ^1H NMR resonances that are very similar in chemical shift to those in compound **1** but with a worse resolution (broad signals).



Scheme 4.

The ferrocenium cation can withdraw electron density from the conjugated system, enhancing the possibility of thermal cyclization by nucleophilic attack on the pyridine nitrogen at the double bond and favouring the attack of the nucleophile at the *para* position of the pyridine ring (see Scheme 5). The role of the PPh_3 is of great importance, because only when the nucleophile is added does the system proceed to the indolizine derivative; in fact, the indolizine derivative **2** can also be obtained by the reaction of **1** with $\text{Ag}(\text{OTf})$ to give **4** and subsequent addition of PPh_3 . This proves that the ferrocenium compound is the intermediate species. We have also checked that no reaction occurs between compound **1** and PPh_3 , consequently the oxidation of the ferrocene moiety by the silver centre seems essential for the course of the reaction.



Scheme 5.

Thermal cyclization by nucleophilic attack on the pyridine nitrogen at the double bond, which favours the attack of the nucleophile at the *para* position of the pyridine ring, produces the aromatization of the five-membered ring. Then the conjugation of π -electrons produces the re-aromatization of the system and subsequent reduction to Fe^{2+} (Scheme 5).

The introduction of the nucleophile opens the way to the functionalization of this position. The particular case of the triarylphosphanes is highly remarkable, since the corresponding tetraarylphosphonium salts have received a great interest during the last years.^[11]

Conclusions

In summary, we have achieved the synthesis of novel ferrocene-containing indolizine systems in only one step and with the simultaneous activation of the 7-position of the heterocyclic ring, by using silver salts as promoters of the cyclization. Furthermore, this is an example of a synthesis of a tetraarylphosphonium salt, a subject of considerable current interest.

Experimental Section

Instrumentation: Infrared spectra were recorded in the range 4000–200 cm^{-1} with a Perkin–Elmer 883 spectrophotometer by using Nujol mulls between polyethylene sheets. Conductivities were measured in acetone solutions (ca. $5 \times 10^{-4} \text{ mol dm}^{-3}$) with a Philips 9509 conductimeter. C, H, N and S analyses were carried out with a Perkin–Elmer 2400 microanalyzer. Mass spectra were recorded with a VG Autospec instrument, by liquid secondary-ion mass spectroscopy (LSIMS), in a nitrobenzyl alcohol matrix. NMR spectra were recorded with a Varian Unity 300 spectrometer and a Bruker ARX 300 spectrometer in CDCl_3 , unless otherwise stated. Chemical shifts are cited relative to SiMe_4 (^1H , external), CFCl_3 (^{19}F , external) and 85% H_3PO_4 (^{31}P , external).

Starting Materials: The starting materials $[\text{Ag}(\text{OTf})(\text{PPh}_3)]$,^[12] were prepared according to published procedures. All other reagents were commercially available.

Caution: perchlorate salts with organic cations may be explosive.

Synthesis of Compounds 2 and 3: To a solution of 2-[3-(ferrocenyl)-1-oxoprop-2-enyl]pyridine (0.063 g, 0.2 mmol) in dichloromethane (20 mL) was added $[\text{Ag}(\text{OTf})(\text{PPh}_3)]$ (0.104 g, 0.2 mmol) or $[\text{Ag}(\text{OTf})(\text{PPh}_2\text{Me})]$ (0.090 g, 0.2 mmol), and the mixture was heated under reflux for 1 d. The metallic silver was filtered off and the solution chromatographed over silica; elution with acetone/methanol (99:1) gave the starting material and the indolizine derivatives **2** or **3**. **Complex 2:** Yield: 0.060 g (41%). $\text{C}_{37}\text{H}_{29}\text{F}_3\text{FeNO}_4\text{PS}$ (727.08); calcd. C 61.08, H 4.01, N 1.92, S 4.40; found C 61.11, H 3.88, N 1.98, S 4.50. ^1H NMR (300 MHz, CDCl_3): δ = 4.15 (m, 2 H, C_5H_4), 4.35 (m, 2 H, C_5H_4), 4.54 (m, 5 H, C_5H_5), 6.03 (t), 6.78 (s), 7.63–7.80 (m, 15 H, Ph), 8.15 (d), 8.57 (d), 10.52 (br. s, 1 H, OH) ppm; $^{31}\text{P}\{^1\text{H}\}$ NMR (121.4 MHz, CDCl_3): δ = 22.0 (s) ppm. MS (LSIMS+): m/z (%) = 578 (100) $[\text{M} - \text{OTf}]^+$. **Complex 3:** Yield: 0.044 g (33%). $\text{C}_{32}\text{H}_{27}\text{F}_3\text{FeNO}_4\text{PS}$ (665.069); calcd. C 57.75, H 4.08, N 2.10, S 4.81; found C 58.32, H 4.38, N 2.18, S 5.10. ^1H NMR (300 MHz, CDCl_3): δ = 2.74 (m, 3 H, Me), 4.16 (m, 2 H, C_5H_4), 4.39 (m, 2 H, C_5H_4), 4.55 (m, 5 H, C_5H_5), 6.00 (m), 6.62

(s), 7.6–7.8 (m, 10 H, Ph), 8.07 (d), 8.39 (d), 10.4 (br., 1 H, OH) ppm; $^{31}\text{P}\{^1\text{H}\}$ NMR (121.4 MHz, CDCl_3): δ = 19.2 (s) ppm. MS (LSIMS+): m/z (%) = 516 (24) $[\text{M} - \text{OTf}]^+$.

Synthesis of Compounds 4 and 5: To a solution of 2-[3-(ferrocenyl)-1-oxoprop-2-enyl]pyridine (0.0317 g, 0.1 mmol) in dichloromethane (20 mL) was added $\text{Ag}(\text{OTf})$ (0.025 g, 0.1 mmol) or $\text{Ag}(\text{ClO}_4)$ (0.020 g, 0.1 mmol), and the mixture was heated under reflux for 1 d. The metallic silver was filtered off, and the green-blue solution was evaporated to ca. 1 mL. Addition of hexane (10 mL) gave compounds 4 or 5. Complex 4: Yield: 0.035 g (79%). $\text{C}_{19}\text{H}_{15}\text{F}_3\text{FeNO}_4\text{S}$ (466.0): calcd. C 48.92, H 3.24, N 3.0, S 6.86; found C 49.11, H 3.38, N 2.98, S 6.50. Complex 5: Yield: 0.035 g (71%). $\text{C}_{18}\text{H}_{15}\text{ClFeNO}_5$ (415.99): calcd. C 51.92, H 3.63, N 3.36; found C 52.17, H 3.49, N 3.02.

Crystal Structure Determination: X-ray structural data for compound $2 \cdot \text{CH}_2\text{Cl}_2$: $\text{C}_{38}\text{H}_{31}\text{Cl}_2\text{F}_3\text{FeNO}_4\text{PS}$, M_r = 812.42, triclinic, space group $P\bar{1}$, a = 11.871(2) Å, b = 12.780(2) Å, c = 13.256(2) Å, α = 68.046(14)°, β = 76.758(14)°, γ = 88.401(14)°, V = 1811.9(5) Å³, Z = 2, D_{calc} = 1.489 Mg m^{-3} , $\mu(\text{Mo-K}\alpha)$ = 0.723 mm^{-1} , $F(000)$ = 832, Siemens P4 diffractometer, $\lambda(\text{Mo-K}\alpha)$ = 0.71073 Å, T = −100 °C. An orange tablet $0.45 \times 0.40 \times 0.25$ mm was used to collect 6544 intensities to $2\theta_{\text{max}}$ = 50°, of which 6232 were unique (R_{int} 0.019). Scan type: ω . An absorption correction was based on ψ -scans, with transmission factors 0.90–0.97. The structure was solved by direct methods and refined anisotropically on F^2 (SHELXL-97).^[13] H atoms were included by using a riding model (but OH refined freely). Refinement proceeded to $wR(F^2)$ 0.095 for 6230 reflections and 461 parameters, conventional $R(F)$ 0.040, $S(F^2)$ 0.967, max $\Delta\rho$ 0.57 $e \text{ Å}^{-3}$. CCDC-146110 contains the supplementary crystallographic data for this paper. These data can be obtained free of charge from The Cambridge Crystallographic Data Centre via www.ccdc.cam.ac.uk/data_request/cif.

Acknowledgments

We thank the Dirección General de Investigación Científica y Técnica (CTQ2007–67273-C02–01) and the Gobierno de Aragón (PM067/2007) for financial support.

- [1] A. Togni, T. Hayashi (Eds.), *Ferrocenes, Homogeneous Catalysis, Organic Synthesis and Materials Science*, VCH, Weinheim, 1995.
- [2] A. Togni, R. L. Halterman (Eds.), *Metallocenes*, VCH, Weinheim, 1998.
- [3] N. J. Long (Ed.), *Metallocenes, An Introduction to Sandwich Complexes*, Blackwell Science, Oxford, 1998.
- [4] P. Štěpnička (Ed.), *Ferrocenes: Ligands, Materials and Biomolecules*, John Wiley & Sons, Chichester, 2008.
- [5] a) T. Uchida, K. Matsumoto, *Synthesis* 1976, 209–239; b) A. Behnisch, P. Behnisch, M. Eggenweiler, T. Wallenhorst, “Indolizine” in *Methods of Organic Chemistry: Synthesis of Peptides and Peptidomimetics (Houben-Weyl)*, Georg Thieme Verlag, Stuttgart and New York, 1994, vol. E6b/1, 2a, pp. 323–450.
- [6] A selection of very recent examples: a) B. Yan, Y. Zhou, H. Zhang, J. Chen, Y. Liu, *J. Org. Chem.* 2007, 72, 7783–7786; b) C. R. Smith, E. M. Bunnelle, A. J. Rhodes, R. Sarpong, *Org. Lett.* 2007, 9, 1169–1171; c) A. R. Hardin, R. Sarpong, *Org. Lett.* 2007, 9, 4547–4550.
- [7] A selection of very recent examples: a) I. Kim, J. Choi, H. K. Won, G. H. Lee, *Tetrahedron Lett.* 2007, 48, 6863–6867; b) I. Kim, H. K. Won, J. Choi, G. H. Lee, *Tetrahedron* 2007, 63, 12954–12960.
- [8] K. Matoba, K. Itoh, K. Kondo, T. Yamazaki, M. Nagata, *Chem. Pharm. Bull.* 1981, 29, 2442–2450.
- [9] P. O. Deane, R. George, P. T. Kaye, *Tetrahedron* 1998, 54, 3871–3876.
- [10] E. C. Constable, A. J. Edwards, R. Martínez-Máñez, P. R. Raithby, A. M. W. Cargill Thompson, *J. Chem. Soc., Dalton Trans.* 1994, 645–650.
- [11] D. Marcoux, A. B. Charette, *J. Org. Chem.* 2008, 73, 590–593.
- [12] M. Bardaji, O. Crespo, A. Laguna, A. K. Fischer, *Inorg. Chim. Acta* 2000, 304, 7.
- [13] G. M. Sheldrick, *SHELXL-97, Program for Crystal Structure Refinement*, University of Göttingen, Göttingen, Germany, 1997.

Received: October 2, 2008

Published Online: December 2, 2008

Transition Metal Complexes of N-Heterocyclic Germylenes

Farman Ullah,^[a] Olaf Kühl,^[a] Gabor Bajor,^[b] Tamas Veszprémi,^{*[b]} Peter G. Jones,^[c] and Joachim Heinicke^{*[a]}**Keywords:** Germanium / Molybdenum / Nickel / Carbenoids / Quantum chemical calculations

The five-membered N-heterocyclic germylenes (NHGe) **1a–3a**, with or without benzo or naphtho anellation, react with $[\text{Mo}(\text{CO})_3(\text{cht})]$ ($\text{cht} = 1,3,5\text{-cycloheptatriene}$) to form the *fac*- $[(\text{NHGe})_3\text{Mo}(\text{CO})_3]$ complexes **1b–3b**. Similarly, $[\text{Ni}(\text{bnNHGe})_4]$ was obtained from the benzo-anellated germylene (bnNHGe) and $\text{Ni}(1,5\text{-cod})_2$; attempts to synthesize less electron-rich complexes with mono- or divalent transition metals failed. The CO valence vibrations in the IR spectra of **1b–3b**, together with their short Ge^{II}–Mo bonds (as determined by X-ray crystallography), hint at the weak donor and good π -acceptor properties of the ligands. Quantum chemical studies on the benzo-anellated germylene, which are supported by the good correlation between calculated

and experimental (PES) orbital ionization potentials, confirm this proposal in terms of the low energy of the Ge lone electron pair and two higher π -MOs. The slight folding about the C–C bridging and N...N axes observed for the benzo-anellated (NHGe)molybdenum and -nickel complexes by X-ray structure analyses, may be due to packing effects. Quantum chemical calculations on slightly bent (for dineopentyl substitution in the gas phase) and planar bnNHGe complexes show that the energy differences between the two are very small.

(© Wiley-VCH Verlag GmbH & Co. KGaA, 69451 Weinheim, Germany, 2009)

Introduction

The discovery of stable acyclic carbenes by Bertrand in 1988^[1] and, in particular, the synthesis of the first stable monomeric N-heterocyclic carbene (NHC) by Arduengo in 1991^[2] have generated great interest in these divalent carbon ligands. Their unique electronic and steric properties,^[3] partly in combination with further functional groups,^[4] have led to burgeoning research activities and to many applications in organic, organometallic and inorganic chemistry.^[5] Unsurprisingly, interest in the chemistry of their homologues has grown in the wake of these developments. This is particularly true for the silylenes,^[6] for which only transient species were known^[7] until the first stable N-heterocyclic representatives were reported in the mid 1990s.^[8] However, the much longer known and more easily accessible diaminogermylenes – both acyclic^[9] and N-heterocyclic germylenes (NHGe)^[10] – have also been the subject of enhanced attention, which has recently been extended to

charged ring-delocalized NHGe compounds.^[11] Neutral donor-substituted and *N,N*-bridged bis(N-heterocyclic stannylenes) and N-heterocyclic plumblylenes are the subject of current studies.^[12] Several quantum chemical studies have been performed to shed light on the nature of the chemical bonding in, and stabilization of, these compounds, including general principles and trends.^[13]

We have a longstanding interest in compounds containing twofold-coordinated (σ^2) group 15^[14] and group 14 elements^[15,16] stabilized in delocalized π -systems, and in the influence of anellation on the stability and ligand properties of these σ^2 -element heterocycles. This includes a series of neutral non-anellated (**1a**), benzo- (**2a**) and naphtho-anellated NHGe compounds (**3a**), and also heterocyclic pyrido- and quinoxaline-anellated NHGe compounds.^[15] Recently, we described the first carbonylmolybdenum(0) complexes of the non-anellated NHGe $\text{C}_2\text{H}_2[\text{N}(\text{CH}_2\text{tBu})_2]\text{Ge}$ (**1a**) and found some interesting structural changes to the ligand upon coordination.^[15a] It remained unclear, however, whether these findings were limited to this particular NHGe or were of a general nature. For this reason, we embarked on a study of anellated NHGe complexes using $[\text{Mo}(\text{CO})_3(\text{cht})]$ ($\text{cht} = 1,3,5\text{-cycloheptatriene}$) as starting material. The IR carbonyl stretching frequencies of the expected *fac*- $[\text{Mo}(\text{CO})_3\text{L}_3]$ complexes can be used as probes^[17] of the electronic properties of the NHGe ligands, thus enabling us to test the recently proposed concept concerning the dependence of the net electron-donating ability of NHGe compounds on anellation.^[18]

[a] Institut für Biochemie – Anorganische Chemie, Ernst-Moritz-Arndt-Universität Greifswald, Felix-Hausdorff-Str. 4, 17487 Greifswald, Germany
Fax: +49-3834-864377
E-mail: heinicke@uni-greifswald.de

[b] Department of Inorganic Chemistry, Technical University of Budapest, 1521 Budapest, Hungary

[c] Institut für Anorganische und Analytische Chemie, Technische Universität Braunschweig, Hagenring 30, 38106 Braunschweig, Germany

Supporting information for this article is available on the WWW under <http://www.eurjic.org> or from the author.

Results and Discussion

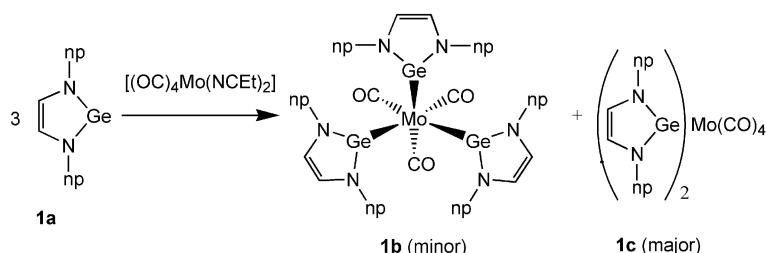
Synthesis

As we reported earlier,^[15a] the reaction between *cis*-[Mo(CO)₄(NCEt)₂] and 2 equiv. of C₂H₂[N(CH₂*t*Bu)]₂Ge (**1a**) yields a mixture of the expected complexes *cis*-[Mo(CO)₄(**1a**)₂] (**1c**) and a small amount of *fac*-[Mo(CO)₃(**1a**)₃] (**1b**; Scheme 1). No trace signal of *mer*-**1b** could be detected in any of the NMR spectra. The solubility of all the NHGe complexes of molybdenum described in this study is very high, even in hydrocarbons. Unfortunately, their sensitivity towards OH groups prevents their chromatographic separation. Neither the oil containing mostly **1c** nor the crystals of **1b** (coated with a thin film of oily **1c**) could be obtained in a completely pure form by fractional crystallization. We therefore searched for a starting material that would provide us with a better defined product and found it in [Mo(CO)₃(cht)]. Thus, treatment of [Mo(CO)₃(cht)] with 3 equiv. of C₆H₄[N(CH₂*t*Bu)]₂Ge (**2a**) or C₁₀H₆[N(CH₂*t*Bu)]₂Ge (**3a**) gave only one product, namely *fac*-[Mo(CO)₃L₃] [L = **2a** (**2b**), **3a** (**3b**); Scheme 2]. Contamination by a small amount of starting material was detected by NMR spectroscopy, but no signals due to any other

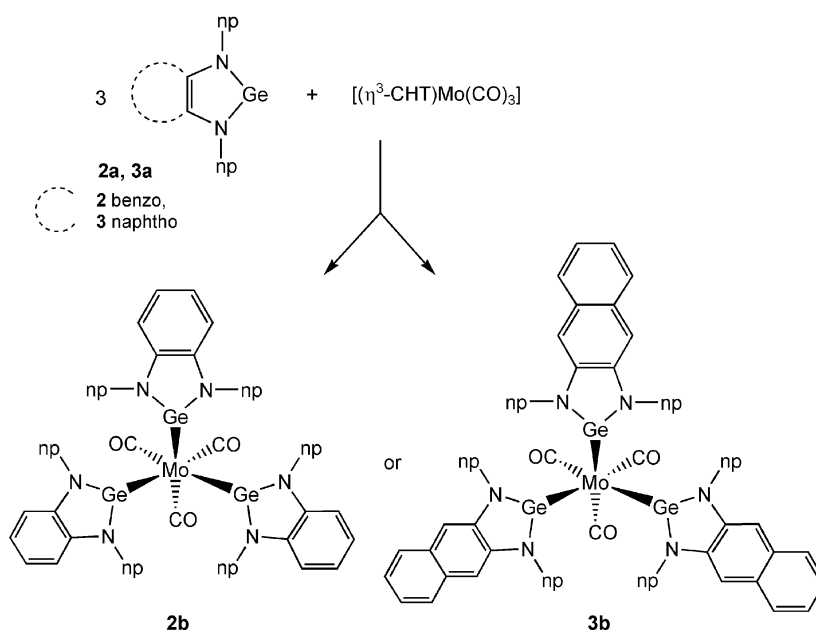
complex were observed. Complex **2b** was isolated in a pure form by layering a solution of **2a** in *n*-hexane on top of a solution of [Mo(CO)₃(CHT)] in thf. The yellow crystals grown in this diffusion-controlled reaction were suitable for an X-ray crystal structure determination. All attempts to crystallise the related complex **3b** failed due to its oily nature.

To synthesize related tungsten complexes, we treated **2a** with [W(CO)₃(mes)] (mes = mesitylene). However, even prolonged reflux in thf did not lead to replacement of the mesitylene ligand. There is no reason to believe that *fac*-[W(CO)₃(**2a**)₃] cannot be synthesised or might not be stable – it simply appears to be the case that mesitylene is not a suitable leaving group for replacement by the germylene **2a**. Heating results in decomposition of the components prior to formation of the intended complex.

[Ni(cod)₂] (cod = 1,5-cyclooctadiene) was selected to synthesize further NHGe complexes as it is usually easy to replace the cod ligands. Treatment of **2a** with [Ni(cod)₂] in thf in a 2:1 molar ratio led to a mixture of unconverted Ni(cod)₂ and the complex [Ni(**2a**)₄] (**2c**) (Scheme 3), which provides evidence that complexes with two or three germylene ligands are less stable. Storage at room temperature resulted in decomposition of Ni(cod)₂ into colloidal nickel

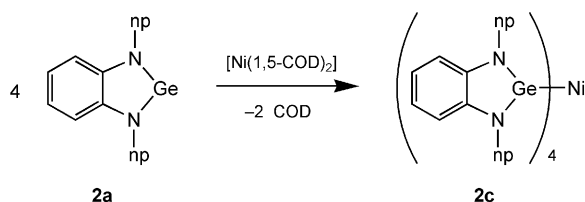


Scheme 1. Synthesis of **1b** and **1c**; np = neopentyl.



Scheme 2. Synthesis of **2b** and **3b**; np = neopentyl.

and cod, whereas **2c** was stable under these conditions. This allowed the facile separation and isolation of complex **2c** as a red solid. This compound can be stored at room temperature for several days and at -4°C for months without decomposition, although it is extremely sensitive to air and moisture. Single crystals were obtained from thf solution upon cooling. An X-ray crystal structure analysis confirmed a tetrahedral coordination similar to the Ni^0 complex of the homologous benzo-anellated NHSi ligand^[19] and two chelating *N,N*-bridged bis(diaminostannylenes) containing benzo-anellated NHSn.^[20] This shows a marked difference of the heavier NHE containing divalent $\text{E} = \text{Si}, \text{Ge}, \text{Sn}$ from the benzimidazol-2-ylidene ligand, which forms only the linear complex $\text{Ni}(\text{NHC})_2$.^[21]



Scheme 3. Synthesis of **2c**; np = neopentyl.

Structural Aspects

The structural assignment of the new germylene complexes was based on conclusive solution NMR spectroscopic data, satisfactory elemental analysis or HRMS data and X-ray crystal structures for three complexes. In an “aromatic” ring system with π -electron delocalisation, electronic changes experienced by the coordinating germanium atom should have add-on effects that are observable in the carbon atoms belonging to this system or the hydrogen atoms bonded to these. It is notable that such effects are absent except for the methylene groups bonded to the nitrogen atoms and for 4-H in the anellated ring, adjacent to the N atoms. The ^1H and ^{13}C NMR spectra of complexes **1b**, **2b**, **3b** and **2c** show only marginal differences with respect to the spectra of the free ligands, with the exception of slight shifts of the signals for the NCH_2 group ($^1\text{H}/^{13}\text{C}$: **1b**: $\Delta\delta = -0.04/-2.35$ ppm; **2b**: $\Delta\delta = -0.03/-2.46$ ppm; **3b**: $\Delta\delta = 0.03/-1.75$ ppm; **2c**: $\Delta\delta = 0.19/-1.80$ ppm) or downfield shifts of 4-H in **2b** ($\Delta\delta \approx 0.80$ ppm) and weakly in **2c** ($\Delta\delta \approx 0.10$ ppm).

Complex **2b** crystallises in the triclinic space group $P\bar{1}$ with two molecules in the unit cell. The compound is the monomeric *fac* isomer with approximate C_3 symmetry (Figure 1). The molybdenum atom is octahedrally coordinated to three carbonyl and three NHGe ligands. Each CO ligand is *trans* to a germylene moiety, with almost linear Ge–Mo–C bond angles [$176.37(5)$, $173.86(5)$ and $176.17(4)^{\circ}$]. The deviation from linearity is, on average, by 1.5° greater than in the closely related complex *fac*-**1b**. The Mo–C bonds in **2b** [$198.38(17)$, $199.01(16)$ and $200.45(17)$ pm] are some 2.5 pm longer than in **1b** and in *fac*- $[\text{Mo}(\text{CO})_3\text{L}_3]$ ($\text{L} = \text{phosphane}$).^[22] The Mo–Ge bond lengths [$252.85(2)$,

$254.45(2)$ and $254.52(3)$ pm] are almost identical to those in **1b** and very similar to those in the closely related chelate complex *cis*- $[\text{Mo}(\text{CO})_4\{(\text{CH}_2\text{CMe}_2\text{CH}_2)[\text{NGeN}(\text{CH}_2t\text{Bu})\text{C}_6\text{H}_4\}_2]]$ (**4**; (Figure 2),^[23] and in the same range as those reported for Mo bonded to Ge^{IV} .^[24] The N–Ge–N bond angles in **2b** [$87.00(6)$ – $87.19(6)^{\circ}$] are 2.2° larger than in the free ligand, whereas the opposite is the case for the non-anellated NHGe complex **1b** [$87.75(6)^{\circ}$ in the free ligand and $85.7(2)$ – $86.5(3)^{\circ}$ in the coordinated ligand]. The Ge–N bond lengths follow the same trend. Thus, whereas the Ge–N bond length contracts by 2.7 pm in **2b** upon complexation, it elongates by 2.0 pm for **1b**. The corresponding N–C_{ring} bond lengths are unchanged in **2b**, but significantly contracted by 5.8 pm for **1b** upon complexation. No comparison with the free ligand can be made for the only other structurally characterised carbonylmolybdenum NHGe complex (**4**) as no crystal structure of the ligand has been reported.^[23]

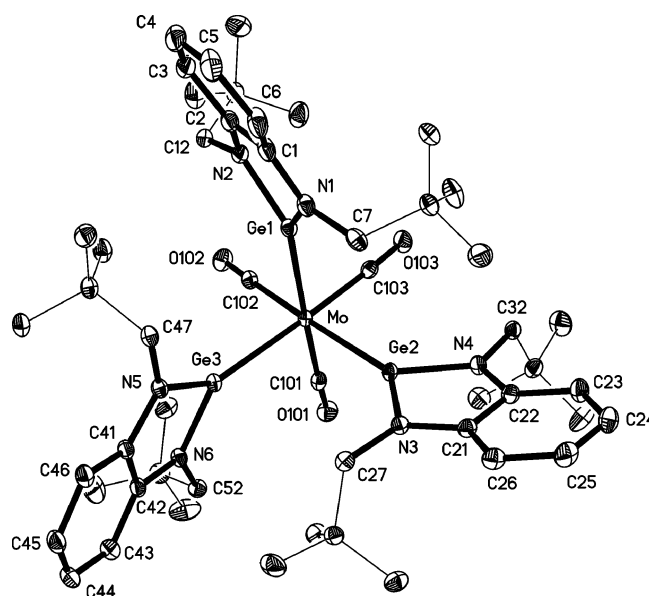


Figure 1. Molecular structure of **2b**. Ellipsoids are shown with 50% probability and hydrogen atoms have been omitted for clarity. Selected bond lengths [pm] and angles [$^{\circ}$]: Mo–C(103) 198.38(17), Mo–C(101) 200.45(17), Mo–Ge(1) 252.85(2), Mo–Ge(3) 254.52(3), Ge(1)–N(2) 183.49(14), Ge(2)–N(3) 183.90(12), N(4)–C(22) 139.26(19), N(5)–C(41) 140.0(2); C(101)–Mo–Ge(1) 176.37(5), C(102)–Mo–Ge(2) 173.86(5), C(103)–Mo–Ge(3) 176.17(4), N(1)–Ge(1)–N(2) 87.19(6), N(6)–Ge(3)–N(5) 87.00(6).

The structure of **2b** is dominated by the mutual avoidance of the three NHGe ligands, which are aligned along the three C–Mo–Ge axes of the molecule with the ligand ring planes oriented perpendicular to each other. The three germanium atoms lie 15, 18 and 19 pm outside the ring planes. This arrangement minimises the interactions between the neopentyl substituents and neighbouring ring systems. There are two short contacts between C–H hydrogen atoms of the neopentyl substituents and nitrogen atoms of neighbouring ligand rings, namely $\text{H50B}\cdots\text{N2}$ (251 pm) and $\text{H31C}\cdots\text{N6}$ (255 pm); C–H $\cdots\pi$ contacts are also observed, with three C–H \cdots centroid distances of 276–306 pm.

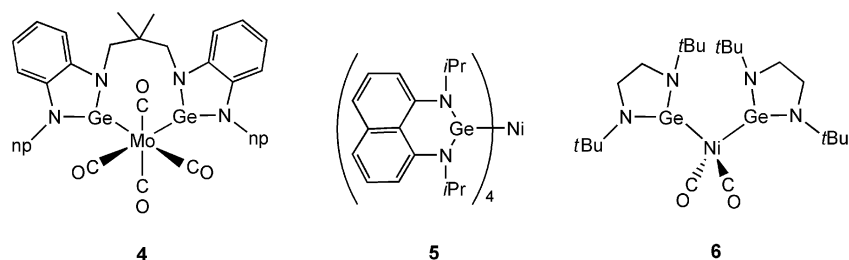


Figure 2. Crystallographically characterised NHGe complexes (**4–6**); np = neopentyl.

The benzo-anellated NHGe in **2b** displays some folding along the N–N and C_N–C_N vectors which makes the NHGe ligands non-planar (see Figure 3) and the [Mo(CO)₃(NHGe)₃] complex formally chiral in consequence. The folding angles average 7.6° for N–N (α) and 3.6° for C_N–C_N (β) between the imidazole and phenyl rings, respectively. The deviation in GeN₂C₂ is smaller ($\alpha = 1.80^\circ$) in the non-anellated NHGe ligand of the molybdenum complex **1b**, although in the nickel complex **2c** with benzo anellation it is similar to that in **2b**.

Compound **2c**·3thf crystallises in the orthorhombic space group $P2_12_12_1$ with four molecules in the unit cell. The compound is monomeric, with the nickel atom coordinated tetrahedrally by four germanium atoms (Figure 4). The Ni–Ge bond lengths [223.24(4), 223.26(4), 223.34(4) and 223.87(4) pm] are similar to those in two other structurally determined Ni⁰–NHGe complexes, namely [Ni{Ge(*i*PrN)₂–C₁₀H₆}]₄ [5; 224.00(16) pm]^[25] and [Ni(CO)₂{Ge(*t*BuN)₂–C₂H₄}]₂ [6; 229.69(4) and 229.13(3) pm],^[26] and also to the Ni–Ge bond lengths in [CpNi{Ge(*N*tBu)₂SiMe₂}₂(μ -Cp)] [7; 208.5(3) and 225.8(3) pm].^[27] The Ge–N bonds in **2c** [184.2(2)–185.4(2) pm, average 184.9(4) pm] are somewhat longer than in **2b** but still 1.5 pm shorter than in the free ligand. Likewise, the N–Ge–N bond angles in **2c** [86.37(9)–86.49(9)°] are marginally smaller than in **2b**, but still some 1.5° larger than in the free ligand. The N–C_{ring} bond lengths [average 139.9(3) pm] are virtually unchanged from the value for the free ligand. The structure of complex **2c** is likewise strongly influenced by the positioning of the neopentyl substituents. In our NiGe₄ tetrahedron there are two sets of perpendicular NHGe–Ni–NHGe moieties whose neopentyl groups are arranged so that they face each other.

This arrangement causes repulsion between these two ligands, which is manifested in a substantial increase of the Ge–Ni–Ge bond angles [114.974(18)° and 115.357(18)°]. At the same time, the remaining four Ge–Ni–Ge bond angles

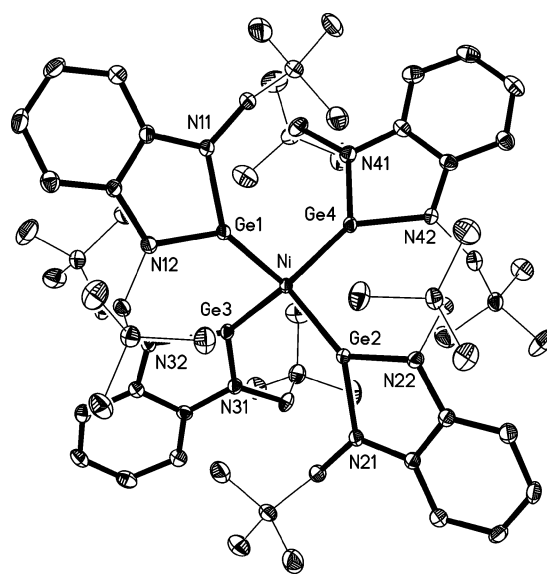


Figure 4. Molecular structure of **2c**·3thf. Ellipsoids are shown with 50% probability, and hydrogen atoms and thf molecules have been omitted for clarity. Selected bond lengths [pm] and angles [°]: Ni–Ge(2) 223.24(4), Ni–Ge(4) 223.87(4), Ge(2)–N(21) 184.2(2), Ge(4)–N(42) 185.4(2), N(11)–C(11) 139.6(3), N(42)–C(412) 146.8(3); Ge(2)–Ni–Ge(3) 107.760(17), Ge(2)–Ni–Ge(1) 114.974(18), Ge(3)–Ni–Ge(1) 104.982(17), Ge(2)–Ni–Ge(4) 104.883(16), Ge(3)–Ni–Ge(4) 115.357(18), Ge(1)–Ni–Ge(4) 109.203(17), N(11)–Ge(1)–N(12) 86.37(9), N(31)–Ge(3)–N(32) 86.49(9).

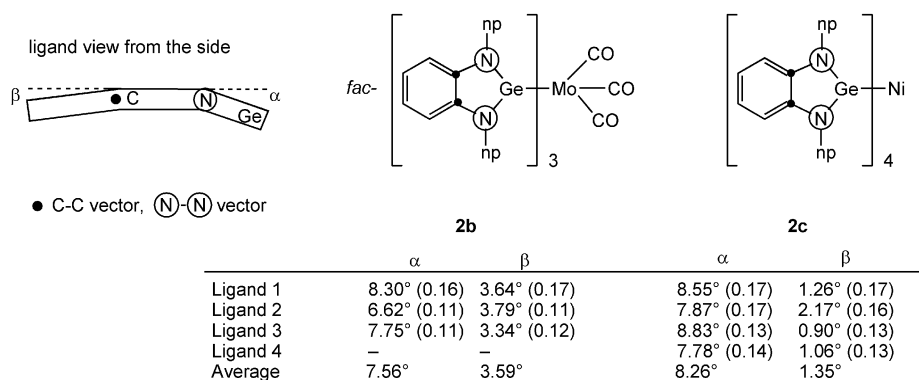


Figure 3. Folding of the coordinated NHGe ligands along the N–N (α) and C_N–C_N (β) vectors; np = neopentyl.

are minimised [107.760(17), 109.203(17), 104.982(17) and 104.883(16)°], with the two smaller angles representing those pairs of ligands whose neopentyl substituents have the maximum distance from each other. This Ge–Ni–Ge pattern is not seen in complex **5**^[25] as the six-membered 7 π -electron ring system experiences twisting upon coordination to the nickel atom, which results in two small [99.23(8)°] and four large [114.82(5)°] Ge–Ni–Ge bond angles. The folding along the N–N and C_N–C_N vectors in the benzo-anellated NHGe in **2c** is similar to that in **2b** and makes the NHGe ligands non-planar. The folding angles average 8.3° for N–N (α) and 1.4° for C_N–C_N (β) between the imidazole and phenyl rings, respectively. Folding of the phenyl rings is significantly less than in **2b** (an average of 1.4° compared to 3.6°). The four germanium atoms lie 18, 18, 20 and 21 pm outside the respective rings. There are no close intra-molecular C–H \cdots N contacts of less than 265 pm and no significant C–H \cdots π contacts, although weak interactions may be possible.

Ligand Properties of N-Heterocyclic Germylenes

Experimental information regarding the electronic properties of the germylene ligands in these complexes can be obtained from the IR spectra of their carbonyl transition metal complexes, particularly the position of the A₁ band in the carbonyl region of the spectrum (Table 1).

Table 1. A₁ stretching vibrations for **1b**, **2b** and **3b**.

Complex	Exp. A ₁ [cm ⁻¹]	Exp. TEP [cm ⁻¹]	Calcd. TEP [cm ⁻¹]
1b	1961	2073.0	(2073)
2b	1970	2077.8	2077.8
3b	1978	2080.6	2081.5
4 ^[23]	2031	2075.4	–
7 ^{[a][23]}	2034	2077.2	–

[a] *cis*-[Mo(CO)₄]{(CH₂)₅[NGeN(CH₂*t*Bu)C₆H₄]₂}.

In order to make comparisons with other ligands, we have to convert the experimental findings to a common standard, in this case the Tolman Electronic Parameter (TEP),^[28] which is derived from the [Ni(CO)₃L] series. Recently, one of us (O. K.) proposed a method for calculating the TEP values for NHGe ligands^[17,18] which allows the TEP values for **2b** and **3b** to be predicted (2077.8 and 2081.5 cm⁻¹, respectively). These values are in excellent agreement with the experimental values. The A₁ bands of compounds **1c**, **2b** and **3b** are found at 1961, 1970 and 1978 cm⁻¹, respectively, which correspond to TEP values of 2073.0, 2077.8 and 2080.6 cm⁻¹, respectively. The increase in wavenumber with increase of anellation from non-anellation via benzo to naphtho translates into a corresponding decline of the net electron-donating ability for the NHGe ligands. This is not, however, mirrored in the M–Ge bond lengths of the metal complexes – the Mo–Ge bond lengths in **1b** and **2b** are virtually the same (Δ = 0.25 pm). Both complexes are members of the *fac*-[Mo(CO)₃L₃] family with identical co-ligands and geometries and are thus ideal for comparison. The only other direct comparison of M–Ge

bond lengths can be made between **2c** and **6**,^[26] both of which are [NiL₂L'₂] complexes (L = NHGe, L' = CO, NHGe) with a tetrahedral geometry. The only difference is that **6** contains a co-ligand with greater π -acceptor strength (carbonyl) that is lacking in **2c**. Thus, whereas the TEP value of the ligand is 8 cm⁻¹ larger, the Ni–Ge bond length in **2c** is 5 pm shorter than in **6**.

These two examples suggest that anellation in NHGe diminishes the σ -donor ability and increases the π -acceptor strength of the germylene. As a consequence, the NHGe ligands will display poor ligating behaviour with metal fragments that show weak π -back-bonding. Indeed, reactions of **2a** with [PdCl₂(cod)], [PdCl₂(NCCH₃)₂] and even [RhCl(cod)]₂ did not give the intended germylene complexes but led to decomposition of the germylene and/or the metal precursor.

PES and Quantum Chemical Calculations

In order to shed more light on the electronic properties of the germylene ligand and compare it to its silylene and carbene homologues, a photoelectron spectrum of **2a** was measured (Figure 5), thereby completing the series of spectra for the series of related benzo-anellated NHE compounds (E = C,^[16a] Si,^[29] Ge). The ionisation potentials of a series of model compounds were also calculated. We chose the *N*-*tert*-butyl-substituted compounds since they feature *N*-substitution and only one stable ground-state conformation. The calculated ionisation energies correlate well with the experimental vertical ionisation energies. Correlation of the calculated ionisation potentials of bnNHC, bnNHSi and bnNHGe (Figure 6) shows the distinct nature of the germylene compared to the homologous silylene and, in particular, the carbene, and clear trends in the electronic properties.

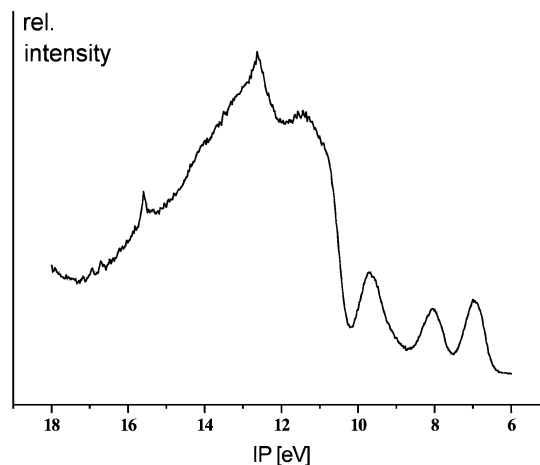


Figure 5. Photoelectron spectrum of **2a** (band 1: IE = 7.00 eV, ring π -orbital; band 2: IE = 8.13 eV, phenyl π -orbital; band 3: IE = 9.7 eV, this band probably contains two peaks, the Ge lone pair and the N lone pairs; band 4: IE = 10.9 eV; band 5: IE = 11.5 eV; band 6: IE = 12.6 eV; band 7: IE = 15.6 eV, N₂ contamination).

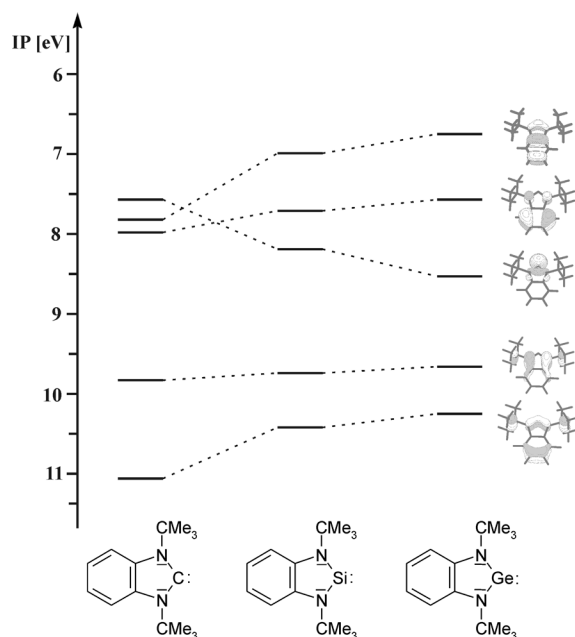


Figure 6. Correlation scheme of the calculated ionization potentials (for the *tert*-butyl model compounds).

The HOMO in the carbene is indeed the carbon atom lone pair. The ionisation potential of the lone pair for heavier group 14 analogs increases, and those of the respective π -orbitals destabilize, in a more pronounced manner for the heteroimidazole π -orbital than for the phenyl π -orbital. As a result, the silicon and germanium lone pair bands in the benzo-anellated NHSi and NHGe can be assigned only to the HOMO-2 (Figure 6). The energetic effect for bnNHGe is about twice that for bnNHSi. The significant increase in the ionisation energy of the germanium lone pair in bnNHGe translates into a substantially reduced σ -donor ability of the ligand.

As regards the influence of element(II) π -bonding, most authors agree that there is a certain degree of π -electron delocalization in the analogous non-anellated carbene and silylene systems, but that this effect is small for the carbenes and much smaller still for the silylenes.^[13] Anellation and the introduction of germanium as the divalent group 14 element further decrease the degree of delocalization. The “aromatic” π -type orbitals in **2a** (see Figure 6) are destabilized in comparison to the respective orbitals of carbenes and silylenes. From this we may conclude that the aromatic stabilization decreases in the order carbene > silylene > germylene and that the main stabilization of the germylene will be achieved through the N–Ge bond.

Coordination of NHGe to a transition metal atom increases the positive charge on the germanium atom, although back-bonding from the metal atom counteracts this to a certain extent. As the germanium atom still experiences a greater Coulomb attraction to the nitrogen atoms, possibly strengthened also by an increase in the π bonding, the Ge–N bond should become shorter. The changes in the Ge–N bond lengths actually seen for the pair **1a/1b** upon coordination to the molybdenum atom are the opposite – the

Ge–N bonds are shorter in the free ligand and increase by 2.0 pm upon complexation. These changes hint at back-bonding and electron repulsion, which shifts π density of the coordinated ligand from Ge to the C=C end of the heterocycle and shortens the N–C_{ring} bond lengths by 5.8 pm. The expected Ge–N bond shortening is observed on complexation for the benzo-anellated pair **2a/2b**. It can therefore be assumed that the π density of the nitrogen lone electron pairs is delocalized into the anellated rings, and the shorter bond is caused mainly by increased Coulomb attractions between the germanium and nitrogen atoms. The folding about the N...N axis, observed particularly for the anellated NHGe complexes, supports this view as deviations from planarity weaken the π delocalization but not electrostatic forces.

Such deviations have been observed before in the closely related N-heterocyclic carbene complex $[\text{W}(\text{CO})_5\{\text{C}_6\text{H}_4\text{N}(\text{CH}_2\text{tBu})_2\text{C}\}]$.^[30] The authors explained the deviations in terms of the steric requirements to obtain a shorter W–C bond, which minimise the interaction between the neopentyl substituents and the equatorial carbonyl ligands. Such effects should cause similar deviations in the structures of **1b** and **2b**, which differ only in the absence of the sterically non-active anellated benzene rings in **1b**. However, the deviations in **2b** are three to four times as large as in **1b** (Ge displacement 19.4 vs. 4.2 pm; Mo displacement 50.8 vs. 20.5 pm). The benzo-anellated bis(NHGe)–Mo(CO)₄ chelate complex **4**^[23] behaves similarly to **2b**, with displacements for Ge of 13.5 pm and for Mo of 65 pm, whereas in a sterically even more challenging but non-anellated (dimesityl-NHGe)Cu^I complex there are no marked deviations from planarity (Ge: 0.8 pm; Cu: 2.8 pm).^[31]

To shed light on the background of the folding observed for the anellated NHGe carbonyl molybdenum(0) and nickel(0) complexes (Figure 3), we calculated the structure of **2a** in the gas phase, along with the structures of $[\text{Ge}\{\text{N}(\text{tBu})_2\text{C}_6\text{H}_4\}]$, the theoretical complex $[\text{Ni}(\text{CO})_3\{\mathbf{2a}\}]$ and the hypothetical complexes $[\text{Ni}(\text{CO})_3\{\text{Ge}(\text{HN})_2\text{C}_6\text{H}_4\}]$, $[\text{Ni}(\mathbf{2a})\{\text{Ge}(\text{HN})_2\text{C}_6\text{H}_4\}_3]$ and $[\text{Ni}(\mathbf{2a})_2\{\text{Ge}(\text{HN})_2\text{C}_6\text{H}_4\}_2]$. The framework of **2a** was found to be non-planar, but with a mere 0.22 kcal mol^{−1} required to enforce planarity. When the neopentyl groups are on opposite sides of the ligand plane, this energy drops to 0.034 kcal mol^{−1}. Compound **2a** is planar in the solid state^[15c] with both neopentyl groups on the same side, but the 0.22 kcal mol^{−1} required to achieve planarity can easily be provided by packing effects. Complexation to the nickel atom does not increase this planarity barrier significantly {0.36 kcal mol^{−1} in $[\text{Ni}(\text{CO})_3\{\mathbf{2a}\}]$. In $[\text{Ni}(\mathbf{2a})\{\text{Ge}(\text{HN})_2\text{C}_6\text{H}_4\}_3]$, the barrier increases to 0.42 kcal mol^{−1} and in $[\text{Ni}(\mathbf{2a})_2\{\text{Ge}(\text{HN})_2\text{C}_6\text{H}_4\}_2]$ to 1.06 kcal mol^{−1}. Assuming about 0.5 kcal mol^{−1} for each ligand, we may expect that the barrier to planarity in **2b** is about 3 kcal mol^{−1}.

It seems that the total energy difference between the planar and nonplanar structures is very small; according to our calculations it is less than or close to 1 kcal mol^{−1}. Thus, both types of bending (α and β) require less than 1 kcal mol^{−1}. This may suggest a corresponding flexibility

of the ring and a very-low-frequency vibrational motion with a possible quasi-planar structure. The low-frequency vibration around the nonplanar equilibrium may cause an effective planar structure (quasi-planarity) in the gas phase if the barrier is lower than the zero-point vibration. Obviously, a more rigid nonplanar geometry is possible in solid crystals because of the constraints imposed by the lattice.

Conclusions

Five-membered N-heterocyclic germylenes (NHGe), which form complexes with electron-rich zero-valent transition metal compounds, are weak donor ligands that allow stabilization by π -back-bonding. Anellation further decreases the donor strength. Several attempts to synthesize complexes of dineopentylbenzodiazagermol-2-ylidene with mono- or divalent transition metals failed, whereas a Cu^I complex with the non-anellated di-*tert*-butyldiazagermol-2-ylidene ligand is known. Compared to N-heterocyclic silylenes, including benzo-anellated representatives, the donor strength is further reduced. This is shown by the CO valence vibrations in mixed NHGe/CO and NHSi/CO complexes and explained by the orbital correlation diagram of benzo-anellated NHC, NHSi and NHGe, which displays a strong decrease in energy of the orbital occupied by the lone electron pair with increasing size of the divalent group 14 element.

Experimental Section

General: All experiments were performed under dry argon or nitrogen by using Schlenk techniques. All glassware was heat-dried in vacuo. Solvents were dried with sodium/benzophenone and freshly distilled before use. KBr was dried by heating under high vacuum; C₆D₆ and [D₈]THF were dried with LiAlH₄ and re-condensed before use. The germylenes **2a** and **3a** were prepared as described earlier. NMR spectra were recorded with an ARX 300 spectrometer (Bruker) at 300.1 and 75.5 MHz (¹H and ¹³C NMR); chemical shifts (δ in ppm) are referenced to internal SiMe₄. Assignment numbers are in accordance with the nomenclature. Mass spectra were measured with a single focusing sector field mass spectrometer AMD40 (Intectra). Elemental analyses were carried out with an elemental analyzer LECO Model CHNS-932 by using standard combustion conditions.

fac-Tricarbonyltris(N,N'-dineopentyl-1,3,2-benzodiazagermol-2-ylidene)molybdenum(0) (2b): A solution of [Mo(CO)₃(cht)] (92 mg, 0.33 mmol) in thf (3 mL) was cooled and added to a solution of **2a** (326 mg, 1.02 mmol) in thf (10 mL) at –78 °C. The colour gradually changed from pale yellow to dark red. After stirring overnight, the solvent was evaporated under reduced pressure, and the crude product was washed with *n*-hexane to give 265 mg (69%) of highly air- and moisture-sensitive orange-yellow **2a** containing a small amount of **1a**. Single crystals of pure **2a** were formed by layering a saturated solution of [Mo(CO)₃(cht)] in thf with a solution of **1a** in hexane (molar ratio 1:3 as above) at room temperature and slow diffusion overnight. ¹H NMR (C₆D₆): δ = 0.90 (s, 18 H, CH₃), 3.74 (br. s, 4 H, NCH₂), 7.00 (m, 2 H, 5-H), 7.89 (m, 2 H, 4-H) ppm. ¹³C{¹H} NMR (C₆D₆): δ = 29.37 (s, CMe₃), 34.55 (s, CMe₃), 54.94 (s, 2 NCH₂), 111.34 (C-4), 118.47 (C-5), 143.52 (C-3a), 218.86 (CO)

ppm. IR (KBr): $\tilde{\nu}$ = 1970, 1901 (ν_{CO}) cm^{–1}. C₅₁H₇₈Ge₃MoN₆O₃ (1137.1): calcd. C 53.87, H 6.91, N 7.39; found C (incomplete combustion), H 6.87, N 7.45. Crystal data are compiled in Table 2.

fac-Tricarbonyltris(N,N'-dineopentyl-1,3,2-naphtho[2,3-*d*]diazagermol-2-ylidene)molybdenum(0) (3b): A cold solution of [Mo(CO)₃(cht)] (54 mg, 0.20 mmol) in thf (3 mL) was slowly added to a solution of **3a** (220 mg, 0.60 mmol) in thf (10 mL) at –78 °C (colour change from yellow to dark red) and stirred for 5 h. The solvent was evaporated in vacuo, and the residue was triturated with hexane to yield 145 mg (56%) of **3b** as an extremely moisture-sensitive orange-yellow viscous material. Attempts to obtain single crystals of **3b** by the diffusion technique described above failed. ¹H NMR (C₆D₆): δ = 0.77 (s, 18 H, CH₃), 3.7–4.0 (v. br, 4 H, NCH₂), 7.33 (m, 2 H, 5-H), 7.40 (s, 2 H, 4-H), 7.77 (m, 2 H, 6-H) ppm. ¹³C{¹H} NMR (C₆D₆): δ = 29.51 (CMe₃), 31.85 (CMe₃), 55.05 (NCH₂), 106.57 (CH-4), 124.65, 127.81 (CH-5, CH-6), 128.49 (C-4a), 143.84 (C-3a), 218.06 (CO) ppm. [The NMR spectra showed contamination by 2,3-bis(neopentylamino)naphthalene due to hydrolysis by traces of moisture in C₆D₆.] IR (KBr): $\tilde{\nu}$ = 1978, 1913 (ν_{CO}) cm^{–1}. C₆₃H₈₄Ge₃MoN₆O₃ (1292.3): calcd. C 58.78, H 6.58, N 6.53; found C (incomplete combustion), H 6.64, N 6.80.

Tetrakis(N,N'-dineopentyl-1,3,2-benzodiazagermol-2-ylidene)-nickel(0) (2c): A solution of Ni(1,5-cod)₂ (169 mg, 0.61 mmol) in thf (3 mL) was added slowly to a solution of **2a** (410 mg, 1.29 mmol) in thf (15 mL) at 0 °C, causing a gradual colour change from yellow to dark red. The solution was stirred for 4 h. Reaction control of a small sample by NMR spectroscopy in C₆D₆ (thf removed in vacuo) showed >95% conversion of **2a** to **2c** and some unconverted Ni(cod)₂. The main part of the reaction mixture in thf was stored at room temperature for 4 d to allow for decomposition of the residual Ni(cod)₂. The nickel powder was removed by filtration, and cod and solvent were evaporated in vacuo to give 370 mg (74%) of red **2c**. Single crystals were grown from a thf solution at –20 °C and separated along with a small amount of mother liquor. The complex can be stored in this form under argon at 4 °C for months, but is extremely air- and moisture-sensitive; even short air contact leads to decomposition to form a violet solution. Crystal structure analysis of the red single crystals showed three molecules of thf per formula unit (see crystal data in Table 2). ¹H NMR (C₆D₆): δ = 0.83 (s, 18 H, CH₃), 3.96 (br. s, 4 H, NCH₂), 7.00 (m, 2 H, 4-H), 7.16 (br., solvent and m, 5-H) ppm. ¹³C{¹H} NMR (C₆D₆): δ = 30.17 (s, CMe₃), 35.00 (s, CMe₃), 55.60 (s, 2 NCH₂), 111.07 (CH-4), 118.22 (CH-5), 143.55 (C_q-3a) ppm. [The NMR spectra displayed trace signals for 1,2-bis(neopentylamino)-benzene due to extreme moisture sensitivity.] The mass spectra (EI) did not display the molecular cation peak but isotopic cluster peaks of decomposition products; base peak: m/z = 320.8 [**2a**⁺].

Crystal Structure Analysis of 2b and 2c. Data Collection: Data were recorded with Bruker area detectors (SMART for **2b**, APEX2 for **2c**) at low temperature. Absorption corrections were performed on the basis of multi-scans. **Structure Refinement:** The structures were refined anisotropically on F^2 by using the program SHELXL-97.^[32] Hydrogen atoms were refined by using rigid methyl groups or a riding model. Crystal data are presented in Table 2. **Special Features of Refinement:** For **2b**, a region of badly resolved residual electron density around an inversion centre was tentatively identified as disordered solvent, but could not be refined adequately. The program SQUEEZE (Prof. A. L. Spek, Univ. of Utrecht, Netherlands) was therefore used to remove the effects of the solvent mathematically. For the calculation of mass-dependent parameters, a composition based on half a benzene molecule per asymmetric unit was assumed. For **2c**, the solvent content of three thf molecules

Table 2. Crystal data and structure refinement (for **1b** see ref.^[15a]).

	2b ·1/2C ₆ H ₆	2c ·3thf
Empirical formula	C ₅₄ H ₈₁ Ge ₃ MoN ₆ O ₃	C ₇₆ H ₁₂₈ Ge ₄ N ₈ NiO ₃
Formula mass	1175.96	1550.93
Temperature	133(2) K	100(2) K
Wavelength	0.71073 Å	0.71073 Å
Crystal system	triclinic	orthorhombic
Space group	<i>P</i> $\bar{1}$	<i>P</i> 2 ₁ 2 ₁
Unit cell dimensions	<i>a</i> = 11.9177(6) Å, <i>a</i> = 70.616(4)° <i>b</i> = 15.2995(8) Å, <i>b</i> = 73.772(4)° <i>c</i> = 17.3158(8) Å, <i>c</i> = 85.640(4)°	<i>a</i> = 15.1654(11) Å, <i>a</i> = 90° <i>b</i> = 19.9918(14) Å, <i>b</i> = 90° <i>c</i> = 26.184(2) Å, <i>c</i> = 90°
Volume	2859.2(2) Å ³	7938.4(10) Å ³
<i>Z</i>	2	4
Density (calcd.)	1.366 Mg m ⁻³	1.298 Mg m ⁻³
Absorption coefficient	1.821 mm ⁻¹	1.779 mm ⁻¹
<i>F</i> (000)	1218	3280
Crystal size	0.35 × 0.25 × 0.20 mm	0.18 × 0.10 × 0.10 mm
θ range for data collection	1.41–30.51°	2.98–28.28°
Index ranges	–17 ≤ <i>h</i> ≤ 16 –21 ≤ <i>k</i> ≤ 21 –24 ≤ <i>l</i> ≤ 24	–20 ≤ <i>h</i> ≤ 20 –26 ≤ <i>k</i> ≤ 26 –34 ≤ <i>l</i> ≤ 34
Reflections collected	67901	418061
Independent reflections	17308 [<i>R</i> (int) = 0.027]	19677 [<i>R</i> (int) = 0.100]
Completeness to θ	99.4% (θ = 30°)	99.8% (θ = 28°)
Absorption correction	semi-empirical from equivalents	semi-empirical from equivalents
Max./min. transmission	0.7122/0.5202	0.8422/0.7283
Refinement method	full-matrix least squares on <i>F</i> ²	full-matrix least squares on <i>F</i> ²
Data/restraints/parameters	17308/0/595	19677/0/853
Goodness-of-fit on <i>F</i> ²	1.07	1.02
Final <i>R</i> indices [<i>I</i> > 2σ(<i>I</i>)]	<i>R</i> 1 = 0.0279 <i>wR</i> 2 = 0.0664	<i>R</i> 1 = 0.0314 <i>wR</i> 2 = 0.0623
<i>R</i> indices (all data)	<i>R</i> 1 = 0.0423 <i>wR</i> 2 = 0.0708	<i>R</i> 1 = 0.0490 <i>wR</i> 2 = 0.0682
Largest diff. peak/hole	0.77/–0.31 e Å ⁻³	0.87/–0.40 e Å ⁻³
Absolute structure parameter	–	–0.007(5)

was well-behaved. CCDC-694679 and -694680 (for **2b** and **2c**, respectively) contain the supplementary crystallographic data for this paper. These data can be obtained free of charge from The Cambridge Crystallographic Data Centre via www.ccdc.cam.ac.uk/data_request/cif.

Photoelectron Spectroscopic Measurements: The He^I photoelectron spectrum of **2a** was recorded as described previously.^[33] The N₂ and He⁺ peaks were used for internal calibration. The resolution during the measurements was 40 meV at the Ar ²P_{1/2} line.

Quantum Chemical Calculations: Quantum chemical calculations for all the investigated molecules were performed with the Gaussian 03 program package.^[34] Structures were optimized at the B3LYP/cc-pVTZ level. The stationary points were characterized by second-derivative calculations. To interpret the PE spectra, we compared the recorded vertical ionization energies with quantum chemical results obtained at the ROVGF/cc-pVDZ level of theory on the optimized geometry.

Supporting Information (see footnote on the first page of this article): Table containing characteristic data of **1a**, **2a**, **1b**, **2b** and **2c** for comparison; ¹³C NMR spectroscopic data for **2b** and **2c**; tables containing data of quantum chemical calculations on model germynes (with NH and NtBu), germylene **2a** (non-planar and planarized, neopentyl group on the same and opposite side), effect of hyperconjugation, orbital representations, (germylene)nickel(0) model complexes and **2c** (non-planar and planarized).

Acknowledgments

A scholarship (F. U.) from the Deutsche Akademische Auslandsdienst is gratefully acknowledged. We thank Dr. M. K. Kindermann and B. Witt for recording the NMR spectra and Dr. G. Fischer (Dept. of Inorganic Chemistry, Ludwig-Maximilians-Universität, München) for mass spectrometric measurements. T. V. thanks the OTKA (T048796) for financial support.

- [1] D. Bourissou, O. Guerret, F. P. Gabbaï, G. Bertrand, *Chem. Rev.* **2000**, *100*, 39–91.
- [2] J. Arduengo III, R. L. Harlow, M. Kline, *J. Am. Chem. Soc.* **1991**, *113*, 361–363.
- [3] S. Díez-González, S. P. Nolan, *Coord. Chem. Rev.* **2007**, *251*, 874–883.
- [4] O. Köhl, *Chem. Soc. Rev.* **2007**, *36*, 592–607.
- [5] Recent reviews: a) F. E. Hahn, M. Jahnke, *Angew. Chem.* **2008**, *120*, 3166–3216; *Angew. Chem. Int. Ed.* **2008**, *47*, 3122–3172; b) E. A. B. Kantchev, C. J. O'Brien, M. G. Organ, *Angew. Chem. Int. Ed.* **2007**, *46*, 2768–2813; c) N. Marion, S. Díez-González, S. P. Nolan, *Angew. Chem.* **2007**, *119*, 3046–3058; *Angew. Chem. Int. Ed.* **2007**, *46*, 2988–3000; d) D. Enders, O. Niemeier, T. Balensiefer, *Angew. Chem.* **2006**, *118*, 1491–1495; *Angew. Chem. Int. Ed.* **2006**, *45*, 1426–1429; e) F. E. Hahn, *Angew. Chem.* **2006**, *118*, 1374–1378; *Angew. Chem. Int. Ed.* **2006**, *45*, 1348–1352; f) J. C. Garrison, W. J. Youngs, *Chem. Rev.* **2005**, *105*, 3978–4008.

- [6] Reviews: a) N. J. Hill, R. West, *J. Organomet. Chem.* **2004**, 689, 4165–4183; b) B. Gehrhus, M. F. Lappert, *J. Organomet. Chem.* **2001**, 617–618, 209–223.
- [7] P. P. Gaspar, R. West, in *The Chemistry of Organic Silicon Compounds*, vol. 2 (Eds.: Z. Rappoport, Y. Apeloig), Wiley, Chichester, **1998**, chapter 43.
- [8] a) M. Denk, R. Lennon, R. Hayashi, R. West, A. V. Belyakov, H. P. Verne, A. Haaland, M. Wagner, N. Metzler, *J. Am. Chem. Soc.* **1994**, 116, 2691–2692; b) B. Gehrhus, M. F. Lappert, J. Heinicke, R. Boese, D. Bläser, *J. Chem. Soc., Chem. Commun.* **1995**, 1931–1932.
- [9] Review: M. F. Lappert, *Main Group Met. Chem.* **1994**, 17, 183–207.
- [10] Recent reviews: a) O. Kühl, *Coord. Chem. Rev.* **2004**, 248, 411–427; b) O. Kühl, *Cent. Eur. J. Chem.* **2008**, 6, 365–372.
- [11] a) W. Wang, S. Yao, C. van Wüllen, M. Driess, *J. Am. Chem. Soc.* **2008**, 130, 9640–9641; b) S. Yao, M. Brym, K. Merz, M. Driess, *Organometallics* **2008**, 27, 3601–3607, and references cited therein.
- [12] a) F. E. Hahn, L. Wittenbecher, D. Le Van, A. V. Zabula, *Inorg. Chem.* **2007**, 46, 7662–7667; b) A. V. Zabula, T. Pape, A. Hepp, F. M. Schappacher, U. Ch. Rodewald, R. Pöttgen, F. E. Hahn, *J. Am. Chem. Soc.* **2008**, 130, 5648–5649; c) F. E. Hahn, D. Heitmann, T. Pape, *Eur. J. Inorg. Chem.* **2008**, 1039–1041.
- [13] a) H. M. Tuononen, R. Roesler, J. L. Dutton, P. J. Ragogna, *Inorg. Chem.* **2007**, 46, 10693–10706; b) J. Oláh, T. Veszprémi, F. De Proft, P. Geerlings, *J. Phys. Chem. A* **2007**, 111, 10815–10823; c) M. Tafipolsky, W. Scherer, K. Öfele, G. Artus, B. Pedersen, W. A. Herrmann, G. S. McGrady, *J. Am. Chem. Soc.* **2002**, 124, 5865–5880; d) J. F. Lehmann, S. G. Urquhart, L. E. Ennis, A. P. Hitchcock, K. Hatano, S. Gupta, M. K. Denk, *Organometallics* **1999**, 18, 1862–1872; e) C. Heinemann, T. Müller, Y. Apeloig, H. Schwarz, *J. Am. Chem. Soc.* **1996**, 118, 2023–2038; f) C. Boehme, G. Frenking, *J. Am. Chem. Soc.* **1996**, 118, 2039–2046.
- [14] a) R. K. Bansal, J. Heinicke, *Chem. Rev.* **2001**, 101, 3549–3578; b) B. R. Aluri, M. K. Kindermann, P. G. Jones, J. W. Heinicke, *Chem. Eur. J.* **2008**, 14, 4328–4335; c) M. S. S. Adam, O. Kühl, M. K. Kindermann, J. W. Heinicke, P. G. Jones, *Tetrahedron* **2008**, 64, 7960–7967.
- [15] a) O. Kühl, P. Lönnecke, J. Heinicke, *Inorg. Chem.* **2003**, 42, 2836–2838; b) O. Kühl, P. Lönnecke, J. Heinicke, *New J. Chem.* **2002**, 26, 1304–1307; c) O. Kühl, P. Lönnecke, J. Heinicke, *Polyhedron* **2001**, 20, 2215–2222; d) J. Heinicke, A. Oprea, M. K. Kindermann, T. Karpati, L. Nyulászi, T. Veszprémi, *Chem. Eur. J.* **1998**, 4, 541–545; e) J. Heinicke, A. I. Oprea, *Heteroat. Chem.* **1998**, 9, 439–444.
- [16] a) F. Ullah, G. Bajor, T. Veszprémi, P. G. Jones, J. Heinicke, *Angew. Chem.* **2007**, 119, 2751–2754; *Angew. Chem. Int. Ed.* **2007**, 46, 2697–2700; b) S. Saravanakumar, A. I. Oprea, M. K. Kindermann, P. G. Jones, J. Heinicke, *Chem. Eur. J.* **2006**, 12, 3143–3154; c) S. Saravanakumar, M. K. Kindermann, J. Heinicke, M. Köckerling, *Chem. Commun.* **2006**, 640–642.
- [17] O. Kühl, *Coord. Chem. Rev.* **2005**, 249, 693–704.
- [18] O. Kühl, K. Lifson, W. Langel, *Eur. J. Org. Chem.* **2006**, 2336–2343.
- [19] A. G. Avent, B. Gehrhus, P. B. Hitchcock, M. F. Lappert, H. Maciejewski, *J. Organomet. Chem.* **2003**, 686, 321–331.
- [20] A. V. Zabula, T. Pape, A. Hepp, F. E. Hahn, *Organometallics* **2008**, 27, 2756–2760.
- [21] a) B. Gehrhus, P. B. Hitchcock, M. F. Lappert, *J. Chem. Soc., Dalton Trans.* **2000**, 3094–3099; b) W. M. Boesfeld, B. Gehrhus, P. B. Hitchcock, M. F. Lappert, P. v. R. Schleyer, *Chem. Commun.* **1999**, 755–756.
- [22] O. Kühl, S. Blaurock, J. Sieler, E. Hey-Hawkins, *Polyhedron* **2001**, 20, 111–117.
- [23] A. V. Zabula, F. E. Hahn, T. Pape, A. Hepp, *Organometallics* **2007**, 26, 1972–1980.
- [24] C. E. Holloway, M. Melnik, *Main Group Met. Chem.* **2002**, 25, 331–410.
- [25] P. Bazinet, G. P. A. Yap, D. S. Richeson, *J. Am. Chem. Soc.* **2001**, 123, 11162–11167.
- [26] W. A. Herrmann, M. Denk, J. Behm, W. Scherer, F.-R. Klimgan, H. Bock, B. Solouki, M. Wagner, *Angew. Chem. Int. Ed. Engl.* **1992**, 31, 1485–1488.
- [27] a) M. Veith, L. Stahl, *Angew. Chem.* **1993**, 105, 123–125; *Angew. Chem. Int. Ed. Engl.* **1993**, 32, 116–119; b) M. Veith, A. Muller, L. Stahl, M. Nötzel, M. Jarzyk, V. Huch, *Inorg. Chem.* **1996**, 35, 3848–3855.
- [28] C. A. Tolman, *Chem. Rev.* **1977**, 77, 313–348.
- [29] P. Blakeman, B. Gehrhus, J. C. Green, J. Heinicke, M. Lappert, M. K. Kindermann, T. Veszprémi, *J. Chem. Soc., Dalton Trans.* **1996**, 1475–1480.
- [30] F. E. Hahn, L. Wittenbecher, R. Boese, D. Bläser, *Chem. Eur. J.* **1999**, 5, 1931–1935.
- [31] J. T. York, V. G. Young Jr, W. A. Tolman, *Inorg. Chem.* **2006**, 45, 4191–4198.
- [32] G. M. Sheldrick, *SHELXL-97, a program for refining crystal structures*, University of Göttingen, **1997**.
- [33] T. Veszprémi, Gy. Zsombok, *Magy. Kem. Foly.* **1986**, 92, 39–40.
- [34] M. J. Frisch, G. W. Trucks, H. B. Schlegel, G. E. Scuseria, M. A. Robb, J. R. Cheeseman, J. A. Montgomery Jr, T. Vreven, K. N. Kudin, J. C. Burant, J. M. Millam, S. S. Iyengar, J. Tomasi, V. Barone, B. Mennucci, M. Cossi, G. Scalmani, N. Rega, G. A. Petersson, H. Nakatsuji, M. Hada, M. Ehara, K. Toyota, R. Fukuda, J. Hasegawa, M. Ishida, T. Nakajima, Y. Honda, O. Kitao, H. Nakai, M. Klene, X. Li, J. E. Knox, H. P. Hratchian, J. B. Cross, V. Bakken, C. Adamo, J. Jaramillo, R. Gomperts, R. E. Stratmann, O. Yazyev, A. J. Austin, R. Cammi, C. Pomelli, J. W. Ochterski, P. Y. Ayala, K. Morokuma, G. A. Voth, P. Salvador, J. J. Dannenberg, V. G. Zakrzewski, S. Dapprich, A. D. Daniels, M. C. Strain, O. Farkas, D. K. Malick, A. D. Rabuck, K. Raghavachari, J. B. Foresman, J. V. Ortiz, Q. Cui, A. G. Baboul, S. Clifford, J. Cioslowski, B. B. Stefanov, G. Liu, A. Liashenko, P. Piskorz, I. Komaromi, R. L. Martin, D. J. Fox, T. Keith, M. A. Al-Laham, C. Y. Peng, A. Nanayakkara, M. Challacombe, P. M. W. Gill, B. Johnson, W. Chen, M. W. Wong, C. Gonzalez, J. A. Pople, *Gaussian 03*, Revision C.02, Gaussian, Inc., Wallingford CT, **2004**.

Received: August 24, 2008

Published Online: October 29, 2008

Syntheses, Structures, and Theoretical Studies of New Ternary Antimonides β -RECoSb₃ ($RE = \text{La-Nd, Sm}$)

Wei-Zhao Cai,^[a,b] Li-Ming Wu,^[a] Long-Hua Li,^[a,b] and Ling Chen^{*[a,c]}

Keywords: Transition metals / Rare earth metal compounds / Cobalt / Antimon / Electronic structure / Calculations / Tight-bonding linear muffin-tin orbital method

Five new intermetallic ternary cobalt antimonides β -RE-CoSb₃ have been prepared by solid state reactions and characterized by single-crystal X-ray diffraction. The title compounds crystallize in β -RENiSb₃-type structure, *Pbcm* (No.57), $Z = 8$, with $a = 12.985(4)$ – $12.5530(13)$ Å, $b = 6.1603(18)$ – $6.1043(4)$ Å, $c = 12.166(4)$ – $12.0267(12)$ Å for $RE = \text{La, Ce, Pr, Nd, and Sm}$. Their structures feature the anionic Sb square nets and CoSb₆ octahedron layers that are separated by RE^{3+} cations along the a axis. The structural relationship among parent-type ($RECrSb_3$), α -type ($RENiSb_3$), and β -type ($RECoSb_3$) has been presented. The electronic

band structure of β -LaCoSb₃ has been calculated with the aid of the tight-bonding linear muffin-tin orbital (TB-LMTO) method and the results suggest that the three types of $RETSb_3$ are metallic in both b and c directions and the electrical conductivities along the a direction are relatively weak. The magnetic calculations indicated that the rare-earth atoms would be the only source for the magnetic properties. Therefore, β -type Co analogues should be magnetically identical to the corresponding Ni members.

(© Wiley-VCH Verlag GmbH & Co. KGaA, 69451 Weinheim, Germany, 2009)

Introduction

Rare-earth transition-metal antimonides have been studied continuously because of their structural diversity, unique bonding interactions, and various interesting physical properties.^[1–3] The main structural motif of the layered $RETSb_3$ family ($RE = \text{La-Nd, Sm, Gd-Dy, Yb; T = V, Cr, and Pd}$) are the condensed TSb₆ octahedron layers and the square Sb nets that are separated by the RE^{3+} cations along the stacking direction.^[4–13] Such anisotropic structure leads to the anisotropic electrical conductivity of LaCrSb₃, and the ferromagnetic behavior corresponds to the existence of an intermediate between Cr^{3+} and Cr^{4+} .^[7] For other $RECrSb_3$ members ($RE = \text{Ce-Nd, Sm}$), the transition metal Cr influences the magnetic behaviors by coupling with RE at about 10 K.^[8,14–16] However, the V analogs ($RE = \text{La-Nd, Sm}$) show no $3d$ moment, and rare-earth cations are the sole magnetic source.^[4,6,14]

The $RENiSb_3$ exhibits interesting α - and β -type polymorphism. The α - $RENiSb_3$ ($RE = \text{Ce, Pr, Nd, Sm}$) differs from $RECrSb_3$ (named “parent type” hereafter) by a tripled c parameter, but similar TSb₆ layer and Sb net. The electrical conductivity perpendicular to the stacking direction is metallic. Unlike the parent structure type, the transition metal in the α -type has no significant contributions on the magnetic properties, and this series of compounds only show effective moments of free RE^{3+} ions.^[17,18]

The β - $RENiSb_3$ ($RE = \text{La, Ce}$) differs from the parent type by a doubled c parameter. And β -type compounds are also metallic perpendicular to the stacking direction; the Ce member shows ferromagnetic ordering of Ce^{3+} free ion only.^[19] The disordered analogs of $RENi(\text{Sn,Sb})_3$ ($RE = \text{Pr, Nd, Sm, Gd, and Tb}$) confirm that the RE^{3+} ions are the sole source of the magnetic properties.^[20] However, the transition metal Ni has no contribution to the magnetic property in both α - and β -type $RENiSb_3$.^[17–19] The replacement of Ni by Co would provide a new opportunity to look for structural and magnetic correlations.

The known $RE/Co/Sb$ compounds are RE_5CoSb_2 ($RE = \text{Gd, Tb, Dy, Ho, Er}$),^[21] $RECo_{1-x}Sb_2$ ($RE = \text{La-Nd, Sm, Gd}$),^[22–24] and α -type $RECoSb_3$ ($RE = \text{Ce, Pr}$).^[25,26]

In this paper, we present the syntheses and structures of a new series of β -type $RECoSb_3$ ($RE = \text{La-Nd, Sm}$). The structural relationship among parent type, α -, and β -type $RETSb_3$ has been presented, and the electronic band structure calculations with the aid of the TB-LMTO method have been reported for the first time; also the electrical conductivity and the magnetic properties are investigated.

[a] State Key Laboratory of Structural Chemistry, Fujian Institute of Research on the Structure of Matter, Chinese Academy of Sciences, Fuzhou, Fujian 350002, People's Republic of China
Fax: +86-591-83704947
E-mail: chenl@fjirsm.ac.cn

[b] Graduate School of the Chinese Academy of Sciences, Beijing 100039, People's Republic of China

[c] State Key Laboratory for Physical Chemistry of Solid Surfaces, Xiamen University, Xiamen 361005, People's Republic of China

Results and Discussion

Structure

β - $RECoSb_3$ ($RE = La-Nd, Sm$) is the isostructural form of the β - $RENiSb_3$ -type compound.^[19] The anionic moiety of the structure consists of two independent parts: slightly distorted Sb square nets and $CoSb_6$ octahedron layers. Both are stacked along the a axis and separated by RE^{3+} cations as shown in Figure 1.

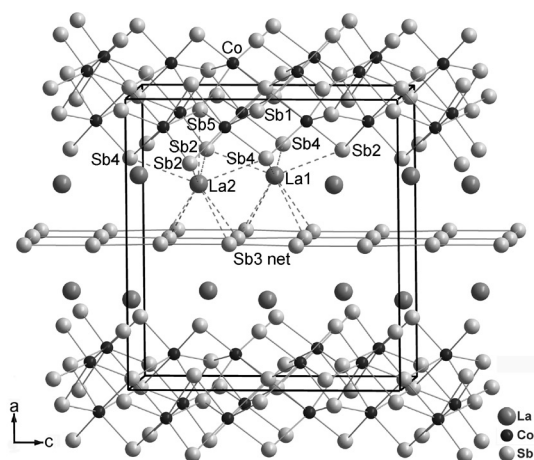


Figure 1. View down the b axis of β - $LaCoSb_3$ with the unit cell outlined. The coordination around the La1 and La2 atom is marked by dashed lines. For clarity, the Co–Co bonds are omitted.

To date, three structure types of antimonides with a common formula $RETSb_3$ ($T =$ transition metal), namely parent-type $RECrSb_3$,^[5] α -type $RENiSb_3$,^[17,18] and β -type $RENiSb_3$ ^[19] have been reported. Each structure has similar anionic building units, Sb square nets and TSb_6 octahedron layers, with RE^{3+} cations inserted between them. The major difference is their c parameters that are determined by the different building units along the c axis. As shown in Figure 2, in the parent-type $RECrSb_3$, the repeat unit is a monooctahedron $[CrSb_6]$ that extends along c through face-sharing. In the β -type, for example $LaCoSb_3$, the building unit is a dimer of the edge-shared octahedra, $[Co_2Sb_{10}]$. While in the α -type, for example $LaNiSb_3$, the building unit is a trimer of the edge-shared octahedra, $[Ni_3Sb_{14}]$. The dimer or trimer along c leads to the approximately doubled or tripled c -parameter for β - or α - $RETSb_3$, respectively. This relationship can also be understood by the stacking sequences of the close-packed layers of Sb atoms along the c direction as shown in Figure 2. Such stacking sequences are AB in parent- $LaCrSb_3$, ABCB in β - $LaCoSb_3$, and AB-ACBC in α - $LaNiSb_3$.

On the other hand, the connection motifs and repeat unit along the b axis are similar for the three types; therefore the b parameters are nearly the same, ranging from 6.160 Å for the β -type to 6.203 Å for the α -type and to 6.212 Å for the parent type.^[5,17] Meanwhile, the a -parameter is determined by the thickness of the TSb_6 octahedron layer, Sb square net, and the size of the interstitial RE^{3+} cations. Therefore, no significant change in a parameters is expected among

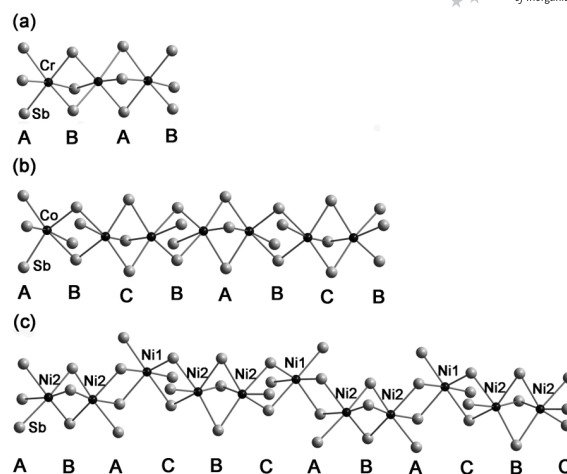


Figure 2. The connection motifs of the TSb_6 octahedra along the c axis of $RETSb_3$. (a): $T = Cr$, (b): $T = Co$, and (c): $T = Ni$. A, B, C represent the stacking sequences of the essentially close-packed Sb atoms.

the three types, for example 13.283 Å for parent-type $LaCrSb_3$ ^[5] and 12.985 Å for β -type $LaCoSb_3$, and 12.634 Å for α -type $CeNiSb_3$.^[17] The β -type $RECoSb_3$ has shown lanthanide contraction as indicated by Figure 3, in which the lattice parameters as well as the cell volumes decrease monotonically with the increase of the atomic number of the lanthanide.

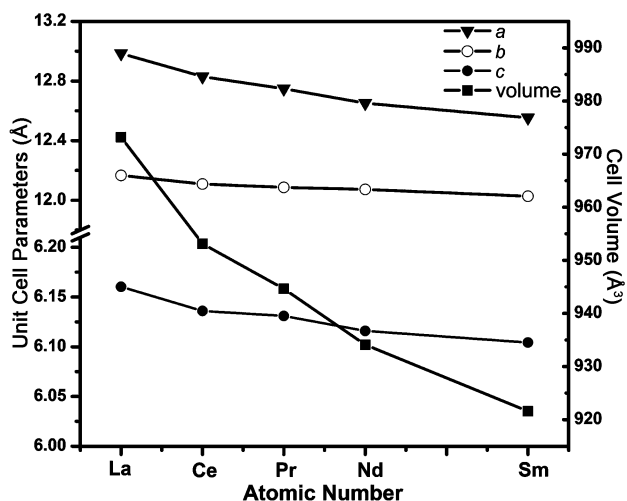


Figure 3. Plots of the lattice parameters [Å] and cell volumes [\AA^3] for β - $RECoSb_3$ ($RE = La-Nd, Sm$).

The five β - $RECoSb_3$ compounds reported here belong to the β -type structure. Taking $LaCoSb_3$ as an example, the Co–Sb bond lengths within the $CoSb_6$ octahedron range from 2.5918(13) Å to 2.6661(12) Å with an average (2.629 Å) similar to 2.588 Å in binary CoSb (NiAs-type),^[27] but slightly longer than that in $CoSb_3$ (2.527 Å).^[28] The distortion of the TSb_6 octahedra is more obvious than that in parent-type $LaCrSb_3$,^[5] but comparable to that in $CoSb_3$.^[28] In addition, the Co–Co distances roughly decrease with a decrease in the size of RE^{3+} cations, 2.756(2) Å for La-, 2.735(2) Å for Ce-, 2.729(2) Å for Pr-, 2.739(2) Å for Nd-,

and 2.718(2) Å for the Sm-member. Such distances are slightly longer than 2.588 Å in binary CoSb.^[27] The Sb–Sb bonds in the Co/Sb layer, such as Sb1–Sb1 [3.1598(9) Å], Sb1–Sb4 [3.1426(14) Å], and Sb1–Sb5 [3.3410(1) Å], are longer than that in the Sb square net, for example Sb3–Sb3 [3.0128(12)–3.0806(9) Å].

There are two crystallographically independent La sites, La1 (Wyckoff site 4c) and La2 (4d) in β -LaCoSb₃. As depicted in Figure 4 (a), the La1 atom adopts a square antiprismatic coordination, which is frequently found in the rare-earth antimonides such as $RECo_{1-x}Sb_2$ ($RE = La, Ce, Pr, Nd, Sm, \text{ and } Gd$)^[22–24] or $RETSb_2$ ($T = Ag, Ga, Mn, Zn, Cd$).^[29–33] One square base is constructed by two Sb2 atoms and two Sb4 atoms from the Co/Sb layer, and the other is defined by four Sb3 atoms from the Sb net. The La2 atom has similar square antiprismatic geometry with an extra La2–Sb5 contact with the Co/Sb layer (Figure 4, b). Compared with the β -RENiSb₃ analogues, RE –Sb distances are not affected significantly by the different transition-metal ions, for example, 3.2573(9)–3.3940(9) Å for β -LaCoSb₃ and 3.2503(5)–3.3942(9) Å for β -LaNiSb₃.^[19] The square Sb nets are composed of Sb3 atoms with bond lengths of 3.0128(12)–3.0806(9) Å, and angle Sb–Sb–Sb: 87.434(5)–92.533(6)° as shown in Figure 5. Compared with the Ni-analogue, different transition metal, Co vs. Ni, slightly changes the bonds and angles. The Sb3 nets are

shown in Figure 5. The Sb nets in the parent type are an ideal square net with Sb–Sb: 3.049(5)–3.108(5) Å; angle Sb–Sb–Sb: 90°,^[5] and distorted in both α -type [3.0620(3)–3.1035(2) Å; 84.953(6)–94.944(6)°]^[17] and β -type [3.0084(7)–3.0702(8) Å; 88.236(19)–91.749(20)°].^[19] Such distortion is caused by the different connection motifs of the TSb₆ octahedra along the c direction as described above. On the other hand, different RE^{3+} cations barely influence the geometry, for example, in the series of β -RE-CoSb₃, from La to Sm, the shorter Sb3–Sb3 bond lengths change 1%, the longer Sb3–Sb3 bond lengths only change 0.9%, and the angular deviation is also negligible.

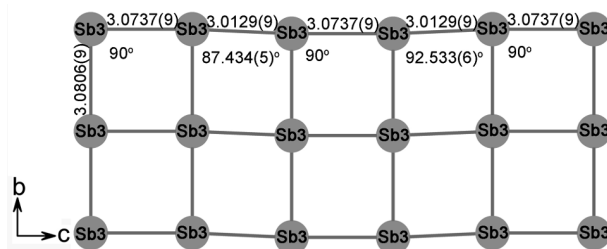


Figure 5. The Sb square nets in β -LaCoSb₃ in the bc -plane with angles and distances [Å] marked.

The structural comparison between β -RECoSb₃ and β -RENiSb₃ suggests that the different transition metal does not alter the crystallographic structure predominantly. The electronic structures have therefore been studied to give some insight into the physical properties.

Electronic Structure

The electronic structure for β -LaCoSb₃ was calculated with the TB-LMTO method. The band structure along the special symmetry lines Γ -X, Γ -Y, and Γ -Z is shown in Figure 6. Along Γ -Y, bands crossing the Fermi level are quite dispersed with contributions largely from the orbitals of either the Sb square net or Co/Sb layer extending along the b axis (Figure 7, parts a, b, d). The bands crossing the

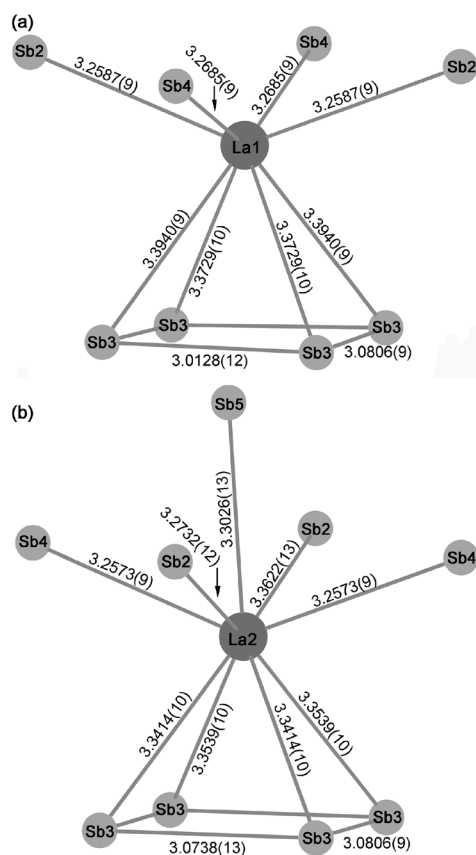


Figure 4. (a) La1 centered square antiprism. (b) La2 centered monocapped square antiprism. The La–Sb, and Sb3–Sb3 bond lengths less than 3.40 Å are indicated.

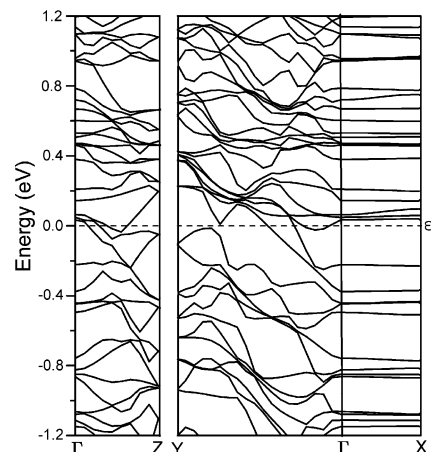


Figure 6. Band dispersion curves for β -LaCoSb₃ along Γ X, Γ Y, and Γ Z. The Fermi level ($\epsilon_f = 0$) is set at zero.

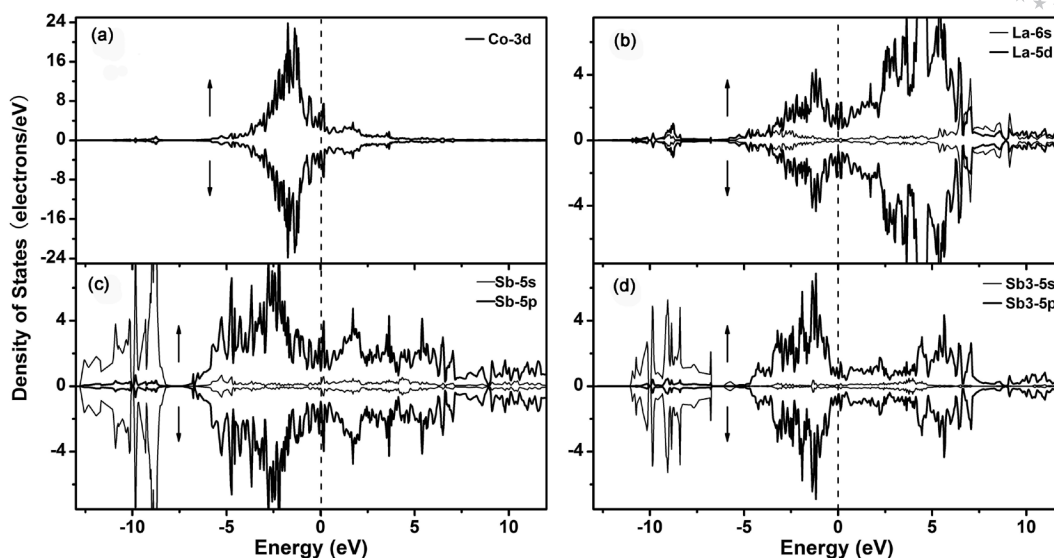


Figure 7. Spin-polarized densities of states (DOS) for β -LaCoSb₃. (a) Partial DOS of Co ions; (b) partial DOS of La cations; (c, d) partial DOS of Sb atoms from Co/Sb layer and Sb₃ atoms of Sb square net, respectively. The Fermi level is marked by a dashed line at 0 eV.

Fermi level along Γ -Z mainly correspond to the contributions of the layers of Co/Sb and Sb square net along the c axis. These features suggest that β -LaCoSb₃ should be metallic in both b and c directions. Meanwhile, the three types of RETSb₃ have similar electronic structures; therefore, their electronic properties should be comparable. This statement has been supported by the experimental measurements on β -LaNiSb₃ that displays metallic electrical conductivity from 1.8 K to 300 K along the b direction.^[19] And the parent-type LaCrSb₃ also exhibits metallic electrical conductivity from 20 K to 300 K along the c direction.^[7] As shown in Figure 6, the bands are flat along Γ -X and no band crosses the Fermi level, which is consistent with the existence of the intervening layers of La³⁺ ions that are weakly bonded to both the Sb net and Co/Sb layers. Therefore, RETSb₃ should show poor conductivity along the a axis. Such a prediction is worthy of further experimental measurement.

The spin-polarized calculations of the partial densities of states (DOS) of La, Co, and Sb atoms and the crystal orbital Hamilton population (COHP) curves for β -LaCoSb₃ are shown in Figure 7 and Figure 8. The Fermi level crosses partially filled bands in the DOS curve, which also indicates the metallic behavior. Most of the La states ($5d$ and $6s$) are unoccupied and locate above the Fermi level, as expected for an electropositive element. The hybridization of La $5d$ and Sb $5p$ states from -3 to 0 eV (Figure 7 b, c, d) implies some bonding character between La and Sb. For instance, La1-Sb bonds range from 3.2587(9) to 3.3940(9) Å, with the integrated $-COHP$ value varying from 1.017 to 0.837 eV/cell. Any La1-Sb bond longer than 3.50 Å is regarded as relatively weak because the integrated $-COHP$ value is only about half of the normal La1-Sb bonds. Similarly, the distances of La2-Sb bonds between 3.2573(9) and 3.3622(13) Å, with an average of 3.3098 Å are slightly

shorter, so the integrated $-COHP$ value of 0.909 eV/cell is larger than that of the La1 sphere. As shown in parts c and d of Figure 7, the partial DOS of Sb atoms in the Co/Sb layer are more delocalized than that of the square net, for example Sb $5p$ (-7 to 0 eV) vs. Sb₃ $5p$ (-4.5 to 0 eV), which illuminates that Sb atoms in the Co/Sb layer show abundant bonding interactions compared with that in the square net. In the region from -5 eV up to the Fermi level, a significant mixture of Co $3d$ and Sb $5p$ states implies the strong covalent character of Co-Sb bonds. As indicated by the COHP curves plotted in Figure 8 (b), the Co-Sb bonds (2.596–2.666 Å) within the CoSb₆ octahedra are almost optimized giving an integrated $-COHP$ value from 1.985 to 2.221 eV/cell. The Sb₃-Sb₃ bonds (3.0128–3.0806 Å) are covalent bonds with the integrated $-COHP$ value of 0.893–1.100 eV/cell. Any Sb-Sb distance beyond 3.3410 Å is not considered since the Sb1-Sb5 (3.3410 Å) only has an $-ICOHP$ about 12% of the strongest Sb₃-Sb₃ bond.

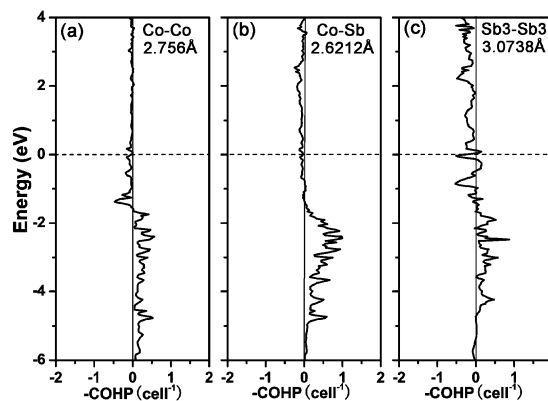


Figure 8. Crystal orbital Hamilton population curves for the Co-Co, Co-Sb, and Sb₃-Sb₃ in β -LaCoSb₃. The Fermi level is set at $\epsilon_F = 0$ eV.

The complex Sb substructure of β -LaCoSb₃ adds difficulty to charge formulation. A simple charge formulation would be $\text{La}^{3+}[\text{CoSb}_3]^{3-}$. The bond orders (v_{ij}) for the Sb atoms can be calculated by $v_{ij} = \exp[(2.80 - d_{ij})/0.37]$, where d_{ij} is the bond length in Å.^[35] The formal charges are thus calculated to be −1.9 for Sb1, −2.5 for Sb2, −1.0 for Sb3, −2.6 for Sb4, and −2.5 for Sb5, giving an overall negative charge of −5.75 per formula unit in β -LaCoSb₃. The calculated charge of Sb3 agrees well with that deduced from the Zintl–Klemm concept, i.e., four-bonded Sb3 atoms (Figure 5) in square nets is assigned to −1.^[2,34] This simple calculation reveals the apparent charge of Co as +2.75.

As shown in Figure 7 (a), the spin-up states (\uparrow) are almost the same as the spin-down states (\downarrow) around the Fermi level (the calculated magnetic moment is 0.000013 μ_{B}), indicating that β -LaCoSb₃ is not a spin-polarized compound. This also agrees with the diamagnetic behavior of Co atoms in many intermetallic compounds such as $\text{Ce}_3\text{Co}_4\text{Sn}_{13}$,^[36] $\text{RE}_5\text{Co}_4\text{Si}_{14}$ ($\text{RE} = \text{Ho}, \text{Er}, \text{Tm}, \text{Yb}$),^[37] $\text{RE}_6\text{Co}_{1.67}\text{Si}_3$ ($\text{RE} = \text{Ce}, \text{Nd}, \text{Gd}, \text{Tb}, \text{Dy}$).^[38] Our calculations allow us to make the statement that for the β -RETSb₃ series the rare-earth atoms are the only magnetic source. Such a statement has been substantiated by the isostructural β -CeNiSb₃ that shows an experimental effective magnetic moment close to the value for free Ce^{3+} cations.^[19] On the basis of these calculations and observations, the magnetism of β -RECoSb₃ should be identical to the corresponding Ni members. And the La members, β -LaCoSb₃ and β -LaNiSb₃, should be diamagnetic.

Conclusions

In summary, we have synthesized five new ternary β -type RECoSb₃ compounds with $\text{RE} = \text{La}, \text{Ce}, \text{Pr}, \text{Nd}, \text{and Sm}$.

The structure features the alternating layers of condensed CoSb₆ octahedra and square Sb nets, with interventional RE^{3+} cations. Electronic structure calculations on β -LaCoSb₃ show anisotropic metallic conductivities in both b and c directions that agree well with previous measurements. The conductivity in the a direction should be weak because of the intervention of RE^{3+} cations via weak bond interactions. The calculations also indicate no spin-polarization occurred around the Fermi level, which means that LaTSb₃ ($\text{T} = \text{Co}, \text{Ni}$) should be diamagnetic.^[19] And for other RE members, the magnetic rare-earth atoms are the only source for the magnetic properties. Therefore, the two series of β -type compounds, RECoSb₃ and RENiSb₃, should be identical in magnetism.

Experimental Section

Synthesis: The handling of all materials was carried out inside a N₂-filled glove box with controlled oxygen and moisture levels below 0.1 ppm. The rare-earth metals, La, Pr, Nd, and Sm (99.5% or higher, Huhhot Jinrui Rare Earth Co. Ltd), Ce foil (99.9%, Alfa Aesar), Co power (99.94%, Shanghai Guoyao group), Sb shot (99.999%, Alfa Aesar), and Sn shot (99.99%, Alfa Aesar) were used as received. Single crystals of β -RECoSb₃ ($\text{RE} = \text{La–Nd}, \text{Sm}$) were prepared with Sn flux. The stoichiometric elemental mixture of RE/Co/Sb (1:1:3 in molar ratio) and 0.3 g Sn was placed in an evacuated fused-silica tube, then flame-sealed under vacuum at 10^{-3} Pa. The sealed tubes were placed into a temperature-controlled tube furnace, heated at 640 °C for 1 d and 1050 °C for 3 d, and then cooled to room temperature over 8 d. The Sn flux was removed by hydrochloric acid, and the plate-like crystals were obtained after being washed with distilled water. These crystals were stable in air over a period of weeks.

The power samples were prepared with RE:Co:Sb ($\text{RE} = \text{La}, \text{Ce}, \text{Pr}, \text{Nd}, \text{and Sm}$) in 1:1:3.15 molar ratio (the excess of Sb was to

Table 1. Crystal data and structural refinements for β -RECoSb₃ ($\text{RE} = \text{La–Nd}, \text{Sm}$).

Chemical formula	LaCoSb ₃	CeCoSb ₃	PrCoSb ₃	NdCoSb ₃	SmCoSb ₃
Formula weight	563.09	564.30	565.09	568.42	574.57
Space group	<i>Pbcm</i> (No.57)	<i>Pbcm</i> (No.57)	<i>Pbcm</i> (No.57)	<i>Pbcm</i> (No.57)	<i>Pbcm</i> (No.57)
a [Å]	12.985(4)	12.829(8)	12.748(6)	12.651(5)	12.5530(13)
b [Å]	6.1603(18)	6.136(4)	6.131(3)	6.116(2)	6.1043(4)
c [Å]	12.166 (4)	12.109(7)	12.086(5)	12.073(4)	12.0267(12)
V [Å ³]	973.19(50)	953.14(10)	944.65(75)	934.13(57)	921.57(15)
Z	8	8	8	8	8
Crystal size [mm]	0.15/0.10/0.05	0.07/0.04/0.02	0.15/0.09/0.05	0.15/0.09/0.04	0.10/0.09/0.08
Temperature [K]	293(2)	293(2)	293(2)	293(2)	293(2)
ρ_{cal} [g/cm ³]	7.686	7.865	7.947	8.084	8.282
Radiation, λ [Å]	Mo- K_{α} , 0.71073	Mo- K_{α} , 0.71073	Mo- K_{α} , 0.71073	Mo- K_{α} , 0.71073	Mo- K_{α} , 0.71073
θ range [°]	3.14–27.48	3.18–27.42	3.20–27.47	3.22–27.47	3.25–27.47
Index ranges	$-16 \leq h \leq 16$ $-7 \leq k \leq 6$ $-14 \leq l \leq 15$	$-16 \leq h \leq 12$ $-7 \leq k \leq 7$ $-15 \leq l \leq 15$	$-16 \leq h \leq 16$ $-7 \leq k \leq 7$ $-13 \leq l \leq 15$	$-14 \leq h \leq 16$ $-7 \leq k \leq 7$ $-15 \leq l \leq 15$	$-16 \leq h \leq 7$ $-7 \leq k \leq 7$ $-15 \leq l \leq 15$
μ [mm ^{−1}]	28.171	29.351	30.293	31.319	33.221
R_{int}	0.0572	0.0375	0.0427	0.0643	0.0672
R_1/wR_2 [$I > 2\sigma(I)$] ^[a]	0.0316/0.0771	0.0232/0.0522	0.0256/0.0619	0.0457/0.1198	0.0326/0.0740
R_1/wR_2 (all data)	0.0355/0.0785	0.0275/0.0541	0.0279/0.0633	0.0463/0.1206	0.0385/0.0778
$\Delta\rho_{\text{max}}$ [e·Å ^{−3}]	2.929	1.265	1.827	4.004	2.576
$\Delta\rho_{\text{min}}$ [e·Å ^{−3}]	−3.329	−1.121	−1.951	−5.434	−2.349
Goodness of fit on F_o^2	1.094	1.092	1.158	1.184	1.094

[a] $R_1 = \sum |F_o| - |F_c| / \sum |F_o|$ for $F_o^2 > 2\sigma(F_o^2)$; $wR_2 = \sum [w(F_o^2 - F_c^2)] / \sum [w(F_o^2)^{1/2}]$, where $w = 1/[\sigma^2(F_o^2) + (AP)^2 + BP]$, and $P = (F_o^2 + 2F_c^2)/3$.

compensate for evaporative losses). The heating profile for each sample is 650 °C for 1 d and 950 °C for 8 d and then cooling to 300 °C at 5 °C/h before switching off the furnace. The X-ray diffraction analyses show the existence of the minor byproducts of CoSb_3 and CoSb_2 . With the purpose to obtain singular β - RE - CoSb_3 , the product was reground several times and pressed into a pellet, sealed in a silica tube, then heated at 900 °C for 8 d, and subsequently cooled to room temperature. Unfortunately, the byproducts, binary CoSb_3 and CoSb_2 (less than 10%), were irremovable by such treatment. The arc-melting technique yields β - RE - CoSb_3 as the major product together with minor CoSb_3 and CoSb_2 byproducts.

Similar reactions were carried out for other rare-earth metals with $RE = \text{Gd-Tm}$ and Y for proposed $RE\text{CoSb}_3$ analogs. However,

$RE\text{Co}_{1-x}\text{Sb}_2$ (HfCuSi_2 -type) with $RE = \text{Gd-Er}$ and Y were produced.^[39] When $RE = \text{Tm}$, binary TmSb was the main product.

In the diagram study of the $RE/\text{Co}/\text{Sb}$ ($RE = \text{Ce, Pr}$) system, two α -type compounds have been identified by XRD patterns, and their annealed temperatures are 400 °C and 600 °C, respectively.^[25,26] Therefore, β - $RE\text{CoSb}_3$ is thought to be a high-temperature stable phase.

Elemental Analysis: Microprobe elemental analysis was performed on some single crystals of $RE\text{CoSb}_3$, including the single crystals used for X-ray diffraction analyses. Spectra were collected on a field emission scanning electron microscope (FESEM, JSM6700F) equipped with an energy dispersive X-ray spectroscopy (EDX, Oxford INCA). The results indicated the presence of all three RE , Co ,

Table 2. Atomic positions, site symmetry, and U_{eq} values for β - $RE\text{CoSb}_3$ ($RE = \text{La-Nd, Sm}$).

Atom	Wyckoff site	x	y	z	$U_{eq} [\text{\AA}^2]^{[a]}$
LaCoSb₃					
La1	4c	0.70093(5)	1/4	0	0.00514(18)
La2	4d	0.30412(5)	0.27003(11)	3/4	0.00490(18)
Co1	8e	0.09764(8)	0.03739(17)	0.86327(7)	0.00630(2)
Sb1	4c	0.97285(5)	1/4	0	0.00630(2)
Sb2	4d	0.79080(5)	0.26224(12)	3/4	0.00590(2)
Sb3	8e	0.50200(3)	0.51089(8)	0.87632(3)	0.00622(18)
Sb4	4c	0.21487(6)	1/4	0	0.00580(2)
Sb5	4d	0.94380(5)	0.88966(12)	3/4	0.00640(2)
CeCoSb₃					
Ce1	4c	0.70037(4)	1/4	0	0.00566(13)
Ce2	4d	0.30463(4)	0.26810(7)	3/4	0.00561(13)
Co1	8e	0.10094(7)	0.03510(13)	0.86292(6)	0.00853(19)
Sb1	4c	0.97276(5)	1/4	0	0.00790(15)
Sb2	4d	0.78711(4)	0.25898(8)	3/4	0.00624(14)
Sb3	8e	0.50195(3)	0.50995(6)	0.87627(3)	0.00675(12)
Sb4	4c	0.21779(5)	1/4	0	0.00628(14)
Sb5	4d	0.94424(4)	0.88655(9)	3/4	0.00780(15)
PrCoSb₃					
Pr1	4c	0.70016(4)	1/4	0	0.00526(15)
Pr2	4d	0.30507(4)	0.26982(8)	3/4	0.00529(14)
Co1	8e	0.10118(7)	0.03578(14)	0.86290(6)	0.00680(2)
Sb1	4c	0.97269(5)	1/4	0	0.00678(16)
Sb2	4d	0.78561(5)	0.25959(9)	3/4	0.00568(16)
Sb3	8e	0.50209(3)	0.51054(6)	0.87628(3)	0.00616(15)
Sb4	4c	0.21956(5)	1/4	0	0.00575(16)
Sb5	4d	0.94333(4)	0.88860(9)	3/4	0.00701(16)
NdCoSb₃					
Nd1	4c	0.70015(6)	1/4	0	0.00640(3)
Nd2	4d	0.30479(6)	0.27282(11)	3/4	0.00620(3)
Co1	8e	0.10065(9)	0.0376(2)	0.86343(9)	0.00850(3)
Sb1	4c	0.97244(7)	1/4	0	0.00760(3)
Sb2	4d	0.78390(7)	0.26240(12)	3/4	0.00660(3)
Sb3	8e	0.50246(4)	0.51204(10)	0.87615(4)	0.00710(3)
Sb4	4c	0.22162(8)	1/4	0	0.00690(3)
Sb5	4d	0.94260(6)	0.89053(12)	3/4	0.00740(3)
SmCoSb₃					
Sm1	4c	0.69968(6)	1/4	0	0.00685(18)
Sm2	4d	0.30568(6)	0.27138(9)	3/4	0.00681(18)
Co1	8e	0.10342(11)	0.03549(18)	0.86301(9)	0.01070(3)
Sb1	4c	0.97241(8)	1/4	0	0.00890(2)
Sb2	4d	0.78138(8)	0.25914(11)	3/4	0.00720(2)
Sb3	8e	0.50244(5)	0.51076(8)	0.87615(4)	0.00769(19)
Sb4	4c	0.22393(8)	1/4	0	0.00730(2)
Sb5	4d	0.94300(7)	0.88831(12)	3/4	0.00900(2)

[a] U_{eq} is defined as one-third of the trace of the orthogonalized U_{ij} tensor.

Table 3. Selected interatomic distances [\AA] in $\beta\text{-RECoSb}_3$ ($RE = \text{La-Nd, Sm}$).

	LaCoSb ₃	CeCoSb ₃	PrCoSb ₃	NdCoSb ₃	SmCoSb ₃
RE1–Sb1	3.5308(14)	3.4950(2)	3.4743(18)	3.4447(17)	3.4237(12)
RE1–Sb2 ($\times 2$)	3.2587(9)	3.2258(18)	3.2125(13)	3.1997(10)	3.1773(5)
RE1–Sb3 ($\times 2$)	3.3729(10)	3.3392(14)	3.3226(12)	3.3052(11)	3.2846(8)
RE1–Sb3 ($\times 2$)	3.3940(9)	3.3568(14)	3.3412(11)	3.3256(11)	3.2988(8)
RE1–Sb4 ($\times 2$)	3.2685(9)	3.2425(18)	3.2317(14)	3.2141(10)	3.1992(4)
RE2–Co1	3.3379(13)	3.2774(16)	3.2676(14)	3.2581(15)	3.2198(14)
RE2–Sb2	3.2732(12)	3.2337(19)	3.2175(15)	3.1975(13)	3.1717(9)
RE2–Sb2	3.3622(13)	3.3381(19)	3.3349(15)	3.3173(14)	3.3124(9)
RE2–Sb3 ($\times 2$)	3.3414(10)	3.3087(14)	3.2887(12)	3.2732(11)	3.2462(8)
RE2–Sb3 ($\times 2$)	3.3539(10)	3.3172(14)	3.3015(11)	3.2879(11)	3.2610(8)
RE2–Sb4 ($\times 2$)	3.2573(9)	3.2277(18)	3.2146(13)	3.1994(10)	3.1797(5)
RE2–Sb5	3.3026(13)	3.2740(2)	3.2494(16)	3.2115(16)	3.2023(12)
Co1–Co1	2.756(2)	2.735(2)	2.7291(19)	2.739(2)	2.718(2)
Co1–Sb1 ($\times 2$)	2.5960(12)	2.5902(13)	2.5889(11)	2.5820(14)	2.5802(12)
Co1–Sb1 ($\times 2$)	2.6661(12)	2.6829(13)	2.6747(11)	2.6528(14)	2.6708(13)
Co1–Sb2 ($\times 2$)	2.6212(13)	2.6081(13)	2.6100(12)	2.6155(15)	2.6047(13)
Co1–Sb4	2.6076(12)	2.5963(13)	2.5977(11)	2.5979(14)	2.5919(13)
Co1–Sb5	2.5918(13)	2.5965(14)	2.5934(13)	2.5849(15)	2.5903(15)
Co1–Sb5	2.6265(14)	2.6183(15)	2.6197(13)	2.6144(15)	2.6125(13)
Sb1–Sb1 ($\times 2$)	3.1598(9)	3.1464(19)	3.1435(14)	3.1365(10)	3.1297(5)
Sb1–Sb4	3.1426(14)	3.1430(2)	3.1472(17)	3.1525(18)	3.1574(14)
Sb1–Sb5 ($\times 2$)	3.3410(1)	3.3166(17)	3.3164(13)	3.3172(10)	3.2985(5)
Sb2–Sb5	3.0356(12)	3.0472(15)	3.0358(13)	3.0338(14)	3.0398(12)
Sb3–Sb3	3.0128(12)	2.9994(19)	2.9940(15)	2.9947(14)	2.9825(10)
Sb3–Sb3	3.0738(13)	3.0580(2)	3.0526(15)	3.0460(14)	3.0344(10)
Sb3–Sb3 ($\times 2$)	3.0806(9)	3.0682(19)	3.0658(14)	3.0586(10)	3.0528(2)

and Sb elements in molar ratios (19–21% RE, 19–20% Co, 58–62% Sb) and no Sn element was detected, which is in good agreement with the stoichiometry refined from the single-crystal X-ray structure determinations.

Structure Determination: The single-crystal X-ray diffraction data were collected with a Rigaku Mercury CCD diffractometer equipped with a graphite-monochromated Mo- K_α radiation source ($\lambda = 0.71073 \text{ \AA}$) at 293 K. The absorption corrections were done by the Multi-scan method.^[40] The space group was determined to be *Pbcm* (No. 57) based on systematic absences, E-value statistics, and subsequent successful refinements of the crystal structure. The structures were solved without events by direct methods and refined by full-matrix least-squares fitting on F^2 by SHELXL-97.^[41] All of the atoms were refined with anisotropic thermal parameters. Crystallographic data and structural refinements are summarized in Table 1. Atomic coordinates and anisotropic displacement parameters are provided in Table 2. Table 3 gives the interatomic distances for $\beta\text{-RECoSb}_3$ ($RE = \text{La-Nd, Sm}$) for comparison.

Further data, in the form of a crystallographic information file (CIF) can be obtained from the Fachinformationszentrum Karlsruhe, Abt. PROKA, 76344 Eggenstein-Leopoldshafen, Germany (Fax: +49-7247-808-666; E-mail: crysdata@fiz.karlsruhe.de) on quoting the depository numbers: CSD-419540 (for LaCoSb₃), CSD-419539 (for CeCoSb₃), CSD-419542 (for PrCoSb₃), CSD-419541 (for NdCoSb₃), and CSD-419538 (for SmCoSb₃).

Electronic Structure Calculations: The electronic structure calculations for $\beta\text{-LaCoSb}_3$ were performed by the linear muffin-tin orbital method^[42] with the aid of the TB-LMTO program.^[43] Exchange and correlation were treated in the local density approximation (LDA).^[44] The basis set included the 4*f*, 5*d*, 6*s*, 6*p* orbitals for La, 3*d*, 4*s*, 4*p* orbitals for Co, and 4*f*, 5*s*, 5*p*, 5*d* orbitals for Sb. The La 6*p*, Co 4*p*, and Sb 4*f*, 5*d* orbitals were treated with the downfolding technique.^[45] The *k*-space integrations were performed

by the tetrahedron method^[46] using a $2 \times 2 \times 4$ *k*-mesh within the Brillouin zone. The Fermi level ($\epsilon_f = 0 \text{ eV}$) was selected as the energy reference.

Acknowledgments

The research was supported by the National Natural Science Foundation of China under Projects (20521101, 20773130, 20733003), “Key Project from Fujian Institute of Research on the Structure of Matter” (SZD08002), and the “Key Project from Chinese Academy of Sciences” (KJCX2-YW-H01).

- [1] A. M. Mills, R. Lam, M. J. Ferguson, L. Deakin, A. Mar, *Coord. Chem. Rev.* **2002**, 233–234, 207–222.
- [2] G. A. Papoian, R. Hoffmann, *Angew. Chem. Int. Ed.* **2000**, 39, 2408–2448.
- [3] S. M. Kauzlarich, *Chemistry, Structure and Bonding of Zintl Phases and Ions*, VCH Publishers, New York, **1996**.
- [4] A. S. Sefat, S. L. Bud'ko, P. C. Canfield, *J. Magn. Magn. Mater.* **2008**, 320, 120–141.
- [5] M. J. Ferguson, R. W. Hushagen, A. Mar, *J. Alloys Compd.* **1997**, 249, 191–198.
- [6] K. Hartjes, W. Jeitschko, M. Brylak, *J. Magn. Magn. Mater.* **1997**, 173, 109–116.
- [7] N. P. Raju, J. E. Greedan, M. J. Ferguson, A. Mar, *Chem. Mater.* **1998**, 10, 3630–3635.
- [8] L. Deakin, M. J. Ferguson, A. Mar, J. E. Greedan, A. S. Wills, *Chem. Mater.* **2001**, 13, 1407–1412.
- [9] L. Deakin, A. Mar, *Chem. Mater.* **2003**, 15, 3343–3346.
- [10] S. J. Crerar, L. Deakin, A. Mar, *Chem. Mater.* **2005**, 17, 2780–2784.
- [11] E. L. Thomas, D. P. Gautreaux, J. Y. Chan, *Acta Crystallogr., Sect. E* **2006**, 62, i96–i98.

- [12] A. Thamizhavel, H. Nakashima, T. Shiromoto, Y. Obiraki, T. D. Matsuda, Y. Haga, S. Ramakrishnan, T. Takeuchi, R. Settai, Y. Ōnuki, *J. Phys. Soc. Jpn.* **2005**, *74*, 2617–2621.
- [13] M. Brylak, W. Jeitschko, *Z. Naturforsch. B: Chem. Sci.* **1995**, *50*, 899.
- [14] M. Leonard, S. Saha, N. Ali, *J. Appl. Phys.* **1999**, *85*, 4759–4761.
- [15] M. L. Leonard, I. S. Dubenko, N. Ali, *J. Alloys Compd.* **2000**, *303–304*, 265–269.
- [16] D. D. Jackson, Z. Fisk, *J. Magn. Magn. Mater.* **2003**, *256*, 106–116.
- [17] R. T. Macaluso, D. M. Wells, R. E. Sykora, T. E. Albrecht-Schmitt, A. Mar, S. Nakatsuji, H. Lee, Z. Fisk, J. Y. Chan, *J. Solid State Chem.* **2004**, *177*, 293–298.
- [18] E. L. Thomas, R. T. Macaluso, H.-O. Lee, Z. Fisk, J. Y. Chan, *J. Solid State Chem.* **2004**, *177*, 4228–4236.
- [19] E. L. Thomas, D. P. Gautreaux, H. O. Lee, Z. Fisk, J. Y. Chan, *Inorg. Chem.* **2007**, *46*, 3010–3016.
- [20] D. P. Gautreaux, C. Capan, J. F. DiTusa, D. P. Young, J. Y. Chan, *J. Solid State Chem.* **2008**, *181*, 1977–1982.
- [21] Y. Verbovytsky, K. Latka, *J. Alloys Compd.* **2008**, *450*, 272–275.
- [22] A. Leithe-Jasper, P. Rogl, *J. Alloys Compd.* **1994**, *203*, 133–136.
- [23] L.-M. Zeng, S.-W. Wu, W. Qin, *Trans. Nonferrous Met. Soc. China* **1997**, *7*, 60–62.
- [24] G. Cordier, H. Schaefer, P. Woll, *Z. Naturforsch., Teil B* **1985**, *40*, 1097–1099.
- [25] R. M. Luo, F. S. Liu, J. Q. Li, X. W. Feng, *J. Alloys Compd.*, DOI:10.1016/j.jallcom.2008.03.061.
- [26] S. Chykhrij, V. B. Smetana, *Inorg. Mater.* **2006**, *42*, 503–507.
- [27] T. Chen, J. C. Mikkelsen, G. B. Charlan, *J. Cryst. Growth* **1978**, *43*, 5–12.
- [28] T. Schmidt, G. Kliche, H. D. Lutz, *Acta Crystallogr., Sect. C* **1987**, *43*, 1678–1679.
- [29] O. Sologub, K. Hiebl, P. Rogl, O. Bodak, *J. Alloys Compd.* **1995**, *227*, 40–43.
- [30] L. Zeng, X. Xie, H. F. Franzen, *J. Alloys Compd.* **2002**, *343*, 122–124.
- [31] O. Sologub, H. Noel, A. Leithe-Jasper, P. Rogl, O. I. Bodak, *J. Solid State Chem.* **1995**, *115*, 441–446.
- [32] H. Flandorfer, O. Sologub, C. Godart, K. Hiebl, A. Leithe-Jasper, P. Rogl, H. Noel, *Solid State Commun.* **1996**, *97*, 561–565.
- [33] R. Wang, H. Steinfink, *Inorg. Chem.* **1967**, *6*, 1685–1692.
- [34] E. Zintl, *Angew. Chem.* **1939**, *52*, 1–6.
- [35] W. Jeitschko, R. O. Altmeyer, M. Schelk, U. C. Rodewald, *Z. Anorg. Allg. Chem.* **2001**, *627*, 1932–1940.
- [36] E. Lyle Thomas, H.-O. Lee, A. N. Bankston, S. MaQuilon, P. Klavins, M. Moldovan, D. P. Young, Z. Fisk, J. Y. Chan, *J. Solid State Chem.* **2006**, *179*, 1642–1649.
- [37] J. R. Salvador, C. Malliakas, J. R. Gour, M. G. Kanatzidis, *Chem. Mater.* **2005**, *17*, 1636–1645.
- [38] B. Chevalier, E. Gaudin, F. Weill, *J. Alloys Compd.* **2007**, *442*, 149–151.
- [39] W.-Z. Cai, L. Chen, unpublished results.
- [40] R. Corp, *CrystalClear*, version 1.3.5, Woodlands, Texas (USA), **1999**.
- [41] G. M. Sheldrick, *SHELXL-97: Program for Crystal Structure Solution*, University of Göttingen, Göttingen (Germany), **1997**.
- [42] a) O. K. Andersen, *Phys. Rev. B* **1975**, *12*, 3060–3083; b) H. L. Skriver, *The LMTO Method*, Springer, Berlin (Germany), **1984**.
- [43] O. Jepsen, O. K. Andersen, *The Stuttgart TB-LMTO Program, Version 4.7*, Max-Planck-Institut für Festkörperforschung, Stuttgart (Germany).
- [44] U. von Barth, L. Hedin, *J. Phys. C* **1972**, *5*, 1629–1642.
- [45] W. R. L. Lambrecht, O. K. Andersen, *Phys. Rev. B* **1986**, *34*, 2439–2449.
- [46] P. E. Blöchl, O. Jepsen, O. K. Andersen, *Phys. Rev. B* **1994**, *49*, 16223–16233.

Received: August 21, 2008

Published Online: December 9, 2008

Nitrogen-Rich Compounds in Pyrotechnics: Alkaline Earth Metal Salts of 5,5'-Hydrazine-1,2-diylbis(1*H*-tetrazole)

Konstantin Karaghiosoff,^[a] Thomas M. Klapötke,^{*[a]} and Carles Miró Sabaté^[a]

Keywords: Nitrogen heterocycles / Nitrogen-rich compounds / Alkaline earth metals / Pyrotechnics

Alkaline earth metal (**2**: Mg, **3**: Ca, **4**: Sr, and **5**: Ba) salts with the nitrogen-rich 5,5'-hydrazine-1,2-diylbis(tetrazolate) anion (HBT²⁻) were synthesized in high purities and yields and fully characterized by spectroscopic and analytical methods. In addition, the crystal structures of the new compounds were determined by X-ray diffraction techniques. Whereas the tetrazole rings in **2** are twisted with respect to one another, as reported for compounds with the same anion, in the heavier-metal salts **3–5** there exists "apparent coplanarity" between the same rings due to disorder, which is discussed. A detailed description of the structures is given. The compounds, obtained as the hydrated species, are insensitive to friction, shock, and electrostatic discharge (BAM testing), but react vigorously in a flame upon loss of water to give the

characteristic flame color for the metal atom. Differential scanning calorimetry (DSC) measurements showed strong bonding of the water of crystallization, which is lost at temperatures equal to or above 130 °C, and great thermal stabilities with decomposition points above 220 °C without melting. Additionally, loss of water was determined by using thermal gravimetry (TG). Lastly, due to the prospective interest in metal salts containing the HBT²⁻ anion as energetic materials, their constant-volume energies of combustion were measured experimentally by bomb calorimetry and their heats of formation were back-calculated from these results.

(© Wiley-VCH Verlag GmbH & Co. KGaA, 69451 Weinheim, Germany, 2009)

Introduction

The chemistry of nitrogen-rich compounds is taking large steps toward the development of new, environmentally friendly energetic materials for use as gas generators,^[1–3] blowing agents,^[2–3] primary explosives,^[4] or ingredients in pyrotechnic and propellant mixtures.^[5] Most currently used stab- and percussion-sensitive mixtures consist of a primary explosive and 2–5% tetrazene (Figure 1). A major problem

with the use of tetrazene as an energetic sensitizer is its poor thermal stability, which leads to depletion and loss of activity.^[6] Pyrotechnics have multiple applications in many diverse fields such as fireworks, airbags, fire extinguishers, (road) flares, matches, or production of nanoporous foams and propellants. Pyrotechnic compositions are generally made up of an oxidizer, a reducing agent, (optionally) a binder, a propellant, coloring agents, and sound- or smoke-producing agents.^[7]

Tetrazene^[8] and tetrazole-based (Figure 1)^[9] energetic compounds are emerging as nitrogen-rich materials with interesting properties. The potential of the 5,5'-azotetrazolate anion to generate nitrogen-rich, highly endothermic metal salts with good performance and high thermal stability has been reported in different studies.^[10–11]

Recently, we reported the synthesis and energetic properties of 5,5'-hydrazine-1,2-diylbis(1*H*-tetrazole) (HBT),^[12] which has a nitrogen content of 83.4%, is thermally stable above 200 °C, and has a high detonation velocity comparable to some of the highest-performing energetic compounds, while being less sensitive.^[13]

As early as 1898, Thiele^[14] described the reduction of the azo bridge in the 5,5'-azotetrazolate anion to form the 5,5'-hydrazine-1,2-diylbis(tetrazolate) anion (HBT²⁻). Some metal salts of the latter have been studied by DSC.^[15] They reveal good thermal stabilities and could be prospectively used as primary explosives and sensitizers^[16] or as ingredients in pyrotechnic mixtures.^[5] Apart from our earlier study

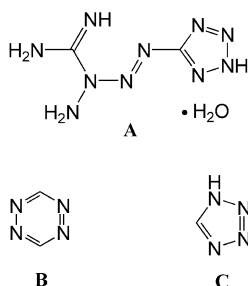


Figure 1. Structural formulas of tetrazene hydrate (A), 1,2,4,5-tetrazine (B), and 5*H*-tetrazole (C).

[a] Department of Chemistry and Biochemistry, Energetic Materials Research, Ludwig-Maximilians-Universität, Butenandstr. 5–13, 81377 München, Germany
Fax: +49-89-2180-77492
E-mail: tmk@cup.uni-muenchen.de

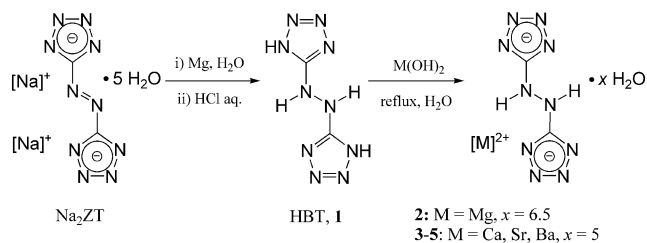
Supporting information for this article is available on the WWW under <http://www.eurjic.org/> or from the author.

on salts containing the HBT^{2-} anion,^[17] no systematic characterization of its metal salts has been performed to date, and only two crystal structures of compounds with the HBT^{2-} anion have been reported. In addition, the potential of such compounds for energetic applications remains to be investigated. Here we would like to report on the synthesis, full analytical and spectroscopic characterization, energetic properties, and X-ray structures of alkaline earth metal salts of HBT.

Results and Discussion

Synthesis

Sodium 5,5'-azotetrazolate pentahydrate^[14] was reduced with magnesium powder. After acid work-up, a white, powdery precipitate of 5,5'-hydrazine-1,2-diylbis(1*H*-tetrazole) (HBT, **1**) formed.^[12] Initially, we prepared the barium salt **5** by two independent methods starting from HBT. The method described in the literature using the sodium salt^[15] gives the product in a low isolated yield (19%). Therefore, an alternative method was developed: **1** was boiled with barium hydroxide in aqueous solution. The method could be extrapolated to synthesize the rest of the metal salts in this study (see **2–4** in Scheme 1).



Scheme 1. Synthesis of alkaline earth metal salts **2–5**.

All compounds were fully characterized by vibrational (IR and Raman) and NMR (^1H and ^{13}C) spectroscopy, elemental analysis, mass spectrometry, and differential scanning calorimetry (DSC). All materials are readily soluble in polar solvents such as water, dmf, or dmsO, they are soluble in hot alcohol and insoluble in less polar or apolar solvents such as acetone, acetonitrile, or ether. Lastly, crystals of the compounds suitable for X-ray analysis were obtained from slow cooling of a solution of the corresponding salt in hot water or by storing in the refrigerator overnight (see Exp. Section).

Vibrational Spectroscopy

The Raman and IR spectra of alkaline earth metal salts of HBT are represented in Figure 2. Both IR and Raman spectra of **3–5** (with some variation in the shifts) look almost identical, whereas those of the magnesium salt **2** are the most different, as expected because of the changes in the crystal structure of the magnesium salt with respect to that of the remainder of the compounds (see the section “Molecular Structures”). The most intense signals in the IR

spectra of alkaline earth metal salts of HBT are broad bands in the X–H (X = O and N) region between ca. 3600 and 2800 cm^{-1} (ca. 3600–2600 cm^{-1} for **2**), corresponding to the stretching modes of the water of crystallization and hydrazine-bridge (observed) protons. In addition, the in-plane carbon–hydrazine–nitrogen stretch (C1–N5 and C2–N10) is observed at about 1630 cm^{-1} (Raman inactive), and the deformation modes (in-plane and out-of-plane) for the hydrazine moiety and ring C–N and N–N stretching modes are observed in the range between 1540 and 1380 cm^{-1} , the ring N–N stretching modes all being found in the region to about 1020 cm^{-1} . In the Raman spectra, the most intense signal corresponds to stretching modes in the tetrazole rings at about 1070 cm^{-1} (hydrazine-bridge deformation mode at 1530 cm^{-1} for **2**). In addition, many other bands of lower intensity can be observed in both IR and Raman spectra, which can be assigned as follows: 735–750 cm^{-1} [$\omega(\text{HN–NH})$], ca. 845 cm^{-1} [$\delta(\text{HN–NH})_{\text{ip}}$], ca. 1020 cm^{-1} [$\nu(\text{C–N})_{\text{ring}}$], ca. 1070 cm^{-1} [$\nu(\text{C–N–N})_{\text{ring}}$ and $\nu(\text{N–N})_{\text{ring}}$], ca. 1130 cm^{-1} [$\nu(\text{N–N})_{\text{ring}}$], ca. 1370 cm^{-1} [$\delta(\text{HN–NH})_{\text{ip}}$ and $\nu(\text{N–N})_{\text{ring}}$], 1384 cm^{-1} [$\delta(\text{HN–NH})_{\text{oop}}$ and $\nu(\text{N–N})_{\text{ring}}$], 1450–1460 cm^{-1} [$\delta(\text{HN–NH})_{\text{ip}}$ and $\nu(\text{N–N})_{\text{ring}}$], 1530–1540 cm^{-1} [$\delta(\text{HN–NH})_{\text{ip}}$ and $\nu(\text{C–N})_{\text{ring}}$], ca. 1630 cm^{-1} [$\nu(\text{C}_{\text{ring}} - \text{N}_{\text{hydr.}})_{\text{ip}}$].^[3b,18]

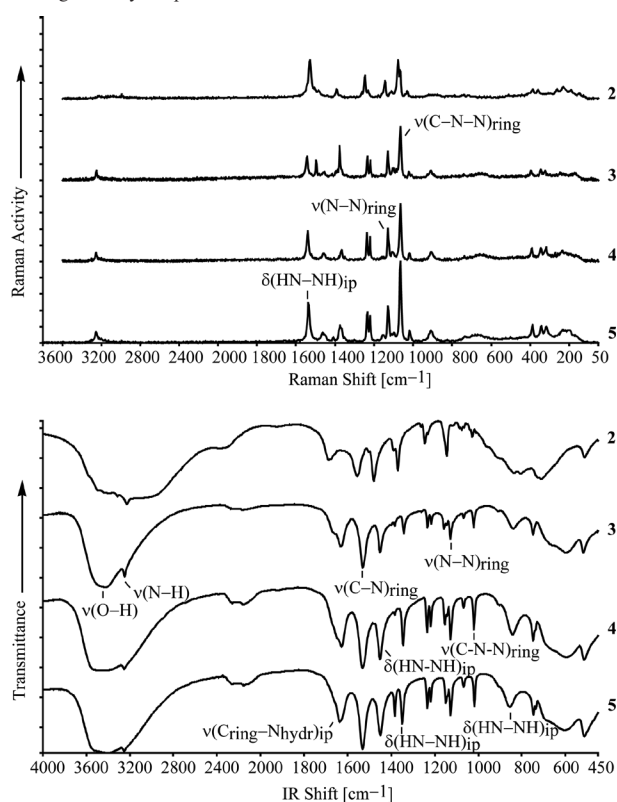


Figure 2. Vibrational spectra: panel plots for alkaline earth metal salts **2–5** [Raman (top) and IR (bottom)].

NMR Spectroscopy

The ^1H NMR spectrum of compounds **2–5** in $[\text{D}_6]\text{dmsO}$ shows two sharp signals, at ca. 7.0 and ca. 4.0 ppm, corre-

sponding to the resonances of the hydrazine hydrogen atoms and the protons of the water molecules of crystallization, respectively. The hydrazine protons are shifted to lower field with respect to the metal hydrazinates reported in the literature containing the same anion, which resonate at ca. 3.5 ppm.^[17] In the ^{13}C NMR spectrum, the resonance of the tetrazolate-ring carbon atoms is found at ca. 167 ppm ($\delta = 166.2$ ppm for **2**), which is well below the resonances at ca. 173 ppm found for the carbon atoms in metal 5,5'-azotetrazolate salts.^[11a] Both ^1H and ^{13}C NMR shifts are in agreement with our previously published results.^[12a,17] No signals were observed in the ^{14}N NMR spectra of any of the compounds, and the compounds were too insoluble to obtain ^{15}N NMR spectra. The lack of protons in the vicinity of nitrogen atoms did not allow the resonances of the tetrazole-ring nitrogen atoms in the ^{15}N solid-state NMR spectrum of **5** to be observed. The only resonance observed in the solid state was that of the hydrazine nitrogen atoms ($\delta = -297$ ppm).

Figure 3 shows the ^{13}C NMR spectrum of the strontium salt (**4**) at different times in $[\text{D}_6]\text{dmsO}$. When the pure compound is dissolved in $[\text{D}_6]\text{dmsO}$, the solvent turns slightly yellow as it dissolves, indicating oxidation to the azo compound (SrZT). However, the ^{13}C NMR spectrum looks clean, and after 1 day, a resonance at ca. 173 ppm starts to become visible. This signal increases in intensity with time, and the initial signal at ca. 167 ppm ends up disappearing, which indicates full oxidation of the HBT to the ZT salt.

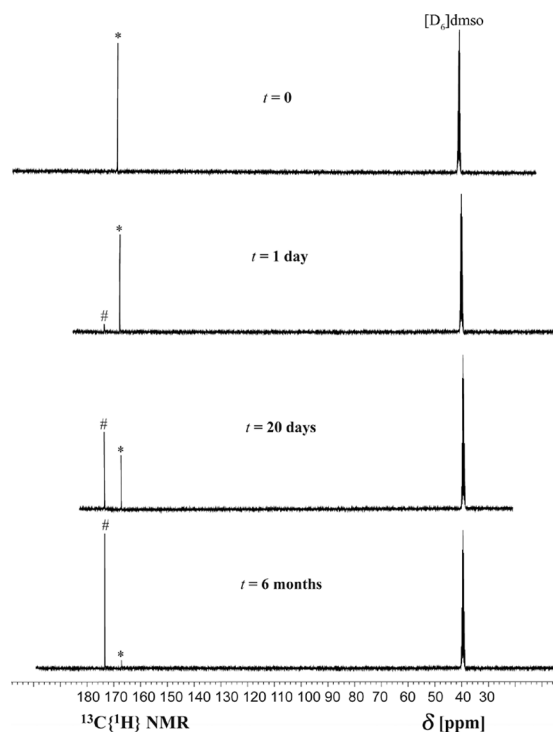


Figure 3. Monitoring of the oxidation of **4** to the 5,5'-azotetrazolate salt (SrZT) by $^{13}\text{C}\{^1\text{H}\}$ NMR spectroscopy in $[\text{D}_6]\text{dmsO}$ (# and * denote SrZT and **4**, respectively).

Molecular Structures

Crystals of the HBT salts **2–5** were obtained as described in the Experimental Section. The X-ray crystallographic data of the compounds were collected with an Oxford Diffraction Xcalibur 3 diffractometer equipped with a CCD detector using graphite-monochromated $\text{Mo-K}\alpha$ radiation ($\lambda = 0.71073$ Å). A multiscan absorption correction was applied to all data sets.^[19a] The structures were solved by direct methods (SHELXS-97 and SIR97) and refined by means of full-matrix least-squares procedures with SHELXL-97.^[19b,19c] Crystallographic data are summarized in Table 6. Selected bond lengths, angles, and hydrogen-bonding geometries are reported in Tables 1, 2, and 4, respectively. In addition, the geometry for the coordination around the cations is tabulated in the Supporting Information (Tables S1–S4). All non-hydrogen atoms were refined anisotropically. All calculations were carried out with the program package G03W.^[20] The structure and frequency calculations were performed with Becke's B3 three-parameter hybrid functional by using the LYP correlation function (B3LYP) and are tabulated in Table 3.^[21] For all H, C, N, and O atoms, a correlation-consistent polarized double-zeta basis set was used (cc-pVDZ).^[22]

The N–N bond lengths in the tetrazolate rings of alkaline earth metal salts **2–5** [1.299(2)–1.366(2) Å] are between N–N single bonds (1.454 Å) and N=N double bonds (1.245 Å)^[23] (Table 1). This indicates conjugation of the negative charge throughout the aromatic rings as seen in the crystal structures of other salts containing the HBT^{2–} anion.^[17] The distances between the two bridging nitrogen atoms [N5–N5ⁱⁱⁱ 1.422(8)–1.432(2) Å and N6–N6^{iv} 1.428(3)–1.442(2) Å] are relatively long (N–N single bond 1.454 Å),^[23] longer than the analogous N–N distances observed in the free acid HBT [1.391(2) Å]^[14] by ca. 0.06 Å, in which no conjugation between the two aromatic rings and the bridging nitrogen atoms is observed. Lastly, the coordination numbers and distances described below are in keeping with salts with anionic nitrogen heterocycles and compounds with alkaline earth metals.^[4a,11a,24]

Compound **5**, in analogy to **3** and **4**, crystallizes in the orthorhombic crystal system in the space group $Pnmm$ with four formula units and with five water molecules each in the unit cell (Table 6). The barium atoms lie on special positions so that half of the water molecules can be generated by symmetry [symmetry code: (i) $x, y, 2 - z$]. Due to the heavy barium atoms in **5**, the hydrogen atoms of the hydrazine bridge could not be found in the difference Fourier map. In the solid state (see Figure 4), "coplanarity" between the two tetrazole rings in the anions is observed, which is in contrast with other previously reported compounds containing the HBT moiety.^[12,17] Calculations were done in order to confirm the "apparent coplanarity" of the two rings. Table 3 presents the computational results obtained for the gas-phase structure of the 5,5'-azotetrazolate anion (ZT^{2-}), 5,5'-azotetrazole (H_2ZT) (see Supporting Information, Figure S1), the nonplanar (HBT^{2-}) and planar (HBT^{2-} planar) 5,5'-hydrazine-1,2-diylbis(tetrazolate) anion, and planar

Table 1. Selected bond lengths [\AA] for alkaline earth metal salts **2–5**.

	2		3	4	5
	A	B			
N1–N2 ^(a)	1.366(2)	1.363(2)	1.352(2)	1.345(3)	1.347(6)
N2–N3	1.299(2)	1.308(2)	1.306(2)	1.306(3)	1.301(6)
N3–N4	1.364(2)	1.352(2)	1.354(2)	1.356(3)	1.361(6)
N4–C1 ^(a)	1.341(2)	1.334(2)	1.328(2)	1.328(3)	1.316(6)
C1–N1	1.337(2)	1.329(2)	1.341(2)	1.342(3)	1.333(6)
C1–N5	1.388(2)	1.405(2)	1.391(3)	1.391(3)	1.397(6)
N5–N5 ⁱⁱⁱ (b)	1.432(2)		1.426(3)	1.423(4)	1.422(8)
N6–N6 ^{iv} (b)		1.442(2)	1.428(3)	1.432(4)	1.431(9)
N6–C2	1.407(2)	1.407(2)	1.397(2)	1.390(3)	1.392(6)
C2–N7	1.335(2)	1.327(2)	1.330(2)	1.330(3)	1.324(6)
N7–N8 ^(c)	1.356(2)	1.356(2)	1.362(2)	1.361(3)	1.344(6)
N8–N9	1.305(2)	1.311(2)	1.300(2)	1.301(3)	1.307(6)
N9–N10 ⁱⁱ (d)	1.361(2)	1.351(2)	1.349(2)	1.351(3)	1.344(6)
C2–N10 ⁱⁱ (e)	1.332(2)	1.332(2)	1.338(2)	1.343(3)	1.336(6)

2: (a–e) no symmetry codes, N5–N5ⁱⁱⁱ = N5–N6 and N6–N6^{iv} = N15–N16. **3:** (b) (iii) $-x, -y, -z$; (iv) $-x, 1-y, -z$. (d) (ii) $-x, -y, -z$. (e) (ii) $-x, -y, -z$. **4:** (b) (iii) $1-x, 1-y, -z$; (iv) $-x, -y, -z$. (c) (ii) $-x, 1-y, -z$. (e) (ii) $-x, 1-y, -z$; **5:** (a) (ii) $1-x, 1-y, -z$; N1–N2ⁱⁱ. (b) (iii) $1-x, -y, -z$; (iv) $2-x, 1-y, -z$.

Table 2. Selected bond angles [$^\circ$] for alkaline earth metal salts **2–5**.

	2		3	4	5
	A	B			
N1–C1–N5	125.9(2)	125.2(2)	123.4(2)	123.1(2)	122.7(4)
N2–N3–N4	109.7(1)	110.0(1)	109.7(1)	109.7(2)	109.6(4)
N7–C2–N6	124.6(2)	125.0(2)	123.3(2)	124.0(2)	125.3(4)
C2–N7–N8 ^(a)	102.7(1)	103.5(1)	103.4(1)	103.6(2)	104.0(4)
N9–N8–N7 ^(a)	110.7(1)	109.9(1)	109.9(1)	110.1(2)	109.7(4)
C1–N5–N5 ⁱⁱⁱ (b)	111.1(1)	111.2(1)	112.1(2)	112.3(2)	112.6(5)
C2–N6–N6 ^{iv} (b)	112.0(1)	112.3(1)	112.6(2)	112.7(2)	111.6(5)
N8–N9–N10 ⁱⁱ (c)	109.2(1)	109.2(1)	109.9(1)	109.5(2)	109.8(4)
C2–N10–N9 ⁱⁱ (c)	103.5(1)	104.1(1)	103.8(1)	104.0(2)	103.6(4)
N6–C2–N10 ⁱⁱ (d)	121.6(2)	121.7(2)	123.6(2)	123.4(2)	121.9(4)
N7–C2–N10 ⁱⁱ (d)	113.7(2)	113.1(2)	112.9(2)	112.6(2)	112.9(4)
N3–N4–C1 ^(e)	103.6(1)	103.6(1)	103.6(1)	103.5(2)	103.7(4)
N1–C1–N4 ^(e)	112.9(2)	113.3(2)	113.2(2)	113.0(2)	113.1(4)
N5–C1–N4 ^(e)	120.9(2)	121.3(2)	123.2(2)	123.9(2)	124.2(4)
N3–N2–N1 ^(e)	110.2(1)	109.4(1)	110.2(1)	110.1(2)	109.6(4)
C1–N1–N2 ^(e)	103.3(1)	103.6(1)	103.1(1)	103.5(2)	103.9(4)
N1–C1–N5–N5 ⁱⁱⁱ (b)	–168.9(2)	–163.1(2)	180.0(1)	180.0(2)	180.0(3)
N7–C2–N6–N6 ^{iv} (b)	–151.1(2)	–146.7(2)	180.0(1)	180.0(2)	180.0(3)

2: (a–e) no symmetry codes, N5ⁱⁱⁱ = N6 and N6^{iv} = N16. **3:** (b) (iii) $-1-x, -y, -z$; (iv) $-x, 1-y, -z$. (c) (ii) $-x, -y, -z$. (d) (ii) $-x, -y, -z$. **4:** (e) (ii) $-x, 1-y, -z$. (b) (iii) $1-x, 1-y, -z$; (iv) $-x, -y, -z$. (c) (ii) $-x, 1-y, -z$. **5:** (a) (iii) $1-x, -y, -z$; (iv) $2-x, 1-y, -z$. (e) (ii) $1-x, 1-y, -z$.

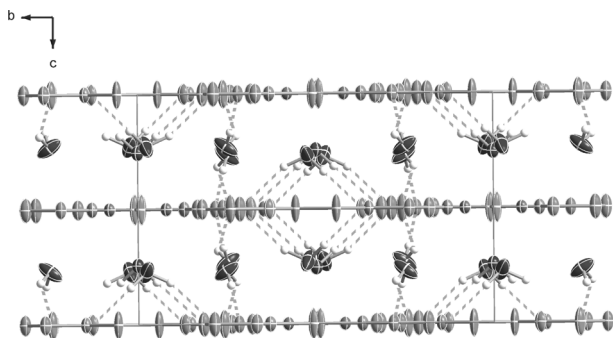


Figure 4. View of the unit cell of compound **5** along the a axis, showing planar parallel layers of anions connected through hydrogen bonds (dotted lines) to water molecules.

(HBT, C_{2h}) and nonplanar (HBT, C_1) 5,5'-hydrazine-1,2-diylbis(1*H*-tetrazole) (see Figure 5). Four of the six computed structures are true minima (TM), i.e. the number of imaginary frequencies equals zero. These results are in agreement with the previously reported structures of 5,5'-azotetrazolates salts,^[11] 5,5'-azotetrazole,^[25] 5,5'-hydrazine-1,2-diylbis(tetrazolate) salts,^[17] and 5,5'-hydrazine-1,2-diylbis(1*H*-tetrazole),^[12] which show planarity of the two tetrazole rings in the case of the azo compounds and torsion angles ranging from ca. 53° (Ba^{2+}) and ca. 86° (hydrazinium) in the HBT^{2-} salts to ca. 115° for neutral HBT. When the structure of HBT is optimized so that it has a planar geometry, i.e. C_{2h} symmetry, one negative frequency is found, and the structure in which both tetrazole rings are planar is a transition state (TS) in the gas phase. Lastly, the

Table 3. Computational results (B3LYP/cc-pVDZ).

	ZT ²⁻	H ₂ ZT	HBT ²⁻	HBT ²⁻ , planar	HBT, C _{2h}	HBT, C ₁
–E [a.u.]	623.631700	624.808041	624.839139	624.822819	626.015826	626.034231
E _{rel.} [kcal mol ^{–1}]			0.0	10.2	11.5	0.0
Point group	C _{2h}	C _{2h}	C _i	C _{2h}	C _{2h}	C ₁
NIMAG	0	0	0	2, –568, –558 cm ^{–1}	1, –59 cm ^{–1}	0
zpe [kcal mol ^{–1}]	36.3	52.6	52.0	50.4	67.5	68.2
d(N–N) [Å]	1.270	1.267	1.474	1.406	1.479	1.424
τ(CNNC) [°] ^[a]	180.0	180.0	180.0	180.0	180.0	85.6
τ(NCNC) [°] ^[a]	0.0	0.0	47, –139	0	62.8	145, –38, 90, –90
μ [D]	0.0	0.0	0.0	0.0	0.0	6.7
Stationary point ^[b]	TM	TM	TM	SP-2	TS	TM

[a] τ: torsion angle. [b] Stationary points: TM: true minimum, TS: transition state, SP-*n*: saddle point of *n*th order.

optimized structure of the HBT²⁻ anion in which both rings are coplanar shows two negative frequencies, which indicates that, in the gas phase, this is a saddle point of second order and not the most stable conformation.

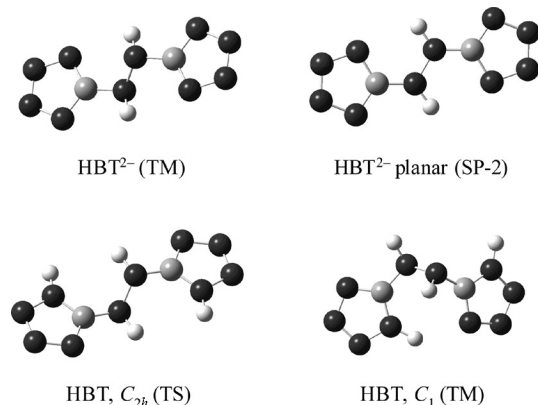


Figure 5. Optimized structures (B3LYP/cc-pVDZ) of HBT²⁻, HBT²⁻ planar, HBT C_{2h}, and HBT C₁.

As represented in Figure 4, the layers of anions are connected to one another by strong, very directional hydrogen bonds (see Table 4) to water molecules [O2...N4^{vii} 2.900(1) Å; symmetry code: (vii) 0.5 + *x*, 0.5 – *y*, 2.5 – *z*]. The water molecules form hydrogen bonds to the ring nitrogen atoms of the tetrazolate anion from the top and from the bottom in five out of the eight ring nitrogen atoms with distances between 2.9 and 3.0 Å and angles between 147(1) and 176(2)°. The coordination of the water molecules is similar to that found in metal 5,5'-azotetrazolate salts.^[3a] The hydrazine-bridge nitrogen atoms are not involved in any hydrogen-bonding interaction. The next electronegative atom that would be available to form a hydrogen bond is O2, placed at more than 3.5 Å away from N5 (sum of the van der Waals radii: *r*_O + *r*_N = 3.07 Å).^[26] There is no indication in the structure for the presence of hydrogen bonds involving the nitrogen atoms at the hydrazine bridge, which is in contrast with the HBT²⁻ salts reported, in which strong hydrogen bonds to the hydrazine hydrogen atoms are always present.^[12,17] The hydrogen-bonding networks identified by

Table 4. Geometry for selected hydrogen bonds for alkaline earth metal salts 2–5.

D–H...A	D–H [Å]	H...A [Å]	D...A [Å]	D–H...A [°]
2				
O9–H9A...O13	0.84(2)	1.90(3)	2.708(2)	159(2)
O4–H4A...O13	0.89(3)	1.83(3)	2.717(2)	169(3)
O3–H3B...N16	0.83(2)	2.13(2)	2.956(3)	177(2)
O6–H11B...N11	0.91(3)	1.80(3)	2.706(2)	176(2)
N16–H16...O2 ⁱⁱ	0.86(2)	2.36(2)	3.219(2)	175(2)
N15–H15...O10 ⁱⁱⁱ	0.87(2)	2.53(2)	3.233(3)	138(2)
N15–H15...O11 ⁱⁱⁱ	0.87(2)	2.44(2)	3.199(2)	147(2)
O2–H2B...N13 ^v	0.85(2)	1.94(2)	2.782(2)	168(2)
O5–H5A...N20 ^{vi}	0.88(2)	1.85(2)	2.729(2)	174(2)
O10–H2B...N12 ^{ix}	0.88(3)	1.86(3)	2.733(2)	172(2)
O9–H9B...N15 ^x	0.82(2)	2.10(2)	2.926(3)	179(2)
O3–H3A...N18 ^x	0.83(2)	1.95(2)	2.770(2)	175(2)
3				
O1–H1...N3 ⁱ	0.88(2)	2.04(2)	2.922(1)	175(2)
O2–H2A...N4 ⁱ	0.87(2)	2.01(2)	2.880(1)	176(2)
O2–H2B...N8 ⁱⁱ	0.81(2)	2.10(2)	2.906(2)	172(2)
O3–H3B...N7 ⁱⁱ	0.86(2)	2.04(2)	2.901(2)	179(2)
O3–H3A...N2 ⁱⁱⁱ	0.82(2)	2.14(2)	2.936(2)	161(2)
4				
O3–H3B...N4 ⁱ	0.84(3)	2.05(3)	2.886(2)	176(2)
O3–H3A...N8 ⁱⁱ	0.77(3)	2.18(3)	2.934(2)	167(2)
O1–H1B...N7 ⁱⁱⁱ	0.81(3)	2.09(3)	2.901(2)	180(3)
O2–H2...N3 ^{iv}	0.80(2)	2.14(2)	2.935(2)	176(2)
O1–H1A...N2 ^v	0.71(3)	2.30(3)	2.978(2)	158(3)
O1–H1A...O3 ^{vi}	0.71(3)	2.65(3)	3.072(2)	120(2)
5				
O3–H3A...N6	0.83(1)	2.06(1)	2.900(1)	176(1)
O3–H3B...N3 ⁱⁱⁱ	0.85(1)	2.25(1)	2.983(1)	147(1)
O1–H1A...N7 ^v	0.84(1)	2.08(1)	2.933(1)	174(2)
O1–H1B...N7 ^{vi}	0.85(1)	2.10(1)	2.910(1)	169(2)
O2–H2A...N4 ^{vii}	0.86(1)	2.06(1)	2.900(1)	176(2)
O2–H2B...N8 ^{viii}	0.84(1)	2.30(1)	3.051(1)	151(1)

Symmetry codes for **2**: (ii) +*x*, *y*, *z*; (iii) –*x*, 1 – *y*, 1 – *z*; (v) 1 – *x*, 1 – *y*, 2 – *z*; (vi) 1 + *x*, *y*, *z*; (ix) *x*, *y*, –1 + *z*; (x) 1 – *x*, 1 – *y*, 1 – *z*; **3**: (i) 0.5 – *x*, –0.5 + *y*, 0.5 – *z*; (ii) 0.5 + *x*, 0.5 – *y*, 0.5 + *z*; (iii) –0.5 + *x*, 0.5 – *y*, 0.5 + *z*; **4**: (i) 0.5 – *x*, 0.5 + *y*, 0.5 + *z*; (ii) 0.5 + *x*, 0.5 – *y*, 0.5 – *z*; (iii) 0.5 – *x*, –0.5 + *y*, –0.5 + *z*; (iv) –0.5 + *x*, 0.5 – *y*, 0.5 – *z*; (v) –0.5 + *x*, 0.5 – *y*, –0.5 – *z*; (vi) –0.5 + *x*, 0.5 – *y*, –0.5 + *z*; **5**: (iii) 0.5 + *x*, 0.5 – *y*, 1.5 – *z*; (v) *x*, *y*, 1 + *z*; (vi) 1 – *x*, 1 – *y*, –1 + *z*; (vii) 0.5 + *x*, 0.5 – *y*, 2.5 – *z*; (viii) 1 – *x*, 1 – *y*, 1 + *z*.

RPLUTO^[27] are of the type D1,1(2), some of which are part of other D1,2(3) and D2,2(*X*) (*X* = 8, 10) dimeric interactions. One forms a C2,2(11) chain pattern and an R2,4(8) motif (all of them at the primary level). The ring motif is formed by two water molecules connecting two anions [O1...N7^{vi} 2.910(1) Å; symmetry code: (vi) 1 - *x*, 1 - *y* - 1 + *z*]. In addition, there exists a characteristic graph-set for this salt of the type D2,1(3) formed by a water molecule, which forms hydrogen bonds to a nitrogen atom of the anion [O3...N6 2.900(1) Å] and to another water molecule [O3...N3ⁱⁱⁱ 2.983(1) Å; symmetry code: (iii) 0.5 + *x*, 0.5 - *y*, 1.5 - *z*]. At the secondary level, the only graph-sets found by the program are finite chains with the label D2,2(*X*) (*X* = 4, 5, 9, 10). Lastly, the coordination number around the metal center in **5** is nine (Figure 6, Table 4) and is completed by interaction to six water molecules (half of which are generated by symmetry) and three tetrazolate rings. The distances between the water oxygen atoms and the barium atoms vary between 2.737(1) and 2.871(1) Å, whereas the distances to the nitrogen atoms are slightly longer [2.962(1) to 2.990(1) Å].

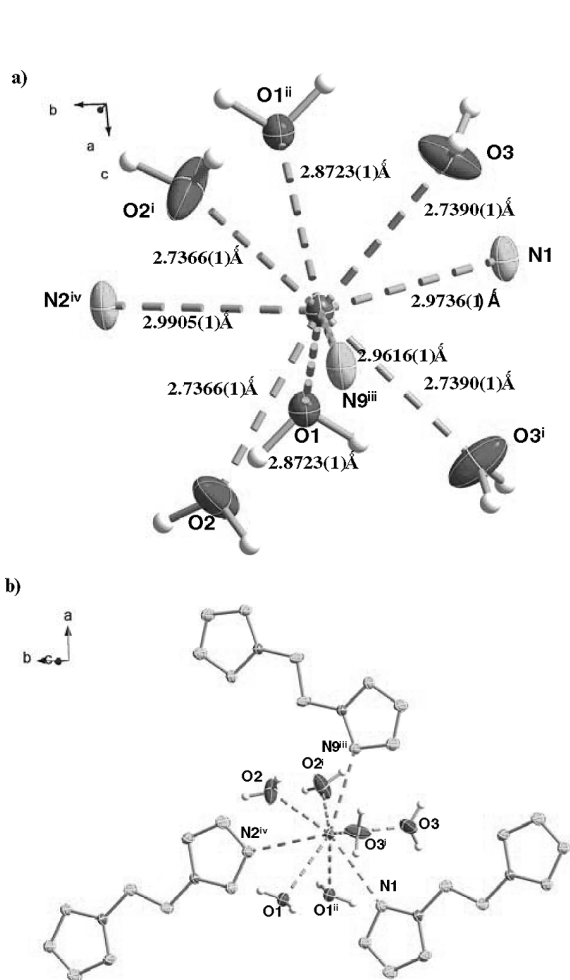


Figure 6. (a) Simplified and (b) full coordination (hydrazine-bridge hydrogen atoms not found) around the metal center in compound **5**. Symmetry codes: (i) *x*, *y*, 2 - *z*; (ii) 1 - *x*, 1 - *y*, 2 - *z*; (iii) 0.5 + *x*, 0.5 - *y*, 1.5 - *z*; (iv) 1 - *x*, 1 - *y*, *z*.

The crystals of the strontium salt **4**, similarly to those of **3** and **5** (see discussions below and above, respectively), also display tetrazole rings, which are apparently “coplanar”. However, in this case the electron density corresponding to the protons of the hydrazine bridge could be found in the difference Fourier map. The elongated ellipsoids found for the bridging nitrogen atoms (N5 and N6) suggest half-occupied positions (Figure 7), so that when the proton on N5 faces up from the “plane of the two tetrazole rings”, the one on N6 faces down and vice versa (Figure 8). The disorder found in the structure applies first of all to the protons. The immediate consequence is that the nitrogen atoms of the bridging hydrazine moiety have, as expected, a pyramidal and not a trigonal planar coordination. This results in a disorder of the nitrogen atoms of the hydrazine bridge and the tetrazole rings (Tz) over two positions, as indicated by the slightly elongated thermal ellipsoids for these atoms. This situation might result in coplanar Tz rings. Unfortunately, we were unable to split the positions of the nitrogen atoms corresponding to the hydrazine bridge and the Tz rings into two sets, but in such a case the deviation from coplanarity would not be expected to be very large.

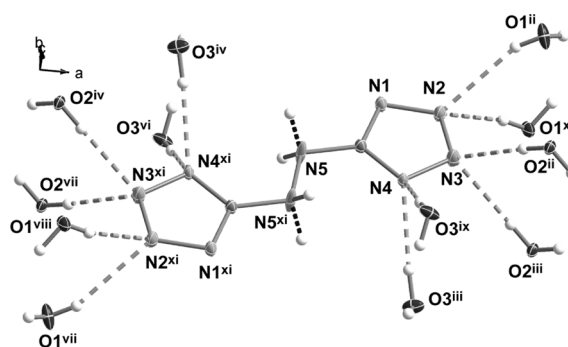


Figure 7. Hydrogen bonding around the HBT²⁻ anion in the crystal structure of **4** showing the elongated ellipsoids for the hydrazine-bridge nitrogen atoms and the (split) positions of the hydrogen atoms. Symmetry codes: (ii) 0.5 + *x*, 0.5 - *y*, 0.5 + *z*; (iii) 0.5 - *x*, -0.5 + *y*, -0.5 + *z*; (iv) -0.5 + *x*, 0.5 - *y*, 0.5 - *z*; (vi) -0.5 + *x*, 0.5 - *y*, -0.5 + *z*; (vii) -0.5 - *x*, -0.5 + *y*, -0.5 + *z*; (viii) -0.5 - *x*, -0.5 + *y*, 0.5 + *z*; (ix) 0.5 - *x*, -0.5 + *y*, 0.5 - *z*; (x) 0.5 + *x*, 0.5 - *y*, -0.5 - *z*; (xi) -*x*, -*y*, -*z*.

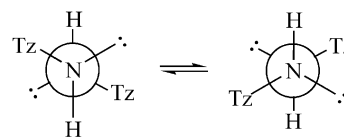


Figure 8. Equilibrium between the two possible configurations of the tetrazole rings in alkaline earth metal salts **3–5** (Tz: tetrazole). View along the NH–NH bond.

On the other hand, the hydrogen-bond lengths between donor and acceptor atoms are (as discussed for **5**) in the range 2.9 to 3.0 Å, and, with the exception of one weaker hydrogen bond between water molecules [O1...O3^{vi} 3.072(2) Å; symmetry code: (vi) -0.5 + *x*, 0.5 - *y*, -0.5 + *z*] with an angle of 120(2)°, also very directional [158(3)–180(3)°]. Lastly, with the exception of the D2,1(3) graph-

set, all the hydrogen-bonding networks discussed for **5** are also present in the structure of **4**. For example, the R2,4(8) network is formed by the interaction between O2 and N3^{iv} over a distance of 2.935(2) Å [symmetry code: (iv) $-0.5 + x, 0.5 - y, 0.5 - z$].

The coordination number around the cation in **4** is nine as in **5** (Figure 9), but as a consequence of the smaller radius of the strontium cation in comparison to that of the barium cation, the contacts are much shorter. Six of the distances are shorter and correspond to coordination of the strontium cations to water molecules with distances between 2.558(2) and 2.697(2) Å, whereas the contacts to the nitrogen atoms (three in total) are looser [2.833(2) to 2.871(2) Å]. Finally, an interesting detail in the structure is the coordination found in a layer of the compound (Figure S2), where every cation participates in the formation of the three Sr–N contacts mentioned above, yielding hexagonal motifs. The space delimited by four anions and four cations is occupied by water of crystallization coordinating from above and below the plane of the layers. As expected, because of the high similarity of the structures, compounds **5** and **3** also form the hexagonal motifs mentioned above.

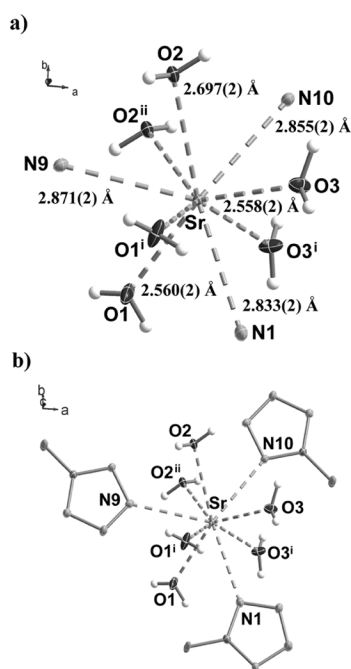


Figure 9. (a) Simplified and (b) full coordination (hydrazine-bridge hydrogen atoms omitted) around the metal center in compound **4**. Symmetry codes: (i) $x, y, -z$; (ii) $-x, 1 - y, -z$.

The relatively small electron density of calcium allowed the hydrazine-bridge protons in compound **3** to be found, which, similarly to **4**, occupy split-positions, as suggested by the elongated ellipsoids of the corresponding nitrogen atoms (N5 and N6). Figure S3 shows a view of the unit cell of the compound along the c axis where the “apparent coplanarity” of the tetrazole rings is obvious. The similarities in the packing between **3**, **4**, and **5** are manifested, first of all, by the similar cell parameters (ca. 7, 11, and 14 Å)

found in the three compounds, which decrease with decreasing size of the cation ($5 > 4 > 3$) and for the coordination to the metal center. Two cations are connected by two bridging water molecules (Figure S3), which are generated by symmetry [$d(\text{Ca}-\text{O}1) = d(\text{Ca}-\text{O}1)^{\text{ii}} = 2.570(1)$ Å; symmetry code: (ii) $-x, -y, -z$]. Each cation has a coordination number of nine (Figure 10) with short distances to oxygen atoms [2.408(1)–2.570(1) Å] and longer contacts to nitrogen atoms [2.788(2)–2.806(2) Å]. Finally, a total of five hydrogen bonds are found in the structure, which are analogous to those discussed for compounds **4** and **5** but slightly more directional [161(2)–179(2)°] and slightly shorter ($\text{O}1 \cdots \text{N}3 \approx 2.9$ Å). As a consequence, the hydrogen-bonding networks [except for the D2,1(3) graph-set found in **5**] are practically identical [e.g. R2,4(8) formed by $\text{O}3 \cdots \text{N}7^{\text{ii}}$ 2.901(2) Å; symmetry code: (ii) $0.5 + x, 0.5 - y, 0.5 + z$].

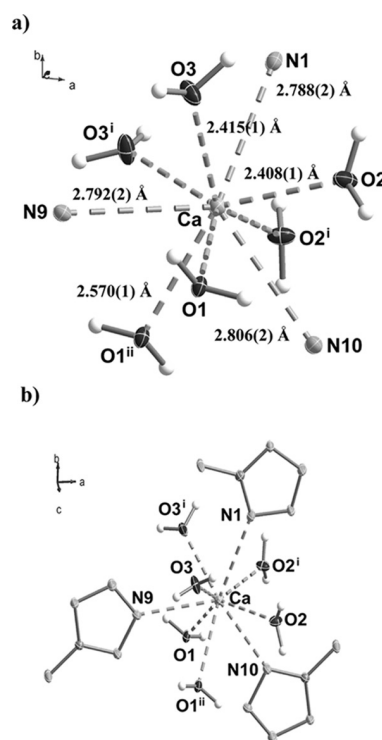


Figure 10. (a) Simplified and (b) full coordination (hydrazine-bridge hydrogen atoms omitted) around the metal center in compound **3**. Symmetry codes: (i) $x, y, -z$; (ii) $-x, -y, -z$.

The crystal structure of the magnesium salt **2** is the most different of all. To start with, the compound is the only one in the series that crystallizes in a triclinic cell (space group $\bar{P}1$) and, regardless of the fact that magnesium has the smallest size among the alkaline earth metals in this study, compound **2** has the largest unit cell [$V_{\text{UC}} = 1219.8(1)$ Å³]. This can be attributed to the higher number of waters of crystallization in the unit cell (6.5 vs. 5). The tetrazole rings are unequivocally noncoplanar; there is an angle of ca. 40° between them. The asymmetric unit (Figure 11) is formed by two crystallographically independent anions, two cations, and thirteen molecules of water. Each cation is surrounded by six water molecules, with very little variation in

the contact distances (ca. 2.0–2.1 Å), forming slightly distorted octahedrons, whereas the remaining water molecule links two octahedrons by hydrogen bonds to water molecules [O9...O13 2.708(2) Å and O4...O13 2.717(2) Å]. Figure 12 shows a view of the unit cell of **2** along the *a* axis, where the anions are oriented approximately parallel to the *c* direction without contacts between nitrogen and magnesium atoms. However, every nitrogen atom in the structure (including the hydrazine-bridge atoms N5/15 and N6/16) is involved in hydrogen bonding, forming a total of twenty eight O...N interactions to water molecules. Figure S4 shows the hydrogen bonding around one of the two crystallographically independent HBT²⁻ anions (type **B**). One type of anions acts as hydrogen-bond acceptor (O...N), with distances to the donor in the range 2.70–2.95 Å, and as hydrogen-bond donor by using the hydrazine-bridge nitrogen

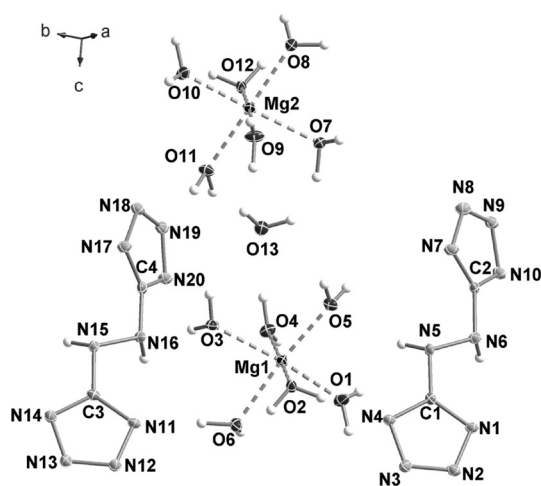


Figure 11. Asymmetric unit of compound **2** with the labeling scheme (the hydrogen bonds to O13 have been omitted for clarity purposes).

atoms (N...O), with weaker interactions (ca. 3.22 Å), whereas the other type of anions shows somewhat different distances with O...N in the range 2.69–3.11 Å and N...O ca. 3.11 Å. A complete record of the distances is found in the Supporting Information (Table S5).

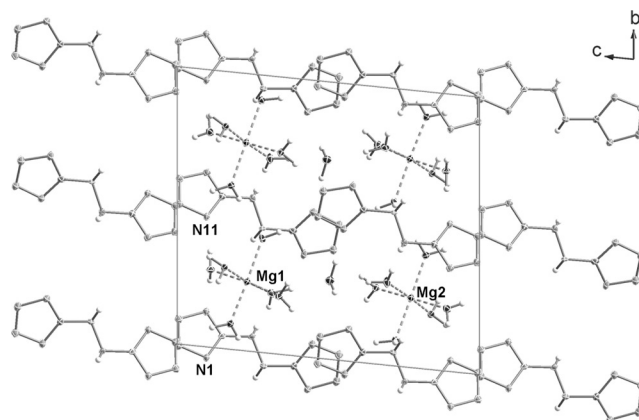


Figure 12. View of the unit cell of compound **2** along the *a* axis showing the contacts to the magnesium atoms (dotted lines).

Stability and Energetic Properties

In order to assess the energetic properties of alkaline earth metal salts of HBT (**2–5**), their thermal stability (decomposition point from DSC measurements), sensitivity to friction, impact, electrostatic discharge (BAM tests),^[28–30] and thermal shock were experimentally determined. The physico-chemical properties of alkaline earth metal salts **2–5** have been summarized in Table 5. At a heating rate of 5 °Cmin^{−1}, the different water molecules of crystallization are lost within a range of 20–30 °C (Figure 13). The strength with which the water molecules coordinate to the

Table 5. Physico-chemical properties of alkaline earth metal salts **2–5**.

	2	3	4	5
Formula	C ₂ H ₁₅ MgN ₁₀ O _{6.5}	C ₂ H ₁₂ CaN ₁₀ O ₅	C ₂ H ₁₂ N ₁₀ O ₅ Sr	C ₂ H ₁₂ BaN ₁₀ O ₅
Formula weight [g mol ^{−1}]	307.55	296.26	343.80	394.00
Impact [J] ^[a]	>30	>30	>30	>30
Friction [N] ^[a]	>360	>360	>360	>360
Electrostatics ^[b]	–	–	–	–
Flame slow heating	burns	burns	burns	burns
Flame fast heating	deflagrates	deflagrates	deflagrates	deflagrates
Flame color	white	red	red	green
Smokeless	+	+	+	+
% N ^[c]	45.6	47.3	40.7	35.6
% O ^[d]	–31.3	–32.4	–27.9	–24.4
T _{H2O} [°C] ^[e]	142–158	140–160	150–185	128–154
Exothermic dec. [°C] ^[f]	220, 250	220, 260	276	260
ρ [g cm ^{−3}] ^[g]	1.675	1.898	2.088	2.210
–Δ _c U [cal g ^{−1}] ^[h]	2000(20)	1300(20)	1360(20)	1310(20)
–Δ _c H° [kJ mol ^{−1}] ^[i]	2560(20)	1590(20)	1940(20)	2150(20)
–Δ _f H° [kJ mol ^{−1}] ^[j]	955(70)	1530(70)	1140(100)	895(70)

[a] Impact and friction sensitivities determined by the standard BAM method.^[28–30] [b] Rough sensitivity to 20 kV electrostatic discharge (ESD testing): + sensitive, –insensitive from an HF-Vacuum-Tester type VP 24. [c] Nitrogen content. [d] Oxygen balance.^[31] [e] Range of temperature of water loss (DSC onset–offset) from the measurement at β = 5 °Cmin^{−1}. [f] Decomposition point (DSC onset) from the measurement at β = 5 °Cmin^{−1}. [g] Calculated density (from X-ray measurements). [h] Experimental (constant-volume) energy of combustion. [i] Experimental molar enthalpy of combustion. [j] Molar enthalpy of formation.

metal center increases in the direction $\text{Ba} < \text{Mg} \approx \text{Ca} < \text{Sr}$. For the strontium salt, the last molecule of water of crystallization is lost at a temperature of ca. 185 °C (DSC offset). No melting is observed for any of the salts, and the trend in the decomposition temperatures is the same as that for the temperatures of water loss. All compounds are thermally stable to temperatures above 220 °C. The lighter-metal salts **2** and **3** show smooth two-step decomposition over a wide range, whereas the heavier-metal compounds (**4** and **5**) show sharp exotherms at ca. 276 (**4**) and 260 (**5**) °C.

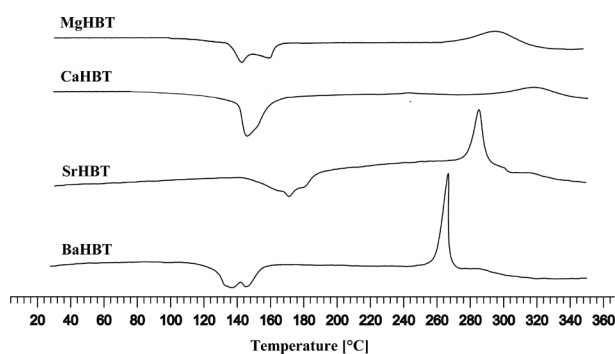


Figure 13. DSC thermographs for alkaline earth metal salts **2–5** (endothermic peaks point down, exothermic peaks point up) for measurements at $\beta = 5\text{ °C min}^{-1}$.

Thermogravimetric (TG) analysis confirmed the results obtained by DSC. Figure 14 shows a typical TG curve for compound **5**. The loss of the five molecules of water of crystallization adds to 21.14% of the sample weight (calculated: 21.34%), and at the decomposition point the weight loss is 66.49%, so that the weight of the residue left in the TG pan is 12.35% the weight of the original sample.

No detonation was observed either in the drop-hammer (ca. 30 J) or in the friction test (ca. 360 N). No explosion occurred either when grinding the compounds in a mortar or when applying an electrostatic discharge by spraying sparks across a small sample of the materials by using an HF-Vacuum-Tester type VP 24 (ca. 20 kV, ESD testing). Thermal shock in a Bunsen burner flame resulted in different responses depending on how the test was conducted. When the compounds were loaded on a spatula and this was heated up slowly from the bottom, compounds **2–5** burned normally, giving the corresponding color for the

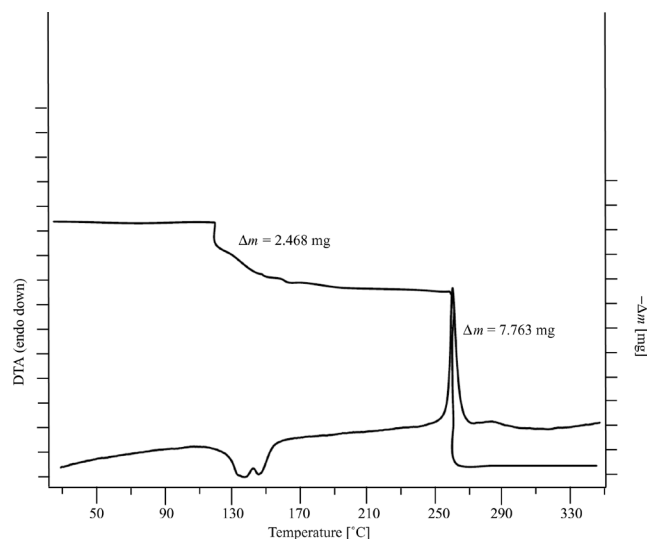
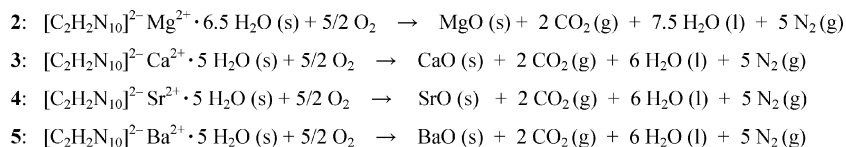


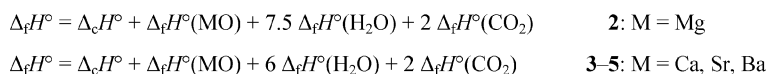
Figure 14. TG curve of **5** showing the DTA curve (left axis) and the loss of mass (right axis) for a measurement at $\beta = 5\text{ °C min}^{-1}$ (sample weight = 11.675 mg).

metal atom (Flame Test, slow heating). However, when the spatula was held so as to allow the compound to come into direct contact with the flame (Flame Test fast heating), a more vigorous response (deflagration) resulted, which showed likewise the characteristic color of the cation.

Due to the energetic nature of the HBT^{2-} anion, the energies of combustion of alkaline earth metal salts **2–5** were determined by using oxygen bomb calorimetry. With the exception of the magnesium salt [**2** $-2000(20)\text{ cal g}^{-1}$], the rest of the materials have similar energies of combustion [**3** $-1300(20)\text{ cal g}^{-1}$, **4** $-1360(20)\text{ cal g}^{-1}$, and **5** $-1310(20)\text{ cal g}^{-1}$]. The standard energies of combustion of the compounds ($\Delta_f H^\circ$) were back-calculated from the heats of combustion on the basis of their combustion equations (Scheme 2), Hess's Law (Scheme 3), the known standard heats of formation for water, carbon dioxide, and the corresponding alkaline earth metal oxide (Table S6),^[32] and a correction for the change in gas volume during combustion. These results were used to calculate the standard heats of combustion according to $\Delta_f H^\circ = \Delta_f U^\circ + \Delta n RT$ [where Δn is the difference in the molar quantities of gases between



Scheme 2. Combustion equations of alkaline earth metal salts **2–5**.



Scheme 3. Calculation of the heats of formation using Hess's law.

products and reagents in the combustion equations, R is the gas constant, and T is the temperature (298.15 K)]. Once again, **2** has an unexpected (abnormally positive) value [$-955(70)$ kJ mol $^{-1}$], whereas the remainder of the compounds show the expected trend [**3** $-1530(70)$ kJ mol $^{-1}$, **4** $-1140(75)$ kJ mol $^{-1}$, and **5** $-895(70)$ kJ mol $^{-1}$], that is, the heats of formation become more positive (less negative) in the direction **3** < **4** < **5**. Lastly, the values for the heats of formation are comparatively less positive than those found for tetrazolate salts with alkali metals.^[33]

Conclusions

Alkaline earth metal salts containing the nitrogen-rich 5,5'-hydrazine-1,2-diylbis(tetrazolate) anion ([HBT] $^{2-}$) have been synthesized in moderate to high yields and high purities and fully characterized by methods including an X-ray structure determination. In contrast to other HBT salts reported in the literature, in the heavier-metal salts (Ca, Sr, and Ba) the two tetrazolate rings are "apparently coplanar" (second-order saddle point in the gas phase) because of disorder; however, the structure of the lighter-metal compound (Mg) agrees with other structural reports with the same anion. The differences in the structure of the Mg salt (already observed in the vibrational spectra) with respect to the other compounds are discussed. All compounds contain tightly bound water of crystallization in the structure, which is lost at temperatures as high as ca. 180 °C (Sr salt), and have great thermal stabilities (>220 °C), as shown by DSC measurements. The presence of water of crystallization accounts for the low sensitivity of the materials to shock (>30 J) and friction (>360 N); however, they deflagrate in the "flame test fast heating", showing the characteristic flame color for the metal center. Lastly, the high thermal stabilities of the salts in combination with a nitrogen-rich anion may make the compounds studied here (except for the barium salt) of interest for future use in environmentally friendly pyrotechnic compositions. The strontium salt is of particular interest as a red color producing agent.

Experimental Section

General Method: All chemical reagents and solvents were obtained from Sigma–Aldrich Fine Chemicals Inc. or Acros Organics (analytical grade) and were used as supplied. 5,5'-Hydrazine-1,2-diylbis(1*H*-tetrazole) (HBT) was prepared as previously reported.^[12] ^1H , ^{13}C , and ^{14}N NMR spectra were recorded in [D_6]dmsO at or near 25 °C with a JEOL Eclipse 400 instrument operating at 400.18 MHz (^1H), 100.63 MHz (^{13}C), and 40.55 MHz (^{14}N). The reported chemical shifts are relative to tetramethylsilane (^1H , ^{13}C) and nitromethane (^{14}N) as external standards. The infrared (IR) spectra were recorded with a Perkin–Elmer Spectrum One FT-IR instrument by using KBr pellets at 20 °C. Transmittance values are qualitatively described as "very strong" (vs), "strong" (s), "medium" (m), and "weak" (w). The Raman spectra were recorded with a Perkin–Elmer Spectrum 2000R NIR FT-Raman instrument equipped with a Nd:YAG laser (1064 nm). The intensities are re-

ported as percentages of the most intense peak and are given in parentheses. Elemental analyses were performed with a Netsch Simultaneous Thermal Analyzer STA 429. The DSC measurements were made with a Linseis DSC PT-10 instrument (calibrated with standard pure indium and zinc)^[34] at a heating rate of 5 °C min $^{-1}$ under a nitrogen flow of 20 mL min $^{-1}$. Lastly, the thermogravimetric analyses were performed with a Setaram DTA-TG machine at 5 °C min $^{-1}$.

CCDC-693858 (for **2**), -693859 (for **3**), -693860 (for **4**), and -693861 (for **5**) contain the supplementary crystallographic data for this paper. This data can be obtained free of charge from The Cambridge Crystallographic Data Centre via www.ccdc.cam.ac.uk/data_request/cif.

Bomb Calorimetry: For all calorimetric measurements, a Parr 1356 bomb calorimeter (static jacket) equipped with a Parr 207A oxygen bomb for the combustion of highly energetic materials was used.^[35] A Parr 1755 printer furnished with the Parr 1356 calorimeter was used to produce a permanent record of all activities within the calorimeter. The samples (ca. 200 mg each) were carefully mixed with analytical grade benzoic acid (ca. 800 mg) and carefully pressed into pellets, which were subsequently burned in a 3.05-MPa atmosphere of pure oxygen. The experimentally determined heats of combustion were obtained as the averages of four single measurements with standard deviations calculated as a measure of experimental uncertainty. The calorimeter was calibrated by the combustion of certified benzoic acid in an oxygen atmosphere at a pressure of 3.05 MPa.

CAUTION! Although the compounds described in this paper are not sensitive to classical stimuli, they are nevertheless energetic materials. Although unlikely, loss of water of crystallization may occur, resulting in compounds that are **very sensitive** to friction and shock. Appropriate safety measures such as the use of Kevlar gloves, safety glasses, face shields, ear plugs, conductive equipment, and grounded shoes are strongly advised specially when working on a larger scale.

5,5'-Hydrazine-1,2-diylbis(1*H*-tetrazole) (1):^[12] The compound was obtained by reduction of sodium 5,5'-azotetrazolate pentahydrate with magnesia in water. The insoluble material was separated by filtration, and the filtrate was treated with an equivalent amount of hydrochloric acid to cause precipitation of the product as a white solid.

Magnesium 5,5'-Hydrazine-1,2-diylbis(tetrazolate) Hexahemihydrate (2): Compound **1** (0.478 g, 2.84 mmol) was suspended in water (5 mL) and treated with one equivalent of magnesium hydroxide (0.165 g, 2.84 mmol). The reaction mixture was heated at reflux for 1.5 h under a stream of nitrogen and left to cool to room temperature. The solvent was stripped under high vacuum (10 $^{-3}$ mbar), yielding a sticky mass, which was recrystallized from the minimum amount of hot water. Slightly yellow crystals of the product suitable for X-ray analysis separated upon slow cooling of the hot solution (Table 6). These were filtered, washed with acetone and ether, and dried under vacuum to yield **2**, which was pure by elemental analysis (0.549 g, 69%). $\text{C}_2\text{H}_{15}\text{MgN}_{10}\text{O}_{6.5}$ (307.55 g mol $^{-1}$): calcd. C 7.82, H 4.92, N 45.60; found C 7.90, H 4.73, N 45.92. DSC (5 °C min $^{-1}$): 142–158 (H $_2$ O loss), 220 and 250 (dec.) °C. IR (KBr): $\tilde{\nu}$ = 3505 (s) 3395 (s), 3319 (s), 3230 (vs), 3054 (s), 2330 (w), 1687 (m), 1557 (m), 1530 (m), 1480 (s), 1371 (m), 1263 (w), 1245 (w), 1146 (m), 1077 (w), 1028 (w), 960 (w), 908 (m), 837 (m), 806 (m), 713 (s), 513 (m) cm $^{-1}$. Raman (400 mW, 25 °C): $\tilde{\nu}$ = 3231 (3), 3082 (3), 2986 (100), 2663 (1), 2409 (1), 1530 (47), 1485 (10), 1393 (11), 1264 (8), 1248 (28), 1233 (10), 1180 (4), 1145 (21), 1111 (9), 1079 (47), 1067 (35), 1031 (9), 888 (5), 739 (5), 387

Table 6. Crystal data and structure refinements for alkaline earth metal salts 2–5.

Parameter	2	3	4	5
Empirical formula	C ₂ H ₁₅ MgN ₁₀ O _{6.5}	C ₂ H ₁₂ CaN ₁₀ O ₅	C ₂ H ₁₂ N ₁₀ O ₅ Sr	C ₂ H ₁₂ BaN ₁₂ O ₅
Formula weight [g mol ⁻¹]	307.55	296.30	343.84	422.01
Temperature [K]	100	100	100	100
Crystal size [mm]	0.30 × 0.15 × 0.10	0.25 × 0.10 × 0.10	0.11 × 0.10 × 0.09	0.20 × 0.12 × 0.07
Crystal system	triclinic	orthorhombic	orthorhombic	orthorhombic
Space group	$\bar{P}1$	<i>Pnmm</i>	<i>Pnmm</i>	<i>Pnmm</i>
<i>a</i> [Å]	7.037(5)	11.0655(2)	11.173(5)	14.2461(3)
<i>b</i> [Å]	12.621(5)	13.6701(3)	13.869(5)	11.2834(3)
<i>c</i> [Å]	13.969(5)	6.8527(1)	7.057(5)	7.3188(2)
α [°]	83.915(5)	90.00	90.00	90.00
β [°]	81.558(5)	90.00	90.00	90.00
γ [°]	87.464(5)	90.00	90.00	90.00
<i>V</i> _{UC} [Å ³]	1219.8(1)	1036.58(3)	1093.51(2)	1176.46(5)
<i>Z</i>	4	4	4	4
ρ_{calc} [g cm ⁻³]	1.675	1.898	2.088	2.210
μ [mm ⁻¹]	0.198	0.648	4.971	3.410
<i>F</i> (000)	644	616	688	752
θ range [°]	3.70–27.00	3.68–27.00	3.72–27.00	2.77–54.93
Index ranges	–8 ≤ <i>h</i> ≤ 8, –12 ≤ <i>k</i> ≤ 16, –17 ≤ <i>l</i> ≤ 17	–14 ≤ <i>h</i> ≤ 14, –17 ≤ <i>k</i> ≤ 17, –8 ≤ <i>l</i> ≤ 8	–14 ≤ <i>h</i> ≤ 14, –17 ≤ <i>k</i> ≤ 17, –9 ≤ <i>l</i> ≤ 9	–18 ≤ <i>h</i> ≤ 18, –14 ≤ <i>k</i> ≤ 14, –9 ≤ <i>l</i> ≤ 8
Reflections collected	8965	10976	11448	8665
Independent reflections	5215	1230	1286	1444
Data / restraints / parameters	5215 / 0 / 472	1230 / 0 / 130	1286 / 0 / 130	1444 / 0 / 118
Goodness-of-fit on <i>F</i> ²	0.816	1.030	1.092	1.162
<i>R</i> _{int}	0.0230	0.0360	0.0296	0.0300
<i>R</i> ₁ [<i>F</i> > 4σ(<i>F</i>)]	0.0314	0.0231	0.0163	0.0222
<i>R</i> ₁ (all data)	0.0665	0.0315	0.0241	0.0244
w <i>R</i> ₂ [<i>F</i> > 4σ(<i>F</i>)]	0.0670	0.0553	0.0362	0.0500
w <i>R</i> ₂ (all data)	0.0735	0.0586	0.0408	0.0508

$$R_1 = \sum \|F_o\| - \|F_c\| / \sum \|F_o\|, R_w = [\sum (F_o^2 - F_c^2) / \sum w (F_o^2)]^{1/2}, w = [\sigma_c^2 (F_o^2) + (xP)^2 + yP]^{-1}, P = (F_o^2 - 2F_c^2) / 3.$$

(11), 361 (10), 262 (11), 231 (14), 193 (11), 150 (7) cm⁻¹. ¹H NMR ([D₆]dmsO, 25 °C): δ = 7.3 (s, 2 H, NH–NH), 3.9 (s, ca. 12 H, H₂O) ppm. ¹³C NMR ([D₆]dmsO, 25 °C): δ = 166.2 (2 C, C_{ring}) ppm. ¹⁴N NMR ([D₆]dmsO, 25 °C): δ = –270 (2N, NH–NH) ppm. MS (FAB[–], xenon, 6 keV, glycerine matrix): *m/z* = 83.0 (6, [CHN₅]^{2–}), 118.1 (4, HCN–gly), 124.1 (2, [C₂H₂N₇][–]), 167.1 (19, [C₂H₃N₁₀][–]), 205.1 (7, [C₂HN₁₀MgO]^{3–}), 259.1 (5, C₂H₄N₁₀–gly), 281.1 (18, C₂H₂N₁₀Mg–gly).

Calcium 5,5'-Hydrazine-1,2-diylbis(tetrazolate) Pentahydrate (3):

Compound **1** (0.354 g, 2.11 mmol) was suspended in water (5 mL) in a Schlenk flask under a stream of nitrogen and treated with calcium hydroxide (0.156 g, 2.11 mmol). The reaction mixture was heated to boiling and stirred for 2 h. Colorless crystals of the desired compound suitable for X-ray structure analysis precipitated upon slow cooling to room temperature, and the solution was stored in the refrigerator overnight. The solid that precipitated was filtered under vacuum and washed with acetone and ether. No further purification was necessary (0.481 g, 77%). C₂H₁₂CaN₁₀O₅ (296.30 g mol⁻¹): calcd. C 8.10, H 4.08, N 47.30; found C 8.13, H 4.01, N 46.40. DSC (5 °C min⁻¹): 140–160 (H₂O loss), 220 and 260 (dec.) °C. IR (KBr): $\tilde{\nu}$ = 3428 (vs), 3251 (s), 2170 (w), 1631 (m), 1531 (s), 1451 (m), 1384 (w), 1343 (m), 1234 (w), 1217 (w), 1158 (m), 1146 (w), 1129 (m), 1067 (w), 1022 (m), 909 (w), 839 (m), 750 (m), 600 (m), 519 (m) cm⁻¹. Raman (400 mW, 25 °C) $\tilde{\nu}$ = 3251 (11), 1546 (29), 1497 (24), 1456 (10), 1377 (41), 1236 (29), 1220 (24), 1131 (35), 1100 (14), 1089 (14), 1066 (65), 1022 (10), 909 (11), 646 (9), 396 (11), 346 (12), 324 (11), 248 (9), 173 (9) cm⁻¹. ¹H NMR ([D₆]dmsO, 25 °C): δ = 7.0 (s, 2 H, NH–NH), 3.8 (s, ca. 10 H, H₂O) ppm. ¹³C NMR ([D₆]dmsO, 25 °C): δ = 167.1 (C_{ring}) ppm. MS

(FAB[–], xenon, 6 keV, glycerine matrix): *m/z* = 83.0 (8, [CHN₅]^{2–}), 118.1 (6, HCN–gly), 124.1 (3, [C₂H₂N₇][–]), 167.1 (35, [C₂H₃N₁₀][–]), 214.0 (3), 221.0 (7, [C₂HN₁₀CaO]^{3–}), 259.1 (8, C₂H₄N₁₀–gly), 297.1 (28) ppm.

Strontium 5,5'-Hydrazine-1,2-diylbis(tetrazolate) Pentahydrate (4):

Compound **1** (0.354 g, 2.11 mmol) was charged in a Schlenk flask under a stream of nitrogen and suspended in water (5 mL). Neat strontium hydroxide octahydrate (0.541 g, 2.11 mmol) was added, and the initial suspension dissolved upon heating. The solution was kept at reflux and stirred for 3 h and then left to slowly crystallize by switching off the oil bath, first at room temperature and then in the refrigerator, upon which crystals of **4** were obtained and were used to measure the crystal structure. The slightly brown solid was filtered and left to dry in air. No further purification was required (0.661 g, 91%). C₂H₁₂N₁₀O₅Sr (343.84 g mol⁻¹): calcd. C 6.99, H 3.52, N 40.74; found C 7.09, H 3.46, N 40.59. DSC (5 °C min⁻¹): 150–185 (H₂O loss), 276 (m.p. + dec.) °C. IR (KBr): $\tilde{\nu}$ = 3416 (vs) 3255 (vs) 2260 (w), 2166 (w), 1628 (m), 1533 (vs), 1451 (s), 1384 (w), 1346 (m), 1236 (m), 1219 (m), 1154 (m), 1144 (m), 1129 (m), 1068 (w), 1021 (m), 843 (m), 749 (m), 598 (s), 515 (s) cm⁻¹. Raman (400 mW, 25 °C): $\tilde{\nu}$ = 3301 (3), 3256 (11), 1541 (37), 1460 (10), 1367 (14), 1238 (35), 1222 (30), 1131 (40), 1108 (12), 1066 (70), 1021 (10), 908 (12), 738 (6), 657 (8), 393 (16), 346 (16), 319 (17), 273 (11), 237 (12) cm⁻¹. ¹H NMR ([D₆]dmsO, 25 °C): δ = 6.9 (s, 2 H, NH–NH), 3.7 (s, ca. 10 H, H₂O) ppm. ¹³C NMR ([D₆]dmsO, 25 °C): δ = 167.2 (C_{ring}) ppm. MS (FAB[–], xenon, 6 keV, glycerine matrix): *m/z* = 83.0 (4, [CHN₅]^{2–}), 118.1 (3, HCN–gly), 124.1 (2, [C₂H₂N₇][–]), 167.1 (28, [C₂H₃N₁₀][–]), 259.1 (7, C₂H₄N₁₀–gly), 269.0 (2, [C₂HN₁₀SrO]^{3–}) ppm.

Barium 5,5'-Hydrazine-1,2-diylbis(tetrazolate) Pentahydrate (5)

Method 1: Compound **1** (0.168 g, 1.0 mmol) was suspended in water (5 mL) and reacted with sodium hydroxide (0.080 g, 2.0 mmol) under a stream of nitrogen. The resulting solution was heated to 65 °C, and a solution of barium chloride dihydrate (0.249 g, 1.0 mmol) in water (5 mL) was added at this temperature. The reaction mixture was stirred for further 15 min, left to cool slowly to room temperature and stored in the refrigerator overnight to yield prismatic colorless crystals of the product, which were filtered and stored under nitrogen (0.058 g, 19%).

Method 2: Alternatively, a Schlenk flask was charged with compound **1** (0.385 g, 2.29 mmol) and water (8 mL) under a stream of nitrogen. Barium hydroxide octahydrate (0.723 g, 2.29 mmol) was added. The suspension was heated at reflux for 1 h under a stream of nitrogen, after which time all the insoluble material had dissolved. The solution was left to slowly cool to room temperature while keeping a nitrogen flow and stored in the refrigerator overnight to yield prismatic colorless crystals of **5**, which were filtered and allowed to dry in air (0.559 g, 80%). $\text{C}_{22}\text{H}_{12}\text{BaN}_{10}\text{O}_5$ (422.01 g mol⁻¹): calcd. C 6.09, H 3.07, N 35.54; found C 6.16, H 3.02, N 35.59. DSC (5 °C min⁻¹): ca. 130–154 (H₂O loss), 260 (m.p. + dec.) °C. IR (KBr): $\tilde{\nu}$ = 3408 (vs) 3255 (vs), 2258 (w), 2150 (w), 1636 (m), 1532 (vs), 1450 (s), 1384 (m), 1349 (m), 1235 (m), 1219 (m), 1149 (m), 1128 (m), 1068 (w), 1019 (m), 856 (m), 748 (m), 736 (m), 603 (s), 514 (s) cm⁻¹. Raman (200 mW, 25 °C) $\tilde{\nu}$ = 3255 (13) 2986 (85) 1536 (48) 1464 (12) 1410 (6), 1376 (21), 1236 (37), 1222 (33), 1157 (9), 1130 (44), 1098 (12), 1066 (100), 1018 (14), 909 (15), 682 (10), 389 (22), 344 (20), 318 (20), 233 (16) cm⁻¹. ¹H NMR ([D₆]-dmsO, 25 °C): δ = 6.9 (s, 2 H, NH–NH), 3.6 (s, ca. 10 H, H₂O) ppm. ¹³C NMR ([D₆]-dmsO, 25 °C): δ = 167.3 (C_{ring}) ppm. MS (FAB⁺, xenon, 6 keV, *m*-NBA matrix): *m/z* = 167.0 [C₂H₃N₁₀]⁺.

Supporting Information (see also the footnote on the first page of this article): Relevant X-ray tables and pictures and the heats of formation of the species involved in the combustion.

Acknowledgments

Financial support of this work by the Ludwig-Maximilians-Universität (LMU), München, the Fonds der Chemischen Industrie (FCI), the European Research Office (ERO) of the U.S. Army Research Laboratory (ARL), and ARDEC (Armament Research, Development and Engineering Center) under contract nos. N 62558-05-C-0027, R&D 1284-CH-01, R&D 1285-CH-01, 9939-AN-01 & W911NF-07-1-0569 and the Bundeswehr Research Institute for Materials, Explosives, Fuels and Lubricants (WIWEB) under contract nos. E/E210/4D004/X5143 & E/E210/7D002/4F088 is gratefully acknowledged. The authors acknowledge collaborations with Dr. M. Krupka (OZM Research, Czech Republic) in the development of new testing and evaluation methods for energetic materials and with Dr. M. Sucasca (Brodarski Institute, Croatia) in the development of new computational codes to predict the detonation parameters of high-nitrogen explosives. We are indebted to and thank Dr. Betsy M. Rice (ARL, Aberdeen, Proving Ground, MD) for many helpful and inspired discussions and support of our work.

- [1] Dynamit Nobel G.m.b.H. (K. Redecker, W. Weuter, U. Bley, D. Schmittner), DE-BP.19730873 (January 22, 1998).
- [2] Chung Shan Institute of Science & Technology (Y. Peng, C. Wong) U.S.5877300 (March 2, 1999).
- [3] a) M. Kaiser, U. Ticmanis, *Inorg. Chem.* **2001**, *40*, 3570–3575; b) K. Karaghiosoff, T. M. Klapötke, P. Mayer, C. Miró Sabaté, A. Penger, J. M. Welch, *Inorg. Chem.* **2008**, *47*, 1007–1019; c)

- T. M. Klapötke, C. Miró Sabaté, *Heteroat. Chem.* **2008**, *19*, 301–306.
- [4] a) Etat Francais (J. Duguet) U.S.4566921 (January 28, 1986); b) T. M. Klapötke, C. Miró Sabaté, *Proceedings of the 10th Seminar New Trends in Research of Energetic Materials*, Pardubice, Czech Republic, Apr. 25–27, 2007.
- [5] L. V. De Yong, G. Campanella, *J. Hazard. Mater.* **1989**, *21*, 125–133.
- [6] D. J. Whelan, R. J. Spear, R. W. Read, *Thermochim. Acta* **1984**, *80*, 149–163.
- [7] T. M. Klapötke, G. Steinhauser, *Angew. Chem. Int. Ed.* **2008**, *47*, 3330–3347.
- [8] a) M. A. Hiskey, D. E. Chavez, D. L. Naud, S. F. Son, H. L. Berghout, C. A. Bolme, *Proc. Int. Pyrotech. Sem.* **2000**, *27*, 3–14; b) H. J. Marcus, A. Remanick, *J. Org. Chem.* **1963**, *28*, 2372–2375; c) D. E. Chavez, M. A. Hiskey, M. H. Huynh, D. L. Naud, S. F. Son, B. C. Tappan, *J. Pyrotech.* **2006**, *23*, 70–80; d) D. E. Chavez, M. A. Hiskey, R. D. Gilardi, *Org. Lett.* **2004**, *6*, 2889–2891; e) D. E. Chavez, B. C. Tappan, M. A. Hiskey, S. F. Son, H. Harry, D. Montoya, S. Hagelberg, *Propellants Explos. Pyrotech.* **2005**, *30*, 412–417; f) D. E. Chavez, M. A. Hiskey, R. D. Gilardi, *Angew. Chem.* **2000**, *112*, 1861–1863; *Angew. Chem. Int. Ed.* **2000**, *39*, 1791–1793; g) M. A. Hiskey, D. E. Chavez, D. Naud, US 6,342,589, 2002.
- [9] a) R. P. Singh, R. D. Verma, D. T. Meshri, J. M. Shreeve, *Angew. Chem.* **2006**, *118*, 3664–3682; *Angew. Chem. Int. Ed.* **2006**, *45*, 3584–3601 and references cited therein; b) J. J. Weigand, Ph. D. Thesis, Ludwig-Maximilians-Universität, München, 2005; c) A. J. Barrat, L. R. Bates, J. M. Jenkins, J. R. White, *Govt. Rep. Announce (U. S.)* **1973**, *73*, 70; d) A. G. Mayants, V. N. Vladimirov, N. M. Razumov, V. A. Shlyapochnikov, *J. Org. Chem. USSR (Engl. Transl.)* **1991**, *27*, 2177–2181; *Zh. Org. Khim.* **1991**, *27*, 2450–2455.
- [10] G. O. Reddy, A. K. Chatterjee, *Thermochim. Acta* **1983**, *66*, 231–244.
- [11] a) A. Hammerl, G. Holl, T. M. Klapötke, P. Mayer, H. Nöth, H. Piotrowski, M. Warchhold, *Eur. J. Inorg. Chem.* **2002**, *4*, 834–845; b) T. M. Klapötke, C. Miró Sabaté, *Chem. Mater.* **2008**, *20*, 1750–1763; c) C. Darwich, T. M. Klapötke, C. Miró Sabaté, *Propellants Explos. Pyrotech.* **2008**, in press.
- [12] a) T. M. Klapötke, C. Miró Sabaté, *Z. Anorg. Allg. Chem.* **2007**, *633*, 2671–2677; b) T. M. Klapötke, C. Miró Sabaté, *Chem. Mater.* **2008**, *20*, 3629–3637.
- [13] J. Koehler, R. Meyer, *Explosivstoffe*, 9th ed., Wiley-VCH, Weinheim, 1998.
- [14] J. Thiele, *Justus Liebigs Ann. Chem.* **1898**, *303*, 57–75.
- [15] G. O. Reddy, A. K. Chatterjee, *J. Hazard. Mater.* **1984**, *9*, 291–303.
- [16] R. J. Spear, P. P. Elischer, *Aust. J. Chem.* **1982**, *35*, 1–13.
- [17] A. Hammerl, G. Holl, M. Kaiser, T. M. Klapötke, H. Piotrowski, *Z. Anorg. Allg. Chem.* **2003**, *629*, 2117–2121.
- [18] N. B. Colthup, L. H. Daly, S. E. Wiberley, *Introduction to Infrared and Raman Spectroscopy*, Academic Press, Boston, 1990.
- [19] a) Oxford Diffraction, *ABSPACK*, CrysAlis CCD and CrysAlis RED. Versions 1.171, Oxford Diffraction Ltd., Abingdon, Oxfordshire, 2006; b) Programs for Crystal Structure Analysis (Release 97-2). G. M. Sheldrick, Institut für Anorganische Chemie der Universität, Tammanstrasse 4, 37077 Göttingen, Germany, 1998; c) A. Altomare, M. C. Burla, M. Camalli, G. L. Cascarano, C. Giacovazzo, A. Guagliardi, A. Moliterni, G. Polidori, R. Spagna, *J. Appl. Crystallogr.* **1999**, *32*, 115–119.
- [20] M. J. Frisch, G. W. Trucks, H. B. Schlegel, G. E. Scuseria, M. A. Robb, J. R. Cheeseman, J. A. Montgomery Jr, T. Vreven, K. N. Kudin, J. C. Burant, J. M. Millam, S. S. Iyengar, J. Tomasi, V. Barone, B. Mennucci, M. Cossi, G. Scalmani, N. Rega, G. A. Petersson, H. Nakatsuji, M. Hada, M. Ehara, K. Toyota, R. Fukuda, J. Hasegawa, M. Ishida, T. Nakajima, Y. Honda, O. Kitao, H. Nakai, M. Klene, X. Li, J. E. Knox, H. P. Hratchian, J. B. Cross, C. Adamo, J. Jaramillo, R. Gomperts, R. E. Stratmann, O. Yazyev, A. J. Austin, R. Cammi, C. Pomelli,

- J. W. Ochterski, P. Y. Ayala, K. Morokuma, G. A. Voth, P. Salvador, J. J. Dannenberg, V. G. Zakrzewski, S. Dapprich, A. D. Daniels, M. C. Strain, O. Farkas, D. K. Malick, A. D. Rabuck, K. Raghavachari, J. B. Foresman, J. V. Ortiz, Q. Cui, A. G. Baboul, S. Clifford, J. Cioslowski, B. B. Stefanov, G. Liu, A. Liashenko, P. Piskorz, I. Komaromi, R. L. Martin, D. J. Fox, T. Keith, M. A. Al-Laham, C. Y. Peng, A. Nanayakkara, M. Challacombe, P. M. W. Gill, B. Johnson, W. Chen, M. W. Wong, C. González, J. A. Pople, *Gaussian 03*, Revision A.1, Gaussian, Inc., Pittsburgh PA, **2003**.
- [21] A. D. Becke, A. Savin, H. Stoll, H. Preuss, *Chem. Phys. Lett.* **1989**, *157*, 200–206.
- [22] a) D. E. Woon, T. H. Dunning Jr, *J. Chem. Phys.* **1993**, *98*, 1358–1371; b) R. A. Kendall, T. H. Dunning Jr, R. J. Harrison, *J. Chem. Phys.* **1992**, *96*, 6796–6806; c) T. H. Dunning Jr, *J. Chem. Phys.* **1989**, *90*, 1007–1023; d) K. A. Peterson, D. E. Woon, T. H. Dunning Jr, *J. Chem. Phys.* **1994**, *100*, 7410–7415; e) A. Wilson, T. van Mourik, T. H. Dunning Jr, *THEOCHEM* **1997**, *388*, 339–349.
- [23] N–N and N=N bond lengths from: *International Tables for X-ray Crystallography*, Vol. C, Kluwer Academic Publishers, Dordrecht, **1992**.
- [24] a) I. D. Brown, *Acta Crystallogr., Sect. B* **1988**, *44*, 545–553; b) J. Hitzbleck, G. B. Deacon, K. Ruhlandt-Senge, *Eur. J. Inorg. Chem.* **2007**, *4*, 592–601; c) B. Lian, C. M. Thomas, O. L. Casagrande Jr, T. Roisnel, J.-F. Carpentier, *Polyhedron* **2007**, *26*, 3817–3824; d) T. Zhang, C. Lu, J. Zhang, K. Yu, *Propellants Explos. Pyrotech.* **2003**, *28*, 271–276; e) N. C. Mosch-Zanetti, M. Ferbinteanu, J. Magull, *Eur. J. Inorg. Chem.* **2002**, *4*, 950–956; f) I. Kobrsi, J. E. Knox, M. J. Heeg, H. B. Schlegel, C. H. Winter, *Inorg. Chem.* **2005**, *44*, 4894–4896.
- [25] A. Hammerl, Ph. D. Thesis, Ludwig-Maximilians Universität, München, **2001**.
- [26] R. Taylor, O. Kennard, *J. Am. Chem. Soc.* **1982**, *104*, 5063–5070.
- [27] a) J. Bernstein, R. E. Davis, L. Shimoni, N.-L. Chang, *Angew. Chem. Int. Ed. Engl.* **1995**, *34*, 1555–1573; b) W. D. S. Motherwell, G. P. Shields, F. H. Allen, *Acta Crystallogr., Sect. B* **2000**, *56*, 466–473; c) W. D. S. Motherwell, G. P. Shields, F. H. Allen, *Acta Crystallogr., Sect. B* **1999**, *55*, 1044–1056; d) <http://www.ccdc.cam.ac.uk/support/documentation/rpluto/TOC.html>.
- [28] Impact, insensitive: >40 J, less sensitive: ≥35 J, sensitive: ≥4 J, very sensitive: ≤3 J. Friction, insensitive: >360 N, less sensitive: 360 N, sensitive: 80–360 N, very sensitive: ≤80 N, extremely sensitive: ≤10 N. All values according to the UN Recommendations on the Transport of Dangerous Goods.
- [29] <http://www.bam.de/>.
- [30] T. M. Klapötke, C. M. Rienäcker, *Propellants Explos. Pyrotech.* **2001**, *26*, 43–47.
- [31] Calculation of the oxygen balance: $\Omega (\%) = (\text{O} - 2\text{C} - \text{H}/2 - x\text{AO}) 1600/M$; M : molecular mass.
- [32] a) *NIST Standard Reference Database Number 69*, **2005**, Web Release: <http://webbook.nist.gov/chemistry/>; b) D. R. Lide, *CRC Handbook of Chemistry and Physics*, 77th ed., **1996–1997**.
- [33] a) V. Ernst, T. M. Klapötke, J. Stierstorfer, *Z. Anorg. Allg. Chem.* **2007**, *633*, 879–887; b) T. M. Klapötke, H. Radies, J. Stierstorfer, *Z. Naturforsch. Teil B* **2007**, *62*, 1343–1352.
- [34] http://www.linseis.net/html_en/thermal/dsc/dsc_pt10.php.
- [35] <http://www.parrinst.com>.

Received: September 22, 2008

Published Online: December 5, 2008

Toward an Allosteric Metallated Container

Helga Szelke,^[a] Hubert Wadepohl,^[a] Morsy Abu-Youssef,^[a,b] and Roland Krämer*^[a]**Keywords:** Allosterism / Supramolecular chemistry / Cage compounds / Iron / Ruthenium

Polytopic ligands L^1 and L^2 in which three 2,2'-bipyridine units are linked to a central tris(pyrid-2-yl)amine (L^1) or tris-(pyrid-2-yl)methanol (L^2) moiety by alkyl spacers were prepared by multistep organic syntheses. The parent tris(pyrid-2-yl)-type ligands were shown to be modest-to-good chelators for Zn^{2+} and Cu^{2+} ions in solution, and bi- and tridentate N-coordination was confirmed by crystal structures of Cu^{II} and Ru^{II} complexes, respectively. Fe^{II} and Ru^{II} smoothly form stable, cage-like 1:1 complexes with L^1 and L^2 , in which the metal ion is coordinated to the tris(bpy) site of the ligands. The vacant tris(pyrid-2-yl) site of these complexes is, however, a poor donor site for Zn^{2+} and Cu^{2+} ions. In addition, Fe^{II} modulates the coordination behaviour of the tris(pyrid-2-yl) site toward Zn^{2+} : Whereas tris(5-methylpyrid-2-yl)amine forms a 2:1 complex with Zn^{2+} in CH_2Cl_2 , $[Fe(L^1)]^{2+}$ forms a

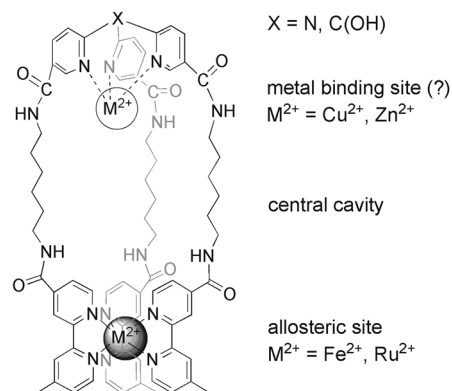
1:1 Zn complex. Spectrophotometric titrations suggest that $[Fe(L^2)]^{2+}$ forms a polynuclear Zn^{2+} complex in CH_2Cl_2 , possibly involving bridging coordination of the alcohol OH group, which contrasts the smooth formation of a 2:1 complex of the parent tris(pyrid-2-yl)-type ligand with Zn. Fe^{II} might therefore be considered as an allosteric effector, which modulates the metal binding properties of the second tris(pyrid-2-yl) site of L^1 and L^2 . Contrary to expectation, Zn^{2+} and Cu^{2+} appear to associate weakly with donor atoms directed toward the exterior of the cage-like complexes $[Fe(L^n)]^{2+}$ and $[Ru(L^1)]^{2+}$, rather than locating in the interior of the container by tripodal coordination to the tris(pyrid-2-yl) site.

(© Wiley-VCH Verlag GmbH & Co. KGaA, 69451 Weinheim, Germany, 2009)

Introduction

Metal-ion cofactors of metalloproteins are often located in discrete cavities that support selective and effective substrate binding and/or protection of reactive metal-bound species. Chemists were inspired early to prepare low-molecular weight coordination compounds that effectively mimic the shielding of such reactive metal sites.^[1] The design of such compounds has meanwhile developed into an important research line in bioinorganic and supramolecular chemistry, including “metallated containers”^[2] and calixarene-based “funnel complexes”.^[3] In this context, complexes of tripodal ligands that mimic the tris(imidazole) donor sites in a number of zinc and copper proteins have attracted considerable attention;^[4] open cavities around the metal site are generated by attachment of bulky substituents to the ligating groups. Substrate selectivity and shielding might be further optimized by complete encapsulation of the metal ion within a cage-like ligand framework without hindering access of the substrate to free metal sites, but synthesis of such compounds is expected to be more challenging and less versatile.

Here we suggest a supramolecular approach to the development of a cage-like compound for incorporation of both a reactive metal ion and a substrate (Scheme 1). A tripodal tris(pyrid-2-yl)amine or -methanol unit serves as an analogue of the biological tris(imidazole) metal-binding site. Substituents are appended at the 5-position (rather than the 6-position) of the pyridyl rings in order to avoid steric hindrance of substrate binding by the metal ion and guarantee adequate cavity size for incorporation of small-molecule substrates. Three bidentate 2,2-bipyridine units are linked to the tripodal moiety by alkyl spacers in a manner that ring closure and formation of a bicyclic cage is achieved by intramolecular, metal-assisted assembly (Scheme 1). This



Scheme 1.

[a] Anorganisch-Chemisches Institut der Universität Heidelberg, Im Neuenheimer Feld 270, 69120 Heidelberg, Germany
Fax: +49-6221-548599
E-mail: roland.kraemer@urz.uni-heidelberg.de

[b] On leave from Chemistry Department, Faculty of Science, Alexandria University, 21321 Alexandria, Egypt

strategy avoids potentially complicated covalent synthesis of a relatively large bicyclic structure. In addition, considering the polytopic ligand as a ditopic receptor, coordination of a metal ion to the tris(bpy) site is expected to modify the metal binding properties of the tris(pyrid-2-yl) site, as described for a variety of synthetic allosteric receptors^[5] for metal ions. Here we will describe the synthesis of the polytopic ligands, their interaction with transition-metal ions and an allosteric relation between the two metal binding sites [tris(bpy) and tri(pyrid-2-yl)] of the ditopic receptors.

Results and Discussion

Ligand Synthesis

The synthetic route to polytopic ligands **L**¹ [tridentate site: tris(pyrid-2-yl)amine] and **L**² [tridentate site: tris(pyrid-2-yl)methanol] is summarized in Scheme 2. 2,2'-Bipyridine derivative **1** was synthesized by coupling the linker *N*-Boc-1,6-diaminohexane to 4'-methyl-2,2'-bipyridine-4-carboxylic acid^[6] by using a standard amide coupling reaction, followed by removal of the Boc protecting group under acidic conditions. Tris(2-pyridyl)amine derivative **2** was prepared by the reaction of 2-amino-5-picoline and 2-bromo-5-methylpyridine over copper bronze. The methyl groups of **2** were oxidized to the corresponding tris(2-nicotinic acid)-amine (**3**) by using potassium permanganate as an oxidant. Finally, **3** was joined to three bipyridine units **1** by amide coupling to yield ligand **L**¹ (Scheme 2).

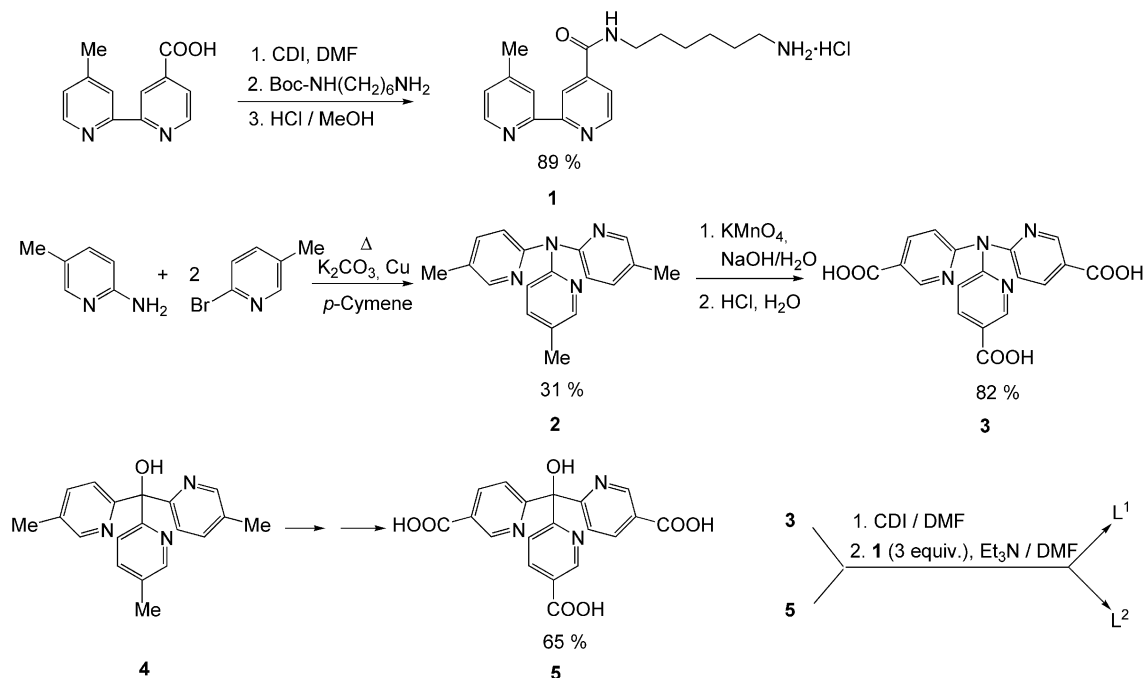
Tris(2-nicotinic acid)methanol (**5**) was synthesized by the oxidation of the methyl groups of tris[(5-methylpyrid-2-yl)]-methanol (**4**)^[7] as described in the literature.^[8] Three units

of bipyridine derivative **1** were coupled to **5** as described for **L**¹ above to give ligand **L**² (Scheme 2). The latter was available in low quantity so that only selected experiments and analytics could be performed (Scheme 3).

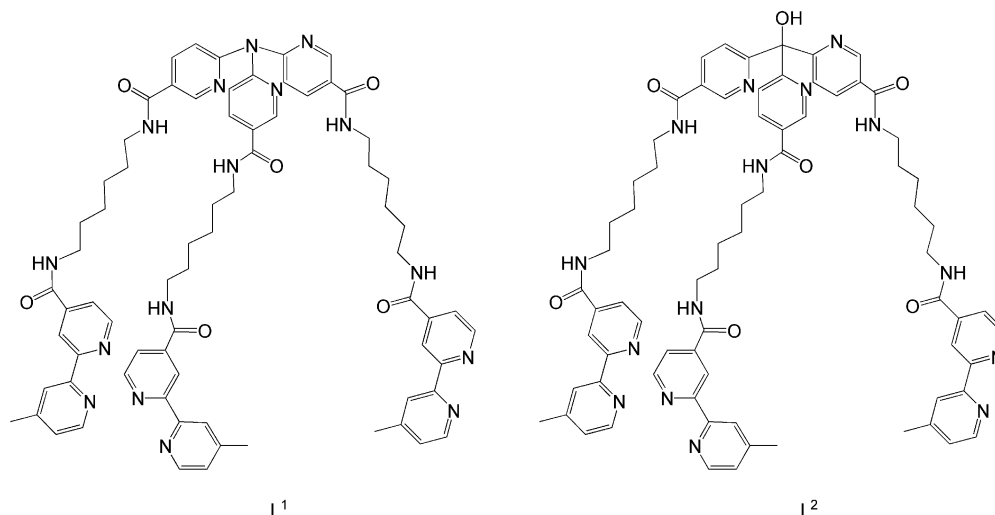
Interaction of **2** and **4** with Zn²⁺ and Cu²⁺ in Solution

We characterized the coordination of Zn²⁺ and Cu²⁺ bio-metals to the simple tripodal ligands **2** and **4** in solution to achieve a better understanding of the interaction of these exchange-labile metal ions with the tris(pyrid-2-yl) site in more complex ligands **L**¹ and **L**².

Tris(pyrid-2-yl)amine was reported to form (depending on the ligand-to-metal ratio) a tetrahedral 1:1 complex with ZnCl₂ and an octahedral 2:1 complex with Zn(O₂CCF₃)₂ in the crystalline state.^[9] In both complexes, tris(pyrid-2-yl)amine coordinates in a bidentate fashion, and planarity around the central N atom is retained. Bidentate coordination, although with fluctuational behaviour, is retained in dichloromethane solution, as evidenced by NMR spectroscopy. Similarly, both 1:1 and 2:1 complexes with Cu^{II} have been reported, again with bidentate coordination of tris(pyrid-2-yl)amine. In contrast, in the presence of weakly coordinating perchlorate counterion, octahedral 2:1 complexes with exchange labile Co^{II} and Ni^{II} were reported in which tris(pyrid-2-yl)amine is tridentate.^[10] The coordination mode of tris(pyrid-2-yl)amine appears to be controlled by specific preferences of the transition metal. Possibly, a loss of *N*-aryl resonance energy due to pyramidalization slightly disfavours a tripodal coordination. On the basis of ball-and-stick models and preliminary force field calculations, we speculated that preorganization of the pyridyl do-



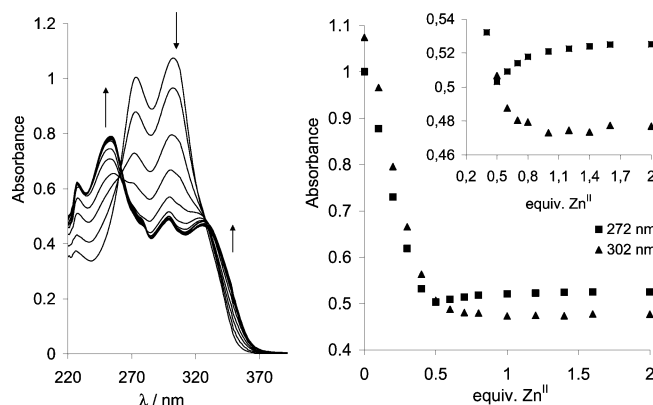
Scheme 2. Synthesis of **L**¹ and **L**².

Scheme 3. Structure of polytopic ligands L^1 and L^2 .

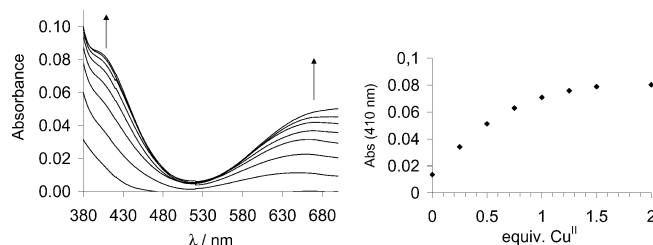
nors in the cage-like structure depicted in Scheme 1 would favour tripodal coordination of Zn and Cu. In addition, coordination of two cage-like moieties to one zinc or copper ion should be disfavoured.

Interaction of **2** with Zn is solvent and counterion dependent; in 50 μM solutions of **2** in water/methanol mixtures the UV/Vis spectra exhibit no changes upon addition of the Zn^{2+} salts, indicating no complexation. Smooth complexation of **2** by Zn is observed in the noncompetitive solvent CH_2Cl_2 in the presence of the weakly coordinated counterion ClO_4^- . Upon the addition of $\text{Zn}(\text{ClO}_4)_2$ (0–0.5 equiv.) to a (50 μM) solution of **2**, a significant and nearly linear decrease in the 272 and 302 nm absorbances of the ligand together with two isosbestic points at 260 and 326 nm is observed (Figure 1). This is compatible with the formation of a complex $[\text{Zn}(\mathbf{2})_2]^{2+}$. The minor changes observed in the UV spectrum upon addition of 0.5–1.0 equiv. of Zn^{2+} (enlarged absorbance diagram, Figure 1, right) might indicate conversion of the 2:1 into a 1:1 complex $[\{\text{Zn}(\mathbf{2})\}^{2+}]$. Formation of 2:1 and 1:1 complexes with Zn^{2+} in CD_2Cl_2 , depending on the ligand-to-metal ratio, was also described of for tris(pyrid-2-yl)amine on the basis of NMR spectroscopic investigations.^[9]

Cu^{2+} forms stronger complexes with **2** than Zn^{2+} , as indicated by the titration of **2** (1 mM) with $\text{Cu}(\text{NO}_3)_2$ solution in competitive solvent water/methanol (3:1) containing 10 mM MOPS buffer at pH 7.0 and 50 mM NaCl. A shoulder appears at about 410 nm together with a broad absorbance at 650 nm (Figure 2). The plot of the absorption intensity at 410 nm against the Cu^{2+} equivalents indicates about 90% complex formation at 1.0 equiv. and saturation at about 2 equiv. Formation of a green 1:1 Cu^{2+} complex with bidentate coordination of tris(5-methylpyrid-2-yl)amine was confirmed by X-ray structural analysis (see below) of the crystalline precipitate formed when the solution was treated with NaClO_4 and allowed to stand for several days at ambient temperature. In the noncompetitive solvent CH_2Cl_2 , the

Figure 1. Spectrophotometric titration of **2** (50 μM in CH_2Cl_2) with $\text{Zn}(\text{ClO}_4)_2$ in 0.1 equiv. steps. Inset: decrease in the absorbance at 272 nm (■) and at 302 nm (▲).

titration of **2** with $\text{Cu}(\text{ClO}_4)_2$ compares well with the Zn titration, suggesting stepwise formation of 2:1 and 1:1 complexes.

Figure 2. Spectrophotometric titration of **2** (1 mM in $\text{H}_2\text{O}/\text{MeOH}$, 3:1; pH 7.0; 10 mM MOPS buffer; 50 mM NaCl) with $\text{Cu}(\text{NO}_3)_2$. Left: increase in the absorbance at 410 nm.

Tris(pyrid-2-yl)methanol (**4**) is expected to form more stable tripodal transition-metal complexes due to better preorganization of the pyridyl groups linked to the central sp^3 carbon atom. In contrast, the coordination mode is am-

biguous due to potential participation of the (deprotonated) OH group in metal binding. Compound **4** in mM concentration was shown by NMR spectroscopy to preferably form a 2:1 Zn^{2+} complex in aqueous solution and a mixture of 1:1 and 2:1 complexes in acetonitrile solution, both with tripodal N,N,N-coordination.^[8,11] Tris(6-methoxypyrid-2-yl)methanol, a ligand related to **4**, was shown to form a distorted octahedral 2:1 complex with Cu^{2+} (crystal structure), again with tridentate N,N,N-coordination of both ligands (Figure 3).^[12]

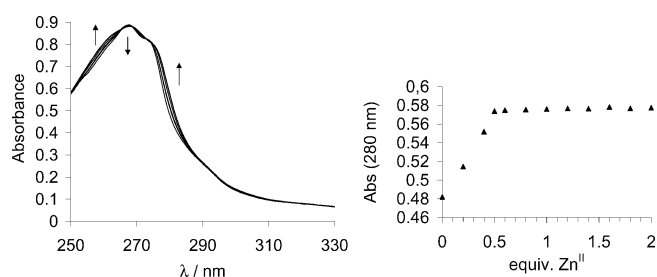


Figure 3. Spectrophotometric titration of **4** (50 μM in $\text{H}_2\text{O}/\text{MeOH}$, 1:1; pH 7.0; 10 mM MOPS buffer; 50 mM NaCl) with ZnSO_4 . Left: increase in the absorbance at 280 nm.

Spectrophotometric titration of **4** (50 μM) with ZnSO_4 in water/methanol (1:1) was followed by relatively small absorbance changes in the UV region of the spectrum and confirms smooth formation of a complex $[\text{Zn}(\textbf{4})_2]^{2+}$ by linear absorbance increase at 280 nm for 0–0.5 equiv. of Zn^{2+} . No further changes are observed at >0.5 equiv. of Zn^{2+} , but conversion into a 1:1 complex with a large excess of Zn^{2+} is not ruled out.

When **4** is titrated with CuSO_4 under the same conditions, a significant increase in the absorbance at 330 nm is observed, together with development of a weak absorbance in the visible spectrum at about 600 nm (Figure 4). The 330 nm absorbance diagram suggests stepwise formation of complexes $[\text{Cu}(\textbf{4})_2]^{2+}$ at 0.5 equiv. of Cu^{2+} and $[\text{Cu}(\textbf{4})]^{2+}$ at 1 equiv. of Cu^{2+} , which might have slightly different absorbance maxima in the optical spectrum.

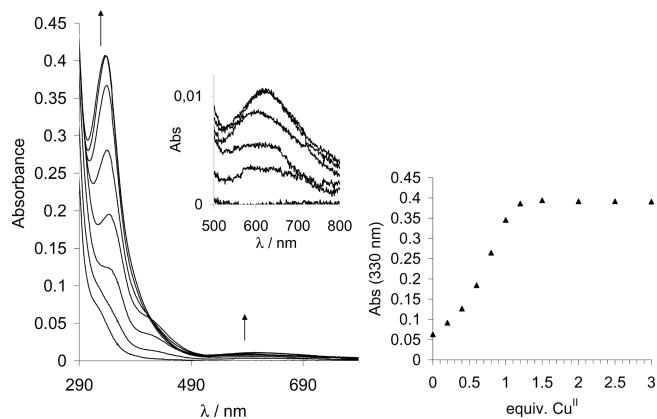


Figure 4. Spectrophotometric titration of **4** (50 μM in $\text{H}_2\text{O}/\text{MeOH}$, 1:1; pH 7.0; 10 mM MOPS buffer; 50 mM NaCl) with CuSO_4 . Inset: increase in the absorbance at 610 nm. Left: increase in the absorbance at 280 nm.

X-ray Crystallography of **2** and Its Metal Complexes

Structure of Tris(3-methyl-pyrid-2-yl)amine

The X-ray crystal structure of tris(pyrid-2-yl)amine was reported only recently,^[9] and **2** has, to the best of our knowledge, not yet been crystallographically characterized.

As in tris(pyrid-2-yl)amine, the central nitrogen atom N1 in **2** is nearly coplanar with the three adjacent carbon atoms; the deviation from the $(\text{C})_3$ plane is only 0.041(1) Å. The dihedral angles between the pyridyl rings and the $(\text{C})_3$ plane were found to be 23.0, 40.2 and 40.9° (Figure 5).

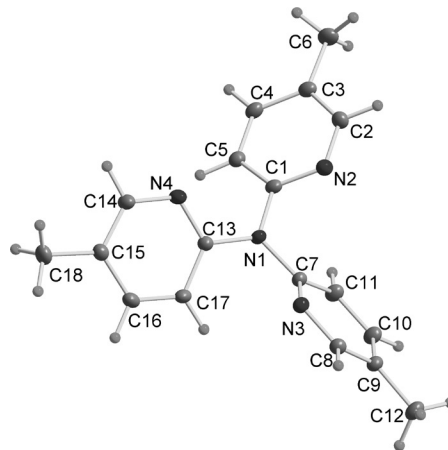


Figure 5. ORTEP diagram showing the structure of **2** with 50% thermal ellipsoids and the atom-labelling scheme.

Structure of $[(2)\text{Cu}(\text{H}_2\text{O})_2(\text{NO}_3)](\text{ClO}_4) \cdot 2\text{H}_2\text{O}$

The X-ray structure of the complex cation of **2**, $[(2)\text{Cu}(\text{H}_2\text{O})_2(\text{NO}_3)](\text{ClO}_4) \cdot 2\text{H}_2\text{O}$, which was obtained by mixing solutions of **2** and $\text{Cu}(\text{NO}_3)_2$ with the addition of NaClO_4 , is shown in Figure 6. The Cu^{2+} ion displays a distorted octahedral environment (CuN_2O_4). Compound **2** acts as an N,N'-bidentate chelating ligand with Cu–N bond lengths of 1.973(3) and 1.981(3) Å and an N–Cu–N angle of 88.7(1)°. Planarity of the central N atom in complex **2**·Cu is retained, where the deviation of N1 from the $(\text{C})_3$ plane [0.014(4) Å] was found to be smaller than that in the free ligand. The dihedral angle between the uncoordinated pyridyl ring and the $(\text{C})_3$ plane was found to be 76.9°.

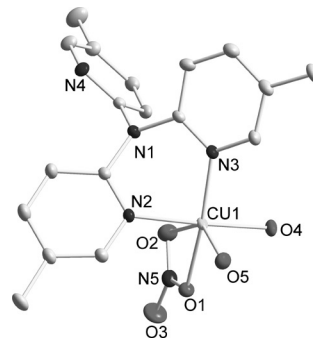


Figure 6. ORTEP diagram showing the structure of $[(2)\text{Cu}(\text{H}_2\text{O})_2(\text{NO}_3)]^+$ complex cation with 50% thermal ellipsoids and the atom-labelling scheme. Hydrogen atoms are omitted for clarity.

whereas the coordinated pyridine rings keep nearly the same 40.9 and 44.4°. The Cu–O(water) bond lengths are 1.944(2) and 2.168(3) Å, whereas the Cu–O(nitrate) distances are 2.034(2) and 2.656(3) Å. Bond angles around the central Cu ion range from 81.5(1) to 98.8(1)°, except the O–Cu–O angle of the chelating nitrate, which was found to be 53.24(9)°. Bidentate coordination by the tris(pyrid-2-yl)-amine moiety is also found in other crystallographically characterized Cu^{II} complexes: [L = tris(pyrid-2-yl)amine]; [Cu₄L₄-μ(OH)₄(F₃CSO₃)₂]·F₃CSO₃·OC(CH₃)₂,^[13] [CuL₂-(NCCH₃)₂]·F₃CSO₃,^[14] [CuL₂(NO₃)₂]^[15] and [CuL₂-(ClO₄)₂].^[16]

Structure of [(2)₂Ru](PF₆)₂

Orange crystals of the complex [Ru(2)₂](PF₆)₂ (Figure 7) were obtained by reaction of **2** with RuCl₂(dmsO)₄, followed by precipitation of the complex cation with PF₆[−] and recrystallization from methanol. The complex cation is octahedral with a crystallographic centre of symmetry. The Ru–N(py) bond lengths range from 2.064(2) to 2.073(2) Å and the N–Ru–N bond angles range from 86.20(7) to 93.80(7)°, indicating a nearly perfect octahedral coordination of Ru^{II} by two tridentate moieties of **2**. Very similar bonding parameters around Ru^{II} have been reported for the following complexes [L = tris(pyrid-2-yl)amine]: [RuL₂]S₂O₆·H₂O and [RuL₂]Cl₂·H₂O.^[17,18]

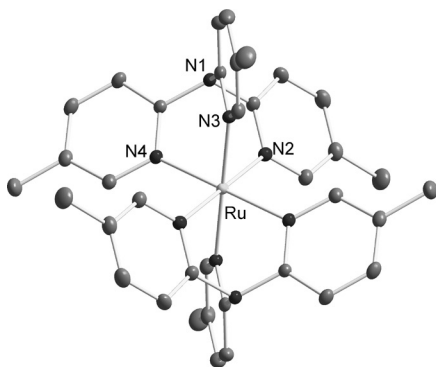


Figure 7. ORTEP diagram showing the structure of Ru[(2)₂]²⁺ complex cation with 50% thermal ellipsoids and the atom-labelling scheme. Hydrogen atoms are omitted for clarity.

Interaction of Polytopic Ligands L¹ and L² with Metal Ions

Binding of Fe^{II} to L¹ and L²

The complexation behaviour of the polytopic ligands L¹ and L² with Fe²⁺ (offered as BF₄[−] salt) in CH₂Cl₂ at 25 °C was monitored by spectrophotometric titration. Smooth formation of a 1:1 complex is indicated by two isosbestic points at 269 and 290 nm (Figure 8).

Absorbance at selected wavelengths 360 and 537 nm increases linearly upon addition of 0–1 equiv. of Fe²⁺. The absorption band around 537 nm is characteristic for the MLCT of the Fe[tris(2,2'-bipyridine)]²⁺ octahedral complex,^[19] which forms in a cooperative manner with a very high stability constant log(β₃) = 21 in water. It is therefore

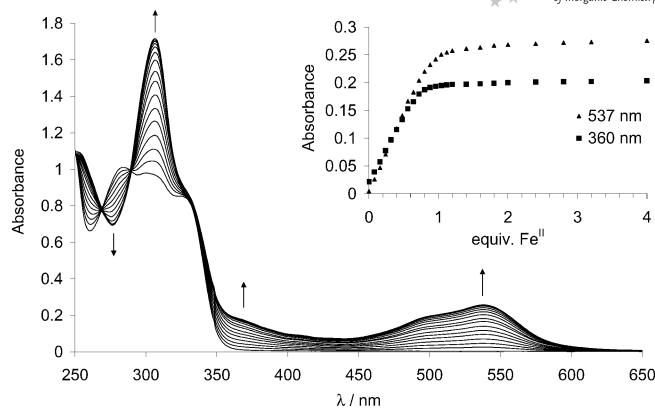


Figure 8. Spectrophotometric titration of **2** (25 μM in CH₂Cl₂) with Fe(BF₄)₂. Inset: increase in the absorbance at 360 nm (■) and at 537 nm (▲).

very likely that Fe²⁺ forms an octahedral complex with the tris(bpy) site of L¹. The red 1:1 complex [Fe(L¹)](ClO₄)₂ could be isolated and characterized by MS (ESI) and elemental analysis. Thus, Fe²⁺ assembles the tricyclic cage-like structure as expected. The same conclusion can be drawn when L¹ is titrated with Fe²⁺ in more competitive solvents (methanol, dmsO/water mixtures). Smooth binding of Fe²⁺ to a tris(bpy) site was described previously for related tri-brachial ligands with three 2,2-bipyridine moieties linked by aza-polyether, aza-thioether or hydroxamic acid containing chains. In these compounds, the Fe²⁺ ion organizes as cryptand-like structures and allosterically controls the binding of alkali-metal ions or transition-metal ions, respectively.^[20] Upon addition of >1 equiv. of Fe to L¹, no further spectral changes are observed between 250 and 650 nm, indicating that even in the noncompetitive solvent CH₂Cl₂, additional Fe²⁺ does not interact with the vacant tris(pyrid-2-yl)amine site of the complex.

Very similar spectrophotometric changes are observed when L² is titrated with 0–1 equiv. of Fe(BF₄)₂ under the same conditions (Figure 9), although the 1:1 complex could not be isolated in pure form. Interestingly and in contrast to the behaviour of L¹, a further linear increase in the 360 nm absorbance of L² is observed upon addition of 1–4 equiv. of Fe and levels off at >4 equiv., whereas the 537 nm band remains unchanged. An increase in the 360 nm band suggests interaction of the free pyridyl groups with Fe, but the L¹:Fe stoichiometry is not compatible with a binding of just a second Fe²⁺ ion to the tris(pyrid-2-yl) site in the interior of the cage. Rather, the OH group in L² might act as a bridging ligand {as observed for the Cu²⁺ ions in the related complex [Cu₃(Br)(L)₃](PF₆)₂,^[21] where L = tris(6-methyl-2-pyridyl)methanol}, for up to three Fe^{II} ions with additional coordination by one pyridyl group each and located at the exterior of the cage.

¹H NMR spectra of [Fe(L¹)](BF₄)₂ were taken in CD₃OD solutions containing 20% [D₆]dmsO. At room temperature, the spectrum of aromatic protons displays broad featureless signals, which overlap a set of sharp signals. When the sample is heated to 60 °C, the intensity of the

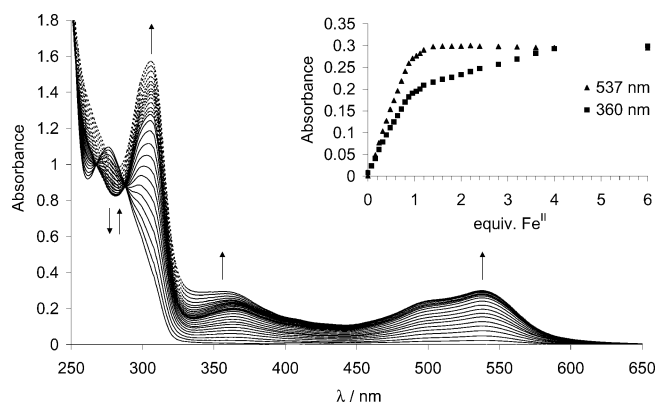


Figure 9. Spectrophotometric titration of **4** (25 μM in CH_2Cl_2) with $\text{Fe}(\text{BF}_4)_2$ in 0–1 equiv. steps (solid lines) and 1–6 equiv. steps (dashed lines). Inset: increase in the absorbance at 360 nm (■) and at 537 nm (▲).

sharp signals increases and that of the broad signals decreases. The final spectrum remains unchanged after cooling to room temperature, even after prolonged standing. A reasonable interpretation of this observation is the formation of two diastereomers due to chirality of both the $\text{Fe}(\text{bpy})_3$ site and the NPy_3 “propeller”, which give rise to different sets of NMR signals (broad and sharp, respectively). When the complex is prepared at room temperature, diastereomer formation is under kinetic control, yielding a mixture of isomers. Upon heating to 60 $^\circ\text{C}$, the configuration of the $\text{Fe}(\text{bpy})_3$ moiety becomes labile, leading to equilibration and enrichment of the thermodynamically favoured second isomer with sharp NMR signals.

Binding of Ru^{II} to L^1

L^1 reacted with 1 equiv. of RuCl_3 at elevated temperature to give the red complex $[\text{Ru}(\text{L}^1)]\text{Cl}_2$. Its composition was confirmed by HRMS (ESI) and elemental analysis. Selective binding of Ru^{II} to the tris(bpy) site is supported by a characteristic MLCT absorbance at $\lambda_{\text{max}} = 460 \text{ nm}$, together with a corresponding fluorescence at $\lambda_{\text{em}} = 630 \text{ nm}$ (Figure 10) as observed for the complex $[\text{Ru}(\text{bpy})_3]^{2+}$.^[22] In contrast, the Ru^{II} complex of **2**, $[\text{Ru}(\text{2})]^{2+}$, is yellow with an absorbance maximum at 396 nm. Whereas the Fe^{2+} ion in $\text{Fe}(\text{L}^1)$ can be removed by prolonged treatment with a

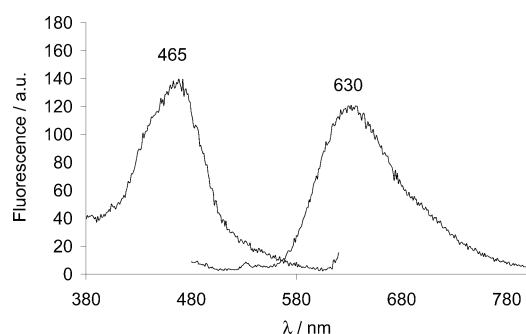


Figure 10. $\text{Ru}(\text{bpy})_3$ centred fluorescence emission spectrum (630 nm) of $[\text{Ru}(\text{L}^1)]\text{Cl}_2$ (5 μM in $\text{EtOH}/\text{H}_2\text{O}$, 1:1; pH 7.0; 10 mM MOPS). Absorbance spectrum ($\lambda_{\text{max}} = 465 \text{ nm}$) is included.

large excess of EDTA or by exchange with an excess amount of Cu^{2+} ions, $[\text{Ru}(\text{L}^1)]\text{Cl}_2$ is not affected by these reagents and, as expected, displays very high kinetic stability.

The ^1H NMR spectra of $[\text{Ru}(\text{L}^1)]\text{Cl}_2$ in CD_3OD look similar to those of the corresponding Fe^{II} complex at room temperature. However, the spectrum remains unchanged after heating to 60 $^\circ\text{C}$. This is consistent with the kinetic inertness of the $\text{Ru}(\text{bpy})_3$ unit, which prevents equilibration of the diastereomer mixture.

Interaction of $\text{Fe}^{\text{II}}(\text{L}^n)$ and $\text{Ru}^{\text{II}}(\text{L}^1)$ with Zn^{2+} and Cu^{2+}

When the 1:1 iron(II) complexes of L^1 and L^2 are exposed to CuSO_4 in aqueous systems, the 537 nm band characteristic of the $\text{Fe}^{\text{II}}(\text{bpy})_3$ unit slowly decreases, indicating replacement of Fe^{2+} by Cu^{2+} at the bpy site of L^n . In contrast, fluorescence titration of the stable $\text{Ru}^{\text{II}}(\text{L}^1)$ complex with Cu^{2+} in aqueous systems indicates an interaction by significant 630 nm fluorescence quenching at 0–1 equiv. of Cu . This is, however, not accompanied by the characteristic absorbance changes in the UV region of the spectrum, which were seen in the titration of **2** with Cu . We therefore suggest association of Cu^{2+} at the exterior of the cage, at a site other than bis- or tris(pyrid-2-yl).

When solutions of $\text{Fe}^{\text{II}}(\text{L}^1)$, $\text{Fe}^{\text{II}}(\text{L}^2)$ and $\text{Ru}^{\text{II}}(\text{L}^1)$ were titrated with ZnSO_4 in aqueous solvent mixtures, no spectral changes were observed between 250 and 650 nm. As observed for **2**, Zn^{2+} does not interact with the tris(pyrid-2-yl) site of $\text{Fe}^{\text{II}}(\text{L}^1)$ in competitive solvents. In the noncompetitive solvent CH_2Cl_2 , however, a titration of $[\text{Fe}(\text{L}^1)](\text{BF}_4)_2$ with $\text{Zn}(\text{ClO}_4)_2$ reveals similar changes in the UV absorbance as observed for **2** (Figure 11), but the 330 nm absorbance diagram indicates formation of a 1:1 complex (whereas a 2:1 ligand/metal complex was formed with **2**, see Figure 1). This observation alone does not allow the conclusion of Zn binding in the interior of the container as depicted in Scheme 1, although a reason for the lack of 2:1 complex formation, which might form by interaction of Zn^{2+} with external binding sites of *two* $\text{Fe}^{\text{II}}(\text{L}^1)$ moieties, is

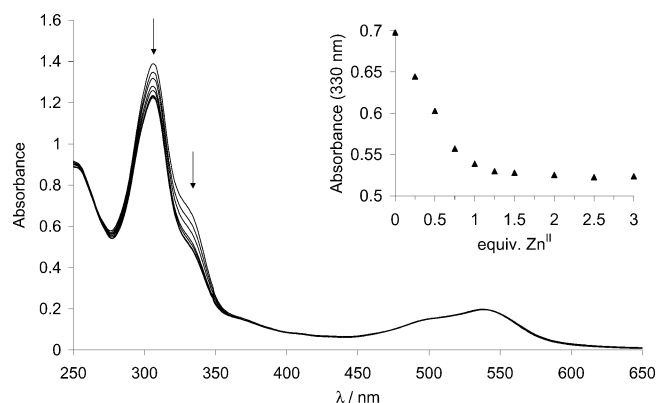


Figure 11. Spectrophotometric titration of $[\text{Fe}(\text{L}^1)](\text{BF}_4)_2$ (20 μM in CH_2Cl_2) with $\text{Zn}(\text{ClO}_4)_2$. Inset: increase in the absorbance at 330 nm.

not obvious. Unfortunately, the NMR spectra of $\text{Fe}^{\text{II}}(\text{L}^1)$ in the presence or absence of Zn^{2+} display broad signals only and are not helpful for determination of Zn binding mode.

The same experimental conditions were kept to study the interaction of $[\text{Fe}(\text{L}^2)](\text{BF}_4)_2$ in CH_2Cl_2 with $\text{Zn}(\text{ClO}_4)_2$ (data not shown). We noticed a small increase in the absorption intensity at 305 nm and a decrease at 285 nm, with an isosbestic point at 296 nm, indicating interaction of Zn^{2+} with the pyridyl units of $[\text{Fe}(\text{L}^2)](\text{BF}_4)_2$. However, as in the titration of $[\text{Fe}(\text{L}^2)](\text{BF}_4)_2$ with excess Fe^{2+} , spectral changes do not level off after 1 equiv. of Zn^{2+} , again indicating formation of polynuclear Zn^{II} complexes at exterior binding sites.

Conclusions

We prepared tribrachial ligands L^1 and L^2 , which offer two distinct sites for metal-ion coordination: a tridentate tris(pyrid-2-yl) site and a tris(bidentate) 2,2'-bipyridyl site. These ligands form stable, cage-like 1:1 complexes with Fe^{II} and Ru^{II} , which coordinate to the tris(bpy) site with high selectivity. Whereas the parent tris(pyrid-2-yl)-type ligands are moderate-to-good binders of exchange-labile metal ions Zn^{2+} and Cu^{2+} in solution, the tris(pyrid-2-yl) site within the cage-type complexes is a poor ligand, indicating negative allostery in transition-metal binding of L^1 and L^2 . Spectrophotometric titrations suggest weak association of Zn^{II} and Cu^{II} with donor groups orientated to the exterior of the cage rather than incorporation of these metal ions in the interior of the container by tridentate coordination to the tris(pyrid-2-yl) site. The reasons for this unexpected behaviour might include stabilization of the "empty" container by intramolecular hydrophobic interactions, intramolecular electrostatic repulsion of the two metal ions and enforced desolvation of the metal ion within the container. Redesign of the polytopic ligand is currently in progress. In addition, we are trying to attach exchange inert transition-metal ions to the tris(pyrid-2-yl) site of L^n , after selective protection of bpy moieties.

Experimental Section

General: Commercially available chemicals were purchased from Sigma–Aldrich (Germany) and used without purification. 4'-Methyl[2,2']bipyridine-4-carboxylic acid,^[6] tris[2-(5-methylpyridyl)]-methanol (**4**),^[7] tris(2-nicotinic acid)methanol (**5**)^[8] and $\text{RuCl}_2(\text{dmsO})_4$ ^[23] were synthesized as described in the literature. NMR spectra were obtained with Bruker Avance 200 and 400 MHz spectrometers, chemical shifts are given in ppm relative to Me_4Si , coupling constants are given in Hz. ESI mass spectra were measured with a Q-TOF Ultima ESI-MS instrument (Waters-Micro-mass). Elemental analyses were performed by Microanalytisches Laboratorium des Organisch-Chemischen Instituts der Universität Heidelberg.

***N*-(Aminohexyl)-4'-methyl-2,2'-bipyridine-4-carboxamide·HCl (1):** A solution of 4'-methyl-2,2'-bipyridine-4-carboxylic acid (1.0 g, 4.7 mmol) and 1,1'-carbonyldiimidazole (CDI; 0.83 g, 4.7 mmol) in dry DMF (15 mL) was stirred at 60 °C under an atmosphere of nitrogen for 30 min. Then, a solution of *N*-Boc-1,6-diaminohexane (1.0 g, 4.7 mmol) in dry DMF (10 mL) was added dropwise and stirring was continued at 60 °C under an atmosphere of nitrogen for 16 h. Solvent was removed under reduced pressure, and the residue was taken up in chloroform (100 mL). This solution was filtered to remove residues of unreacted carboxylic acid, and the filtrate was extracted with saturated NH_4Cl (50 mL) and brine (50 mL). The organic phase was dried with MgSO_4 , filtered and the solvent was removed under reduced pressure to afford the Boc-protected amide (1.59 g, 83%) as a white solid. ^1H NMR (200 MHz, CDCl_3): δ = 1.34–1.53 (m, 6 H), 1.40 (s, 9 H), 1.59–1.69 (m, 2 H), 2.42 (s, 6 H), 3.11 (q, J = 7.2 Hz, 2 H), 3.44 (q, J = 6.4 Hz, 2 H), 4.57 [br. s, 1 H, NHC(O)], 6.72 [br. s, 1 H, NHC(O)], 7.17 (d, J = 5.0 Hz, 1 H), 7.78 (dd, J = 5.0 Hz, J = 1.6 Hz, 1 H), 8.26 (s, 1 H), 8.53 (d, J = 5.0 Hz, 1 H), 8.61 (s, 1 H), 8.78 (d, J = 5.0 Hz, 1 H) ppm. MS (ESI+): m/z = 413.2 $[\text{M} + \text{H}]^+$. The Boc protecting group was removed by dissolving the protected amide (1.59 g, 3.9 mmol) in methanol (30 mL) and adding $\text{HCl}/\text{H}_2\text{O}$ (1:1, 30 mL). After stirring at room temperature for 16 h, the solvent was removed under reduced pressure. The residue was taken up in methanol, and the product was precipitated with ether. The precipitate was filtered, washed with diethyl ether and vacuum dried to give a white solid (1.20 g, 89%). ^1H NMR (200 MHz, $[\text{D}_6]\text{dmsO}$): δ = 1.32–1.41 (m, 4 H), 1.48–1.62 (m, 4 H), 2.57 (s, 3 H), 2.75 (q, J = 6.4 Hz, 2 H), 3.32 (q, J = 6.0 Hz, 2 H), 7.65 (d, J = 5.2 Hz, 1 H), 7.99 (d, J = 5.0 Hz, 1 H), 8.05 (br. s, 3 H), 8.65 (s, 1 H), 8.69 (d, J = 5.4 Hz, 1 H), 8.91 (d, J = 5.0 Hz, 1 H), 8.96 (s, 1 H), 9.23 [br. t, 1 H, NHC(O)] ppm. HRMS (ESI+): calcd. for $\text{C}_{18}\text{H}_{25}\text{N}_4\text{O}$ $[\text{M} + \text{H}]^+$ 313.2028; found 313.2018.

Tris[2-(5-methylpyridyl)]amine (2): 2-Bromo-5-methylpyridine (6.52 g, 38 mmol), 5-methylpyridin-2-amine (2.05 g, 19 mmol), potassium carbonate (4.36 g, 44 mmol), potassium iodide (trace) and potassium bromide (trace) were heated at reflux (60 h) with continuous stirring over copper (0.95 g, 15 mmol) in *p*-cymene (30 mL). The product mixture was filtered hot and washed with ethanol, and the solvent was removed under reduced pressure. The product was purified by column chromatography (silica gel, 3% methanol in dichloromethane) and recrystallized from acetone/hexane to afford a yellow crystalline product (1.67 g, 30%). X-ray quality crystals were grown by slow crystallization at room temperature from ethanol. ^1H NMR (200 MHz, CDCl_3): δ = 2.27 (s, 9 H), 6.95 (d, J = 8.2 Hz, 3 H), 7.42 (dd, J = 8.2 Hz, J = 2.2 Hz, 3 H), 8.18 (d, J = 1.6 Hz, 3 H) ppm. HRMS (ESI+): calcd. for $\text{C}_{18}\text{H}_{19}\text{N}_4$ $[\text{M} + \text{H}]^+$ 291.1610; found 291.1590. UV/Vis (MeOH): λ_{max} (ϵ , $\text{M}^{-1}\text{cm}^{-1}$) = 270 (18730), 303 (21010) nm; λ_{cm} = 400 nm.

Tris(2-nicotinic acid)amine (3): Amine **2** (1.14 g, 3.9 mmol), KMnO_4 (5.12 g, 32.4 mmol) and NaOH (1.41 g, 35.3 mmol) were added to distilled water (150 mL). The reaction mixture was stirred at 60 °C for 4 h. To this mixture a second portion of KMnO_4 (4.23 g, 26.8 mmol) was added and stirring was continued at 60 °C for 16 h. The reaction was quenched with methanol, and the brown precipitate (MnO_2) was filtered off and washed with water. The combined aqueous phase was acidified with $\text{HCl}/\text{H}_2\text{O}$ (1:1) to pH 2.5 and was cooled to 5 °C. The resulting white precipitate was filtered off, washed with water and dried in vacuo to give triacid **3** (1.2 g, 82%) as a white powder. ^1H NMR (200 MHz, MeOD): δ = 7.27 (d, J = 8.6 Hz, 3 H), 8.34 (dd, J = 8.5 Hz, J = 2.2 Hz, 3 H), 8.92 (d, J = 2.2 Hz, 3 H) ppm. HRMS (ESI+): calcd. for $\text{C}_{18}\text{H}_{13}\text{N}_4\text{O}_6$ $[\text{M} + \text{H}]^+$ 381.0835; found 381.0845.

L¹: A solution of triacid **3** (0.25 g, 0.66 mmol) and 1,1'-carbonyl-diimidazole (CDI; 0.39 g, 2.17 mmol) in dry DMF (20 mL) was stirred at 60 °C under an atmosphere of nitrogen for 30 min. Then, a solution of aminobipyridine **1** (0.76 g, 2.17 mmol) and Et₃N (0.4 mL, 2.89 mmol) in dry DMF (20 mL) was added dropwise and stirring was continued at 60 °C under an atmosphere of nitrogen for 16 h. The solvent was removed under reduced pressure, and the residue was taken up in methanol/chloroform (1:2, 15 mL). An insoluble white powder was filtered off, and the remaining solution was concentrated in vacuo. The residue was purified by column chromatography (neutral alumina, 5% methanol in chloroform) followed by precipitation from methanol/chloroform (1:2) with ether to give the product (0.19 g, 23%) as a white powder. ¹H NMR (200 MHz, CDCl₃): δ = 1.28–1.36 (m, 12 H), 1.46–1.58 (m, 12 H), 2.38 (s, 9 H), 3.26–3.37 (m, 12 H), 6.94 (d, *J* = 8.4 Hz, 3 H), 7.11 (d, *J* = 4.6 Hz, 3 H), 7.66 [br. t, 3 H, NHC(O)], 7.68 (d, *J* = 4.2 Hz, 3 H), 8.00 (dd, *J* = 8.8 Hz, *J* = 1.2 Hz, 3 H), 8.14 (s, 3 H), 8.39 (d, *J* = 5.0 Hz, 3 H), 8.53 (s, 3 H), 8.65 (s, 3 H), 8.67 (d, *J* = 5.4 Hz, 3 H) ppm. HRMS (ESI⁺): calcd. for C₇₂H₈₀N₁₆O₆ [M + H]⁺ 1264.6447; found 1264.6438. UV/Vis (CH₂Cl₂): λ_{max} (ε, M⁻¹ cm⁻¹) = 284 (50530), 300 (49000), 324 (sh.) nm; λ_{em} = 400 nm.

L²: A solution of triacid **5** (0.1 g, 0.25 mmol) and 1,1'-carbonyl-diimidazole (CDI; 0.12 g, 0.75 mmol) in dry DMF (10 mL) was stirred at 60 °C under an atmosphere of nitrogen for 30 min. Then, a solution of aminobipyridine **1** (0.25 g, 0.72 mmol) and Et₃N (0.16 mL, 0.84 mmol) in dry DMF (15 mL) was added dropwise and stirring was continued at 60 °C under an atmosphere of nitrogen for 16 h. The solvent was removed under reduced pressure, and the residue was purified by column chromatography (silica gel, 5% methanol in chloroform) followed by precipitation from methanol/chloroform (1:2) with ether to give the product (93 mg, 30%) as an off-white powder. ¹H NMR (400 MHz, CDCl₃): δ = 1.18–1.23 (m, 12 H), 1.38–1.46 (m, 12 H), 2.34 (s, 9 H), 3.24–3.29 (m, 12 H), 7.04 (d, *J* = 4.8 Hz, 3 H), 7.48–7.57 (m, 6 H), 7.62 (dd, *J* = 4.8 Hz, *J* = 1.6 Hz, 3 H), 7.72 [br. t, 3 H, NHC(O)], 7.98 (d, *J* = 8.8 Hz, 3 H), 8.12 (s, 3 H), 8.34 (d, *J* = 5.2 Hz, 3 H), 8.59 (s, 3 H), 8.61 (d, *J* = 4.8 Hz, 3 H), 8.83 (s, 3 H) ppm. HRMS (ESI⁺): calcd. for C₇₃H₈₁N₁₅O₇ [M + H]⁺ 1279.6443; found 1279.6490. UV/Vis (CH₂Cl₂): λ_{max} (ε, M⁻¹ cm⁻¹) = 275 (45570) nm; λ_{em} = 360 nm.

[(2)Cu(NO₃)(H₂O)₂](ClO₄)·2H₂O: To a solution of ligand **2** (67 mg, 0.23 mmol) dissolved in acetone (5 mL) was added a solution of Cu(NO₃)₂ in water (0.5 M, 0.46 mL), and the mixture was stirred at room temperature for 2 h. Then, a solution of NaClO₄ (28 mg, 0.23 mmol) in water (5 mL) was added, and the mixture was allowed to stand overnight. Dark-green crystals appeared that were filtered off, washed with diethyl ether and dried to afford the product (91 mg, 72%). MS (ESI⁺): *m/z* (%) = 415.0 (100) [⁶³Cu(2)(NO₃)₂]⁺, 417.0 (65) [⁶⁵Cu(2)(NO₃)₂]⁺, 452.0 (49) [⁶³Cu(2)(NO₃)₂]⁺, 454.0 (32) [⁶⁵Cu(2)(NO₃)₂]⁺. UV/Vis (MeOH/H₂O, 1:1): λ_{max} (ε, M⁻¹ cm⁻¹) = 265 (22200), 300 (23900), 400 (80), 658 (52) nm.

[Ru(2)₂](PF₆)₄: A mixture of ligand **2** (25 mg, 0.087 mmol) and RuCl₂(dmsO)₄ (20 mg, 0.041 mmol) was heated in ethylene glycol (10 mL) at 125 °C for 10 min under an atmosphere of nitrogen. After cooling down to room temperature, water (10 mL) was added, and the product was precipitated with saturated NH₄PF₆. The precipitate was filtered off, washed with water and vacuum dried to afford a yellow solid (25 mg, 61%). ¹H NMR (200 MHz, CDCl₃): δ = 2.08 (s, 18 H), 7.40 (br. s, 6 H), 8.00 (d, *J* = 1.4 Hz, 6 H), 8.04 (s, 16 H) ppm. MS (ESI⁺): *m/z* (%) = 341.4 (100) [¹⁰¹Ru(2)₂]²⁺, 827.1 (49) [¹⁰¹Ru(2)₂](PF₆)₂⁺. UV/Vis (MeOH): λ_{max} (ε, M⁻¹ cm⁻¹) = 252 (9650), 266 (sh.), 340 (4910), 396 (12070) nm.

[Fe(L¹)](ClO₄)₂·4H₂O: To a solution of ligand L¹ (20 mg, 0.016 mmol) dissolved in methanol/dichloromethane (1:1, 5 mL) was added a solution of Fe(ClO₄)₂·xH₂O in acetonitrile (0.1 M, 0.158 mL), and the mixture was stirred at room temperature for 2 h. A dark-red precipitate appeared upon standing that was filtered off, washed with dichloromethane and dried to afford a red solid (9.1 mg, 38%). HRMS (ESI⁺): calcd. for C₇₂H₇₈N₁₆O₆Fe [M + H]⁺ 1318.5640; found 1318.5616. C₇₂H₈₆Cl₂N₁₆O₁₈Fe (1590.30): calcd. C 54.38, H 5.45, N 14.09; found C 54.59, H 5.53, N 14.25. UV/Vis (dmsO/H₂O, 4:1): λ_{max} (ε, M⁻¹ cm⁻¹) = 255 (53900), 308 (93700), 365 (sh.), 539 (10460) nm. ¹H NMR after heating to 60 °C, only signals of one diastereomer are given (400 MHz; [D₆]dmsO/MeOD, 1:5): δ = 1.62–1.77 (m, 18 H), 1.79–1.88 (m, 6 H), 3.13–3.22 (m, 6 H), 3.42–3.51 (m, 9 H), 3.81–3.52 (m, 6 H), 7.13 (d, 3 H, *J* = 5.6 Hz), 7.16 (d, 3 H, *J* = 8.8 Hz), 7.38 (d, 3 H, *J* = 5.6 Hz), 7.58 (d, 3 H, *J* = 5.6 Hz), 7.92 (d, 3 H, *J* = 5.6 Hz), 8.20 (dd, 3 H, *J* = 8.8 Hz, *J* = 2.4 Hz), 8.48 (d, 3 H, *J* = 2.4 Hz), 8.69 (s, 3 H), 8.97 (s, 3 H).

[Ru(L¹)]Cl₂·4H₂O: A mixture of ligand L¹ (33 mg, 0.026 mmol) and RuCl₂·3H₂O (6.5 mg, 0.025 mmol) was heated in ethanol (95%, 10 mL) at 78 °C for 16 h under an atmosphere of nitrogen. After cooling down to room temperature, the solvent was removed under reduced pressure and the residue was purified by column chromatography (neutral alumina, 1% AcOH, 15% methanol in chloroform) followed by precipitation from methanol with ether to afford an orange solid (18 mg, 44%). HRMS (ESI⁺): calcd. for C₇₂H₇₈N₁₆O₆Ru [M + H]⁺ 1364.5334; found 1364.5268. C₇₂H₈₆Cl₂N₁₆O₁₀Ru (1507.53): C 57.36, H 5.75, N 14.87; found C 57.71, H 5.75, N 14.99. UV/Vis (MeOH/H₂O, 1:1): λ_{max} (ε, M⁻¹ cm⁻¹) = 297 (84172), 325 (sh.), 459 (14180) nm; λ_{em} = 630 nm. ¹H NMR, only sharp signals of one diastereomer are given (400 MHz, MeOD): δ = 1.39–1.50 (m, 12 H), 1.61–1.73 (m, 12 H), 3.36–3.48 (m, 12 H), 7.14 (d, 3 H, *J* = 8.4 Hz), 7.27 (d, 3 H, *J* = 4.4 Hz), 7.76 (d, 3 H, *J* = 4.4 Hz), 8.15 (d, 3 H, *J* = 8.4 Hz, *J* = 2.4 Hz), 8.18 (s, 3 H), 8.52 (d, 3 H, *J* = 4.8 Hz), 8.60 (s, 3 H), 8.74 (s, 3 H), 8.76 (d, 3 H, *J* = 5.0 Hz).

Spectrophotometric and Fluorescence Titrations: Fluorescence spectra were acquired with a Varian Cary Eclipse fluorescence spectrophotometer, UV/Vis experiments were performed with a Varian Cary 100 Bio UV/Vis spectrophotometer by using 1 cm optical path quartz or PMMA macrocuvettes with a sample volume of 2 mL.

X-ray Crystal Structure Determinations: Crystal data and details of the structure determinations are listed in Table 1. Intensity data were collected at low temperature with a Bruker AXS Smart 1000 CCD diffractometer and corrected for Lorentz, polarization and absorption effects (semiempirical, SADABS).^[24] The structures were solved by the heavy atom method combined with structure expansion by direct methods applied to difference structure factors^[25] or by conventional direct methods^[26] (compound **2**) and refined by full-matrix least-squares methods based on *F*² against all reflections.^[27] All non-hydrogen atoms were given anisotropic displacement parameters. For compound **2** the positions of most hydrogen atoms (except those of the methyl groups, which were treated as variable metric rigid groups) were taken from difference Fourier syntheses and refined. For all other structures, hydrogen atoms were input at calculated positions and refined with a riding model. In the structure of [(2)Cu(H₂O)₂(NO₃)](ClO₄)·2H₂O the hydrogen atoms of the water molecules could not be unambiguously located. The perchlorate anion in this structure was found to be severely disordered; Cl–O and O···O distances were restrained to sensible values during refinement. CCDC-690411 (for **2**), -690412

Table 1. Details of the crystal structure determinations of compounds **2**, [(2)Cu(H₂O)₂(NO₃)](ClO₄)·2H₂O and [(2)₂Ru](PF₆)₂.

	2	[(2)Cu(H ₂ O) ₂ (NO ₃)](ClO ₄)·2H ₂ O	[(2) ₂ Ru](PF ₆) ₂
Formula	C ₁₈ H ₁₈ N ₄	C ₁₈ H ₂₆ ClCuN ₅ O ₁₁	C ₃₆ H ₃₆ F ₁₂ N ₈ P ₂ Ru
Crystal system	monoclinic	monoclinic	monoclinic
Space group	<i>P</i> ₂ ₁ / <i>c</i>	<i>P</i> ₂ ₁ / <i>c</i>	<i>P</i> ₂ ₁ / <i>n</i>
<i>a</i> / Å	9.6470(6)	8.9902(5)	9.862(2)
<i>b</i> / Å	10.8779(7)	16.742(1)	11.342(2)
<i>c</i> / Å	15.2615(8)	16.293(1)	18.251(3)
β / °	110.420(3)	99.600(1)	104.539(3)
<i>V</i> / Å ³	1500.9(2)	2418.0(2)	1976.1(6)
<i>Z</i>	4	4	2
<i>M_r</i>	290.36	587.43	971.74
<i>d</i> _{calc.} / Mg m ^{−3}	1.285	1.614	1.633
<i>F</i> (000)	616	1212	980
μ(Mo- <i>K</i> _α) / mm ^{−1}	0.079	1.081	0.574
Max., min. transmission factors	0.9799, 0.9705	0.8246, 0.7230	0.7464, 0.6759
X-radiation, λ / Å	Mo- <i>K</i> _α , graphite monochromated, 0.71073		
Data collection temperature / K	100(2)	100(2)	100(2)
θ range / °	2.3 to 32.0	1.8 to 31.5	2.1 to 31.5
Index ranges (indep. set) <i>h</i> , <i>k</i> , <i>l</i>	−14 to 13, −15 to 0, −22 to 12	−13 to 13, 0 to 24, 0 to 23	−14 to 13, 0 to 16, 0 to 26
Reflections measured	14297	60716	49713
Unique [<i>R</i> _{int}]	5100 [0.0352]	7986 [0.0471]	6542 [0.0589]
Observed [<i>I</i> ≥ 2σ(<i>I</i>)]	3842	6252	4908
Parameters refined	232	328	271
<i>R</i> indices [<i>F</i> > 4σ(<i>F</i>)] <i>R</i> (<i>F</i>), <i>wR</i> (<i>F</i> ²)	0.0537, 0.1425	0.0785, 0.2488	0.0370, 0.0809
<i>R</i> indices (all data) <i>R</i> (<i>F</i>), <i>wR</i> (<i>F</i> ²)	0.0718, 0.1538	0.0933, 0.2652	0.0638, 0.0984
GooF on <i>F</i> ²	1.067	1.138	1.077
Largest residual peaks / e Å ^{−3}	0.612, −0.236	3.682, −3.277	1.199, −0.514

{for [(2)Cu(H₂O)₂(NO₃)](ClO₄)·2H₂O} and -690413 {for [(2)₂Ru](PF₆)₂} contain the supplementary crystallographic data for this paper. These data can be obtained free of charge from The Cambridge Crystallographic Data Centre via www.ccdc.cam.ac.uk/data_request/cif.

Acknowledgments

This work was supported by the Deutsche Forschungsgemeinschaft (SFB 623) and by the European Commission (Marie Curie Intra-European Fellowship for H. S.).

- a) J. P. Collman, R. R. Gagné, C. A. Reed, *J. Am. Chem. Soc.* **1974**, *96*, 2629–2630; b) N. Kitajima, K. Fujisawa, C. Fujimoto, Y. Morooka, S. Hashimoto, T. Kitagawa, K. Toriumi, K. Tatsumi, A. Nakamura, *J. Am. Chem. Soc.* **1992**, *114*, 1277–1291.
- B. Kersting, *Z. Anorg. Allg. Chem.* **2004**, *630*, 765–780 and references cited therein.
- N. Le Poul, M. Campion, B. Douziech, Y. Rondelez, L. Le Clainche, O. Renaud, Y. Le Mest, *J. Am. Chem. Soc.* **2007**, *129*, 8801–8810 and references cited therein.
- a) H. Vahrenkamp, *Acc. Chem. Res.* **1999**, *32*, 589–596; b) L. M. Mirica, X. Ottenwaelder, T. D. P. Stack, *Chem. Rev.* **2004**, *104*, 1013–1046.
- L. Kovbasyuk, R. Krämer, *Chem. Rev.* **2004**, *104*, 3161–3187.
- B. H. Peek, G. T. Ross, S. W. Edwards, G. J. Meyer, T. J. Meyer, B. W. Ericksson, *Int. J. Peptide Protein Res.* **1991**, *38*, 114–123.
- X. Li, C. L. D. Gibb, M. E. Kuebel, B. C. Gibb, *Tetrahedron* **2001**, *57*, 1175–1182.
- J. Gong, B. C. Gibb, *Org. Lett.* **2004**, *6*, 1353.
- W. Yang, H. Schmider, Q. Wu, Y.-Sh. Zhang, S. Wang, *Inorg. Chem.* **2000**, *39*, 2397–2404.
- W. R. McWhinnie, G. C. Kulasingam, J. C. Draper, *J. Chem. Soc.* **1966**, 1199–1203.
- a) L. J. Childs, M. Pascu, A. J. Clarke, N. W. Alcock, M. J. Hannon, *Chem. Eur. J.* **2004**, *10*, 4291–4300; b) E. S. Zvargulis, I. E. Buis, T. W. Hambley, *Polyhedron* **1995**, *14*, 2267–2273; c) R. K. Boggess, A. H. Lamson, S. York, *Polyhedron* **1991**, *10*, 2791–2798.
- R. T. Jonas, T. D. P. Stack, *Inorg. Chem.* **1998**, *37*, 6615–6629.
- P. L. Dedert, T. Sorrell, T. J. Marks, J. A. Ibers, *Inorg. Chem.* **1982**, *21*, 3506–3517.
- P. L. Dedert, J. S. Thompson, J. A. Ibers, T. J. Marks, *Inorg. Chem.* **1982**, *21*, 969–977.
- P. A. Anderson, F. R. Keene, J. M. Gulbis, E. R. T. Tiekink, *Z. Kristallogr.* **1993**, *206*, 275.
- D. Boys, C. Escobar, W. Zamudio, *Acta Crystallogr., Sect. C: Cryst. Struct. Commun.* **1992**, *48*, 1118.
- F. R. Keene, M. R. Snow, P. J. Stephenson, E. R. T. Tiekink, *Inorg. Chem.* **1988**, *27*, 2040–2045.
- N. Nagao, *Meiji Daigaku Kagaku Gijutsu Kenkyusho Nenpo* **1999**, *41*, 59.
- H. Irving, D. H. Mellor, *J. Chem. Soc.* **1962**, 5222–5237.
- a) T. Nabeshima, Y. Tanaka, T. Saiki, S. Akine, C. Ikeda, S. Sato, *Tetrahedron Lett.* **2006**, *47*, 3541–3544; b) E. Krenske, L. R. Gahan, *Aust. J. Chem.* **2002**, *55*, 761–766; c) L. Zelikovich, J. Libman, A. Shanzer, *Nature* **1995**, *374*, 790–792. A redox-dependent translocation of a single Fe ion between the two sites was also observed.
- M. Kodera, Y. Tachi, T. Kita, H. Kobushi, Y. Sumi, K. Kano, M. Shiro, M. Koikawa, T. Tokii, M. Ohba, H. Okawa, *Inorg. Chem.* **2000**, *39*, 226–234.
- G. A. Crosby, W. G. Perkins, D. M. Klassen, *J. Chem. Phys.* **1965**, *43*, 1498–1503.
- T. Bora, M. M. Singh, *J. Inorg. Nucl. Chem.* **1976**, *38*, 1815–1820.
- G. M. Sheldrick, *SADABS*, Bruker AXS, **2004–2008**.
- a) P. T. Beurskens in *Crystallographic Computing 3* (Eds.: G. M. Sheldrick, C. Krüger, R. Goddard), Clarendon Press, Oxford, UK, **1985**, p. 216; b) P. T. Beurskens, G. Beurskens, R. de Gelder, J. M. M. Smits, S. Garcia-Granda, R. O. Gould,

- DIRDIF-2008*, Raboud University Nijmegen, The Netherlands, **2008**.
- [26] a) G. M. Sheldrick, *SHELXS-86*, University of Göttingen, **1986**; b) G. M. Sheldrick, *Acta Crystallogr., Sect. A* **1990**, *46*, 467.
- [27] G. M. Sheldrick, *SHELXL-97*, University of Göttingen, **1997**; G. M. Sheldrick, *Acta Crystallogr., Sect. A* **2008**, *64*, 112.
- Received: October 17, 2008
Published Online: December 2, 2008

Pd/MO_x Materials Synthesized by Sol-Gel Coprecipitation as Catalysts for Carbon–Carbon Coupling Reactions of Aryl Bromides and Chlorides

Wolfgang Kleist,^{[a],‡} Jae-Kyu Lee,^[a] and Klaus Köhler*^[a]

Keywords: C–C Coupling / Heck reaction / Palladium / Sol-gel processes / Supported catalysts

In order to control the interaction of palladium species with oxide supports, a sol-gel coprecipitation synthesis has been developed for Pd/MO_x. The resulting Pd/MO_x catalysts are characterized by a rather strong interaction between the highly dispersed Pd²⁺ species and the alumina and silica lattices. During coupling reactions of the Heck type the catalytically active species is generated by partial dissolution of Pd from the support surface. Due to the strong bonding of Pd to the support this dissolution occurs to significant extent only at comparatively high temperatures (≥ 160 °C). These temperatures are exactly necessary for the activation of less-re-

active substrates like bromobenzene and aryl chlorides. In this way we are able to synthesize supported catalysts that facilitate a controlled release of soluble Pd species under reaction conditions that are required for the activation of aryl bromides and chlorides. The Pd/MO_x catalysts show excellent activity in the Heck reaction of bromobenzene (TON up to 10000; TOF up to 5000 h⁻¹) and 4-chloroacetophenone (TON up to 9300; TOF up to 1550 h⁻¹).

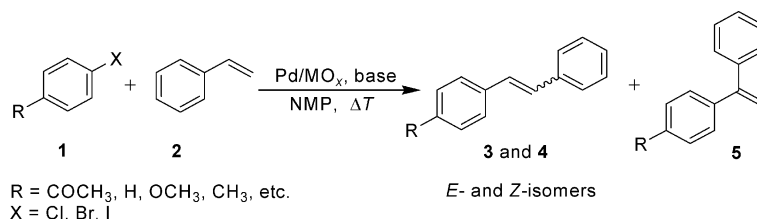
(© Wiley-VCH Verlag GmbH & Co. KGaA, 69451 Weinheim, Germany, 2009)

Introduction

A large number of detailed investigations on Heck-type coupling reactions (Scheme 1) in the presence of supported catalysts within the last years led to an eminent improvement of the mechanistic understanding in this area.^[1–5] It could be shown independently by different groups that the reaction is catalyzed by soluble Pd species that are temporarily dissolved from the surface of the support.^[6–12] In the original catalyst Pd has to be provided as an effective precursor species from which the active form can be generated in situ. Optimized procedures for the synthesis of such highly active Pd catalysts have been reported in the literature.^[13,14] In general, these materials contain Pd²⁺ species

in a high dispersion which facilitates an efficient in-situ reduction (Pd⁰ is required for the oxidative addition of the aryl halide as the first step of the catalytic cycle) and dissolution under typical reaction conditions.^[15] Beside an optimized synthetic procedure for the catalyst material, especially the right choice of reaction conditions during the catalytic reaction was found to be essential.

It emerged to be crucial that the dissolution and re-precipitation equilibria are controlled effectively at any time during the catalytic reaction. Here it is important that the right amount of dissolved (= active) Pd species is provided in the reaction solution. While a too low Pd concentration might be not sufficient to achieve high reaction rates, agglomeration (and consequently deactivation) processes



Scheme 1. Heck reaction of aryl halides and styrene.

[a] Department of Chemistry, Technische Universität München, Lichtenbergstr. 4, 85747 Garching, Germany
 Fax: +49-89-289-13183
 E-mail: klaus.koehler@ch.tum.de

[‡] Present Address: Department of Chemistry and Applied Biosciences, Institute for Chemical and Bioengineering, ETH Zurich, Wolfgang-Pauli-Str. 10, 8093 Zurich, Switzerland

might occur if too much Pd is leached from the catalyst support simultaneously.

One of the most important parameters that influences these dissolution/re-precipitation processes is the reaction temperature. Higher reaction temperatures can increase the total amount of dissolved Pd species, but they also acceler-

ate deactivation of active species by Pd black formation. Higher reaction temperatures might be needed, however, for the activation of certain substrates. While aryl iodides and activated aryl bromides can be activated easily by a great variety of different Pd catalysts at reaction temperatures below 100 °C (due to their lower C–X binding energies),^[16,17] the activation of less reactive aryl bromides and especially chlorides requires in general harsher reaction conditions and higher temperatures.^[18] Consequently, an efficient catalyst for the activation of such less-reactive substrates should facilitate a controlled release of the supported Pd into the reaction solution at these higher reaction temperatures avoiding agglomeration and deactivation of Pd in solution. The development of such materials being more robust and applicable for a broader range of experimental conditions in particular for higher temperatures would be of particular interest for practical application of supported palladium catalysts.

In this work we present a new strategy to cope with this challenge. A sol-gel coprecipitation synthesis procedure has been developed for metal oxide supported Pd catalysts. It results in a stronger Pd-support interaction (compared to conventionally prepared supported catalysts) and leaching of Pd species into reaction solution starts at 160 °C only. Such high temperatures have to be applied for an efficient conversion of less-reactive substrates like bromobenzene and aryl chlorides.^[19] Since leaching and stabilization of dissolved Pd species against Pd black formation may be influenced by ammonium halides, a variety of these salts have been tested as additives/promoters in the catalytic reaction too.

Results and Discussion

To achieve a strong Pd/support interaction, the Pd catalysts were prepared by combined sol-gel (metal alkoxides) and coprecipitation (palladium salt) procedures. Al(OⁱPr)₃, which was used as the precursor for Pd/Al₂O₃ catalysts, was dissolved in 2-propanol at elevated temperature (65 °C). Precipitation of the metal oxide was induced by controlled addition of water and finally a solution of PdCl₂ in hydrochloric acid. After a reaction time of one and three days, respectively (see Exp. Sect.), two different Pd/Al₂O₃ materials (denoted as “Pd/Al-1” and “Pd/Al-3”) were obtained. In the case of Pd/SiO₂ catalysts a different procedure had to be applied. A preformed gel, which was obtained by addition of water to a solution of Si(OEt)₄ in ethanol, was dissolved again in 1-butanol. Coprecipitation of Pd/SiO₂ (“Pd-Si”) was then achieved by addition of a solution of PdCl₂ in hydrochloric acid. Note that these different procedures had to be applied in order to obtain an incorporation of the Pd into the outermost layers of the MO_x lattice for both types of materials. The raw materials were divided in two portions each which were calcined at 100 (“Pd/Al-1-100”, etc.) or 450 °C (“Pd/Al-1-450”, etc.). Each of these two fractions was split again and one part was treated at 200 °C for 2 hours in H₂ stream to reduce Pd²⁺ to Pd⁰ (“Pd/

Al-1-100-red” and “Pd-Al-1-450-red”, etc.), the other was used without further treatment. Detailed information on the thermal treatment of the catalyst series can be found in Table 1.

Table 1. Nomenclature used and thermal treatments of the various palladium-metal oxide catalysts prepared by combined sol-gel coprecipitation. Samples denoted as “100” were dried in air atmosphere at a temperature of 100 °C for 2 h, those denoted as “450” at a temperature of 450 °C for 6 h. All of these catalysts were divided again into two portions: one was used without further treatment; the other was treated in a H₂ stream at 200 °C for 2 h (denoted as “red”).

Catalyst	Thermal treatment	Reduction (H ₂ stream)
Pd/Al-1-100	100 °C, 2 h	–
Pd/Al-1-100-red	100 °C, 2 h	200 °C, 2 h
Pd/Al-1-450	450 °C, 6 h	–
Pd/Al-1-450-red	450 °C, 6 h	200 °C, 2 h
Pd/Al-3-100	100 °C, 2 h	–
Pd/Al-3-100-red	100 °C, 2 h	200 °C, 2 h
Pd/Al-3-450	450 °C, 6 h	–
Pd/Al-3-450-red	450 °C, 6 h	200 °C, 2 h
Pd/Si-100	100 °C, 2 h	–
Pd/Si-100-red	100 °C, 2 h	200 °C, 2 h
Pd/Si-450	450 °C, 6 h	–
Pd/Si-450-red	450 °C, 6 h	200 °C, 2 h

The influence of these different reaction parameters (see Table 1) on the activity of the resulting catalysts was studied by comparing the catalytic activity of the different systems in the Heck reaction of bromobenzene and styrene. First, the influence of the pre-treatment (atmosphere) and calcination temperature was investigated in order to get information on the role of the oxidation state of Pd (0 or +2). For this purpose the four catalysts of the Pd/Al-1 series were tested in the Heck coupling of bromobenzene and styrene (Pd amount: 0.01 mol-% based on bromobenzene). After 2 hours at 160 °C the reaction was stopped and the mixtures were analyzed by GLC and GC/MS (Figure 1). The best results were achieved with the unreduced catalyst calcined at 450 °C (Pd/Al-1-450; 99% conversion, 90% yield of *E*-stilbene 3). The unreduced catalyst calcined at 100 °C (Pd/Al-1-100; 65% conversion, 60% yield) and the reduced catalyst calcined at 450 °C (Pd/Al-1-450-red; 61% conversion, 56% yield) provided similar results. Only the reduced catalyst calcined at 100 °C (Pd/Al-1-100-red; 6% conversion and yield) showed low activity.

Although Pd⁰ is the catalytically active species, Pd²⁺ on the catalyst surface exhibits a higher activity compared to Pd⁰. This is explained by the fact that Pd species can be dissolved easier when a single (pre-reduced) Pd⁰ surface atom is bound to a palladium oxide or hydroxide surface compared to metallic Pd⁰. Dissolution is then induced by an oxidative addition of an aryl halide molecule.^[4,15] Another conclusion that can be drawn from this comparison is that higher calcination temperatures also lead to higher catalytic performance. Calcination at high temperatures causes a stronger interaction between Pd and the catalyst support. As a consequence, Pd dissolution is hampered and occurs only at higher temperatures. In the case of Pd/Al-1-450 a controlled Pd leaching is possible, whereas the weaker

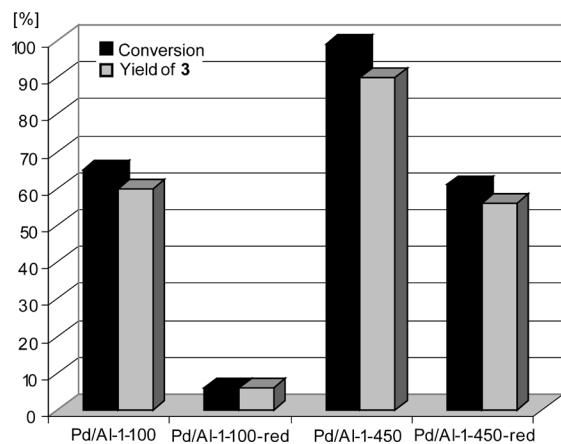


Figure 1. Influence of thermal treatment on the activity of the Pd-metal oxide catalysts; reaction conditions: 10 mmol bromobenzene, 15 mmol styrene, 12 mmol NaOAc, 10 mL NMP, 0.01 mol-% Pd, 160 °C, 2 h, argon atmosphere.

Pd-support interaction in Pd/Al-1-100 leads to a higher Pd leaching. Therefore in the latter case agglomeration of Pd particles and loss in activity are observed. Synergy of high temperature calcination and presence of Pd²⁺ leads to extremely active catalysts, while the combination of the undesired properties (weakly bound Pd⁰) causes a dramatic decrease in activity.

In Figure 2 two modified preparation routes for Pd/Al₂O₃ catalysts are compared and the influence of the oxidic support (Al₂O₃ vs. SiO₂) is investigated. All catalysts were tested in the same reaction and under the same conditions mentioned above. First, the differences between the Pd/Al-1 and the Pd/Al-3 series are discussed. Both catalyst series were prepared using different conditions during the coprecipitation process: While coprecipitation of Pd/Al-1 catalysts was performed at room temp. for 1 day, Pd/Al-3 catalysts were stirred at 65 °C for 3 days. The latter procedure causes, again, a stronger interaction between Pd and the support (or even partial incorporation of Pd into the Al₂O₃ lattice). This is demonstrated by the fact that Pd can be removed completely from the Al-1 surface by washing with acetonitrile at room temp., whereas no dissolution from Al-3 catalysts is observed. The Pd/Al-3 series shows qualitatively the same influence of thermal treatment as the Pd/Al-1 catalysts discussed above. However, catalysts of the Al-3 series exhibit higher activity. Complete conversion of bromobenzene is observed for both unreduced Al-3 and the reduced Al-3-450-red catalysts. Even Al-3-100-red which contains comparably weakly bound Pd⁰ (an undesired combination) reaches 84% conversion (compared to 6% for Al-1-100-red).

Pd/SiO₂ catalysts show similar tendencies concerning thermal treatment. Only small differences in activity are observed for the first three catalysts (100, 100-red and 450) of the Pd/Al-1 and the Pd/Si series. This means that the influence of the support is negligible and the differences can be explained by small variations in Pd dispersion. Pd/Al₂O₃ catalysts do not show XRD signals from metallic or oxid-

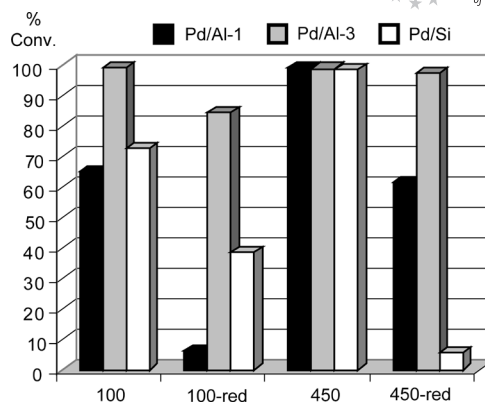


Figure 2. Comparison of the different Pd-metal oxide (SiO₂, Al₂O₃) catalyst series; reaction conditions: 10 mmol bromobenzene, 15 mmol styrene, 12 mmol NaOAc, 10 mL NMP, 0.01 mol-% Pd, 160 °C, 2 h, argon atmosphere.

ized Pd. Therefore a very high Pd dispersion (and stronger Pd-support interaction) is postulated in these catalysts. In contrast, the presence of larger crystalline Pd species can be observed by X-ray powder diffraction investigations for the catalysts of the Pd/SiO₂ series. The high catalytic activity of Pd/Si-450 is explained by the presence of crystalline PdO particles, whereas a lower activity was observed for the other three catalysts that exhibit signals from metallic Pd⁰.

Investigations on the influence of the reaction temperature on the catalyst activity were performed using several of the catalysts. The results for the coupling of bromobenzene and styrene with Pd/Al-3-100-red as catalyst at different temperatures are shown in Table 2. While only 31% conversion are reached after 2 hours at 140 °C catalyst performance increases significantly at 160 °C (84% conversion). For almost complete conversion in the same time a temperature of 180 °C is needed. This temperature dependence is consistent with the concept of a strong Pd-support interaction. Therefore high temperatures are necessary to release Pd from the surface and generate catalytically active species in solution.

Table 2. Influence of the reaction temperature on the catalytic activity and selectivity in the Heck reaction of bromobenzene with styrene; reaction conditions: 10 mmol bromobenzene, 15 mmol styrene, 12 mmol NaOAc, 10 mL NMP, 0.01 mol-% Pd (Pd/Al-3-100-red), 2 h, argon atmosphere.

Temperature [°C]	% Conversion	% Yield of 3
140	31	31
160	84	83
180	92	91

Kinetic investigations were performed to study the correlation of the progress of the reaction and the content of leached Pd in solution. In Figure 3 the results for the reaction of bromobenzene and styrene in presence of 0.025 mol-% Pd/Al-3-450 are shown. The reaction was performed simultaneously in 14 pressure tubes; after the respective reaction time each reaction was stopped and one sample was taken to determine the conversion via GLC and another to

quantify the Pd content in solution via AAS. A slightly elevated catalyst concentration of 0.025 mol-% was used to minimize fluctuations of Pd concentrations in the different tubes.

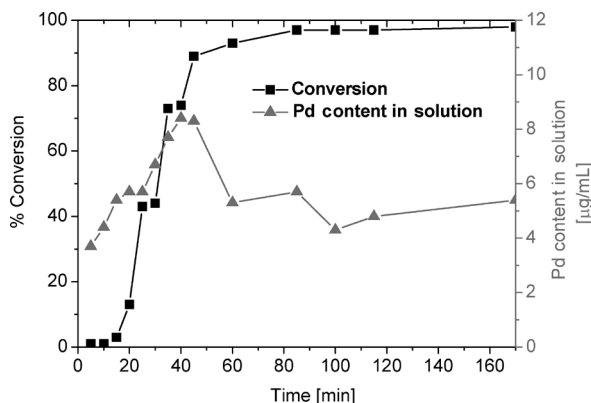


Figure 3. Correlation of the progress of the Heck reaction with Pd leaching (during the reaction): 10 mmol bromobenzene, 15 mmol styrene, 12 mmol NaOAc, 10 mL NMP, 0.025 mol-% Pd/Al-3-450, 160 °C, argon atmosphere.

Figure 3 shows a conversion curve that is typical for heterogeneously catalyzed Heck reactions. During an induction period (first 15 minutes) no conversion is observed and Pd dissolution is initiated. After a critical Pd concentration in solution is reached the reaction proceeds very fast. Nearly complete conversion of bromobenzene is achieved in the next 30 minutes. The concentration of leached Pd increases and reaches a maximum in the same timeframe. At the end of the reaction most of the dissolved Pd is re-deposited onto the support and only a small amount remains in solution. Figure 3 shows a clear correlation between the reaction progress and Pd leaching. The same qualitative behavior has also been observed for corresponding reactions in the presence of “conventionally” prepared supported Pd catalysts. However, the applied reaction temperatures for the successful coupling of bromobenzene and styrene are different. While in the presence of a “normal” Pd/TiO₂ catalyst 140 °C were sufficient,^[11] an elevated reaction temperature of 160 °C had to be applied in this work using the sol-gel catalysts. Note that in both cases a maximum of ca. 35% of the total Pd amount was found in solution in the period between 20 and 40 minutes, which is exactly the timeframe in which complete conversion of the substrates is achieved. When we compare the results from Figure 3 with kinetic studies of the reaction of 4-chloroacetophenone and styrene,^[12] one can clearly see that in this case exactly the same reaction temperature of 160 °C is necessary to generate a sufficient Pd concentration in solution. All these observations confirm the “quasi-homogeneous” reaction mechanism that has been proven in various similar studies of several groups.^[6–12,15]

Investigations on the recovery and reuse of the catalysts show that Pd/MO_x can be easily filtered off and used for further experiments after washing with dichloromethane. In these experiments a higher Pd concentration of 0.1 mol-% was used to minimize losses of Pd during catalyst separa-

tion and washing. While complete conversion in the reaction of bromobenzene with styrene is achieved in the first run, in the second run a slight decrease to 95% conversion is observed. This marginal loss in activity of the catalyst can be attributed to a partial reduction of Pd²⁺ to Pd⁰ and to a lowered Pd dispersion after the re-deposition of the dissolved Pd species at the end of the first run. However, the catalysts retain a high activity in recycling experiments.

In the first part of the investigations we showed that a high content and dispersion of Pd²⁺ at the surface of the support is crucial for the generation of highly active catalysts. As a second main condition the presence of a strong Pd-support interaction was found to be necessary for the generation of dissolved Pd species in the right concentration at the right reaction temperature. The Pd/Al-3-450 catalyst exhibits an extremely high activity (TON up to 10000; TOF up to 5000 h⁻¹) in the reaction of bromobenzene with styrene due to a combination of these positive properties. The required reaction temperature of 160 °C was quite high for reactions of aryl bromides; however, the catalyst released the optimum amount of Pd at these elevated temperatures. For the reaction of industrially important aryl chlorides, in general, harsher conditions are necessary. Due to an increased C–X bond energy quite high temperatures are required to insert Pd into the aryl–X bond in the oxidative addition step. Therefore Pd/Al-3-450 was chosen as the catalyst in the reaction of 4-chloroacetophenone with styrene.

Reactions of 4-chloroacetophenone were performed using 0.01 mol-% Pd and the same reaction conditions as described for reactions of bromobenzene with the only difference of 6 hours reaction time (compared to 2 hours for bromobenzene). In spite of this extended reaction time, only poor conversion (14%; Table 3, entry 1) was obtained. It is widely accepted that addition of salts like tetra-*n*-butylammonium bromide N(C₄H₉)₄Br exhibits a promoting effect in Heck reactions.^[2,15,20,21] The influence of different tetra-*n*-alkylammonium halides was studied and the results obtained are presented in Table 3. A comparison of the four different tetra-*n*-butylammonium halides (entries 2–5) showed that the bromide salt had the strongest promoting effect (although in this case only 1 mmol was applied, compared to 10 mmol of the fluoride, chloride and iodide). By addition of 1 mmol N(C₄H₉)₄Br the conversion of 4-chloroacetophenone could be raised to 93%. Addition of the corresponding chloride and iodide yielded a comparable low conversion of 26%. Note that this conversion is still twice as high as without additional salt. The exceptionally high conversion obtained by using the fluoride salt (51%) may be explained by the fact that in this case a trihydrate salt was applied. The promoting effect of water in the reaction mixture is also a well known fact.^[13,14] A comparison of differently substituted tetra-*n*-alkylammonium bromides showed only marginal influence of the length of the alkyl chains (Table 3, entries 4, 6–9). In all different cases conversions of 88 to 94% could be obtained. There are only a few heterogeneous catalysts known up to now that exhibit such high TON (8600–9300) and TOF (1450–1550 h⁻¹) in the reaction of an aryl chloride.^[11,12,22–25] In the reaction of

nonactivated aryl chlorides like chlorobenzene only conversions lower than 10% were observed. A further optimization of the variety of reactions parameters like base or solvent is necessary for improvements in this complex reaction system.

Table 3. Substituted ammonium halides as promoters in the Heck reaction of 4-chloroacetophenone with styrene; reaction conditions: 10 mmol 4-chloroacetophenone, 15 mmol styrene, 12 mmol NaOAc, 1 mmol NR₄X, 10 mL NMP, 0.01 mol-% Pd (Pd/Al-3-450), 6 h, 160 °C, argon atmosphere.

NR ₄ X	% Conversion	% Yield of 3	TON	TOF [h ⁻¹]
None	14	11	1370	230
N(C ₄ H ₉) ₄ F·3H ₂ O ^[a]	51	37	5180	860
N(C ₄ H ₉) ₄ Cl ^[a]	26	24	2420	400
N(C ₄ H ₉) ₄ Br	93	81	8900	1480
N(C ₄ H ₉) ₄ I ^[a]	26	10	2430	410
N(C ₆ H ₁₃) ₄ Br	88	71	8680	1450
N(C ₇ H ₁₅) ₄ Br	93	85	9180	1530
N(C ₈ H ₁₇) ₄ Br	94	81	9310	1550
N(C ₁₂ H ₂₅) ₄ Br	91	85	9010	1500

[a] 10 mmol NR₄X.

Conclusions

In this work the synthesis of heterogeneous Pd/MO_x catalysts via combined sol-gel coprecipitation routes has been presented. Since it is known that in heterogeneously catalyzed Heck reactions the active Pd species are generated by dissolution of Pd from the catalyst surface, the control of this leaching process is essential. Coprecipitation of Pd and the metal oxide leads to a comparably strong Pd-support interaction and as a consequence quite high temperatures are necessary to dissolve Pd and generate the catalytically active species. However, the same high reaction temperatures are, in general, necessary to activate non-activated aryl bromides and aryl chlorides. Pd/MO_x catalysts prepared by optimized sol-gel methods exhibit a high dispersion of Pd²⁺ and they release exactly the right amount of Pd into the reaction mixture at these elevated temperatures. Therefore they were found to be highly active in Heck reactions of bromobenzene (TON up to 10000; TOF up to 5000 h⁻¹) and 4-chloroacetophenone (TON up to 9300; TOF up to 1550 h⁻¹). Kinetic investigations confirm the postulated “quasi-homogeneous” reaction mechanism by showing a clear correlation of the reaction rate and the Pd content in solution.

Experimental Section

Preparation of Catalysts: Pd/Al₂O₃ catalysts are prepared from Al(OiPr)₃ and PdCl₂. Al(OiPr)₃ (10 g, 49.0 mmol) is suspended in 2-propanol (300 mL) and heated to 65 °C. Water (15 mL) and, subsequently, a solution of PdCl₂ (42.5 mg, 0.24 mmol) in hydrochloric acid (30 mL) are added dropwise under vigorous stirring. The mixture is stirred for 24 h at room temp. and afterwards the solvent is evaporated. From the resulting raw material four different catalysts (Pd/Al-1 series) are prepared by thermal treatment (see Table 1).

A second charge of Pd/Al₂O₃ catalysts (Pd/Al-3 series) is prepared the same way, but the mixture is stirred for 3 days at 65 °C after the addition of the PdCl₂ solution. After evaporation of the solvent four different catalysts are prepared by thermal treatment (see Table 1).

Pd/SiO₂ catalysts are prepared from Si(OEt)₄ and PdCl₂. Si(OEt)₄ (22.2 mL, 100.0 mmol) is dissolved in ethanol (250 mL) and heated to 80 °C. Water (30 mL) is added dropwise under vigorous stirring and the reaction mixture is stirred for 3 h at 80 °C and another 10 h at room temp. Afterwards the solvent is evaporated and the resulting colorless gel is dissolved in 1-butanol (60 mL) and heated to 80 °C. A solution of PdCl₂ (102.0 mg, 0.58 mmol) in hydrochloric acid (60 mL) is added dropwise under vigorous stirring and the mixture is stirred for 2.5 h at 80 °C and another 24 h at room temp. After evaporation of the solvent four different catalysts (Pd/Si series) are prepared from the raw material (see Table 1).

Typical Procedure for Heck Reactions: Catalytic reactions are performed in sealed pressure tubes after 5 minutes of purging with argon. Reactants and solvents are used without additional drying.

Aryl halide (10 mmol), styrene (15 mmol), sodium acetate (12 mmol), NR₄X (1 mmol, only for reactions of 4-chloroacetophenone), and Pd catalyst (0.01 mol-% Pd based on aryl halide) are dissolved/suspended in 1-methyl-2-pyrrolidone (NMP, 10 mL) and heated to 160 °C for 2 h (bromobenzene) or 6 h (4-chloroacetophenone).

Filtered samples are extracted with water/CH₂Cl₂ and dried with MgSO₄. Products are identified by GC/MS. Conversion and yields are quantified by GLC using diethylene glycol dibutyl ether as internal standard ($\Delta_{\text{rel}} = \pm 5\%$).

The Pd content in solution during the reaction was determined as follows: After the desired reaction time, the pressure tube was removed from the oil bath. 5 mL of the reaction mixture were sampled and immediately filtered into a 10 mL flask. Subsequently, all liquid components were carefully evaporated by thermal treatment in a heating block. After cooling, the solid residue was treated with H₂SO₄ (98%, 2 mL) and heated to reflux for 1 h. HNO₃ (65%, 0.5 mL) was added and the resulting mixture was refluxed for 24 h. Subsequently, again HNO₃ (65%, 0.5 mL) was added and the mixture is refluxed for 24 h and cooled down to room temp. Afterwards, HCl (37%, 5 mL) and an aqueous solution of LaCl₃ (10%, 5 mL) were added. The mixture was diluted with bidistilled water to a total volume of 50 mL. The palladium content was determined by using a flame atomic absorption spectrometer Varian SpectrAA 400.

Acknowledgments

Manfred Barth and his co-workers (Mikroanalytisches Labor, TU München) are gratefully acknowledged for performing the Pd trace analysis.

- [1] A. Biffis, M. Zecca, M. Basato, *J. Mol. Catal. A* **2001**, 173, 249–274.
- [2] M. T. Reetz, J. G. de Vries, *Chem. Commun.* **2004**, 1559–1563.
- [3] N. T. S. Phan, M. van der Sluys, C. W. Jones, *Adv. Synth. Catal.* **2006**, 348, 609–679.
- [4] K. Köhler, S. S. Pröckl, W. Kleist, *Curr. Org. Chem.* **2006**, 10, 1585–1601.
- [5] V. Polshettiwar, A. Molnár, *Tetrahedron* **2007**, 63, 6949–6976.
- [6] A. Biffis, M. Zecca, M. Basato, *Eur. J. Inorg. Chem.* **2001**, 1131–1133.

- [7] F. Zhao, M. Shirai, Y. Ikushima, M. Arai, *J. Mol. Catal. A* **2002**, *180*, 211–219.
- [8] F. Zhao, M. Arai, *React. Kinet. Catal. Lett.* **2004**, *81*, 281–289.
- [9] A. F. Schmidt, V. V. Smirnov, *J. Mol. Catal. A* **2003**, *203*, 75–78.
- [10] A. F. Schmidt, A. Al-Halalqa, V. V. Smirnov, *J. Mol. Catal. A* **2006**, *250*, 131–137.
- [11] S. S. Pröckl, W. Kleist, M. A. Gruber, K. Köhler, *Angew. Chem. Int. Ed.* **2004**, *43*, 1881–1882.
- [12] S. S. Pröckl, W. Kleist, K. Köhler, *Tetrahedron* **2005**, *61*, 9855–9859.
- [13] K. Köhler, R. G. Heidenreich, J. Krauter, J. Pietsch, *Chem. Eur. J.* **2002**, *8*, 622–631.
- [14] R. G. Heidenreich, J. Krauter, J. Pietsch, K. Köhler, *J. Mol. Catal. A* **2002**, *182–183*, 499–509.
- [15] K. Köhler, W. Kleist, S. S. Pröckl, *Inorg. Chem.* **2007**, *46*, 1876–1883.
- [16] J. M. Richardson, C. W. Jones, *J. Catal.* **2007**, *251*, 80–93.
- [17] M. B. Thathagar, J. E. ten Elshof, G. Rothenberg, *Angew. Chem. Int. Ed.* **2006**, *45*, 2886–2890.
- [18] J. G. de Vries, *Dalton Trans.* **2006**, 421–429.
- [19] W. Kleist, S. S. Pröckl, K. Köhler, *Catal. Lett.* **2008**, *125*, 197–200.
- [20] T. Jeffery, *Tetrahedron Lett.* **1985**, *26*, 2667–2670.
- [21] C. Amatore, M. Azzabi, A. Jutand, *J. Am. Chem. Soc.* **1991**, *113*, 8375–8384.
- [22] M. R. Buchmeiser, K. Wurst, *J. Am. Chem. Soc.* **1999**, *121*, 11101–11107.
- [23] B. M. Choudary, S. Madhi, N. S. Chowdari, M. L. Kantam, B. Sreedhar, *J. Am. Chem. Soc.* **2002**, *124*, 14127–14136.
- [24] R. Srivastava, N. Venkatathri, D. Srinivas, P. Ratnasamy, *Tetrahedron Lett.* **2003**, *44*, 3649–3651.
- [25] S. Jana, B. Dutta, R. Bera, S. Koner, *Inorg. Chem.* **2008**, *47*, 5512–5520.

Received: August 22, 2008

Published Online: December 4, 2008

Rational Design of a Novel Chiral Palladacycle: Synthesis, Optical Resolution, and Stereochemical Evaluation

Yi Ding,^[a] Yongxin Li,^[a] Sumod A. Pullarkat,^[a] See Leng Yap,^[a] and Pak-Hing Leung*^[a]

Keywords: Asymmetric synthesis / Palladium / Chiral resolution / Cycloaddition

A novel palladacycle was designed and prepared by direct cyclopalladation of the ligand 1-(3,6-dimethylnaphthalen-1-yl)-*N,N*-dimethylethanamine, which was synthesized by a multistep sequence starting from 2,7-dimethylnaphthalene. The palladacycle structure and ring conformations of its triphenylphosphane derivative was investigated by X-ray structural analysis in the solid state and 2D ¹H–¹H ROESY NMR spectroscopy in solution. The *ortho*-palladated ring is stereochemically rigid, and the five-membered ring conformation is locked by repulsive interactions between the methyl group on the prochiral carbon atom and its neighboring naphthylene proton. The racemic cyclopalladated complex could be efficiently resolved through the formation of its (*S*)-prolinato derivatives, and efficient separation of the resulting diastereomeric complexes was achieved by simple silica-gel chromatography. The structures and absolute con-

figurations of the two optically resolved palladium complexes were determined by X-ray crystallography. Both the (*R,R*)- and (*S,S*)-di- μ -chloride dimeric palladium complexes could be obtained chemoselectively by treating the corresponding prolinato derivatives with 1 M hydrochloric acid. Despite the severe interchelate steric constraints within this new organo-palladium complex, the bulky monodentate ligand 3,4-dimethyl-1-phenylphosphole (dmpp) was coordinated regio-specifically to the *ortho*-palladated amine unit *trans* to the NMe₂ group. In comparison to its naphthylamine analogue, the new palladacycle showed a much higher stereoselectivity in the chiral template-promoted asymmetric Diels–Alder reaction of coordinated dmpp and *N,N*-dimethylacrylamide.

(© Wiley-VCH Verlag GmbH & Co. KGaA, 69451 Weinheim, Germany, 2009)

Introduction

Recently, a great deal of attention has been focused on the development of enantiomerically pure cyclopalladated complexes, because these compounds play important roles in many aspects of synthetic stereochemistry. Many chiral cyclopalladated complexes have been reported,^[1] and they could be used as resolving agents for chiral ligands,^[2] clear and reliable references for the NMR spectroscopic assignment of unknown absolute configurations,^[3] diamagnetic chiral shift reagents for the determination of optical purity of organic compounds,^[3b,3h,3f,4] and efficient chiral catalysts for asymmetric reactions.^[5]

In the past decade, we have chosen *ortho*-metalated dimethyl[1-(α)-naphthyl]ethylamine [(*S*)-**1**; Figure 1] and its (*R*) enantiomer as chiral templates for the asymmetric [4+2] Diels–Alder reaction between 3,4-dimethyl-1-phenylphosphole (dmpp) and a range of dienophiles.^[6] A unique stereochemical feature of (*S*)-**1** is that there is an internal steric repulsion between the methyl substituent on the stereogenic carbon atom and its neighboring naphthylene

proton H⁸, and this interaction confines the methyl group in the axial position, and hence, the λ absolute conformation of the five-membered ring is fixed and not interconvertible, both in the solid state and in solution.^[7] Due to this unique ring conformation, the chirality of the naphthylamine ring is transmitted efficiently through its prochiral NMe groups onto the neighboring coordination site. A series of functionalized P-chiral phosphanes have been generated stereoselectively by using both chiral forms of **1** as the chiral reaction template.^[6] However, this naphthylamine auxiliary does not exhibit good stereoselectivity in certain reactions. For example, when *N,N*-dimethylacrylamide was used as the dienophile, the two possible diastereomeric *endo* cycloadducts were obtained as a 1:2 mixture.^[6j] This experiment shows that the chiral naphthylethylamine auxiliary exerts a weak stereochemical influence on the reaction site. In the transition state, the dmpp group enjoys a certain degree of free rotation around the P–Pd bond, and thus, poor stereoselectivity was observed. It has been established that the coordination site *cis* to the N atom is controlled stereochemically by the two prochiral NMe groups.^[5f] We believe that by introducing a spacer on the aromatic carbon atom adjacent to the Pd–C bond on the template, this class of *ortho*-palladated complexes may induce better stereoselectivity in similar reactions.^[6k–6m]

[a] Division of Chemistry and Biological Chemistry, School of Physical and Mathematical Sciences, Nanyang Technological University, 637371, Singapore
E-mail: pakhing@ntu.edu.sg

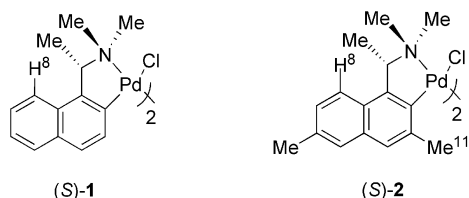


Figure 1. Stereochemical features of complexes (S)-1 and (S)-2.

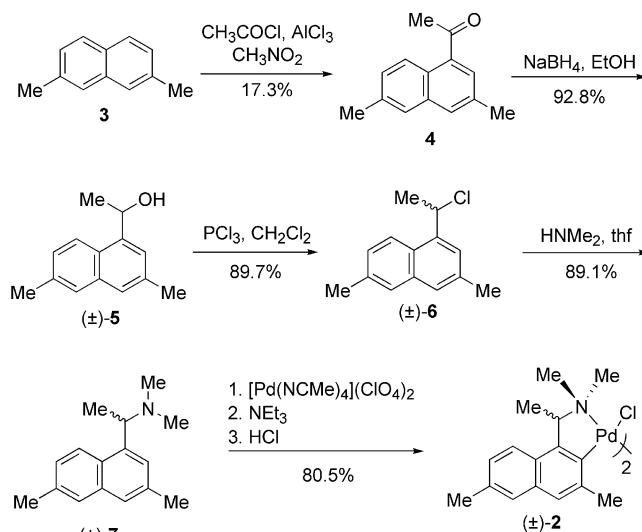
Therefore, we report the synthesis and optical resolution of novel chiral palladacycle (S)-2. Chiral complex (S)-2 exhibits the key stereochemical features of the chiral naphthylamine chelate ring in (S)-1. The internal steric repulsion between the methyl substituent on the stereogenic carbon atom and its neighboring aromatic proton H⁸ is expected to lock the five-membered organometallic ring conformation. Furthermore, a methyl group^[11] (Figure 1) was introduced on the aromatic ring, which was designed to exert a stronger stereochemical influence on the neighboring reaction site as compared to (S)-1. For comparison purposes, the application of this new chiral palladacycle in the asymmetric Diels–Alder reaction was examined.

Results and Discussion

Synthesis and Characterization of *ortho*-Palladium Complex (±)-2

The racemic form of the amine was prepared according to Scheme 1. On the basis of the reported procedure with 2,7-dimethylnaphthalene (3)^[8] as the starting material, ketone 4 was obtained as the minor product in 17.3% yield.^[6m,9] Reduction of ketone 4 by NaBH₄ gave racemic alcohol (±)-5 in 92.8% yield. Conversion of (±)-5 into chloride (±)-6 was achieved by treatment with an excess amount of PCl₃ in CH₂Cl₂ in 89.7% yield. Reaction between (±)-6 and aqueous dimethylamine afforded target *N,N*-dimethylamine (±)-7 in 89.1% yield. Treatment of (±)-7 with [Pd(MeCN)₄](ClO₄)₂ in the presence of NEt₃ followed by the addition of 1 M HCl led to chloride-bridged dimeric complex (±)-2 in the form of a light-yellow powder in 80.5% isolated yield.

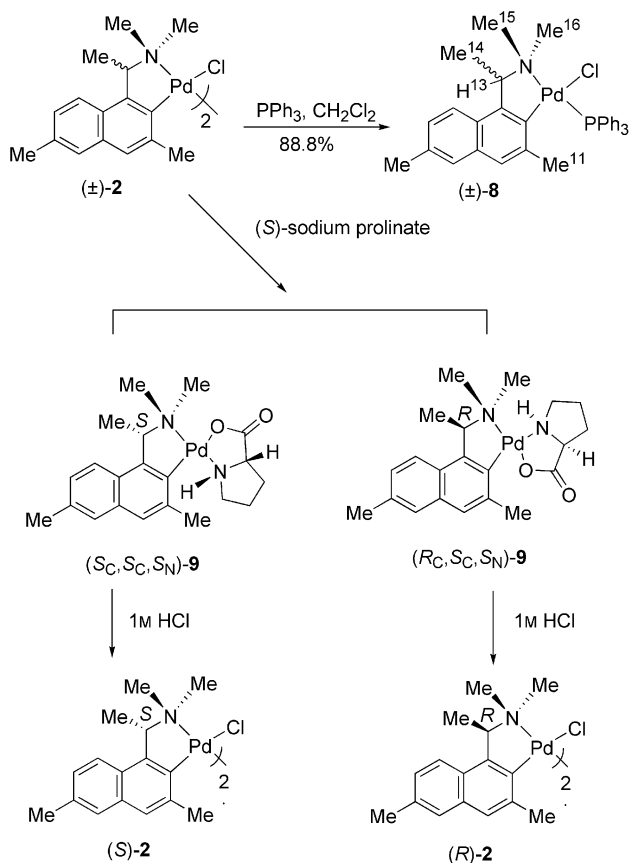
The dynamic *cis*–*trans* interconversion and the stereoisomeric properties of dimeric complex (±)-2 rendered difficulties in the characterization of its ¹H NMR signals. Thus, the dimer was converted into its monomeric form (±)-8 by treatment with PPh₃. Complex (±)-8 was prepared efficiently from the reaction of (±)-2 with PPh₃ through a standard μ-Cl bridge cleavage reaction (Scheme 2). In CDCl₃, the ³¹P NMR spectrum of (±)-8 shows only a singlet resonance at δ = 30.1 ppm, indicating the presence of a sole isomer in solution. The NMR spectroscopic analysis of racemic adduct (±)-8 showed that in solution the five-membered palladacycle exists preferentially in the δ(*R*) or λ(*S*) conformation with the α-methyl substituent in the axial position. This conclusion may be inferred from the ⁴J_{H,P} value of 6.4 Hz for the α-methane proton and confirmed by



Scheme 1.

the results of ROESY measurements (Figure 2). The conformational behavior of the five-membered palladacycle was deduced from NOE data obtained from the ¹H–¹H ROESY NMR spectra of (±)-8. The interaction between the α-methane H¹³ and methyl protons are the key interactions to the conformational state of the palladacycle, which gave rise to the existence of NOE interactions (C and D) between H¹³ and the two NMe groups (Me¹⁶ and Me¹⁵) and the interaction between H¹³ and Me¹⁴ (E). In contrast, the α-methane group Me¹⁴ interacts strongly with the equatorial NMe group Me¹⁶ (B). The driving force for Me¹⁴ to assume mainly the axial position can be attributed to the repulsive interactions, that is, H¹³–H⁸ (F) and Me¹⁴–H⁸ (I). Other expected NOE interactions of H³–Me¹¹ (J), Me¹⁵–Me¹⁶ (A), Me¹²–H⁵, and Me¹²–H⁷ (G and H) are also observed. The above NMR spectroscopic investigations of (±)-8 in solution indicates that the α-methyl group Me¹⁴ is located in the axial position and the interaction between the Me¹⁴ and H⁸ can confine the five-membered organometallic ring conformation and the λ and δ conformations are adopted in the (*S*) and (*R*) enantiomers, respectively.

In the solid state, the structure of (±)-8 was reaffirmed crystallographically. The X-ray molecular structure of (±)-8 and selected bond lengths and angles are presented in Figure 3 and Table 1, respectively. Complex (±)-8 has a distorted square-planar coordination geometry. There is a strong steric repulsion between the PPh₃ ligand and the organometallic chelate; hence, the bond angle C1–Pd1–P1 was enlarged to 100.2(4)°. With these structural features, the Pd–P bond would not be able to rotate freely, as all the possible rotational motions are blocked by the chloride ligand and the projecting methyl group. Therefore, among the three P–Ph phenyl rings, the C29–C34 ring experiences the most intramolecular ligand–ligand repulsion. As a result, the bond angle Pd1–P1–C29 is enlarged to 119.6(5)°, which is larger than the two less affected Pd1–P1–C23 and Pd1–P1–C17 angles [109.6(5) and 117.6(5)°, respectively]. The distance between H¹³ and H⁸ is 2.176 Å; the distance



Scheme 2.

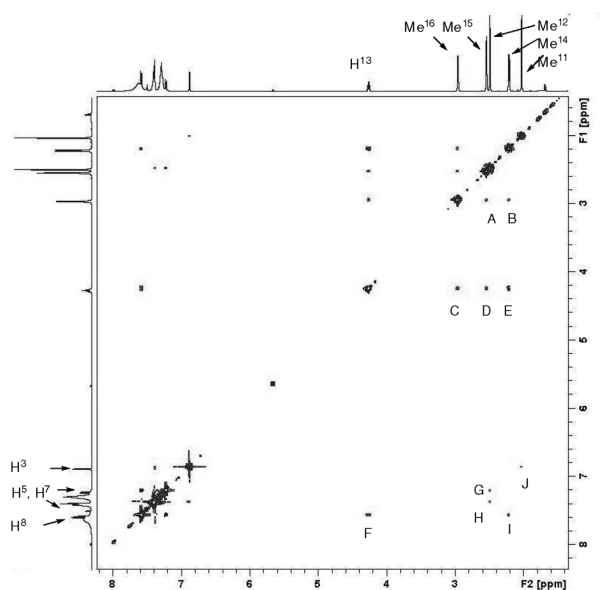
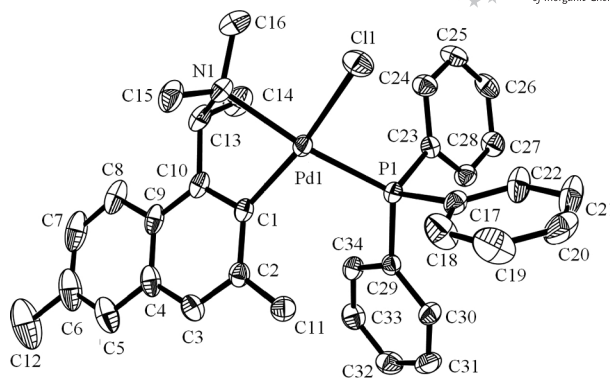


Figure 2. 2D ¹H–¹H ROESY NMR spectrum of (\pm)-8 in CDCl₃ [refer to Figure 3 for the numbered structure of (\pm)-8]. Selected NOE interactions: (A) Me¹⁵–Me¹⁶; (B) Me¹⁴–Me¹⁶; (C) H¹³–Me¹⁶; (D) H¹³–Me¹⁵; (E) H¹³–Me¹⁴; (F) H⁸–H¹³; (G, H) Me¹²–H⁵, Me¹²–H⁷; (I) Me¹²–Me¹⁶; (J) H³–Me¹¹.

between C14 and the methyl carbon atoms (both axial and equatorial methyl groups) were found to be 2.872 and 3.875 Å, respectively.

Figure 3. Molecular structure of (\pm)-8.Table 1. Selected bond lengths [Å] and angles [°] for complex (\pm)-8.

Pd1–C1	2.017(2)	Pd1–N1	2.146(1)
Pd1–P1	2.259(4)	Pd1–C11	2.385(5)
P1–C23	1.836(2)	P1–C17	1.829(2)
P1–C29	1.819(2)	P1–Pd1–C11	100.2(4)
C1–Pd1–N1	79.6(6)	C1–Pd1–P1	101.7 (1)
N1–Pd1–P1	158.4(4)	C1–Pd1–C11	165.6(4)
N1–Pd1–C11	94.1(4)	P1–Pd1–C11	90.4(2)

Optical Resolution of Racemic Dimer (\pm)-2

The resolution of racemic dimeric complex (\pm)-2 was achieved by using (*S*)-prolinato as the resolving agent (Scheme 2). By treating of the racemic dimer with two molar equivalents of sodium (*S*)-prolinato, the expected 1:1 mixture of diastereomeric adducts (*R_C,S_C,S_N*)-9 and (*S_C,S_C,S_N*)-9 was formed and confirmed by ¹H NMR spectroscopy. Initial attempts to separate the two diastereomers by fractional crystallization were unsuccessful, as crystallization could not be induced despite the use of an array of solvent systems. Nevertheless, the neutral nature of these complexes presented the alternate option of diastereomeric separation by column chromatography. Thus, the 1:1 diastereomeric mixture was slowly eluted through a silica gel column with CH₂Cl₂/acetone (2:1) as the mobile phase. The eluted fractions were checked by ¹H NMR spectroscopy for their optical purities. Thus, by column chromatography, both diastereomers were separated efficiently. Diastereomer (*R_C,S_C,S_N*)-9, which eluted first, was crystallized from CH₂Cl₂ and hexane as light-yellow prisms in an overall yield of 90.6% with [α]₃₆₅ = +160 (*c* = 0.5, CH₃OH) and with >99% *de* (according to ¹H NMR spectroscopy). The other diastereomer, (*S_C,S_C,S_N*)-9, was isolated as a light-yellow powder and also crystallized from CH₂Cl₂ and hexane in 88.4% yield with [α]₃₆₅ = +916 (*c* = 0.5, CH₃OH) and with >99% *de* (according to ¹H NMR spectroscopy).

X-ray diffraction analysis of diastereomer (*R_C,S_C,S_N*)-9 was performed (Figure 4), and selected bond lengths and angles are provided in Table 2. The X-ray crystallographic study reveals the (*R*) absolute configuration of the α -carbon stereocenter. The α -methyl group Me¹⁴ occupies the expected axial position and the conformation of the five-membered palladacycle is δ . This complex adopts a *cis*-

(*N,N*) arrangement, as observed in similar prolinato complexes.^[6k] The tetrahedron distortion of the palladium coordination environment is minimal, with the angle between the {Pd1C1N1} and {Pd1N2O1} planes equal to 5.01°.

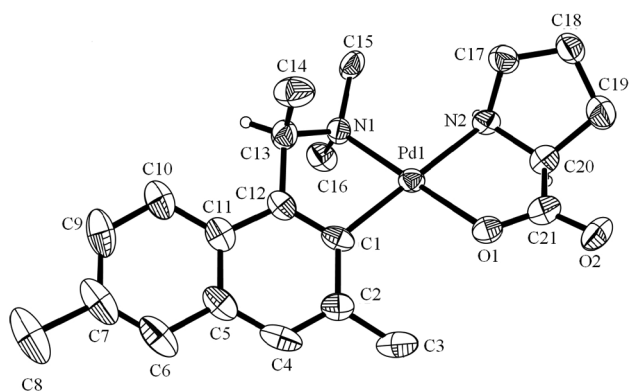


Figure 4. Molecular structure of (*R_C*, *S_C*, *S_N*)-**9**.

Table 2. Selected bond lengths [Å] and angles [°] for complex (*R_C*, *S_C*, *S_N*)-**9**.

Pd1–C1	2.030(6)	Pd1–O1	2.039(4)
Pd1–N1	2.047(5)	Pd1–N2	2.141(5)
N1–C16	1.477(8)	C17–N2	1.503(8)
C21–O2	1.221(9)	C21–O1	1.300(9)
C1–Pd1–N1	79.8(2)	C1–Pd1–N2	178.5(2)
N1–Pd1–O1	175.5(2)	N2–Pd1–O1	80.8(2)
C1–Pd1–O1	99.7(2)	N1–Pd1–N2	99.8(2)

For the other diastereomer, (*S_C*, *S_C*, *S_N*)-**9**, yellow crystals suitable for X-ray crystallography were obtained by slow evaporation of a CH₂Cl₂/hexane solution. There are two crystallographically distinguished molecules in the asymmetrical unit with the same stereochemistry but slightly different bond lengths and angles. For clarity, only one of them (molecule A) is depicted in Figure 5. Selected bond lengths and angles are listed in Table 3. The absolute configuration of (*S_C*, *S_C*, *S_N*)-**9** was determined from its X-ray molecular structure and confirmed from the Flack parameter of 0.04(2). Like the previously reported (*S*)-prolinated complex, complex (*S_C*, *S_C*, *S_N*)-**9** adopts a *trans*-(*N,N*) arrangement.^[6k] However, due to the repulsive interaction between the *ortho* methyl group Me³ and the pyrrolidine, the C1–Pd1–N2 angle is enlarged to 104.6(1)° in comparison to the value of 99.9(1)° for a similar benzylamine derivative.^[10]

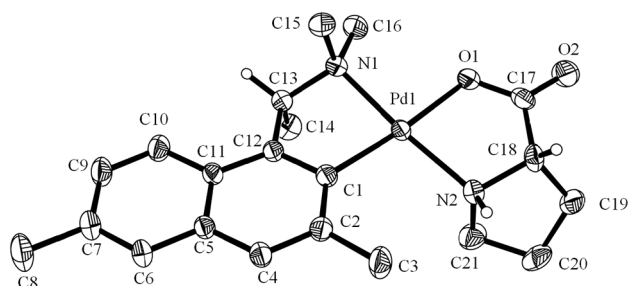


Figure 5. Molecular structure of (*S_C*, *S_C*, *S_N*)-**9**.

Table 3. Selected bond lengths [Å] and angles [°] for complex (*S_C*, *S_C*, *S_N*)-**9**.

Molecule A		Molecule B	
Pd1–C1	2.009(3)	Pd2–C22	2.002(3)
Pd1–N1	2.062(2)	Pd2–N4	2.061(3)
Pd1–N2	2.074(2)	Pd2–N3	2.062(3)
Pd1–O1	2.083(2)	Pd2–O3	2.083(2)
C1–Pd1–N1	81.8(1)	C22–Pd2–N4	102.3(1)
C1–Pd1–N2	104.6(1)	C22–Pd2–N3	80.7 (1)
N1–Pd1–N2	172.7(1)	N4–Pd2–N3	174.5(1)
C1–Pd1–O1	174.3(1)	C22–Pd2–O3	176.0(1)
N1–Pd1–O1	92.6(1)	N4–Pd2–O3	81.7(1)

Synthesis of the Palladacycle in Its Optically Active Form

Optical chloride dimer (*S*)-**2** was obtained by mixing (*S_C*, *S_C*, *S_N*)-**9** with 1 M HCl and isolated as a yellow powder in 95.6% yield with $[\alpha]_D = +120$ ($c = 0.5$, CH₂Cl₂). Single crystals were obtained from a mixture of CH₂Cl₂ and hexane. The structure of chiral dimeric complex (*S*)-**2** was determined by X-ray crystallography (Figure 6) and selected bond lengths and angles are listed in Table 4. X-ray crystallographic analysis confirms the expected (*S*) absolute configuration of the α -carbon stereocenter of the palladacycle. In line with most of the recorded X-ray structures of similar μ -chloride-bridged dimeric *ortho*-palladated amines or related dimers of C,N-type, complex (*S*)-**2** reveals the expected *trans* relationship between two nitrogen atoms and two carbon donor atoms. The coordination spheres of both the palladium centers are in a distorted square-planar geometry, with tetrahedral distortions of 10.4 and 11.0°. The most interesting feature of (*S*)-**2** is that the central four-membered ring (Pd1–C11–Pd1A–C11A) is bent along the C11–C11A axis by 52.9°. This can be partially attributed to the repulsive interactions between the methyl groups (C11, C11A) and the two bridged Cl atoms. Both the C11–C11 and C11A–C11A distances were found to be 3.230 Å, which is less than the sum of the van der Waals radii of the two atoms (3.8 Å). Furthermore, the interaction between the NMe group (C16, C16A) and the bridged Cl atoms (C11, C11A) also contributed to the large angle observed, because the C16–C11 and C16A–C11A distances were 3.285 Å. The interactions mentioned above project the naphthalene ring away from the chloride bridges to thus form butterfly-like dimeric complex (*S*)-**2**.

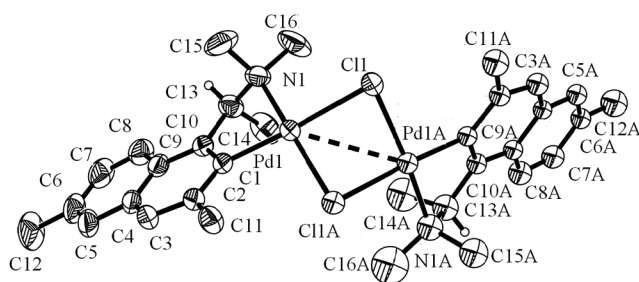


Figure 6. Molecular structure of (*S*)-**2**.

Table 4. Selected bond lengths [Å] and angles [°] for complex (S)-2.

Pd1–C1	1.996(2)	Pd1–N1	2.075(2)
Pd1–C11A	2.355(6)	Pd1–C11	2.489(5)
Pd1–Pd1A	3.225(3)	C11–Pd1A	2.355(6)
C1–Pd1–N1	80.6(8)	C1–Pd1–C11A	98.7(6)
N1–Pd1–C11A	168.6(6)	C1–Pd1–C11	176.3(6)
N1–Pd1–C11	97.4(5)	C11A–Pd1–C11	83.9(2)
C1–Pd1–Pd1A	137.1(5)	N1–Pd1–Pd1A	123.9(6)
C11A–Pd1–Pd1A	50.1(1)	C11–Pd1–Pd1A	46.5 (1)
Pd1A–C11–Pd1	83.4 (2)	C15–N1–Pd1	111.2(2)
C16–N1–Pd1	113.8(2)	C13–N1–Pd1	104.4(1)

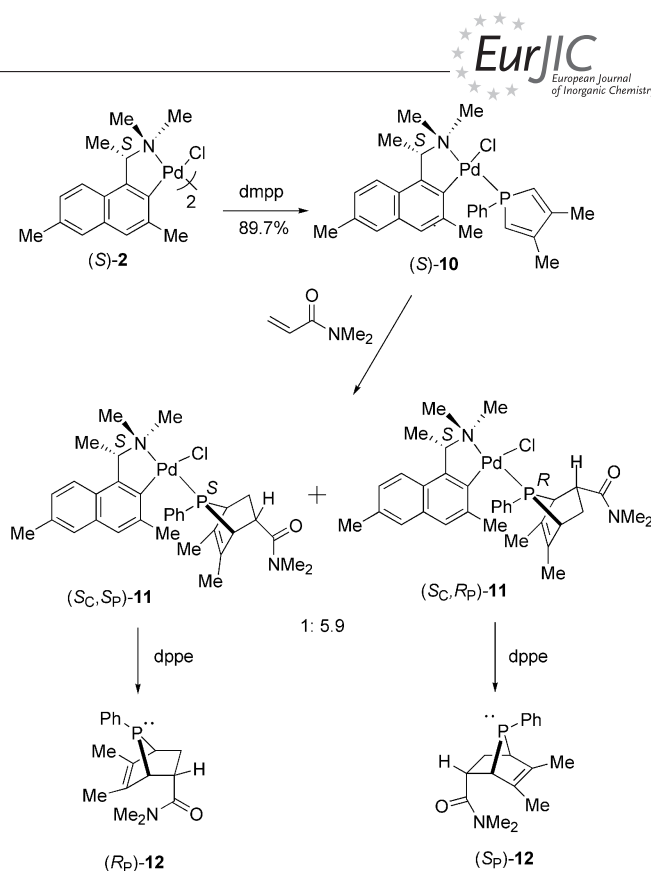
Enantiomeric palladacycle (*R*)-2 could be prepared from (*R_CS_CS_N*)-9 in a similar manner: [α]_D = –142, (*c* = 0.5, CH₂Cl₂).

Synthesis of dmpp Complex (S)-10 and Its *endo* Diels–Alder Reactions with *N,N*-Dimethylacrylamide

In order to evaluate the efficiency of the new palladacycle as a chiral template for intermolecular Diels–Alder cycloaddition reactions, the intermediate 3,4-dimethyl-1-phenylphosphole (dmpp) complex (S)-10 was synthesized by a cleavage reaction of dimeric complex (S)-2 with dmpp. The reaction between (S)-10 and *N,N*-dimethylacrylamide was subsequently investigated.

As shown in Scheme 3, the dichloride bridge in (S)-2 could be split readily by dmpp at room temperature to afford (S)-10 as a yellow powder in 89.7% yield. The ³¹P NMR spectrum of (S)-10 in CDCl₃ shows only one singlet signal at δ = 28.4 ppm. In the ¹H NMR spectrum, the long-range P,H coupling constants of 3.4 and 6.5 Hz observed for the resonance signals of NMe(eq) and the proton borne on the chiral center indicate that the dmpp group is coordinated *trans* to the nitrogen atom in solution.

Single crystals of (S)-10 were obtained from a solution of chloroform and hexane. The solid structure of this complex was determined by X-ray crystallography. Figure 7 presents the molecular structure of (S)-10, and Table 5 tabulates selected interatomic distance and angles. The coordinated geometry is square planar and the phosphole group is in the *trans* position with respect to the amine nitrogen. The complex has a distorted square-planar coordination geometry with a tetrahedral distortion angle of 13.2°. As expected, the five-membered palladacycle has an envelop-like geometry with the N1 atom 0.848 Å above the C13–C12–C1–Pd1 mean plane. The bond angles around P1 are significantly different. The angle C22–P1–Pd1 [123.22(5)°] is significantly larger than those of C17–P1–Pd1 [112.55(6)°] and C23–P1–Pd1 [113.81(5)°]. This difference can be attributed to the repulsive interactions between the coordinated dmpp group and the “spacer” methyl C3 (Figure 7). The C3–P1 distance (3.439 Å) is shorted than the sum of the van der Waals radii of the two groups (3.8 Å). As a result of this repulsion, the C3 atom is not strictly coplanar with the phenyl ring C1–C2–C4–C5–C11–C12, but with a distance of 0.222 Å to the mean plane.



Scheme 3.

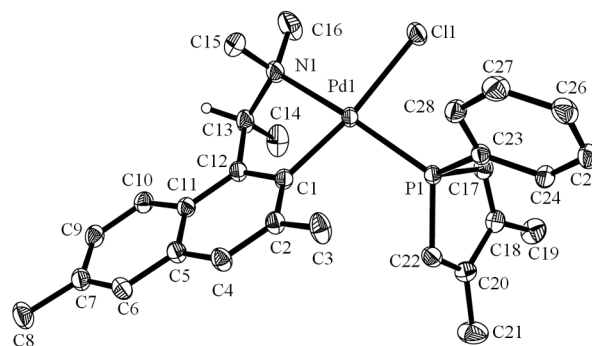


Figure 7. Molecular structure of (S)-10.

Table 5. Selected bond lengths [Å] and angles [°] for complex (S)-10.

Pd1–C1	2.018(2)	Pd1–N1	2.133(1)
Pd1–P1	2.244(3)	Pd1–C11	2.395(4)
C1–Pd1–N1	80.1(6)	C1–Pd1–P1	99.6(4)
N1–Pd1–P1	167.9(5)	C1–Pd1–C11	171.6(5)
N1–Pd1–C11	94.1(4)	P1–Pd1–C11	87.4(1)
C12–C1–Pd1	111.3(1)	C2–C1–Pd1	129.2(1)
C17–P1–Pd1	112.6(6)	C22–P1–Pd1	123.2(5)

The intermolecular *endo*-cycloaddition reaction between (S)-10 and *N,N*-dimethylacrylamide was carried out at room temperature in CH₂Cl₂. The reaction was monitored by ³¹P NMR spectroscopy and found to be complete in 20 d. Prior to purification, the ³¹P NMR spectrum of the

crude reaction product in CDCl_3 exhibited two sharp singlets at $\delta = 114.3$ and 115.3 ppm in a ratio of 1:5.9, indicating that two diastereomeric products were formed in the *endo*-cycloaddition reaction.

The diastereomeric cycloadducts could be separated by column chromatography efficiently. The mixture was slowly eluted through a silica gel column with CH_2Cl_2 /ethyl acetate (10:1) as the mobile phase. The two diastereomers were readily distinguished as two well-separated bands. Minor diastereomer (S_C, S_P)-**11** was isolated as a pale-yellow powder in 11.9% yield, $[\alpha]_D = +120$, ($c = 0.5$, CH_2Cl_2). The other diastereomer, (S_C, R_P)-**11**, was also isolated as a yellow powder in 69.5% yield with $[\alpha]_D = +60$ ($c = 0.5$, CH_2Cl_2). Known optically active phosphanorbornene (S_P)-**12** and (R_P)-**12** could be liberated efficiently by treating enantiomerically pure complex (S_C, R_P)-**11** and (S_C, S_P)-**11** with 1,2-bis(diphenylphosphanyl)ethane, respectively.^[6e,6j,6p] The apparent inversion of configuration that takes place at the phosphorus center when the functionalized phosphane is liberated from the reaction promoter is merely a consequence of the Cahn–Ingold–Prelog (CIP) sequence rules.^[11]

Conclusions

In this article, the synthesis of novel palladacycle (*S*)-**2** was readily accomplished from 2,7-dimethylnaphthalene and then resolved by separation of the (*S*)-proline diastereomeric derivatives. When naphthylamine auxiliary (*S*)-**1** was used as a chiral template for the asymmetric Diels–Alder reaction between dmp and *N,N*-dimethylacrylamide at room temperature, the cycloadducts were obtained in a ratio of 1:2. However, in this study, this ratio was improved to 1:5.9. Clearly, the 1-(3,6-dimethylnaphthalen-1-yl)-*N,N*-dimethylethanamine palladium complex exhibits a better stereoselectivity for this class of intermolecular cycloaddition reactions. Therefore, the introduction of a methyl group on the aromatic ring next to the Pd–C bond indeed exerts an influence on the selectivity in this asymmetric cycloaddition reaction. Currently, investigations of chiral palladacycles with different substituents and synthetic applications of newly prepared palladacycle (*S*)-**2** are in progress.

Experimental Section

General: Reactions involving air-sensitive compounds were performed under positive pressure of purified nitrogen by using standard Schlenk techniques. ^1H and ^{13}C NMR spectroscopy were performed with Bruker Avance 300, 400, or 500 NMR spectrometers. Multiplicities were given as: s (singlet), br. (broad), d (doublet), t (triplet), q (quartet), dd (doublets of doublet), m (multiplet). The number of protons (n) for a given resonance is indicated by $n\text{H}$. Coupling constants are reported as a J values in Hz. Chemical shifts are reported as δ in units of parts per million (ppm) downfield from SiMe_4 ($\delta = 0.0$ ppm), relative to the signal of $[\text{D}]\text{chloroform}$ ($\delta = 77.00$ ppm, triplet; ^{13}C NMR) and 85% H_3PO_4 (^{31}P NMR) (300 K). All the ^{31}P NMR spectra were recorded at 121 MHz with a Bruker Avance DPX300 NMR spectrometer. Mass spectra were recorded with a Thermo Finnigan MAT 95 XP

Mass Spectrometer with EI mode and Waters Q-ToF Premier Mass Spectrometer with ESI mode. Melting points were determined with an SRS-Optimelt MPA-100 apparatus and are uncorrected. Optical rotations were measured with the specified solution in 0.1-dm cell at 20 °C with a Perkin–Elmer model 341 polarimeter. Elemental analyses were performed by the Elemental Analysis Laboratory of the Division of Chemistry and Biological Chemistry at the Nanyang Technological University of Singapore. Compound **4** was previously reported; however, its synthesis experimental details were not available.^[9]

1-(3,6-Dimethyl-1-naphthyl)ethanone (4): A solution of 2,7-dimethylnaphthalene (**3**; 7.30 g, 46.73 mmol) in CH_3NO_2 (100 mL) was added whilst stirring to a mixture of anhydrous AlCl_3 (7.33 g, 54.97 mmol) and acetyl chloride (3.34 mL, 46.80 mmol) in the same solvent (20 mL). The resultant red solution was stirred at room temperature for 20 h and poured into a mixture of ice (50 g) and concentrated HCl (20 mL). After vigorous stirring for 30 min, the yellowish organic layer was separated, washed with H_2O , and dried (MgSO_4). Removal of the solvent gave a brown color oil. The residue was thus passed through a silica gel column (Et_2O /hexane, 1:40), and **4** (1.60 g, 17.3%) was separated as the minor product. Colorless solid. M.p. 78–80 °C. ^1H NMR (300 MHz, CDCl_3): $\delta = 2.49$ (s, 3 H, CH_3), 2.53 (s, 3 H, CH_3), 2.72 (s, 3 H, COCH_3), 7.36 (dd, $^3J_{\text{H,H}} = 8.8$ Hz, $^4J_{\text{H,H}} = 1.7$ Hz, 1 H, aromatic proton), 7.53 (s, 1 H, aromatic proton), 7.65 (s, 1 H, aromatic proton), 7.69 (s, 1 H, aromatic proton), 8.60 (d, $^3J_{\text{H,H}} = 8.8$ Hz, 1 H, aromatic proton) ppm. ^{13}C NMR (75 MHz, CDCl_3): $\delta = 21.5$, 29.9, 125.6, 126.7, 126.8, 129.4, 130.2, 131.4, 133.9, 134.6, 135.2, 136.1, 201.9 ppm. HRMS (ESI): calcd. for $\text{C}_{14}\text{H}_{15}\text{O}$ [$\text{M} + \text{H}$] $^+$ 199.1123; found 199.1118. $\text{C}_{14}\text{H}_{14}\text{O}$ (198.26): calcd. C 84.81, H 7.12; found C 84.98, H 7.09.

1-(3,6-Dimethyl-1-naphthyl)ethanol [(±)-5]: To a solution of **4** (1.60 g, 8.07 mmol) in ethanol (30 mL) was added a solution of NaBH_4 (0.60 g, 15.86 mmol) in the same solvent (20 mL). The mixture was stirred at room temperature for 24 h, followed by treatment with dilute NaOH solution. The ethanol in the resulting solution was removed under vacuum, and the aqueous phase was then extracted with CH_2Cl_2 . The organic layers were combined, washed with H_2O , and dried with MgSO_4 . Removal of the solvent gave product (±)-**5** (1.50 g, 92.8%) as a white solid. ^1H NMR (300 MHz, CDCl_3): $\delta = 1.65$ (d, $^3J_{\text{H,H}} = 6.4$ Hz, 3 H, CHCH_3), 2.33 (s, 1 H, OH), 2.55 (s, 6 H, aryl- CH_3), 5.58 (q, $^3J_{\text{H,H}} = 6.4$ Hz, 1 H, CHCH_3), 7.30 (d, $^3J_{\text{H,H}} = 8.7$ Hz, $^4J_{\text{H,H}} = 1.6$ Hz, aromatic proton), 7.45 (s, 1 H, aromatic proton), 7.46 (s, 1 H, aromatic proton), 7.56 (s, 1 H, aromatic proton), 7.93 (d, $^3J_{\text{H,H}} = 8.7$ Hz, 1 H, aromatic proton) ppm. ^{13}C NMR (75 MHz, CDCl_3): $\delta = 21.6$, 21.8, 24.4, 67.1, 122.8, 123.4, 126.2, 126.7, 127.3, 127.4, 134.5, 135.1, 135.2, 141.1 ppm. HRMS (ESI): calcd. for $\text{C}_{14}\text{H}_{15}$ [$\text{M} - \text{OH}$] $^+$ 183.1174; found 183.1166. $\text{C}_{14}\text{H}_{16}\text{O}$ (200.27): calcd. C 83.96, H 8.05; found C 83.71, H 8.08.

1-(1-Chloroethyl)-3,6-dimethylnaphthalene [(±)-6]: A solution of (±)-**5** (1.50 g, 7.49 mmol) in CH_2Cl_2 (20 mL) was dropped slowly into a solution of PCl_3 (4.50 g, 32.8 mmol) in the same solvent (30 mL). The mixture was stirred overnight at room temperature and quenched by the addition of ice water at 0 °C. The organic layer was separated, washed with water, and dried with MgSO_4 . Removal of the solvent gave product (±)-**6** (1.47 g, 89.7%) as a colorless oil. ^1H NMR (300 MHz, CDCl_3): $\delta = 2.06$ (d, $^3J_{\text{H,H}} = 6.5$ Hz, 3 H, CHCH_3), 2.53 (s, 6 H, aryl- CH_3), 5.87 (q, $^3J_{\text{H,H}} = 6.5$ Hz, 1 H, CHCH_3), 7.36 (d, $^3J_{\text{H,H}} = 8.4$ Hz, 1 H, aromatic proton), 7.49 (s, 1 H, aromatic proton), 7.52 (s, 1 H, aromatic proton), 7.57 (s, 1 H, aromatic proton), 8.03 (d, $^3J_{\text{H,H}} = 8.4$ Hz, 1 H, aro-

matic proton) ppm. ^{13}C NMR (75 MHz, CDCl_3): δ = 21.5, 21.8, 25.2, 54.8, 122.7, 125.0, 126.9, 127.3, 127.5, 127.8, 134.5, 134.9, 135.5, 137.3 ppm. HRMS (EI) calcd. for $\text{C}_{14}\text{H}_{15}[\text{M} - \text{Cl}]$ 183.1174; found 183.1175.

***N*-[1-(3,6-dimethyl-1-naphthyl)ethyl]-*N,N*-dimethylamine [(±)-7]:** A solution of (±)-6 (1.47 g, 6.72 mmol) in CH_2Cl_2 (20 mL) was added to a solution of dimethylamine (2 M in THF, 10 mL) and stirred vigorously for 48 h. The solvent was removed under vacuum, and the residue was then dissolved in CH_2Cl_2 . The solution was washed with H_2O , dried with MgSO_4 , and the solvents evaporated to dryness. The pure amine was obtained as a light-yellow oil (1.36 g, 89.1%) after silica gel chromatography (ethyl acetate). ^1H NMR (300 MHz, CDCl_3): δ = 1.50 (d, $^3J_{\text{H,H}}$ = 6.6 Hz, 3 H, CHCH_3), 2.32 (s, 6 H, CH_3), 2.53 (s, 6 H, CH_3), 3.96 (q, $^3J_{\text{H,H}}$ = 6.6 Hz, 1 H, CHCH_3), 7.30 (dd, $^3J_{\text{H,H}}$ = 8.3 Hz, $^4J_{\text{H,H}}$ = 1.6 Hz, 1 H, aromatic proton), 7.42 (s, 1 H, aromatic proton), 7.46 (s, 1 H, aromatic proton), 7.57 (s, 1 H, aromatic proton), 8.25 (d, $^3J_{\text{H,H}}$ = 8.7 Hz, 1 H, aromatic proton) ppm. ^{13}C NMR (75 MHz, CDCl_3): δ = 19.9, 21.5, 21.8, 43.9, 62.4, 123.5, 125.7, 125.7, 127.0, 127.2, 128.1, 134.7, 134.9, 135.1, 140.7 ppm. HRMS (ESI): calcd. for $\text{C}_{16}\text{H}_{22}\text{N}[\text{M} + \text{H}]^+$ 228.1752; found 228.1746.

Palladium Complex (±)-2: A mixture of $[\text{Pd}(\text{MeCN})_4](\text{ClO}_4)_2$ (1.56 g, 6.00 mmol) and AgClO_4 (2.48 g, 12.0 mmol) in CH_3CN (30 mL) was stirred in the dark at room temperature for 1 h. The AgCl precipitate was filtered off, and the filtrate was added dropwise to a stirred mixture of (±)-7 (1.36 g, 6.00 mmol) and NEt_3 (0.60 g, 6.00 mmol) in CH_2Cl_2 (20 mL). The resulting mixture was stirred at room temperature for 24 h and filtered through Celite. The filtrate was evaporated, and the residue was dissolved in CH_2Cl_2 (100 mL). Dilute HCl (1 M, 50 mL) was then added to the solution, and the mixture was vigorously stirred for 1 h. The organic layer was separated, washed with H_2O , and dried with MgSO_4 . After removing the solvent, the residue was passed through a silica gel column (CH_2Cl_2) to give yellow powder (±)-2 (1.78 g, 80.5%). M.p. 196–198 °C (decomp.). ^1H NMR (300 MHz, CDCl_3): δ = 2.26–2.28 (m, 6 H, CH_3), 2.44 (br. s, 6 H, CH_3), 2.62–2.72 (m, 18 H, CH_3), 4.12–4.13 (m, 2 H, CHCH_3), 7.11–7.14 (m, 4 H, aromatic protons), 7.43 (m, 4 H, aromatic protons) ppm. $\text{C}_{32}\text{H}_{40}\text{Cl}_2\text{N}_2\text{Pd}_2$ (736.42): calcd. C 52.19, H 5.47, N 3.80; found C 52.52, H 5.34, N 3.59.

Palladium Complex (±)-8: A CH_2Cl_2 solution of (±)-2 (0.18 g, 0.25 mmol) and PPh_3 (0.13 g, 0.50 mmol) was stirred for 30 min at room temperature and concentrated to ca. 5 mL. The residue liquid was chromatographed on silica gel (CH_2Cl_2) to give a light-yellow powder, which was recrystallized from CH_2Cl_2 /hexane to afford light-yellow crystals of (±)-8 (0.28 g, 88.8%). M.p. 192–194 °C (decomp.). ^{31}P NMR (121 MHz, CDCl_3): δ = 30.1 (s) ppm. ^1H NMR (400 MHz, CDCl_3): δ = 2.00 (s, 3 H, aryl- CH_3), 2.18 (d, $^3J_{\text{H,H}}$ = 6.4 Hz, 3 H, CHCH_3), 2.46 (s, 3 H, aryl- CH_3), 2.51 [s, 3 H, $\text{NCH}_3(\text{ax})$], 2.92 [d, $^4J_{\text{P,H}}$ = 3.0 Hz, 3 H, $\text{NCH}_3(\text{eq})$], 3.76 (quint, $^4J_{\text{P,H}}$ = $^3J_{\text{H,H}}$ = 6.4 Hz, 1 H, CHCH_3), 6.86 (s, 1 H, aromatic proton), 7.19–7.60 (m, 18 H, aromatic protons) ppm. ^{13}C NMR (125 MHz, CDCl_3): δ = 21.4, 22.2, 26.8 (d, $J_{\text{C,P}}$ = 9.2 Hz), 49.0, 50.6 (d, $J_{\text{C,P}}$ = 2.7 Hz), 74.1 (d, $J_{\text{C,P}}$ = 3.0 Hz), 122.6, 124.9, 125.2, 126.8 (d, $J_{\text{C,P}}$ = 14.4 Hz), 126.8 (d, $J_{\text{C,P}}$ = 10.3 Hz), 130.1, 132.2, 133.2, 134.7 (br. s), 134.8 (br. s), 139.9 (d, $J_{\text{C,P}}$ = 2.3 Hz), 146.3, 156.6 ppm. HRMS (ESI): calcd. for $\text{C}_{34}\text{H}_{35}\text{NPPd}[\text{M} - \text{Cl}]^+$ 594.1542; found 594.1559. $\text{C}_{34}\text{H}_{35}\text{ClNPPd}$ (630.50): calcd. C 64.77, H 5.60, N 2.22; found C 64.40, H 5.42, N 2.22.

(*R*_C,*S*_C,*S*_N)-9 and (*S*_C,*S*_C,*S*_N)-9: To racemic dimer (±)-2 (1.47 g, 2.00 mmol) was added a solution of (*S*)-sodium proline (0.55 g, 4.00 mmol) in MeOH (30 mL). The mixture was stirred at room

temperature for 1 h, and the solvent was removed under reduced pressure. The solution of the residue in CH_2Cl_2 was washed with H_2O and dried with MgSO_4 . After removing the solvent, the 1:1 diastereomeric mixture was slowly eluted through a silica gel column (CH_2Cl_2 /acetone, 2:1), and the first eluted diastereomer (*R*_C,*S*_C,*S*_N)-9 was crystallized slowly from CH_2Cl_2 and hexane as light-yellowish crystals (0.81 g, 90.6%, based on half of the dimer used), >99% *de* (according to ^1H NMR spectroscopy). M.p. 190–192 °C (decomp.). $[\alpha]_{436}^{\text{D}} = +38$; $[\alpha]_{365}^{\text{D}} = +160$ (*c* = 0.5, CH_3OH). ^1H NMR (500 MHz, CDCl_3): δ = 1.64–1.65 (m, 1 H, $\text{CH}_2\text{CH}_2\text{CH}_2$), 1.68–1.73 (m, 2 H, $\text{CH}_2\text{CH}_2\text{CH}_2$, COCHCH_2), 1.98 (d, $^3J_{\text{H,H}}$ = 6.3 Hz, 3 H, CHCH_3), 2.30–2.32 (m, 1 H, COCHCH_2), 2.40 (s, 3 H, aryl- CH_3), 2.44 (s, 3 H, aryl- CH_3), 2.61 [s, 3 H, $\text{NCH}_3(\text{ax})$], 2.64 [s, 3 H, $\text{NCH}_3(\text{eq})$], 3.15–3.22 (m, 1 H, NHCH_2), 3.42–3.44 (m, 1 H, NHCH_2), 4.00–4.03 (m, 1 H, *NH*), 4.07–4.10 (m, 2 H, COCH , CHCH_3), 7.13–7.16 (m, 2 H, aromatic protons), 7.38 (s, 1 H, aromatic proton), 7.43 (d, $^3J_{\text{H,H}}$ = 8.5 Hz, 1 H, aromatic proton) ppm. ^{13}C NMR (125 MHz, CDCl_3): δ = 21.3, 22.9, 23.1, 25.3, 28.7, 29.1, 48.3, 51.1, 66.8, 72.9, 122.6, 124.5, 125.0, 126.8, 127.2, 131.9, 133.5, 139.8, 143.7, 148.4, 178.4 ppm. HRMS (ESI): calcd. for $\text{C}_{21}\text{H}_{29}\text{N}_2\text{O}_2\text{Pd}[\text{M} + \text{H}]^+$ 447.1264; found 447.1274. $\text{C}_{21}\text{H}_{28}\text{N}_2\text{O}_2\text{Pd} \cdot \text{CH}_2\text{Cl}_2$ (531.82): calcd. C 49.69, H 5.69, N 5.27; found C 49.85, H 5.32, N 5.39. The second eluted diastereomer (*S*_C,*S*_C,*S*_N)-9 was also crystallized slowly from CH_2Cl_2 and hexane as yellowish crystals (0.79 g, 88.4%, based on half of the dimer used), >99% *de* (according to ^1H NMR spectroscopy). M.p. 190–192 °C (decomp.). $[\alpha]_{\text{D}}^{\text{D}} = +194$; $[\alpha]_{578}^{\text{D}} = +206$; $[\alpha]_{546}^{\text{D}} = +234$; $[\alpha]_{436}^{\text{D}} = +446$; $[\alpha]_{365}^{\text{D}} = +916$ (*c* = 0.5, CH_3OH). ^1H NMR (500 MHz, CDCl_3): δ = 1.61–1.73 (m, 1 H, $\text{CH}_2\text{CH}_2\text{CH}_2$), 2.01–2.04 (m, 1 H, $\text{CH}_2\text{CH}_2\text{CH}_2$), 2.07 (d, $^3J_{\text{H,H}}$ = 6.4 Hz, 3 H, CHCH_3), 2.22–2.34 (m, 2 H, COCHCH_2), 2.44 (s, 3 H, aryl- CH_3), 2.58 (s, 3 H, aryl- CH_3), 2.64 [s, 3 H, $\text{NCH}_3(\text{ax})$], 2.78 [s, 3 H, $\text{NCH}_3(\text{eq})$], 3.10–3.24 (m, 2 H, NHCH_2), 4.09–4.10 (m, 1 H, COCH), 4.11 (q, $^3J_{\text{H,H}}$ = 6.5 Hz, 1 H, CHCH_3), 4.38–4.42 (m, 1 H, *NH*), 7.16 (dd, $^3J_{\text{H,H}}$ = 8.7 Hz, $^4J_{\text{H,H}}$ = 1.1 Hz, 1 H, aromatic proton), 7.19 (s, 1 H, aromatic proton), 7.45 (s, 1 H, aromatic proton), 7.46 (d, $^3J_{\text{H,H}}$ = 8.3 Hz, 1 H, aromatic proton) ppm. ^{13}C NMR (100 MHz, CDCl_3): δ = 21.3, 23.2, 24.3, 25.3, 30.2, 48.0, 53.0, 53.3, 65.2, 73.0, 123.4, 124.9, 124.9, 126.7, 127.2, 131.7, 133.3, 139.4, 145.9, 147.7, 181.1 ppm. HRMS (ESI): calcd. for $\text{C}_{21}\text{H}_{29}\text{N}_2\text{O}_2\text{Pd}[\text{M} + \text{H}]^+$ 447.1264; found 447.1274. $\text{C}_{21}\text{H}_{28}\text{N}_2\text{O}_2\text{Pd} \cdot \text{H}_2\text{O}$ (464.89): calcd. C 54.25, H 6.50, N 6.03; found C 54.47, H 7.04, N 5.88.

Palladium Complex (S)-2: Dilute HCl (20 mL, 1 M) was added to a CH_2Cl_2 solution (10 mL) of diastereomer (*S*_C,*S*_C,*S*_N)-9 (0.80 g, 1.79 mmol), and the resulting solution was vigorously stirred for 30 min at room temperature. The organic layer was separated and washed with H_2O and dried with MgSO_4 , and the solvent was evaporated to dryness to afford (S)-2 as a yellow powder. Recrystallization from CH_2Cl_2 and diethyl ether afforded yellow crystals of 2 (0.63 g, 95.6%). M.p. 172–174 °C (decomp.). $[\alpha]_{\text{D}}^{\text{D}} = +120$; $[\alpha]_{578}^{\text{D}} = +122$; $[\alpha]_{546}^{\text{D}} = +120$ (*c* = 0.5, CH_2Cl_2). ^1H NMR (400 MHz, CD_2Cl_2): δ = 2.25–2.28 (m, 6 H), 2.46 (s, 6 H), 2.61–2.73 (m, 18 H), 4.12–4.18 (m, 2 H, CHCH_3), 7.11–7.13 (m, 2 H, aromatic protons), 7.17–7.19 (m, 2 H, aromatic protons), 7.47 (m, 4 H, aromatic protons) ppm. ^{13}C NMR (100 MHz, CDCl_3): δ = 21.4, 23.3, 25.4, 25.6, 49.5, 50.3, 53.4, 53.8, 54.0, 74.6, 74.7, 122.6, 124.7, 124.9, 125.0, 126.8, 126.9, 132.1, 133.5, 141.1, 143.1, 143.2, 146.5 ppm. $\text{C}_{32}\text{H}_{40}\text{Cl}_2\text{N}_2\text{Pd}_2$ (736.42): calcd. C 52.19, H 5.47, N 3.80; found C 52.52, H 5.34, N 3.59.

Palladium Complex (R)-2: Prepared from (*R*_C,*S*_C,*S*_N)-9 in a similar manner to that of (S)-2. $[\alpha]_{\text{D}}^{\text{D}} = -118$ (*c* = 0.4, CH_2Cl_2). $[\alpha]_{578}^{\text{D}} = -113$ (*c* = 0.4, CH_2Cl_2). $[\alpha]_{546}^{\text{D}} = -118$ (*c* = 0.4, CH_2Cl_2).

Palladium Complex (S)-10: To a solution of (S)-2 (0.37 g, 0.50 mmol) in CH₂Cl₂ (20 mL) was added a solution of 3,4-dimethyl-1-phenylphosphole (dmpp; 0.20 g, 1.06 mmol) in the same solvent (10 mL). The resulting light-yellow solution was stirred at room temperature for 1 h, and the solvent was removed under reduced pressure. The solid residue was chromatographed on silica gel (CH₂Cl₂/ethyl acetate, 1:1) to give a pale-yellow powder, which was recrystallized from chloroform/hexane as yellow prisms (0.50 g, 89.7%). [α]_D = +456; [α]₅₇₈ = +484; [α]₅₄₆ = +572; [α]₄₃₆ = +1348 (*c* = 0.5, CH₂Cl₂). M.p. 188–190 °C (decomp.). ³¹P NMR (121 MHz, CDCl₃): δ = 28.4 (s) ppm. ¹H NMR (500 MHz, CDCl₃): δ = 1.94 (d, ⁴J_{P,H} = 1.6 Hz, 3 H, C=CCH₃), 1.95 (d, ³J_{H,H} = 6.8 Hz, 3 H, CHCH₃), 2.02 (s, 3 H, C=CCH₃), 2.37 (s, 3 H, aryl-CH₃), 2.47 (s, 3 H, aryl-CH₃), 2.54 [d, ⁴J_{P,H} = 2.0 Hz, 3 H, NCH_{3(ax)}], 2.87 [d, ⁴J_{P,H} = 3.4 Hz, 3 H, NCH_{3(eq)}], 3.72 (quint, ³J_{H,H} = ⁴J_{P,H} = 6.5 Hz, 1 H, CH₃CH), 6.17 (d, ²J_{P,H} = 33.2 Hz, 1 H, C=CH), 6.81 (d, ²J_{P,H} = 32.1 Hz, 1 H, C=CH), 7.18 (dd, ³J_{H,H} = 8.6 Hz, ⁴J_{H,H} = 1.6 Hz, 1 H, aromatic proton), 7.24 (s, 1 H, aromatic proton), 7.35–7.41 (m, 3 H, *p*-Ph, 2 × *m*-Ph), 7.47 (s, 1 H, aromatic proton), 7.52 (d, ³J_{H,H} = 8.6 Hz, 1 H, aromatic proton), 7.88–7.92 (m, 2 H, 2 × *o*-Ph) ppm. ¹³C NMR (100 MHz, CDCl₃): δ = 17.1 (d, *J*_{C,P} = 12.7 Hz), 17.7 (d, *J*_{C,P} = 12.2 Hz), 21.3, 22.7, 27.8 (d, *J*_{C,P} = 9.7 Hz), 48.4, 50.6 (d, *J*_{C,P} = 2.7 Hz), 73.4 (d, *J*_{C,P} = 3.3 Hz), 122.6, 124.0, 125.6 (d, *J*_{C,P} = 49.2 Hz), 125.7, 126.8 (d, *J*_{C,P} = 21.4 Hz), 127.6 (d, *J*_{C,P} = 43.9 Hz), 128.4 (d, *J*_{C,P} = 10.8 Hz), 129.3 (d, *J*_{C,P} = 52 Hz), 130.4 (d, *J*_{C,P} = 2.5 Hz), 131.9, 133.1, 133.2, 133.4, 141.0 (d, *J*_{C,P} = 6.1 Hz), 147.3 (d, *J*_{C,P} = 1.3 Hz), 148.1 (d, *J*_{C,P} = 10.1 Hz), 151.1, 153.5 (d, *J*_{C,P} = 10.3 Hz) ppm. HRMS (ESI): calcd. for C₂₈H₃₃NPPd [M – Cl]⁺ 520.1385; found 520.1398. C₂₈H₃₃ClNPPd (556.37): calcd. C 60.44, H 5.98, N 2.52; found C 60.08, H 6.40, N 2.52.

Preparation of (S_C,R_P)-11 and (S_C,S_P)-11 by the Asymmetric Diels–Alder Reaction of (S)-10 and *N,N*-Dimethylacrylamide: A solution of (S)-10 (0.50 g, 0.9 mmol) in CH₂Cl₂ (10 mL) was stirred with *N,N*-dimethylacrylamide (0.30 g, 3.03 mmol) at room temperature for 20 d. Removal of the solvent left a brownish oil. The ³¹P NMR (CDCl₃) spectrum of the crude product prior to purification indicated a 1:5.9 mixture of the diastereomeric cycloadducts at δ = 114.3 and 115.3 ppm. Products (S_C,S_P)-11 and (S_C,R_P)-11 were isolated after silica gel chromatography (ethyl acetate/CH₂Cl₂, 1:10). The first eluted complex was minor diastereomer (S_C,S_P)-11 (0.07 g, 11.9%). M.p. 181–183 °C (decomp.). [α]_D = +120; [α]₅₇₈ =

+124; [α]₅₄₆ = +142; [α]₄₃₆ = +164 (*c* = 0.5, CH₂Cl₂). ³¹P NMR (121 MHz, CDCl₃): δ = 114.3 (s). ¹H NMR (400 MHz, CDCl₃): δ = 1.24 (s, 3 H, C=CCH₃), 1.79 (s, 3 H, C=CCH₃), 1.94–2.05 (m, 2 H, CH₂), 2.15 (d, ³J_{H,H} = 6.4 Hz, 3 H, CHCH₃), 2.28 (s, 3 H, aryl-CH₃), 2.46 (s, 3 H, aryl-CH₃), 2.50 [s, 3 H, NCH_{3(ax)}], 2.74 (br. s, 1 H, CH₂CHP), 2.86 [d, ⁴J_{P,H} = 2.4 Hz, 3 H, NCH_{3(eq)}], 2.89 [s, 3 H, NCH_{3(amide)}], 3.34 [s, 3 H, NCH_{3(amide)}], 3.67 (br. s, 1 H, CHCHP), 4.24 (quint, ³J_{H,H} = ⁴J_{P,H} = 6.2 Hz, 1 H, CHCH₃), 4.58 (m, 1 H, COCH), 7.19 (d, ³J_{H,H} = 8.5 Hz, 1 H, aromatic proton), 7.24 (s, 1 H, aromatic proton), 7.39–7.41 (m, 3 H, *p*-Ph, 2 × *m*-Ph), 7.46 (s, 1 H, aromatic proton), 7.53 (d, ³J_{H,H} = 8.6 Hz, 1 H, aromatic proton), 7.98–8.02 (m, 2 H, 2 × *o*-Ph) ppm. ¹³C NMR (100 MHz, CDCl₃): δ = 14.3 (d, *J*_{C,P} = 3.4 Hz), 14.9 (d, *J*_{C,P} = 4.0 Hz), 21.4, 22.4, 28.3, 35.9, 37.6, 41.0 (d, *J*_{C,P} = 30.5 Hz), 48.2 (d, *J*_{C,P} = 38.3 Hz), 48.6, 51.2 (d, *J*_{C,P} = 3.3 Hz), 54.8 (d, *J*_{C,P} = 60.1 Hz), 73.0 (d, *J*_{C,P} = 3.9 Hz), 122.8, 124.6, 125.7, 127.0 (d, *J*_{C,P} = 35.4 Hz), 127.9 (d, *J*_{C,P} = 12.5 Hz), 129.9 (d, *J*_{C,P} = 2.8 Hz), 130.2, 130.6, 131.0, 132.1, 133.7 (d, *J*_{C,P} = 3.3 Hz), 133.9, 134.5, 140.2 (d, *J*_{C,P} = 8.1 Hz), 147.2 (d, *J*_{C,P} = 1.9 Hz), 152.5, 171.8 (d, *J*_{C,P} = 21.1 Hz) ppm. HRMS (ESI): calcd. for C₃₃H₄₂N₂OPPd [M – Cl]⁺ 619.2070; found 619.2056. C₃₃H₄₂ClN₂OPPd·C₄H₁₀O (729.67): calcd. C 60.90, H 7.18, N 3.84; found C 60.78, H 7.52, N 4.08. The second eluted complex was major diastereomer (S_C,R_P)-11 (0.41 g, 69.5%). M.p. 180–182 °C (decomp.). [α]_D = +60; [α]₅₇₈ = +64; [α]₅₄₆ = +66 (*c* = 0.5, CH₂Cl₂). ³¹P NMR (121 MHz, CDCl₃): δ = 115.3 (s) ppm. ¹H NMR (500 MHz, CDCl₃): δ = 1.38 (s, 3 H, C=CCH₃), 1.56 (s, 3 H, C=CCH₃), 1.63 [s, 3 H, NCH_{3(amide)}], 2.10 (d, ³J_{H,H} = 6.5 Hz, 3 H, CHCH₃), 2.11–2.18 (m, 1 H, CH₂), 2.21 (m, 1 H, PCH), 2.34 (s, 3 H, aryl-CH₃), 2.40 (s, 3 H, aryl-CH₃), 2.43 [s, 3 H, NCH_{3(ax)}], 2.57 [s, 3 H, NCH_{3(amide)}], 2.80 [s, 3 H, NCH_{3(eq)}], 2.90–2.93 (m, 1 H, CH₂), 3.42 (br. s, 1 H, PCH), 3.53 (br. s, 1 H, COCH), 4.19 (quint, ³J_{H,H} = ⁴J_{P,H} = 6.1 Hz, 1 H, CHCH₃), 7.14 (d, ³J_{H,H} = 8.5 Hz, 1 H, aromatic proton), 7.21 (s, 1 H, aromatic proton), 7.31–7.35 (m, 4 H, aromatic protons), 7.47 (d, ³J_{H,H} = 8.6 Hz, 1 H, aromatic proton), 7.94–7.98 (m, 2 H, 2 × *o*-Ph) ppm. ¹³C NMR (100 MHz, CDCl₃): δ = 13.9 (d, *J*_{C,P} = 3.0 Hz), 15.7 (d, *J*_{C,P} = 1.9 Hz), 21.5, 22.3, 28.1 (d, *J*_{C,P} = 9.4 Hz), 29.3 (d, *J*_{C,P} = 14.4 Hz), 35.5 (d, *J*_{C,P} = 22.7 Hz), 39.9 (d, *J*_{C,P} = 27.4 Hz), 48.5, 50.9 (d, *J*_{C,P} = 30.1 Hz), 51.2 (d, *J*_{C,P} = 1.9 Hz), 52.1 (d, *J*_{C,P} = 33.8 Hz), 73.2 (d, *J*_{C,P} = 2.6 Hz), 122.6, 124.8, 125.8, 126.6, 127.5, 128.0 (d, *J*_{C,P} = 9.0 Hz), 129.3, 129.9 (d, *J*_{C,P} = 1.4 Hz), 130.7 (d, *J*_{C,P} = 30.9 Hz), 132.1, 133.6 (d, *J*_{C,P} = 8.8 Hz), 133.8, 134.5, 140.3 (d, *J*_{C,P} = 6.1 Hz), 147.6, 152.9, 171.7 (d, *J*_{C,P} =

Table 6. Crystallographic data for complexes (±)-8, (R_C,S_C,S_N)-9, (S_C,S_C,S_N)-9, (S)-2, and (S)-10.

	(±)-8	(R _C ,S _C ,S _N)-9	(S _C ,S _C ,S _N)-9	(S)-2	(S)-10
Formula	C ₃₄ H ₃₅ ClNPPd	C ₂₁ H ₂₈ N ₂ O ₂ Pd	C ₂₁ H ₂₉ N ₂ O _{2.50} Pd	C ₃₂ H ₄₀ Cl ₂ N ₂ Pd ₂	C ₂₉ H ₃₄ Cl ₄ NPPd
Formula weight	630.45	446.8	455.86	736.36	675.74
Space group	P2 ₁ /n	P2 ₁	P2 ₁	P2 ₁ 2 ₁ 2	P2 ₁
Crystal system	monoclinic	monoclinic	monoclinic	orthorhombic	monoclinic
<i>a</i> [Å]	15.0712(6)	9.7485(2)	11.7939(4)	12.2080(4)	10.9885(3)
<i>b</i> [Å]	12.1873(4)	11.5735(2)	10.4704(4)	18.1509(6)	7.5360(2)
<i>c</i> [Å]	16.3450(6)	9.9185(2)	16.8695(6)	7.0581(2)	18.3493(4)
<i>V</i> [Å ³]	2983.28(19)	1012.51(3)	2044.13(13)	1563.98(9)	1519.38(7)
<i>Z</i>	4	2	4	2	2
<i>T</i> [K]	173(2)	173(2)	173(2)	296(2)	173(2)
ρ _{calcd.} [g cm ^{−3}]	1.404	1.466	1.481	1.564	1.477
λ [Å]	0.71073(Mo)	0.71073(Mo)	0.71703(Mo)	0.71073(Mo)	0.71073(Mo)
μ [mm ^{−1}]	0.788	0.933	0.928	1.344	1.034
Flack parameters		0.09(6)	−0.036(17)	−0.03(2)	−0.013(12)
<i>R</i> ₁ (obsd. data) [a]	0.0269	0.0492	0.0343	0.0274	0.0268
<i>wR</i> ₂ (obsd. data) [b]	0.0659	0.1326	0.0797	0.0579	0.0580

[a] *R*₁ = Σ||*F*_o| − |*F*_c||/Σ|*F*_o|. [b] *wR*₂ = √{Σ[*w*(*F*_o² − *F*_c²)²]}/Σ(*F*_o²) + (*aP*)² + *bP*.

= 16.5 Hz) ppm. HRMS (ESI): calcd. for $C_{33}H_{42}N_2OPPd$ [$M - Cl$] + 619.2070; found 619.2056. $C_{33}H_{42}ClN_2OPPd \cdot C_4H_{10}O$ (729.67): calcd. C 60.90, H 7.18, N 3.84; found C 60.78, H 7.52, N 4.08.

Crystal Structure Determination: Crystal data and a summary of the crystallographic analyses are given in Table 6. Diffraction data were collected with a Bruker X8 CCD diffractometer with Mo- K_α radiation (graphite monochromator). SADABS absorption corrections were applied. All non-hydrogen atoms were refined anisotropically, whereas hydrogen atoms were introduced at calculated positions and refined riding on their carrier atoms. The absolute configurations of the chiral complexes were determined unambiguously by using the Flack parameter.^[12] CCDC-702081 [for (\pm)-**8**], -702083 [for (S_C, S_C, S_N)-**9**], -702085 [for (R_C, S_C, S_N)-**9**], -702082 [for (S)-**2**], and -702084 [for (S)-**10**] contain the supplementary crystallographic data for this paper. These data can be obtained free of charge from The Cambridge Crystallographic Data Centre via www.ccdc.cam.ac.uk/data_request/cif.

Acknowledgments

We are grateful to Nanyang Technological University for supporting this research and for a research scholarships to Y. D.

- [1] For examples, see: a) J. Vicente, I. Saura-Llamas, M. G. Palin, P. G. Jones, *J. Chem. Soc., Dalton Trans.* **1995**, 2535–2540; b) J. Albert, J. Granell, A. Luque, J. Minguez, R. Moragas, M. Font-Bardia, X. Solans, *J. Organomet. Chem.* **1996**, 522, 87–95; c) Y. Fuchita, K. Yoshinaga, Y. Ikeda, J. Kinoshita-Kawashima, *J. Chem. Soc., Dalton Trans.* **1997**, 2495–2500; d) V. V. Dunina, L. G. Kuz'mina, M. Y. Kazakova, O. N. Gorunova, Y. K. Grishin, E. I. Kazakova, *Eur. J. Inorg. Chem.* **1999**, 1029–1039; e) B. Calmuschi, U. Englert, *Acta Crystallogr., Sect. C* **2002**, 58, m545–m548; f) B. Calmuschi, A. Erik, U. Englert, *Acta Crystallogr., Sect. C* **2004**, 60, m320–m323; g) J. Vicente, I. Saura-Llamas, D. Bautista, *Organometallics* **2005**, 24, 6001–6004; h) J. Vicente, I. Saura-Llamas, J.-A. Garcia-Lopez, B. Calmuschi-Cula, D. Bautista, *Organometallics* **2007**, 26, 2768–2776.
- [2] For examples, see: a) S. Chatterjee, M. D. George, G. Salem, A. C. Willis, *J. Chem. Soc., Dalton Trans.* **2001**, 1890–1896; b) N. K. Roberts, S. B. Wild, *J. Am. Chem. Soc.* **1979**, 101, 6254–6260; c) N. K. Roberts, S. B. Wild, *J. Chem. Soc., Dalton Trans.* **1979**, 2015–2021; d) G. He, K. F. Mok, P.-H. Leung, *Organometallics* **1999**, 18, 4027–4031; e) V. V. Dunina, E. B. Golovan, *Tetrahedron: Asymmetry* **1995**, 6, 2747–2754; f) M. Pabel, A. C. Willis, S. B. Wild, *Inorg. Chem.* **1996**, 35, 1244–1249; g) A. Bader, M. Pabel, A. C. Willis, S. B. Wild, *Inorg. Chem.* **1996**, 35, 3874–3877; h) M. Pabel, A. C. Willis, S. B. Wild, *Tetrahedron: Asymmetry* **1995**, 6, 2369–2374; i) S. Y. M. Chooi, S. Y. Siah, P.-H. Leung, K. F. Mok, *Inorg. Chem.* **1993**, 32, 4812–4818; j) S. Otsuka, A. Nakamura, T. Kano, K. Tani, *J. Am. Chem. Soc.* **1971**, 93, 4301–4303; k) K. Tani, L. D. Brown, J. Ahmed, J. A. Ibers, M. Yokota, A. Nakamura, S. Otsuka, M. Yokota, *J. Am. Chem. Soc.* **1977**, 99, 7876–7886; l) D. G. Allen, G. M. McLaughlin, G. B. Robertson, W. L. Steffen, G. Salem, S. B. Wild, *Inorg. Chem.* **1982**, 21, 1007–1014; m) J. Albert, J. M. Cadena, J. Granell, *Tetrahedron: Asymmetry* **1997**, 8, 991–994; n) J. Albert, J. M. Cadena, J. Granell, G. Muller, J. I. Ordinas, D. Panyella, C. Puerta, C. Sanudo, P. Valerga, *Organometallics* **1999**, 18, 3511–3518; o) J. Albert, J. M. Cadena, J. Granell, G. Muller, D. Panyella, C. Sañudo, *Eur. J. Inorg. Chem.* **2000**, 1283–1286; p) J. Albert, J. M. Cadena, S. Delgado, J. Granell, *J. Organomet. Chem.* **2000**, 603, 235–239; q) J. Albert, R. Bosque, J. M. Cadena, J. R. Granell, G. Muller, J. I. Ordinas, *Tetrahedron: Asymmetry* **2000**, 11, 3335–3343; r) E. Duran, E. Gordo, J. Granell, M. Font-Bardia, X. Solans, D. Velasco, F. Lopez-Calaborra, *Tetrahedron: Asymmetry* **2001**, 12, 1987–1997; s) J. Albert, R. Bosque, J. M. Cadena, S. Delgado, J. Granell, G. Muller, J. I. Ordinas, M. F. Bardia, X. Solans, *Chem. Eur. J.* **2002**, 8, 2279–2287; t) V. V. Dunina, E. D. Razmyslova, O. N. Gorunova, M. V. Livantsov, Y. K. Grishin, *Tetrahedron: Asymmetry* **2003**, 14, 2331–2333; u) J.-M. Camus, P. Roy-Garcia, J. Andrieu, P. Richard, R. Poli, *J. Organomet. Chem.* **2005**, 690, 1659–1668; v) J. Albert, J. Granell, G. Muller, *J. Organomet. Chem.* **2006**, 691, 2101–2106.
- [3] For examples, see: a) S. B. Wild, *Coord. Chem. Rev.* **1997**, 166, 291–311; b) V. V. Dunina, O. N. Gorunova, M. V. Livantsov, Y. K. Grishin, *Tetrahedron: Asymmetry* **2000**, 11, 2907–2916; c) F. Levrat, H. Stoeckli-Evans, N. Engel, *Tetrahedron: Asymmetry* **2002**, 13, 2335–2344; d) J. Albert, J. Granell, G. Muller, D. Sainz, M. Font-Bardia, X. Solans, *Tetrahedron: Asymmetry* **1995**, 6, 325–328; e) V. V. Dunina, E. B. Golovan, N. S. Gulyukina, A. V. Buyevich, *Tetrahedron: Asymmetry* **1995**, 6, 2731–2746; f) C. Lopez, R. Bosque, D. Sainz, X. Solans, M. Font-Bardia, *Organometallics* **1997**, 16, 3261–3266; g) J. R. Moncarz, N. F. Laritcheva, D. S. Glueck, *J. Am. Chem. Soc.* **2002**, 124, 13356–13357; h) S. Y. M. Chooi, P.-H. Leung, C. C. Lim, K. F. Mok, G. H. Quek, K. Y. Sim, M.-K. Tan, *Tetrahedron: Asymmetry* **1992**, 3, 529–532; i) C.-C. Lim, P.-H. Leung, K. Y. Sim, *Tetrahedron: Asymmetry* **1994**, 5, 1883–1886; j) B.-H. Aw, S. Selvaratnam, P.-H. Leung, N. H. Ress, W. McFarlane, *Tetrahedron: Asymmetry* **1996**, 7, 1753–1762.
- [4] G. Uccello-Barretta, R. Bernardini, R. Lazzaroni, P. Salvadori, *Org. Lett.* **2000**, 2, 1795.
- [5] For examples, see: a) J. F. van Baar, J. M. Klerks, P. Overbosch, D. J. Stufkens, K. Vrieze, *J. Organomet. Chem.* **1976**, 112, 95–103; b) Y. Yamamoto, H. Yamazaki, *Inorg. Chim. Acta* **1980**, 41, 229–232; c) J. Vicente, I. Saura-Llamas, M. C. R. de Arelano, P. G. Jones, *Organometallics* **1999**, 18, 2683–2693; d) J. Vicente, I. Saura-Llamas, C. Alcaraz, P. G. Jones, D. Bautista, *Organometallics* **2002**, 21, 3587–3595; e) W. E. Lindsell, D. D. Palmer, P. N. Preston, G. M. Rosair, R. V. H. Jones, A. J. Whitton, *Organometallics* **2005**, 24, 1119–1133; f) P.-H. Leung, *Acc. Chem. Res.* **2004**, 37, 169–177; g) W.-C. Yeo, S. Y. Tee, H.-B. Tan, G.-K. Tan, L. L. Koh, P.-H. Leung, *Inorg. Chem.* **2004**, 43, 8102–8109; h) S. A. Pullarkat, D. Yi, Y. Li, G.-K. Tan, P.-H. Leung, *Inorg. Chem.* **2006**, 45, 7455–7463; i) M. L. Bungabong, K. W. Tan, Y. Li, S. V. Selvaratnam, K. G. Dongol, P.-H. Leung, *Inorg. Chem.* **2007**, 46, 4733–4736; j) W.-C. Yeo, J. J. Vittal, L. L. Koh, P.-H. Leung, *Organometallics* **2006**, 25, 1259–1269; k) Y. Zhang, L. Tang, Y. Ding, J.-H. Chua, Y. Li, P.-H. Leung, *Tetrahedron: Lett.* **2008**, 49, 1762–1767.
- [6] a) B. H. Aw, P.-H. Leung, *Tetrahedron: Asymmetry* **1994**, 5, 1167–1170; b) B. H. Aw, P.-H. Leung, A. J. P. White, D. J. Williams, *Organometallics* **1996**, 15, 3640–3643; c) S. Selvaratnam, K. F. Mok, P.-H. Leung, A. J. P. White, D. J. Williams, *Inorg. Chem.* **1996**, 35, 4798–4800; d) A. M. Liu, K. F. Mok, P.-H. Leung, *Chem. Commun.* **1997**, 2397–2398; e) P.-H. Leung, S. K. Loh, J. J. Vittal, A. J. P. White, D. J. Williams, *Chem. Commun.* **1997**, 1987–1988; f) P.-H. Leung, S. Y. Siah, A. J. P. White, D. J. Williams, *J. Chem. Soc., Dalton Trans.* **1998**, 893–900; g) G. He, S. K. Loh, J. J. Vittal, K. F. Mok, P.-H. Leung, *Organometallics* **1998**, 17, 3931–3936; h) Y. C. Song, J. J. Vittal, S. H. Chan, P.-H. Leung, *Organometallics* **1999**, 18, 650–655; i) P.-H. Leung, A. M. Liu, K. F. Mok, *Tetrahedron: Asymmetry* **1999**, 10, 1309–1314; j) P.-H. Leung, G. He, H. Lang, A. Liu, S. K. Loh, S. Selvaratnam, K. F. Mok, A. J. P. White, D. J. Williams, *Tetrahedron* **2000**, 56, 7–15; k) Y. Li, S. Selvaratnam, J. J. Vittal, P.-H. Leung, *Inorg. Chem.* **2003**, 42, 3229–3236; l) Y. Li, K.-H. Ng, S. Selvaratnam, G.-K. Tan, J. J. Vittal, P.-H. Leung, *Organometallics* **2003**, 22, 834–842; m) Y. Ding, Y. Li, Y. Zhang, S. A. Pullarkat, P.-H. Leung, *Eur. J. Inorg. Chem.* **2008**, 11, 1880–1891; n) M. Ma, S. A. Pullarkat, Y. Li, P.-H. Leung, *Inorg. Chem.* **2007**, 46, 9488–9494; o) W.-C. Yeo, S. Chen, G.-K. Tan, P.-H. Leung, *J. Organomet. Chem.* **2007**, 692, 2539–2547; p) S.-K. Loh, G.-K. Tan, L. L. Koh, S. Selvaratnam, P.-

- H. Leung, *J. Organomet. Chem.* **2005**, 690, 4933–4938; q) Y. Qin, H. Lang, J. J. Vittal, G.-K. Tan, S. Selvaratnam, A. J. P. White, D. J. Williams, P.-H. Leung, *Organometallics* **2003**, 22, 3944–3950.
- [7] B. H. Aw, S. Selvaratnam, P.-H. Leung, N. H. Rees, W. McFarlane, *Tetrahedron: Asymmetry* **1996**, 7, 1753–1762.
- [8] D. Carol, K. Isabelle, G. Marc, *Organic. Synth.* **2002**, 78, 42–50.
- [9] P. H. Gore, A. S. Siddiquei, *J. Chem. Soc. Perkin Trans. 1* **1972**, 1442–1445.
- [10] a) R. Urban, R. Kramer, K. Polborn, B. Wagner, W. Beck, *J. Organomet. Chem.* **1996**, 517, 191–200; b) V. V. Dunina, E. D. Razmyslova, L. G. Kuz'mina, A. V. Churakov, M. Y. Rubina, Y. K. Grishin, *Tetrahedron: Asymmetry* **1999**, 10, 3147–3155.
- [11] R. S. Cahn, C. K. Ingold, V. Prelog, *Angew. Chem. Int. Ed. Engl.* **1966**, 5, 385–415.
- [12] H. D. Flack, *Acta Crystallogr., Sect. A* **1983**, 39, 876–881.

Received: September 16, 2008

Published Online: December 2, 2008

Binuclear Copper(II) Chelates with Heptadentate Ligands: Synthesis, Structure, Magnetic Properties, DFT Studies, and Catecholase and Hydrolytic DNA Cleavage Activity

Atanu Banerjee,^[a] Reena Singh,^[a] Enrique Colacio,^[b] and Kajal Krishna Rajak^{*[a]}

Keywords: Copper / Magnetic properties / Density functional calculations / DNA cleavage

Two binucleating heptadentate ligands 2,6-bis[[(2-hydroxybenzyl)(*N,N*-(dimethylamino)ethyl)amino)methyl]-4-methylphenol (H_3L^1) and 2,6-bis[[(2-hydroxybenzyl)(*N*-(2-pyridylmethyl)amino)methyl]-4-methylphenol (H_3L^2) were used to synthesize the two new copper(II) complexes $[Cu_2(L^1)(N_3)] \cdot 2H_2O$ (**1**·2 H_2O) and $[Cu_2(HL^2)(O_2CPh)(H_2O)] \cdot PhCO_2 \cdot H_2O$ (**2**· H_2O). X-ray diffraction studies disclose that **1** is made up from bridging phenoxido and azido group in an equatorial fashion, whereas **2** is bridged axially–equatorially through a central cresolato and *syn-syn* benzoate moiety. The geometry around the copper(II) centers is distorted square pyramid in both cases. Variable-temperature magnetic susceptibility data reveals that **1** is moderately antiferromagnetically coupled ($J = -119 \text{ cm}^{-1}$) and **2** is very weakly

antiferromagnetic ($J = -1.0 \text{ cm}^{-1}$). The structural features, as well as the presence of orbital countercomplementary effects, are associated with the magnetic behavior. Theoretical calculations with the use of broken symmetry density functional theory also establish the experimental values of the exchange coupling constants (J). In our case, only **2** exhibits catalytic activity in the oxidation of 3,5-di-*tert*-butylcatechol (3,5-DTBC) at pH 9.5 and hydrolytic cleavage of plasmid DNA in the absence of any added cofactor, whereas complex **1** cannot display catecholase activity or DNA interaction as a result of strong Cu^{II} –azido binding.

(© Wiley-VCH Verlag GmbH & Co. KGaA, 69451 Weinheim, Germany, 2009)

Introduction

The coordination chemistry of copper with binucleating ligands with a central phenol moiety is a notable frontier of inorganic research.^[1,2] This is because copper(II) ions in their close proximity play an important role in various enzymatic reactions,^[3] such as catechol oxidase.^[4] The binuclear metal complexes, either coordinatively unsaturated or containing easily replaceable binding sites, are also successful devices for the receptor of different small molecules as well as biomolecules. Among the biomolecules, the interaction of DNA to such centers becomes a fascinating area of research in terms of their DNA cleavage activity. The cleavage of DNA molecules by synthetic metal complexes takes place mainly by two processes: oxidative and hydrolytic. However, hydrolytic DNA strand scission is more important than the oxidative process due to various reasons.^[5] The metal complexes that promote the hydrolytic cleavage of the DNA molecule has widespread application in the area of molecular biology, drug development,^[6] and in the elucidation of the precise roles of the metal centers in enzy-

matic reactions. Besides the chemistry of biologically relevant polynuclear complexes of copper, the study of variable-temperature magnetic moments is also important as a means to examine the type of magnetic interactions involved in such species. Theoretical interpretation of magnetic behavior by DFT methods^[7] is an emerging field of research as a method to learn the pathways of magnetic exchange interactions as well as the electronic structure of the biologically relevant coordination compounds. The above state of development has generated a lot of interest in the search of new binuclear copper(II) complexes containing N_4O_3 coordinating heptadentate ligands.

In this paper we wish to report the synthesis, characterization, magnetic properties, and DFT calculation of two binuclear copper(II) complexes. The oxidation of catechol to quinone and the hydrolytic cleavage of supercoiled pUC19 DNA by using one of the synthesized complex are also scrutinized.

Results and Discussion

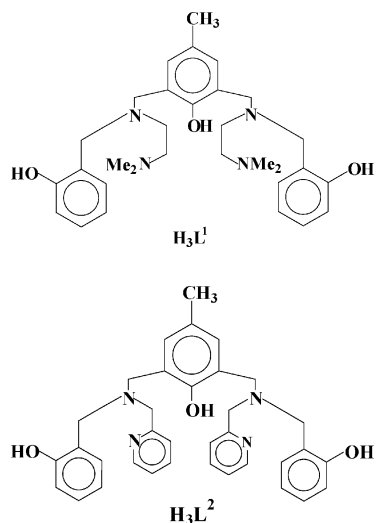
Synthesis

The two symmetrical N_4O_3 -coordinating heptadentate ligands H_3L^1 and H_3L^2 having a central phenol moiety are used in this work. The efficacy of the H_3L^1 and H_3L^2 li-

[a] Inorganic Chemistry Section, Department of Chemistry, Jadavpur University, Kolkata 700032, India
E-mail: kajalrajak@hotmail.com
kkrajak@chemistry.jdvu.ac.in

[b] Departamento de Química Inorgánica, Facultad de Ciencias, Universidad de Granada, 18071 Granada, Spain

gands in the formation of binuclear complexes and their capability in stabilizing dinuclear frameworks during reaction cycles was reported earlier.^[1a,8] The reaction of $\text{CuCl}_2 \cdot 2\text{H}_2\text{O}$ with sodium azide and H_3L^1 in methanol affords brown crystals of $[\text{Cu}_2(\text{L}^1)(\text{N}_3)]$ (**1**) in good yields. When the same reaction is carried out in the presence of pyridinium benzoate and H_3L^2 , green crystals of $[\text{Cu}_2(\text{HL}^2)(\text{O}_2\text{CPh})(\text{H}_2\text{O})](\text{PhCO}_2)$ (**2**) are obtained.



Spectral and Electrochemical Behavior

IR and UV/Vis spectra of the complexes were recorded as KBr disks and in methanol solution, respectively. The relevant experimental data are given in the Experimental Section. The $\text{Cu}^{\text{II}}-\mu\text{-O}_{\text{phenoxido}}$ and $\text{C}-\text{O}_{\text{phenoxido}}$ vibrations for both complexes are observed at ca. 758 and 1295 cm^{-1} , respectively. The *syn-syn* carboxylate stretches occur at 1601 and 1458 cm^{-1} for **2**, whereas the $\mu_{1,1}-\text{N}_3$ vibration appears at 2077 cm^{-1} for **1**.

The complexes exhibit a d-d absorption band near 660 nm, which is characteristic of a square pyramidal geometry around the copper(II) centers. The allowed intense peak near 390 nm is believed to be due to a ligand-(phenoxido, benzoate, azido)-to-metal Cu^{II} charge-transfer transition, and the peaks near 250 and 280 nm are assigned to an intraligand $\pi-\pi^*$ transition.

Both complexes are electroactive at the platinum electrode vs. SCE in acetonitrile solution. Cyclic voltammetry reduction potential data are given in the Experimental Section. Both complexes display two responses near 0.85 and -0.70 V. The anodic peak potential at ca. 0.85 V is assigned to $\text{Cu}^{\text{II}} \rightarrow \text{Cu}^{\text{III}}$ oxidation,^[9] whereas the cathodic peak potential at ca. -0.70 V is believed to be $\text{Cu}^{\text{II}} \rightarrow \text{Cu}^{\text{I}}$ reduction.

The X-band EPR spectra of the complexes were recorded at 77 K for polycrystalline samples in frozen solution (DMF/toluene). The spectroscopic data are included in the Experimental Section. Complex **1** is EPR silent, in agreement with the antiferromagnetic coupling between the two copper(II) centers. In contrast, complex **2** is EPR active,

and the result is quite similar to other Cu^{II} complexes that are weakly coupled or uncoupled having a tetragonally elongated square pyramid geometry.^[11]

Crystal Structure

Rectangular-shaped greenish brown and green crystals of complexes **1** and **2**, respectively, were obtained by slow evaporation of their methanolic solutions. The ORTEP projection of **1** and the cationic part of **2** are shown in Figures 1 and 2, and selected bond lengths and angles are presented in Tables 1 and 2, respectively.

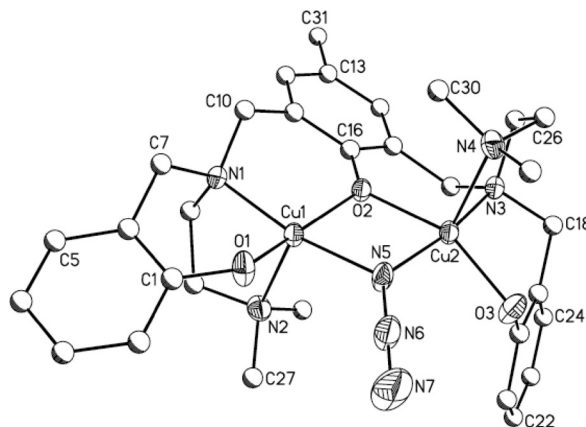


Figure 1. ORTEP view of complex **1**. Hydrogen atoms are omitted for clarity and all coordinating atoms are represented by their 25% thermal probability ellipsoids.

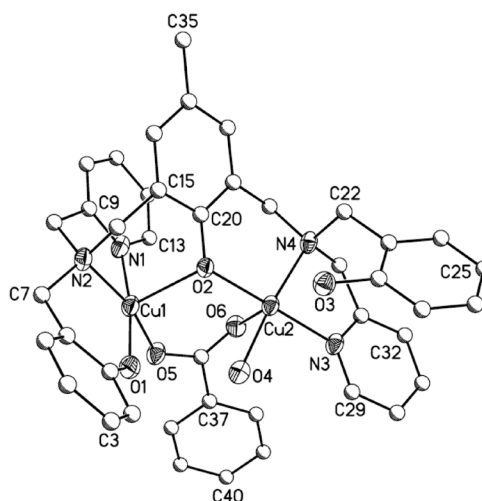


Figure 2. ORTEP view of the cationic part of **2**. Hydrogen atoms are omitted for clarity and all coordinating atoms are represented by their 25% thermal probability ellipsoids.

Complex **1** crystallizes as a water solvate in the $P2_1/n$ space group with four formula units present per unit cell. The binuclear core comprises two copper(II) ions bridged equatorially by the endogenous cresolato group and exogenous azide ion. The $\text{Cu} \cdots \text{Cu}$ separation in the complex is 3.100(7) Å. Both copper centers are surrounded by penta-coordinated identical N_3O_2 donor sets. The CuN_3O_2 poly-

Table 1. Selected bond lengths and angles for complex **1**.

Distances / Å			
Cu1–O1	1.913(3)	Cu2–O3	1.939(3)
Cu1–O2	1.973(3)	Cu2–N3	2.020(3)
Cu1–N1	2.034(3)	Cu2–N4	2.227(4)
Cu1–N2	2.317(4)	Cu2–N5	1.977(4)
Cu1–N5	1.985(3)	Cu1...Cu2	3.100(5)
Cu2–O2	2.014(3)		
Angles / °			
O1–Cu1–O2	159.90(12)	O2–Cu2–N3	91.88(12)
O1–Cu1–N1	95.78(13)	O2–Cu2–N4	98.06(12)
O1–Cu1–N2	102.36(14)	O2–Cu2–N5	77.08(12)
O1–Cu1–N5	90.21(14)	O3–Cu2–N3	94.47(13)
O2–Cu1–N1	93.81(12)	O3–Cu2–N4	108.43(15)
O2–Cu1–N2	96.24(13)	O3–Cu2–N5	93.52(15)
O2–Cu1–N5	77.86(13)	N3–Cu2–N4	84.82(14)
N1–Cu1–N2	83.46(14)	N3–Cu2–N5	168.07(14)
N1–Cu1–N5	169.27(15)	N4–Cu2–N5	101.01(16)
N2–Cu1–N5	103.99(16)	Cu1–O2–Cu2	102.06(12)
O2–Cu2–O3	153.21(14)	Cu1–N5–Cu2	102.94(16)

Table 2. Selected bond lengths and angles for complex **2**.

Distances / Å			
Cu1–O1	1.921(4)	Cu2...O3	2.562(3)
Cu1–O2	2.249(3)	Cu2–O4	1.965(4)
Cu1–O5	1.968(3)	Cu2–O6	2.396(3)
Cu1–N1	2.004(4)	Cu2–N3	2.013(4)
Cu1–N2	2.056(4)	Cu2–N4	2.043(4)
Cu2–O2	1.924(3)	Cu1...Cu2	3.562(4)
Angles / °			
O1–Cu1–O2	96.41(14)	O2–Cu2–O4	90.40(16)
O1–Cu1–O5	86.24(15)	O2–Cu2–N3	173.66(16)
O1–Cu1–N1	172.03(16)	O2–Cu2–N4	95.25(13)
O1–Cu1–N2	93.09(15)	O4–Cu2–O6	90.16(17)
O2–Cu1–O5	104.02(12)	O4–Cu2–N3	91.55(18)
O2–Cu1–N1	90.51(14)	O4–Cu2–N4	174.05(18)
O2–Cu1–N2	90.14(14)	O6–Cu2–N3	85.52(14)
O5–Cu1–N1	95.94(16)	O6–Cu2–N4	91.85(13)
O5–Cu1–N2	165.82(15)	N3–Cu2–N4	83.02(15)
N1–Cu1–N2	82.91(16)	Cu1–O2–Cu2	116.95(14)

hedron is best described as distorted square pyramid^[10] ($\tau_{\text{Cu1}} = 0.14$ and $\tau_{\text{Cu2}} = 0.24$), where the tripodal and azido nitrogen atoms and bridging and terminal phenoxido group occupy the position *trans* to each other in the basal plane, whereas the sidearm nitrogen atoms are in the apical position. The Cu–N (basal), Cu–O (basal), and Cu–N (apical) bond lengths and angles in the coordination sphere are usual.

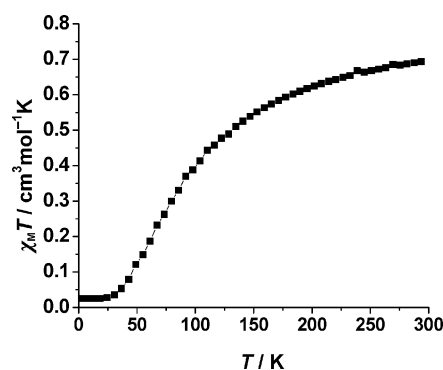
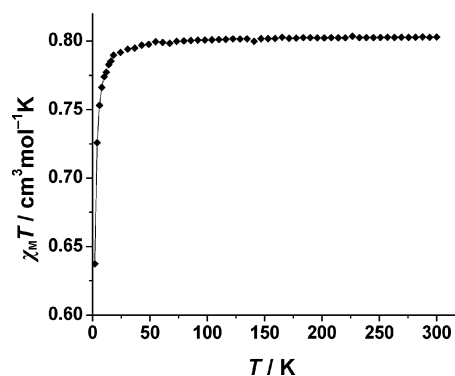
Complex **2** crystallizes in the $P2_12_12_1$ space group with $Z = 4$. In this case, two copper centers are linked by bridging phenoxido and *syn-syn* benzoate groups in an axial-equatorial fashion.

The geometry of each copper(II) center appears to be distorted square pyramid ($\tau_{\text{Cu1}} = 0.13$ and $\tau_{\text{Cu2}} = 0.01$), in which the tripodal N2 nitrogen, the pyridine ring N1 nitrogen, the terminal O1 phenoxido, and the benzoate group O5 bridging oxygen atoms form the basal plane of the Cu1 ion; the bridging cresolato O2 oxygen atom occupies the axial position. In contrast, the equatorial plane of the Cu2

center is made up from the N3 and N4 nitrogen atoms, the oxygen O2 atom of the bridging phenoxido group, and the O4 atom of the coordinated water molecule, whereas the O6 oxygen atom of the benzoate group is engaged in the apical position. In the complex, one uncoordinated water molecule is also present per formula unit. The complexes possess intramolecular hydrogen bonding between the O1 atom of the terminal phenoxido group and the O4 atom of the coordinated water molecule with a O...O distance of 2.70(5) Å. In addition to intramolecular hydrogen bonding, the counter benzoate anion is also engaged in hydrogen bonding with the uncoordinated phenolic OH group and the coordinated water molecule; the O...O distances are 2.52(5) and 2.61(4) Å, respectively.

Magnetic Studies

Variable-temperature magnetic susceptibility measurements were performed in the temperature range 2–300 K. Figures 3 and 4 show the $\chi_{\text{M}}T$ vs. T plots for complexes **1** and **2**, respectively. The experimental $\chi_{\text{M}}T$ values of 0.70 and 0.813 cm³ mol^{−1} K for **1** and **2**, respectively, at 300 K are characteristic for isolated Cu^{II} ions with a g value close to 2.10.

Figure 3. Plot of $\chi_{\text{M}}T$ vs. T for **1**. Closed squares represent the experimental data and the solid line represents the best-fit data.Figure 4. $\chi_{\text{M}}T$ vs. T for **2**. Closed diamonds represent the experimental data and solid line represents the best-fit data.

In **1**, the value of $\chi_{\text{M}}T$ (0.70 cm³ mol^{−1} K at 300 K) decreases gradually with a steady rate to 0.03 cm³ mol^{−1} K at 19 K and then the values of $\chi_{\text{M}}T$ remain almost constant

up to 2 K; this behavior suggests an antiferromagnetic interaction in complex **1** ($J = -119 \text{ cm}^{-1}$). In the case of complex **2**, the value of χ_{MT} ($0.81 \text{ cm}^3 \text{ mol}^{-1} \text{ K}$ at 300 K) remains almost unaltered up to 10 K and then decreases rapidly to $0.64 \text{ cm}^3 \text{ mol}^{-1} \text{ K}$ at 2 K; this trend is consistent with a very weak antiferromagnetic interaction in complex **2**.

It is well documented in the literature that alkoxido/phenoxido-bridged species exhibit antiferromagnetic interaction when the angle is larger than 97.60° ; the antiferromagnetic character increases with increasing angle.^[11] Therefore, the expected coupling in $[\text{Cu}_2(\text{L}^1)(\text{N}_3)]$ through the phenoxido group ($\text{Cu}-\text{O}-\text{Cu}$ 102°) should be antiferromagnetic. In contrast, for $\mu_{1,1}-\text{N}_3$ bridges, the ferromagnetic character decreases with an increase in the $\text{Cu}-\text{N}-\text{Cu}$ angle from 85° and shows antiferromagnetic behavior for $\text{Cu}-\text{N}-\text{Cu}$ angle $\geq 104^\circ$.^[12] In complex **1**, the $\text{Cu}-\text{N}-\text{Cu}$ angle (102.93°) is close to the cutoff value of 104° for ferromagnetic character and very weak ferromagnetic coupling may be expected through the bridging azido group. The magnetic behavior of $[\text{Cu}_2(\text{L}^1)(\text{N}_3)]$ depends on the orbital countercomplementary effect^[13] operated by the phenoxido and azido groups. However, in the present case, the $\mu_{1,1}-\text{N}_3$ group shows a small or negligible orbital countercomplementary effect, which results in medium antiferromagnetic coupling.

Now for **2**, the copper(II) atoms are connected by bridging phenoxido and *syn-syn* carboxylate groups as axial and equatorial binding modes. It was reported that axially-equatorially bonded phenoxido groups exhibit very weak ferro-^[14] and antiferromagnetic^[14a,15] interactions. It is also known that antiferromagnetic interactions result from $\text{O}\cdots\text{H}\cdots\text{O}$ hydrogen bonding^[16] and bridging $\mu_{\text{syn-syn}}$ -carboxylate groups.^[7d] It is believed that these types of structural features may generate either very weak ferro- or antiferromagnetic interactions in the complex. In our case, we observed very weak antiferromagnetic behavior with $J = -1.0 \text{ cm}^{-1}$.

Theoretical Calculations

We calculated the spin density of the triplet states for the two cases to understand the electronic structure and, hence, the behavior of the magnetic properties. The exchange interaction of the complexes is mainly governed by the delocalization of the spin density of the unpaired electron between the paramagnetic centers. The antiferromagnetic interaction originates from the delocalization of the unpaired electron through the suitable orbital of the bridging ligand. It is to be noted that the participation of the coordinating atoms of the ligand in the singly occupied molecular orbital (SOMO) leads to an enhancement in the degree of delocalization of the unpaired electron, which increase the antiferromagnetism of the molecule.

It is seen from the spin density plot (Figure 5) of **2** that spin densities mainly belong to the $d_{x^2-y^2}$ orbital of the Cu^{II} atoms and the hybrid orbital of the ligands on the equato-

rial plane; no electron densities are directed towards the d_{z^2} orbital of the Cu^{II} ion. As a result, a spin delocalization mechanism is not operating through the axial-equatorial coordinated $\mu\text{-O}_{\text{phenoxido}}$ and *syn-syn* benzoate group. However, some spin delocalization takes place through the $\text{O}\cdots\text{H}\cdots\text{O}$ bond in the ground state, resulting in very weak antiferromagnetic interactions in **2**. The calculated exchange coupling constants with the use of different basis sets are listed in Table 3.

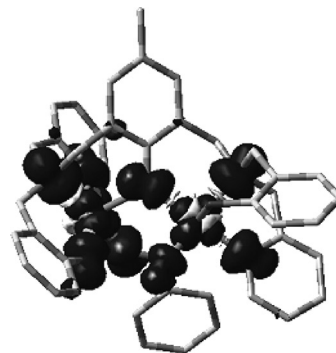


Figure 5. Spin density plot corresponding to the triplet state of **2** (isosurface cut off value 0.001).

Table 3. Calculated exchange coupling constants J for **1** and **2** by using different basis sets.

	Cu	C, N and O	H	$J_{\text{calcd.}} / \text{cm}^{-1}$	$J_{\text{exp.}} / \text{cm}^{-1}$
1	ae TZP	ae DZ	6-31G	-110	-119
2	ae TZP	ae DZ	6-31G	-0.68	-1.0

In contrast, in the case of **1**, the overlap (Figure 6) between the $d_{x^2-y^2}$ orbitals of the copper atoms occurs through the hybrid orbital of the equatorially coordinated, bridging phenoxido group, which exhibits moderate antiferromagnetic interaction (Table 3).

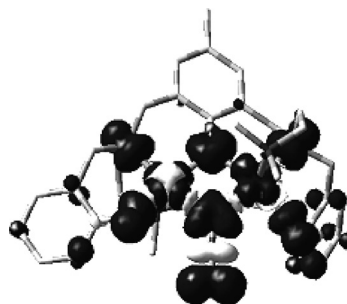


Figure 6. Spin density plot corresponding to the triplet state for **1** (isosurface cut off value 0.001).

Catecholase Activity

The catalytic oxidation of 3,5-di-*tert*-butylcatechol (3,5-DTBC) was studied to investigate the catecholase activity of the complexes, and it was found that only complex **2** shows catecholase activity in oxygen-saturated methanolic

solution. It is to be noted that in the neutral pH range almost no activity was observed. Above pH 8, catalytic activity developed that leveled off around pH 10 (Figure 7).

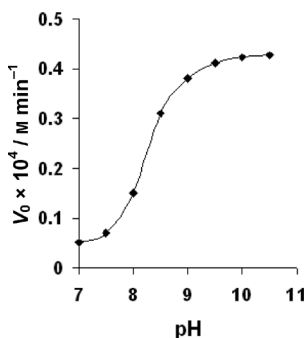


Figure 7. Dependence of the reaction rates on pH for the oxidation of 3,5-DTBC catalyzed by complex **2**. The reactions were performed in methanol/aqueous buffer saturated with O₂ (TRIS/HCl pH 7.0 and TRIS pH 7.5, 8.0, 8.5, 9.0 and NaOH solution pH 9.5, 10.0, and 10.5). [Complex] = 1 × 10^{−4} M and [3,5-DTBC] = 5 × 10^{−3} M at 25 °C.

Thus, the catalytic activity experiments were performed at pH 9.5 and to minimize the effect of pH on the spontaneous reaction the same solution was used without adding the complex as an internal reference. The catalytic oxidation of 3,5-DTBC to 3,5-di-*tert*-butylquinone (3,5-DTBQ) was studied by monitoring the increase in the absorbance of 3,5-DTBQ at 400 nm. The time-dependent growth of 3,5-DTBQ is shown in Figure 8. The initial rate method was used to determine the rate of the reaction. The first-order dependence on the 3,5-DTBC concentration was confirmed from the linear relationship between the initial rates and the concentration of the substrate. Saturation kinetics were observed for the initial rate versus 3,5-DTBC concentration and the data was analyzed on the basis of the Michaelis–Menten approach.^[4b,4d,17]

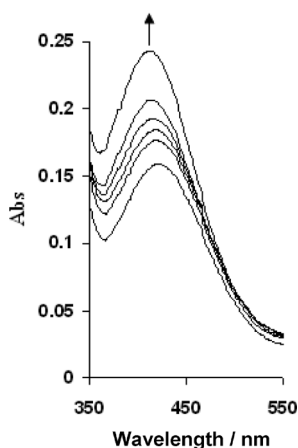


Figure 8. Absorbance at ca. 400 nm of the solution of complex **2** and 3,5-DTBC in methanol, 25 °C. The spectra were recorded at various time intervals from 2 to 60 min.

The kinetic parameters $K_M = 7.4 \times 10^{-4}$ M, $k_{cat} = 0.43 \text{ min}^{-1}$, and $V_{max} = 4.3 \times 10^{-5} \text{ M min}^{-1}$ were evaluated by using both the Michaelis–Menten equation and a Li-

neweaver–Burk plot (Figure 9). The observed kinetic parameters fall in the range of the previously reported Cu^{II} complexes incorporating binucleating ligands.^[1f,2a,16a,18]

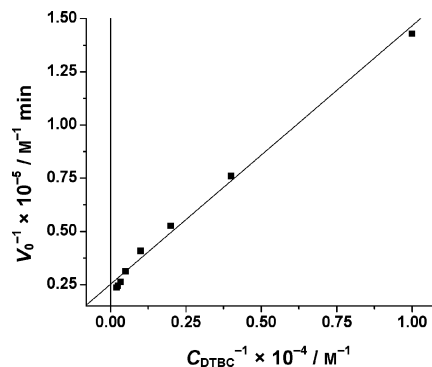


Figure 9. Lineweaver–Burk plot for aerobic oxidation of 3,5-DTBC by complex **2**.

It has been established^[18a] that in case of pH dependence, the dianionic form of catechol binds to the metal center as a bridging ligand prior to intermolecular electron transfer in the oxidation of 3,5-DTBC to 3,5-DTBQ. Therefore, the catecholase activity is mainly regulated by the steric match between the dicopper(II) center and the substrate.

In the case of **1**, the strongly bonded azido ion and the axially disposed *trans* sidearm nitrogen atoms of the ligand are believed to be responsible for the inactivity towards catechol oxidation. However, in complex **2**, binding of the stronger catecholato ligand to the dicopper(II) center [Cu...Cu 3.562(6) Å] is much easier when the weakly bonded benzoate group is replaced; in this case, complex **2** exhibits moderate catecholase activity (turnover rate = 26 h^{−1}). It is known^[19] that the oxidation of catechol to quinone is facilitated by Cu²⁺ ions at pH 6.7. In the present study, complex **2** shows maximum activity at pH 9.5, which suggests that free Cu²⁺ ions have an insignificant role in the oxidation of catechol.

Hydrolytic Cleavage of DNA

Complex **2** is prone to hydrolytic cleavage of DNA molecules under anaerobic conditions. The gel electrophoresis separation of supercoiled plasmid pUC19 DNA induced by complex **2** is shown in Figure 10. It can be seen that the complex converts plasmid supercoiled pUC19 DNA into a

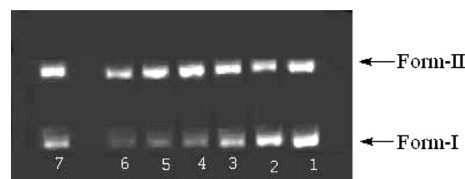


Figure 10. Agarose gel electrophoresis patterns for the cleavage of pUC19 DNA with various concentrations of complex **2**. Lane 1: DNA control; lane 2: DNA + 50 μM complex; lane 3: DNA + 125 μM complex; lane 4: DNA + 250 μM complex; lane 5: DNA + 375 μM complex; lane 6: DNA + 500 μM complex; lane 7: DNA + 125 μM complex + 0.4 M DMSO.

mixture of the supercoiled (Form-I) and nicked (Form-II) forms.

The cleavage activity increases remarkably with increasing concentration of the complexes and shows maximum cleavage at 5.0 times the concentration with respect to the base pair concentration of DNA. A further increase in the complex concentration led to precipitation of plasmid DNA as a white solid, and this is probably due to the neutralization of charge by the binding of metal complexes. We also performed the reaction in the presence of 0.4 M DMSO and no appreciable inhibition of cleavage was observed; this indicates that the reaction pathway takes place by the hydrolytic cleavage path way.

Conclusions

Herein we presented the synthesis, crystal structure, magnetic properties, and interaction of DNA and catechol substrates of two new complexes synthesized from copper(II) chloride, H_3L^1 or H_3L^2 benzoate, and azido ligands. In complex **2**, the involvement of axially–equatorially bonded cresolato and *syn–syn* benzoato groups resulted in very weak antiferromagnetic coupling with $J = -1.0 \text{ cm}^{-1}$. In complex **1**, the magnetic core is $[Cu_2(\mu-O_{phen})(\mu_{1,1}-N_3)]^{2+}$ and the antiferromagnetic character with a medium J value ($J = -119 \text{ cm}^{-1}$) can be attributed from the orbital counter-complementary phenomenon. The exchange pathway was evaluated by using broken symmetry DFT calculations. Complex **2** is able to promote the cleavage of plasmid DNA under hydrolytic conditions and also exhibits catecholase activity at pH 9.5.

Experimental Section

Materials: All the starting chemicals were analytically pure and used without further purification. The ligands were prepared according to literature procedures.^[8c] Supercoiled pUC19 DNA, agarose (molecular biology grade), and ethidium bromide were purchased from Bangalore Genei.

Physical Measurements: UV/Vis spectra were recorded with a Perkin–Elmer LAMBDA 25 spectrophotometer and IR spectra were measured with a Perkin–Elmer L-0100 spectrometer. Electrochemical measurements were performed (acetonitrile solution) with a CHI 620A electrochemical analyzer by using a platinum electrode. Tetraethylammonium perchlorate (TEAP) was used as a supporting electrolyte, and the potentials are referenced to the saturated calomel electrode (SCE) without junction correction. The cyclic voltammograms were recorded with a scan rate of 50 mV s^{-1} with iR compensation in all cases. Electron paramagnetic resonance experiments were performed with a Varian E-112 (X band, 9.1 GHz) spectrometer at a microwave power of 5 mW and modulation amplitude of 2.0 gauss, and spectra were collected by using a quartz dewar. Tetracyanoethylene (tcne, $g = 2.00277$) was used to calibrate the spectra. Magnetic measurements were carried out on polycrystalline samples with a Quantum Design MPMS XL SQUID susceptometer operating at a magnetic field of 0.1 T between 2 and 300 K. The diamagnetic corrections were evaluated from Pascal's constants. Elemental analyses (C, H, N) were performed with a Perkin–Elmer 2400 Series II elemental analyzer.

The catecholase activity was studied in methanol at 25 °C by reaction of the complexes with 3,5-di-*tert*-butylcatechol (3,5-DTBC). For this purpose, 10^{-4} M solutions of the complexes were treated with 3,5-DTBC (50 equiv.) under aerobic conditions. The increase in the absorption band at 400 nm, characteristic of the quinone formed, was followed spectrophotometrically at various time intervals from 2 to 60 min. The kinetic parameters were evaluated for $1 \times 10^{-4} \text{ M}$ solutions of the complexes and 1×10^{-4} to $5 \times 10^{-3} \text{ M}$ solutions of the substrate in oxygen-saturated methanol/aqueous NaOH solutions (pH 9.5).

DNA cleavage experiments were done by using plasmid pUC19 DNA. Reactions were performed by incubating pUC19 DNA ($50.5 \mu\text{M}$ base pair in 10 mM Tris-HCl, pH 8.0) at 37 °C for 6 h by varying the concentration (50 – $750 \mu\text{M}$) of the complexes in 10 mM Tris-HCl (pH 7.5; containing 5 mM NaCl) buffer. To examine the presence of $\cdot\text{OH}$, the incubation was also performed in the presence of radical scavengers with the use of DMSO. Gel electrophoresis was performed on 1% agarose gel in TBE (Tris–boric acid–EDTA) buffer (pH = 8). Free Cu^{II} ions produced hardly any cleavage of plasmid pUC19 DNA under identical conditions.^[20] After electrophoresis, the gel was stained with ethidium bromide solution and photographed under UV light (UVipro Platinum, UVitec).

DFT Study and Computational Details: DFT calculations were carried out to get better insights into the electronic structure, energy, and magnetic behavior. The X-ray coordinates of the complexes were used for DFT calculations. The magnetic exchange interactions between the transition-metal ions were studied on the basis of density functional theory coupled with the broken symmetry approach^[21] for weakly interacting magnetic ions in the polynuclear complexes.^[22] Here, we performed the DFT calculation with the BS solution to calculate the exchange coupling parameters. To evaluate the exchange coupling constant, J , the following equation was applied:^[7a]

$$E_{\text{HS}} - E_{\text{BS}} = -(2S_1S_2 + S_2)J$$

where S_1 and S_2 are the total spin for the paramagnetic centers, and in this case $S_1 = S_2 = 1/2$, $E_{\text{HS}} - E_{\text{BS}} = -J$ by using the Heisenberg Hamiltonian, $\hat{H} = -J\hat{S}_1\hat{S}_2$. The term E_{HS} corresponds to the energy of the high-spin state (triplet state) and E_{BS} corresponds to the broken symmetry state. The positive and negative values of the coupling constant J indicate the ferromagnetic and antiferromagnetic ground states of the system, respectively.

Ground-state electronic structure calculations of the complexes were carried out by using density functional theory (DFT)^[23] methods with the Gaussian 03W program.^[24] The Becke's hybrid function^[25] with Lee–Yang–Parr (LYP) correlation function^[26] was used throughout the study. We used a triple- ζ quality all-electron basis set for copper atoms (TZP)^[27] and a double- ζ all-electron basis set^[28] for C, N, and O atoms, and a 6-31G basis set was applied for H. All energy calculations were performed by using the *SCF* = *Tight* option of Gaussian to ensure sufficiently well-converged values of the state energies.

Crystallographic Studies: Single crystals of suitable quality for single-crystal X-ray diffraction studies of $[Cu_2(L^1)(N_3)] \cdot 2H_2O$ (**1**· $2H_2O$) and $[Cu_2(HL^2)(O_2CPh)(H_2O)](PhCO_2) \cdot H_2O$ (**2**· H_2O) were grown by slow evaporation of their methanolic solutions. The X-ray intensity data were measured at 293 K with a Bruker AXS SMART APEX CCD diffractometer ($Mo-K\alpha$, $\lambda = 0.71073 \text{ \AA}$). The detector was placed at a distance of 6.03 cm from the crystal. A total of 606 frames were collected with a scan width of 0.3° in different settings of ϕ . The data were reduced in SAINTPLUS^[29] and empirical absorption correction was applied by using the SAD-

ABS package.^[29] Metal atoms were located by direct methods and the rest of the non-hydrogen atoms emerged from successive Fourier synthesis. The structures were refined by full-matrix least-square procedure on F^2 . All non-hydrogen atoms were refined anisotropically. The H4B and H4C hydrogen atoms of the coordinated water molecule in **2** were directly observed in difference Fourier maps and the hydrogen atoms of the uncoordinated solvent water molecule for both cases were solved by using a riding model. The remaining hydrogen atoms were included in calculated positions. Calculations were performed by using the SHELXTL^[30] program package. Molecular structure plots were drawn by using ORTEP.^[31] Relevant crystal data are given in Table 4. CCDC-698746 and -698745 contain the supplementary crystallographic data for this paper. These data can be obtained free of charge from The Cambridge Crystallographic Data Centre via www.ccdc.cam.ac.uk/data_request/cif.

Table 4. Crystal data and structure refinement parameters for complexes **1**·2H₂O and **2**·H₂O.

	1 ·2H ₂ O	2 ·H ₂ O
Formula	C ₃₁ H ₄₅ N ₇ O ₅ Cu ₂	C ₄₉ H ₄₈ N ₄ O ₉ Cu ₂
F_w	722.82	964.01
Crystal system	monoclinic	orthorhombic
Space group	$P2_1/n$	$P2_12_12_1$
$a / \text{\AA}$	10.3599(9)	13.501(5)
$b / \text{\AA}$	28.656(3)	17.842(7)
$c / \text{\AA}$	12.4381(11)	18.982(7)
$\alpha / ^\circ$	90.00	90.00
$\beta / ^\circ$	109.5800(10)	90.00
$\gamma / ^\circ$	90.00	90.00
$V / \text{\AA}^3$	3479.0(6)	4573(3)
Z	4	4
$D_{\text{calcd.}} / \text{Mg m}^{-3}$	1.380	1.400
μ / mm^{-1}	1.270	0.991
$\theta / ^\circ$	1.88 to 25.00	1.85 to 25.00
T / K	293(2)	293(2)
Unique reflections / R_{int}	6126/0.0366	8041/0.0506
$R_1^{[a]} wR_2^{[b]} [I > 2\sigma(I)]$	0.0549, 0.1255	0.0555, 0.1033
GOF on F^2	1.128	1.102

[a] $R_1 = \Sigma |F_o| - |F_c| / \Sigma |F_o|$. [b] $wR_2 = [\Sigma w(F_o^2 - F_c^2)^2 / \Sigma w(F_o^2)^2]^{1/2}$.

[Cu₂(L¹)(N₃) (1**):** To a solution of copper(II) chloride dihydrate (0.171 g, 1.0 mmol) in methanol (30 mL) was added H₃L¹ (0.258 g, 0.50 mmol), and the mixture was stirred for 0.5 h. Triethylamine (0.2 mL, 1.5 mmol) and an aqueous solution of sodium azide (0.0325 g, 0.50 mmol) was then added. The resulting brown solution was stirred for another 0.5 h at room temperature. Slow evaporation of the solution yielded a brown crystalline product. Yield: 72% (0.260 g). UV/Vis (CH₃OH): λ (ϵ , M⁻¹cm⁻¹) = 237 (15460), 284 (9250), 386 (2645), 667 (236) nm. IR (KBr): $\tilde{\nu}$ = 1295 (C–O_{phenoxido}), 2077 ($\mu_{1,1}$ -N₃) cm⁻¹. Epa (Cu^{II} → Cu^{III}): 0.87 (irr) V. Epc (Cu^{II} → Cu^I): –0.72 (irr) V. C₃₁H₄₁Cu₂N₇O₃ (722.82): calcd. C 54.055, H 5.999, N 14.23; found C 54.03, H 5.98, N 14.26.

[Cu₂(HL²)(O₂CPh)(H₂O)](PhCO₂) (2**):** To a solution of copper(II) chloride dihydrate (0.171 g, 1.0 mmol) in methanol (25 mL) was added H₃L² (0.280 g, 0.50 mmol), and the mixture was stirred at room temperature for 0.5 h. A solution of benzoic acid (0.120 g, 1.0 mmol) in methanol (5 mL) and pyridine (0.08 mL, 1.00 mmol) was the added, and the solution was stirred for another 0.5 h to afford a greenish solution. Slow evaporation of the solution yielded a dark-green crystalline product. Yield: 70% (0.337 g). UV/Vis (CH₃OH): λ (ϵ , M⁻¹cm⁻¹) = 253 (11200), 280 (7620), 386 (1356), 667 (180) nm. IR (KBr): $\tilde{\nu}$ = 1293 (C–O_{phenoxido}), 1601 and 1458 ($\mu_{\text{syn-syn}}$ -carboxylate) cm⁻¹. Epa (Cu^{II} → Cu^{III}): 0.88 (irr) V. Epc

(Cu^{II} → Cu^I): –0.65 (irr) V. EPR: g_{\parallel} = 2.22; g_{\perp} = 2.09. C₄₉H₄₆Cu₂N₄O₈ (964.01): calcd. C 62.15, H 4.90, N 5.92; found C 62.20, H 4.87, N 5.87.

Acknowledgments

Financial support from Department of Science and Technology, New Delhi, India and the Council of Scientific and Industrial Research, New Delhi, India. University Grant Commission, New Delhi is greatly acknowledged. We are also thankful to Prof. T. N. Guru Row, Solid State and Structural Chemistry Unit (SSCU), Indian Institute of Science, for helping us with the data collection at the CCD facility setup (Indian Institute of Science, Bangalore, India) under IRHPA-DST program. The authors also acknowledge SAIF, Indian Institute of Technology Bombay, India, for EPR measurements. We are also thankful to the Department of Life Science and Biotechnology of this university for their help in gel documentation.

- a) A. Banerjee, S. Sarkar, D. Chopra, E. Colacio, K. K. Rajak, *Inorg. Chem.* **2008**, *47*, 4023–4031; b) N. A. Rey, A. Neves, A. J. Bortoluzzi, C. T. Pich, H. Terenz, *Inorg. Chem.* **2007**, *46*, 348–350; c) F. Fondo, A. M. Gartia-Deibe, J. Sanmartin, M. R. Bermejo, L. Lezama, T. Rojo, *Eur. J. Inorg. Chem.* **2003**, 3703–3706; d) P. Dapporto, M. Formica, V. Fusi, L. Giorgi, M. Micheloni, P. Paoli, R. Pontellini, P. Rossi, *Inorg. Chem.* **2001**, *40*, 6186–6192; e) A. Neves, L. M. Rossi, A. J. Bortoluzzi, A. S. Mangrich, W. Hasse, R. J. Werner, *J. Braz. Chem. Soc.* **2001**, *12*, 747–754; f) S. Torelli, C. Belle, I. Gautier-Luneau, J. L. Pierre, E. Saint-Aman, J. M. Latour, L. LePape, D. Luneau, *Inorg. Chem.* **2000**, *39*, 3526–3536; g) T. N. Sorrell, *Tetrahedron* **1989**, *45*, 3–68; h) J. M. Latour, *Bull. Soc. Chim. Fr.* **1988**, 508–520; i) A. Neves, L. M. Rossi, I. Vencato, V. Drago, W. Hasse, R. Werner, *Inorg. Chim. Acta* **1998**, *281*, 111–115; j) R. C. Holz, J. M. Brink, F. T. Gobena, C. J. O'Connor, *Inorg. Chem.* **1994**, *33*, 6086–6092; k) K. D. Karlin, Z. Tykier, *Bioinorganic Chemistry of Copper*; Chapman and Hill: New York, **1993**; l) N. Kitajima, *Adv. Inorg. Chem.* **1992**, *39*, 1–77; m) P. A. Vigato, S. Tamburini, D. Fenton, *Coord. Chem. Rev.* **1990**, *106*, 25–170.
- a) J. Ackermann, S. Buchler, F. Meyer, *C. R. Chim.* **2007**, *10*, 421–432; b) C. H. Weng, S. C. Cheng, H. M. Wei, H. H. Wei, C. J. Lee, *Inorg. Chim. Acta* **2006**, *359*, 2029–2040; c) R. A. Peralta, A. Neves, A. J. Bortoluzzi, A. dos Anjos, F. R. Xavier, B. Szpoganicz, H. Terenzi, M. C. B. de Oliveira, E. Castellano, G. R. d. Friedermann, A. S. Mangrich, M. A. Novak, *J. Inorg. Biochem.* **2006**, *100*, 992–1004; d) R. C. Holz, J. M. Bradshaw, B. Bennet, *Inorg. Chem.* **1998**, *37*, 1219–1225.
- M. C. Linder, C. A. Goode, *Biochemistry of Copper*, Plenum, New York, **1991**.
- a) S. Torelli, C. Belle, S. Hamman, J. L. Pierre, E. Saint-Aman, *Inorg. Chem.* **2002**, *41*, 3983–3989; b) C. Gerdemann, C. Eicken, B. Krebs, *Acc. Chem. Res.* **2002**, *35*, 183–191; c) C. Eicken, B. Krebs, J. C. Sacchettini, *Curr. Opin. Struct. Biol.* **1999**, *9*, 677–683; d) J. Reim, B. Krebs, *J. Chem. Soc., Dalton Trans.* **1997**, 3793–3804; e) E. I. Solomon, U. M. Sundaram, T. E. Machonkin, *Chem. Rev.* **1996**, *96*, 2563–2606; f) A. Sanchez-Ferrer, J. N. Rodriguez-Lopez, F. Garcia-Canovas, F. Garcia-Carmona, *Biochim. Biophys. Acta* **1995**, *1247*, 1–11; g) M. Tremolieres, J. B. Bieth, *Phytochemistry* **1984**, *23*, 501–505.
- a) F. Mancin, P. Scrimin, P. Tecilla, U. Tonellato, *Chem. Commun.* **2005**, 2540–2548 and references cited therein; b) C. Liu, S. Yu, D. Li, Z. Liao, X. Sun, H. Xu, *Inorg. Chem.* **2002**, *41*, 913–922; c) N. H. William, B. Takasaki, M. Wall, J. Chin, *Acc. Chem. Res.* **1999**, *32*, 485–493; d) E. L. Hegg, K. A. Deal, L. L. Kiessling, J. N. Burstyn, *Inorg. Chem.* **1997**, *36*, 1715–1718.
- a) C. Liu, M. Wang, T. Zhang, H. Sun, *Coord. Chem. Rev.* **2004**, *248*, 147–168; b) A. Sreedhara, J. A. Cowan, *J. Biol. In-*

- org. Chem. **2001**, 6, 337–347; c) M. Komiyama, N. Takeda, H. Shigekawa, *Chem. Commun.* **1999**, 1443–1451; d) E. L. Hegg, J. N. Burstyn, *Coord. Chem. Rev.* **1998**, 173, 133–165.
- [7] a) E. Ruiz, A. Rodriguez-Fortea, J. Tercero, T. Cauchy, C. Mas-sobrio, *J. Chem. Phys.* **2005**, 123, 74102–74111 and references cited therein; b) E. Ruiz, S. Alvarez, *ChemPhysChem* **2005**, 6, 1094–1099; c) J. H. Rodriguez, J. K. Mc Cusker, *J. Chem. Phys.* **2002**, 116, 6253–6270; d) O. Kahn, *Molecular Magnetism*, VCH, New York, **1993**.
- [8] a) R. Singh, C. de-Graaf, E. Colacio, K. K. Rajak, *Polyhedron* **2008**, 27, 2751–2756; b) A. Mondal, S. Basak, S. Sarkar, D. Chopra, R. Das, K. K. Rajak, *Eur. J. Inorg. Chem.* **2006**, 1824–1829; c) A. Mondal, S. Sarkar, D. Chopra, T. N. Guru Row, K. Pramanik, K. K. Rajak, *Inorg. Chem.* **2005**, 44, 703–708; d) V. D. Campbell, E. J. Parsons, W. T. Pennington, *Inorg. Chem.* **1993**, 32, 1773–1778.
- [9] E. Franco, E. Lopez-Torres, M. A. Mendiola, M. T. Sevilla, *Polyhedron* **2000**, 19, 441–451.
- [10] C. O'Sullivan, G. Murphy, B. Murphy, B. J. Hathaway, *J. Chem. Soc., Dalton Trans.* **1999**, 1835–1844.
- [11] V. H. Crawford, H. W. Richardson, J. R. Hodgson, D. J. Was-son, W. E. Hatfield, *Inorg. Chem.* **1976**, 15, 2107–2110.
- [12] E. Ruiz, J. Cano, S. Alvarez, P. Alemany, *J. Am. Chem. Soc.* **1998**, 120, 11122–11129.
- [13] a) M. S. El Fallah, R. Vecente, J. Tercero, C. Elpelt, E. Rentschler, X. Solans, M. Font-Bardia, *Inorg. Chem.* **2008**, 47, 6322–6328; b) M. S. El Fallah, F. Badyine, R. Vecente, A. Es-cuer, X. Solans, M. Font-Bardia, *Dalton Trans.* **2006**, 2934–2942; c) Y. Nishida, S. Kida, *J. Chem. Soc., Dalton Trans.* **1986**, 2633–2640; d) V. Mckee, M. Zwagulis, J. V. Dagdigian, M. G. Patch, C. A. Reed, *J. Am. Chem. Soc.* **1984**, 106, 4765–4772.
- [14] a) J. Manzur, H. Mora, A. Vega, E. Spodine, D. V. Yazigi, M. T. Garland, M. S. E. Fallah, A. Escuer, *Inorg. Chem.* **2007**, 46, 6924–6932; b) H. P. Berends, D. W. Stephan, *Inorg. Chem.* **1987**, 26, 749–754.
- [15] A. Mukherjee, M. K. Saha, I. Rudra, S. Ramasesha, M. Ne-thaji, A. R. Chakravarty, *Inorg. Chim. Acta* **2004**, 357, 1077–1082.
- [16] a) S. Sarkar, A. Dutta, A. Mondal, D. Chopra, J. Ribas, K. K. Rajak, S. M. Sairam, S. K. Pati, *J. Phys. Chem. B* **2006**, 110, 12–15; b) C. Desplanches, E. Ruiz, A. R. Fortea, S. Alvarez, *J. Am. Chem. Soc.* **2002**, 124, 5197–5205; c) J. B. Goodenough, *Magnetism and the Chemical Bond*, New York, **1996**.
- [17] R. Than, A. A. Feldman, B. Krebs, *Coord. Chem. Rev.* **1999**, 182, 211–241.
- [18] a) I. A. Koval, G. Patrick, C. Belle, K. Selmezi, J. Reedijk, *J. Chem. Soc. Rev.* **2006**, 35, 814–840; b) A. Neves, L. M. Rossi, A. J. Bortoluzzi, B. Szpoganicz, C. Wiezbicki, E. Schwingel, W. Hasse, S. Ostrovsky, *Inorg. Chem.* **2002**, 41, 1788–1794.
- [19] P. Kamau, R. B. Jordon, *Inorg. Chem.* **2002**, 41, 3076–3083.
- [20] a) C. Siss, F. Mancin, M. Gatos, M. Palumbo, P. Tecilla, U. Tonellato, *Inorg. Chem.* **2005**, 44, 2310–2317; b) R. Ren, P. Yang, W. Zheng, Z. Hua, *Inorg. Chem.* **2000**, 39, 5454–5463.
- [21] a) L. Noodleman, D. A. Case, *Adv. Inorg. Chem.* **1992**, 38, 423–470; b) L. Noodleman, E. J. Baerends, *J. Am. Chem. Soc.* **1984**, 106, 2316–2327; c) L. Noodleman, *J. Chem. Phys.* **1981**, 74, 5737–5743.
- [22] a) J. E. Mc Grady, R. Stranger, *J. Am. Chem. Soc.* **1997**, 119, 8512–8522; b) L. Noodleman, J. G. Morman Jr, *J. Chem. Phys.* **1979**, 70, 4903–4906.
- [23] R. G. Parr, W. Yang, *Density Function Theory of Atoms and Molecules*, Oxford University Press, Oxford, **1989**.
- [24] M. J. Frisch, G. W. Trucks, H. B. Schlegel, G. E. Scuseria, M. A. Robb, J. R. Cheeseman, J. A. Montgomery Jr, T. Vreven, K. N. Kudin, J. C. Burant, J. M. Millam, S. S. Iyengar, J. Tom-asi, V. Barone, B. Mennucci, M. Cossi, G. Scalmani, N. Rega, G. A. Petersson, H. Nakatsuji, M. Hada, M. Ehara, K. Toyota, R. Fukuda, J. Hasegawa, M. Ishida, T. Nakajima, Y. Honda, O. Kitao, H. Nakai, M. Klene, X. Li, J. E. Knox, H. P. Hratch-ian, J. B. Cross, V. Bakken, C. Adamo, J. Jaramillo, R. Gom-perts, R. E. Stratmann, O. Yazyev, A. J. Austin, R. Cammi, C. Pomelli, J. W. Ochterski, P. Y. Ayala, K. Morokuma, G. A. Voth, P. Salvador, J. J. Dannenberg, V. G. Zakrzewski, S. Dap-prich, A. D. Daniels, M. C. Strain, O. Farkas, D. K. Malick, A. D. Rabuck, K. Raghavachari, J. B. Foresman, J. V. Ortiz, Q. Cui, A. G. Baboul, S. Clifford, J. Cioslowski, B. B. Stefanov, G. Liu, A. Liashenko, P. Piskorz, I. Komaromi, R. L. Martin, D. J. Fox, T. Keith, M. A. Al-Laham, C. Y. Peng, A. Nanayak-kara, M. Challacombe, P. M. W. Gill, B. Johnson, W. Chen, M. W. Wong, C. Gonzalez, J. A. Pople, *Gaussian 03*, revision C.02, Gaussian, Inc., Wallingford, CT, **2004**.
- [25] A. D. Becke, *J. Chem. Phys.* **1993**, 98, 5648–5652.
- [26] C. Lee, W. Yang, R. G. Parr, *Phys. Rev. B* **1988**, 37, 785–789.
- [27] A. Schaefer, H. Horn, R. Ahlrichs, *J. Chem. Phys.* **1994**, 100, 5829–5835.
- [28] A. Schaefer, H. Horn, R. Ahlrichs, *J. Chem. Phys.* **1992**, 97, 2571–2577.
- [29] *SMART, SAINT, SADABS, XPREP, SHELXTL*, Bruker AXS Inc., Madison, WI, **1998**.
- [30] G. M. Sheldrick, *SHELXTL*, v.6.14, Bruker AXS Inc., Madi-son, WI, **2003**.
- [31] C. K. Johnson, *ORTEP*, Report ORNL-5138, Oak Ridge National Laboratory, Oak Ridge, TN, **1976**.

Received: September 20, 2008

Published Online: December 9, 2008

Palladium(II) Complexes with Benzimidazolin-2-ylidene and Phosphane Ligands and their Catalytic Activity in Mizoroki–Heck Coupling Reactions

Hayati Türkmen,^{*[a]} Tania Pape,^[b] F. Ekkehardt Hahn,^{*[b]} and Bekir Çetinkaya^[a]

Keywords: N ligands / Phosphanes / Palladium / Carbene ligands / Cross-coupling

Symmetrically and unsymmetrically substituted benzimidazolium bromides (**1a–d** = NHC·HBr) were synthesized, incorporating bulky benzyl and/or methoxyethyl substituents (**a**: R = pentamethylbenzyl, R' = 2-methoxyethyl; **b**: R = 2,3,5,6-tetramethylbenzyl, R' = methoxyethyl; **c**: R, R' = pentamethylbenzyl; **d**: R, R' = 2,3,5,6-tetramethylbenzyl). The salts were used to prepare NHC palladium complexes. Reaction of **1a–d** with Pd(OAc)₂ and NaBr in a 1:1:3 ratio in dmsO gave mono or dinuclear, bromide-bridged complexes of type **2**. Complexes of type **2** react with monodentate or bidentate phosphanes in CH₂Cl₂ to afford the mixed benz-

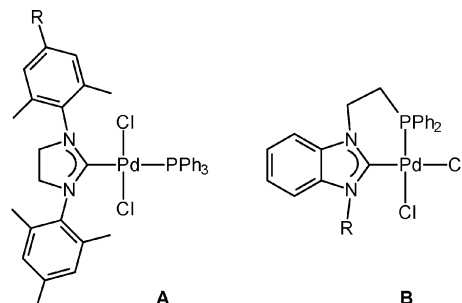
imidazolin-2-ylidene-phosphane complexes **3–6**. Reaction of salts **1a–d** with Pd(OAc)₂ in a 1:2 ratio, in the absence of NaBr, gave complexes *trans*-[PdBr₂(NHC)₂] (**7**). All compounds were fully characterized by NMR spectroscopy, mass spectrometry (MALDI), and elemental analysis. In addition, the molecular structures of **2c**, **3c**, **3d**, and **5b** were determined by X-ray diffraction. The catalytic activities of **2–7** in Mizoroki–Heck C–C coupling reactions of aryl halides with *n*-butyl acrylate are described and compared.

(© Wiley-VCH Verlag GmbH & Co. KGaA, 69451 Weinheim, Germany, 2009)

Introduction

Complexes with N-heterocyclic carbene (NHC) ligands, particularly those bearing imidazolin-2-ylidene and imidazolidin-2-ylidene moieties, have been employed widely as ligands in organometallic chemistry.^[1–4] The steric and electronic properties of such ligands are easily modified through variation of the substituents at the nitrogen and carbon atoms, and they have been used as ancillary ligands for the preparation of various catalytically active complexes.^[5] Palladium NHC complexes, for example, have been used as highly active precatalysts for C–C coupling reactions such as the Mizoroki–Heck and the Suzuki–Miyaura reaction, as well as for the copolymerization of CO and olefins.^[6] In a recent study, we observed that variation of the *para* substituents at the phenyl rings of 1,3-diarylimidazolidin-2-ylidene palladium(II) complexes had a significant influence on the catalytic behavior of complexes of type **A** in Suzuki C–C coupling reactions.^[7b]

Several groups have reported superior catalytic activity of mixed NHC–phosphane palladium(II) complexes in comparison to those of their bis(NHC) analogues.^[6,8] We described some related palladium(II) complexes either with a mixed phosphane–NHC donor set of type **A**^[7b] or with



phosphane-substituted benzimidazolin-2-ylidene ligands of type **B**.^[9]

In spite of the useful catalytic properties of complexes of types **A** and **B**, palladium complexes with a mixed donor set made up from benzannulated NHCs and phosphanes have not been studied in detail so far. Neither have they been tested as catalysts for C–C coupling reactions. We describe herein the synthesis and characterization of a series of palladium(II) complexes containing benzimidazolin-2-ylidene and phosphane ligands. The Mizoroki–Heck reaction was used to study the catalytic activity of the complexes in C–C coupling reactions. Some related palladium(II) complexes bearing triphenylphosphane and *N,N'*-(diisopropyl)benzimidazolin-2-ylidene ligands were reported as active Suzuki–Miyaura coupling catalysts^[10] while this work was in progress.

Results and Discussion

Synthesis of 1,3-Dialkylbenzimidazolium Bromides **1**

The preparation of benzimidazolium bromides **1** started from benzimidazole. Both symmetrically and unsymmetrically

[a] Department of Chemistry, Ege University, 35100 Bornova-Izmir, Turkey

Fax: +90-232-3888264

E-mail: hayatituerkmen@hotmail.com

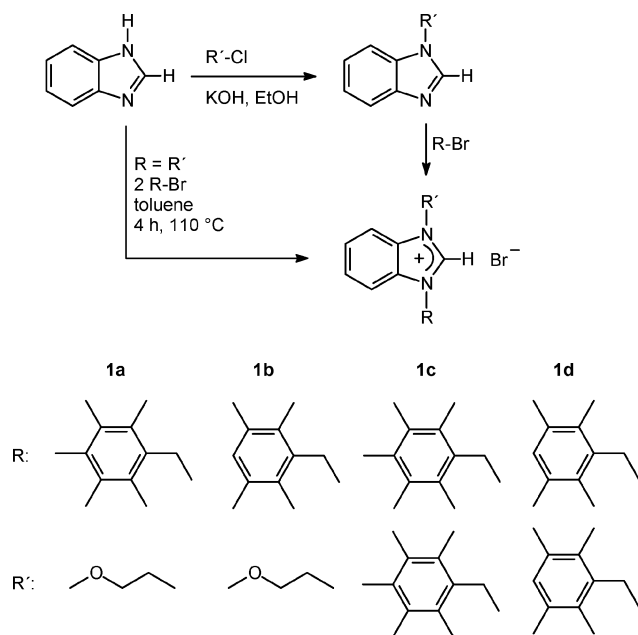
[b] Institut für Anorganische und Analytische Chemie, Westfälische Wilhelms-Universität Münster,

Corrensstraße 36, 48149 Münster, Germany

Fax: +49-251-8333108

E-mail: fehahn@uni-muenster.de

cally N^1,N^3 -substituted benzimidazolium salts^[11] can be prepared in analogy to published procedures according to the methods depicted in Scheme 1. Unsymmetrically substituted derivatives **1a,b** were synthesized in a stepwise manner, whereas symmetrically substituted derivatives **1c,d** were prepared from benzimidazole and alkylated benzyl bromides in the presence of KOH.

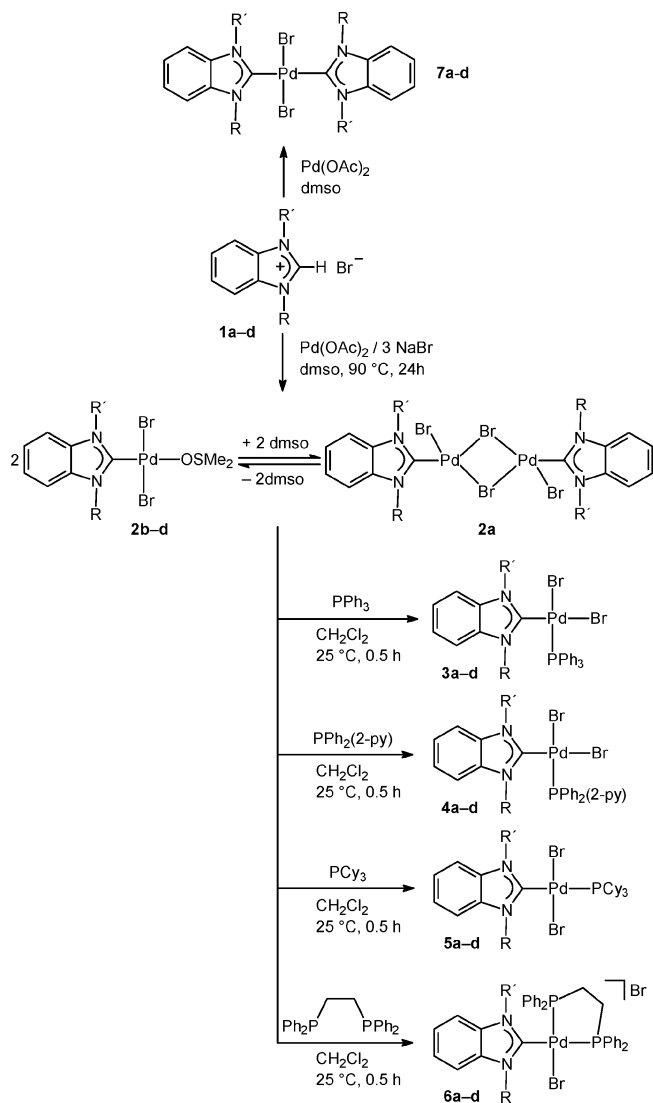


Scheme 1. Synthesis of benzimidazolium salts **1a–d**.

Benzimidazolium salts **1a–d** are white, air-stable solids. The ^1H NMR spectra of these salts exhibit characteristic NCHN resonance around $\delta = 9.73$ – 9.83 ppm. The formation of salts **1** is also supported by a resonance around $\delta = 141.3$ – 141.8 ppm in the ^{13}C NMR spectrum for the NCN carbon atom. The mass spectra of all four benzimidazolium salts exhibited peaks for the $[\text{M} - \text{Br}]^+$ ions as base peaks.

Synthesis of Palladium(II) NHC Complexes

Stoichiometric amounts of benzimidazolium salts **1a–d** react with $\text{Pd}(\text{OAc})_2$ in dmsO in the presence of a threefold excess of NaBr to yield palladium(II) NHC complexes **2**. We assume that an equilibrium between the dinuclear bis(μ -bromido) and the mononuclear dmsO solvate complexes exist in solution. Similar equilibria between mononuclear and dinuclear palladium NHC complexes have been observed previously.^[10] At this stage, it is not known which factors determine the position of the equilibrium. Complex mixtures of **2** react readily with mono- or bidentate phosphanes to yield the neutral (**3–5**) or cationic (**6**) complexes, respectively. For comparison, *trans*-bis(NHC) complexes **7** were prepared directly from salts **1a–d** and $\text{Pd}(\text{OAc})_2$ employed in a 2:1 stoichiometry in the absence of NaBr (Scheme 2).



Scheme 2. Synthesis of palladium(II) NHC complexes **2–7**.

Complexes **2–7** are yellow-orange and soluble in chlorinated solvents. The absence of a downfield signal for the NCHN proton in the ^1H NMR spectra was taken as an indication for the formation of the complexes. ^{13}C NMR chemical shifts, which serve as a useful diagnostic tool for the detection of metal NHC complexes, show that $\text{C}_{\text{carbene}}$ resonances are substantially deshielded in comparison to the benzimidazolium salts at $\delta = 160.3$, 158.5 , 157.9 , and 157.8 ppm for complexes **2a**, **2b**, **2c**, and **2d**, respectively. The MALDI mass spectrometry data point to a dinuclear skeletal structure for **2a** ($m/z = 1125$ corresponding to $[\text{2a} - \text{Br}]^+$). In contrast, the ^1H NMR spectra in CDCl_3 of **2b–d** clearly showed the coordination of one dmsO molecule to the palladium center. Single-crystal X-ray diffraction analysis of **2c** (Figure 1) confirmed the formation of a mononuclear complex containing one dmsO molecule coordinated in *trans* position to the NHC ligand.

Complexes **2** proved to be useful starting materials for the synthesis of mixed ligand complexes **3–6** under mild conditions. The NMR spectra of complexes **3–6** showed

that the phosphane ligands are coordinated to the palladium center, and their position relative to the NHC ligands was inferred from ¹³C NMR chemical shifts and ²J_{C,P} coupling constants, which are consistent with previous observations.^[7] The molecular geometry of selected complexes (*cis*-**3c**·2CH₂Cl₂, *cis*-**3d**·2CH₂Cl₂, and *trans*-**5b**) confirmed the geometry of complexes **3** and **5** depicted in Scheme 2. The reaction of **2** with diphosphanylene resulted in the formation of the cationic dicarbene complexes **6** (Scheme 2). The presence of two phosphane and one NHC donor groups is clearly demonstrated by ³¹P NMR spectroscopy, where two doublets corresponding to *trans* and *cis* phosphanes were observed at δ ≈ 52 ppm and δ ≈ 59 ppm (²J_{P,P} ≈ 11 Hz).

Both *cis* and *trans* isomers of palladium complexes of types [PdX₂L(NHC)]^[12] and [PdX₂(NHC)₂]^[13] are known. We assume that *trans* complexes **5** formed owing to the larger steric demand of tricyclohexylphosphane ligand compared to the triarylphosphanes PPh₃ and PPh₂(2-py).

X-ray Diffraction Studies

The molecular structures of complexes **2c**, **3c**·2CH₂Cl₂, **3d**·CH₂Cl₂, and **5b** were determined by single-crystal X-ray diffraction studies. Selected bond parameters for these complexes are summarized in Table 1.

Table 1. Selected bond lengths [Å] and angles [°] in **2c**, **3c**·CH₂Cl₂, **3d**·CH₂Cl₂, and **5b**.

Parameter	2c	3c ·2CH ₂ Cl ₂	3d ·CH ₂ Cl ₂	5b
Pd–C1	1.924(7)	1.979(3)	1.982(3)	2.031(4)
Pd–P1/O1	2.101(5)	2.2574(10)	2.2823(10)	2.3563(11)
Pd–Br1	2.4232(11)	2.4695(6)	2.4787(5)	2.4298(7)
Pd–Br2	2.4143(11)	2.4762(5)	2.4559(5)	2.4394(7)
N1–C1	1.353(9)	1.344(5)	1.352(4)	1.341(5)
N2–C1	1.341(9)	1.348(4)	1.354(4)	1.391(4)
Br1–Pd–Br2	175.78(4)	93.99(2)	89.70(2)	173.26(2)
Br1–Pd–P1/O1	92.6(2)	87.11(3)	174.83(3)	92.34(3)
Br1–Pd–C1	90.6(2)	88.15(10)	86.65(10)	86.90(11)
Br2–Pd–P1/O1	91.1(2)	87.11(3)	91.47(3)	94.35(3)
Br2–Pd–C1	85.7(2)	175.06(10)	176.26(10)	86.54(11)
P1/O1–Pd–C1	176.7(2)	90.85(10)	92.09(10)	173.30(11)
N1–C1–N2	108.0(6)	108.0(3)	107.9(3)	107.3(3)

The structure determination of complex **2c** reveals a mononuclear square-planar Pd^{II} atom coordinated by the NHC, two bromido ligands, and one dimethyl sulfoxide ligand in a *trans* arrangement (Figure 1). Apparently for steric reasons, the Br1–Pd–Br2 vector is oriented almost perpendicular to the NHC plane. The Pd–C1 bond length [1.924(7) Å] is shorter than the equivalent value found in the related acetonitrile complex *trans*-[PdBr₂(NHC)-(NCCH₃)] [NHC = *N,N'*-diisopropylbenzimidazolin-2-ylidene; 1.936(2) Å].^[10]

The molecular structures of complexes **3c** and **3d** exhibit the proposed square-planar geometry with a *cis* arrangement of the two bromido ligands. The Pd–C1 bond lengths in **3c** [1.979(3) Å] and **3d** [1.982(3) Å] (Table 1, Figure 2)

compare well with the corresponding parameters in palladium(II) NHC complexes with a *trans* arrangement of the NHC ligand relative to a halogenato ligand.^[13a,14]

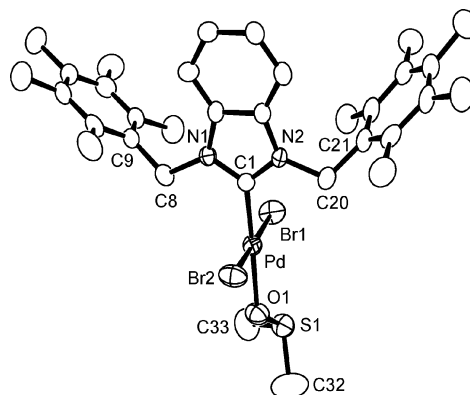


Figure 1. Molecular structure of **2c**.

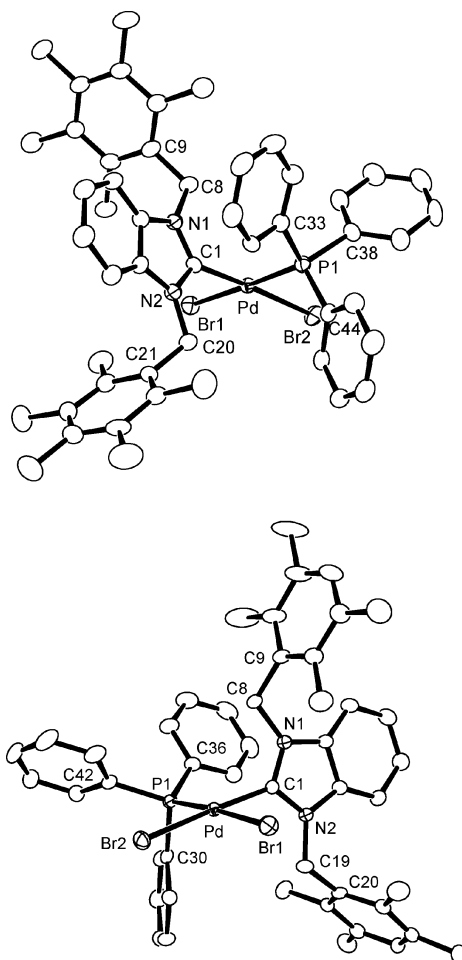


Figure 2. Molecular structures of **3c** (top) and **3d** (bottom).

The Br1–Pd–Br2 [173.26(2)°] and C1–Pd–P1 [173.30(11)] angles in *trans* complex **5b** (Figure 3) do not measure 180°. Apparently, for steric reasons, the bromido ligands are bent towards the NHC ligand. In both complexes, the planar ring of the NHC ligand is oriented in a perpendicular fashion to the plane that is formed by the approximately square-

planar coordination of the palladium(II) center. The C1–Pd bond length measures 2.031(4) Å. Similar Pd^{II}–C_{carbene} bond lengths were observed for complexes of the type *trans*-[PdX₂(NHC)PR₃].^[15] The Pd–C_{carbene} bond length in **5b** is significantly longer than the equivalent parameter in **3c** and **3d**. This lengthening is attributable to the stronger *trans* influence of the phosphane ligands than the *trans* bromido ligands in complexes **3**.

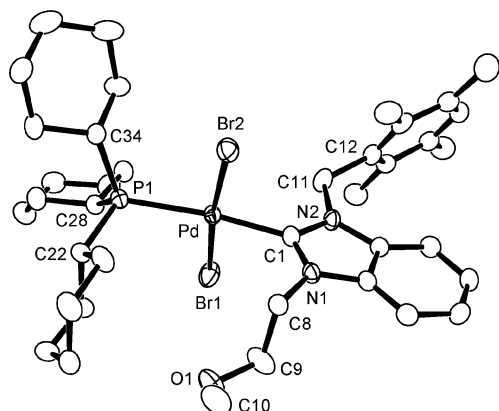


Figure 3. Molecular structure of **5b**.

Catalytic Studies

Palladium(II) catalysts derived from a mixed donor set made up from phosphanes and NHCs have been shown to display an increased activity in carbon–carbon bond-forming reactions.^[7,8] Our recent studies indicated that complexes bearing MeOCH₂CH₂/CH₂Ar substituted NHC ligands are more active than those derived from simple alkyl-substituted NHC ligands.^[16] We therefore became interested to find out if such substituents are important for the catalytic activity of palladium(II) complexes with a mixed phosphane/benzimidazolin-2-ylidene ligand set.

Pd^{II} NHC complexes **2–7** were screened in the model reaction between *n*-butyl acrylate and aryl halides under identical conditions (in dma at 100 °C, reaction time 2 h, Cs₂CO₃ as base). The results of the catalytic reactions are summarized in Table 2. No difference in activity was observed for dinuclear complexes **2a** relative to the mononuclear complexes of the type [PdBr₂(NHC)(dmsol)] (**2b–d**; Table 2, entries 1–4). *trans*-Biscarbene complexes **7a–d** exhibited the lowest activities in the coupling reactions (Table 2, entries 21–24). The catalytic activity of palladium complexes with a mixed phosphane/benzimidazolin-2-ylidene ligand set compares favorably with the data reported for other palladium NHC complexes. The NHC complexes containing a 2-methoxyethyl substituent on N³ (**a** and **b**) display slightly better activity than the **c** and **d** series, presumably due to the hemilabile OMe group.

Trialkylphosphane (PCy₃)-ligated complexes **5** exhibit a lower catalytic activity relative to that of the complexes bearing triarylphosphane (PPh₃, PPh₂py) ligands **3** and **4**.

Table 2. Palladium-catalyzed C–C coupling reaction of *n*-butyl acrylate with aryl halides.

Entry	Catalyst	mol-% Pd	X	Yield [%]
1	2a	3.0	Br	42
2	2b	3.0	Br	43
3	2c	3.0	Br	45
4	2d	3.0	Br	44
5	3a	3.0	Br	60
6	3b	3.0	Br	59
7	3c	3.0	Br	58
8	3d	3.0	Br	59
9	4a	3.0	Br	67
10	4b	3.0	Br	69
11	4c	3.0	Br	64
12	4d	3.0	Br	65
13	5a	3.0	Br	68
14	5b	3.0	Br	63
15	5c	3.0	Br	65
16	5d	3.0	Br	60
17	6a	3.0	Br	88
18	6b	3.0	Br	90
19	6c	3.0	Br	74
20	6d	3.0	Br	72
21	7a	3.0	Br	37
22	7b	3.0	Br	39
23	7c	3.0	Br	25
24	7d	3.0	Br	22
25	6a	3.0	Cl	21
26	6b	3.0	Cl	24
27	6a	3.0	Cl	56 ^[a]
28	6b	3.0	Cl	61 ^[a]
29	6a	3.0	Cl	98 ^[b]
30	6b	3.0	Cl	94 ^[b]
31	6a	1.0	Br	39
32	6b	1.0	Br	42
33	6b	0.5	Br	24
34	6b	0.1	Br	10
35	6b	0.01	Br	2
36	PdBr ₂ (PPh ₃) ₂	3.0	Br	5

[a] With the addition of 1.5 equiv. of [N(*n*C₄H₉)₄]Br. [b] Reaction time 24 h.

The data in Table 2 also indicate that cationic complexes **6** with a carbene/diphosphane ligand set are highly efficient in the coupling reaction of aryl bromides (Table 2, entries 16–20) under similar conditions. With catalysts **6a** and **6b**, 4-bromoacetophenone can be coupled with good yields but the catalysts are not active in the case of 4-chloroacetophenone under standard conditions. The general activity trend is as follows: **6** > **5** > **4** > **3** > **2** > **7**, and this trend is consistent with the previous studies on Pd^{II}NHC complexes.^[7b,8,17] Heck reactions were then attempted at lower catalysts loadings. The activity decreased dramatically and only poor conversions were obtained under the same conditions (Table 2, entries 31–35).

Conclusions

Mixed palladium(II) complexes of NHCs and phosphanes were prepared and characterized inclusive of the deter-

mination of the molecular structures of complexes **2c**, **3c**·2CH₂Cl₂, **3d**·CH₂Cl₂, and **5b**. The molecular structures reveal no unexpected features. Palladium(II) complexes with unsymmetrically *N,N'*-substituted benzimidazolin-2-ylidene ligands generally exhibit a higher catalytic activity in the Mizoroki–Heck coupling reaction than those with symmetrically substituted NHC ligands. The highest catalytic activity was observed for cationic palladium(II) complexes **6** bearing unsymmetrically substituted NHC ligands in addition to a diphosphane ligand.

Experimental Section

General Considerations: All reactions for the preparation of **2–7** were carried out under an atmosphere of argon in flame-dried standard Schlenk-type flasks. Anhydrous solvents were either distilled from appropriate drying agents or purchased from Merck and degassed prior to use by purging with dry argon and kept over molecular sieves. All other reagents were commercially available and used as received. NMR spectra were recorded at 297 K with a Varian Mercury AS 400 spectrometer at 400 (¹H) or 100.56 MHz (¹³C). Elemental analyses were carried out by the analytical service of TUBITAK with a Carlo Erba Instrumentazione Model 1106 apparatus. Mass spectra were measured with a Varian MAT 212 instrument.

***N*-(Pentamethylbenzyl)-*N'*-(2-methoxyethyl)benzimidazolium Bromide (**1a**):** Yield: 0.39 g, 94.0%. ¹H NMR (400 MHz, CDCl₃): δ = 9.83 (s, 1 H, NCHN), 7.94 (m, 1 H, Ar-H), 7.60 (m, 1 H, Ar-H), 7.54 (m, 1 H, Ar-H), 7.52 (m, 1 H, Ar-H), 5.73 [s, 2 H, CH₂C₆(CH₃)₅], 4.90 (t, *J* = 2.4 Hz, 2 H, NCH₂CH₂OCH₃), 3.82 (t, *J* = 2.4 Hz, 2 H, NCH₂CH₂OCH₃), 3.24 (s, 3 H, NCH₂CH₂OCH₃), 2.25 [s, 3 H, *p*-C₆(CH₃)₅], 2.24 [s, 6 H, *m*-C₆(CH₃)₅], 2.22 [s, 6 H, *o*-C₆(CH₃)₅] ppm. ¹³C NMR (100 MHz, CDCl₃): δ = 141.5 (NCHN), 137.3, 133.9, 133.4, 132.2, 131.0, 128.6, 127.0, 124.3, 114.2, 113.0 [Ar-C and C₆(CH₃)₅], 69.9 (NCH₂CH₂OCH₃), 58.8 (NCH₂CH₂OCH₃), 47.7 (NCH₂CH₂OCH₃), 47.6 [NCH₂C₆(CH₃)₅], 17.2 [*p*-C₆(CH₃)₅], 20.5 [*m*-C₆(CH₃)₅], 20.4 [*o*-C₆(CH₃)₅] ppm. MS (MALDI): *m/z* = 337 [M – Br]⁺. C₂₂H₂₉BrN₂O (417.4): calcd. C 63.31, H 7.00, N 6.71; found C 63.22, H 7.01, N 6.88.

***N*-(2,3,5,6-Tetramethylbenzyl)-*N'*-(2-methoxyethyl)benzimidazolium Bromide (**1b**):** Yield: 0.38 g, 95.0%. ¹H NMR (400 MHz, CDCl₃): δ = 9.83 (s, 1 H, NCHN), 7.98 (m, 1 H, Ar-H), 7.94 (m, 1 H, Ar-H), 7.62 (m, 1 H, Ar-H), 7.54 [s, 1 H, C₆H(CH₃)₄], 7.52 (m, 1 H, Ar-H), 5.73 [s, 2 H, CH₂C₆H(CH₃)₄], 4.91 (t, *J* = 2.4 Hz, 2 H, NCH₂CH₂OCH₃), 3.83 (t, *J* = 2.4 Hz, 2 H, NCH₂CH₂OCH₃), 3.25 (s, 3 H, NCH₂CH₂OCH₃), 2.24 [s, 6 H, *m*-C₆H(CH₃)₄], 2.23 [s, 6 H, *o*-C₆H(CH₃)₄] ppm. ¹³C NMR (100 MHz, CDCl₃): δ = 141.8 (NCHN), 135.1, 133.4, 133.5, 133.2, 131.0, 127.2, 127.1, 114.1, 113.6, 113.0 [Ar-C and C₆H(CH₃)₄], 69.9 (NCH₂CH₂OCH₃), 58.8 (NCH₂CH₂OCH₃), 47.8 (NCH₂CH₂OCH₃), 47.2 [NCH₂C₆H(CH₃)₄], 20.5 [*m*-C₆H(CH₃)₄], 20.4 [*o*-C₆H(CH₃)₄] ppm. MS (MALDI): *m/z* = 323 [M – Br]⁺. C₂₁H₂₇BrN₂O (403.4): calcd. C 62.53, H 6.75, N 6.95; found C 62.42, H 6.73, N 7.00.

***N,N'*-Bis(pentamethylbenzyl)benzimidazolium Bromide (**1c**):** Yield: 0.47 g, 91.0%. ¹H NMR (400 MHz, CDCl₃): δ = 9.73 (s, 1 H, NCHN), 7.43–7.41 (m, 4 H, Ar-H), 7.35 [s, 4 H, CH₂C₆(CH₃)₅], 2.24 [s, 6 H, *p*-C₆(CH₃)₅], 2.21 [s, 12 H, *m*-C₆(CH₃)₅], 2.19 [s, 12 H, *o*-C₆(CH₃)₅] ppm. ¹³C NMR (100 MHz, CDCl₃): δ = 141.6 (NCHN), 137.0, 133.7, 133.3, 131.7, 127.0, 125.0, 113.7 [Ar-C and C₆(CH₃)₅], 48.4 [NCH₂C₆(CH₃)₅], 17.2 [*p*-C₆(CH₃)₅], 16.9 [*m*-C₆(CH₃)₅], 16.8 [*o*-C₆(CH₃)₅] ppm. MS (MALDI): *m/z* = 439 [M –

Br]⁺. C₃₁H₃₉BrN₂ (519.6): calcd. C 71.66, H 7.57, N 5.39; found C 71.72, H 7.58, N 5.28.

***N,N'*-Bis(2,3,5,6-tetramethylbenzyl)benzimidazolium Bromide (**1d**):** Yield: 0.43 g, 88.0%. ¹H NMR (400 MHz, CDCl₃): δ = 9.74 (s, 1 H, NCHN), 7.40–7.36 [m, 6 H, NCH₂C₆H(CH₃)₄ and Ar-H], 7.25 [s, 4 H, CH₂C₆H(CH₃)₄], 2.27 [s, 12 H, *m*-C₆H(CH₃)₄], 2.21 [s, 12 H, *o*-C₆H(CH₃)₄] ppm. ¹³C NMR (100 MHz, CDCl₃): δ = 141.3 (NCHN), 137.1, 134.2, 133.1, 131.2, 127.5, 125.0, 112.9 [Ar-C and C₆H(CH₃)₄], 48.3 [NCH₂C₆H(CH₃)₄], 17.3 [*m*-C₆H(CH₃)₄], 16.8 [*o*-C₆H(CH₃)₄] ppm. MS (MALDI): *m/z* = 411 [M – Br]⁺. C₂₉H₃₅BrN₂ (491.5): calcd. C 70.87, H 7.18, N 5.70; found C 70.72, H 7.17, N 5.58.

***trans*-Dibromido(μ-dibromido)bis[*N*-(pentamethylbenzyl)-*N'*-(2-methoxyethyl)benzimidazolin-2-ylidene]dipalladium(II) (**2a**):** A dmsO solution (10 mL) containing 1,3-alkylbenzimidazolium bromide **1** (0.417 g, 1.0 mmol), Pd(OAc)₂ (0.225 g, 1.0 mmol), and NaBr (0.309 g, 3.0 mmol) was stirred at 90 °C for 24 h. The dmsO was then removed in vacuo, and the remaining solid was washed with diethyl ether. The solid residue was crystallized from CH₂Cl₂/EtOH. Yield: 0.93 g, 77%. ¹H NMR (400 MHz, CDCl₃): δ = 7.52 (d, *J* = 4.0 Hz, 2 H, Ar-H), 7.15 (t, *J* = 3.9 Hz, 2 H, Ar-H), 6.90 (t, *J* = 3.8 Hz, 2 H, Ar-H), 6.32 [s, 4 H, NCH₂C₆(CH₃)₅], 6.25 (d, *J* = 4.2 Hz, 2 H, Ar-H), 5.08 (br. m, 4 H, NCH₂CH₂OCH₃), 4.21 (t, *J* = 2.3 Hz, 4 H, NCH₂CH₂OCH₃), 3.35 (s, 6 H, NCH₂CH₂OCH₃), 2.33 [s, 12 H, *o*-C₆(CH₃)₅], 2.25 [s, 6 H, *p*-C₆(CH₃)₅], 2.23 [s, 12 H, *m*-C₆(CH₃)₅] ppm. ¹³C NMR (100 MHz, CDCl₃): δ = 160.3 (NCN), 136.4, 134.9, 134.7, 134.3, 132.6, 131.1, 122.9, 122.5, 111.8, 111.1 [Ar-C and C₆(CH₃)₅], 71.9 (NCH₂CH₂OCH₃), 59.4 (NCH₂CH₂OCH₃), 51.7 [NCH₂C₆H(CH₃)₄], 48.4 (NCH₂CH₂OCH₃), 21.3 [*p*-C₆(CH₃)₅], 20.8 [*m*-C₆(CH₃)₅], 17.0 [*o*-C₆(CH₃)₅] ppm. MS (MALDI): *m/z* = 1125 [M – Br]⁺. C₄₄H₅₆Br₄N₄O₂Pd₂ (1205.4): calcd. C 43.84, H 4.68, N 4.65; found C 43.83, H 4.63, N 4.59.

***trans*-Dibromido(dimethyl sulfoxide)[*N*-(2,3,5,6-tetramethylbenzyl)-*N'*-(2-methoxyethyl)benzimidazolin-2-ylidene]palladium(II) (**2b**):** The complex was prepared as described for **2a** by using **1b**. Yield: 0.53 g, 77%. ¹H NMR (400 MHz, CDCl₃): δ = 7.53 (d, *J* = 4.2 Hz, 1 H, Ar-H), 7.37 (m, 1 H, Ar-H), 7.14 [s, 1 H, C₆H(CH₃)₄], 6.92 (m, 1 H, Ar-H), 6.32–6.27 [m, 3 H, Ar-H and NCH₂C₆H(CH₃)₄], 5.10 (br. m, 2 H, NCH₂CH₂OCH₃), 4.33 (t, *J* = 2.3 Hz, 1 H, NCH₂CH₂OCH₃), 3.73 (t, *J* = 2.3 Hz, 1 H, NCH₂CH₂OCH₃), 3.39 (s, 6 H, dmsO), 3.36 (s, 3 H, NCH₂CH₂OCH₃), 2.29 [s, 6 H, *o*-C₆H(CH₃)₄], 2.25 [s, 6 H, *m*-C₆H(CH₃)₄] ppm. ¹³C NMR (100 MHz, CDCl₃): δ = 158.5 (NCN), 136.0, 135.3, 134.8, 134.5, 132.6, 131.1, 122.9, 122.5, 111.8, 111.1 [Ar-C and C₆H(CH₃)₄], 71.9 (NCH₂CH₂OCH₃), 59.4 (NCH₂CH₂OCH₃), 51.7 [NCH₂C₆H(CH₃)₄], 48.4 (NCH₂CH₂OCH₃), 20.8 [*m*-C₆H(CH₃)₄], 17.0 [*o*-C₆H(CH₃)₄] ppm. MS (MALDI): *m/z* = 509 [M – Br – dmsO]⁺. C₂₃H₃₂Br₂N₂O₂PdS (666.8): calcd. C 41.43, H 4.84, N 4.20; found C 41.29, H 5.00, N 4.19.

***trans*-Dibromido(dimethyl sulfoxide)bis[*N,N'*-bis(pentamethylbenzyl)benzimidazolin-2-ylidene]dipalladium(II) (**2c**):** The complex was prepared as described for **2a** by using **1c**. Yield: 0.65 g, 83.0%. ¹H NMR (400 MHz, CDCl₃): δ = 6.81 (m, 2 H, Ar-H), 6.35 (m, 2 H, Ar-H), 6.30 [s, 4 H, CH₂C₆(CH₃)₅], 3.39 (s, 6 H, dmsO), 2.29 [s, 12 H, *o*-C₆(CH₃)₅], 2.25 [s, 12 H, *m*-C₆(CH₃)₅], 2.25 [s, 6 H, *p*-C₆(CH₃)₅] ppm. ¹³C NMR (100 MHz, CDCl₃): δ = 157.9 (NCN), 136.4, 135.2, 135.0, 132.9, 129.1, 122.1, 111.6 [Ar-C and C₆(CH₃)₅], 52.3 [CH₂C₆(CH₃)₅], 18.9 [*p*-C₆(CH₃)₅], 17.9 [*m*-C₆(CH₃)₅], 17.4 [*o*-C₆(CH₃)₅] ppm. MS (MALDI): *m/z* (%) = 625 [M –

Br – dmsol⁺. C₃₃H₄₄Br₂N₂OPdS (783.0): calcd. C 50.62, H 5.66, N 3.58; found C 50.43, H 5.55, N 3.63.

trans-Dibromido(dimethyl sulfoxide)bis[*N,N'*-bis(2,3,5,6-tetramethylbenzyl)benzimidazolin-2-ylidene]dipalladium (2d): The complex was prepared as described for **2a** by using **1d**. Yield: 0.60 g, 80.0%. ¹H NMR (400 MHz, CDCl₃): δ = 6.78 (m, 2 H, Ar-H), 6.39 (m, 2 H, Ar-H), 6.35 [s, 2 H, CH₂C₆H(CH₃)₄], 6.31 [s, 4 H, CH₂C₆H(CH₃)₄], 3.37 (s, 6 H, dmsol), 2.31 [s, 12 H, *o*-C₆H(CH₃)₄], 2.27 [s, 12 H, *m*-C₆H(CH₃)₄] ppm. ¹³C NMR (100 MHz, CDCl₃): δ = 157.8 (NCN), 136.3, 135.1, 135.0, 132.3, 129.2, 122.2, 111.7 [Ar-C and C₆H(CH₃)₄], 52.1 [CH₂C₆H(CH₃)₄], 17.2 [*m*-C₆H(CH₃)₄], 16.9 [*o*-C₆H(CH₃)₄] ppm. MS (MALDI): *m/z* = 597 [M – Br – dmsol]⁺. C₃₁H₄₀Br₂N₂OPdS (754.9): calcd. C 49.32, H 5.34, N 3.71; found C 49.39, H 5.35, N 3.63.

cis-Dibromido[*N*-(pentamethylbenzyl)-*N'*-(2-methoxyethyl)benzimidazolin-2-ylidene](triphenylphosphane)palladium (3a): A sample of **2a** (1.205 g, 1.0 mmol) and PPh₃ (0.524 g, 2.0 mmol) was dissolved in dichloromethane (10 mL). The mixture was stirred at ambient temperature for 20 min. The solvent was then removed in vacuo. The solid residue obtained was dissolved in a few milliliters of dichloromethane, and the resulting solution was added dropwise to diethyl ether (30 mL). The bright yellow precipitate obtained was collected by filtration, washed with diethyl ether (10 mL), and dried in vacuo. Yield: 1.68 g, 93.0%. ¹H NMR (400 MHz, CDCl₃): δ = 7.96 (br. m, 4 H, PPh₃-H), 7.43 (br. m, 6 H, PPh₃-H), 6.57–6.34 (m, 7 H, PPh₃-H and Ar-H), 5.72–5.56 (m, 2 H, Ar-H), 5.09, [s, 2 H, CH₂C₆H(CH₃)₅], 4.89 (t, *J* = 1.8 Hz, 2 H, NCH₂CH₂OCH₃), 3.99 (m, 2 H, NCH₂CH₂OCH₃), 3.33 (s, 3 H, NCH₂CH₂OCH₃), 2.20 [s, 6 H, *o*-C₆H(CH₃)₅], 2.13 [s, 6 H, *m*-C₆H(CH₃)₅], 1.89 [s, 3 H, *p*-C₆H(CH₃)₅] ppm. ¹³C NMR (100 MHz, CDCl₃): δ = 175.4 (NCN), 135.6, 135.3, 134.7, 133.1, 128.9, 128.6, 126.2, 122.3, 111.9 [Ar-C and PPh₃-C and C₆H(CH₃)₅], 71.0 (NCH₂CH₂OCH₃), 58.3 (NCH₂CH₂OCH₃), 51.8 [CH₂C₆H(CH₃)₅], 50.1 (NCH₂CH₂OCH₃), 20.7 [*p*-C₆H(CH₃)₅], 18.2 [*m*-C₆H(CH₃)₅], 17.5 [*o*-C₆H(CH₃)₅] ppm. ³¹P NMR (162.0 MHz, CDCl₃): δ = 26.7 ppm. MS (MALDI): *m/z* = 785 [M – Br]⁺. C₄₀H₄₃Br₂N₂OPd (864.98): calcd. C 55.54, H 5.01, N 3.24; found C 55.41, H 5.13, N 3.19.

cis-Dibromido[*N*-(2,3,5,6-tetramethylbenzyl)-*N'*-(2-methoxyethyl)benzimidazolin-2-ylidene](triphenylphosphane)palladium (3b): A sample of **2b** (0.667 g, 1.0 mmol) and PPh₃ (0.262 g, 1.0 mmol) was dissolved in dichloromethane (15 mL). The mixture was stirred at ambient temperature for 20 min. The solvent was removed in vacuo. The solid residue obtained was dissolved in a few milliliters of dichloromethane, and the resulting solution added dropwise to diethyl ether (30 mL). The bright yellow precipitate obtained was collected by filtration, washed with diethyl ether (10 mL), and dried in vacuo. Yield: 0.76 g, 90.0%. ¹H NMR (400 MHz, CDCl₃): δ = 7.92 (br. m, 4 H, PPh₃-H), 7.33 (br. m, 6 H, PPh₃-H), 6.54 [s, 1 H, C₆H(CH₃)₄], 6.48–6.39 (m, 6 H, PPh₃-H and Ar-H), 5.72 (t, *J* = 1.8 Hz, 2 H, Ar-H), 5.54 (d, *J* = 1.7 Hz, 1 H, Ar-H), 5.09, [s, 2 H, CH₂C₆H(CH₃)₄], 4.90 (t, *J* = 1.8 Hz, 2 H, NCH₂CH₂OCH₃), 3.98 (m, 2 H, NCH₂CH₂OCH₃), 3.34 (s, 3 H, NCH₂CH₂OCH₃), 2.13 [s, 6 H, *o*-C₆H(CH₃)₄], 1.89 [s, 6 H, *m*-C₆H(CH₃)₄] ppm. ¹³C NMR (100 MHz, CDCl₃): δ = 175.2 (NCN), 136.4, 135.2, 134.7, 133.3, 128.7, 128.6, 126.2, 122.1, 111.9 [Ar-C and PPh₃-C and C₆H(CH₃)₄], 70.7 (NCH₂CH₂OCH₃), 58.0 (NCH₂CH₂OCH₃), 51.4 [CH₂C₆H(CH₃)₄], 51.1 (NCH₂CH₂OCH₃), 20.7 [*m*-C₆H(CH₃)₄], 17.5 [*o*-C₆H(CH₃)₄] ppm. ³¹P NMR (162.0 MHz, CDCl₃): δ = 25.9 ppm. MS (MALDI): *m/z* = 771 [M – Br]⁺. C₃₉H₄₁Br₂N₂OPd (850.95): calcd. C 55.05, H 4.86, N 3.29; found C 55.52, H 5.00, N 3.31.

cis-Dibromido[*N,N'*-bis(pentamethylbenzyl)benzimidazolin-2-ylidene](triphenylphosphane)palladium(II) (3c): The complex was pre-

pared as described for **3b** by using **2c**. Yield: 0.88 g, 91.0%. ¹H NMR (400 MHz, CDCl₃): δ = 7.96 (br. m, 4 H, PPh₃-H), 7.40 (br. m, 6 H, PPh₃-H), 6.54 (m, 7 H, PPh₃-H and Ar-H), 5.72 (m, 2 H, Ar-H), 5.07, [s, 2 H, CH₂C₆H(CH₃)₅], 5.01 [s, 2 H, CH₂C₆H(CH₃)₅], 2.20 [s, 12 H, *o*-C₆H(CH₃)₅], 2.10 [s, 12 H, *m*-C₆H(CH₃)₅], 1.89 [s, 6 H, *p*-C₆H(CH₃)₅] ppm. ¹³C NMR (100 MHz, CDCl₃): δ = 175.1 (NCN), 136.3, 135.7, 134.7, 133.2, 128.8, 128.6, 127.2, 122.5, 111.4 [Ar-C and PPh₃-C and C₆H(CH₃)₅], 52.2 [CH₂C₆H(CH₃)₅], 17.7 [*p*-C₆H(CH₃)₅], 17.5 [*m*-C₆H(CH₃)₅], 17.1 [*o*-C₆H(CH₃)₅] ppm. ³¹P NMR (162.0 MHz, CDCl₃): δ = 26.7 ppm. MS (MALDI): *m/z* = 887 [M – Br]⁺. C₄₉H₅₃Br₂N₂PPd (967.16): calcd. C 60.85, H 5.52, N 2.90; found C 60.81, H 5.53, N 2.79.

cis-Dibromido[*N,N'*-bis(2,3,5,6-tetramethylbenzyl)benzimidazolin-2-ylidene](triphenylphosphane)palladium (3d): The complex was prepared as described for **3b** by using **2d**. Yield: 0.85 g, 91.0%. ¹H NMR (400 MHz, CDCl₃): δ = 8.06 (br. m, 4 H, PPh₃-H), 7.48 (br. m, 6 H, PPh₃-H), 7.02 [s, 2 H, C₆H(CH₃)₄], 6.59 (m, 7 H, PPh₃-H and Ar-H), 5.72 (m, 2 H, Ar-H), 5.12 [s, 2 H, CH₂C₆H(CH₃)₄], 5.08 [s, 2 H, CH₂C₆H(CH₃)₄], 2.19 [s, 12 H, *o*-C₆H(CH₃)₄], 1.92 [s, 12 H, *m*-C₆H(CH₃)₄] ppm. ¹³C NMR (100 MHz, CDCl₃): δ = 175.4 (NCN), 135.6, 135.2, 134.4, 133.0, 129.7, 128.8, 128.7, 122.6, 111.3 [Ar-C and PPh₃-C and C₆H(CH₃)₄], 51.5 [CH₂C₆H(CH₃)₄], 20.7 [*m*-C₆H(CH₃)₄], 16.7 [*o*-C₆H(CH₃)₄] ppm. ³¹P NMR (162.0 MHz, CDCl₃): δ = 26.8 ppm. MS (MALDI): *m/z* = 859 [M – Br]⁺. C₄₇H₄₉Br₂N₂PPd (939.1): calcd. C 60.11, H 5.26, N 2.98; found C 60.11, H 5.33, N 2.99.

cis-Dibromido[*N*-(2-methoxyethyl)-*N'*-(pentamethylbenzyl)benzimidazolin-2-ylidene](diphenyl-2-pyridylphosphane)palladium (4a): The complex was prepared as described for **3a** by using **2a** and PPh₂(2-py). Yield: 0.81 g, 94.0%. ¹H NMR (400 MHz, CDCl₃): δ = 7.91 [m, 4 H, PPh₂(2-py)-H], 7.51–7.33 [m, 8 H, PPh₂(2-py)-H], 7.21 [br. m, 1 H, PPh₂(2-py)-H], 7.20 (d, *J* = 2 Hz, 1 H, Ar-H), 7.02 (td, *J* = 2, 1 Hz, Ar-H), 6.94 [br., 1 H, PPh₂(2-py)-H], 6.76 (td, *J* = 2 Hz, 1 H, Ar-H), 6.36 [d, *J* = 3.2 Hz, 1 H, CHHC₆(CH₃)₅], 5.80 (d, *J* = 2 Hz, 1 H, Ar-H), 5.35 [d, *J* = 3.6 Hz, 1 H, CHHC₆(CH₃)₅], 4.80 (t, *J* = 1.7 Hz, 1 H, NCH₂CH₂OCH₃), 4.08 (t, *J* = 1.7 Hz, 1 H, NCH₂CH₂OCH₃), 3.91 (m, 2 H, NCH₂CH₂OCH₃), 3.21 (s, 3 H, NCH₂CH₂OCH₃), 2.29 [s, 6 H, *o*-C₆H(CH₃)₅], 2.20 [s, 6 H, *m*-C₆H(CH₃)₅], 2.02 [s, 3 H, *p*-C₆H(CH₃)₅] ppm. ¹³C NMR (100 MHz, CDCl₃): δ = 174.5 (NCN), 148.4 [d, ¹*J*_{PC} = 15.7 Hz, PPh₂(2-py)-C], 137.7 [d, ³*J*_{PC} = 8.9 Hz, PPh₂(2-py)-C], 136.1, 135.3, 133.8, 133.6, 129.1, 127.5, 126.6, 123.3, 111.4 [Ar-C and PPh₂(2-py)-C and C₆H(CH₃)₅], 71.3 (NCH₂CH₂OCH₃), 59.0 (NCH₂CH₂OCH₃), 52.1 [CH₂C₆H(CH₃)₅], 52.3 (NCH₂CH₂OCH₃), 19.5 [*p*-C₆H(CH₃)₅], 18.1 [*m*-C₆H(CH₃)₅], 17.2 [*o*-C₆H(CH₃)₅] ppm. ³¹P NMR (162.0 MHz, CDCl₃): δ = 25.8 ppm. MS (MALDI): *m/z* = 786 [M – Br]⁺. C₃₉H₄₂Br₂N₃OPd (865.97): calcd. C 54.09, H 4.89, N 4.85; found C 54.12, H 5.01, N 4.88.

cis-Dibromido[*N*-(2-methoxyethyl)-*N'*-(2,3,4,5-tetramethylbenzyl)benzimidazolin-2-ylidene](diphenyl-2-pyridylphosphane)palladium (4b): The complex was prepared as described for **3a** by using **2b** and PPh₂(2-py). Yield: 0.74 g, 87%. ¹H NMR (400 MHz, CDCl₃): δ = 7.94–7.84 [m, 4 H, PPh₂(2-py)-H], 7.54–7.46 [m, 6 H, PPh₂(2-py)-H], 7.22–6.93 [m, 3 H, PPh₂(2-py)-H and Ar-H], 6.83 [br. m, 2 H, PPh₂(2-py)-H], 6.76 (t, *J* = 1.9 Hz, 1 H, Ar-H), 6.50 (d, *J* = 3.2 Hz, 1 H, Ar-H), 6.26 [s, 1 H, C₆H(CH₃)₄], 5.71 (d, *J* = 1.1 Hz, 1 H, Ar-H), 5.35 [s, 1 H, CHHC₆H(CH₃)₄], 5.29 [s, 1 H, CHHC₆H(CH₃)₄], 4.20 (br. m, 2 H, NCH₂CH₂OCH₃), 4.08 (t, *J* = 1.7 Hz, 2 H, NCH₂CH₂OCH₃), 3.21 (s, 3 H, NCH₂CH₂OCH₃), 2.26 [s, 6 H, *o*-C₆H(CH₃)₄], 2.03 [s, 6 H, *m*-C₆H(CH₃)₄] ppm. ¹³C NMR (100 MHz, CDCl₃): δ = 174.1 (NCN), 148.1 [d, ¹*J*_{PC} = 16.2 Hz, PPh₂(2-py)-C], 137.3 [d, ³*J*_{PC} = 9.0 Hz, PPh₂(2-py)-C],

131.3, 128.6, 128.3, 125.7, 123.4, 122.9, 122.1, 111.5, 111.2, 111.0 [Ar-C and PPh₂(2-py)-C and C₆(CH₃)₅], 71.5 (NCH₂CH₂OCH₃), 59.1 (NCH₂CH₂OCH₃), 51.6 [CH₂C₆H(CH₃)₄], 49.1 (NCH₂CH₂OCH₃), 20.6 [m-C₆H(CH₃)₄], 16.6 [o-C₆H(CH₃)₄] ppm. ³¹P NMR (162.0 MHz, CDCl₃): δ = 26.6 ppm. MS (MALDI): *m/z* = 771 [M – Br]⁺. C₃₈H₄₀Br₂N₃OPPd (851.9): calcd. C 53.57, H 4.73, N 4.93; found C 53.62, H 4.85, N 4.98.

cis-Dibromido[N,N'-bis(pentamethylbenzyl)benzimidazolin-2-ylidene](diphenyl-2-pyridylphosphane)palladium (4c): The complex was prepared as described for **3a** by using **2c** and PPh₂(2-py). Yield: 0.90 g, 93.0%. ¹H NMR (400 MHz, CDCl₃): δ = 7.95 [br. m, 4 H, PPh₂(2-py)-H], 7.45 [d, *J* = 0.8 Hz, 6 H, PPh₂(2-py)-H], 7.13 [s, 1 H, PPh₂(2-py)-H], 6.83 [br. m, 3 H, PPh₂(2-py)-H], 6.58 [s, 2 H, Ar-H], 6.50 (d, *J* = 3.2 Hz, 2 H, Ar-H), 5.81 (d, *J* = 3.2 Hz, 2 H, Ar-H), 5.29–5.22 [m, 4 H, CH₂C₆(CH₃)₅], 2.27 [s, 12 H, o-C₆(CH₃)₅], 2.18 [s, 12 H, m-C₆(CH₃)₅], 2.03 [s, 6 H, p-C₆(CH₃)₅] ppm. ¹³C NMR (100 MHz, CDCl₃): δ = 173.9 (NCN), 149.6 [d, ¹J_{PC} = 16.1 Hz, PPh₂(2-py)-C], 136.8 [d, ³J_{PC} = 9.1 Hz, PPh₂(2-py)-C], 136.4, 135.6, 134.9, 133.2, 131.6 [Ar-C and PPh₂(2-py)-C and C₆(CH₃)₅], 128.9 [d, ²J_{PC} = 10.7 Hz, PPh₂(2-py)-C], 127.5, 122.2, 111.4 [Ar-C, PPh₂(2-py)-C], 52.3 [CH₂C₆(CH₃)₅], 17.6 [p-C₆(CH₃)₅], 17.5 [m-C₆(CH₃)₅], 17.0 [o-C₆(CH₃)₅] ppm. ³¹P NMR (162.0 MHz, CDCl₃): δ = 27.3 ppm. MS (MALDI): *m/z* = 888 [M – Br]⁺. C₄₈H₅₂Br₂N₃PPd (968.14): calcd. C 59.55, H 5.41, N 4.34; found C 59.71, H 5.43, N 4.29.

cis-Dibromido[N,N'-bis(2,3,5,6-tetramethylbenzyl)benzimidazolin-2-ylidene](diphenyl-2-pyridylphosphane)palladium (4d): The complex was prepared as described for **3a** by using **2d** and PPh₂(2-py). Yield: 0.85 g, 90.0%. ¹H NMR (400 MHz, CDCl₃): δ = 7.94 [br. m, 4 H, PPh₂(2-py)-H], 7.49 [d, *J* = 0.7 Hz, 6 H, PPh₂(2-py)-H], 7.12 [s, 1 H, PPh₂(2-py)-H], 6.90 [br. m, 3 H, PPh₂(2-py)-H], 6.53 [s, 2 H, CH₂C₆H(CH₃)₄], 6.50 (d, *J* = 3.0 Hz, 2 H, Ar-H), 5.83 (d, *J* = 3.0 Hz, 2 H, Ar-H), 5.27–5.20 [m, 4 H, CH₂C₆H(CH₃)₄], 2.25 [s, 12 H, o-C₆H(CH₃)₄], 2.19 [s, 12 H, m-C₆(CH₃)₅] ppm. ¹³C NMR (100 MHz, CDCl₃): δ = 172.9 (NCN), 149.7 [d, ¹J_{PC} = 16.0 Hz, PPh₂(2-py)-C], 136.3 [d, ³J_{PC} = 9.3 Hz, PPh₂(2-py)-C], 136.1, 135.2, 134.7, 134.2, 132.0 [Ar-C and PPh₂(2-py)-C and C₆H(CH₃)₄-C], 128.9 [d, ²J_{PC} = 10.0 Hz, PPh₂(2-py)-C], 127.6, 121.9, 111.1 [Ar-C and PPh₂(2-py)-C and C₆H(CH₃)₄-C], 52.0 [CH₂C₆H(CH₃)₄], 17.6 [m-C₆H(CH₃)₅], 17.1 [o-C₆H(CH₃)₄] ppm. ³¹P NMR (162.0 MHz, CDCl₃): δ = 27.8 ppm. MS (MALDI): *m/z* = 860 [M – Br]⁺. C₄₆H₄₈Br₂N₃PPd (940.1): calcd. C 58.77, H 5.15, N 4.47; found C 58.71, H 5.18, N 4.46.

trans-Dibromido[N-(2-methoxyethyl)-N'-(pentamethylbenzyl)benzimidazolin-2-ylidene](tricyclohexylphosphane)palladium (5a): The complex was prepared as described for **3a** by using **2a** and PCy₃. Yield: 0.83 g, 94.0%. ¹H NMR (400 MHz, CDCl₃): δ = 7.44 (d, *J* = 2.0 Hz, 1 H, Ar-H), 7.09 (t, *J* = 1.9 Hz, 1 H, Ar-H), 6.84 (t, *J* = 2.0 Hz, 1 H, Ar-H), 6.21 (d, *J* = 2.1 Hz, 1 H, Ar-H), 6.06 [s, 4 H, CH₂C₆(CH₃)₅], 4.92 (t, *J* = 1.3 Hz, 2 H, NCH₂CH₂OCH₃), 4.16 (t, *J* = 1.3 Hz, 2 H, NCH₂CH₂OCH₃), 3.37 (s, 3 H, NCH₂CH₂OCH₃), 2.56 (m, 3 H, PCy₃-H), 2.32 [s, 6 H, o-C₆(CH₃)₅], 2.26 [s, 6 H, m-C₆(CH₃)₅], 2.06 [s, 3 H, p-C₆(CH₃)₅], 1.81–1.68 (m, 14 H, PCy₃-H), 1.30–1.20 (m, 16 H, PCy₃-H) ppm. ¹³C NMR (100 MHz, CDCl₃): δ = 179.4 (d, ²J_{CP} = 174.7 Hz, NCN), 136.2, 136.1, 136.0, 135.2, 133.3, 128.4, 122.8, 122.4, 111.8, 111.0 [Ar-C and C₆(CH₃)₅], 71.4 (NCH₂CH₂OCH₃), 59.3 (NCH₂CH₂OCH₃), 52.0 [CH₂C₆(CH₃)₅], 48.1 (NCH₂CH₂OCH₃), 32.6 (d, ¹J_{PC} = 19.0 Hz, PCy₃-C), 30.4 (PCy₃-C), 27.9 (d, ²J_{PC} = 10.7 Hz, PCy₃-C), 26.9, 26.5, 25.8 (PCy₃-C), 17.9 [p-C₆(CH₃)₅], 17.5 [m-C₆(CH₃)₅], 17.1 [o-C₆(CH₃)₅] ppm. ³¹P NMR (162.0 MHz, CDCl₃): δ = 23.4 ppm. (MALDI): *m/z* = 803 [M – Br]⁺. C₄₀H₆₁Br₂N₂OPPd (883.12): calcd. C 54.40, H 6.96, N 3.17; found C 54.51, H 6.83, N 3.19.

trans-Dibromido[N-(2-methoxyethyl)-N'-(2,3,5,6-tetramethylbenzyl)benzimidazolin-2-ylidene](tricyclohexylphosphane)palladium (5b): The complex was prepared as described for **3b** using **2b** and PCy₃. Yield: 0.80 g, 92.0%. ¹H NMR (400 MHz, CDCl₃): δ = 7.48 (d, *J* = 4 Hz, 1 H, Ar-H), 7.11 (t, *J* = 4.1 Hz, 1 H, Ar-H), 6.85 (t, *J* = 4.1 Hz, 1 H, Ar-H), 6.25 (d, *J* = 4.1 Hz, 1 H, Ar-H), 6.18 [s, 1 H, CH₂C₆H(CH₃)₄], 6.06 [s, 2 H, CH₂C₆H(CH₃)₄], 4.94 (t, *J* = 3 Hz, 2 H, NCH₂CH₂OCH₃), 4.17 (t, *J* = 3.2 Hz, 2 H, NCH₂CH₂OCH₃), 3.38 (s, 3 H, NCH₂CH₂OCH₃), 2.54 (m, 3 H, PCy₃-H), 2.33 [s, 6 H, o-C₆H(CH₃)₄], 2.27 [s, 6 H, m-C₆H(CH₃)₄], 2.05–1.67 (m, 14 H, PCy₃-H), 1.30–1.20 (m, 16 H, PCy₃-H) ppm. ¹³C NMR (100 MHz, CDCl₃): δ = 180.3 (d, ²J_{CP} = 174.7 Hz, NCN), 135.9, 134.8, 133.0, 128.6, 128.1, 122.6, 122.1, 111.6, 111.4, 110.7 [Ar-C and C₆H(CH₃)₄], 71.1 (NCH₂CH₂OCH₃), 59.0 (NCH₂CH₂OCH₃), 51.7 [CH₂C₆(CH₃)₅], 47.8 (NCH₂CH₂OCH₃), 32.2 (d, ¹J_{PC} = 20.0 Hz, PCy₃-C), 30.0 (PCy₃-C), 27.9 (d, ²J_{PC} = 9.1 Hz, PCy₃-C), 26.9, 26.7, 26.1 (PCy₃-C), 17.7 [m-C₆H(CH₃)₄], 17.2 [o-C₆H(CH₃)₄] ppm. ³¹P NMR (162.0 MHz, CDCl₃): δ = 21.6 ppm. MS (MALDI): *m/z* = 789 [M – Br]⁺. C₃₉H₅₉Br₂N₂OPPd (869.10): calcd. C 53.90, H 6.84, N 3.22; found C 53.81, H 6.83, N 3.24.

trans-Dibromido[N,N'-bis(pentamethylbenzyl)benzimidazolin-2-ylidene](tricyclohexylphosphane)palladium (5c): The complex was prepared as described for **3b** by using **2c** and PCy₃. Yield: 0.91 g, 92.0%. ¹H NMR (400 MHz, CDCl₃): δ = 6.68 (m, 2 H, Ar-H), 6.22 (m, 2 H, Ar-H), 6.18 [s, 4 H, CH₂C₆(CH₃)₅], 2.58 (m, 3 H, PCy₃-H), 2.37 [s, 12 H, o-C₆(CH₃)₅], 2.33 [s, 6 H, p-C₆(CH₃)₅], 2.27 [s, 12 H, m-C₆(CH₃)₅], 2.07 (m, 6 H, PCy₃-H), 1.83–1.68 (m, 15 H, PCy₃-H), 1.31 (m, 9 H, PCy₃-H) ppm. ¹³C NMR (100 MHz, CDCl₃): δ = 179.6 (d, ²J_{CP} = 175.4 Hz, NCN), 136.0, 135.7, 135.1, 133.2, 128.6, 122.1, 111.6 [Ar-C and C₆(CH₃)₅], 52.3 [CH₂C₆(CH₃)₅], 32.6 (d, ¹J_{PC} = 19.1 Hz, PCy₃-C), 30.4 (PCy₃-C), 27.9 (d, ²J_{PC} = 9.9 Hz, PCy₃-C), 26.9, 26.7, 26.0 (PCy₃-C), 18.5 [p-C₆(CH₃)₅], 17.5 [m-C₆(CH₃)₅], 17.1 [o-C₆(CH₃)₅] ppm. ³¹P NMR (162.0 MHz, CDCl₃): δ = 22.9 ppm. MS (MALDI): *m/z* = 906 [M – Br]⁺. C₄₉H₇₁Br₂N₂PPd (985.30): calcd. C 59.73, H 7.26, N 2.84; found C 59.81, H 7.23, N 2.79.

trans-Dibromido[N,N'-bis(2,3,5,6-tetramethylbenzyl)benzimidazolin-2-ylidene](tricyclohexylphosphane)palladium (5d): The complex was prepared as described for **3b** by using **2d** and PCy₃. Yield: 0.88 g, 92.0%. ¹H NMR (400 MHz, CDCl₃): δ = 6.67 (m, 2 H, Ar-H), 6.22 (m, 2 H, Ar-H), 6.18 [s, 2 H, CH₂C₆H(CH₃)₄], 6.08 [s, 4 H, CH₂C₆H(CH₃)₄], 2.56 (m, 3 H, PCy₃-H), 2.35 [s, 12 H, o-C₆H(CH₃)₄], 2.28 [s, 12 H, m-C₆H(CH₃)₄], 2.03 (m, 6 H, PCy₃-H), 1.83–1.67 (m, 15 H, PCy₃-H), 1.31 (m, 9 H, PCy₃-H) ppm. ¹³C NMR (100 MHz, CDCl₃): δ = 180.0 (d, ²J_{CP} = 175.4 Hz, NCN), 136.0, 135.6, 135.0, 133.4, 128.3, 122.9, 111.5 [Ar-C and C₆H(CH₃)₄], 52.0 [CH₂C₆H(CH₃)₄], 32.3 (d, ¹J_{PC} = 19.0 Hz, PCy₃-C), 30.2 (PCy₃-C), 27.9 (d, ²J_{PC} = 9.7 Hz, PCy₃-C), 26.7, 26.5, 26.1 (PCy₃-C), 18.5 [m-C₆H(CH₃)₄], 17.1 [o-C₆H(CH₃)₄] ppm. ³¹P NMR (162.0 MHz, CDCl₃): δ = 22.3 ppm. MS (MALDI): *m/z* = 877 [M – Br]⁺. C₄₉H₇₁Br₂N₂PPd (957.25): calcd. C 58.97, H 7.05, N 2.93; found C 58.96, H 7.03, N 3.00.

Bromido[N-(2-methoxyethyl)-N'-(pentamethylbenzyl)benzimidazolin-2-ylidene][1,2-bis(diphenylphosphanyl)ethane]palladium (6a): The complex was prepared as described for **3a** by using **2a** and PPh₂CH₂CH₂PPh₂. Yield: 0.85 g, 85.0%. ¹H NMR (400 MHz, CDCl₃): δ = 8.13 (m, 2 H, Ph-H), 8.08 (m, 4 H, Ph-H), 7.91 (m, 2 H, Ph-H), 7.66 (m, 2 H, Ar-H), 7.60–7.21 (m, 13 H, Ar-H, Ph-H), 6.90 (t, *J* = 1.2 Hz, 1 H, Ar-H), 5.93 [s, 1 H, CHHC₆(CH₃)₅], 5.00 [s, 1 H, CHHC₆(CH₃)₅], 4.88 (t, *J* = 1.2 Hz, 2 H, NCH₂CH₂OCH₃), 4.23 (t, *J* = 1.2 Hz, 2 H, NCH₂CH₂OCH₃), 3.86–3.72 (m, 2 H,

PPh_2CH_2), 3.60–3.56 (m, 2 H, PPh_2CH_2), 3.02 (s, 3 H, $\text{NCH}_2\text{CH}_2\text{OCH}_3$), 2.30, 2.28, 1.98 [s, 15 H, $\text{C}_6(\text{CH}_3)_5$] ppm. ^{13}C NMR (100 MHz, CDCl_3): δ = 135.6, 135.5, 134.7, 134.0, 133.7, 132.7, 129.0, 128.8, 127.5, 122.2, 111.8 [Ar-C and Ph-C and $\text{C}_6(\text{CH}_3)_5$], 70.5 ($\text{NCH}_2\text{CH}_2\text{OCH}_3$), 66.0 ($\text{NCH}_2\text{CH}_2\text{OCH}_3$), 51.8 [$\text{CH}_2\text{C}_6(\text{CH}_3)_5$], 48.9 ($\text{NCH}_2\text{CH}_2\text{OCH}_3$), 48.1 (PPh_2CH_2), 20.6 [$p\text{-C}_6(\text{CH}_3)_5$], 16.3 [$m\text{-C}_6(\text{CH}_3)_5$], 15.5 [$o\text{-C}_6(\text{CH}_3)_5$] ppm. ^{31}P NMR (162.0 MHz, CDCl_3): δ = 59.5 (d, J_{PP} = 11.8 Hz), 52.2 (d, J_{PP} = 11.8 Hz) ppm. The signal for the carbene carbon atom was not detected under the given conditions. MS (MALDI): m/z = 921 [$\text{M} - \text{Br}$] $^+$. $\text{C}_{48}\text{H}_{52}\text{Br}_2\text{N}_2\text{OP}_2\text{Pd}$ (1000.1): calcd. C 57.59, H 5.24, N 2.80; found C 57.61, H 5.21, N 2.79.

Dibromido[*N*-(2-methoxyethyl)-*N'*-(2,3,5,6-tetramethylbenzyl)benzimidazolin-2-ylidene][1,2-bis(diphenylphosphanyl)ethane]palladium (6b): The complex was prepared as described for **3b** by using **2b** and $\text{PPh}_2\text{CH}_2\text{CH}_2\text{PPh}_2$. Yield: 0.89 g, 90.0%. ^1H NMR (400 MHz, CDCl_3): δ = 8.11 (m, 2 H, Ph-H), 8.07 (m, 4 H, Ph-H), 7.88 (m, 1 H, Ph-H), 7.64 (m, 3 H, Ar-H), 7.60–7.21 [m, 14 H, Ar-H and Ph-H and $\text{C}_6\text{H}(\text{CH}_3)_4$], 6.89 (t, J = 1.2 Hz, 1 H, Ar-H), 5.93 [s, 1 H, $\text{CHHC}_6\text{H}(\text{CH}_3)_4$], 5.01 [s, 1 H, $\text{CHHC}_6\text{H}(\text{CH}_3)_4$], 4.90 (t, J = 1.2 Hz, 2 H, $\text{NCH}_2\text{CH}_2\text{OCH}_3$), 4.23 (t, J = 1.2 Hz, 2 H, $\text{NCH}_2\text{CH}_2\text{OCH}_3$), 3.86–3.72 (m, 2 H, PPh_2CH_2), 3.60–3.56 (m, 2 H, PPh_2CH_2), 2.92 (s, 3 H, $\text{NCH}_2\text{CH}_2\text{OCH}_3$), 2.28, 2.25, 1.98 [s, 12 H, $\text{C}_6\text{H}(\text{CH}_3)_4$] ppm. ^{13}C NMR (100 MHz, CDCl_3): δ = 135.4, 135.1, 134.7, 134.2, 133.9, 132.7, 129.1, 128.9, 127.4, 122.2, 111.6 [Ar-C and Ph-C and $\text{C}_6(\text{CH}_3)_5$], 71.1 ($\text{NCH}_2\text{CH}_2\text{OCH}_3$), 66.4 ($\text{NCH}_2\text{CH}_2\text{OCH}_3$), 51.4 [$\text{CH}_2\text{C}_6(\text{CH}_3)_5$], 48.4 ($\text{NCH}_2\text{CH}_2\text{OCH}_3$), 48.2 (PPh_2CH_2), 18.6 [$m\text{-C}_6\text{H}(\text{CH}_3)_4$], 16.3 [$o\text{-C}_6\text{H}(\text{CH}_3)_4$] ppm. ^{31}P NMR (162.0 MHz, CDCl_3): δ = 60.1 (d, J_{PP} = 11.0 Hz), 52.6 (d, J_{PP} = 10.8 Hz) ppm. The signal for the carbene carbon atom was not detected under the given conditions. MS (MALDI): m/z = 907 [$\text{M} - \text{Br}$] $^+$. $\text{C}_{47}\text{H}_{50}\text{Br}_2\text{N}_2\text{OP}_2\text{Pd}$ (987.1): calcd. C 57.19, H 5.11, N 2.84; found C 57.21, H 5.17, N 2.89.

Dibromido[*N,N'*-bis(pentamethylbenzyl)benzimidazolin-2-ylidene]-[1,2-bis(diphenylphosphanyl)ethane]palladium (6c): The complex was prepared as described for **3b** by using **2c** and $\text{PPh}_2\text{CH}_2\text{CH}_2\text{PPh}_2$. Yield: 0.96 g, 87.0%. ^1H NMR (400 MHz, CDCl_3): δ = 8.05 (m, 2 H, Ph-H), 7.48 (m, 8 H, Ph-H), 7.25 (m, 6 H, Ph-H), 6.71 (m, 2 H, Ar-H), 6.55 (t, J = 1.2 Hz, 2 H, Ph-H), 6.36 [s, 4 H, $\text{CH}_2\text{C}_6(\text{CH}_3)_5$], 6.00 (m, 2 H, Ar-H), 5.93 (t, J = 1.2 Hz, 2 H, Ph-H), 3.56 (d, J = 1.7 Hz, 1 H, PPh_2CH_2), 3.48 (d, J = 1.8 Hz, 1 H, PPh_2CH_2), 2.88 (d, J = 1.9 Hz, 1 H, PPh_2CH_2), 2.80 (d, J = 2.1 Hz, 1 H, PPh_2CH_2), 2.34, 2.28, 2.25, 2.22, 2.18, 2.15 [s, 30 H, $\text{C}_6(\text{CH}_3)_5$] ppm. ^{13}C NMR (100 MHz, CDCl_3): δ = 136.3, 135.5, 134.9, 134.0, 133.1, 128.9, 128.8, 128.5, 127.5, 122.2, 111.4 [Ar-C and Ph-C and $\text{C}_6(\text{CH}_3)_5$], 53.6 [$\text{CH}_2\text{C}_6(\text{CH}_3)_5$], 52.3 (PPh_2CH_2), 17.5 [$p\text{-C}_6(\text{CH}_3)_5$], 17.1 [$m\text{-C}_6(\text{CH}_3)_5$], 15.4 [$o\text{-C}_6(\text{CH}_3)_5$] ppm. ^{31}P NMR (162.0 MHz, CDCl_3): δ = 58.5 (d, J_{PP} = 10.8 Hz), 52.1 (d, J_{PP} = 10.8 Hz) ppm. The signal for the carbene carbon atom was not detected under the given conditions. MS (MALDI): m/z = 1023 [$\text{M} - \text{Br}$] $^+$. $\text{C}_{57}\text{H}_{62}\text{Br}_2\text{N}_2\text{P}_2\text{Pd}$ (1103.3): calcd. C 62.05, H 5.60, N 2.54; found C 62.07, H 5.51, N 2.60.

Dibromido[*N,N'*-bis(2,3,5,6-tetramethylbenzyl)benzimidazolin-2-ylidene]-[1,2-bis(diphenylphosphanyl)ethane]palladium (6d): The complex was prepared as described for **3b** by using **2d** and $\text{PPh}_2\text{CH}_2\text{CH}_2\text{PPh}_2$. Yield: 0.53 g, 84.0%. ^1H NMR (400 MHz, CDCl_3): δ = 8.12 (m, 2 H, Ph-H), 7.58 (m, 8 H, Ph-H), 7.25–7.23 (m, 4 H, Ph-H), 7.00 [s, 2 H, $\text{CH}_2\text{C}_6\text{H}(\text{CH}_3)_4$], 6.83 (br., 2 H, Ar-H), 6.59 (t, J = 1.2 Hz, 2 H, Ph-H), 6.33 [s, 4 H, $\text{CH}_2\text{C}_6\text{H}(\text{CH}_3)_4$], 6.01 (m, 2 H, Ar-H), 5.93 (t, J = 1.3 Hz, 2 H, Ph-H), 3.57 (d, J = 1.6 Hz, 1 H, PPh_2CH_2), 3.48 (d, J = 1.7 Hz, 1 H, PPh_2CH_2), 2.90 (d, J = 1.8 Hz, 1 H, PPh_2CH_2), 2.80 (d, J = 1.8 Hz, 1 H, PPh_2CH_2),

2.31, 2.22, 2.20, 2.15, 2.15 [s, 24 H, $\text{C}_6\text{H}(\text{CH}_3)_4$] ppm. ^{13}C NMR (100 MHz, CDCl_3): δ = 136.9, 136.0, 134.2, 134.0, 133.1, 128.6, 128.2, 128.0, 127.0, 122.9, 111.1 [Ar-C and Ph-C and $\text{C}_6\text{H}(\text{CH}_3)_4$], 53.0 [$\text{CH}_2\text{C}_6\text{H}(\text{CH}_3)_4$], 52.0 (PPh_2CH_2), 17.9 [$m\text{-C}_6\text{H}(\text{CH}_3)_4$], 16.0 [$o\text{-C}_6\text{H}(\text{CH}_3)_4$] ppm. ^{31}P NMR (162.0 MHz, CDCl_3): δ = 58.8 (d, J_{PP} = 11.0 Hz), 52.2 (d, J_{PP} = 11.0 Hz) ppm. The signal for the carbene carbon atom was not detected under the given conditions. MS (MALDI): m/z = 995 [$\text{M} - \text{Br}$] $^+$. $\text{C}_{55}\text{H}_{58}\text{Br}_2\text{N}_2\text{P}_2\text{Pd}$ (1075.23): calcd. C 61.44, H 5.44, N 2.61; found C 61.47, H 5.53, N 2.67.

trans-Dibromido[*N*-(2-methoxyethyl)-*N'*-(pentamethylbenzyl)benzimidazolin-2-ylidene]palladium (7a): A mixture of **1a** (0.450 g, 1.08 mmol) and $\text{Pd}(\text{OAc})_2$ (0.121 g, 0.54 mmol) in dmso (10 mL) was stirred at 60 °C for 3 h and then at 110 °C for another 2 h. The dmso was removed in vacuo, and the remaining solid was washed with diethyl ether. The residue was crystallized from $\text{CH}_2\text{Cl}_2/\text{EtOH}$. Yield: 0.40 g, 78%. ^1H NMR (400 MHz, CDCl_3): δ = 7.40 (m, 2 H, Ar-H), 7.03 (m, 2 H, Ar-H), 6.79 (m, 2 H, Ar-H), 6.26 [s, 4 H, $\text{NCH}_2\text{C}_6(\text{CH}_3)_5$], 6.16 (m, 2 H, Ar-H), 5.01 (m, 4 H, $\text{NCH}_2\text{CH}_2\text{OCH}_3$), 4.32 (m, 4 H, $\text{NCH}_2\text{CH}_2\text{OCH}_3$), 3.21 (s, 6 H, $\text{NCH}_2\text{CH}_2\text{OCH}_3$), 2.32 [s, 12 H, $o\text{-C}_6(\text{CH}_3)_5$], 2.26 [s, 12 H, $m\text{-C}_6(\text{CH}_3)_5$], 2.21 [s, 6 H, $p\text{-C}_6(\text{CH}_3)_5$] ppm. ^{13}C NMR (100 MHz, CDCl_3): δ = 182.4 (NCN), 136.2, 135.9, 135.0, 134.8, 133.3, 128.4, 122.9, 122.4, 111.8, 111.2 [Ar-C and $\text{C}_6(\text{CH}_3)_5$], 67.3 ($\text{NCH}_2\text{CH}_2\text{OCH}_3$), 59.4 ($\text{NCH}_2\text{CH}_2\text{OCH}_3$), 52.4 [$\text{NCH}_2\text{C}_6(\text{CH}_3)_5$], 48.5 ($\text{NCH}_2\text{CH}_2\text{OCH}_3$), 17.9 [$p\text{-C}_6(\text{CH}_3)_5$], 17.4 [$m\text{-C}_6(\text{CH}_3)_5$], 17.1 [$o\text{-C}_6(\text{CH}_3)_5$] ppm. MS (MALDI): m/z = 859 [$\text{M} - \text{Br}$] $^+$. $\text{C}_{44}\text{H}_{56}\text{Br}_2\text{N}_4\text{O}_2\text{Pd}$ (939.1): calcd. C 56.27, H 6.01, N 5.97; found C 56.41, H 6.13, N 5.99.

trans-Dibromido[*N*-(2-methoxyethyl)-*N'*-(2,3,5,6-tetramethylbenzyl)benzimidazolin-2-ylidene]palladium (7b): The complex was prepared as described for **7a** by using **1b**. Yield: 0.38 g, 77%. ^1H NMR (400 MHz, CDCl_3): δ = 7.49 (m, 2 H, Ar-H), 7.15 (m, 2 H, Ar-H), 7.11 (m, 2 H, Ar-H), 7.05 [s, 2 H, $\text{C}_6\text{H}(\text{CH}_3)_4$], 6.88 [m, 4 H, $\text{NCH}_2\text{C}_6\text{H}(\text{CH}_3)_4$], 6.25 (m, 2 H, Ar-H), 5.11 (m, 4 H, $\text{NCH}_2\text{CH}_2\text{OCH}_3$), 4.25 (m, 4 H, $\text{NCH}_2\text{CH}_2\text{OCH}_3$), 3.32 (s, 6 H, $\text{NCH}_2\text{CH}_2\text{OCH}_3$), 2.31 [s, 12 H, $o\text{-C}_6\text{H}(\text{CH}_3)_4$], 2.25 [s, 12 H, $m\text{-C}_6\text{H}(\text{CH}_3)_4$] ppm. ^{13}C NMR (100 MHz, CDCl_3): δ = 182.4 (NCN), 136.0, 135.3, 134.8, 134.5, 132.6, 131.1, 122.9, 122.5, 111.8, 111.1 [Ar-C and $\text{C}_6\text{H}(\text{CH}_3)_5$], 71.9 ($\text{NCH}_2\text{CH}_2\text{OCH}_3$), 59.4 ($\text{NCH}_2\text{CH}_2\text{OCH}_3$), 51.7 [$\text{NCH}_2\text{C}_6\text{H}(\text{CH}_3)_4$], 48.4 ($\text{NCH}_2\text{CH}_2\text{OCH}_3$), 20.8 [$m\text{-C}_6\text{H}(\text{CH}_3)_4$], 17.0 [$o\text{-C}_6\text{H}(\text{CH}_3)_4$] ppm. MS (MALDI): m/z = 831 [$\text{M} - \text{Br}$] $^+$. $\text{C}_{42}\text{H}_{52}\text{Br}_2\text{N}_4\text{O}_2\text{Pd}$ (911.1): calcd. C 55.37, H 5.75, N 6.15; found C 55.31, H 5.83, N 6.29.

trans-Dibromido[*N,N'*-bis(pentamethylbenzyl)benzimidazolin-2-ylidene]palladium (7c): The complex was prepared as described for **7a** by using **1c**. Yield: 0.50 g, 81%. ^1H NMR (400 MHz, CDCl_3): δ = 6.71 (m, 4 H, Ar-H), 6.37 [s, 4 H, $\text{NCH}_2\text{C}_6(\text{CH}_3)_5$], 6.32 (m, 4 H, Ar-H), 2.40 [s, 24 H, $o\text{-C}_6(\text{CH}_3)_5$], 2.28 [s, 24 H, $m\text{-C}_6(\text{CH}_3)_5$], 2.23 [s, 12 H, $p\text{-C}_6(\text{CH}_3)_5$] ppm. ^{13}C NMR (100 MHz, CDCl_3): δ = 182.8 (NCN), 135.9, 135.6, 134.7, 133.2, 128.7, 122.1, 111.8 [Ar-C and $\text{C}_6(\text{CH}_3)_5$], 52.4 [$\text{NCH}_2\text{C}_6(\text{CH}_3)_5$], 18.1 [$p\text{-C}_6(\text{CH}_3)_5$], 18.0 [$m\text{-C}_6(\text{CH}_3)_5$], 17.4 [$o\text{-C}_6(\text{CH}_3)_5$] ppm. MS (MALDI): m/z = 1063 [$\text{M} - \text{Br}$] $^+$. $\text{C}_{62}\text{H}_{76}\text{Br}_2\text{N}_4\text{Pd}$ (1143.5): calcd. C 65.15, H 6.70, N 4.90; found C 65.20, H 6.83, N 4.99.

trans-Dibromido[*N,N'*-bis(2,3,5,6-tetramethylbenzyl)benzimidazolin-2-ylidene]palladium (7d): The complex was prepared as described for **7a** by using **1d**. Yield: 0.49 g, 83%. ^1H NMR (400 MHz, CDCl_3): δ = 7.04 [s, 4 H, $\text{C}_6\text{H}(\text{CH}_3)_4$], 6.72 (m, 4 H, Ar-H), 6.39 [s, 4 H, $\text{NCH}_2\text{C}_6\text{H}(\text{CH}_3)_4$], 6.30 (m, 4 H, Ar-H), 2.25 [s, 24 H, $m\text{-C}_6\text{H}(\text{CH}_3)_4$], 2.35 [s, 24 H, $o\text{-C}_6\text{H}(\text{CH}_3)_4$] ppm. ^{13}C NMR (100 MHz, CDCl_3): δ = 182.8 (NCN), 111.7, 122.3, 131.4, 132.5, 134.4, 135.2, 135.4 [Ar-C and $\text{C}_6\text{H}(\text{CH}_3)_4$], 51.9 [$\text{NCH}_2\text{C}_6\text{H}$ -

(CH₃)₄], 20.7 [*m*-C₆H(CH₃)₄], 17.1 [*o*-C₆H(CH₃)₄] ppm. MS (MALDI): *m/z* = 1008 [M – Br]⁺. C₅₈H₆₈Br₂N₄Pd (1087.4): calcd. C 64.06, H 6.30, N 5.15; found C 64.10, H 6.33, N 5.21.

General Procedure for the Heck Coupling Reactions: A two-necked, 25-mL flask fitted with a reflux condenser was charged with the aryl halide (1.0 mmol), the olefin (1.5 mmol), Cs₂CO₃ (1.5 mmol), diethylene glycol di-*n*-butyl ether (internal standard), dma (3 mL), and catalyst **2–7** (3.0 mol-%) under an atmosphere of argon. The flask was placed in a preheated oil bath (100 °C) for 2 h. Yields were determined by gas chromatography for an average of two runs.

X-ray Diffraction Studies: Diffraction data for all complexes were collected with a Bruker AXS APEX CCD diffractometer equipped with a rotation anode at 153(2) K by using graphite monochromated Mo-*K*_α radiation (λ = 0.71073 Å). Diffraction data were collected over the full sphere and were corrected for absorption. The data reduction was performed with the Bruker SMART¹¹⁸¹ program package. Structure solutions were found with the SHELXS-97¹¹⁹¹ package by using the heavy-atom method and were refined with SHELXL-97¹²⁰¹ against $|F^2|$ by using first isotropic and later anisotropic thermal parameters for all non-hydrogen atoms. Hydrogen atoms were added to the structure models on calculated positions. CCDC-703113 (for **2c**), -703114 (for **3c**·2CH₂Cl₂), -73115 (for **3d**·CH₂Cl₂), and -703116 (for **5b**) contain the supplementary crystallographic data for this paper. These data can be obtained free of charge from The Cambridge Crystallographic Data Centre via www.ccdc.cam.ac.uk/data/request/cif.

Crystal Data for **2c:** C₃₃H₄₄N₂Br₂OPdS, *M* = 782.98, μ = 3.143 mm^{–1}, ρ = 1.611 g cm^{–3}, monoclinic, *P*2₁/*c*, *Z* = 4, *a* = 10.3854(14) Å, *b* = 19.389(3) Å, *c* = 16.854(3) Å, β = 107.925(3)°, *V* = 3229.0(8) Å³, 25694 measured reflections ($3.3^\circ \leq 2\theta \leq 50.0^\circ$), 5675 unique reflections (*R*_{int} = 0.0621), *R* = 0.0588, *wR* = 0.1408 for 4233 contributing reflections [$I \geq 2\sigma(I)$] and 373 parameters, refinement against $|F^2|$ with anisotropic thermal parameters for all non-hydrogen atoms and hydrogen atoms on calculated positions. The asymmetric unit contains one molecule of **2c**.

Crystal Data for **3c·2CH₂Cl₂:** C₅₁H₅₇N₂Br₂Cl₄PPd, *M* = 1136.96, μ = 2.281 mm^{–1}, ρ = 1.530 g cm^{–3}, triclinic, *P*1̄, *Z* = 2, *a* = 10.298(2) Å, *b* = 12.239(2) Å, *c* = 20.297(3) Å, α = 101.929(3)°, β = 90.023(3)°, γ = 99.374(3)°, *V* = 2467.8(7) Å³, 24219 measured reflections ($3.4^\circ \leq 2\theta \leq 55.0^\circ$), 11301 unique reflections (*R*_{int} = 0.0334), *R* = 0.0436, *wR* = 0.1048 for 8520 contributing reflections [$I \geq 2\sigma(I)$] and 560 parameters, refinement against $|F^2|$ with anisotropic thermal parameters for all non-hydrogen atoms and hydrogen atoms on calculated positions. The asymmetric unit contains one molecule of **3c** and two molecules of CH₂Cl₂.

Crystal Data for **3d·CH₂Cl₂:** C₄₈H₅₁N₂Br₂Cl₂PPd, *M* = 1024.0, μ = 2.400 mm^{–1}, ρ = 1.525 g cm^{–3}, monoclinic, *P*2₁/*c*, *Z* = 4, *a* = 18.861(2) Å, *b* = 11.3521(14) Å, *c* = 21.034(3) Å, β = 98.075(3)°, *V* = 4459.1(9) Å³, 50366 measured reflections ($3.9^\circ \leq 2\theta \leq 60.1^\circ$), 12997 unique reflections (*R*_{int} = 0.0495), *R* = 0.0505, *wR* = 0.1368 for 9866 contributing reflections [$I \geq 2\sigma(I)$] and 503 parameters, refinement against $|F^2|$ with anisotropic thermal parameters for all non-hydrogen atoms and hydrogen atoms on calculated positions. The asymmetric unit contains one molecule of **3d** and one molecule of CH₂Cl₂ with disordered chloride atoms.

Crystal Data for **5b:** C₃₉H₅₉N₂Br₂OPPd, *M* = 869.07, μ = 2.656 mm^{–1}, ρ = 1.514 g cm^{–3}, triclinic, *P*1̄, *Z* = 2, *a* = 11.111(3) Å, *b* = 12.678(3) Å, *c* = 14.646(3) Å, α = 83.382(4)°, β = 69.563(4)°, γ = 81.363(4)°, *V* = 1907.0(8) Å³, 18318 measured reflections ($3.5^\circ \leq 2\theta \leq 55.0^\circ$), 8745 unique reflections (*R*_{int} = 0.0443), *R* = 0.0434, *wR* = 0.0911 for 6073 contributing reflections [$I \geq 2\sigma(I)$]

and 420 parameters, refinement against $|F^2|$ with anisotropic thermal parameters for all non-hydrogen atoms and hydrogen atoms on calculated positions. The asymmetric unit contains one molecule of **5b**.

Acknowledgments

Financial support from Ege University and the University of Münster is gratefully acknowledged. F. E. H thanks the Deutsche Forschungsgemeinschaft and the Fonds der Chemischen Industrie for financial support.

- [1] a) D. J. Cardin, B. Çetinkaya, M. F. Lappert, *Chem. Rev.* **1972**, 72, 545–573; b) D. J. Cardin, B. Çetinkaya, M. J. Doyle, M. F. Lappert, *J. Chem. Soc.* **1973**, 2, 99–144; c) M. F. Lappert, *J. Organomet. Chem.* **2005**, 690, 5467–5473.
- [2] a) D. Bourissou, O. Guerret, F. P. Gabbaï, G. Bertrand, *Chem. Rev.* **2000**, 100, 39–91; b) F. E. Hahn, M. C. Jahnke, *Angew. Chem. Int. Ed.* **2008**, 47, 3122–3172.
- [3] For a special issue dedicated to modern trends in NHC chemistry, see: *Coord. Chem. Rev.* **2007**, 251, 595–896.
- [4] A. T. Normand, K. J. Cavell, *Eur. J. Inorg. Chem.* **2008**, 2781–2800.
- [5] a) W. A. Herrmann, *Angew. Chem. Int. Ed. Engl.* **1997**, 36, 2162–2187; b) S. P. Nolan (Ed.), *N-Heterocyclic Carbenes in Synthesis*, Wiley-VCH, Weinheim, **2006**; F. Glorius (Ed.), *Topics in Organometallic Chemistry Vol. 21: N-Heterocyclic Carbenes in Transition Metal Catalysis*, Springer, Berlin, **2007**.
- [6] a) R. B. Bedford, C. S. Z. Cazin, D. Holder, *Coord. Chem. Rev.* **2004**, 248, 2283–2321; b) E. A. B. Kantchev, C. J. O'Brien, M. G. Organ, *Angew. Chem. Int. Ed.* **2007**, 46, 1768–2813.
- [7] a) A. Bertogg, F. Camponovo, A. Togni, *Eur. J. Inorg. Chem.* **2005**, 347–356; b) H. Türkmen, B. Çetinkaya, *J. Organomet. Chem.* **2006**, 691, 3749–3759.
- [8] a) W. A. Herrmann, V. P. W. Böhm, C. W. K. Gstöttmayr, M. Grosche, C.-P. Reisinger, T. Weskamp, *J. Organomet. Chem.* **2001**, 617–618, 616–628; b) C. Yang, H. M. Lee, S. P. Nolan, *Org. Lett.* **2001**, 3, 1511–1514; c) J. Pytkowicz, S. Roland, P. Mangeney, G. Meyer, A. Jutand, *J. Organomet. Chem.* **2003**, 678, 166–179; d) J.-S. Shi, P.-Y. Yang, Q. Tang, Y. Wu, Y. Peng, *J. Mol. Catal. A* **2006**, 259, 7–10; e) T. Weskamp, V. P. W. Böhm, W. A. Herrmann, *J. Organomet. Chem.* **1999**, 585, 348–352.
- [9] F. E. Hahn, M. C. Jahnke, T. Pape, *Organometallics* **2006**, 25, 5927–5936.
- [10] H. V. Huynh, Y. Han, J. H. H. Ho, G. K. Teng, *Organometallics* **2006**, 25, 3267–3274.
- [11] a) F. E. Hahn, B. Heidrich, T. Lügger, T. Pape, *Z. Naturforsch.* **2004**, 59b, 1519–1523; b) F. E. Hahn, C. Holtgrewe, T. Pape, M. Martin, E. Sola, L. A. Oro, *Organometallics* **2005**, 24, 2203–2209; c) C. Holtgrewe, C. Diedrich, T. Pape, S. Grimme, F. E. Hahn, *Eur. J. Org. Chem.* **2006**, 3116–3124; d) F. E. Hahn, B. Heidrich, T. Pape, A. Hepp, M. Martin, E. Sola, L. A. Oro, *Inorg. Chim. Acta* **2006**, 359, 4840–4846; e) F. E. Hahn, B. Heidrich, A. Hepp, T. Pape, *J. Organomet. Chem.* **2007**, 692, 4630–4638.
- [12] B. Çetinkaya, E. Çetinkaya, M. F. Lappert, *J. Chem. Soc., Dalton Trans.* **1973**, 906–912.
- [13] a) F. E. Hahn, M. Foth, *J. Organomet. Chem.* **1999**, 585, 241–245; b) H. V. Huynh, J. H. H. Ho, T. C. Neo, L. L. Koh, *J. Organomet. Chem.* **2005**, 690, 3845–3860.
- [14] F. E. Hahn, T. Lügger, M. Beinhoff, *Z. Naturforsch.* **2004**, 59b, 196–201.
- [15] a) A. G. Gökçe, H. Türkmen, M. Aygün, B. Çetinkaya, C. Kazak, *Acta Crystallogr., Sect. C* **2004**, 60, m254–m255; b) R. Sevinç, H. Türkmen, M. Aygün, B. Çetinkaya, S. García-Granda, *Acta Crystallogr., Sect. C* **2007**, 63, m277–m279.

- [16] a) Y. Gök, N. Gürbüz, I. Özdemir, B. Çetinkaya, E. Çetinkaya, *Appl. Organomet. Chem.* **2005**, *19*, 870–874; b) I. Özdemir, S. Yaşar, S. Demir, B. Çetinkaya, *Heteroat. Chem.* **2005**, *16*, 557–561.
- [17] a) H. M. Lee, P. L. Chiu, J. Y. Zeng, *Inorg. Chim. Acta* **2004**, *357*, 4313–4321; b) A. A. D. Tulloch, A. A. Danopoulos, R. P. Tooze, S. M. Cafferkey, S. Kleinhenz, M. B. Hursthouse, *Chem. Commun.* **2000**, 1247–1248; c) V. César, S. Bellemin-Laponnaz, L. H. Gade, *Organometallics* **2002**, *21*, 5204–5208; d) D. S. McGuinness, K. J. Cavell, B. W. Skelton, A. H. White, *Organometallics* **1999**, *18*, 1596–1605; e) D. S. McGuinness, K. J. Cavell, *Organometallics* **2000**, *19*, 741–748.
- [18] *SMART*: Bruker AXS, **2000**.
- [19] *SHELXS-97*: G. M. Sheldrick, *Acta Crystallogr., Sect. A* **1990**, *46*, 467.
- [20] G. M. Sheldrick, *SHELXL-97*, University of Göttingen, **1997**.

Received: September 25, 2008

Published Online: December 4, 2008

Mechanism of Hydride Abstraction by Cyclopentadienone-Ligated Carbonylmetal Complexes (M = Ru, Fe)

Megan K. Thorson,^[a] Kortney L. Klinkel,^[a] Jianmei Wang,^[a] and Travis J. Williams^{*[a]}

Keywords: Cyclopentadienone ligands / C–H bond activation / Oxidation / Hydrides / Reaction mechanisms

Cyclopentadienone-ligated ruthenium complexes, such as Shvo's catalyst, are known to oxidize reversibly alcohols to the corresponding carbonyl compounds. The mechanism of this reaction has been the subject of some controversy, but it is generally believed to proceed through concerted transfer of proton and hydride, respectively, to the cyclopentadienone ligand and the ruthenium center. In this paper we further study the hydride transfer process as an example of a coordinatively directed hydride abstraction by adding quantitative understanding to some features of this mechanism that are not well understood. We find that an oxidant as weak as ace-

tone can be used to re-oxidize the intermediate ruthenium hydride without catalyst re-oxidation becoming rate-limiting. Furthermore, C–H cleavage is a significantly electrophilic event, as demonstrated by a Hammett reaction parameter of $\rho = -0.89$. We then describe how the application of our mechanistic insights obtained from the study have enabled us to extend the ligand-directed hydride abstraction strategy to include a rare example of an iron(0) oxidation catalyst.

(© Wiley-VCH Verlag GmbH & Co. KGaA, 69451 Weinheim, Germany, 2009)

Introduction

C–H bond oxidation by hydride abstraction is an important reaction for organic synthesis and has a central role in applications ranging from utilization of hydrocarbon feedstocks to fine chemical synthesis,^[1] yet its mechanism is underexplored and its applications are scarcely exploited. Our group is developing ligand–metal bifunctional catalysts for hydride abstraction from general organic substrates to enable nucleophilic substitution reactions in which hydride is activated as a leaving group (Scheme 1, A). Our strategy is to devise a bifunctional catalyst in which the ligand “addresses” the catalyst to a particular C–H bond by placing an electrophilic metal atom in its immediate proximity. Following hydride transfer to metal atom, the resulting M–H group must be re-oxidized under mild conditions.

We have adopted the cyclopentadienone-ligated metal scaffold (e.g. **3**) as a starting point for development of coordination-directed hydride abstraction reactions because of the apparently significant role of the cyclopentadienone as a redox non-innocent ligand. “Shvo's catalyst” (Scheme 1, **1**),^[2] is an example of this type of reactivity. Compound **1** itself, an air-stable, commercially available, crystalline solid, is the heterodimer of reduced (**2**) and oxidized (**3**) forms. The mixture of **2** and **3**, generated by dissociation of **1**, is

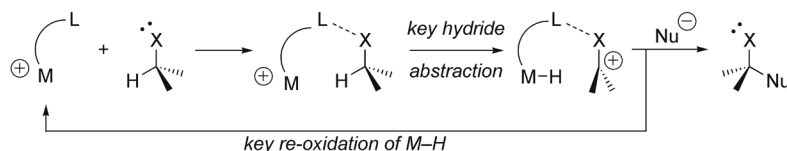
known to catalyze reversibly the interconversion of carbonyl and alcohol compounds (Scheme 1, C). Although **1** was first introduced as a hydrogenation catalyst, its utility in the corresponding oxidation reaction has also been examined.^[1f,3] Data collected to date regarding the mechanism of oxidation reactions catalyzed by **1** are most consistent with a mechanism involving transfer of both hydrogen atoms (O–H and C–H) in or before a single rate-determining transition state when the reaction is conducted under strongly oxidative conditions (tetrafluorobenzoquinone).^[3b] Thus, **3** is a bifunctional metal–ligand scaffold in which H⁺ (from O–H) acts as a coordinating direction element “L” that disposes an electrophilic ruthenium center “M⁺” in the proximity of a C–H bond.

We believe that coordination-directed hydride abstraction will be an excellent strategy for our program of designing and developing efficient, selective, inexpensive, and environmentally benign catalysts for C–H oxidation, and we believe that identification of mild conditions of re-oxidation of metal hydrides (such as **2**) will be essential to the identification of high-value catalytic systems because this is a key to realizing catalytic turnover. Moreover, an improved understanding of the polarization and energetics of hydride abstraction mediated at a cyclopentadienone-ligated metal center (such as **3**) is essential to effective catalyst design. In this paper we address these issues for the case of some Shvo-related complexes, and add quantitative understanding to some features of this mechanism that are a key to our goal (Scheme 1, A): *an oxidant as weak as acetone can be used, and catalyst re-oxidation does not become rate-limiting; replacement of a single phenyl group of*

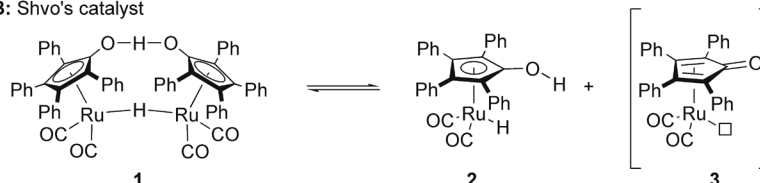
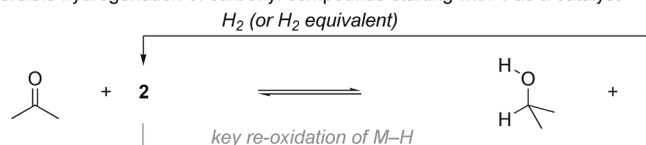
[a] Loker Hydrocarbon Research Institute and Department of Chemistry, University of Southern California, 837 Bloom Walk, Los Angeles, CA 90089-1661, USA
Fax: +1-213-740-6679
E-mail: travisw@usc.edu

Supporting information for this article is available on the WWW under <http://www.eurjic.org> or from the author.

A: Coordination-directed hydride abstraction as a strategy for C–H oxidation



B: Shvo's catalyst

C: Reversible hydrogenation of carbonyl compounds starting with **1** as a catalyst

Scheme 1. Shvo's system as a platform for hydride abstraction reactions.

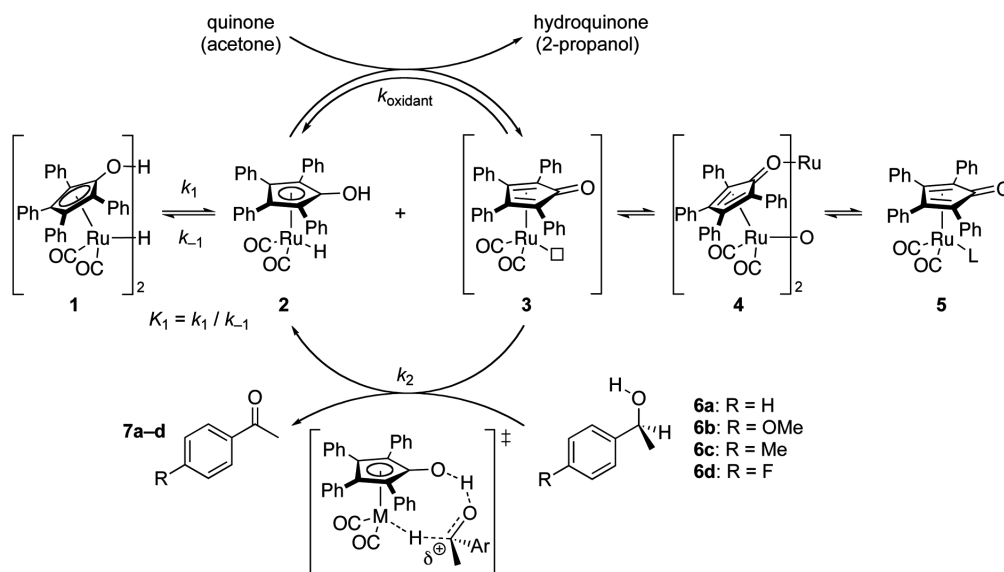
the cyclopentadienone ring can reduce the efficiency of oxidation significantly; and C–H cleavage is a significantly electrophilic event. We then describe how the application of this weakly oxidizing medium and our mechanistic insights obtained from the study have enabled us to extend the strategy to include a rare example of an iron(0)-based oxidation catalyst.

Results and Discussion

Studies on **1** conducted by Shvo et al.,^[2] Casey et al.,^[4] Bäckvall et al.,^[1f,3] and others^[5] have shown that in aromatic solvents the catalyst resting state in these reactions is dimer **1**, which must dissociate to reduced (**2**) and oxidized

(**3**) forms (very small K_1) for a reaction to occur. Alcohol oxidation with **1** has isotope effects on both C–H ($k_H/k_D = 2.6$) and O–H ($k_H/k_D = 1.8$).^[3b] Bäckvall et al. have explained that these kinetic isotope effect (KIE) data, along with a k_H/k_D value of 4.61 for a fully deuterated substrate is consistent with a concerted transition state for hydride and proton transfer (Scheme 2).^[3b]

We started our study by switching to acetone, a milder, environmentally more benign medium to effect oxidation with catalyst **1**. Upon dissolving dimer **1** in $[D_6]$ acetone with alcohol **6a**, we find dissociation and oxidation of dimer **1** as is evident from the disappearance of the characteristic μ^2 -H peak ($\delta = -18.1$ ppm) and appearance of $[D_6]$ 2-propanol ($\delta = +3.9$ ppm), which indicates that the dissoci-



Scheme 2. Alcohol oxidation in Shvo's system.

ation equilibrium of **1** lies to the right under these conditions. This transformation is complete within the first acquisition of a kinetics run (see Supporting Information for an illustration). We perceive that the result is an acetone- or substrate-ligated dicarbonylruthenium complex (**5**, $L = [D_6]$ acetone or **6**). Using this catalyst, we verify that **6a** can be converted to **7a** in 97% isolated yield on a 1 mmol scale.^[6]

Systematic kinetics experiments on the conversion of **6a** to **7a** (Table 1) in $[D_6]$ acetone solution support a rate law of $d[6a]/dt = -k_2 \cdot [1]^{1/2} \cdot [6a] \cdot [\text{oxidant}]^0$ with $k_2 = 1.67(6) \times 10^{-2} \text{ M}^{-1/2} \text{ s}^{-1}$. This is analogous to what Bäckvall et al. observed for quinone conditions (**1**, $[D_6]$ benzene, tetrafluorobenzoquinone), but is interesting because we observe no kinetic order in the re-oxidation step even though it is a significantly milder oxidant than tetrafluorobenzoquinone. Kinetic order on **1** is illustrated in a plot of $\ln(k_{\text{obs}})$ versus $\ln[1]$ (Figure 1, left). A slope of 0.40(6) in this plot is consistent with a half-order dependence on **1**. This indicates that dimerization of **2** and **3** is occurring during the catalysis even though this equilibrium lies well to the right under the reaction conditions. The dependence of the reaction rate on [acetone] is shown graphically in Figure 1 (right). The observed rate constants (k_{obs}) decrease only slightly with [acetone] in a mixed $[D_2]$ dichloromethane/ $[D_6]$ acetone solution. The high y intercept of this plot is inconsistent with the kinetic order on [acetone], but is more likely interpreted as a medium effect: the data in Figure 1 (right) represent variation from 25% to 100% acetone. This means that re-oxidation of **2** from **3** does not impact

the rate of the overall reaction, and thus that $[D_6]$ acetone is as efficient as a quinone in regenerating **3** from **2** in a solution.

In cases in which we introduced benzoquinone to compete with acetone in acetone solution (Table 1, Entries 4 and 5), acetone was the major oxidant because of its high concentration. By comparison of ^1H NMR peaks for benzoquinone and $[D_6]$ 2-propanol, we can estimate the ratio of rates of reduction of benzoquinone and acetone ($k_{\text{BQ}}/k_{\text{acetone}}$) as 414(4). Although we observe this ratio to be constant over the course of the conversion, we must interpret it as an upper bound because $[D_6]$ 2-propanol can reduce benzoquinone (by re-formation of $[D_6]$ acetone) in the presence of **1**. Moreover, Table 1 (Entry 5) shows that an excess of quinone can slow the reaction. We perceive that this is a result of competitive binding of **3** by benzoquinone or hydroquinone.

An internal competition isotope effect experiment with $[D]$ benzyl alcohol $[\text{PhC(D)HOH}]$ afforded a value of $k_{\text{H}}/k_{\text{D}} = 3.7(2)$ at 323 K through the first 40% of conversion. We assign our value to a primary KIE [as opposed to an equilibrium isotope effect (EIE) or a combination of both] because it is constant over the course of conversion. This value is higher than a literature value^[3b] ($k_{\text{H}}/k_{\text{D}} = 2.6$ by independent runs) observed for the conversion of **6d** to **7d**, possibly because of the relative strength of the primary (versus secondary) C–H bond. The difference in these values can also be attributed to the role of an EIE in the literature measurement. By contrast, we observe full dissociation of **1**.

We also show that the C–H cleavage is an electrophilic event by measuring a Hammett ρ value of $-0.89(5)$ by comparing the rates of oxidation of alcohols **6a–6d** in independent runs (Figure 2).^[7] A Hammett reaction parameter of $\rho = -0.89$ is larger than expected for a transition state involving β -hydride elimination or free-radical hydrogen atom transfer. Kaneda et al. report $\rho = -0.43$ for the oxidation of **6** with a ruthenium catalyst immobilized on hydroxyapatite and proposes a β -hydride elimination mechanism.^[8] Kuria-cose et al. report $\rho = -0.3$ for the same reaction with a

Table 1. Kinetics data for the **1**-catalyzed conversion of **6a** to **7a**.^[a]

Entry	$k_{\text{obs}} (\times 10^5 \text{ s}^{-1})$	1 [mM]	6a [mM]	BQ [mM]	$k_{\text{BQ}}/k_{\text{acetone}}$
1	7.55(26)	1.5	120	0	—
2	11.1(1)	2.9	120	0	—
3	7.46(3)	1.5	240	0	—
4	8.49(31)	1.5	120	72	410
5	4.13(7)	1.5	120	144	418

[a] $k_{\text{obs}} = k_2 \cdot [6]$. BQ = benzoquinone; $k_2 = 1.67(6) \times 10^{-2} \text{ M}^{-1/2} \text{ s}^{-1}$.

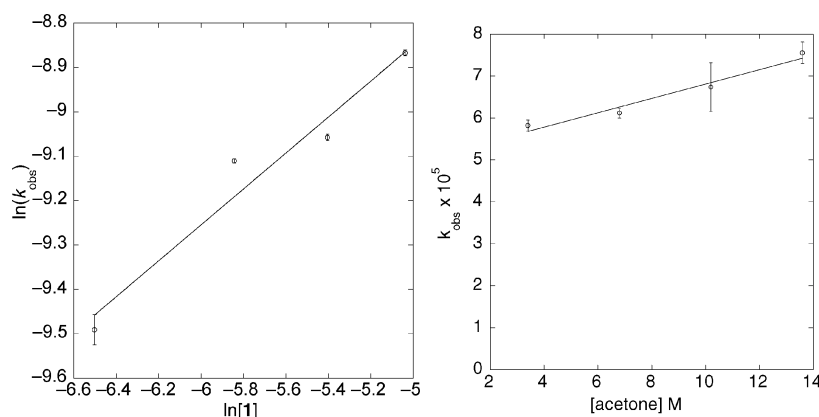


Figure 1. Left: plot of $\ln(k_{\text{obs}})$ versus $\ln[1]$; slope = 0.40(6). Right: plot of k_{obs} versus [acetone] in a mixed medium of $[D_6]$ acetone and $[D_2]$ dichloromethane. Kinetics data were processed as described in the Exp. Sect.

ruthenium trichloride catalyst in the presence of *N*-methylmorpholine *N*-oxide. These authors propose a hydrogen atom (radical) abstraction by an (oxido)ruthenium(V) intermediate.^[9] Our observation is more in line with benzyl alcohol oxidation by quinolinium chlorochromate ($\rho = -1.2$).^[10] Thus, with catalyst **1**, we interpret that a significant cationic character is evolved at the carbon atom in the rate-determining transition state, which is only slightly compensated by electron donation from the concurrent deprotonation of the O–H bond.

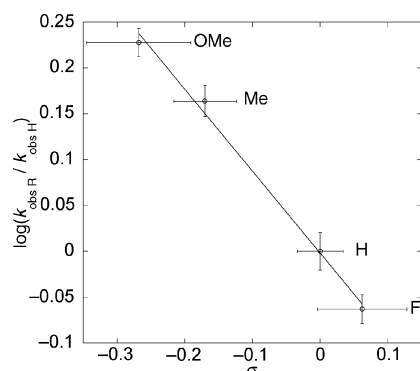
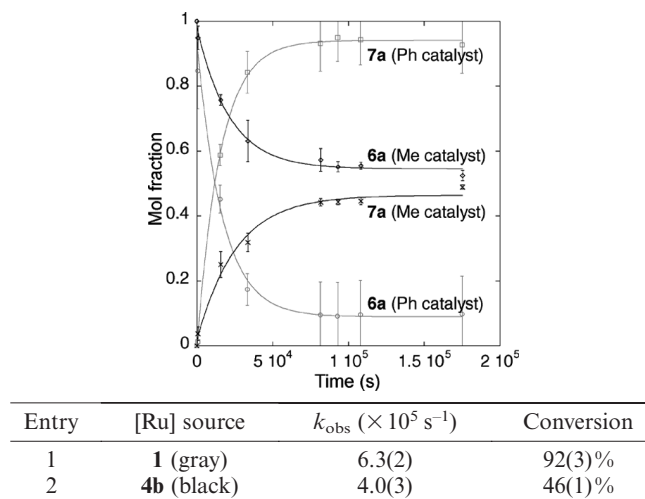


Figure 2. Hammett plot for the **1**-catalyzed conversion of **6** to **7**. Kinetics data were acquired and processed as described in the Exp. Sec. $\rho = -0.89(5)$.

Furthermore, we have studied other ruthenium complexes based on electronically differentiated cyclopentadienones to compare the reaction rates. We attempted to prepare catalyst precursors analogous to **4** by treating $[\text{Ru}_3(\text{CO})_{12}]$ ^[4b] with the corresponding cyclopentadienone **9**^[11] (Table 2). Only methyl-substituted compound **9b** participated in the formation of **4b** cleanly. Surprisingly, although **4b** appears monomeric under the reaction conditions used in Table 1, it reacts with **6a** ca. 10^1 times slower than the parent (**1**). Because **4b** is only sparingly soluble acetone, the experiment was repeated in a solvent system of $[\text{D}_2]$ dichloromethane/ $[\text{D}_6]$ acetone (1:1). Under these conditions, both **1** and **4b** are completely dissolved and dissociated to active forms, and the parent system is only 60% faster: $k_2(\text{Ph})/k_2(\text{Me}) = 1.6(1)$. We observe, however, that the methyl-substituted system stalls at 46(1)% conversion, whereas the parent reached 92(3)%. This, along with a dark color that develops over time, indicates that the cyclopentadienone ligand is being lost in the course of the reaction. We thus assign the deficiencies of **4b** as: (1) solubility, (2)

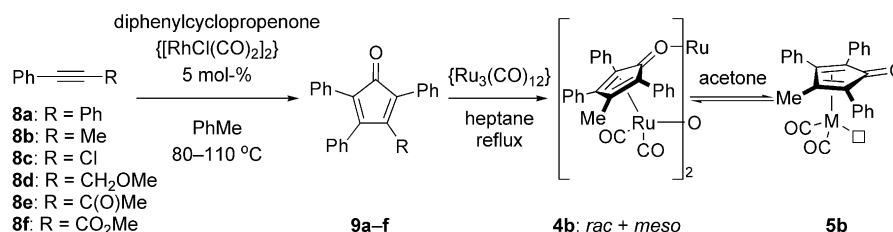
stability, and (3) rate in the C–H oxidation step (k_2). We further hypothesized that a more electron-deficient catalyst based on chloroalkyne **8c** would facilitate hydride abstraction and afford a faster oxidation reaction, but this complex is apparently unreactive (Scheme 3).

Table 2. Conversion of **6a** to **7a** with catalyst precursors **1** (gray) and **4b** (black).^[a]



[a] A solvent system of $[\text{D}_2]$ dichloromethane/ $[\text{D}_6]$ acetone (1:1) was used.

Having identified mild oxidative conditions in which catalyst **1** operates smoothly, and having developed an understanding of the mechanistic details of the reaction under these conditions, we turned our attention to the possibility of replacing the catalytic ruthenium atom by an iron atom. To do so would involve hydride abstraction to a formal iron(0) center. Although biological oxidases such as cytochrome p450^[12] rely on iron-based oxidation systems, these and related non-heme iron-based oxidation catalysts^[13] generally feature an iron(II) or iron(III) precursor that is supported by several nitrogen ligands. These systems typically activate C–H bonds through the generation of a high-valent (oxido)iron intermediate^[13c] from which hydrogen atoms (not hydride ions) are abstracted in a radical (or radical rebound) mechanism.^[13a,13b] Several outstanding examples of C–H oxidation have been reported recently based on this strategy.^[14] An iron homolog of **1**, however, would be structurally and mechanistically distinct: such a system would be supported by a redox-noninnocent cyclopentadienone li-

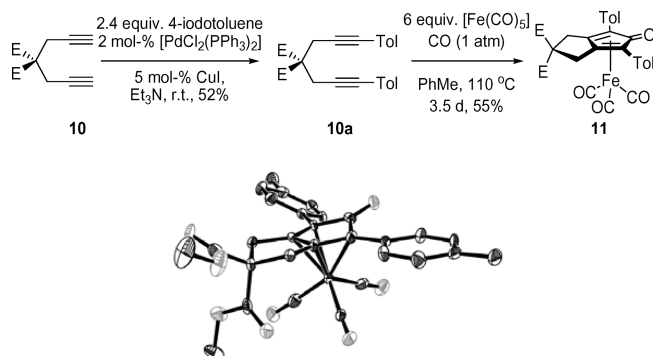


Scheme 3. Syntheses of **9** and **4**.

gand that would be an integral part of the catalyst's ligand-metal bifunctional nature, and C–H abstraction would involve transfer of a hydride ion, rather than a hydrogen radical. More closely related to our strategy are some examples of iron-catalyzed transfer hydrogenation catalysts in which a secondary alcohol is the hydrogen source. Some examples include a porphyrin-ligated system,^[15] [(PP3)Fe(H)(H₂)⁺][BPh₄][−] [PP3 = P(CH₂CH₂PPh₃)₃],^[16] and a cyclopentadienone-based system.^[17] The first two appear to have little homology with our system, but the third suggests a starting point.

Surprisingly, (cyclopentadienone)iron(0) complexes do participate in productive hydride abstraction reactions in oxidative media. We first investigated this by preparing bicyclic complex **11** (Scheme 4)^[18] and treating it with benzoquinone and alcohol **6a** in [D₆]benzene, which afforded only a trace amount of **7a** (Table 3, Entry 1). Curiously, we observe neither iron oxide formation nor ligand displacement from **11** under these conditions. Data in Table 2 suggested that this system could be improved by switching from doubly arylated complex **11** to fully phenylated complex **12**.^[19] This worked moderately (Entry 2) and enabled a yield of 24%. Much as in the case of **1**, application of acetone con-

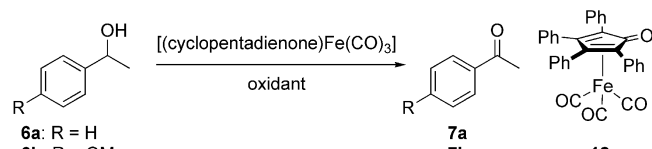
ditions for re-oxidation of our catalyst is advantageous. In this case, a yield of 38% of **7a** is realized (Entry 3). As predicted by Hammett analysis, rate, and thus conversion, are higher with alcohol **6b**: this substrate can be oxidized in up to 79% yield of **7b**.



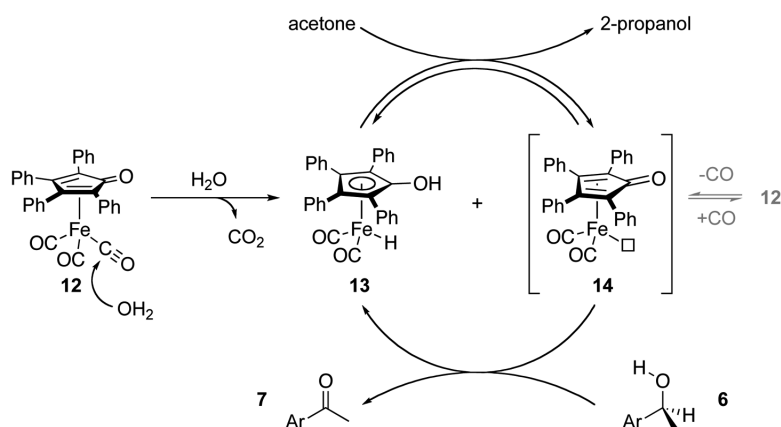
Scheme 4. Syntheses and X-ray structure of **11**.^[20] E = CO₂Me.

Although significant improvement remains to be made in the efficiency of this iron(0)-based oxidation system, we have gathered some data regarding its mechanism. An iso-

Table 3. Iron-catalyzed conversion of **6** to **7**.^[a]

						
Entry	[Fe]	Alcohol	Oxidant	Solvent	<i>T</i> [°C]	Yield (conv.), time
1	11 (0.1 equiv.)	6a	BQ	C ₆ D ₆	65	1% (1%), 16 h
2	12 (0.1 equiv.)	6a	BQ	C ₆ D ₆	65	11% (14%), 17 h
3	12 (0.1 equiv.)	6a	–	(CD ₃) ₂ CO	54	24% (26%), 4 d
4 ^[b]	12 (0.2 equiv.)	6b	–	(CD ₃) ₂ CO	80	38% (44%), 4 d
5 ^[b]	12 (0.5 equiv.)	6b	–	(CD ₃) ₂ CO	80	52% (79%), 4 d
						79% (97%), 2 d

[a] Yield and conversion were determined by NMR spectroscopy. BQ = benzoquinone. All reactions were run in screw-capped NMR tubes and prepared in air. [b] Experiments 4 and 5 were run with 1 equiv. (relative to **12**) of D₂O at 80 °C (bath temp.) in a J. Young NMR tube under reduced pressure after rigorous degassing.



Scheme 5. Proposed mechanisms for alcohol oxidation with catalyst precursor **12**.

tope effect (determined as above through 20% conversion at 50 °C) of 3.6(9) indicates that C–H bond cleavage occurs in the rate-limiting step. The relative facility of oxidation of **6b** relative to **6a** is consistent with the view that this cleavage is an electrophilic event, as is observed in the ruthenium system. To the extent that direct comparison is possible, iron-based system **12** is slower than ruthenium-based system **1**. In both cases, we perceive that the active catalytic species is a dicarbonyl(cyclopentadienone)metal complex (**14** or **3**) and that hydride abstraction by that species is rate-determining. For alcohol **6a**, we observe an initial turnover frequency of $7.8(1) \text{ h}^{-1}$ for ruthenium (**1**-based) and $0.10(1) \text{ h}^{-1}$ for iron (**12**-based) under analogous conditions. Although we believe that this reflects the relative energetics of hydride abstraction, an induction period for the initiation of **12** cannot be excluded.

Because complexes **11** and **12** are coordinatively saturated species (18 electrons), these are most likely precursors that enter a catalytic cycle by ligand dissociation. We perceive based on previous literature^[17b] that the mechanism of activation involves hydrolysis of one CO ligand to give CO_2 and intermediate **13** (Scheme 5). Thermal or photochemical dissociation of CO from **12** (highlighted in gray) is also a possibility. Once initiated, we believe that this mechanism proceeds analogously to Scheme 2.

Conclusions

Herein we describe mechanistic paradigms regarding the oxidation of alcohols with cyclopentadienone-ligated metal catalysts that are a key to our ongoing program in directed hydride abstraction: alcohol oxidation by **1** is a directed hydride abstraction, and even with an oxidant as weak as acetone, and under these mild conditions re-oxidation of intermediate ruthenium hydride **2** is rapid relative to k_2 . We also find that substituting even one phenyl group on parent complex **1** significantly attenuates the oxidation reactivity. Using these insights we have discovered a rare example of C–H oxidation that occurs at a (formal) iron(0) center within the ligand–metal bifunctional scaffold. This offers significant potential advantages over ruthenium, such as cost, toxicity, and environmental impact. Further studies regarding directed hydride abstraction reactions are ongoing in our laboratory.

Experimental Section

General: General procedures and instrumentation are defined fully in the Supporting Information. Preparative details for all other materials and graphical ^1H NMR spectra are provided in the Supporting Information. $[\text{D}_6]\text{Benzene}$ was vacuum-distilled from sodium/benzophenone ketyl for kinetics experiments. $[\text{D}_6]\text{Acetone}$ was used as received from Alfa Aesar. Shvo's catalyst (**1**) was purchased from Strem and used as received. Pentacarbonyliron(0) $[\text{Fe}(\text{CO})_5]$ and nonacarbonyliron(0) $[\text{Fe}_2(\text{CO})_9]$ were purchased from Strem, manipulated under air-free conditions and protected from light. Benzoquinone was recrystallized from ethanol and used as a yellow crystal. Alcohols **6a–d** were purchased from common suppliers and

distilled on a small scale immediately prior to use. Compound **9a** is commercially available, and compounds **9b–e** are known.^[11] Spectroscopy and data: NMR spectra were measured with a Varian Mercury 400 NMR spectrometer. NMR spectroscopic data were processed and analyzed with Varian vnmr 6.1c or Acorn NMR NUTS. Spectra acquired for kinetics analysis were taken with a 5 s pulse sequence ($> 5 \times T_1$). Charts and graphs were generated with Synergy Software KaleidaGraph 4. Error values were calculated and propagated by using traditional methods.

Kinetics: Sample procedure: A standard solution of Shvo's catalyst **1** (700 μL , 1.5 mM **1**, in $[\text{D}_6]\text{acetone}$) was added to an oven-dried screw-cap NMR tube. No further precautions were taken to exclude air or water. The sample was placed into the NMR spectrometer pre-warmed to 323(1) K, and 10.2 μL (1.01 mmol, to make 120 mM, 2.5 mol-% Ru atom) of alcohol **6a** was added by syringe, and timing begun. The tube was reinserted into the NMR spectrometer. Integrations were recorded in comparison to a 1,2-dichloroethane (4.7 μL) internal standard. Kinetic constants (pseudo-first order k_{obs}) were determined by statistical agreement of k_{obs} values measured individually for aryl, methyl, benzyl (**6a**), and isopropyl C–H signals in multiple runs. Air sensitivity: For the case of ruthenium complexes, independence of rate from air and water exposure was verified by side-by-side runs conducted in $[\text{D}_6]\text{benzene}$ with benzoquinone. One was prepared from solvent distilled from sodium/benzophenone ketyl and manipulated under air-free conditions, and the other was prepared with commercial materials on the bench top. Rate constants observed in these experiments were identical within error. This was not repeated in $[\text{D}_6]\text{acetone}$ because anhydrous acetone is known to undergo dehydrative dimerization.^[121] Kinetic isotope effects: Internal competition KIEs ($k_{\text{H}}/k_{\text{D}}$) were measured by comparison of [benzaldehyde] and $[\text{D}]\text{benzaldehyde}$ as observed in ^1H NMR integrations for benzaldehyde and $[\text{D}]\text{benzyl alcohol}$. For catalyst **1**, 25 points throughout the first 40% of conversion were used. For complex **12**, 4 points through 20% conversion were used. Error was calculated as the standard deviation of these measurements. To insure comparability of integrations, spectra were acquired with a calibrated 90° pulse, 5 s ac-

Table 4. Kinetic dependence on **[1]** as shown in Figure 1 (left).

Entry	[1] [mM]	$k_{\text{obs}} (\times 10^5 \text{ s}^{-1})$	$\ln [\textbf{1}]$	$\ln(k_{\text{obs}})$
1	1.50	7.55(26)	−6.50	−9.49(3)
2	2.90	11.1(1)	−5.84	−9.11(1)
3	4.50	11.6(1)	−5.40	−9.06(1)
4	6.50	14.1(1)	−5.04	−8.87(1)

Table 5. Kinetic dependence on [acetone] as shown in Figure 1 (right).

Entry	[acetone] [M]	$k_{\text{obs}} (\times 10^5 \text{ s}^{-1})$
1	13.6 (100 vol.-%)	7.55(26)
2	10.2 (75 vol.-%)	6.74(58)
3	6.80 (50 vol.-%)	6.12(12)
4	3.40 (25 vol.-%)	5.82(13)

Table 6. Data for Hammett plot (Figure 2).

Entry	Alcohol: R	$\sigma^{[7]}$	$k_{\text{obs}} (\times 10^5 \text{ s}^{-1})$	$\ln(k_{\text{obs}})$
1	6b : OMe	−0.268(77)	12.8(2)	0.228(15)
2	6c : Me	−0.170(46)	11.0(2)	0.164(17)
3	6a : H	0.000(34)	7.55(26)	0.000(20)
4	6d : F	+0.062(66)	6.53(11)	−0.063(32)

quisition time, and 45 s pulse delay. A control spectrum of [H_6]benzaldehyde showed < 5% error in ^1H integrations under these conditions (Tables 4, 5, and 6).

Preparative Details: Sample procedure of the oxidation of 1-phenylethanol: **1** (21.7 mg, 20.0 μmol), acetone (3 mL), and **6a** (121 μL , 1.00 mmol) were combined in a test tube with a stir bar. The resulting solution was subjected to reflux for 2 d, and the reaction mixture was cooled to room temperature, concentrated, and purified by flash column chromatography to afford **7a** (118 mg, 97%) as a colorless liquid.

Synthesis of 11: By cannulation, a 25 mL solution of **10**^[22] (0.42 g, 2.00 mmol) in NEt_3 was added to a 25 mL solution of 4-iodotoluene (1.09 g, 5.01 mmol), $[\text{PdCl}_2(\text{PPh}_3)_2]$ (0.03 g, 0.04 mmol), and $[\text{CuI}]$ (0.02 g, 0.10 mmol) under nitrogen. The mixture was stirred at room temperature for 18 h at which time all volatiles were removed under reduced pressure. The resulting oil was dissolved in CH_2Cl_2 and washed once each with ca. 20 mL of $\text{Na}_2\text{S}_2\text{O}_3$ solution and brine, respectively. The organic layer was then dried with MgSO_4 . Upon removal of all volatiles under reduced pressure, a golden-colored oil resulted. The oil was dissolved in 20 mL of hexanes and placed in a -15°C freezer overnight. The product was isolated and recrystallized from hexanes resulting in 0.37 g (57% yield) of off-white crystals of **10a**; m.p. 68–71 $^\circ\text{C}$. ^1H NMR ($[\text{D}]\text{-chloroform}$, 400 MHz): δ = 7.28 (d, $^3J_{\text{H,H}}$ = 7.5 Hz, 4 H, Ar-H), 7.09 (d, $^3J_{\text{H,H}}$ = 7.5 Hz, 4 H, Ar-H), 3.80 (s, 6H, OCH_3), 3.26 (s, 4 H, CH_2), 2.34 (s, 6 H, CH_3) ppm. ^{13}C NMR ($[\text{D}]\text{-chloroform}$, 100 MHz): δ = 169.5 (2 C), 138.2 (2 C), 131.6 (4 C), 129.0 (4 C), 120.0 (2 C), 83.9 (2 C), 83.2 (2 C), 57.3, 53.1 (2 C), 23.9 (2 C), 21.5 (2 C) ppm. FTIR (NaCl): $\tilde{\nu}$ = 3291 (w), 3030 (w), 2954 (m), 2923 (w), 1743 (s), 1734 (s), 1511 (s), 1436 (m), 1327 (m), 1294 (m), 1263 (m), 1212 (br., s), 1107 (w), 1076 (m), 1058 (m), 1022 (w), 991 (w), 943 (w), 853 (w), 817 (s), 668 (w) cm^{-1} . $\text{C}_{25}\text{H}_{24}\text{O}_4$ (388.46): calcd. C 77.30, H 6.23; found C 76.73, H 6.11. The reaction was run air-free in a method similar to that described by Pearson et al.^[18] Specifically, **10a** (0.11 g, 0.27 mmol) was dissolved in 600 mL of toluene (distilled from calcium hydride) in a 50 mL Strauss flask equipped with a stir bar. Next, $[\text{Fe}(\text{CO})_5]$ (0.22 mL, 1.63 mmol), previously degassed with N_2 was syringed into the flask. The flask was then flushed three times with CO gas and tightly sealed and placed into a 110 $^\circ\text{C}$ oil bath for 4 d. All volatiles were then removed under reduced pressure, resulting in the crude product as a powdery solid. The solid was treated with warm hexanes and filtered, resulting in 80 mg (55% yield) of pure **11** as a mustard-yellow solid; decomposition 201–204 $^\circ\text{C}$. ^1H NMR ($[\text{D}]\text{-chloroform}$, 400 MHz): δ = 7.94 (d, $^3J_{\text{H,H}}$ = 7.9 Hz, 4 H, Ar-H), 7.23 (d, $^3J_{\text{H,H}}$ = 7.5 Hz, 4 H, Ar-H), 4.22 (d, $^2J_{\text{H,H}}$ = 16.6 Hz, 2 H, CH_2), 3.52 (d, $^2J_{\text{H,H}}$ = 16.6 Hz, 2 H, CH_2), 3.92 (s, 3 H, OCH_3), 3.89 (s, 3 H, OCH_3), 2.38 (apparent s, 6 H, CH_3) ppm. FTIR (NaCl): $\tilde{\nu}$ = 3437 (br., s), 2067 (s), 2029 (m), 1987 (s), 1739 (m), 1653 (m), 1645 (m), 1623 (s), 1309 (w), 1260 (w), 1206 (w), 1189 (w), 1166 (m), 1134 (w), 1050 (w), 872 (w), 822 (m), 752 (w), 732 (w), 711 (w), 615 (m), 588 (w), 568 (w) cm^{-1} . $\text{C}_{29}\text{H}_{24}\text{FeO}_8$ (556.34): calcd. C 62.61, H, 4.35; found C 62.76, H 4.35.

Supporting Information (see footnote on the first page of this article): Complete general procedures, details of kinetics analysis (including graphical spectra), preparative details and graphical spectra for new compounds, and line-listed X-ray crystallographic data for **11**.

Acknowledgments

This research was supported by the University of Southern California, the Loker Hydrocarbon Research Institute, and the ACS

Petroleum Research Fund (grant 47987-G1). We thank Robert Bau and Tim Stewart for assistance with X-ray crystallography. T. J. W. thanks colleagues for insightful discussions: Kyung Jung, Surya Prakash, Mark Thompson, George Olah, Charles McKenna, Richard Brutchey, Tom Flood, and Nicos Petasis.

- [1] Regarding hydride transfer, see: a) N. C. Deno, H. J. Peterson, G. S. Saines, *Chem. Rev.* **1960**, *60*, 7–14. Some examples include: b) Z. Li, D. S. Bohle, C.-J. Li, *Proc. Natl. Acad. Sci. USA* **2006**, *103*, 8928–8933; c) S. J. Pastine, K. M. McQuaid, D. Sames, *J. Am. Chem. Soc.* **2005**, *127*, 12180–12181; d) W. H. N. Nijhuis, W. Verboom, A. A. El-Fadl, S. Harkema, D. N. Reinhoudt, *J. Org. Chem.* **1989**, *54*, 199–209. via SET; e) S. Fukuzumi, K. Ohkubo, T. Okamoto, *J. Am. Chem. Soc.* **2002**, *124*, 14147–14155; f) for a review, see: J.-E. Bäckvall, *J. Organomet. Chem.* **2002**, *652*, 105–111.
- [2] Y. Blum, D. Czarkie, Y. Rahamim, Y. Shvo, *Organometallics* **1985**, *4*, 1459–1461.
- [3] a) M. L. S. Almeida, M. Beller, G.-Z. Wang, J.-E. Bäckvall, *Chem. Eur. J.* **1996**, *2*, 1533–1536; b) J. B. Johnson, J.-E. Bäckvall, *J. Org. Chem.* **2003**, *68*, 7681–7684.
- [4] a) C. P. Casey, S. E. Beetner, J. B. Johnson, *J. Am. Chem. Soc.* **2008**, *130*, 2285–2295; b) C. P. Casey, S. W. Singer, D. R. Powell, R. K. Hayashi, M. Kavana, *J. Am. Chem. Soc.* **2001**, *123*, 1090–1100.
- [5] For a computational study of **1**-catalyzed hydrogenation of ketones, see: A. Comas-Vives, G. Ujaque, A. Lledós, *Organometallics* **2007**, *26*, 4135–4144.
- [6] Further information on the synthetic applications of **1** and its related system $[(\text{PPh}_3)_2\text{RuCl}_2]/\text{K}_2\text{CO}_3$ has been reported: M. L. S. Almeida, M. Beller, G.-Z. Wang, J.-E. Bäckvall, *Chem. Eur. J.* **1996**, *2*, 1533–1536.
- [7] L. P. Hammett, *J. Am. Chem. Soc.* **1937**, *59*, 96–103.
- [8] K. Kaneda, K. Mori, T. Hara, T. Mizugaki, K. Ebitani, *Catal. Surv. Asia* **2004**, *8*, 231–239.
- [9] K. Vijayasri, J. Rajaram, J. C. Kuriacose, *J. Mol. Catal.* **1987**, *39*, 203–217.
- [10] H. B. Özgün, N. Değirmenbaşı, *J. Chem. Res. (S)* **1997**, 32–33.
- [11] P. A. Wender, T. J. Paxton, T. J. Williams, *J. Am. Chem. Soc.* **2006**, *128*, 14814–14815.
- [12] J. T. Groves, Y.-Z. Han, in *Cytochrome P450: Structure, Mechanism, and Biochemistry*, 2nd ed. (Ed.: P. R. Ortiz de Montelano), Plenum Press, New York, **1995**.
- [13] a) M. Costas, M. P. Mehn, M. P. Jensen, L. Que Jr, *Chem. Rev.* **2004**, *104*, 939–986; b) M. M. Abu-Omar, A. Loaiza, N. Hontzas, *Chem. Rev.* **2005**, *105*, 2227–2252. Regarding the first mechanistic evidence implicating the role of a non-heme $\text{Fe}^{\text{V}}=\text{O}$ species in alkane hydroxylation, see: c) K. Chen, L. Que Jr, *J. Am. Chem. Soc.* **2001**, *123*, 6327–6337.
- [14] a) A. Company, L. Gómez, X. Fontrodona, X. Ribas, M. Costas, *Chem. Eur. J.* **2008**, *14*, 5727–5731; b) P. C. A. Bruijninx, I. L. C. Buurmans, S. Gosiewska, M. A. H. Moelands, M. Lutz, A. L. Spek, G. van Koten, R. J. M. Klein Gebbink, *Chem. Eur. J.* **2008**, *14*, 1228–1237; c) M. S. Chen, M. C. White, *Science* **2007**, *318*, 783–787; d) G. J. P. Britovsek, J. England, S. K. Spitzmesser, A. J. P. White, D. J. Williams, *Dalton Trans.* **2005**, 945–955.
- [15] S. Enthaler, G. Erre, M. K. Tse, K. Junge, M. Beller, *Tetrahedron Lett.* **2006**, *47*, 8095–8099.
- [16] C. Bianchini, E. Farnetti, M. Graziani, M. Peruzzini, A. Polo, *Organometallics* **1993**, *12*, 3753–3761.
- [17] Regarding a cyclopentadienone-ligated iron(II) catalyst for ketone hydrogenation, see: a) C. P. Casey, H. Guan, *J. Am. Chem. Soc.* **2007**, *129*, 5816–5817; b) H.-J. Knölker, E. Baum, H. Goessmann, R. Klaus, *Angew. Chem. Int. Ed.* **1999**, *38*, 2064.
- [18] Prepared according to a known procedure: A. J. Pearson, R. J. Shively, R. A. Dubbert, *Organometallics* **1992**, *11*, 4096–4104.

- [19] Prepared from $\text{Ph}_4\text{C}_5\text{O}$ and $[\text{Fe}_2(\text{CO})_9]$: G. N. Schrauzer, *J. Am. Chem. Soc.* **1959**, *81*, 5307–5310.
- [20] CCDC-690601 contains the supplementary crystallographic data for this paper. These data can be obtained free of charge from The Cambridge Crystallographic Data Centre via www.ccdc.cam.ac.uk/data_request/cif.
- [21] W. L. F. Armarego, C. L. L. Chai, *Purification of Laboratory Chemicals*, 5th ed., Elsevier, San Francisco, **2003**.
- [22] R. S. Atkinson, M. J. Grimshire, *J. Chem. Soc. Perkin Trans. 1* **1986**, 1215–1224.

Received: October 6, 2008

Published Online: December 2, 2008

Spin-Crossover 2D Metal–Organic Frameworks with a Redox-Active Ligand: $[\text{Fe}(\text{tff-adpy})_2\text{M}(\text{CN})_4] \cdot n\text{H}_2\text{O}$ (tff-adpy = 4-Tetrathiafulvalenylcarboxamidopyridine; $\text{M}^{\text{II}} = \text{Ni}, \text{Pd}, \text{Pt}$)

Víctor Martínez,^[a] Ana Belén Gaspar,^{*[a]} M. Carmen Muñoz,^[b] Rafael Ballesteros,^[c] Norma Ortega-Villar,^[d] Víctor M. Ugalde-Saldívar,^[d] Rafael Moreno-Esparza,^[d] and José Antonio Real^{*[a]}

Keywords: Metal–organic frameworks / Polymers / Spin crossover / Cooperative effects / Conducting materials

A new ttf (tetrathiofulvalene) ligand containing an amidopyridine moiety was synthesized and characterized. The electrochemical study of the 4-tetrathiofulvalenylcarboxamidopyridine (tff-adpy) ligand showed two reversible oxidation processes at $E'_{1/2} = 0.08 \text{ V/Fc}^+ - \text{Fc}$ and $E''_{1/2} = 0.26 \text{ V/Fc}^+ - \text{Fc}$. The crystal structure of $[(\text{tff-adpyH})_2\text{Pt}(\text{CN})_4]$ (**1**) was solved at 293 K, where **1** displays the triclinic space group $P\bar{1}$. The tff-adpyH⁺ molecule is planar, and the bond lengths within the ttf core are in the usual range for neutral ttf moieties. The tff-adpyH⁺ molecules and the $[\text{Pt}(\text{CN})_4]^{2-}$ anions organize in a three-dimensional network by means of hydrogen bonds and short S...S contacts. In the network, the tff-adpy molecules order following the pattern -D-A-D-A- (D = donor, pyridine; A = acceptor, ttf moieties). Reaction of the $\text{Fe}(\text{BF}_4)_2 \cdot 6\text{H}_2\text{O}$ salt, tff-adpy ligand and the $[\text{M}(\text{CN})_4]^{2-}$ coordinating counterions led to the 2D Hofmann-like polymers $[\text{Fe}(\text{tff-adpy})_2\text{M}(\text{CN})_4] \cdot n\text{H}_2\text{O}$ [$\text{M} = \text{Ni}^{\text{II}}$; $n = 1.5$ (**2**), 0 (**5**); Pd^{II} ;

$n = 2$ (**3**), 0 (**6**); Pt^{II} $n = 2$ (**4**), 0 (**7**)]. A 2D structure for **2–7** was proposed on the basis of analytical data. Compounds **2–4** present a complete thermally induced two-step spin transition. It is observed in the temperature interval from 100 to 200 K for **2**; whereas for **3** and **4** it occurred in the interval of 200–250 K. The spin-transition properties of **2–4** were found to be strongly dependent on the water content, as non-hydrated materials **5–7** are paramagnetic in the studied temperature range (5–350 K). The thermodynamic parameters associated with the spin transition estimated from DSC measurements are: $\Delta H_1 = 5.7 \text{ kJ mol}^{-1}$ (**3**), 6.2 kJ mol^{-1} (**4**), $\Delta H_2 = 6.5 \text{ kJ mol}^{-1}$ (**3**), 7.2 kJ mol^{-1} (**4**) and $\Delta S_1 = 24 \text{ J K}^{-1} \text{ mol}^{-1}$ (**3**), $26.6 \text{ J K}^{-1} \text{ mol}^{-1}$ (**4**), $\Delta S_2 = 30.4 \text{ J K}^{-1} \text{ mol}^{-1}$ (**3**) and $32.8 \text{ J K}^{-1} \text{ mol}^{-1}$ (**4**).

(© Wiley-VCH Verlag GmbH & Co. KGaA, 69451 Weinheim, Germany, 2009)

Introduction

Electrical conductivity is a fundamental property of matter that is currently being investigated with respect to molecular science. Since the discovery of electrical conductivity in perylene bromide,^[1] considerable effort has been invested to obtain high T_c superconductors based on organic^[2] and organometallic charge-transfer complexes and radical-ion salts.^[3–5] Presently, the trend in the field of molecular conductors aims towards the design of multifunctional materi-

als combining in a synergetic fashion a second interesting physical property^[2–5] [i.e., spin crossover^[6] (SCO), optical or magnetic properties^[4]]. The tailoring of this kind of molecular materials represents a challenge for synthetic chemists due to the difficulties found in controlling the self-assembly of the molecular building blocks.

The spin-crossover phenomenon is one of the best examples of molecular bistability.^[6] SCO materials display labile electronic configurations that can switch between the high-spin (HS) and low-spin (LS) states leading to distinct changes in magnetism, colour and structure, which may be driven by variations in temperature and/or pressure and by light irradiation (LIESST effect).^[7] Their magnetic, optical and structural properties may be altered drastically in a narrow range of temperatures and/or pressures for cooperative spin transitions. Cooperativity may be accompanied by hysteresis (memory effect) when the cohesive forces communicating between the SCO centres in the solid state propagate the structural changes cooperatively throughout the whole lattice. A crossover between the HS and LS configurations occurs when the change in the Gibbs free energy $\Delta G_{\text{HL}} = G_{\text{HS}} - G_{\text{LS}}$ is in the range of thermal energy.

[a] Institut de Ciència Molecular (ICMOL)/Departament de Química Inorgànica, Universitat de València, Edifici de Instituts de Paterna,

Apartat de Correus 22085, 46071 València, Spain

[b] Departament de Física Aplicada, Universitat Politècnica de València, Camí de Vera s/n, 46022 València, Spain

[c] Departament de Química Orgànica, Facultat de Farmàcia, Avd. Vicente Andrés Estellés s/n, 46100 Burjassot, València, Spain

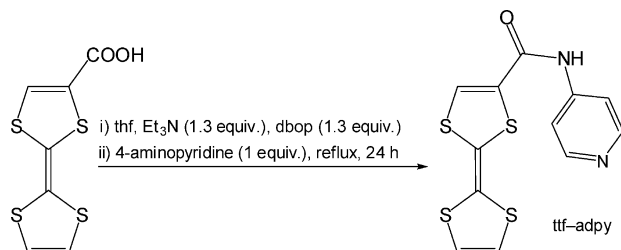
[d] Facultad de Química, Departamento de Química Inorgànica, Universidad Nacional Autónoma de México, Av. Universidad 3000, México, D.F. 04510, México

Supporting information for this article is available on the WWW under <http://www.eurjic.org> or from the author.

With regard to the combination of spin-crossover and electrical conductivity properties in a single material, two different synthetic approaches can be underlined. From one side, the assembly of switchable molecular spin-crossover building blocks with radical ionic salts has recently been proposed as a strategy to tune the conducting properties by acting on the bistable cation.^[8–10] This strategy has already led to some interesting results, such as, the $\{[\text{Fe}(\text{sal}_2\text{-trien})][\text{Ni}(\text{dmit})_2]_3\}$ ^[8] and $\{[\text{Fe}(\text{qsal})_2][\text{Ni}(\text{dmit})_2]_3\} \cdot \text{CH}_3\text{CN} \cdot \text{H}_2\text{O}$ ^[9] salts obtained from electrolysed solutions of $\{[\text{Fe}(\text{sal}_2\text{-trien})][\text{Ni}(\text{dmit})_2]\}$ and $\{[\text{Fe}(\text{qsal})_2][\text{Ni}(\text{dmit})_2]\} \cdot 2\text{CH}_3\text{CN}$, respectively. The cationic units undergo cooperative SCO behaviour and the $[\text{Ni}(\text{dmit})_2]^{2-}$ layers enable electron transport. At room temperature, the electrical conductivity of these molecular compounds is 0.20 and 2.0 Scm^{-1} , respectively. Another achievement in this research line is represented by $\{[\text{Ni}(\text{dmit})_2]_5[\text{Fe}(\text{salEen})_2]_2\} \cdot 6\text{CH}_3\text{CN}$,^[10] a fractional oxidation state complex, which behaves like a semiconductor and exhibits a gradual but complete spin transition between 300 and 4 K. However, to the best of our knowledge no interplay/synergy was observed between the physical properties gathered in these molecular materials.

Another approach currently under investigation in this context consists of a covalent linkage of paramagnetic metal ions to redox-active ligands. The association of redox-active moieties and heteroatom-based ligands capable of coordinating to the metallic centre provides a novel perspective for the modulation of collective electronic properties of the resulting bifunctional material.^[11] The suitability of the ligand bedt-ttf-bipy [4,5-ethylenedithio-4',5'-(4'-methyl-2,2'-dipyrid-4-ylethylenedithio)tetrathiafulvalene] to induce spin-crossover behaviour in Fe^{II} compounds was investigated by Ouahab and coworkers.^[12] In the synthesized compound, $[\text{Fe}(\text{bedt-ttf-bipy})_2(\text{NCS})_2]$, no spin-crossover behaviour was observed. Approximately 50% of the iron(II) ions are in the LS state at 300 K, whereas the rest remains in the HS state in the range of temperatures investigated (5–300 K).

Taking into account the well-known suitability of pyridine and pyridine-substituted ligands to induce a crystal field strength around the iron(II) centre near to the crossover point,^[6,14–16] we decided to investigate the suitability of the ligand ttf-adpy (4-tetrathiofulvalenylcarboxamidopyridine) for the synthesis of Fe^{II} metal–organic frameworks with spin-crossover properties. In this contribution we shall present a detailed study of the synthesis and characterization of the new ligand ttf-adpy (Scheme 1), as well



Scheme 1. Synthesis of the ttf-adpy ligand.

as the synthesis and physical characterization of a novel family of Hofmann-like spin-crossover polymers obtained by self assembly of the $\text{Fe}(\text{X})_2$ salt, the ttf-adpy ligand and $[\text{M}(\text{CN})_4]^{2-}$ coordinating counterions. The general formula of these polymers obey to $\{[\text{Fe}(\text{ttf-adpy})_2][\text{M}(\text{CN})_4]\} \cdot n\text{H}_2\text{O}$ [$\text{M} = \text{Ni}^{\text{II}}$; $n = 1.5$ (2), 0 (5); Pd^{II} ; $n = 2$ (3), 0 (6); Pt^{II} $n = 2$ (4), 0 (7)].

Results and Discussion

The synthesis of the ttf-adpy ligand was performed by following the procedure shown in Scheme 1 by coupling ttfCOOH with 4-aminopyridine with the use of dbop as a catalyst. Further details concerning the synthesis are given in the Experimental Section.

Electrochemistry of the ttf-adpy Ligand

The electrochemical study of the ttf-adpy ligand is presented in Figure 1 and in the Supporting Information. The study was performed by dissolving 1.57 mg of the ttf-adpy ligand in dmsO (spectroscopic grade) and by using tetrabutylammonium hexafluorophosphate (0.1 M) as the electrolyte on a glassy carbon electrode. The typical voltammograms for ttf-adpy when the potential scans were started in the negative and positive directions present differences (Figure S5a, Supporting Information). Therefore, the oxidation processes were investigated in the potential interval between -0.86 and 0.74 V. Analysis of the different inverse anodic potentials for the ttf-adpy ligand (Figure S5b, Supporting Information) allows the half-wave potentials for this system to be evaluated:

$\text{ttf-adpy} \rightarrow \text{ttf-adpy}^+ + 1\text{e}^-$ first oxidation, $E'_{1/2} = 0.08 \text{ V}/\text{Fc}^+/\text{Fc}$

$\text{ttf-adpy}^+ \rightarrow \text{ttf-adpy}^{++} + 1\text{e}^-$ second oxidation, $E''_{1/2} = 0.26 \text{ V}/\text{Fc}^+/\text{Fc}$

$\text{ttf-adpy} + \text{ttf-adpy}^{++} \rightarrow 2 \text{ttf-adpy}^+$ comproportionation, $E'_{1/2} = 0.08 < E''_{1/2} = 0.26 \text{ V}$

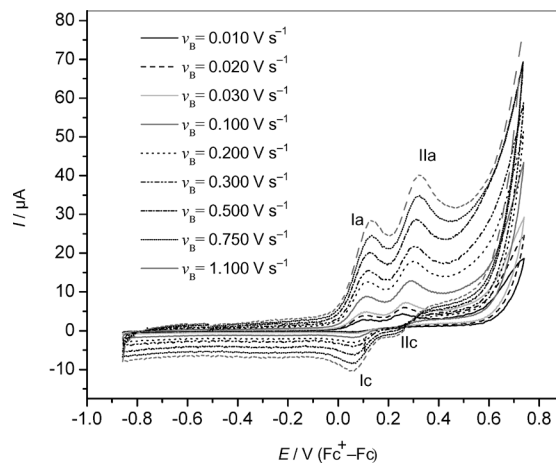


Figure 1. Cyclic voltammograms of the ttf-adpy ligand recorded in dmsO.

In addition, the electrochemical study was performed at different scan rates (Figure 1). This study confirmed that both oxidation steps are reversible and associated to Ia–Ic and IIa–IIc processes, respectively. The characteristics of the oxidation and reduction peaks in the second process suggest that a chemical reaction is connected with the product of the second oxidation (ttf-adpy^{++}). Unfortunately, we do not have sufficient information to propose anything more specific. From this study it is concluded that the ttf-adpy ligand is more prone to oxidation than the ttf -based ligands reported by Batail and coworkers.^[11] Indeed, the oxidation potentials for the first and second processes are 0.67 and 0.92 V/ $\text{F}_c^+ - \text{F}_c$, respectively, for the tightly related ligand $\text{edt-ttf-CONH-}p\text{-py}$ [= 4,5-ethylenedithio-4'-(*p*-pyridylcarbamoyl)tetrathiafulvalene]. Most likely, these differences stem from the ethylenedithio moiety attached to the $\text{ttf-CONH-}p\text{-py}$ group, which protects it from oxidation. However, we have to be careful with this comparison, as Batail and coworkers^[11] do not give details of the experimental conditions employed, and this prevents knowing how they used the saturated calomel electrode (ECS). This can provoke a small variation in the “real” potentials of approximately 20–40 mV. Anyhow, this difference is much smaller than the difference observed between the oxidation potentials measured for the ttf-adpy and $\text{edt-ttf-CONH-}p\text{-py}$ ligands and confirms that the former is more easily oxidized than the latter.

UV/Vis Spectrum of ttf-adpy

The UV/Vis spectrum of ttf-adpy was recorded at 293 K in different solvents: CH_3CN , CH_3OH and dmf . The spectra reveal mainly three peaks independent of the solvent used: one has a low intensity band at low energy (440 nm), whereas the other two appear at higher energies (315 and 290 nm) and show strong intensities (Figure 2). The spectra obtained are in reasonable agreement with that observed for the ttf molecule in cyclohexane.^[13] The band observed at 440 nm corresponds to the lowest allowed transition (π –

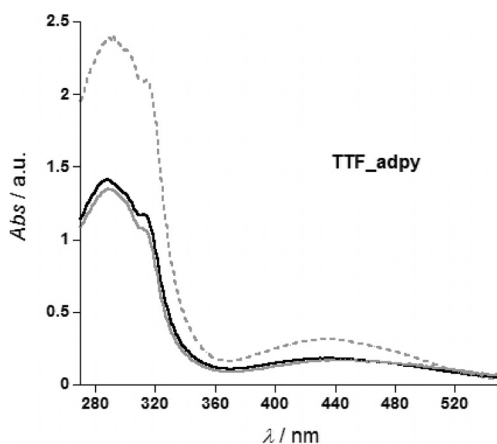


Figure 2. UV/Vis spectra of the ttf-adpy ligand recorded in CH_3CN (black line), CH_3OH (grey line) and dmf (dashed grey line).

σ). MO calculations for the ttf molecule indicate that the next band in order of increasing energy should be a weak π – σ transition. The spectrum of ttf-adpy , as well as that of ttf , show that this weak π – σ transition (368 nm) lies on the tail of the band as a result of the π – π transition being located at 315 nm for the ttf-adpy ligand (317 nm for ttf). The next allowed π – π transition presumably corresponds to the maxima observed at 290 nm for the ttf-adpy ligand (303 nm for ttf). Further allowed π – π transitions fall out of the UV/Vis energy range and are not seen in the spectra.

Crystal Structure of $[(\text{ttf-adpyH})_2\text{Pt}(\text{CN})_4]$ (**1**)

The crystal structure determination was performed at 293 K for **1**. At 293 K, **1** displays the triclinic space group $P\bar{1}$. A selection of crystallographic data and bond lengths and angles is given in Tables 1, 2 and 3. An ORTEP diagram of **1** with the corresponding atom numbering scheme is shown in Figure 3. The unit cell contains two molecules of ttf-adpyH^+ and one $[\text{Pt}(\text{CN})_4]^{2-}$ group. The ttf-adpyH^+ molecule is planar with dihedral angles Φ , θ_1 , θ_2 and θ_3 equal to, 2.30(7), 5.89(8), 1.3(3) and 3.1(2)°, respectively (Scheme 2). Bond lengths within the ttf core are in the usual range for neutral ttf moieties^[11,17] (Table 1). An illustration

Table 1. Geometrical characteristics of the ttf core in **1** at 293 K.

C=C Bond lengths / Å			
C6–C5	1.334(9)	C2–C1	1.297(13)
C3–C4	1.338(9)		
C–S Bond lengths / Å			
S4–C6	1.756(6)	S3–C5	1.719(7)
S4–C4	1.758(6)	S3–C4	1.756(7)
S1–C1	1.745(9)	S2–C2	1.735(9)
S1–C3	1.766(6)		

Table 2. Selected bond lengths and angles for **1** at 293 K.

Bond lengths / Å			
N1–C7	1.357(8)	C11–C12	1.364(10)
N1–C8	1.383(8)	C8–C12	1.400(9)
C8–C9	1.397(8)	Pt–C13	2.003(7)
C10–C9	1.373(9)	Pt–C14	1.995(7)
N2–C10	1.326(9)	C14–N4	1.144(9)
N2–C11	1.335(9)	C13–N3	1.151(9)
Bond angles / °			
O1–C7–N1	123.7(6)	C5–C6–C7	129.4(6)
O1–C7–C6	118.9(6)	C7–N1–C8	127.1(5)
N1–C7–C6	117.4(5)	C13–Pt–C14 ^[a]	90.5(3)

[a] $i = 2 - x, -y, -z$.

Table 3. Intermolecular contacts (Å) for **1** at 293 K.

N1–N3	3.194(8)
N2–N4 ⁱ ; $i = 1 - x, 1 - y, -z$	2.791(9)
O1–C9 ⁱⁱ ; $ii = 1 - x, 1 - y, 1 - z$	3.260(8)
O1–C10 ⁱⁱ ; $ii = 1 - x, 1 - y, 1 - z$	3.128(9)
S3–S3 ⁱⁱⁱ ; $iii = 2 - x, -y - 1, 1 - z$	3.512(2)

of the crystal packing of **1** in the yz plane is shown in Figure 4. Table 3 gathers the most representative intermolecular distances. The ttf-adpyH^+ molecules and $[\text{Pt}(\text{CN})_4]^{2-}$ anions organize in a three-dimensional network

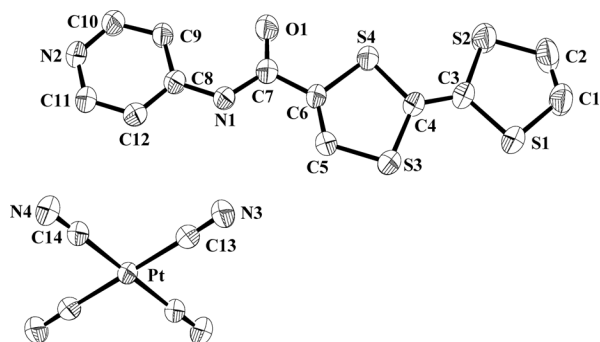
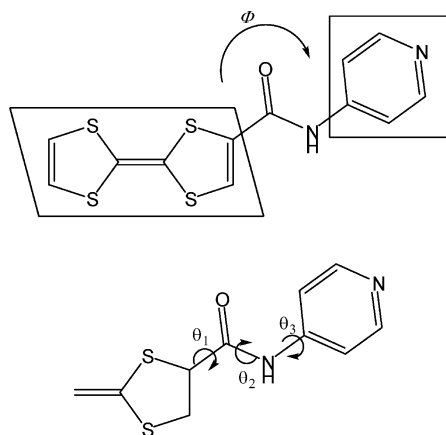


Figure 3. ORTEP diagram of $[(\text{ttf-adpyH})_2\text{Pt}(\text{CN})_4]$ (**1**) at 293 K with the corresponding atom numbering scheme. Displacement ellipsoids are shown at the 50% probability levels.



Scheme 2. Intramolecular dihedral angles of the ttf-adpy ligand.

through hydrogen bonds and short $\text{S}\cdots\text{S}$ contacts. Infinite chains of the ttf-adpyH^+ molecules running along the y axis are sustained by hydrogen bonds and short $\text{S}\cdots\text{S}$ contacts (Figure 4a,b). The chains are organized in such a way that the ttf-adpyH^+ molecules stack in a “head-to-tail” fashion along the x axis thereby forming an infinite stable two-dimensional -D-A-D-A- array (D = donor, pyridine; A = acceptor, ttf moieties). The shortest interactions between the ttf-adpyH^+ molecules are $\text{O1}\cdots\text{H}(\text{C9})$ 3.260(8) Å, $\text{O1}\cdots\text{H}(\text{C10})$ 3.128(9) Å and $\text{S3}\cdots\text{S3}$ 3.512(2) Å. In addition, hydrogen bonds are present between the N1 atom of the amide groups of the ttf-adpy ligand and the N3 and N4 atoms of the $[\text{Pt}(\text{CN})_4]^{2-}$ groups [$\text{N1}\cdots\text{H}(\text{N3})$ 3.194(8) Å and $\text{N2}\cdots\text{H}(\text{N4})$ 2.791(9) Å]. These intermolecular contacts together with those previously mentioned lead to the formation of a three-dimensional network (Figure 4c). In contrast, the crystal packing of the $\text{edt-ttf-CONH-}p\text{-py}$ ligand consists of a one-dimensional infinite chain of molecules sustained by a hydrogen bond defined by $\text{CO}\cdots\text{H-C}$ and donor-acceptor electrostatic interactions leading to an infinite stable -D-A-D-A- assembly.

IR Spectroscopic Study of 2–7

The information about the coordination mode of the $[\text{M}(\text{CN})_4]^{2-}$ groups and the ttf-adpy ligand in complexes **2–7** can be derived directly from the IR spectra measured at room temperature. For compounds **2–4** the IR spectra are given in Figure S3 (Supporting Information). Those corresponding to **5–7** are not given, because they match the IR spectra of their respective hydrated form. For the noncoordinated ttf-adpy ligand, a band at 1640 cm^{-1} assigned to the C=N bond stretches of the ring is observed. It is shifted to the high-frequency region in the case of coordination. Indeed, the value of this band in coordination polymers lies

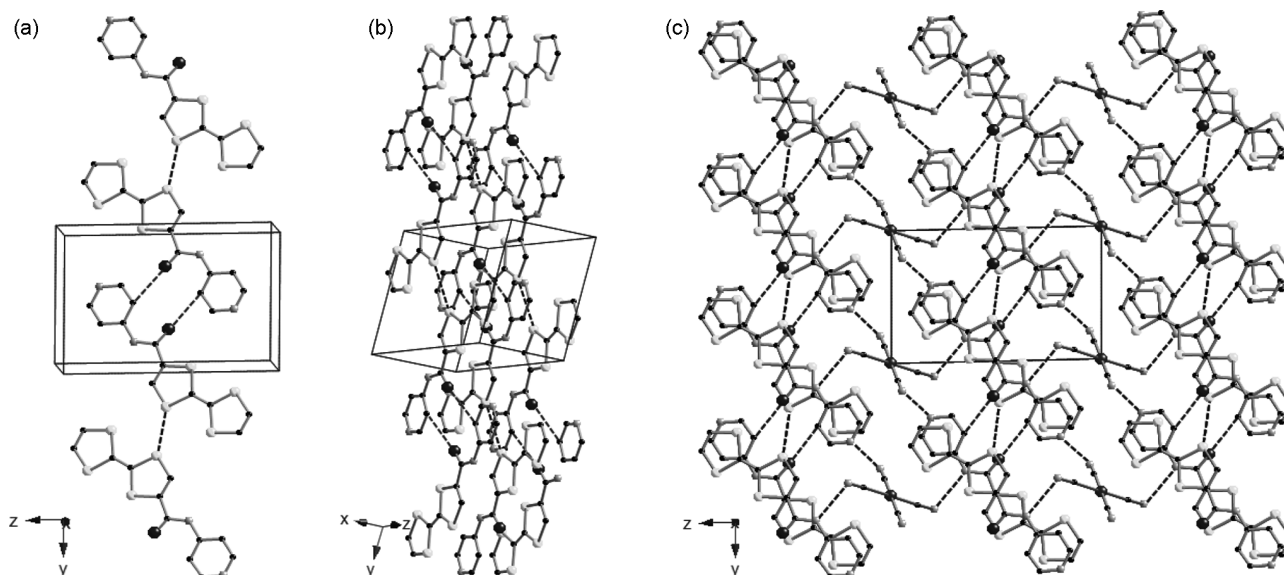


Figure 4. (a) View of the -D-A-D-A stack of ttf-adpy molecules along the y axis; (b) packing along the x axis; (c) view of the crystal packing of **1** in the yz plane. Intermolecular contacts are plotted as dash lines, $\text{S}\cdots\text{S}$; $\text{O}\cdots\text{C}$ and $\text{N}\cdots\text{N}$.

typically 15–30 cm^{−1} higher relative to that of the free ligand, and for compounds **2–4** these bands are observed at 1670, 1672 and 1672 cm^{−1}. For the [M(CN)₄]^{2−} groups, it is a common observation that the vibrational frequency associated with the stretching mode of the cyanide bridge is above that of the corresponding terminal cyanide (2120–2130 cm^{−1}, noncoordinated). In fact, for compounds **2–4** it appears at 2155, 2160 and 2158 cm^{−1}.

X-ray Powder Diffraction of **2**

X-ray powder diffraction patterns (XRPD) for **2–4** were recorded at 293 K (Figure S6, Supporting Information). Compounds **2–4** have very similar profiles, where the representative peaks are as follow: 2 θ : 5.08, 10.31, 12.13, 15.50, 16.83, 17.85, 19.71, 22.90, 23.88°. From these XRPD profiles one can conclude that compounds **3** and **4** are isostructural, whereas the structure of **2** must be closely related to them. Taking into account the analytical data [IR, energy-dispersive X-ray microanalysis (EDXA) and CHN analysis] of compounds **2–4** it is reasonable to propose a similar 2D structure as reported for {Fe(py)₂[M(CN)₄]} (py = pyridine, M = Ni^{II},^[14a] Pd^{II},^[14b] Pt^{II},^[14b] see the Supporting Information, Figure S7). It consists of two-dimensional extended metal cyanide sheets constructed by the alternate linkage of square-planar M^{II} (Ni, Pd or Pt) and octahedral Fe^{II} ions through cyano bridges. The Fe^{II} ion is coordinated in an octahedral fashion by four terminal N atoms of the cyano groups and two N atoms of two py ligands in a *trans* configuration.^[14]

Magnetic Properties of **2–7**

The magnetic data expressed in the form of $\chi_M T$ vs. T , where χ_M is the molar magnetic susceptibility and T the temperature, is shown in Figure 5 for compounds **2–7**. The temperature dependence of the magnetic susceptibility was recorded on microcrystalline samples over range from 300 to 5 K in a field of 1 T at a rate of 1 K min^{−1}. At 300 K, the $\chi_M T$ value is 3.72 (**2**), 3.60 (**3**) and 3.75 (**4**) cm³ K mol^{−1}, which is in the range of values expected for an Fe^{II} ion in the HS state. For **2**, this value is practically temperature independent between 300 and 185 K. Then, below 185 K it decreases abruptly and reaches a plateau centred at around 2.13 cm³ K mol^{−1} in the temperature range 164–141 K, over which $\chi_M T$ varies smoothly. The $\chi_M T$ value in this flat region corresponds to about 50% of the complete spin transition taking place in two differentiated steps. The first step has a characteristic temperature $T_{1/2}^1 = 172$ K ($T_{1/2}$ and T_c are the characteristic temperature at which the number of molecules in both spin states is equal, $T_{1/2}$ is used in the case of second-order phase transitions and T_c for first-order phase transitions). Below $T = 140$ K, a second drop in the value of $\chi_M T$ centred at $T_{1/2}^2 = 110$ K is observed; this corresponds to a second spin transition that is much more continuous than the first one. The two-step spin transition observed in **2** can be considered practically complete as far as

the $\chi_M T$ value at 5 K is 0.50 cm³ K mol^{−1}. In the warming mode, the temperature dependence of $\chi_M T$ matches that of the cooling mode.

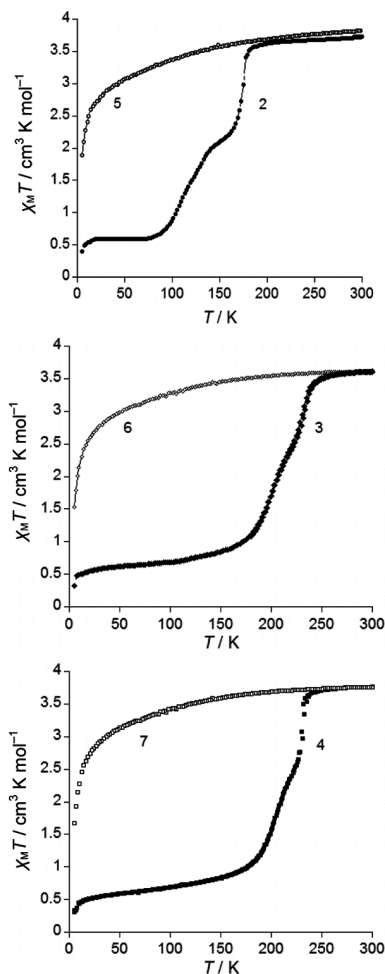


Figure 5. Temperature-dependent magnetic susceptibility measurements for **2–7** at atmospheric pressure (rate of measurements: 1 K min^{−1}).

Like **2**, compounds **3** and **4** undergo a two-step spin transition but at higher temperatures. The first spin transition is more abrupt than the second one for both compounds being centred in the cooling mode at $T_c^{1\downarrow} = 228$ K [$T_c^{2\downarrow} = 197$ K] (**3**) and $T_c^{1\downarrow} = 228$ K [$T_c^{2\downarrow} = 202$ K] (**4**). In contrast to that observed for **2**, the plateau region between the two spin transitions is less pronounced for **3** and **4**. The $\chi_M T$ values found for **3** and **4** at low temperature (5 K) are equal to 0.48 (**3**) and 0.46 (**4**) cm³ K mol^{−1}, which indicate that the $S = 2 \leftrightarrow S = 0$ transition is practically complete. The temperature dependence of the magnetic susceptibility recorded in the warming mode denotes a very narrow hysteresis that is 2 K in width for both **3** and **4**.

The magnetic properties of dehydrated complexes **5–7** were investigated (Figure 5). Dehydration of the complexes is complete at 350 K as TGA analysis confirms (Figure S4, Supporting Information). However, after dehydration compounds **5–7** lose crystallinity, which is recovered after rehy-

dration. The dehydration/hydration is a reversible process, as compounds **2–4** are recovered after compounds **5–7** are suspended in water for 1 d. The samples were heated from 300 to 350 K and then kept at this temperature for 15 min in the SQUID magnetometer under vacuum. Subsequently, the magnetic susceptibility of the dehydrated samples was recorded from 300 down to 5 and up to 300 K. The temperature dependence of the magnetic susceptibility of compounds **5–7** shows a paramagnetic behaviour in the whole temperature range under study. At 300 K, the $\chi_{\text{M}}T$ value is 3.72 (**5**), 3.60 (**6**) and 3.75 (**7**) $\text{cm}^3 \text{K mol}^{-1}$ and remains constant down to 100 K, where it diminishes most probably due to zero-field splitting of the $S = 2$ spin state of the Fe^{II} ions and/or intermolecular antiferromagnetic interactions.

Differential Scanning Calorimetry

Differential scanning calorimetry (DSC) measurements for **3** and **4** were carried out in the 170–300 K temperature range at a rate of 5 K min^{-1} . Due to the low temperature of the spin transition of **2**, we were not able to record the complete DSC profile, because the lower working temperature of the DSC setup is 120 K. The thermal dependence of the anomalous heat capacity, ΔC_p , obtained from DSC measurements is shown for **3** and **4** in Figure 6. For **3**, anomalies in the heat capacity appear in the cooling mode at $T_{\text{c}}^{\downarrow} = 236 \text{ K}$ and at $T_{\text{c}}^{\downarrow} = 213 \text{ K}$. In the warming mode, the anomalies in ΔC_p appear at different temperatures, denoting that the spin transition is accompanied by a few Kelvin hysteresis width ($T_{\text{c}}^{\uparrow} = 239 \text{ K}$ and at $T_{\text{c}}^{\uparrow} = 215 \text{ K}$). These values agree reasonably well with those observed from the

$\chi_{\text{M}}T$ vs. T plot. Compound **4** exhibits anomalies in the heat capacity at $T_{\text{c}}^{\downarrow} = 233 \text{ K}$, $T_{\text{c}}^{\downarrow} = 216 \text{ K}$, $T_{\text{c}}^{\uparrow} = 237 \text{ K}$ and at $T_{\text{c}}^{\uparrow} = 219 \text{ K}$, which are comparable with those obtained from magnetic data. The small differences in critical temperatures between the DSC and magnetic data have their origin in the different rate at which the experiments were done. Table 4 summarizes the derived thermodynamic parameters ΔH_{SCO} and ΔS_{SCO} for compounds **3** and **4**; the values obtained are in the range of the values expected for spin transitions in Fe^{II} compounds.^[6,18]

Table 4. Thermodynamic parameters ΔH and ΔS for **3** and **4** deduced from DSC analysis.

	$\Delta H / \text{kJ mol}^{-1}$		$\Delta S / \text{J K}^{-1} \text{mol}^{-1}$	
	ΔH_1	ΔH_2	ΔS_1	ΔS_2
3	5.7	6.5	24	30.4
4	6.2	7.2	26.6	32.8

Conclusions

In this contribution we reported the synthesis of the redox-active ttf-adpy ligand and demonstrated its suitability in combination with the $[\text{M}(\text{CN})_4]^{2-}$ coordinating counterions for the synthesis of Fe^{II} metal–organic frameworks exhibiting spin-crossover properties. Although many attempts were performed to obtain single crystals of the $\{\text{Fe}(\text{ttf-adpy})_2[\text{M}(\text{CN})_4] \cdot n\text{H}_2\text{O}\}$ polymers, all were unsuccessful. H-shaped tube slow diffusion experiments resulted in the formation of microcrystalline powders of the polymers, whereas **1** was accidentally obtained as a byproduct during the synthesis of **4**. Concerning the spin-transition behaviour in the $\{\text{Fe}(\text{ttf-adpy})_2[\text{M}(\text{CN})_4] \cdot n\text{H}_2\text{O}\}$ polymers, it is noticeable that the water molecules contained in the lattice plays a dominant role in defining the spin-crossover behaviour. Indeed, the hydrated polymers undergo relatively abrupt two-step spin transition, whereas the nonhydrated polymers are in the HS state in the temperature range investigated. This result is in agreement with the general observation for SCO compounds: stabilization of the LS state through hydrogen bonding of the water molecule with the ligand.^[6] Most probably, this is the case for the polymers under study, as the amide group of the ttf-adpy ligand is prone to form hydrogen bonds. At variance with the precedent systems $\{\text{Fe}(\text{py})_2[\text{M}(\text{CN})_4]\}$ ($\text{M} = \text{Ni}^{\text{II}}$,^[14a] Pd^{II} ,^[14b] Pt^{II} ^[14b]) the spin transition is less cooperative in the ttf-adpy-based polymers, because the distance between the 2D sheets is longer and separated by flexible ttfCONH moieties, which probably work as shock absorbers instead of transmitters of the spin-transition structural changes. Thus, cooperative intersheet interactions are less efficient.

A further step in this research is to achieve conductivity in these SCO polymers. Ongoing work is focused on the oxidation of the ttf moieties by using electrocrystallization techniques and chemical agents.

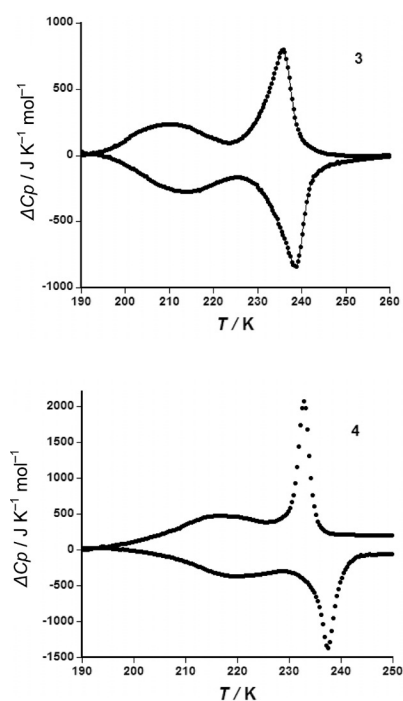


Figure 6. DSC measurements performed at a rate of 5 K min^{-1} for **3** and **4**.

Experimental Section

Materials: Starting reagents and solvents were purchased from commercial sources and used as received or dried in the case of solvents.

Measurements: IR spectra were recorded at 293 K by using a Nicolet 5700 FTIR spectrometer with the samples prepared as KBr discs. Elemental analyses were done with an Elemental Analyzer CE Instrument EA 1110 CHNS. ^1H NMR spectroscopic measurements were done with an Avance DRX Bruker 300 MHz spectrometer. Mass spectroscopy was done with a Bruker Esquire 3000 ion trap spectrometer. Microanalysis was done by using PV 9760 EDAX Microanalysis with a PHILIPS XL 30 ESEM scanning electron microscope.

Synthesis of ttf-adpy : To a mixture of 4-carboxytetrathiafulvalene (ttfCOOH ; 1 g, 1 equiv.), Et_3N (0.733 mL, 1.3 equiv.) and diphenyl(2,3-dihydroxy-2-thioxo-3-benzoxazoly)phosphonate (dbop ; 1.84 g 1.3 equiv.) in dry thf (300 mL) was added 4-aminopyridine (0.379 g, 1 equiv.). The final mixture was heated at reflux for 24 h and then filtered to eliminate solid impurities. The solvent was evaporated under reduced pressure. The obtained dark brown oil was dried under vacuum (10^{-2} Torr) for 4 h. H_2O (300 mL) was poured over the dry thick brown oil, and the mixture was sonicated (5×15 min). The resulting crude precipitate was filtered, washed with water and dried under vacuum. The crude was then dissolved in dmf (100 mL) and H_2O (ca. 1 L) was poured onto this solution to precipitate the pure ttfadpy ligand. The product was filtered, washed with water and dried under vacuum. Yield: 998 mg (81%). MS (EI): m/z (%) = 125.1 (96) $[\text{M}]^+$, 108.1 (100) $[\text{M} - \text{O}]^+$. ^1H NMR (300 MHz, $[\text{D}_6]\text{dmsO}$): δ = 10.57 (s, 1 H, NH), 8.45 (d, J = 6.25 Hz, 2 H, PyH), 7.9 (s, 1 H, tthf), 7.6 (d, J = 6.25 Hz, 2 H, PyH), 6.76 (s, 2 H, tthf) ppm. FTIR (KBr): $\tilde{\nu}$ = 3523 [br., $\nu(\text{O}-\text{H})$], 3072, 3027 $[\nu(\text{CONH})]$, 1640, 1592 $[\nu(\text{C}=\text{N}, \text{Py})]$, 1519 $[\nu(\text{NH})]$, 1415 $[\nu(\text{C}=\text{C})]$, 1332, 1295 $[\nu(\text{C}_{\text{Ar}}-\text{N})]$, 1235, 1207 $[\nu(\text{CH}, \text{Py})]$, 1090 $[\nu(\text{C}=\text{C}, \text{tthf})]$, 1001, 908 $[\nu(\text{CH}, \text{tthf})]$, 818 $[\nu(\text{CH}, \text{Py})]$, 773 $[\nu(\text{CH}, \text{tthf})]$, 714 $[\nu(\text{NH})]$, 649 $[\nu(\text{CC}, \text{tthf})]$, 569, 534 $[\nu(\text{ring vibrations})]$ cm^{-1} . $\text{C}_{12}\text{H}_8\text{N}_2\text{O}_5\text{S}_4$ (324): calcd. C 44.42, H 2.49, N 8.63, S 39.53; found C 44.38, H 2.51, N 8.60, S 39.49.

Synthesis of $[(\text{ttf-adpy})_2\text{Pt}(\text{CN})_4]$ (1): Compound 1 was obtained as a byproduct in the synthesis of 4 in an H-shaped tube by the slow diffusion method. A solution of $\text{Fe}(\text{BF}_4)_2 \cdot 6\text{H}_2\text{O}$ (0.06 mmol, 20.2 mg) and ttf-adpy (0.12 mmol, 38.9 mg) in N,N -dimethylformamide (1.2 mL) was placed in one side of the H-tube, while the other side was filled with an aqueous solution of $\text{K}[\text{Pt}(\text{CN})_4] \cdot \text{H}_2\text{O}$ (0.9 mL, 0.06 mmol, 22.6 mg). N,N -Dimethylformamide was used as diffusion medium. Red crystals of 1 suitable for single-crystal X-ray diffraction were obtained after 4 weeks together with a microcrystalline powder of compound 4. Yield: 3 mg (8%).

General Procedure for the Synthesis of 2–4: To a constantly stirred solution of $\text{K}_2[\text{M}(\text{CN})_4]$ (0.075 mmol, 18.1 mg for Ni^{II} ; 21.6 mg for Pd^{II} ; 28.3 mg for Pt^{II}) under an argon atmosphere in H_2O (10 mL) was dropwise added a solution containing stoichiometric amounts of ttf-adpy (0.15 mmol, 48.7 mg) and $\text{Fe}(\text{BF}_4)_2 \cdot 6\text{H}_2\text{O}$ (0.075 mmol, 25.3 mg) in MeOH (100 mL) over 12 h. Compounds 2–4 precipitated as reddish-brown microcrystalline powders. The precipitates were filtered off, washed with water and MeOH and dried in air.

$[\text{Fe}(\text{tff-adpy})_2\text{Ni}(\text{CN})_4] \cdot 1.5\text{H}_2\text{O}$ (2): Yield: 53.6 mg (76%). FTIR (KBr): $\tilde{\nu}$ = 3077 $[\nu(\text{C}-\text{H}_{\text{ar}})]$; 2156 $[\nu(\text{C}\equiv\text{N})]$; 1670, 1591, 1508, 1421 $[\nu(\text{C}=\text{C}, \text{C}=\text{N})]$; 1335, 1290, 1212 $[\nu(\text{C}-\text{N})]$; 1035 $[\nu(\text{C}-\text{H in-plane})]$; 827, 798, 779, 701, 656, 582, 535, 503, 435 $[\nu(\text{C}-\text{H out-of-plane})]$ cm^{-1} . $\text{C}_{28}\text{H}_{19}\text{FeN}_8\text{O}_{3.5}\text{PdS}_8$ (942.24): calcd. C 35.69, H 2.03, N

11.89, S 27.22; found C 35.64, H 2.01, N 11.90, S 27.25. EDXA: Fe 9.8%, Ni 9.7%, S 80.5%.

$[\text{Fe}(\text{tff-adpy})_2\text{Pd}(\text{CN})_4] \cdot 2\text{H}_2\text{O}$ (3): Yield 57.1 mg (80%). FTIR (KBr): 3076 $[\nu(\text{C}-\text{H}_{\text{ar}})]$; 2161 $[\nu(\text{C}\equiv\text{N})]$; 1672, 1591, 1509, 1424 $[\nu(\text{C}=\text{C}, \text{C}=\text{N})]$; 1333, 1290, 1212 $[\nu(\text{C}-\text{N})]$; 1035 $[\nu(\text{C}-\text{H in-plane})]$; 828, 797, 778, 702, 655, 582, 534, 507, 418 $[\nu(\text{C}-\text{H out-of-plane})]$ cm^{-1} . $\text{C}_{28}\text{H}_{20}\text{FeN}_8\text{O}_4\text{PdS}_8$ (951.24): calcd. C 35.35, H 2.12, N 11.78, S 26.97; found C 35.31, H 2.08, N 11.81, S 27.01. EDXA: Fe 9.9%, Pd 9.9%, S 80.2%.

$[\text{Fe}(\text{tff-adpy})_2\text{Pt}(\text{CN})_4] \cdot 2\text{H}_2\text{O}$ (4): Yield 62.3 mg (80%). FTIR (KBr): 3076 $[\nu(\text{C}-\text{H}_{\text{ar}})]$; 2158 $[\nu(\text{C}\equiv\text{N})]$; 1672, 1591, 1509, 1421 $[\nu(\text{C}=\text{C}, \text{C}=\text{N})]$; 1333, 1291, 1211 $[\nu(\text{C}-\text{N})]$; 1035 $[\nu(\text{C}-\text{H in-plane})]$; 828, 797, 778, 701, 654, 582, 534, 504, 459 $[\nu(\text{C}-\text{H out-of-plane})]$ cm^{-1} . $\text{C}_{28}\text{H}_{20}\text{FeN}_8\text{O}_4\text{PtS}_8$ (1039.93): calcd. C 32.34, H 1.94, N 10.77, S 24.67; found C 32.26, H 1.92, N 10.80, S 24.62. EDXA: Fe 9.8%, Pt 9.9%, S 80.3%.

$[\text{Fe}(\text{tff-adpy})_2\text{Ni}(\text{CN})_4]$ (5), $[\text{Fe}(\text{tff-adpy})_2\text{Pd}(\text{CN})_4]$ (6) and $[\text{Fe}(\text{tff-adpy})_2\text{Pt}(\text{CN})_4]$ (7): Compounds 5–7 were obtained by heating hydrated compounds 2–4 in an oven at 350 K for 30 min or in a SQUID magnetometer from 300 to 350 K and then kept at this temperature for 15 min under vacuum.

Physical Measurements: Variable-temperature magnetic susceptibility measurements of samples 2–7 (20–30 mg) were recorded with a Quantum Design MPMS2SQUID susceptometer equipped with a 5.5 T magnet operating at 1 T and at temperatures from 1.8–300 K. The susceptometer was calibrated with $(\text{NH}_4)_2\text{Mn}(\text{SO}_4)_2 \cdot 12\text{H}_2\text{O}$. Experimental susceptibilities were corrected for diamagnetism of the constituent atoms by the use of Pascal's constants. Electrochemical measurements were carried out in a potentiostat-galvanostat PAR model 263A, with a three-electrode system in a 0.1 M $\text{Bu}_4\text{N}(\text{PF}_6)$ acetonitrile solution as the supporting electrolyte. A carbon glass disc (0.071 cm^2) was used as the working electrode, a Pt wire as the auxiliary electrode and 0.1 M $(\text{Bu}_4\text{N})\text{Br}/\text{AgBr}(\text{s})/\text{Ag}$ was used as the reference electrode. The working electrode (C) was polished with alumina to ensure the absence of residues on the surface. All voltammograms were initiated from the null current potential ($E_i = 0$), and the scan was initiated in both positive and negative potential directions. In order to report the potentials used according to the IUPAC convention, voltammograms were obtained for approximately 10^{-3} M solution of ferrocene (Fc) in a supporting electrolyte. For the working conditions, the electroactive domain was between -3.26 and $0.94 \text{ V}/\text{Fc}^+/\text{Fc}$. The halfwave potentials were estimated from $E_{1/2} = (E_p + E_c)/2$, where E_p and E_c are the anodic and cathodic peak potentials, respectively. $E_{1/2}(\text{Fc}^+/\text{Fc}) = 0.659 \text{ V}/\text{AgBr}-\text{Ag}$. Calorimetric measurements were performed by using a differential scanning calorimeter (Mettler Toledo DSC 821e). Low temperatures were obtained with an aluminum block, which was attached to the sample holder, refrigerated with a flow of liquid nitrogen and stabilized at a temperature of 110 K. The sample holder was kept in a dry box under a flow of dry nitrogen gas to avoid water condensation. The measurements were carried out by using around 20 mg of a powdered sample sealed in aluminum pans with a mechanical crimp. Temperature and heat flow calibrations were made with standard samples of indium by using its melting (429.6 K, 28.45 J g^{-1}) transition. An overall accuracy of 0.2 K in the temperature and 2% in the heat flow is estimated. The thermodynamic parameters were analyzed with Netzsch Proteus software (NETZSCH-Geraetebau GMBH, <http://www.e-thermal.com/proteus.htm>). The UV/Vis spectra were performed with an Agilent 8453 UV/Vis spectrophotometer in the region between 250 and 1000 nm. TGA measurements were performed with a Mettler Toledo TGA/SDTA 851e in the 300–700 K

temperature range under a nitrogen atmosphere with a rate of 10 K min⁻¹.

Single-Crystal X-ray Diffraction: Diffraction data for **1** was collected with a Nonius Kappa-CCD single-crystal diffractometer by using Mo- K_α radiation ($\lambda = 0.71073$ Å). A multiscan absorption correction was found to have no significant effect on the refinement results. The structures were solved by direct methods by using SHELXS-97 and refined by full-matrix least-squares on F^2 by using SHELXL-97.^[19] All non-hydrogen atoms were refined anisotropically. The crystallographic data for **1** are summarized in Table 5. CCDC-674105 (for **1**) contains the supplementary crystallographic data for this paper. These data can be obtained free of charge from The Cambridge Crystallographic Data Centre via www.ccdc.cam.ac.uk/data_request/cif.

Table 5. Crystal data for **1** at 293 K.

	1
Formula	C ₂₈ H ₁₈ N ₈ O ₂ PtS ₈
M_r	950.07
Space group	P $\bar{1}$
a / Å	7.1330(3)
b / Å	8.7130(3)
c / Å	13.5710(7)
α / °	87.6210(10)
β / °	84.4730(10)
γ / °	78.512(3)
V / Å ³	822.48(6)
Z	1
$D_{\text{calcd.}}$ / mg cm ⁻³	1.918
$F(000)$	464
$\lambda(\text{Mo-}K_\alpha)$ / Å	0.71073
$\mu(\text{Mo-}K_\alpha)$ / mm ⁻¹	4.816
Crystal size / mm	0.04 × 0.04 × 0.06
Temperature / K	293(2)
No. of total reflections	4794
No. of unique reflections	3691
No. of reflections [$I > 2\sigma(I)$]	3211
$R(\text{int})$	0.0315
R_1 [$I > 2\sigma(I)$] ^[a]	0.0437
wR ^[b]	0.1098
S	0.999

[a] $R_1 = \sum ||F_o| - |F_c|| / \sum |F_o|$. [b] $wR = \{\sum [w(F_o^2 - F_c^2)^2] / \sum [w(F_o^2)^2]\}^{1/2}$, $w = 1 / [\sigma^2(F_o^2) + (mP)^2 + nP]$, where $P = (F_o^2 + 2F_c^2) / 3$; $m = 0.0734$; $n = 1.2733$.

X-ray Powder Diffraction (XRPD): The equipment used for XRPD characterization of compounds **2–4** was a Seifert XRD 3003 TT diffractometer, with Bragg–Brentano geometry and Cu tube working at 40 kV with a Ni filter (0.3 mm primary slit, 0.3 mm secondary slit, 0.2 mm detector slit and scintillation detector).

Supporting Information (see footnote on the first page of this article): Schematic of the synthesis of the ttf–adpy ligand; ¹H NMR and MS of the ttf–adpy ligand; IR spectra of the ttf–adpy ligand and compounds **2–4**; TGA analysis for **2–4**; cyclic voltammograms of the ttf–adpy ligand; XRPD and view of the crystal structure of [Fe(py)₂Ni(CN)₄].

Acknowledgments

Financial support is acknowledged from the Spanish Ministerio de Educación y Ciencia (MEC) (CTQ 2007-64727 and CTQ 2006-15672-C05-03), from the Generalitat Valenciana (GVPRE/2008/150) and from the European network of excellence MAGMANET (Contract: NMP3-CT-2005-515767-2). A. B. G. thanks the Spanish MEC for a research contract (Programa Ramón y Cajal).

- [1] H. Akamatu, H. Inokuchi, Y. Matsunaga, *Nature* **1954**, 173, 168.
- [2] M. Mas-Torrent, C. Rovira, *J. Mater. Chem.* **2006**, 16, 433.
- [3] a) L. Ouahab, *Coord. Chem. Rev.* **1998**, 178–180, 1501; b) L. Ouahab, *Chem. Mater.* **1997**, 9, 1909.
- [4] A. Miyazaki, T. Enoki, *Chem. Rev.* **2004**, 104, 5549.
- [5] E. Coronado, J. R. Galán-Mascarós, *J. Mater. Chem.* **2005**, 15, 66.
- [6] a) P. Gülich, H. A. Goodwin (Eds.), *Topics in Current Chemistry Vols. 233–236: Spin Crossover in Transition Metal Compounds*, Springer, Berlin, **2004**; b) J. A. Real, A. B. Gaspar, M. C. Muñoz, *Dalton Trans.* **2005**, 2062; c) A. B. Gaspar, V. Ksenofontov, M. Seredyuk, P. Gülich, *Coord. Chem. Rev.* **2005**, 249, 2661; d) J. A. Real, A. B. Gaspar, V. Niel, M. C. Muñoz, *Coord. Chem. Rev.* **2003**, 236, 121; e) P. Gülich, A. Hauser, H. Spiering, *Angew. Chem. Int. Ed. Engl.* **1994**, 33, 2024.
- [7] a) S. Decurtins, P. Gülich, C. P. Köhler, H. Spiering, A. Hauser, *Chem. Phys. Lett.* **1984**, 105, 1–4; b) J.-F. Létard, *J. Mater. Chem.* **2006**, 16, 2550.
- [8] S. Dorbes, L. Valade, J. A. Real, C. Faulmann, *Chem. Commun.* **2005**, 69.
- [9] K. Takahashi, H. B. Cui, Y. Okano, H. Kobayashi, Y. Einaga, O. Sato, *Inorg. Chem.* **2006**, 45, 5739.
- [10] C. Faulmann, S. Dorbes, S. Lampert, I. Malfant, M.-L. Doublet, L. Valade, J. A. Real, *Inorg. Chem.* **2007**, 46, 8548.
- [11] T. Devic, N. Avarvari, P. Batail, *Chem. Eur. J.* **2004**, 10, 3697.
- [12] K. Hervé, S. X. Liu, O. Cadot, S. Golhen, Y. Le Gal, A. Bousseksou, H. Stoeckli-Evans, S. Decurtins, L. Ouahab, *Eur. J. Inorg. Chem.* **2006**, 3498.
- [13] D. L. Coffen, Q. Chambers, D. R. William, P. E. Garrett, N. D. Canfield, *J. Am. Chem. Soc.* **1971**, 93, 2258.
- [14] a) T. Kitazawa, Y. Gomi, M. Takahashi, M. Takeda, A. Enemoto, T. Miyazaki, T. Enoki, *J. Mater. Chem.* **1996**, 6, 119; b) V. Niel, J. M. Martínez-Agudo, M. C. Muñoz, A. B. Gaspar, J. A. Real, *Inorg. Chem.* **2001**, 40, 3838.
- [15] A. B. Gaspar, J. A. Real, M. C. Muñoz, *J. Mater. Chem.* **2006**, 16, 2522.
- [16] a) K. Nakano, S. Kawata, K. Yoneda, A. Fuyuhiko, T. Yagi, S. Nasu, S. Morimoto, S. Kaizaki, *Chem. Commun.* **2004**, 2892; b) S. Kawata, S. Kaizaki, K. Yoneda, K. Adachi, S. Hayami, Y. Maeda, M. Katada, A. Fuyuhiko, *Chem. Commun.* **2006**, 45; c) K. Nakano, N. Suemura, K. Yoneda, S. Kawata, S. Kaizaki, *Dalton Trans.* **2005**, 740.
- [17] a) S. S. Kuduva, N. Avarvari, M. Fourmigué, *J. Chem. Soc., Dalton Trans.* **2002**, 3686; b) K. Heuzé, M. Fourmigué, P. Batail, *J. Mater. Chem.* **1999**, 9, 2373.
- [18] M. Sorai, M. Nakano, Y. Miyazaki, *Chem. Rev.* **2006**, 106, 976.
- [19] G. M. Sheldrick, *SHELX97: Program for Crystal Structure Determination*, University of Göttingen, Germany, **1997**.

Received: October 7, 2008

Published Online: December 9, 2008

Group 4 Metal Complexes That Contain a Thioether-Functionalized Phenolato Ligand: Synthesis, Structure, and 1-Hexene Polymerization

Bing Lian,^[a] Klaus Beckerle,^[a] Thomas P. Spaniol,^[a] and Jun Okuda*^[a]

Keywords: Hafnium / Zirconium / Titanium / Oligomerization / Polymerization / Regioselectivity

Reaction of group 4 metal tetrabenzyl complexes $[M(\text{CH}_2\text{Ph})_4]$ ($M = \text{Ti, Zr, Hf}$) with 1 or 2 equiv. of a thioether-functionalized phenol 2,4-*t*Bu₂-6-(PhSCH₂)C₆H₂OH afforded dibenzyl complexes $[M(\text{L})_2(\text{CH}_2\text{Ph})_2]$ ($M = \text{Ti, 1; M = Zr, 2; M = Hf, 3}$) and the tribenzyl zirconium complex $[\text{Zr}(\text{L})(\text{CH}_2\text{Ph})_3]$ (**4**). Benzyl abstraction with a Lewis acid gave the zirconium monobenzyl cation $[\text{Zr}(\text{L})_2\text{CH}_2\text{Ph}]^+[\text{PhCH}_2\text{B}(\text{C}_6\text{F}_5)_3]^-$ (**5**) and the di-

benzyl cation $[\text{Zr}(\text{L})(\text{CH}_2\text{Ph})_2]^+[\text{PhCH}_2\text{B}(\text{C}_6\text{F}_5)_3]^-$ (**6**). The monobenzyl cation **5** oligomerized 1-hexene to low molecular-weight atactic oligo(1-hexene) ($M_n = 560\text{--}820$), while the dibenzyl cation **6** polymerized 1-hexene isospecifically ($[mmmm] > 90\%$).

© Wiley-VCH Verlag GmbH & Co. KGaA, 69451 Weinheim, Germany, 2009

Introduction

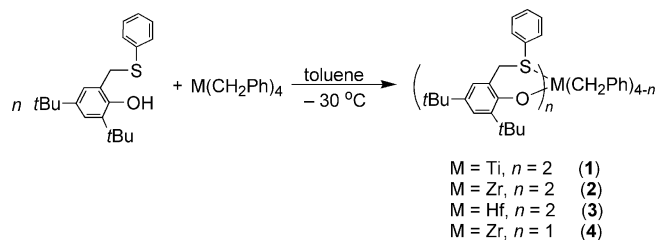
Group 4 metal complexes based on non-metallocene frameworks^[1] such as alkoxo/aryloxo complexes are single-site catalyst precursors for the polymerization of α -olefins, with performance profiles distinct from those of metallocene catalysts.^[2] Complexes containing an [OSSO]-type bis-(phenolato) ligand polymerize styrene isospecifically,^[3a–3d] whereas α -olefins are oligomerized regioselectively.^[3e] Living methyl methacrylate polymerization was also achieved with a titanium enolate complex featuring this type of ligand.^[3f] This mixed hard–soft donor-based tetradentate ligand apparently ensures the C_2 -symmetric *cis- α* configuration in an octahedral environment, required for the isospecific polymerization of styrene and related monomers.^[4] Given the prominence of the phenoxyimine ligand for highly active α -olefin polymerization catalysts,^[2a–2d] we wondered how group 4 metal catalysts with a bidentate phenolato [OS]-type ligand would behave. We report here on the synthesis, structure, and polymerization behavior of group 4 metal complexes that contain a phenylthiomethyl-substituted phenoxy ligand toward 1-hexene.

Results and Discussion

Group 4 Metal Benzyl Complexes

Reaction of $[M(\text{CH}_2\text{Ph})_4]$ ($M = \text{Ti, Zr, Hf}$) with 2 equiv. of the phenylthiomethyl-substituted phenol 2,4-*t*Bu₂-6-(PhSCH₂)C₆H₂OH (LH) in toluene at $-30\text{ }^\circ\text{C}$ led to the dibenzyl complexes $[M(\text{L})_2(\text{CH}_2\text{Ph})_2]$ ($M = \text{Ti, 1; M = Zr, 2; M = Hf, 3}$) and the tribenzyl zirconium complex $[\text{Zr}(\text{L})(\text{CH}_2\text{Ph})_3]$ (**4**).

$M = \text{Hf, 3}$) (Scheme 1), which were isolated as crystals in high yield (81–85%) and characterized by elemental analysis as well as by NMR spectroscopy. The ¹H NMR spectrum of the titanium complex **1** in C₆D₆ at room temperature exhibits one singlet for the SCH₂ group at $\delta = 3.85$ ppm and one singlet for the TiCH₂ group at $\delta = 3.36$ ppm. This may indicate a symmetric molecular structure with a mirror plane (*trans* benzyl groups) or a highly fluxional structure in solution. The tribenzyl zirconium complex $[\text{Zr}(\text{L})(\text{CH}_2\text{Ph})_3]$ (**4**) was synthesized from $[\text{Zr}(\text{CH}_2\text{Ph})_4]$ and LH in a 1:1 molar ratio (Scheme 1) and obtained as yellow crystals in 86% yield. The ¹H NMR spectrum in C₆D₆ shows one singlet for the CH₂Ph group at $\delta = 2.34$ ppm, which indicates the absence of a rigid η^2 coordination of the benzyl ligand to the zirconium center.



Scheme 1.

Recrystallization of the hafnium complex **3** from pentane gave crystals that are suitable for X-ray diffraction. Details of the crystal structure determination are given in Table 2 (see Experimental Section). The molecular structure in the solid state as well as selected interatomic distances and angles are shown in Figure 1. The octahedrally coordinated hafnium center is coordinated by two *trans* oxygen atoms, two *cis* sulfur donor atoms, and the *cis* arranged benzyl groups (Figure 1). The two benzyl ligands point in opposite

[a] Institute of Inorganic Chemistry, RWTH Aachen University, Landoltweg 1, 52074 Aachen, Germany
 Fax: +49-241-80-92644
 E-mail: jun.okuda@ac.rwth-aachen.de

directions, and their planes are nearly perpendicular to each other. Both benzyl groups have a similar coordination mode [Hf–C43, 2.270(7) Å; Hf–C50, 2.240(7) Å; Hf–C43–C44, 111.9(5)°; Hf–C50–C51, 124.2(5)°], and no significant Hf··· η^2 -benzyl interactions are indicated [Hf–C44, 3.3145(8) Å; Hf–C51, 3.106(7) Å]. The interatomic distances of Hf–S1 [2.8722(18) Å] and Hf–S2 [2.837(2) Å] are comparable to those of [Hf(OC₆H₂-*t*Bu₂-{S(CH₂)}(CH₂-Ph)₂)] {2.9222(9), 2.8260(8) Å^[3a]} and an [OSO]-type bis-(phenolato)hafnium complex [Hf–S, 2.796(4) Å].^[5a] Both phenyl groups attached to the sulfur atoms adopt an almost parallel configuration in the solid state.

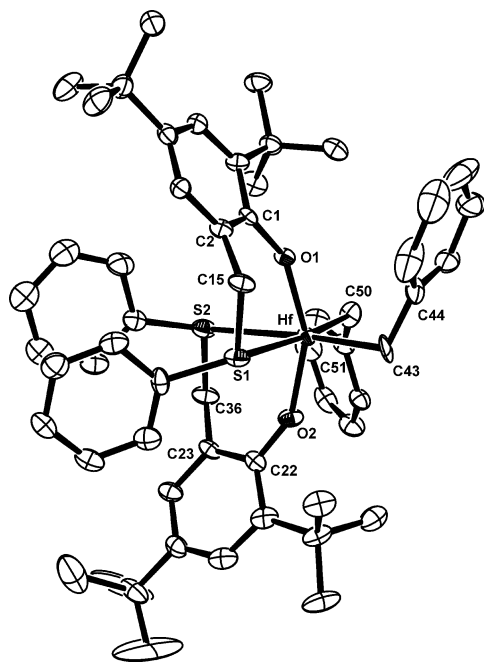


Figure 1. Molecular structure of [Hf(L)₂(CH₂Ph)₂] (**3**) (hydrogen atoms are omitted for clarity). Selected bond lengths (Å) and angles (°): Hf–O1 1.962(5), Hf–O2 1.975(5), Hf–C43 2.270(7), Hf–C50 2.240(7), Hf–S1 2.8722(18), Hf–S2 2.837(2), S1–C15 1.807(7), O1–C1 1.343(8), O1–Hf–O2 154.1(2), S1–Hf–S2 88.76(6), C43–Hf–C50 99.1(3), Hf–C43–C44 111.9(5), Hf–C50–C51 124.2(5), O1–Hf–S1 77.10(14), O1–Hf–S2 82.90(15), O2–Hf–S1 84.47(16).

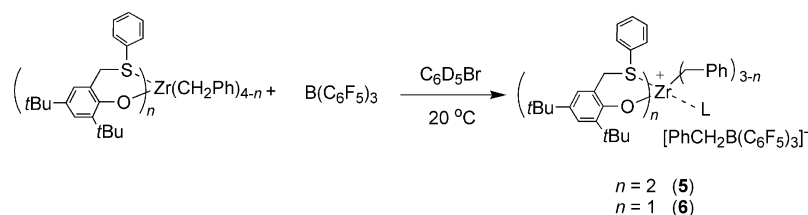
Cationic Zirconium Alkyl Complexes

Upon addition of the electrophilic borane B(C₆F₅)₃ in C₆D₅Br to **2**, the cationic species [Zr(L)₂CH₂Ph]⁺[PhCH₂B(C₆F₅)₃][–] (**5**) could be cleanly generated and was

found to be stable at room temperature for at least 24 h (Scheme 2). Compound **5** was characterized by ¹H, ¹³C, ¹¹B, and ¹⁹F spectroscopy and may act as a model for the key intermediate in the 1-hexene polymerization reaction (vide infra). The ¹H NMR spectrum in C₆D₅Br at room temperature exhibits one singlet at δ = 3.58 ppm for the PhCH₂B group. The absence of signals for an η^6 -coordinated arene ring indicates the free anionic character of [PhCH₂B(C₆F₅)₃][–]. The cationic dibenzyl zirconium species [Zr(L)(CH₂Ph)₂]⁺[PhCH₂B(C₆F₅)₃][–] (**6**) was generated analogously in the solvent C₆D₅Br with **4** (Scheme 2). The cationic species **6** was thermally more stable at room temperature than cation **5**. The ¹H NMR spectrum of **6** shows one singlet at δ = 2.39 ppm for the Zr(CH₂Ph)₂ group, which suggests the absence of an η^2 -coordinated benzyl group at the zirconium center.

1-Hexene Polymerization

Polymerization of 1-hexene using benzyl complexes **1–4** was investigated. The results are summarized in Table 1. When the dibenzyl complexes **1–3** were combined in situ with 1-hexene as a monomer and the activator (Entries 1–5), neither did the titanium complex **1** nor the hafnium complex **3** polymerize 1-hexene within 24 h (Entries 1 and 5); only the zirconium complex **2** showed moderate activity towards 1-hexene (Entries 2–4). The yield of poly(1-hexene)s could not be significantly improved by changing the solvent to C₆H₅Br (Entry 3) and by using Al(C₆F₅)₃ as an activator (Entry 4). The obtained poly(1-hexene)s have low molecular weights (M_n = 560–820) and show relatively narrow polydispersities (M_w/M_n = 1.77–2.15). The degree of polymerization for the obtained oligo(1-hexene)s is between 6 and 10. The oligomers produced by the zirconium complex **2** (Entry 2) show olefine ¹H NMR resonances at δ = 5.34 ppm, in agreement with the presence of vinylene groups [(*E*)- and (*Z*)-R¹CH=CHR²], whereas no signals for vinylidene end groups (R¹R²C=CH₂) (expected around 4.6 ppm) are observed (Figure 2a). In the ¹³C NMR spectrum of the oligomers, the signals around 130 ppm are assigned to the vinylene group [(*E*)- and (*Z*)-R¹CH=CHR²], and no signals for vinylidene end groups (R¹R²C=CH₂), expected around 150 and 110 ppm, are observed (Figure 2b). This indicates that the oligo(1-hexene)s are formed by β -H elimination from a 2,1-enriched zirconium alkyl and that the 2,1-regioselectivity is close to 100%. According to the literature,^[3e,6] the reason for this unusual 2,1-regiose-



Scheme 2.

lectivity of the zirconium complex **2** in 1-hexene oligomerization is still not understood. The resultant oligo(1-hexene)s produced by **2**/ $\text{B}(\text{C}_6\text{F}_5)_3$ are atactic according to the ^{13}C NMR spectrum (Figure 2b).

Table 1. Polymerization of 1-hexene with the system **1**–**4**/ $\text{E}(\text{C}_6\text{F}_5)_3$ (E = B, Al).^[a]

Entry	Catalyst	Activator	Solvent	Yield [%]	$M_n^{[b]}$	$M_w/M_n^{[b]}$
1	1	$\text{B}(\text{C}_6\text{F}_5)_3$	toluene	<1	n.d.	n.d.
2	2	$\text{B}(\text{C}_6\text{F}_5)_3$	toluene	53	820	1.77
3	2	$\text{B}(\text{C}_6\text{F}_5)_3$	$\text{C}_6\text{H}_5\text{Br}$	50	770	1.82
4	2	$\text{Al}(\text{C}_6\text{F}_5)_3$	toluene	12	560	2.15
5	3	$\text{B}(\text{C}_6\text{F}_5)_3$	toluene	<1	n.d.	n.d.
6	4	$\text{B}(\text{C}_6\text{F}_5)_3$	toluene	10	50600	5.96
7	4	$\text{B}(\text{C}_6\text{F}_5)_3$	$\text{C}_6\text{H}_5\text{Br}$	12	58700	5.01
8	4	$\text{Al}(\text{C}_6\text{F}_5)_3$	toluene	9	48000	6.82

[a] Polymerization conditions: solvent = 10 mL; cat. = 0.02 mmol; 1-hexene/cat./activator = 600:1:1; polymerization time = 24 h; protocol: cat. + 1-hexene, then activator. [b] Determined by GPC in thf vs. polystyrene standards.

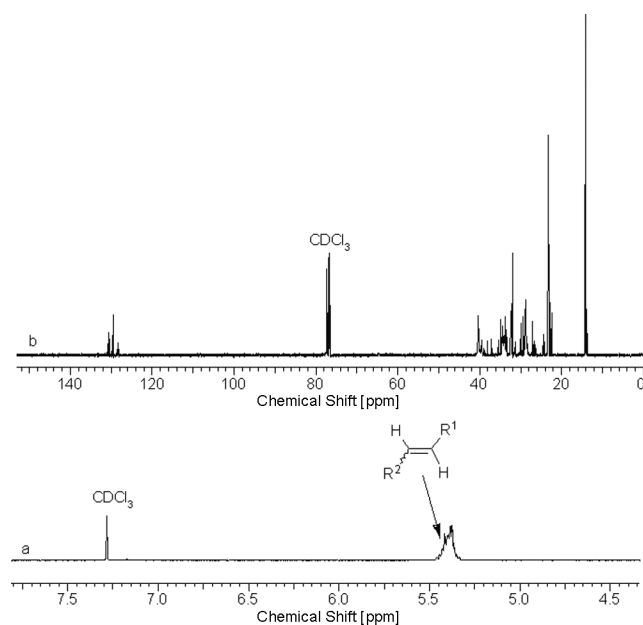


Figure 2. (a) ^1H NMR spectrum (400 MHz, CDCl_3) of the reaction mixture produced by the zirconium catalyst **2**/ $\text{B}(\text{C}_6\text{F}_5)_3$ and 1-hexene at 20 °C (Entry 2); the selected region shows the end groups for the oligo(1-hexene)s. (b) ^{13}C NMR (101 MHz, CDCl_3) spectrum of oligo(1-hexene)s produced by zirconium catalyst **2**/ $\text{B}(\text{C}_6\text{F}_5)_3$ (Entry 2).

The tribenzyl zirconium complex **4** was also investigated in the polymerization of 1-hexene activated by $\text{B}(\text{C}_6\text{F}_5)_3$ or $\text{Al}(\text{C}_6\text{F}_5)_3$ in solution (Entries 6–8). The yield was generally low (9–16%). The resultant polymers have molecular weights of around 50000 and broad polydispersities ($M_w/M_n = 5.01$ –6.82). Surprisingly, the activator influences the microstructure of the polymer. The poly(1-hexene) obtained with **4**/ $\text{B}(\text{C}_6\text{F}_5)_3$ is highly isotactic ($[mmmm] > 90\%$) (Figure 3a), whereas the polymer produced by **4**/ $\text{Al}(\text{C}_6\text{F}_5)_3$ is

atactic (Figure 3b). This unusual counterion effect is mostly caused by the non-single-site characteristics with the **4**/activator system.

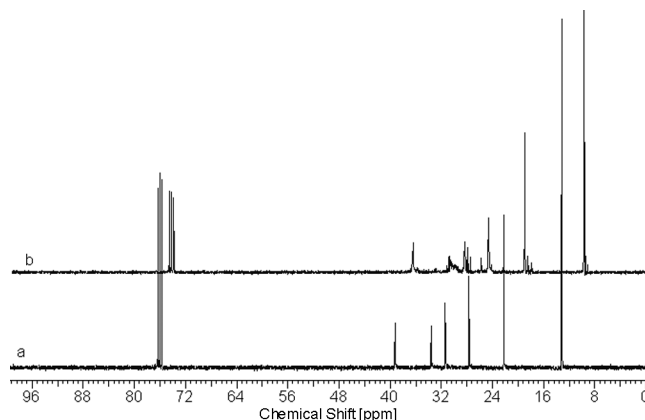


Figure 3. $^{13}\text{C}\{^1\text{H}\}$ NMR spectra (101 MHz, CDCl_3 , selected regions) of the poly(1-hexene)s produced by the catalyst systems **4**/ $\text{B}(\text{C}_6\text{F}_5)_3$ (a, Entry 6) and **4**/ $\text{Al}(\text{C}_6\text{F}_5)_3$ (b, Entry 8), both at 20 °C.

Conclusions

In conclusion, we have synthesized group 4 metal catalyst precursors that contain an [OS]-type bidentate phenolato ligand similar to the intensely studied phenoxyimine and related functionalized phenoxy ligands. Upon activation with a Lewis acid $\text{E}(\text{C}_6\text{F}_5)_3$ (E = B, Al), the dibenzyl zirconium complex **2** oligomerizes 1-hexene and the tribenzyl zirconium complex **4** polymerizes 1-hexene. Further studies are underway to establish a structure–activity and –stereoselectivity relationship for 1-hexene polymerization by using this type of group 4 metal catalysts.^[7]

Experimental Section

All experiments were carried out under purified argon by using standard Schlenk techniques or in a glove box (<1 ppm O_2 , 1 ppm H_2O). Toluene, pentane, diethyl ether, dichloromethane, and thf were purified from an MBraun SPS-800 system prior to use. Deuterated solvents were purchased from Aldrich and purified before use. All other chemicals were commercially available and used after appropriate purification. The compounds 2,4-di-*tert*-butyl-6-hydroxymethylphenol,^[8] 2,4-di-*tert*-butyl-6-(chloromethyl)phenol,^[9] $[\text{M}(\text{CH}_2\text{Ph})_4]$ (Ti, Zr, Hf),^[10] and $\text{Al}(\text{C}_6\text{F}_5)_3 \cdot 0.5\text{C}_7\text{H}_8$ ^[11] were synthesized according to literature methods. NMR spectra were recorded on a Bruker Avance 400 (^1H , 400 MHz; ^{13}C , 101 MHz) or a Varian Mercury 200 spectrometer in Teflon-valved NMR tubes at 25 °C unless otherwise stated. ^1H and ^{13}C NMR chemical shifts were determined by using residual solvent resonances and are reported referenced to SiMe_4 . Signal assignment was made from ^1H – ^{13}C HMQC and ^1H – ^{13}C HMBC 2D NMR experiments. Coupling constants are given in Hz. Elemental analyses were performed by the Microanalytical Laboratory of this department. Molecular weights of polymers were determined by gel permeation chromatography (GPC) at room temperature in thf and calibrated with respect to polystyrene standards. The microstructure of the

polymer was determined by ^1H NMR and ^{13}C NMR spectroscopy in CDCl_3 .

2,4-*t*Bu₂-6-(PhSCH₂)C₆H₂OH (LH): To a solution of thiophenol (2.6 g, 23.5 mmol) in methanol (30 mL) was added NaOH (0.94 g, 23.5 mmol), and the mixture was heated until all NaOH was completely dissolved. After cooling to room temperature, 2,4-*t*Bu₂-6-(ClCH₂)C₆H₂OH (6.0 g, 23.5 mmol) was slowly added, and the mixture was heated at reflux for 2 h. After evaporation of the volatiles under vacuum, water was added, and the organic phase was extracted diethyl ether (2 × 30 mL). The solution was dried with MgSO_4 , and diethyl ether was removed under vacuum. The crude product was recrystallized from pentane to give colorless crystals of 2,4-*t*Bu₂-6-(PhSCH₂)C₆H₂OH (6.60 g, 85%). ^1H NMR (CDCl_3): δ = 7.33–7.19 (m, 5 H, SC_6H_5), 7.29 (d, $^4J_{\text{HH}}$ = 2.4 Hz, 1 H, Ph-3-*H*), 6.79 (d, $^4J_{\text{HH}}$ = 2.4 Hz, 1 H, Ph-5-*H*), 6.13 (s, 1 H, OH), 4.12 (s, 2 H, CH_2S), 1.41 [s, 9 H, $\text{C}(\text{CH}_3)_3$], 1.19 [s, 9 H, $\text{C}(\text{CH}_3)_3$] ppm. $^{13}\text{C}\{^1\text{H}\}$ NMR (CDCl_3): δ = 151.47 (C_6H_2 -C1), 142.36 (C_6H_2 -C4), 137.05 (C_6H_2 -C2), 133.96 (SPh-C1), 131.59 (C_6H_2 -C3), 128.89 (SPh-C3), 127.41 (SPh-C2), 125.42 (C_6H_2 -C5), 123.73 (SPh-C4), 121.78 (C_6H_2 -C6), 37.80 (SCH_2), 34.95 [$\text{C}(\text{CH}_3)_3$], 34.16 [$\text{C}(\text{CH}_3)_3$], 31.50 [$\text{C}(\text{CH}_3)_3$], 29.83 [$\text{C}(\text{CH}_3)_3$] ppm. $\text{C}_{21}\text{H}_{28}\text{OS}$ (328.51): calcd. C 76.78, H 8.59; found C 77.54, H 8.94.

[Ti(L)₂(CH₂Ph)₂] (1): To a solution of $[\text{Ti}(\text{CH}_2\text{Ph})_4]$ (0.35 g, 0.85 mmol) in toluene (15 mL), a toluene solution (20 mL) of LH (0.56 g, 1.70 mmol) was slowly added at -30°C . The reaction mixture was warmed to room temperature and stirred further for 2 h. After evaporation of the volatiles under vacuum, the residue was recrystallized from pentane to give $[\text{Ti}(\text{L})_2(\text{CH}_2\text{Ph})_2]$ (1) as red crystals (0.62 g, 82%). ^1H NMR (C_6D_6): δ = 7.47 (d, $^4J_{\text{HH}}$ = 2.4 Hz, 2 H, C_6H_2 -3-*H*), 7.26–6.82 (m, 20 H, SC_6H_5 and $\text{TiCH}_2\text{C}_6\text{H}_5$), 6.91 (d, $^4J_{\text{HH}}$ = 2.4 Hz, 2 H, C_6H_2 -5-*H*), 3.85 (s, 4 H, CH_2S), 3.36 (s, 4 H, TiCH_2Ph), 1.57 [s, 18 H, $\text{C}(\text{CH}_3)_3$], 1.23 [s, 18 H, $\text{C}(\text{CH}_3)_3$] ppm. $^{13}\text{C}\{^1\text{H}\}$ NMR (C_6D_6): δ = 161.50 (C_6H_2 -C1), 147.79 (CH_2Ph -C1), 143.81 (C_6H_2 -C4), 136.94 (C_6H_2 -C2), 133.47 (SPh-C1), 129.03 (C_6H_2 -C5), 128.56 (SPh-C3), 127.67 (CH_2Ph -C3), 127.51 (C_6H_2 -C3), 127.30 (SPh-C2), 127.20 (CH_2Ph -C2), 125.28 (SPh-C4), 122.97 (C_6H_2 -C6), 121.75 (CH_2Ph -C4), 95.91 (CH_2Ph), 35.41 (SCH_2), 35.31 [$\text{C}(\text{CH}_3)_3$], 34.03 [$\text{C}(\text{CH}_3)_3$], 31.13 [$\text{C}(\text{CH}_3)_3$], 30.24 [$\text{C}(\text{CH}_3)_3$] ppm. $\text{C}_{56}\text{H}_{68}\text{O}_2\text{S}_2\text{Ti}$ (885.13): calcd. C 75.99, H 7.74; found C 75.62, H 8.17.

[Zr(L)₂(CH₂Ph)₂] (2): Following a procedure analogous to the preparation of 1, starting from $[\text{Zr}(\text{CH}_2\text{Ph})_4]$ (0.20 g, 0.44 mmol) and LH (0.29 g, 0.88 mmol), the product $[\text{Zr}(\text{L})_2(\text{CH}_2\text{Ph})_2]$ (2) was obtained as pale yellow crystals (0.33 g, 81%). ^1H NMR (C_6D_6): δ = 7.46 (d, $^4J_{\text{HH}}$ = 2.4 Hz, 2 H, C_6H_2 -3-*H*), 7.24–6.72 (m, 20 H, SC_6H_5 and $\text{ZrCH}_2\text{C}_6\text{H}_5$), 6.70 (d, $^4J_{\text{HH}}$ = 2.4 Hz, 2 H, C_6H_2 -5-*H*), 3.79 (s, 4 H, CH_2S), 2.81 (s, 4 H, ZrCH_2Ph), 1.56 [s, 18 H, $\text{C}(\text{CH}_3)_3$], 1.32 [s, 18 H, $\text{C}(\text{CH}_3)_3$] ppm. $^{13}\text{C}\{^1\text{H}\}$ NMR (C_6D_6): δ = 158.21 (C_6H_2 -C1), 146.51 (CH_2Ph -C1), 141.59 (C_6H_2 -C4), 137.03 (C_6H_2 -C2), 133.58 (SPh-C1), 128.57 (C_6H_2 -C5), 128.43 (SPh-C3), 127.80 (CH_2Ph -C3), 127.32 (SPh-C2), 127.20 (CH_2Ph -C2), 125.32 (SPh-C4), 124.05 (C_6H_2 -C3), 123.81 (C_6H_2 -C6), 121.70 (CH_2Ph -C4), 72.03 (ZrCH_2Ph), 37.51 (SCH_2), 35.21 [$\text{C}(\text{CH}_3)_3$], 33.66 [$\text{C}(\text{CH}_3)_3$], 31.32 [$\text{C}(\text{CH}_3)_3$], 30.07 [$\text{C}(\text{CH}_3)_3$] ppm. $\text{C}_{56}\text{H}_{68}\text{O}_2\text{S}_2\text{Zr}$ (928.49): calcd. C 72.44, H 7.38; found C 72.25, H 7.51.

[Hf(L)₂(CH₂Ph)₂] (3): An analogous procedure was followed for the preparation of 1, starting from $[\text{Hf}(\text{CH}_2\text{Ph})_4]$ (0.20 g, 0.37 mmol) and LH (0.24 g, 0.74 mmol). The product $[\text{Hf}(\text{L})_2(\text{CH}_2\text{Ph})_2]$ (3) was obtained as colorless crystals (0.32 g, 85%). A crystal of 3 suitable for X-ray diffraction analysis was grown from pentane. ^1H NMR (C_6D_6): δ = 7.45 (d, $^4J_{\text{HH}}$ = 2.4 Hz, 2 H, C_6H_2 -3-*H*), 7.23–6.69 (m, 20 H, SC_6H_5 and $\text{HfCH}_2\text{C}_6\text{H}_5$), 6.83 (d, $^4J_{\text{HH}}$

= 2.4 Hz, 2 H, C_6H_2 -5-*H*), 3.84 (s, 4 H, CH_2S), 2.69 (s, 4 H, HfCH_2Ph), 1.50 [s, 18 H, $\text{C}(\text{CH}_3)_3$], 1.31 [s, 18 H, $\text{C}(\text{CH}_3)_3$] ppm. $^{13}\text{C}\{^1\text{H}\}$ NMR (C_6D_6): δ = 158.53 (C_6H_2 -C1), 147.79 (CH_2Ph -C1), 141.52 (C_6H_2 -C4), 137.63 (C_6H_2 -C2), 133.55 (SPh-C1), 128.52 (SPh-C3), 127.86 (CH_2Ph -C3), 127.35 (SPh-C2), 127.26 (CH_2Ph -C2), 127.01 (C_6H_2 -C5), 125.29 (SPh-C4), 124.07 (C_6H_2 -C3), 123.58 (C_6H_2 -C6), 121.78 (CH_2Ph -C4), 79.22 (CH_2Ph), 38.04 (SCH_2), 35.34 [$\text{C}(\text{CH}_3)_3$], 34.25 [$\text{C}(\text{CH}_3)_3$], 31.71 [$\text{C}(\text{CH}_3)_3$], 30.29 [$\text{C}(\text{CH}_3)_3$] ppm. $\text{C}_{56}\text{H}_{68}\text{HfO}_2\text{S}_2$ (1015.76): calcd. C 66.22, H 6.75; found C 65.93, H 6.36.

[Zr(L)(CH₂Ph)₃] (4): Following a procedure analogous to that of 1, starting from $[\text{Zr}(\text{CH}_2\text{Ph})_4]$ (0.28 g, 0.61 mmol) and LH (0.20 g, 0.61 mmol), the product $[\text{Zr}(\text{L})(\text{CH}_2\text{Ph})_3]$ (4) was obtained as yellow crystals (0.36 g, 86%). ^1H NMR (C_6D_6): δ = 7.45 (d, $^4J_{\text{HH}}$ = 2.4 Hz, 1 H, C_6H_2 -3-*H*), 7.19–6.80 (m, 20 H, SC_6H_5 and $\text{ZrCH}_2\text{C}_6\text{H}_5$), 6.52 (d, $^4J_{\text{HH}}$ = 2.4 Hz, 1 H, C_6H_2 -5-*H*), 3.50 (s, 2 H, CH_2S), 2.34 (s, 6 H, ZrCH_2Ph), 1.72 [s, 9 H, $\text{C}(\text{CH}_3)_3$], 1.17 [s, 9 H, $\text{C}(\text{CH}_3)_3$] ppm. $^{13}\text{C}\{^1\text{H}\}$ NMR (C_6D_6): δ = 158.82 (C_6H_2 -C1), 142.61 (CH_2Ph -C1), 142.31 (C_6H_2 -C4), 136.02 (C_6H_2 -C2), 132.75 (SPh-C1), 128.26 (SPh-C3), 127.67 (CH_2Ph -C3), 127.28 (SPh-C2), 127.06 (CH_2Ph -C2), 125.88 (C_6H_2 -C5), 125.07 (SPh-C4), 123.25 (C_6H_2 -C3), 122.76 (C_6H_2 -C6), 121.57 (CH_2Ph -C4), 71.89 (ZrCH_2Ph), 39.10 (SCH_2), 35.06 [$\text{C}(\text{CH}_3)_3$], 34.01 [$\text{C}(\text{CH}_3)_3$], 31.10 [$\text{C}(\text{CH}_3)_3$], 29.81 [$\text{C}(\text{CH}_3)_3$] ppm. $\text{C}_{42}\text{H}_{48}\text{OSZr}$ (692.12): calcd. C 72.88, H 6.99; found C 72.54, H 7.06.

Generation of the Ion Pair $[\text{Zr}(\text{L})_2(\text{CH}_2\text{Ph})]^+[\text{PhCH}_2\text{B}(\text{C}_6\text{F}_5)_3]^-$ (5):

In a glove box, a Teflon-valved NMR tube was charged with $[\text{Zr}(\text{L})_2(\text{CH}_2\text{Ph})_2]$ (2) (18.6 mg, 0.02 mmol) and $\text{B}(\text{C}_6\text{F}_5)_3$ (10.2 mg, 0.02 mmol). $\text{C}_6\text{D}_5\text{Br}$ (ca. 0.5 mL) was added by syringe. The tube was sealed, and NMR spectra revealed the quantitative formation of the cation $[\text{Zr}(\text{L})_2(\text{CH}_2\text{Ph})]^+[\text{PhCH}_2\text{B}(\text{C}_6\text{F}_5)_3]^-$ (5). All volatiles were removed under vacuum, and the oily residue was washed with pentane (3 × 1 mL) and dried under vacuum to leave 5 as a pale yellow powder (23 mg, 80%). ^1H NMR ($\text{C}_6\text{D}_5\text{Br}$): δ = 7.59 (d, $^4J_{\text{HH}}$ = 2.2 Hz, 2 H, C_6H_2 -3-*H*), 7.49–6.97 (m, 20 H, aromatic signals), 6.76 (d, $^4J_{\text{HH}}$ = 2.2 Hz, 2 H, C_6H_2 -5-*H*), 3.95 (s, 4 H, CH_2S), 3.58 (s, 2 H, PhCH_2B), 3.27 (s, 2 H, ZrCH_2Ph), 1.70 [s, 18 H, $\text{C}(\text{CH}_3)_3$], 1.28 [s, 18 H, $\text{C}(\text{CH}_3)_3$] ppm. $^{13}\text{C}\{^1\text{H}\}$ NMR ($\text{C}_6\text{D}_5\text{Br}$): δ = 157.80 (C_6H_2 -C1), 149.25 (BCH_2Ph -C1), 145.53 (C_6H_2 -C4), 137.08 (C_6H_2 -C2), 133.24 (Ph-C), 129.82 (Ph-C), 129.23 (Ph-C), 127.27 (Ph-C), 126.87 (C_6H_2 -C5), 125.52 (C_6H_2 -C3), 125.37 (Ph-C), 122.77 (Ph-C), 122.91 (Ph-C), 74.15 (ZrCH_2Ph), 41.52 (SCH_2), 35.22 [$\text{C}(\text{CH}_3)_3$], 34.22 [$\text{C}(\text{CH}_3)_3$], 32.11 (PhCH_2B), 31.26 [$\text{C}(\text{CH}_3)_3$], 30.43 [$\text{C}(\text{CH}_3)_3$] ppm. ^{11}B NMR ($\text{C}_6\text{D}_5\text{Br}$): δ = -11.9 (s, BCH_2Ph) ppm. ^{19}F NMR ($\text{C}_6\text{D}_5\text{Br}$): δ = -129.7 (d, $^3J_{\text{FF}}$ = 24 Hz, 6 F, *o*-F), -163.4 (t, $^3J_{\text{FF}}$ = 24 Hz, 3 F, *p*-F), -166.0 (m, $^3J_{\text{FF}}$ = 24 Hz, 6 F, *m*-F) ppm.

Generation of the Ion Pair $[\text{Zr}(\text{L})(\text{CH}_2\text{Ph})_2]^+[\text{PhCH}_2\text{B}(\text{C}_6\text{F}_5)_3]^-$ (6):

In a glove box, a Teflon-valved NMR tube was charged with $[\text{Zr}(\text{L})(\text{CH}_2\text{Ph})_3]$ (4) (14.0 mg, 0.02 mmol) and $\text{B}(\text{C}_6\text{F}_5)_3$ (10.2 mg, 0.02 mmol). $\text{C}_6\text{D}_5\text{Br}$ (ca. 0.5 mL) was added by syringe. After sealing the tube, NMR spectra were recorded, which revealed the quantitative formation of the cationic species $[\text{Zr}(\text{L})(\text{CH}_2\text{Ph})_2]^+[\text{PhCH}_2\text{B}(\text{C}_6\text{F}_5)_3]^-$ (6). All volatiles were removed under vacuum, and the oily residue was washed with pentane (3 × 1 mL) and dried under vacuum to give 6 as a pale yellow powder (20 mg, 82%). ^1H NMR ($\text{C}_6\text{D}_5\text{Br}$): δ = 7.55 (d, $^4J_{\text{HH}}$ = 2.2 Hz, 1 H, C_6H_2 -3-*H*), 7.36–6.94 (m, 20 H, aromatic signals), 6.78 (d, $^4J_{\text{HH}}$ = 2.2 Hz, 1 H, C_6H_2 -5-*H*), 4.12 (s, 2 H, CH_2S), 3.50 (s, 2 H, PhCH_2B), 2.39 (s, 4 H, ZrCH_2Ph), 1.48 [s, 9 H, $\text{C}(\text{CH}_3)_3$], 1.30 [s, 9 H, $\text{C}(\text{CH}_3)_3$] ppm. $^{13}\text{C}\{^1\text{H}\}$ NMR ($\text{C}_6\text{D}_5\text{Br}$): δ = 158.48 (C_6H_2 -C1), 149.17 (BCH_2Ph -C1), 146.62 (C_6H_2 -C4), 138.02 (C_6H_2 -C2),

133.48 (Ph-C), 128.28 (Ph-C), 127.32 (Ph-C), 126.54 (C₆H₂-C5), 125.62 (Ph-C), 125.42 (C₆H₂-C3), 122.97 (Ph-C), 121.77 (Ph-C), 75.32 (ZrCH₂Ph), 42.80 (SCH₂), 34.88 [C(CH₃)₃], 34.36 [C(CH₃)₃], 31.37 (PhCH₂B), 30.03 [C(CH₃)₃], 30.43 [C(CH₃)₃] ppm. ¹¹B NMR (C₆D₅Br): δ = -11.7 (s, BCH₂Ph) ppm. ¹⁹F NMR (C₆D₅Br): δ = -130.6 (d, ³J_{FF} = 24 Hz, 6 F, *o*-F), -163.5 (t, ³J_{FF} = 24 Hz, 3 F, *p*-F), -166.2 (m, ³J_{FF} = 24 Hz, 6 F, *m*-F) ppm.

Typical 1-Hexene Polymerization Procedure: Into a 30 mL-flask equipped with a magnetic stirrer, the catalyst (0.02 mmol), 1-hexene (1.01 g, 12 mmol), and toluene (8 mL) were added. The solution was kept at the desired polymerization temperature. The activator B(C₆F₅)₃ or Al(C₆F₅)₃·0.5C₇H₈ (0.02 mmol) in toluene (2 mL) was rapidly added by syringe. The polymerization was carried out over a specified time period. The reaction was quenched by adding acidified methanol (3% HCl, 1 mL). The reaction mixture was dried under vacuum. The poly(1-hexene)s were purified by CHCl₃/CH₃OH, and the oligo(1-hexene)s were purified by passing their hexane solution through a pipette containing silica gel. The polymer or oligomer was dried overnight under vacuum.

Crystal Structure Determination of Complex 3: The X-ray diffraction measurement was performed on a Bruker AXS diffractometer with Mo-K α radiation using ω -scans. Crystal parameters and the results of the structure refinement are given in Table 2. The investigated crystal was non-merohedrally twinned. The program system PLATON was used to create an intensity data set with indices for both twinned domains.^[12] The structure was solved by direct methods (SHELXS-86)^[13a] and refined (SHELXS-97)^[13b] against all *F*² data. All non-hydrogen atoms were refined with anisotropic displacement parameters. Hydrogen atoms were included into calculated positions. For the graphical representations, the program ORTEP was used as implemented in the program system WinGX.^[14] CCDC-696292 (3) contains the supplementary crystallographic data for this paper. These data can be obtained free of charge from The Cambridge Crystallographic Data Centre via www.ccdc.cam.ac.uk/data_request/cif.

Table 2. Crystal data and structure refinement for 3.

Empirical formula	C ₅₆ H ₆₈ HfO ₂ S ₂
<i>M_r</i> [g mol ⁻¹]	1015.71
Crystal size [mm]	0.26 × 0.12 × 0.10
Crystal color and habit	colorless prism
Crystal system	triclinic
Space group	<i>P</i> $\bar{1}$
<i>a</i> [Å]	12.670(3)
<i>b</i> [Å]	12.932(3)
<i>c</i> [Å]	15.229(4)
α [°]	89.756(4)
β [°]	88.091(4)
γ [°]	79.012(4)
<i>Z</i>	2
<i>D</i> _{calcd.} [g cm ⁻³]	1.378
<i>T</i> (K)	130(2)
μ (Mo-K α) [mm ⁻¹]	2.256
<i>F</i> (000)	1048
θ range [°]	2.06–31.12
Number of reflections collected	14019
Number of reflections observed [<i>I</i> > 2 σ (<i>I</i>)]	11134
Data/restraints/parameters	14019/5/564
Goodness-of-fit on <i>F</i> ²	1.051
<i>R</i> ₁ , <i>wR</i> ₂ [<i>I</i> > 2 σ (<i>I</i>)]	0.0716/0.1827
<i>R</i> ₁ , <i>wR</i> ₂ (all data)	0.0880/0.1910
Largest difference in peak and hole [e Å ⁻³]	6.084/–4.362

Acknowledgments

We thank the Deutsche Forschungsgemeinschaft and the Fonds der Chemischen Industrie for financial support. We are grateful to Mr. Y.-T. Wang for collecting the X-ray data and to Prof. U. Englert for helpful discussions.

- a) G. J. P. Britovsek, V. C. Gibson, D. F. Wass, *Angew. Chem. Int. Ed.* **1999**, *38*, 428–447; b) V. C. Gibson, S. K. Spitzmesser, *Chem. Rev.* **2003**, *103*, 283–316.
- For selected references, see: a) J. Saito, M. Mitani, J.-I. Mohri, Y. Yoshida, S. Matsui, S.-I. Ishii, S.-I. Kojoh, N. Kashiwa, T. Fujita, *Angew. Chem. Int. Ed.* **2001**, *40*, 2918–2920; b) M. Mitani, R. Furuyama, J.-I. Mohri, J. Saito, S. Ishii, H. Terao, N. Kashiwa, T. Fujita, *J. Am. Chem. Soc.* **2002**, *124*, 7888–7889; c) J. Tian, G. W. Coates, *Angew. Chem. Int. Ed.* **2000**, *39*, 3626–3629; d) J. Tian, P. D. Hustad, G. W. Coates, *J. Am. Chem. Soc.* **2001**, *123*, 5134–5135; e) E. Y. Tshuva, I. Goldberg, M. Kol, *J. Am. Chem. Soc.* **2000**, *122*, 10706–10707; f) V. Busico, R. Cipullo, N. Friederichs, S. Ronca, M. Togrou, *Macromolecules* **2003**, *36*, 3806–3808; g) A. Yeori, I. Goldberg, M. Shuster, M. Kol, *J. Am. Chem. Soc.* **2006**, *128*, 13062–13063; h) V. Busico, R. Cipullo, R. Pellicchia, S. Ronca, G. Roviello, G. Talarico, *Proc. Natl. Acad. Sci. USA* **2006**, *103*, 15321–15326; i) E. Kirillov, L. Lavanant, C. Thomas, T. Roisnel, Y. Chi, J.-F. Carpentier, *Chem. Eur. J.* **2007**, *13*, 923–935; j) R. L. Long, V. C. Gibson, A. J. P. White, *Organometallics* **2008**, *27*, 235–245.
- a) C. Capacchione, A. Proto, H. Ebeling, R. Mülhaupt, K. Möller, T. P. Spaniol, J. Okuda, *J. Am. Chem. Soc.* **2003**, *125*, 4964–4965; b) C. Capacchione, R. Manivannan, M. Barone, K. Beckerle, R. Centore, L. Oliva, A. Proto, A. Tuzi, T. P. Spaniol, J. Okuda, *Organometallics* **2005**, *24*, 2971–2982; c) K. Beckerle, R. Manivannan, T. P. Spaniol, J. Okuda, *Organometallics* **2006**, *25*, 3019–3026; d) K. Beckerle, R. Manivannan, B. Lian, G.-J. M. Meppelder, G. Raabe, T. P. Spaniol, H. Ebeling, F. Pelascini, R. Mülhaupt, J. Okuda, *Angew. Chem. Int. Ed.* **2007**, *46*, 4790–4793; e) B. Lian, K. Beckerle, T. P. Spaniol, J. Okuda, *Angew. Chem. Int. Ed.* **2007**, *46*, 8507–8510; f) B. Lian, T. P. Spaniol, J. Okuda, *Organometallics* **2007**, *26*, 6653–6660.
- a) C. Capacchione, A. Proto, V. Venditto, J. Okuda, *Macromolecules* **2003**, *36*, 9249–9251; b) C. Capacchione, M. D'Acunzi, O. Motta, L. Oliva, A. Proto, J. Okuda, *Macromol. Chem. Phys.* **2004**, *205*, 370–373; c) C. Capacchione, A. Proto, J. Okuda, *J. Polym. Sci. Part A: Polym. Chem.* **2004**, *42*, 2815–2822; d) C. Capacchione, F. De Carlo, C. Zannoni, J. Okuda, A. Proto, *Macromolecules* **2004**, *37*, 8918–8922; e) C. Capacchione, A. Proto, H. Ebeling, R. Mülhaupt, J. Okuda, *J. Polym. Sci. Part A: Polym. Chem.* **2006**, *44*, 1908–1913; f) C. Capacchione, A. Avagliano, A. Proto, *Macromolecules* **2008**, *41*, 4573–4575; g) B. T. Gall, F. Pelascini, H. Ebeling, K. Beckerle, J. Okuda, R. Mülhaupt, *Macromolecules* **2008**, *41*, 1627–1633.
- a) D. Wiśniewska, Z. Janas, P. Sobota, L. B. Jerzykiewicz, *Organometallics* **2006**, *25*, 6166–6169; for other Hf-S bond lengths, see: b) J. J. W. Eshuis, Y. Y. Tan, A. Meetsma, J. H. Teuben, J. Renkema, G. G. Evens, *Organometallics* **1992**, *11*, 362–369; c) E. Y. Tshuva, S. Groysman, M. Kol, Z. Goldschmidt, *Organometallics* **2002**, *21*, 662–670; d) R. Hart, W. Levason, B. Patel, G. Reid, *J. Chem. Soc., Dalton Trans.* **2002**, 3153–3159.
- a) H. Makio, Y. Tohi, J. Saito, M. Onda, T. Fujita, *Macromol. Rapid Commun.* **2003**, *24*, 894–899; b) H. Tsurugi, K. Mashima, *Organometallics* **2006**, *25*, 5210–5212.
- The fluxionality as well as polymerization behavior of a more extensive series of similar group 4 metal complexes have been independently studied by: M. Lamberti, M. Mazzeo, C. Pellicchia, Abstract no. P136, International Conference on Organometallic Chemistry, Rennes, France, **2008**; C. Pellicchia, private communication.

- [8] I. Cepanec, H. Mikuldaš, V. Vinković, *Synth. Commun.* **2001**, *31*, 2913–2919.
- [9] M. Lanznaster, H. P. Hratchian, M. J. Heeg, L. M. Hryhorczuk, B. R. McGarvey, H. B. Schlegel, C. N. Verani, *Inorg. Chem.* **2006**, *45*, 955–957.
- [10] U. Zucchini, E. Albizzati, U. Giannini, *J. Organomet. Chem.* **1971**, *26*, 357–372.
- [11] S. Feng, G. R. Roof, E. Y.-X. Chen, *Organometallics* **2002**, *21*, 832–839.
- [12] A. L. Spek, *PLATON, A Multipurpose Crystallographic Tool*, Utrecht University, Utrecht, The Netherlands, **1999**.
- [13] a) G. M. Sheldrick, *SHELXS-86, A Program for Crystal Structure Solution*, University of Göttingen, Germany, **1986**; b) G. M. Sheldrick, *SHELXL-97, A Program for Crystal Structure Refinement*, University of Göttingen, Germany, **1997**.
- [14] L. J. Farrugia, *J. Appl. Crystallogr.* **1999**, *32*, 837.

Received: August 14, 2008

APublished Online: December 2, 2008